

Robotic Tower Crane Modelling Control (RTCMC)

Thein Moe Win

A thesis in fulfilment of the requirements for the degree of
Doctor of Philosophy



School of Electrical Engineering & Telecommunication
Faculty of Engineering
The University of New South Wales

April 2017

Abstract

Fast and accurate positioning and swing minimization of payloads in large standing tall tower crane operation are challenging as well as conflicting tasks. Juggling the trolley back-and-forth manually by crane operator to suppress payload swing can make time consuming and cause fatigue. Minimizing the load swing is also primarily limited by the existence of wind disturbance effect triggering higher tower vibration, especially in the high speed course and load is in the end of tower region. Unstable load swing due to wind disturbance, vibration, and operational error would subsequently cause the crane collapse as well risk the whole working environment. Tower Crane Incidents World statistic shows 23% of crane accidents are due to wind disturbance while 38% are operational error.

Motivated by Robotic Tower Crane (RTC), this work investigates solutions to a class of problem where swing suppression is critical to overcoming poor performance of highly nonlinear trolley-tower-payload crane operational control. Since having uneasy tasks for the researchers to explore research works on operating crane, controllers proposed in the past have as well been based on lab-scale prototype or mathematical sketch which would rather become impractical.

While risk free crane operation is desirable in a crane modelling and control, the problem in swing minimization is that disturbance predictions are prone to error due to the variability and complexity of trolley-payload interaction forces. However, the use of robotic tower crane model control (RTCMC) with disturbance rejection observer and linear estimator integral approaches could significantly improve the rejection of disturbances (crane vibration due to wind disturbance, unknown dynamics, and noise) as well as achieve reference tracking of control system beyond the limitations of feedback.

Cranes in construction and shipyard sectors still entirely rely on human operator with manual joystick to perform costly-time consuming tasks since proposed mathematical linear-nonlinear models have never been practical to date. Ignoring some essential parameters in linear model optimization could also pamper the control performance. Vibration impact on the large standing tall tower crane is also another huge contributing factor as it can cause instability during crane operation and windy weather condition. Though wind disturbance issue has been paid much attention in wind turbine control, the vibration impact of wind disturbance on tower crane in construction sectors has widely been ignored. Therefore, to explicitly address the use RTCMC in this new technological era, the principles of crane modelling, optimization, vibration impact, swing minimization, and control issues are required to be reviewed.

This work proposes a range of issues in implementing RTCMC. Firstly, SimMechanics-visualized RTC model development using real tower crane Morrow (Liebherr 71EC) datasheet has been considered. Secondly, wind disturbance model is designed based on Gawronski approach, applies different wind patterns on RTC model, and analyses the vibration impact on the payload swing instability. Thirdly, The best optimized mathematical linear model is derived using improved-linear least square algorithm. Fourthly, to actively reject the disturbances caused by undesired source of inputs or unknown dynamics, LQR-Disturbance Rejection Observer (DRO) Control with Luenberger-based Extended State Observer is introduced. This research further examines the combination of error space approach with estimator, from which it is argued that the LQR-Estimator-Integral Control (LEIC) for linear model is necessary to achieve robust tracking. Finally, in order to achieve robust tracking control of highly nonlinear trolley translation-payload swing working environment fuelled by wind disturbance, LQR-DRO control with torque compensator actuation is implemented on the interaction joints between trolley and payload cables. Several combinations of joints-sensors-actuators-extra links implementations on payload swing were initially tried before considering proposed method.

During simulation trials, proposed RTCMC demonstrated the ability to iteratively achieve desired trolley translation-loadswing geometry. Under this iterative method, all weighting Q-R matrices, Observer gains L matrix, and uncertainties gains have adapted to different input conditions and passes were repeated autonomously until pre-specified trajectories of trolley-loadswing were achieved. Evidences of improvements in LQR-DRO and LEIC-Antiwindup controls for linear models as well as LQR-DRO for nonlinear RTCMC are presented.

Tower crane payload swing minimization is one of the oldest challenges in the field of construction automation; despite decades of research, no commercial deployment of a fully autonomous swing minimization has been reported to date in regards to large standing-tall operational tower crane. In the literature, proposed solutions have required stringent preconditions, such as visual scanning of terrain profiles in construction sites, the design of vibration suppression control using sway angle observer with friction disturbance, neural network with GA-based training, etc.. These considerations increase the difficulty of implementing the controller in time. Control solutions in this research focused on simplicity of implementation: general and straightforward reference-tracking control methods were preferred over Tower crane-tailored formulations. The benefit is that, the proposed RTCMC has potential applications to other types of crane operations and global crane research.

ACKNOWLEDGEMENTS

My profound gratitude goes first and foremost to my supervisor Associate Professor Timothy Hesketh and Co-Supervisor Dr. Ramond Eaton for their great encouragement, support and guidance. Tim and Ray have always been open and friendly in every aspect of research discussion. From the very first step of sketch to the every improvement of research stage, their valuable inputs were quite substantial. With their enthusiastic help, I have achieved three international journal papers, three poster-presentation competitions, the precious IEEE-iToF best poster-presentation award, certificated of commended caper for my 3rd paper in prestigious IREACO journal, and appreciation of acknowledgement in UNSW-GRS June-2016 Newsletter. I am very grateful for being their research student and I believe those memorable days would last forever.

I would like to wholeheartedly express my sincere gratitude to Islamic Development Bank (IDB, Jeddha) for alleviating my life from a hard-labour man to a PhD Graduate. Without that merit scholarship support to study abroad, my life would have been in struggles.

In particular, I would like to thank my beloved wife, Theingi Aye for her profound supports, great patience, and courage throughout our life struggles. I am very much indebted to her. And of course, dedication goes to my lovely children: Min htat, Su Myat Moe, and Si Thu.

My ultimate gratitude goes to my mother who sacrificed everything in raising me, and her thoughts and prayers have always been with me towards the success. Finally, I would like to say Alhamdullilah (being thankful) to Allah Almighty, The Creator and the Sustainer of the whole Universe, for granting my life endeavour.

Abbreviations

autoCAD	Computer-Aided-Design software
SimMechanics	Set of block libraries with mechanical Modelling and
RNEA	Recursive Newton-Euler Algorithm
Liebherr71EC	Standing Tall Tower Crane from Morrow Crane Industry
LLS	Linear least square
LQR	Linear Quadratic Regulator
PID	Proportional-Integral-Derivative
LEIC	LQR-Estimator-Integral Control
DRO	Disturbance Rejection Observe
NARX	Nonlinear Autoregressive exogenous
RTCMC	Robotic Tower Crane Modelling Control
SMS	Sliding Mode Control
DOF	Degree of Freedom
ESO	Extended State Observer
RMSE	Root Mean Square Error
RFID	Radio Frequency Identification
PDA	Personal Data Assistant
LCD	Liquid-Crystal Display
PIV	Proportional-Integral-Velocity Compensator
FTC	Fault Tolerant Control

Symbols

J	Cost Function
P	Riccati Equation
Ma	Moment at Pivot point A
$F_{counterjib}$	Acting Force at the end of counterjib
y_{ss}	Steady State Output
v_{ws}	Wind Static Velocity
v_{wg}	Wind Gust Velocity
$\Delta_{v_0}(t)$	Initial wind gust speed
F_{ws}	Wind-static Force
K_{df}	Dragging Force Coefficient
F_t	Wind Force Total
$\Delta_v(t)$	Standard Deviation
y_{ls}	Measurement Output
y_i	Actual Output

List of Figures

Figure 1.1	Large Standing Tall Operating Tower Crane	1
Figure 1.2	Tower Crane Collapse and Environmental Risk	1
Figure 1.3	Tower Crane Incidents Statistic by Health and Safety Executive (HSE)	2
Figure 1.4	SimMechanics-Visualized Tower Crane Model development based on	3
Figure 2.1	Tower cranes working in a construction Site	9
Figure 2.2	Overhead crane free-body diagram in	10
Figure 2.3	Three-dimensional overhead crane free-body diagram	11
Figure 2.4a	Lab-scale tower crane model developed by Quanser	12
Figure 2.4b	Lab-scale tower crane model developed by Inteco	12
Figure 2.5a	Overhead crane lab-scale model used by	12
Figure 2.5b	Overhead crane lab-scale model free-body diagram in	12
Figure 2.6	Deformed shape of crane structure with the spherical pendulum	13
Figure 2.7	Tower Crane Model built using Soliworks and Auto CAD graphic software to analyse the crane strength in	13
Figure 2.8	Overhead Crane free-body diagram	15
Figure 2.9	Tower crane illustration with Kinematic nonlinearity of trolley-payload Oscillation	16
Figure 2.10	Tower crane model free-body diagram with wind disturbance	18
Figure 2.11a	Free-body diagram of swing oscillation with jib vibration	19
Figure 2.11b	Input Shaper design for vibration suppression	19
Figure 2.12	Comparisons of Input shaper with other filters	19
Figure 2.13	Vibration damping for flexible-link	20
Figure 2.14	Disturbance Observer implementation	21
Figure 2.15	Pulse frequency signal with input shaping	23
Figure 2.16a	HiBay crane model at Georgia Institute of Technology	24
Figure 2.16b	Input Shaper for position control	24
Figure 2.17	The illustration of payload trajectory along the pre-specified reference	25
Figure 2.18a	Vision Based position Measurement	26
Figure 2.18b	Wand controller with PD disturbance	27
Figure 2.18c	Hook with Circular reflective material which updates hook's relative Position	26
Figure 2.19a	Load location transmission to operator	27
Figure 2.19b	Video camera mounting	27
Figure 3.1	Free-body diagram of Jib System	30
Figure 3.2a	Trolley-Payload Models Excitation	34
Figure 3.2b	Trolley-Payload System Response	34
Figure 3.3	3D tower crane positions identification (Cartesian coordinate)	36
Figure 3.4	Trolley translational motion along jib	37
Figure 3.5	2D SimMechanics Visualized Overhead	46
Figure 3.6	Measurements and Moment of Inertia for Rectangle	47
Figure 3.7	Measurement and Moment of Inertia for Rectangle form Jib	47
Figure 3.8	Measurements and Moment of Inertia for	48
Figure 3.9	SimMechanics model visualization of the crane system with payload	50

Figure 3.10 Pseudo-Random Input Signal at Frequency 10, range -1 to 1	50
Figure 3.11 2D Overhead Crane Model excitation and Trolley-Payload	51
Figure 3.12 3D Overhead Gantry Crane Model Free-body Diagram	52
Figure 3.13a Spherical joint used between trolley and steel cable	53
Figure 3.13b Spherical joint and its specifications	53
Figure 3.14 Spherical joint sensor outputs in 3D load swing angles	54
Figure 3.15 Force Signals for Trolley-Jib X-Y Run	55
Figure 3.16 3D Overhead Crane Visualized Model	55
Figure 3.17 3D Overhead Crane SimMechanics Model to generate Visualization	56
Figure 3.18a Load-swings in X-Y-Z Directions	57
Figure 3.18b Lissajous Graph for X-Y-Z Load-swings	57
Figure 3.19a Training and Checking Model	59
Figure 3.19b RMSE Comparison between actual and predicted models	60
Figure 3.20a Den 3 Num 3 Trolley model	61
Figure 3.20b Den 3 Num 2 Load Swing model	61
Figure 3.21 Improved LLS Algorithm to compute lowest RMSE	63
Figure 3.22 RMSEs from high to low with respective models	64
Figure 3.23a Den 4 Num 4 Trolley model	66
Figure 3.23b Den 3 Num 4 Load Swing model	66
Figure 3.24a RMSE Comparison for Normal LLS and Improved LLS for	67
Figure 3.24b RMSE Comparison for Normal LLS and Improved LLS for Trolley Case	67
Figure 3.25 LQR Controller Design	69
Figure 3.26 LQR-Controlled models response comparison	70
Figure 3.27a Full state feedback-LQR Reference Tracking Control	71
Figure 3.27b Full state feedback-LQR with pre-compensator \bar{N}	71
Figure 3.28 Full-state feedback-LQR Reference Tracking Control	78
Figure 3.29a Full-state feedback-LQR Control Responses Trolley Models with Different QR Weighting Matrices	73
Figure 3.29b Full-state feedback-LQR Control Responses Payload Models with Different QR Weighting Matrices	73
Figure 3.30 Libherr 71-EC Morrow Tower Crane Datasheet	75
Figure 3.31a Concrete Base Visualization	76
Figure 3.31b Concrete Base SimMechanics	76
Figure 3.32a Concrete Footing in angle view	76
Figure 3.32b Measure style for Rectangle block	76
Figure 3.33a One side of Base Frame 4-m Visualization	78
Figure 3.33b One side of Base Frame 4-m SimMechanics	78
Figure 3.34a Base Frame Visualization	79
Figure 3.34b Base Frame SimMechanics	79
Figure 3.35a One side of Hub Frame 12-m Visualization	80
Figure 3.35b One side of Hub Frame 12-m SimMechanics	80
Figure 3.36a Hub Frame 12-m Visualization	81
Figure 3.36b Hub Frame 12-m SimMechanics	81
Figure 3.37a Hub Frame 6-m Visualization	82
Figure 3.37b Hub Frame 12-m SimMechanics	82
Figure 3.38a Hub Frame 6-m Visualization	83
Figure 3.38b Hub Frame 6-m SimMechanics	83

Figure 3.39a Visualized Tower Crane Hub 22.2 m	84
Figure 3.39b SimMechanics Tower Hub 22.2 m	84
Figure 3.40 Slewing Assembly from Morrow data sheet	84
Figure 3.41a Visualized Slewing Assembly	85
Figure 3.41b SimMechanics Slewing Assembly	85
Figure 3.42 Complete Counter Jib shown in Morrow data sheet	86
Figure 3.43a Combined Counter-jib SimMechanics design	87
Figure 3.43b Combined Counter-jib visualized-view	87
Figure 3.44a one side of tower jib 12-m extension SimMechanics	88
Figure 3.44b one side of tower jib 12-m extension Visualization	88
Figure 3.45 SimMechanics Visualized tower jib extension (12+12+2.31m)	90
Figure 3.46a SimMechanics trolley rail cart-attached load	91
Figure 3.46b Visualised trolley rail cart-attached load	91
Figure 3.47 Visualized Tower Crane Model	92
Figure 3.48 SimMechanics Design of developed Tower Crane Model	93
Figure 3.49 Libherr Crane Drive Info and its motor with pulley attached	94
Figure 3.50 Frictions and Brakes Dampers Design	95
Figure 3.51 Libherr Crane Drive Info and its motor with pulley attached	96
Figure 4.1 Identify Counter weight at Crane's equilibrium position	98
Figure 4.2 Establish equilibrium position	99
Figure 4.3 Jib Moment M_a at Pivot A	100
Figure 4.4 Moment of Inertia at pivot A using different payloads	102
Figure 4.5a Moments at pivot A for payload 1000 Kg	102
Figure 4.5b Moments at pivot A for payload 3000 Kg	102
Figure 4.6 Rigid Crane Model with Trolley Translational Motion	103
Figure 4.7 Rigid Crane Model Simulations results	105
Figure 4.8 Worst Case results for (3000W_1000Kg) in Rigid Crane Model	105
Figure 4.9 Ideal Crane Model with Trolley Translational Motion	106
Figure 4.10 Ideal Crane Model Trolley Translation with results	107
Figure 4.11 Ideal Crane Model Trolley Translation with results for 3000W_1000Kg	107
Figure 4.12 Wind surface terrain ($x=0.12m, y=0.12m$)	109
Figure 4.13 Apply Wind Disturbance Model on Ideal Model	111
Figure 4.14 Wind Model Surface Area ($x=0.12m, y=0.12m$), 1s notch wind strike	112
Figure 4.15 Load swing , Jip Tip, Hub Top Oscillations changes due to different wind model strikes	113
Figure 4.16 Load Swing-Jib tip-Hub top relationship due to	113
Figure 4.17a Load Swings of without Wind and with Wind Pattern (22-43-017) in Trolley Translation Case	114
Figure 4.17b Jib Oscillation of without Wind and with Wind Pattern (22-43-017) in Trolley Translation Case	114
Figure 4.17c Load Swings of without Wind and with Wind Pattern (41-86-1010) in Trolley Translation Case	114
Figure 4.17d Jib Oscillation of without Wind and with Wind Pattern (41-86-1010) in Translation Case	114
Figure 4.18 Jib/Hub Oscillation of Tower rotation	115
Figure 4.19 Load swing and Jib-Hub Oscillation of Tower rotation	116
Figure 4.20a Load Swing X-Y-Z responses for 6.3kW_3000Kg without wind	117

Figure 4.20b Jib tip-Hub top Oscillations for 6.3kW_3000Kg without wind	117
Figure 4.21 Ideal Tower Rotation with Wind Disturbance and Trolley at 24 m	118
Figure 4.22a Load Swing X-Y-Z responses	119
Figure 4.22b Jib tip-Hub top Oscillations	119
Figure 4.23a Load Swings without Wind and with Wind Pattern (22-43-017) in Tower Rotation Case	120
Figure 4.23b Jib Oscillation of without Wind and with Wind Pattern (22-43-017) in Tower Rotation Case	120
Figure 4.23c Load Swings without Wind and with Wind Pattern (41-86-1010) in Tower Rotation Case	120
Figure 4.23d Jib Oscillation of without Wind and with Wind Pattern (41-86-1010) in Tower Rotation Case	120
Figure 4.24a Parallel Operation of Tower Rotation and Trolley Translation	121
Figure 4.24b Swing angles in (X-Y-Z) directions	121
Figure 4.24c Jib-Tip Oscillation with Wind Pattern (22-43-1017)	121
Figure 4.24d Hub-Top Oscillation with Wind Pattern (22-43-1017)	121
Figure 4.25 Wind Disturbance strikes on Tower Crane	123
Figure 4.26a The Best Fit Tower Angular Rotational Linear Model vs Nonlinear Actual Output	124
Figure 4.26b The Best Fit Payload swing Linear Model vs Nonlinear Actual Output	125
Figure 4.27 Full state feedback-LQR Control for Tower rotation and loadswing	127
Figure 4.28a LQR Full State Feedback Control for Tower Rotation	127
Figure 4.28b Comparison of LQR Full-State Feedback Controlled Load Swing and Nonlinear Load Swing	127
Figure 4.29 Simple PID Controller Design	128
Figure 4.30a Full state feedback-LQR Control for Tower rotation	128
Figure 4.30b Full state feedback-LQR Control for Payload swing	128
Figure 5.1 Tower Crane SimMechanics-Visualized 3D Model based on (Liebheer 71 EC: Morrow Crane data sheet)	131
Figure 5.2 Trolley Translation in Control Canonical Form	133
Figure 5.3 Disturbance Rejection Observer Implementation	136
Figure 5.4 LQR-DRO Control	139
Figure 5.5 LQR-DRO Controller performance with different Observer columns	140
Figure 5.6 LQR-DRO Controlled Trolley-Loadswing	141
Figure 5.7 LQR-Estimator-Integral Control (LEIC) for Linear Model	142
Figure 5.8 LQR-Estimator-Integral Control (LEIC) in Simulink	145
Figure 5.9 LQR, LQR-DRO, and LEIC Comparison	146
Figure 5.10a Simple LQR Controlled Loadswing output	147
Figure 5.10b LQR-DRO Controlled Loadswing output	147
Figure 5.10c LEIC-Controlled Loadswing output	147
Figure 5.11 Trolley-Payload Free Body Diagram	148
Figure 5.12 Training and Validating Trolley Model using NARX	149
Figure 5.13 Nonlinear Autoregressive exogenous (NARX) Structure	150
Figure 5.14 LEIC-Antiwindup Controller Design for Linear ARX Trolley Model	152
Figure 5.15 Trolley position Tracking using LEIC-antiwindup Control	152
Figure 5.16 LQR, LQR-DRO, LQR-LEIC, LQR-LEIC Antiwindup Controllers	153
Figure 5.17a LQR, LQR-DRO, LQR-LEIC, LQR-LEIC Antiwindup Performance Comparison for Trolley Model	154

Figure 5.17b LQR, LQR-DRO, LQR-LEIC, LQR-LEIC Antiwindup Performance Comparison for Trolley Model	154
Figure 5.18a LQR Control Effort	155
Figure 5.18b DRO Control Effort	155
Figure 5.18c LEIC Control Effort	155
Figure 5.18d LEIC-Antiwindup Control Effort	155
Figure 5.19 Training and Validating Payload Model using NARX	156
Figure 5.20 Torque to Power Conversion	157
Figure 5.21 LQR, LQR-DRO, LQR-LEIC, LQR-LEIC Antiwindup Controls for Payload Swing Models	158
Figure 5.22a LQR, LQR-DRO, LQR-LEIC, LQR-LEIC Antiwindup Payload Swing Responses	159
Figure 5.22b LQR, LQR-DRO, LQR-LEIC, LQR-LEIC Antiwindup Performance Comparison for Payload Swing	159
Figure 6.1 Nonlinear Robotic Tower Crane Modelling Control (RTCMC)	163
Figure 6.2a Using One-link Payload Swing	164
Figure 6.2b Trolley-Payload results from One-link cable	164
Figure 6.3a Using Cross-link Payload Swing	165
Figure 6.3b Trolley-Payload results from Cross-link cable	165
Figure 6.4a Case 1 W-link	166
Figure 6.4b Case 2 W-link	166
Figure 6.4c Case 3 W-link	166
Figure 6.5a Case 1 Connector-link	166
Figure 6.5b Case 2 Connector-link	166
Figure 6.5c Trolley-Payload responses from Connector-link trial	166
Figure 6.6a Using Reverse T-link Payload Swing	167
Figure 6.6b Trolley-Payload results from Reverse T-link cable	167
Figure 6.7a Using two cable-link	168
Figure 6.7b Trolley-Payload results from two cable-link	168
Figure 6.8 Feedback Forces and Torques consideration on nonlinear	169
Figure 6.9 Joints, Sensors, and Actuators for Nonlinear Trolley-Payload Control	170
Figure 6.10 Torque Compensation Actuators Implementation. τ is Torque	171
Figure 6.11 Nonlinear RTCMC with LQR-DRO for Trolley Loadswing Operation	172
Figure 6.12 RMSE Comparison of Square Reference and Semi-Hexagonal	173
Figure 6.13a Nonlinear Trolley-Loadswing result for Square Reference 1m	174
Figure 6.13b Nonlinear Trolley-Loadswing result for Square Reference 20m	174
Figure 6.14 Nonlinear Trolley-Loadswing result for Semi-Hexagonal Ref 1-m	175
Figure 6.15 Nonlinear Trolley-Loadswing result for Semi-Hexagonal Ref 20-m	176
Figure 6.16 Sudden Trolley velocity change and Response of Nonlinear RTCMC	177

List of Tables

Table 3.1 Linear Least Square System Identified Models	60
Table 3.2a RMSE(Training) and RMSE (Checking) for Trolley Model	61
Table 3.2b from lowest to highest RMSE for Trolley Model	61
Table 3.3a RMSE(Training) and RMSE (Checking) for Loadswing Model	61
Table 3.3b from lowest to highest RMSE for Load Swing Model	61
Table 3.4a Generated Models and respective RMSEs	64
Table 3.4b RMSEs from high to low and respective models	64
Table 3.5a RMSE(Training) and RMSE(Checking) for Trolley Model	65
Table 3.5b From lowest to highest RMSE for Trolley Model	65
Table 3.6a RMSE(Training) and RMSE(Checking) for Loadswing Model	65
Table 3.6b From lowest to highest RMSE for Loadswing Model	65
Table 3.7 RMSE Comparison for Normal LLS and Improved LLS	66
Table 3.8 Linear Trolley-Loadswing Models based on LLS and ILLS	68
Table 3.9 Concrete Footing in mass-measurements-moment of inertia	77
Table 3.10 One side of 4-m frame in mass-measurements-moment of inertia	78
Table 3.11 One side of 12-m frame in mass-measurements-moment of inertia	80
Table 3.12 One side of 6-m frame in mass-measurements-moment of inertia	82
Table 3.13 Slew Assembly in mass-measurements-moment of inertia	85
Table 3.14 Slew right extension in mass-measurements-moment of inertia	86
Table 3.15 Combined Counter-jib mass-measurements-moment of inertia	88
Table 3.16 tower jib 12-m extension mass-measurements-moment of inertia	89
Table 3.17 Trolley rail-cart mass-measurements-moment of inertia	91
Table 4.1 Load positions VS Moments at pivot A	101
Table 4.2 Mass, Measurements and Moment of Inertia for Rigid Structure	104
Table 4.3 Rigid Crane Model Simulations results	104
Table 4.4 Ideal Crane Model Trolley Translation with results	106
Table 4.5 Ideal Tower Rotation without Wind Disturbance and Stationary Trolley 24 m	116
Table 4.6 Ideal Tower Rotation with Wind Disturbance and Stationary Trolley at 24m	118
Table 4.7 Oscillation VS Load Swing comparison Case Analysis	122
Table 4.8 Tower Rotation with Wind Disturbance 6.3kW_3000Kg case	124
Table 6.1 RMSE Comparison in both Sque_Ref and Semi-Hex_Ref inputs	173
Table 6.2 Comparison of swing RMSEs for both Square-Reference and Square-Reference and Semi-Hexagonal Reference inputs cases	176

Table of Contents

Acknowledgements	i
Abbreviations and Symbols	ii
List of Figures	iii
List of Tables	viii
Chapter 1. Introduction	
1.1 Overview	1
1.2 Approaches to the Crane Modelling	2
1.3 Model Linearization and Optimization	3
1.4 Vibration Impact and Disturbance Rejection	4
1.5 Swing Minimization and crane Control Approaches	5
1.6 Thesis Outline	5
1.7 Thesis related Poster-Presentations, Publications, Appreciation & Award	6
Chapter 2. Background 9	
2.1 Modelling of Tower Crane	10
2.1.1 Modelling based-on Mathematical Sketch	10
2.1.2 Modelling based-on Lab-scale prototype	11
2.1.3 Modelling based-on Graphic Software	13
2.1.4 Modelling based-on SimMechanics-Visualization	13
2.2 Linearization and Optimization	14
2.2.1 Proposed Linearization Methods	15
2.2.2 Model Optimization by linear least square	16
2.3 Vibration impact on tower crane	17
2.3.1 Vibration due to Wind Disturbance	18
2.3.2 Vibration due to unstable crane operation	18
2.3.3 Vibration and Swing suppression	19
2.3.4 Disturbance Rejection	20
2.4 Anti-swing control	22
2.4.1 Swing Control methods in literature	22
2.4.2 Trajectory Tacking Control	24
2.4.3. Vision-based Swing Control	26
Chapter 3. Modelling and Linearization 28	
3.1 2D Mathematical Modelling of Payload attached-Trolley Cart	28

3.1.1 Free body diagram of Jib System	28
3.1.2 Linear Model Derivation	29
3.1.3 2D Model Linearization using simple assumption	31
3.1.4 Model Excitation with simple step input	33
3.1.5 Nonlinear Model Derivation for 2D model	33
3.1.6 3D Tower Crane Free-body Diagram modelling	34
3.1.7 Nonlinear Model Derivation for 3D model	35
3.1.8 Trolley-Payload Nonlinear Equations of motion	43
3.1.9 3D Model Simplification using parameters assumption	44
 3.2 SimMechanics-Visualized Crane model Development	44
3.2.1 2D Overhead Crane Design	45
3.2.2 Mass and Moment of Inertia tensor calculation	46
3.2.3 Actuators, sensors and connectors used in the model	48
3.2.4 The SimMechanics visualization of the crane model	48
3.2.5 Force Input Signal	49
3.2.6 Simulation of Trolley Cart forward/Reverse motion in X-direction	50
3.2.7 3D Overhead Crane Design	50
3.2.8 SimMechanics visualization of Overhead Gantry Crane	54
3.2.9 Simulation of Jib-Trolley motion in Overhead Crane	55
 3.3 Linearization of 2D Overhead Crane using Linear Least Square Approach	56
3.3.1 Denominator and Numerator Coefficients consideration	57
3.3.2 Training and Checking Model	57
3.3.3 Root Mean Square Error Calculation	58
3.3.4 Linearization using Improved Least Square with 7 past inputs-outputs	60
3.3.5 Improved LLS Algorithm	62
3.3.6 Den2-Num2 to Den4-Num4 Models Development using Improved LLS	64
3.3.7 RMSE comparison and Linear Models selection	65
3.3.8 Linear Quadratic Regulator (LQR) Design	67
3.3.9 Full state feedback-LQR Reference Tracking control	69
3.3.10 Results and Discussion	71
 3.4 3D Tower Crane Modelling using SimMechanics-Visualization	73
3.4.1 SimMechanics-Visualization Development	73
3.4.2 Liebherr 71 EC Morrow Crane Data Sheet	74
3.4.3 Base Concrete Footing	75
3.4.4 Base Section 4 m	76
3.4.5 Hub Section 12 m	78
3.4.6 Hub Section 6 m	80
3.4.7 Tower Crane Hub with Concrete Base	82
3.4.8 Slew Assembly	83
3.4.9 Combined Counterjib	85
3.4.10 Tower Jib Butt Extension	87
3.4.11 Complete Tower Jib Extension (12m+12m+2.31m)	88
3.4.12 Trolley Rail-Cart-attached Load	89
3.4.13 Complete Ideal Tower Crane SimMechanics Visualized Model	91

3.4.14 Input Trolley Drive for Translational Motion	93
3.4.15 Trolley Brake and Friction Design	93
3.4.16 Input Tower Rotation Drive	94
 3.5 Conclusion	 95
 Chapter 4. Tower Vibration Impact on Payload Swing Analysis	 96
4.0 Crane Vibration Analysis	96
4.1 Jib Moment Calculation	96
4.1.1 Equilibrium Establishment	96
4.1.2 Jib Moment at pivot A	99
4.2 Vibration Analysis on Rigid Model Translation without wind Disturbance	102
4.2.1 Mass, Measurements, and Moment of Inertia for rigid structure	102
4.3 Vibration Analysis on Ideal Model Translation without wind Disturbance	104
4.4 Wind Disturbance Model Development	107
4.4.1 Obtaining Wind Static Force from Wind Static Velocity	108
4.4.2 Dragging Force Coefficient Derivation	109
4.4.3 Wind-gust Force	109
4.5 Vibration Impact Analysis on Trolley Translation with wind Disturbance	110
4.5.1 Vibration impact Analysis with Different Wind Surface Area	111
4.6 Vibration Impact Analysis on Tower Rotation without Wind Disturbance	114
4.6.1 Oscillation Analysis while trolley-payload is at the beginning of jib tower	114
4.6.2 Oscillation Analysis while trolley-payload is at the end of jib tower	114
4.7 Vibration Impact Analysis on Tower Rotation with Wind Disturbance	116
4.7.1 Vibration Impact Analysis of Tower Rotation-Trolley Translation with Wind Disturbance	120
4.8 Vibration Impact Analysis on Tower Rotation-Trolley Translation With Wind Disturbance	119
4.9 Discussion and Analysis	120
4.10 Linearized System Identification and Optimization of 6kW-3000Kg case	121
4.10.1 System Identification and Model Optimization	122
4.11 LQR Full State Feedback Controller With Reference Tracking	125
4.11.1 Tower Crane Rotation and LQR Swing Control	126
4.11.2 Simulations and Results Comparison with PID	127

4.12 Conclusion	128
Chapter 5. Linear Controllers Development	128
5.0 Controllers Implementation	130
5.1 LQR-Disturbance Rejection Observer Control	130
5.1.1 Disturbance Rejection Observer (DRO)	131
5.1.2 Trolley Model in Control Canonical Form	132
5.1.3 Disturbance Realisation	134
5.1.4 Extended State Observer (ESO) Design	135
5.1.5 Extended State Observer Gains	136
5.1.6 LQR-DRO Trolley Model Control	138
5.1.7 LQR-DRO Trolley and Loadswing controls	140
5.2 LQR-Estimator-Integral Control (LEIC) Development	141
5.2.1 Error Space Approach	142
5.2.2 LQR Gains	143
5.2.3 Full-order Estimator	144
5.2.4 Estimator Gains	144
5.2.5 LQR-LEIC for Trolley Model	145
5.2.6 LQR, LQR-DRO, and LEIC Performance Comparison for Trolley-Loadswing	146
5.3 LEIC- Antiwindup Control for Linear Models	147
5.3.1 Linear System Identification from NARX Structure	148
5.3.2 Linear ARX Model Development	149
5.3.3 LEIC-Antiwindup Control for Linear ARX Trolley Model	151
5.3.4 Weighting Matrices Q, and R	151
5.3.5 Result and Discussion	152
5.3.6 DRO,LEIC,LEIC-Antiwindup performance Comparison for Trolley	153
5.3.7 Control Efforts Comparison	155
5.3.8 Linear ARX Payload Plant	155
5.3.9 DRO, LEIC, LEIC-Antiwindup performance Comparison for Payload	157
5.4 Summary	159
Chapter 6. Nonlinear Robotic Tower Crane Modelling Control (RTCMC)	159
6.0 Robotic Tower Crane Modelling	159
6.1 Nonlinear RTCMC Flowchart	159
6.2 Cable structure impact on Payload Swing Minimization	160
6.2.1 Applying One-link Payload Swing Cable	161
6.2.2 Applying Cross-link Payload Swing Cable	161
6.2.3 Applying W-link Payload Swing Cable	162

6.2.4 Applying Connector-link Payload Swing Cable	163
6.2.5 Applying T-link Payload Swing Cable	164
6.2.6 Applying Two-link Payload Swing Cable	165
6.3 Reaction Forces and Torques Investigation	165
6.4 Joints, Sensors, and Actuators, implementation	166
6.5 Torque Compensation in Swing Minimization	167
6.6 Nonlinear RTCMC	168
6.7 Comparison of Square Reference and Semi-Hexagonal Reference	169
6.8 Results and Discussion of Square Reference Input applications	173
6.9 Sudden Trolley Velocity Change and RTCMC Response	176
6.9 Conclusion	173
Chapter 7. Thesis Conclusion and Future Work	175
7.1 Thesis Conclusion	175
7.1.1 Tower Crane Modelling	175
7.1.2 Linearization and Optimization	176
7.1.3 Vibration Impact Analysis	176
7.1.4 Controllers for Linear Models	178
7.1.5 Nonlinear Robotic Tower Crane Modelling Control (RTCFC)	179
7.2 Future Work	180
Bibliography	185
Appendix A: IEEE-iToF 2015 Award, Certificate of Commended Paper, Appreciation in UNSW-GRS June-2016, Participations & Competitions	190
Appendix B: "Robotic Tower Crane Modelling and Control (RTCFC) with LQR-DRO and LQR-LEIC for Linear and Nonlinear Payload Swing Minimization"	201
Appendix C: "Construction Tower Crane SimMechanics-Visualized Modelling Tower Vibration Impact on Payload Swing Analysis and LQR Swing Control"	216
Appendix D: "SimMechanics-Visualization of Experimental Model Overhead Crane, Its Linearization And Reference Tracking-LQR Control"	232
Appendix E: Responses to Examiners' Reports	249

Chapter 1

Introduction

1.1 Overview

Large and tall Tower cranes are widely used for the heavy loads transfer in Fig. 1.1. In each crane operation like: hoist up-down motion, trolley forward-backward motion, and flat-top rotation, the level of payload swing uncertainty eventually develops. To stabilize payload swing, skilled operators apply mental map and use manual joysticks to juggle the trolley back-and-forth so that the operation can be brought under control. However in busy working environments such as construction sites and shipyard docks, meeting the customers demand/deadline are crucial. And therefore, employer concern is to complete the tasks in shorter time with low operational cost whereby operator concern is to perform the operation without environmental risk as shown in Fig. 1.2 [1].



Figure 1.1 Large Standing Tall Operating Tower Crane



Figure 1.2 Tower Crane Collapse and Environmental Risk

Unfortunately, that workplace pressure might have caused operator's fatigue which may lead to operational failure. Tower Crane Incidents World statistic by Health and Safety Executive (HSE) shows 23% of crane accidents are due to wind disturbance,

38% are operational error, and the rest 31% are caused by assembly/disassembly as shown in Fig. 1.3 [1],

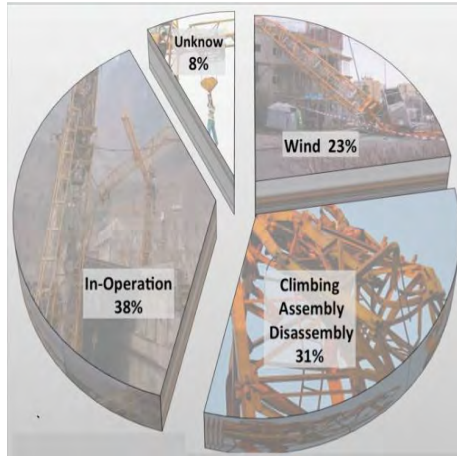


Figure 1.3 Tower Crane Incidents Statistic by Health and Safety Executive (HSE)

To ease the burden on operator while having safe and efficient tower crane operation, practical controller automation becomes necessary. Nevertheless, the major obstacle is, the researchers around the globe find it hard to operate large standing tall live operating tower crane on site which forces them to rely on mathematically derived models or lab-scaled models with several assumptions. Since majority of those models do not represent real crane's factors, the credibility of proposed swing minimization controllers to sort out challenging control problem is in question. This research initially identifies the significant role of having the ideal model which represents actual crane followed by the consideration of suitable linear-nonlinear controller implementations to further improve safe and sound working environment.

1.2 Approaches to the Crane Modeling

A number of crane modeling strategies from a set of mathematical equations, lab-scale prototype, solid works, autoCAD, to finite elements approaches have been proposed in the past. F. Ju [2], presented the tower crane model which was built on finite element approach and demonstrated the payload oscillation effect on the crane structure deformation due to pendulum-induced vibration. Several approaches on dynamics and stress analysis of articulating cranes also exist in the literature. From modeling point of view, crane's dynamics and structural analysis can be tackled by a set of algorithms: Recursive Newton-Euler Algorithm (RNEA), Composite Rigid Body Algorithm (CRBA), and finite element method to analyze structural members of a complex shape [3, 4] and references given therein. Detail review of recently proposed crane modeling and swing minimization control methods are provided in Chapter 2.

In contrast to the approaches described, as in [2]-[3]-[4], this paper presents a practical solutions to the modeling and control of 3D construction tower crane where the trolley motion, tower rotation, and payload swing are all together in the modeling and control. Considering the real crane facts and visualization, this research recently developed Tower crane model based on SimMechanics-visualized modelling approach Fig. 1.4 in [5]. SimMechanics provides a multi-body simulation environment for 3-Dimensional (3D) mechanical system which contains joints, constraints, actuator elements, and sensors. Another reason using this approach was: it can deal with the equations of motion for the complete mechanical system and integrate the controller implementation.

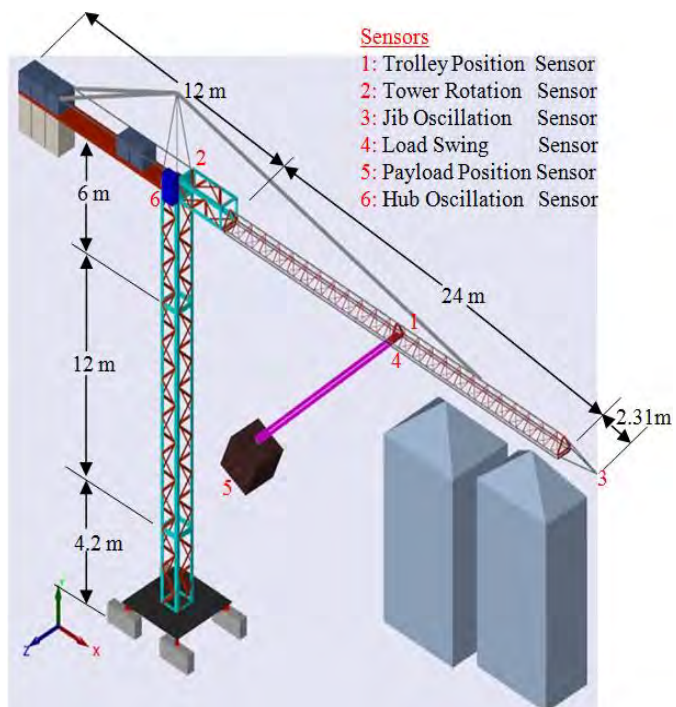


Figure 1.4 SimMechanics-Visualized Tower Crane Model development based on Liebherr-71EC Morrow crane

1.3 Model Linearization and Optimization

Linear least square (LLS) approach is one useful way to develop linear model from the simulated nonlinear result and it uses past consecutive data to compute the states [6]. This research applies existing LLS approach to linearize the model and further developed improved version of LLS algorithm to achieve the best fit linear model. The algorithm aims to pick 7 past inputs-outputs data randomly to maximize the better fit while minimizing the error. By selecting every possible combination of the columns from a large matrix with 7 past inputs and 7 past outputs according to the model needs, the matrix, X, is formed to compute estimated states, [7].

1.4 Vibration Impact and Disturbance Rejection

As a standing tall construction tower crane with only hub support, shouldering counterweight in one side and payload-attached trolley runs on the other side of the jib could eventually cause jib-hub vibration making huge impact on load swing instability. Not only it is difficult to view jib vibration by naked eyes but also hard to do much research work on operating crane.

Therefore, researchers have to rely on small model crane prototype to develop anti-sway control strategies. Ref. [8] envisages that, residual vibration would occur on completion of a trolley traverse due to the operator's manual control, different containers size and load lengths causing more friction and unstable load swing. In [9], transient sway and residual oscillation appear for certain types of payload and riggings, the payload mass is comparable to the cable mass, or the mass hangs from a hook without a cable in which the dynamics can become slightly different from a single pendulum due to the effects of inertia.

To date, the extensive researches have taken considerations on swing uncertainties problem due to wind or frictional disturbances, vibrations, cable nonlinearities, and trolley-tower (jib) dynamical systems, etc.. Z. Gao [10], discussed about the Active Disturbance Rejection Control which included stability analysis and the characteristics of new significance paradigm to reduce from complex nonlinear to the simple problem using active estimation and rejection. H. Sano, as in [8], emphasized on nonlinear friction disturbance of trolley and delay time from vision sensor response would deteriorate the control performance. Frictional force between trolley-rail was also considered as disturbance and time correction observer was further implemented to eliminate disturbance, as in [8]. Since the dynamics of a trolley-payload system is similar to inverted pendulum dynamical system, another important method of compensating measurement disturbances using PID (Proportional-Integral-Derivative) control was proposed to nonlinear flywheel inverted pendulum model, as in [11]. Furthermore, M. Olivares introduced full state feedback control with state estimator/observer to overcome an unstable open-loop pole and a zero at the origin, as in [11]. Likewise, Both PID-LQR and 2PID-LQR control techniques have been implemented on the nonlinear inverted pendulum-cart system with continuous disturbance input, as in [12]. The cause of flexible cable vibration is the major concern for unstable overhead crane operation and therefore, A. Elharfi came up with boundary feedback law implementation to bring the cable vibrations to the desired zero equilibrium, as in [13].

However in this research, sensors have been mounted on the developed SimMechanics-visualized tower crane model to monitor jib-hub vibration and analyze their impacts on payload swing. To analyze jib vibration impact on the crane and payload swing in particular, this research checked jib moment calculation, and tested the model with and without Wind Disturbance. After obtaining the nonlinear model and the best fit linearized model, this paper further discussed the combination of LQR-Disturbance Rejection Observer (LQR-DRO) aiming to reject disturbance, minimize payload swing, and achieve robust reference tracking.

1.5 Swing Minimization and crane Control Approaches

In the case of construction tower crane load swing minimization and control, diverse field of techniques can be presented in many different ways. Some literatures proposed payload trajectory controls using model predictive control and feedback linearization methods. Model Predictive Control scheme based on direct method with path-following was introduced [14]. D. Chwa in [15], proposed the feedback linearization control using swing angle and angular rate to eliminate the nonlinear characteristics of the system as well as achieve payload swing suppression. Regarding those unmeasured states such as: trolley and swing angular rate, numerical backward difference technique and low-pass filtering were also applied [15].

This paper discussed control strategies in twofold, one: tower crane linear model controls and, two: nonlinear model control. Considering the disturbance in the system, Luenberger-based LQR-Disturbance Rejection Observer was introduced. LQR-Estimator-Integral Control which consists of error-space approach and full-order estimator is further discussed. LEIC is then reconstructed by adding antiwindup and saturation. Linear model derived from Nonlinear Autoregressive exogenous (NARX) has then been applied in LEIC-Antiwindup control. Finally, LQR-DRO controller is considered suitable for nonlinear crane model as it is proven to be robust in the case of linear model control.

1.6 Thesis Outline

The remainder of this thesis is arranged as follow.

- Chapter 2 reviews the related works in tower crane modelling, system identification and linearization, anti-swing control strategies, and payload trajectory tracking controls.
- Chapter 3 presents 2-dimensional overhead crane linear and nonlinear mathematical models, 3-dimensional tower crane nonlinear mathematical models, SimMechanics-visualized 2-D overhead crane and 3D gantry crane

models development, linearization and model optimization, simple Linear Quadratic Regulator (LQR) control for developed linear model, full-state feedback LQR control for reference tracking, and details of 3D Tower Crane Modeling using SimMechanics-Visualization.

- Chapter 4 describes the vibration impact analysis. Details include: jib tower moment calculation, trials on both rigid-structure tower crane model and SimMechanics-visualized 3-D tower crane, Wind disturbance model development based on Garonski approach, apply wind disturbance on tower rotation, case studies on combinations of tower rotation speed-payload, identified and linearized worst case scenario, and finally implement full-state feedback LQR control.
- Chapter 5 discussed about linear model controllers development. It introduced LQR-Disturbance Rejection Observer (DRO) Control with Luenberger-based Extended State Observer to actively reject the disturbances caused by undesired source of inputs or unknown dynamics. This chapter further elaborates on: the combination of error space approach with estimator as LQR-Estimator-Integral Control (LEIC) for linear model, the derivation of linear model using Nonlinear Autoregressive eXogenous (NARX) approach, the development of LEIC-Antiwindup control to investigate robust reference tracking.
- Chapter 6 introduces Robotic Tower Crane Modelling Control (RTCMC) which includes: cable structure impact on payload swing minimization, reaction forces-torques investigation, joints-sensors-actuators implementation, torque compensator design in swing minimization, complete nonlinear RTCMC, and comparison of trajectory tracking performance based on square reference and semi-hexagonal reference inputs.
- Chapter 7 summarises the main results of this work and the directions for future work

1.7 Thesis related Poster-Presentations, Publications, Appreciation & Award

During the course of the research work, the following poster-presentations, competitions, and Journal publications have been made:

- Thein Moe Win, Tim Hesketh, and Ray Eaton, “Experimental Model Tower Crane Using SimMechanics Visualization and Load Swing Control with

Reference Tracking Compensation". IEEE Technology of the Future (iTof 2013) Poster-Presentation Competition. 6th November 2013, <http://www.cse.unsw.edu.au/~ieee/itof2013/index.html>

- Thein Moe Win, Tim Hesketh, and Ray Eaton, "Construction Tower Crane SimMechanics-Visualized Modeling, Tower Vibration Impact on Payload Swing Analysis, and LQR Swing Control". IEEE Technology of the Future (iTof 2014) Poster-Presentation Competition. 5th November 2014, <http://www.cse.unsw.edu.au/~ieee/archive/itof2014/index.html>
- Thein Moe Win, Tim Hesketh, and Ray Eaton, "Tower Crane SimMechanics-Visualized Modeling, Vibration Impact Analysis, and Linear/Nonlinear Trolley-Loadswing Control using LQR-DRO". IEEE Technology of the Future (iTof 2015) Poster-Presentation Competition. 29th October 2015, <http://cgi.cse.unsw.edu.au/~ieee/itof2015/index.html>
- Thein Moe Win, Tim Hesketh, and Ray Eaton. SimMechanics Visualization of Experimental Model Overhead Crane, Its Linearization And Reference Tracking-LQR Control, *AIRCC International Journal of Chaos, Control, Modeling and Simulation (IJCCMS)*, Volume 2 (Issue 3):1-16, September 2013.
- Thein Moe Win, Tim Hesketh, and Ray Eaton. Construction Tower Crane SimMechanics-Visualized Modelling Tower Vibration Impact on Payload Swing Analysis and LQR Swing Control, *International Review on Modeling and Simulations (IREMOS)*, Volume 7 (Issue 6):979-994, December 2014.
- Thein Moe Win, Tim Hesketh, and Ray Eaton. Robotic Tower Crane Modeling and Control (RTCMC) with LQR-DRO and LQR-LEIC for Linear and Nonlinear Payload Swing Minimization, *International Review of Automatic Control (IREACO)*, Volume 9 (Issue 2):72-87, March 2016.
- Thein Moe Win, Tim Hesketh, and Ray Eaton, "Tower Crane SimMechanics-Visualized Modeling, Vibration Impact Analysis, and Linear/Nonlinear Trolley-Loadswing Control using LQR-DRO". iTof 2015, Poster-Presentation Award in Modeling and Simulation Category. 29th October 2015. <http://cgi.cse.unsw.edu.au/~ieee/itof2015/prize.html>

- Certificate of Publication:(Commended Paper): Robotic Tower Crane Modeling and Control (RTCMC) with LQR-DRO and LQR-LEIC for Linear and Nonlinear Payload Swing Minimization, International Review of Automatic Control (IREACO), Volume 9 (Issue 2):72-87, March 2016
<http://www.praiseworthyprize.org/jsm/index.php?journal=ireaco>
- Appreciation News: Graduate Research Newsletter (June-2016 Issue)
<http://us2.campaign-archive2.com/?u=7b3c52328a8b98d8218ba4bf4&id=2840e099eb&e=1b52cb1504>
- 2016 Postgraduate Research Symposium, UNSW Faculty of Engineering (26-29 Sept 2016) <https://www.engineering.unsw.edu.au/all-events/2016-postgraduate-research-symposium>

Chapter 2

Background

In modern industrial systems, shipyards, warehouses, and construction, tower cranes are widely used for the transfer of heavy loads. Each type of crane has its own function and their motions are inherently different. This research focus is on tower cranes. The 3D tower cranes are in widespread use in construction as shown in Fig. 2.1. They have three degrees of freedom which giving the capability to independently translate, rotate and elevate heavy building blocks especially during the construction of tall buildings. Their small footprint on the ground and large workspace make them ideal for these types of applications.



Figure 2.1 Tower cranes working in a construction Site

The dynamics of tower cranes are inherently complicated due to their rotational nature. Transferring loads in a shorter time, perfect safety with no load swing or damage, and low operation cost are the main concerns. However, the crane acceleration can cause undesirable load swing, which normally has negative consequences on the whole operation and safety performance. It is essential to minimize the load transfer time and load swing angle with proper control action to avoid operational risks. This research categorizes four important aspects which contribute to the tower crane control such as; tower crane modelling, system identification and optimization, vibration impact analysis, and swing suppression control.

2.1 Modelling of Tower Crane

The modelling techniques of the crane proposed to date are mostly based on; derivation from free-body diagrams and mathematical sketches, use of lab-prototypes, and designing using graphic software.

2.1.1 Modelling based-on Mathematical Sketch

Most of the proposed tower crane mathematical models obtain dynamic equations using mathematical sketch and free-body diagrams in 2 as well as 3-Dimensional forms. For instance, a simple free body diagram as shown in Fig. 2.2 below is developed to represent a 2-Dimensional (2D) crane model. A trolley cart is mounted on a jib (rail) along x direction, [16]. Trolley cart mass (M), payload mass (m), and load length (l) are assigned certain values while (θ) is load swing angle in the XY plane. For 2D simple motion, payload length is initially considered unchanged and frictionless between trolley and jib. An applied force (F) pushes the trolley to move along the X direction and potentially a large swing angle θ appears which needs to be minimized to as small as possible. H Sano [8] then derived mathematical model of the crane based-on Lagrange equation.

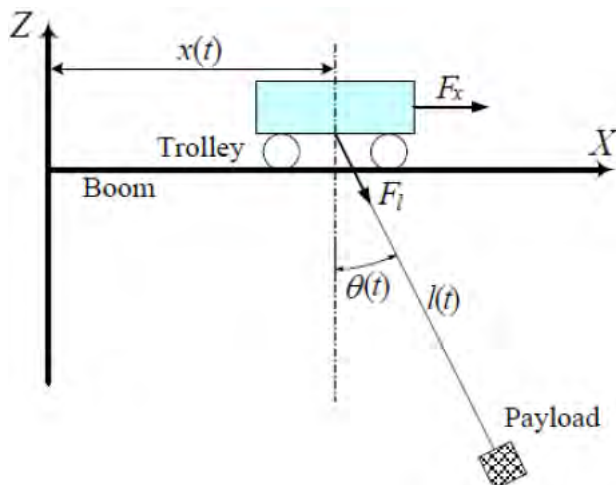


Figure 2.2 Overhead crane free-body diagram in [16]

In another approach, a new dynamic model of a three-dimensional overhead crane as shown in Fig. 2.3 is derived based on a newly defined two-degree-of-freedom swing angle [17]. The dynamic model describes the simultaneous traveling, traversing, and hoisting motions of the crane and the resulting load swing.

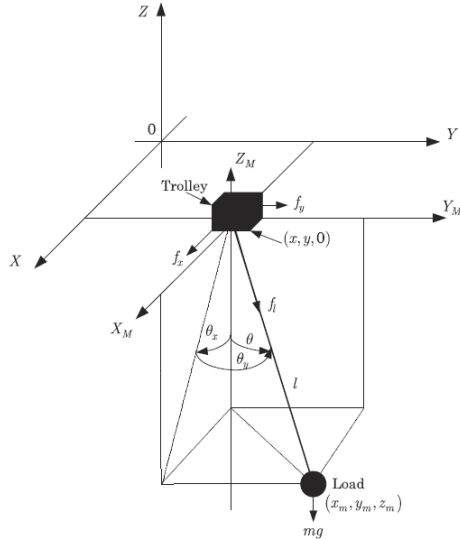


Figure 2.3 Three-dimensional overhead crane free-body diagram [17]

Omar proposed a mathematical model [18] using free body sketch by ignoring interaction forces between the swing and trolley, actual measurements, location of load cable, joint between hub and tower, friction during trolley stop, etc. In [14], the mathematical model was developed based on a labs-scale prototype which has no counter weight while the jib tower comprises only one link, while reference to any specific tower crane mechanisms are omitted. In the early stage of this research, 2-D overhead crane and 3D tower crane mathematical models were also derived from free-body diagrams. Linear and nonlinear models are presented in Chapter 3.

2.1.2 Modelling based-on Lab-scale prototype

The Tower crane lab-prototype as shown in Fig. 2.4a is sold by Quanser and has the crane model with a mounted trolley on the rotary arm. The suspended cable is also attached underneath using a gimbal joint to measure pendulum deflection angle. The three separated subsystems; payload, jib, and tower models are derived from the 3D crane plant [19]. Another crane model developer, Inteco, designed an overhead 3D gantry crane with jib-trolley-pendulum system. The Inteco further provides nonlinear equations describing the dynamics of the crane with varying pendulum length as depicted in Fig. 2.4b [20].



Figure 2.4a Lab-scale tower crane model developed by Quanser



Figure 2.4b Lab-scale tower crane model developed by Inteco

An experimental overhead crane prototype is used in [8] to develop antisway control for suppressing vibrations Fig. 2.5a. In this container crane control case, a trolley moves along a girder, hoisting ropes which are let out to drop a spreader, and a container is gripped and hoisted by the ropes. The trolley then moves along the girder and the container is loaded on a truck waiting on the quay. Dynamic equations were first derived from a 2D free-body diagram as shown in Fig. 2.5b.

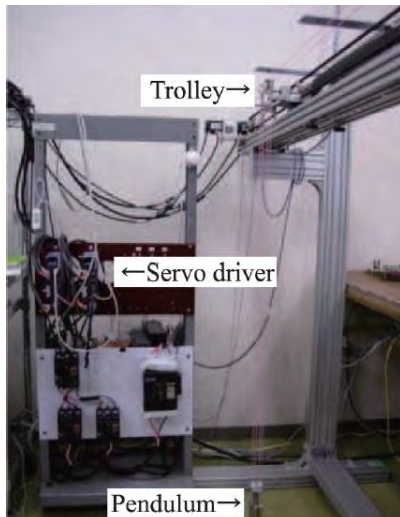


Figure 2.5a Overhead crane lab-scale model used by [8]

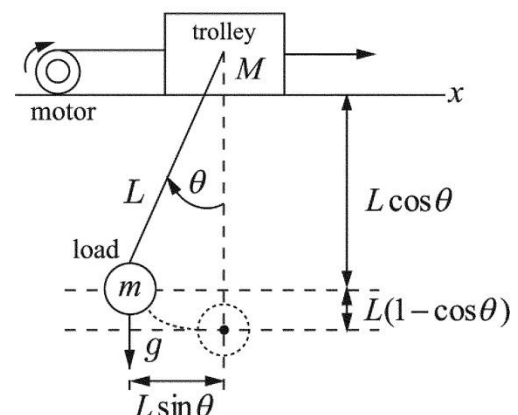


Figure 2.5b Overhead crane lab-scale model free-body diagram in [8]

Omar H [18] uses the Lagrangian approach to derive the equations governing the nonlinear motion based-on an experimental lab-scale tower crane. To simplify the controller design, the author assumes the swing angles are small and neglects the

Chapter 2 Background

cable length variations. However, most of the payload swing models including the above-mentioned laboratory crane in the literature employ only one swing cable while an actual live crane has two suspended cables with a hook attached at the end. Also, proper sensors-actuators implementation have not been addressed.

2.1.3 Modelling based-on Graphic Software

Some research has introduced crane model design using graphic software. F. Ju, as in [2], presented the tower crane model which was built on a finite element approach and demonstrated the payload oscillation effect on the crane structure deformation as shown in Fig. 2.6. Likewise, [3]-[4] developed crane dynamics and structural analysis using a Recursive Newton-Euler Algorithm (RNEA), a Composite Rigid Body Algorithm (CRBA), and the finite element method. In [21], a tower crane is modelled in 3D using Solidworks computer software, and the strength of the tower crane parts are calculated according to FEM standards are suggested in Fig. 2.7.

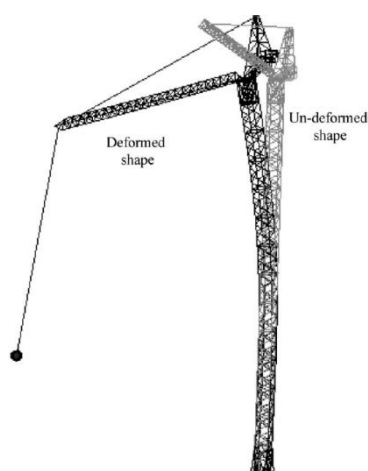


Figure 2.6 Deformed shape of crane structure with the spherical pendulum motion of the payload designed in [2]

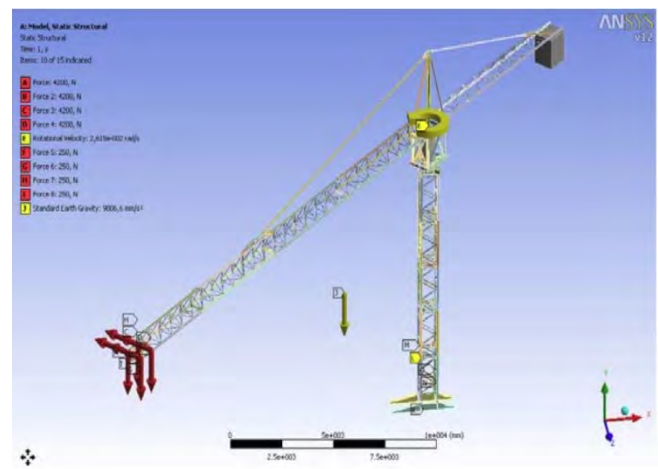


Figure 2.7 Tower Crane Model built using Solidworks and Auto CAD graphic software to analyse the crane strength in [21]

2.1.4 Modelling based-on SimMechanics-Visualization

It is usually hard to conduct research on the real operating crane on site and therefore, most research derives a mathematical crane model for simulation purposes. An alternative is to employ models built in graphic software as discussed above. To further simplify the crane modelling, researchers may assume or ignore various crane related parameters such as: friction, noise and disturbance, actuator dynamic, and sensor, etc.. The resulting proposed control methods may be impractical. Therefore,

Chapter 2 Background

this research aims to apply a SimMechanics approach in developing a crane model which not only represents an actual crane, but also which can be practical for further control implementation, [22].

The SimMechanics-Visualization tool is a block diagram modelling environment with ability to undertake multi-body machine simulation, [22]. The Physical modelling blocks in SimMechanics represent physical components, geometric, and kinematic relationships directly. This is not only more intuitive, it also saves time and effort required to derive the equations of motion [23]. Furthermore, SimMechanics uses the standard Newtonian dynamics. Based on Physical Principles, it allows modeling and simulation of mechanical systems with a suite of tools to specify bodies and their mass properties, their possible motions, kinematic constraints, and coordinate systems, and to initiate and measure body motions, [24]-[25]. Designing with detailed parameters, and applying for each part a mass/moment of inertia, can produce reliable crane operating data from which suitable controllers can be achieved, [26]. In alternative approach [27], the researcher incorporated an AutoCAD predesigned model on the SimMechanics platform which then offers merely a graphic display and does not contain actual “Mass, Inertia, and Measurements”.

SimMechanics offers industrially proved features and reliable simulation result. This research designs a tower crane model based on a MORROW TOWER (Liebherr 71EC) crane datasheet, as in [28]. The model will include the trolley cart, rail jib, steel cable, load, sensors and actuators, actual mass-moment of inertia-densities, and frictions. This computer-based physical model offers a milestone development for crane research since a wide range of crane research can be done using this model such as, tower rotation, trolley translation, load swing control, and safety issues. Researchers will be able to do real time research without having trouble in dealing with real cranes on a working site.

2.2 Linearization and Optimization

Almost every physical system contains nonlinearity, often its behaviour within a certain operating range of an equilibrium point can be reasonably approximated by a linear model. The reason for approximating the nonlinear system by a linear model is that, by so doing, one can apply rather simple linear control design techniques. This section discusses previous linearization and optimization methods implemented for tower cranes and 2D overhead cranes. Methods include linearization around equilibrium point, assumptions, some use adopted of an extended Kalman filter, linear least squares approaches.

2.2.1 Proposed Linearization Methods

Three-dimensional equations of motions for overhead cranes have been derived using Lagrange equations [31]. Payload is considered a point mass and stiffness of the rope is neglected. After obtaining the dynamic model for the free-body diagram as shown in Fig. 2.8, the paper assumed acceleration and velocity components to be zero in order to reduce two two-dimensional model forms. For small swing, $\sin \theta_x \cong \theta_x$, $\sin \theta_y \cong \theta_y$, $\cos \theta_x \cong 1$, $\cos \theta_y \cong 1$ [30]. In this case, with the trigonometric functions approximated, the high order terms in the nonlinear model can be neglected to form a linearized model [29].

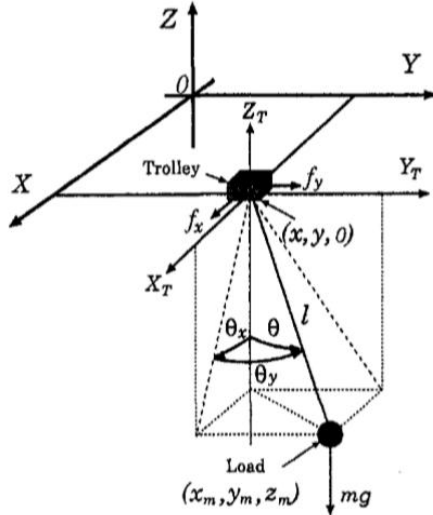


Figure 2.8 Overhead Crane free-body diagram [29]

Sien K [30] found that large changes in the rope length would lead to linear controller instability while a nonlinear controller remained stable. Sein K further details a method to implement a nonlinear control using a dynamic exact linearization controller which transforms a nonlinear system into a linear normal form followed by a reverse transformation to correct the system states. However, his work does not describe any practical implementation of the controller, nor if cart positioning and rope length control was achieved. Thus, there may be no guarantee that the controller will behave as in the simulation when implemented in a practical scenario.

Another strategy is to employ inverse and forward kinematic converters to linearize system dynamics in the control loop. This strategy is particularly well suited to systems with a joint or kinematic nonlinearity, such as a robot arm as shown in Fig. 2.9. The idea is to take the desired command in joint space and convert it into the desired path in Cartesian space. Because, motions in Cartesian space are linear, a standard input shaper will eliminate residual vibration. Then, the shaped command is converted

back into joint space. This strategy was used by Vaughan Joshua [31] for input shaping a two-link, manipulator.

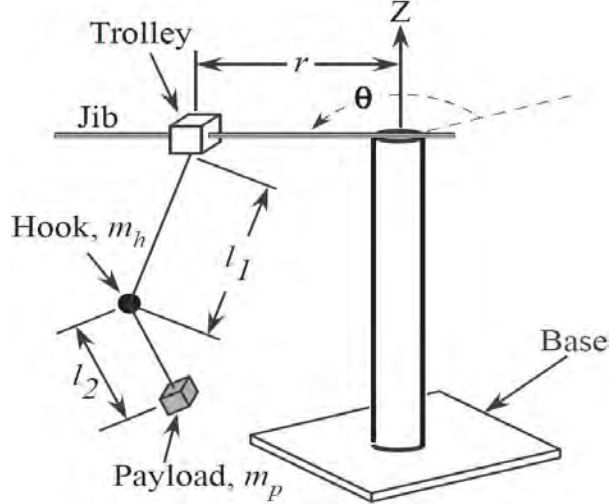


Figure 2.9 Tower crane illustration with Kinematic nonlinearity of trolley-payload oscillation [31]

A continuous-time extended Kalman filter (EKF) is presented, which allows the parameters of nonlinear systems to be estimated. The extended Kalman filter augments the linearized Kalman filter to directly estimate the states of a nonlinear system linearizing the nonlinear system around the Kalman filter estimate [32].

The problem of determining a mathematical model for an unknown system by observing its input-output data pairs is generally referred to as system identification. The purposes of system identification are; to predict systems behaviour, to explain the interactions and relationships between inputs and outputs, and to design a controller or simulation of the system [6]. The linear Least Square approach is widely used in system identification of linear models. It aims to establish two main goals: one is to determine the number of parameters required in the plant model dynamics Eq.(2.1), and the second is to find the value of parameters b_1, \dots, b_m and a_1, \dots, a_n [33].

$$\Delta y(k) = \frac{b_1 z^{-1} + b_2 z^{-2} + \dots + b_m z^{-m}}{1 + a_1 z^{-1} + a_2 z^{-2} + \dots + a_n z^{-n}} \Delta u(k) \quad (2.1)$$

2.2.2 Model Optimization by linear least square

The concept of least squares is to fit a linear curve which fits that data the best according to some criterion. One such common criterion is the minimization of sum of the squared differences between the actual data and the predicted data due to the least squares line [34]. The error thus defined is given in Eq.(2.2) as

$$E = \sum_{i=1}^M [y_i - y_{LS}(x_i)]^2 \quad (2.2)$$

Chapter 2 Background

where $i = 1, 2, \dots, M$ is the number of data points, and y_{LS} is the approximating curve's predicted y at the point x_i . The problem of solving overdetermined linear simultaneous equations of the form Eq.(2.3) can be written as

$$\begin{bmatrix} y_1 \\ y_2 \\ y_3 \\ \vdots \\ y_m \end{bmatrix} = \begin{bmatrix} x_{11} & x_{12} & x_{13} & \cdots & x_{1n} \\ x_{21} & x_{22} & x_{23} & \cdots & x_{2n} \\ x_{31} & x_{32} & x_{33} & \cdots & x_{3n} \\ \vdots & \vdots & \vdots & \ddots & \vdots \\ x_{m1} & x_{m2} & x_{m3} & \cdots & x_{mn} \end{bmatrix} \begin{bmatrix} \theta_1 \\ \theta_2 \\ \theta_3 \\ \vdots \\ \theta_n \end{bmatrix} \quad (2.3)$$

Or in a compact form Eq.(2.4) $y = X\theta$ (2.4)

where $X \in R^{m \times n}$ is the coefficient matrix and $y \in R^{m \times 1}$ is the observation vector, and $\theta \in R^{n \times 1}$ is the vector of unknowns to be solved. The least square method aims to find the solution $\hat{\theta} = [\hat{\theta}_1, \hat{\theta}_2, \dots, \hat{\theta}_n]$ that minimizes their estimated values, $\hat{\theta}$ to equation (4) is given by the following normal equation

$$[X^T X]\theta = X^T y$$

In this research, an improved version of existing linear least square approaches is proposed which considers every possible combination of columns from the matrix X to compute estimated states [7]. Details are discussed in section 3.

2.3 Vibration impact on tower crane

Having tall construction tower crane on standing tower hub, the vibration impact will be unavoidable. Since most of the researchers around the globe refer to the respective crane prototypes in proposing any control strategies, those developed models cannot provide reliable vibration impact analysis. There can be many forms of vibration impact on the crane due to: the crane unstable operation itself with higher load swing, the wind disturbance, unbalance counterweight and payload, trolley translational and tower rotation speeds, etc. In order to achieve the real crane automation and control, it is important to analyse the vibration impact on a reliable crane model in the case of real crane is inaccessible.

2.3.1 Vibration due to Wind Disturbance

Wind impact is one of the major loads affecting buildings and other constructions, among which the most affected is large-standing construction tower crane which can be seriously damaged by wind, resulting in serious collateral damage to its surrounding environments [35]. The destructive irregular wind disturbance would also be the reason for tower vibration causing higher unstable payload swing during the operation. In order to design a controller with wind disturbance rejection properties, wind disturbance should be known at the input to the crane model. Therefore, Gawronski [35] proposed a “wind force acting on the dish” model for the large standing tall antenna at 34-m height. However, instead of deriving wind gust speed $\Delta_{v_0}(t)$ through a Davenport Spectrum as mentioned [35], this research will consider available inputs from Sydney Metrological Weather Office) which provides static wind (static) and wind gust (variable). The free-body diagram with wind disturbance strike on the jib is shown in Fig. 2.10, [5].

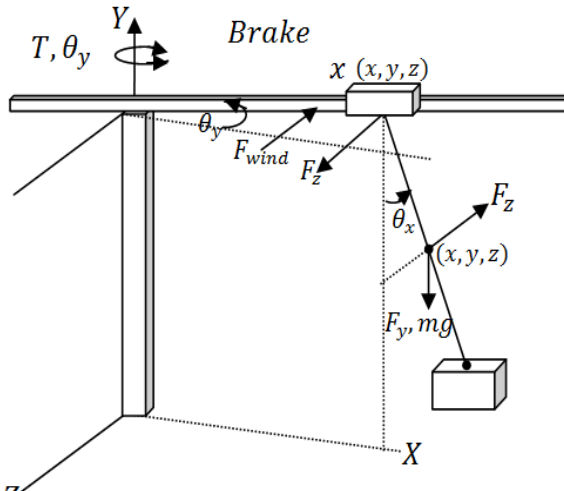


Figure 2.10 Tower crane model free-body diagram with wind disturbance [5]

2.3.2 Vibration due to unstable crane operation

Trolley vibration of the crane can cause excessive load swing, system instability, property damage, and place lives at risk. To eliminate the vibrations, researchers in [36]-[37]-[38] developed shaped command model, back-stepping boundary control approach, fuzzy logic control, and high gain feedback control. Jason W. Lawrence [37] discovered that the radial, tangential, and residual vibration appeared when testing an experimental tower crane in Tokyo Tech, Japan, Fig. 2.11a. Once the velocity command pulse is given to move the payload, each impulse would excite some amount of vibration which result in vibrating or eventually load swinging [37], Fig. 2.11b. Interestingly, Jason W. Lawrence used a shaped command with

Chapter 2 Background

convolution filter to reduce the payload vibration. Though he achieved zero vibration for a lab model, perhaps he should have considered external factors like wind disturbance and viscous friction to achieve the same result in a real operational crane.

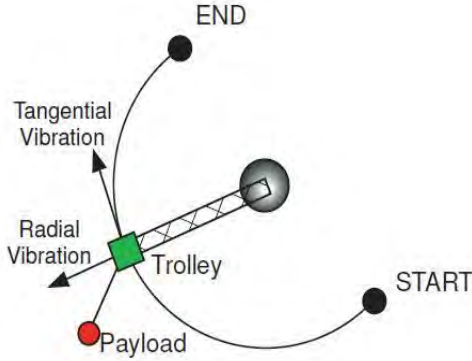


Figure 2.11a Free-body diagram of swing oscillation with jib vibration [37]

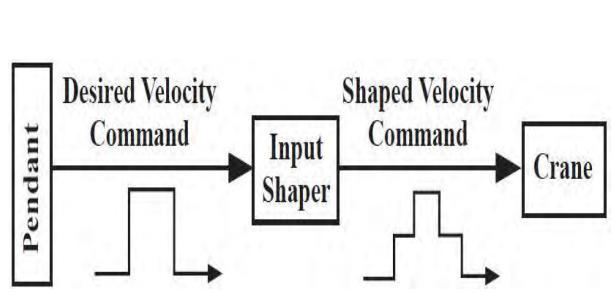


Figure 2.11b Input Shaper design for vibration suppression [37]

Yu Y. [38] in their perceptive research, validated the feasibility of reducing trolley vibration using a wireless inclinometer. Vaughan Joshua [31] followed similar approach to that of [37] but the author emphasized that each impulse required one multiplication and one addition in shaping the command using real-time convolution. The implication is, input shapers contain 3-5 impulses and filters can often contain 64, 128, or 256 impulses and if hundreds of impulses are run, it can burden the control computer [31], Fig. 2.12. Since Vaughan realized that vibration cannot be totally eliminated but only reduced below a tolerable level, he came up with Modified Input Shaping (MIS) technique. However, MIS could not simply suppress vibration due to a larger number of impulses and longer shaper duration.

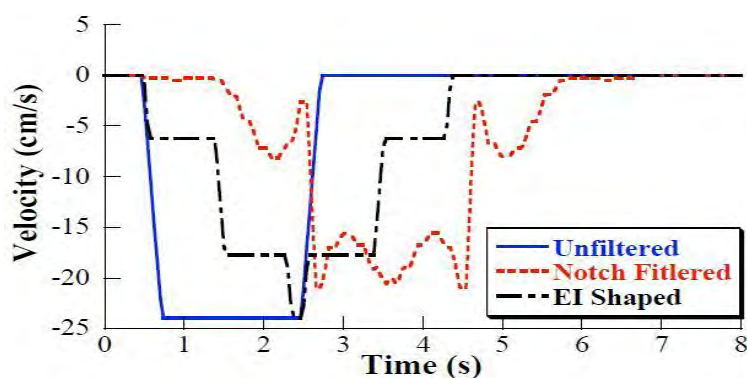


Figure 2.12 Comparisons of Input shaper with other filters [31]

2.3.3 Vibration and Swing suppression

Trabia [39] in the journal of vibration used fuzzy logic control with inverse dynamic to suppress the payload swing to be within +5 to -5 degree and to lower vibration. Baicu, C. [40] identified that high-gain current feedback increases the motor

bandwidth frequency which link to vibration. So, a backstepping control approach using partial differential equations is applied to compensate the motor electrical dynamics in [40]. After combining Lyapunov theory and Galerkin's method in their strategy, they develop Numerical simulations which demonstrate the improved vibration damping characteristics. Fig. 2.13 in [40] shows that the controller can stabilize the flexible-link vibrations and regulate the gantry position by using the control voltage $E(t)$ and gantry position $w(x,t)$ and shear force sensors. This approach remains a theoretical prediction. Further considerations and new approaches must be viewed within the context of vibration.

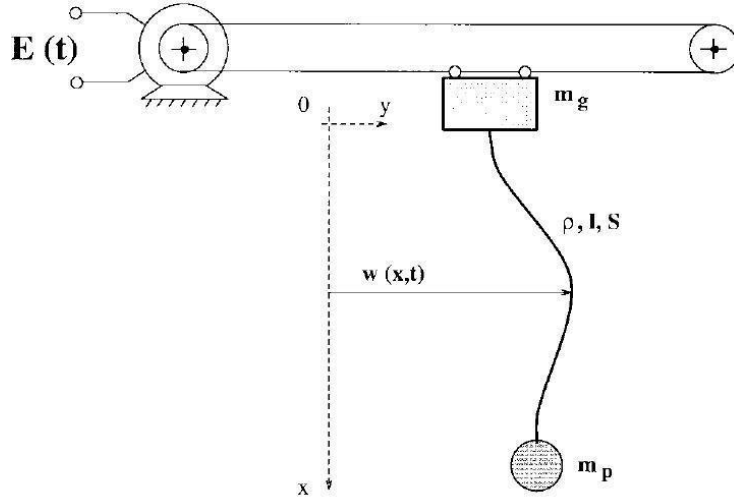


Figure 2.13 Vibration damping for flexible-link [40]

Controlling load swing and vibration and trajectory tracking are part of the cranes operation systems. Yet, it still needs to integrate the best measurement techniques to achieve the state-of-art crane system. Several measurements systems on the cranes are discussed in the coming section.

2.3.4 Disturbance Rejection

There are swing uncertainties problem due to wind or frictional disturbances, vibrations, cable nonlinearities, and trolley-tower (jib) dynamical systems [10]. Z. Gao further discussed Active Disturbance Rejection Control which included stability analysis and the characteristics of a new paradigm to reduce a complex nonlinear problem to a simpler one using active estimation and rejection.

Many types of observers have been proposed in the literature, including the unknown input observer, the disturbance observer, the perturbation observer, and the extended state observe. For instance, N Uchiyama in [41] highlighted that, the observer

Chapter 2 Background

consists of a high gain will be insensitive to external disturbances. Therefore, modeling errors will cause large deviations of the observed states from the actual states due to the high gain component. Neupert J. [42] also examined reconstruction of the rope angles from the gyroscope data using disturbance observers to damp the load sway, Fig. 2.14. The authors in [43] give a model-free anti-swing controller which has a PID structure. However, the main challenges of their concepts in [42]-[43] are the coupling of the moving axes due to centrifugal forces, and parameter variations.

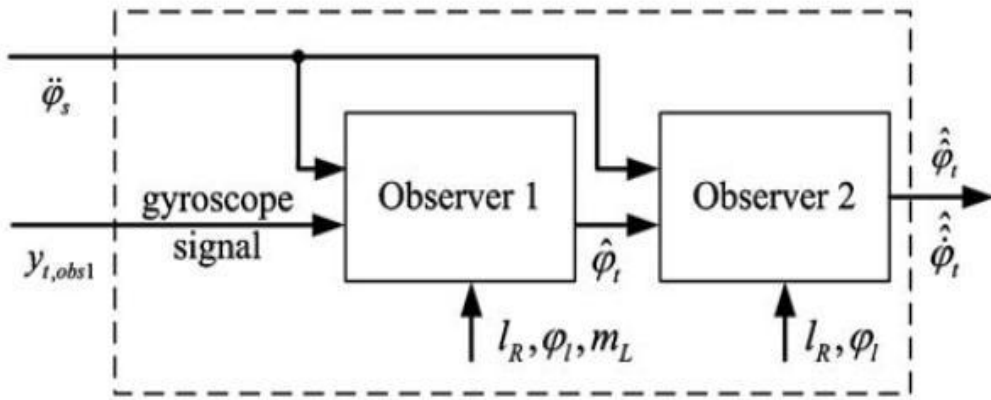


Figure 2.14 Disturbance Observer implementation [42]

H. Sano [8] emphasized nonlinear friction disturbance of trolley and delay time from vision sensor response would deteriorate the control performance. Frictional force between the trolley and rail was also considered as a disturbance and a time correction observer was implemented to eliminate disturbance, as in [8]. Since the dynamics of a trolley-payload system is similar to that of an inverted pendulum dynamical system, another important method of compensating measurement disturbances using PID (Proportional-Integral-Derivative) control was proposed for a nonlinear flywheel inverted pendulum model, as in [11]. Furthermore, M. Olivares introduced full state feedback control with state estimator/observer to overcome an unstable open-loop pole and a zero at the origin, as in [11]. Likewise, Both PID-LQR and 2PID-LQR control techniques have been implemented on the nonlinear inverted pendulum-cart system with continuous disturbance input, as in [12]. Flexible cable vibration is a major concern for unstable overhead crane operation and therefore, A. Elharfi came up with boundary feedback law implementation to bring the cable vibrations to the desired zero equilibrium, as in [13].

In [8], researchers propose a full-order friction disturbance observer with sensor-delay correction for a lab scale 1D overhead crane prototype to eliminate swing caused by vibration-affected nonlinear friction. Though nonlinear friction is considered due to vibration, the analysis of vibration was not discussed. A vision sensor system is used to

Chapter 2 Background

detect the sway angle however as it has a delay time when determining the angle, it sometimes leads to deterioration of control performance. In order to overcome this problem, this research proposes a new antisway crane control system based on a dual-state observer with sensor-delay correction. However, because of nonlinear friction in the crane, the estimation accuracy achieved by using the observer is poor. To overcome this problem, this paper proposes a disturbance observer considering friction disturbance. A Time Delay Filtering method for cancelling vibration has also been proposed, as in [9]. Likewise, Ref. [44] considered vibration in a rotary crane system (which is similar to tower jib rotation) and proposed a three-layered neural network GA-based training controller.

2.4 Anti-swing control

The load suspended from the trolley by cable is subject to swing caused by improper control input and/or disturbances. Therefore, minimizing the load swing with proper control action during operation is essential to avoid several risks. Even though researchers worldwide have proposed many forms of approaches using manual joy stick with human operators is still the norm. The cranes use open loop systems to control position while anti-swing control is done manually by skilled operators using joysticks with analogue control. Since a skilled operator always needs to focus on the operational trajectory, it creates fatigue problems and eventually affects the whole operation. Higher running costs, operational delay, and environmental damages have to be taken into account. Several anti-swing control methods have been developed based on different considerations and conditions. Many of those findings are discussed in this section.

2.4.1 Swing Control methods in literature

All cranes use cables to hoist and support the payload and because of this structure, the payload has the tendency to swing during transport operations. Swinging degrades the speed, accuracy, and safety of transport operations; these three factors are of paramount importance to crane operation. They lower the speed of transport operations because the payload swing must die out before the payload can be safely lowered into position. The swing makes it difficult to perform alignment, positioning, or other accuracy driven tasks. Swing also causes safety problems because of the potential for collisions with objects or people.

Other approaches (including the one undertaken in this thesis) aim to minimise the swing angle throughout the entire load journey. One solution to the problem is to apply a sliding mode control (SMC)-LQR control strategy, as in Ailane [45], for an inverted pendulum with and without disturbances. Wind disturbances affect tower vibration creating higher unstable load swing; the payload begins to oscillate and it takes a long time for the oscillations to decay. Park M-Soo, [43] and Chen [46] have discussed the asymptotic stability of output feedback control using a sliding mode approach. Clearly using a sliding mode approach to output feedback control will ensure the robustness of the control when the controller is faced with uncertainties. The limitation in [43] is that the controller is made up of a set of derivatives of the output state and this is clearly not practical. The stiffness and mass of the rope are also neglected and the load is considered as a point mass.

Several crane-related input shaping techniques have been developed that go beyond the standard implementations. For instance, the payload and its rope often create a second vibration mode causing the crane to exhibit double-pendulum load swing dynamics. Jason W. Lawrence [37] derived multi-mode shapers with PI controller while Garrido [47] designed Specified Insensitivity (SI) shapers to suppress that vibration across a range of frequencies as shown in Fig. 2.15.

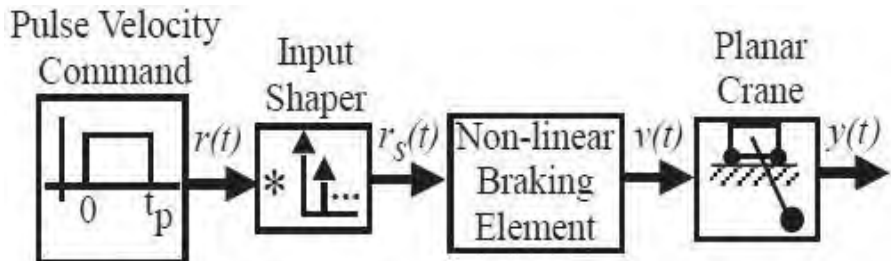


Figure 2.15 Pulse frequency signal with input shaping [47]

J. W. Lawrence [37] noted that if the modeling frequency is not exact then the input shaping methods would not completely cancel the swing angle. Thus, in using input shaping, one must have a superior knowledge of the systems to generate an appropriate pulse frequency signal. This is also required to position the impulse at the correct time location in order to minimize any system vibrations. In simulation this is clearly possible, but in a practical environment, this method would produce an ineffective control signal since this consists of noise and changing system parameters. Vaughan J [31] proposed input shaper with adaptive technique which is then implemented on a HiBay crane and jib cranes at Sandia National Labs and Oakridge National Labs at Georgia Institute of Technology as shown in Fig. 2.16a. One

constraint in this approach is, trolley velocity is measured to calculate the load swing angle.

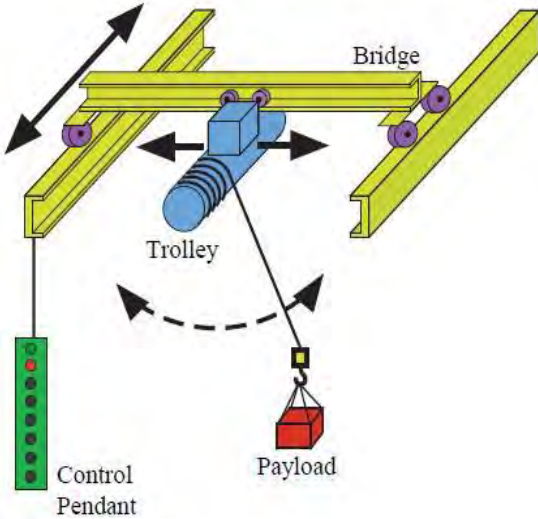


Figure 2.16a HiBay crane model at Georgia Institute of Technology [31]

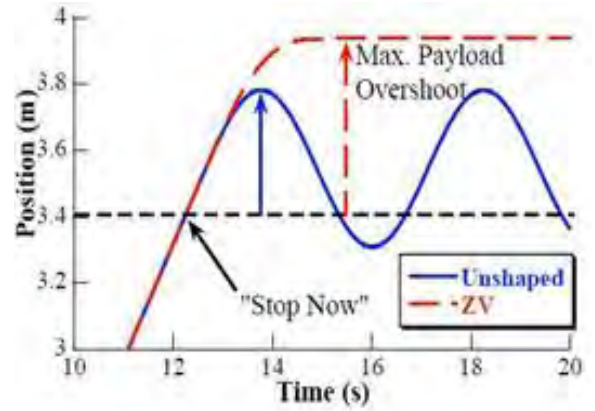


Figure 2.16b Input Shaper for position control [31]

Vaughan J [31] also compared the performances of input shapers with notch filter, time optimal commands. It was shown that compared to the time optimal trajectory, input shaping reduced position overshoot efficiently and reached steady state within a few seconds, in Fig. 2.16b. However, the level of effectiveness is uncertain on hoisting motions especially when the large hoisted suspension length changes.

Although these methods were proven to work both theoretically and in implementation, the underlying models did not take into account physical properties of the system such as: friction. To overcome the resultant steady state errors arising from these physical properties, [19] implemented high-pass filtering in the lab-scale tower crane model to measure payload position in the lab-scale model. Then a Proportional-Integral-Velocity Compensator (PIV) Control with high gain observer is introduced. On the other hand, another lab-scale tower crane model developer, inteco [20], uses a PID control approach to minimize the load swing. However, the additional level of complexity did not produce adequate swing angle minimization or residual response dampening.

2.4.2 Trajectory Tacking Control

Recently interest has also arisen in producing systems that utilize swing minimizing trajectories instead of relying on system stabilization techniques for anti-swing control. Load is transferred from the start to destination point on an arbitrary trajectory through the commands of the crane operator via the hand levers. That

Chapter 2 Background

arbitrary trajectory makes the load sway and it needs proper trajectory tracking to become sway-free transportation as shown in Fig. 2.17. For all types of cranes, the unactuated sway dynamics is heavily coupled with actuated dynamics through trolley acceleration, hoisting velocity and hoisting rope length. As a result, that coupling becomes an obstacle in trajectory tracking control. Liu and Iven [48] derived an optimal control law for the tracking problem. They show that the optimal control law is a function of the desired trajectory's future value. Neupert and Oliver [42], and Jason W. Lawrence [37] extend this solution to a special class of the tracking problem, known as the model following problem for a boom crane. They use the dynamics of the model which generates the desired trajectory in the formulation of the control law.

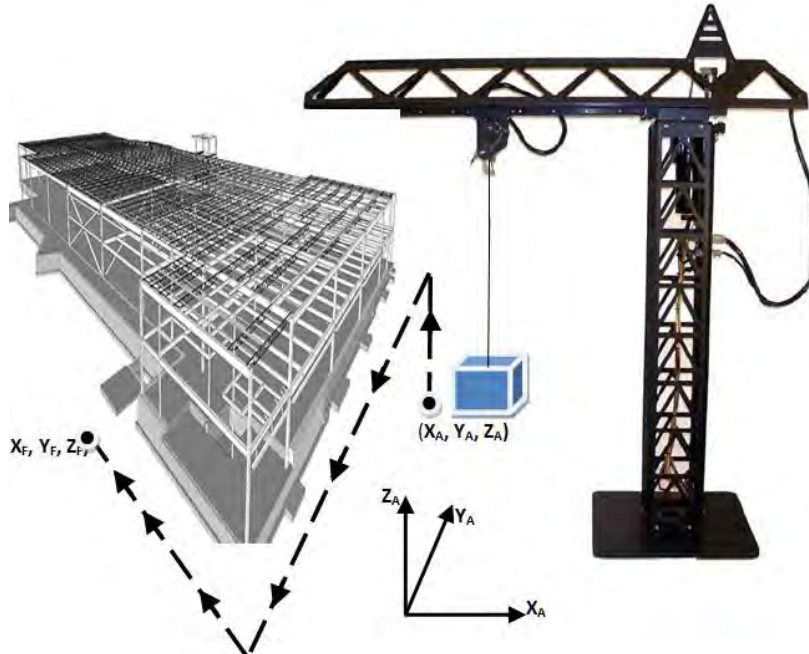


Figure 2.17 The illustration of payload trajectory along the pre-specified reference input

In [42], Neupert J and Oliver tried to linearize and stabilize the nonlinear system and calculate the reference trajectories under the input constraints. Since, tracking of a reference trajectory is based on the operator's hand lever signals, it is considered as semi-automatic system. Besides, the implementations of these control concepts have never outperformed experimental setups or scale models. Further consideration, e.g. whether their approach impose any constraint on Perfect Model Matching (the order of the desired trajectory must be the same as the order of the plant) still needs to be verified. Park Mun-Soo [43] and Chwa [49] took fuzzy sliding mode control approach to find optimal trajectories for overhead cranes in shipyards. Su Steven [50] used a nonlinear model predictive control method to find optimal trajectories for tower cranes. Their solution was obtained by discretizing the equations and using sequential

quadratic programming. Omer Hanafy [18] illustrated tracking controller using input shaping method where gains values are first chosen to obtain good tracking.

Kim J, Dong [51] and Giam [52] found that an optimal control approach decreased motion times and heavy computational burden especially for industrial cranes. Therefore, they come up with a kinematic approach which can improve an on-line minimum-time trajectory planning algorithm. However, by using the constant kinematic constraints that neglect the manipulator dynamics the global efficiency of the manipulator's dynamic capability may be decreased.

2.4.3. Vision-based Swing Control

Another method of tackling the swing minimisation problem is to implement vision-based swing monitoring system. Chen C [53] implemented hand-held wand control on an industrial bridge crane at the Georgia Institute of Technology, Fig. 2.18a. An image processing module tracks position and the crane is driven by a PD disturbance controller, Fig. 2.18b. Circular reflective materials with Siemens intelligent camera mounted between the trolley and hook will constantly provide hook relative position to Fig. 2.18c. The captured position is calculated using a blob detection algorithm. Though their conceptual design offers an inspiration, other dynamic controllers offer better performance than using a PD controller alone. Another important issue is the fact that sunlight or ambient lighting may have on measurement accuracy.

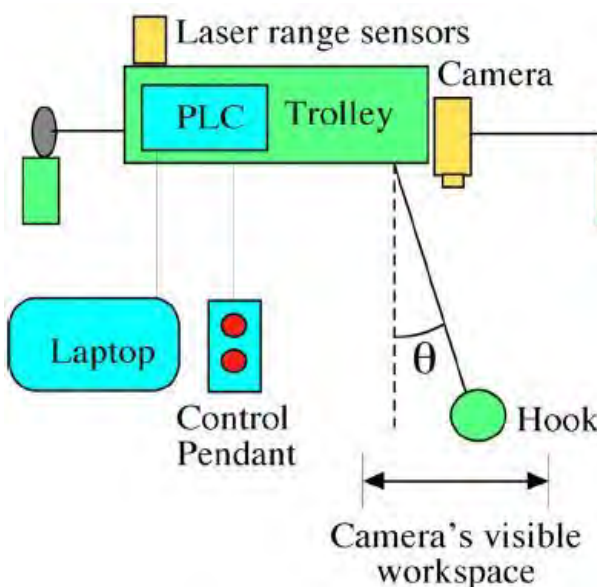


Figure 2.18a Vision Based position Measurement [53]



Figure 2.18c Hook with Circular reflective material which updates hook's relative position[53]

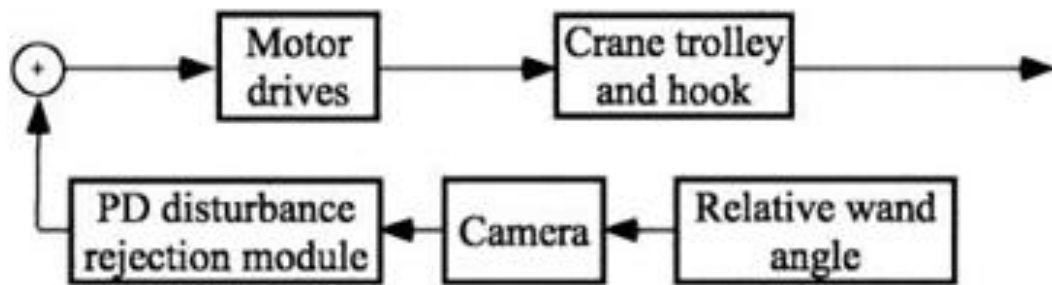


Figure 2.18b Wand controller with PD disturbance [53]

Lee [54] attempted to implement RFID-based wireless technology to demonstrate state-of-the-art for tower cranes. Donghyun Kim [55] have proposed GPS devices to explore ways of automating cranes and/or preventing conflicts between cranes and neighbouring buildings. Fig. 2.19a shows how the load location has been transmitted to the operator through RFID tag and PDA. The wireless video camera is also mounted pointing downward under the trolley to monitor the payload positions, Fig. 2.19b. However, many questions could be raised such as; different load positions with different RFID tags can have disadvantages in the wireless camera image processing unit. And that makes hard for the crane operator to identify the exact load location. Wireless transmission to control video camera may be inaccurate due to noise disturbance. Instead, direct cable connection for camera should have been considered to prevent image distortion while site supervisor to be in command control.

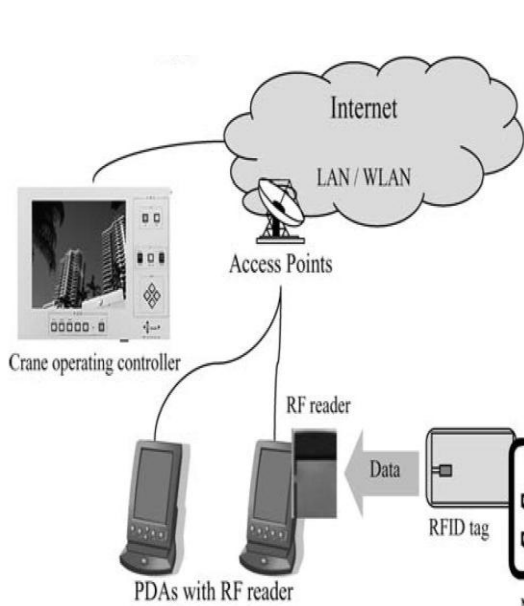


Figure 2.19a Load location transmission to operator [54]

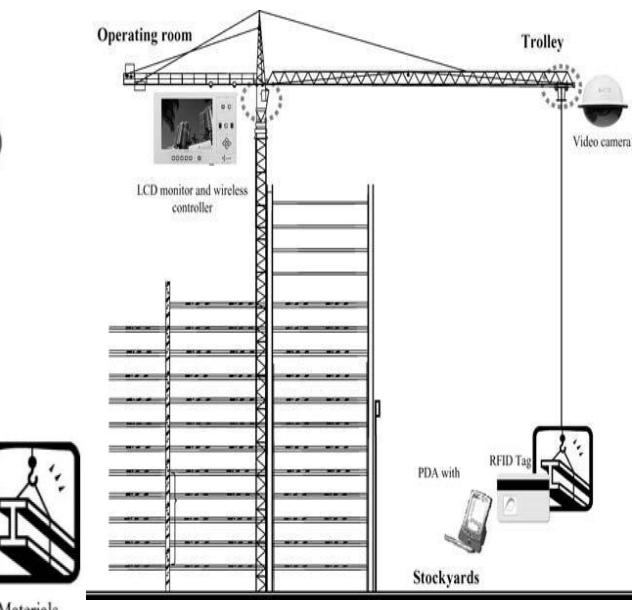


Figure 2.19b Video camera mounting [54]

Chapter 2 Background

The works mentioned above are only representative of the many previously devised solutions for the tower crane control and swing minimization problems. Although the background literature is extensive in scope, there exists one striking similarity between all the solutions: they treat the system as two separate control entities, crane trolley movement with anti-swing control and crane tower rotation with anti-swing control. This adds another level of complexity to the system and increases the difficulties of practical implementations. Portability of the presented solutions beyond research into industry is further inhibited by the extensive requirements for system parameter information prior to installation, and the difficulties in implementing the complex controller design and theoretical models. This thesis aimed to address these issues of controller and model complexity, and implementation difficulties, through the development of simmichenics-based modeling and trajectory tracking control which achieves maximal transit speed and minimal swing.

Chapter 3

Modelling and Linearization

3.1 2D Mathematical Modelling of Payload attached-Trolley Cart

In this section, the 2-DOF crane jib plant with trolley-payload assembly is presented. From the free-body diagram, nonlinear and linearized models are then derived. Using the developed linear models, a feedback control system can be designed to control the position of trolley while keeping the swings of the payload to a minimum.

3.1.1 Free body diagram of Jib System

A trolley cart is placed on a jib (rail) which is fixed over the ground along x direction. Trolley cart mass (M), payload mass (m), and load length (l) are assigned certain values while (θ) is considered load swing angle in XY plane. For 1D simple motion, load length is unchanged and frictionless between trolley and jib. Since applied force F pushes trolley to move along X direction, large swing angle θ appears which needs to be minimized to as small as possible. Therefore, simple free body diagram, as shown in Fig. 3.1, below is developed to represent 1D crane model. Furthermore, Lagrange's equations would be used to define mathematical models of the crane.

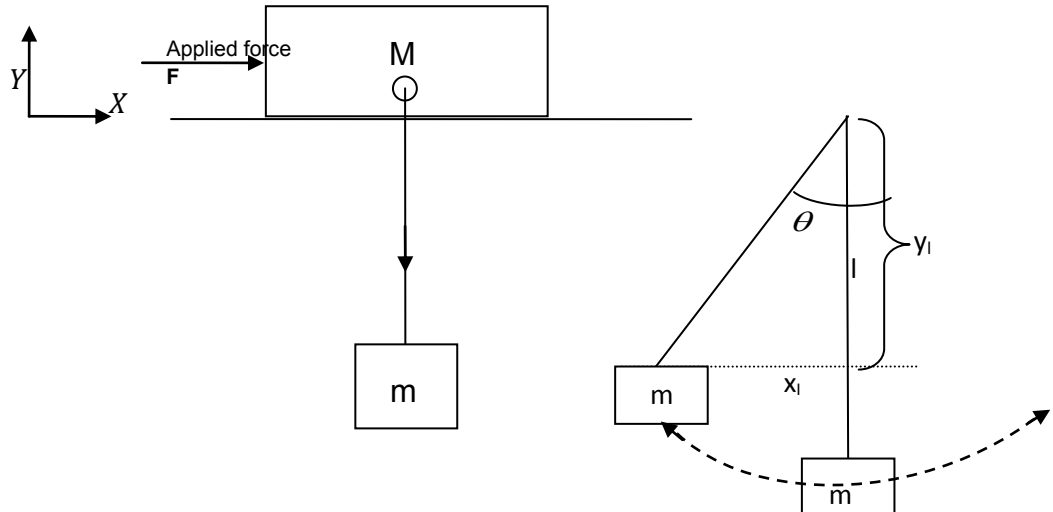


Figure 3.1 Free-body diagram of Jib System

3.1.2 Linear Model Derivation

The jib is modeled as a two-dimensional linear gantry by assuming the payload is at a fixed height and is also fixed about θ gimble angle, which is the motion perpendicular to the jib length. In other words, it is assumed the payload only rotates about gimble angle θ . The payload is connected to the trolley with the steel cable. Assuming the cable remains rigid, the payload is modeled as a suspended pendulum. As illustrated in Figure (1), when the trolley goes positive towards the right, the pendulum angle θ turns clockwise. This is defined as positive rotational velocity. Using Figure (1), the position of the payload's center of mass with respect to the Cartesian coordinate system is

$$\begin{aligned}x_l &= x_t + l \sin \theta, \text{ and } y_l = -l \cos \theta \\ \dot{x}_l &= \dot{x}_t + l \dot{\theta} \cos \theta, \quad \dot{y}_l = l \dot{\theta} \sin \theta \\ (\dot{x}_l)^2 &= (\dot{x}_t + l \dot{\theta} \cos \theta)^2 = \dot{x}_t^2 + l^2 \dot{\theta}^2 \cos^2 \theta + 2\dot{x}_t l \dot{\theta} \cos \theta \\ (\dot{y}_l)^2 &= l^2 \dot{\theta}^2 \sin^2 \theta \\ v_l^2 &= (\dot{x}_l)^2 + (\dot{y}_l)^2 = \dot{x}_t^2 + l^2 \dot{\theta}^2 \cos^2 \theta + 2\dot{x}_t l \dot{\theta} \cos \theta + l^2 \dot{\theta}^2 \sin^2 \theta \\ v_l^2 &= \dot{x}_t^2 + l^2 \dot{\theta}^2 + 2\dot{x}_t l \dot{\theta} \cos \theta\end{aligned}$$

The kinetic energy can then be shown to be $K = \frac{1}{2}M(\dot{x}_t)^2 + \frac{1}{2}mv_l^2$

$$K = \frac{1}{2}M(\dot{x}_t)^2 + \frac{1}{2}m[\dot{x}_t^2 + l^2 \dot{\theta}^2 + 2\dot{x}_t l \dot{\theta} \cos \theta]$$

and the potential energy of the system is

$$P = -mg l \cos \theta$$

Trolley cart with suspended pendulum nonlinear system is modelled below in which the Lagrange method is used to find the nonlinear dynamics of the system.

The Lagrangian equation in Eq.(3.1) is therefore

$$L = \frac{1}{2}M(\dot{x}_t)^2 + \frac{1}{2}m[\dot{x}_t^2 + l^2\dot{\theta}^2 + 2\dot{x}_t l\dot{\theta} \cos \theta] + mgl\cos\theta \quad (3.1)$$

Now carrying out the differentiations gives for the support coordinate x

$$x_t, \frac{d}{dt}\left(\frac{\partial L}{\partial \dot{x}_t}\right) - \frac{\partial L}{\partial x_t} = F - b\dot{x} \quad \text{where } b \text{ is viscous friction.}$$

$$\frac{\partial L}{\partial \dot{x}_t} = M\dot{x}_t + \frac{1}{2}m(2\dot{x}_t + 0 + 2l\dot{\theta} \cos \theta) + 0$$

$$\frac{d}{dt}\left(\frac{\partial L}{\partial \dot{x}_t}\right) = M\ddot{x}_t + m\ddot{x}_t + ml\ddot{\theta} \cos \theta - ml\dot{\theta}^2 \sin \theta$$

$$\frac{\partial L}{\partial x_t} = 0$$

$$\frac{d}{dt}\left(\frac{\partial L}{\partial x_t}\right) - \frac{\partial L}{\partial x_t} = F - b\dot{x}$$

Nonlinear Dynamic equation form in Eq.(3.2) is then

$$M\ddot{x}_t + m\ddot{x}_t + ml\ddot{\theta} \cos \theta - ml\dot{\theta}^2 \sin \theta = F - b\dot{x} \quad (3.2)$$

For Swing Angle, θ , $\frac{d}{dt}\left(\frac{\partial L}{\partial \dot{\theta}}\right) - \frac{\partial L}{\partial \theta}$

$$L = \frac{1}{2}M(\dot{x}_t)^2 + \frac{1}{2}m[\dot{x}_t^2 + l^2\dot{\theta}^2 + 2\dot{x}_t l\dot{\theta} \cos \theta] + mgl\cos\theta$$

$$\frac{\partial L}{\partial \dot{\theta}} = 0 + \frac{1}{2}m[0 + 2l^2\dot{\theta} + 2\dot{x}_t l \cos \theta] + 0$$

$$\frac{d}{dt}\left(\frac{\partial L}{\partial \dot{\theta}}\right) = m[l^2\ddot{\theta} + \dot{x}_t l \cos \theta - \dot{x}_t l \dot{\theta} \sin \theta]$$

$$\frac{\partial L}{\partial \theta} = \frac{1}{2}m[0 + 0 - 2\dot{x}_t l \dot{\theta} \sin \theta] - mgl \sin \theta = -m\dot{x}_t l \dot{\theta} \sin \theta - mgl \sin \theta$$

Torque Equation

$$\frac{d}{dt}\left(\frac{\partial L}{\partial \dot{\theta}}\right) - \frac{\partial L}{\partial \theta} = m[l^2\ddot{\theta} + \dot{x}_t l \cos \theta - \dot{x}_t l \dot{\theta} \sin \theta] + m\dot{x}_t l \dot{\theta} \sin \theta + mgl \sin \theta = I\ddot{\theta} + c\dot{\theta}$$

Where "c" is viscous friction coefficient and I is moment of inertia of the load about pivot.

$$ml^2\ddot{\theta} + m\dot{x}_t l \cos \theta - m\dot{x}_t l \dot{\theta} \sin \theta + m\dot{x}_t l \dot{\theta} \sin \theta + mgl \sin \theta = I\ddot{\theta} + c\dot{\theta}$$

$$m\dot{x}_t l \cos \theta + mgl \sin \theta - c\dot{\theta} = \ddot{\theta}(I - ml^2) \quad (3.3)$$

Referring to the nonlinear dynamic force and torque equations Eq.(3.2) and Eq.(3.3), the following nonlinear equations of motions Eq.(3.4) and Eq.(3.5) are derived as

$$\ddot{x}_t = \frac{1}{(M+m)}[F - ml(\ddot{\theta} \cos \theta - \dot{\theta}^2 \sin \theta) - b\dot{x}] \quad (3.4)$$

$$\ddot{\theta} = \frac{1}{(I - ml^2)}[ml(\ddot{x}_t \cos \theta + g \sin \theta) - c\dot{\theta}] \quad (3.5)$$

Using these derived nonlinear equations Eq.(3.4) and Eq.(3.5), linearized models are developed in the next section.

3.1.3 2D Model Linearization using simple assumption

In several literatures, approximate parameters such as: $\sin \theta = 0, \cos \theta = 1$ (OR) $\sin \theta = \tan \theta = \theta, \cos \theta = 1$, have been substituted in the nonlinear model to linearize nonlinear equations of crane model. By assuming the system at an equilibrium point, load swing angle θ and its velocity $\dot{\theta}$ are considered as small, and this research considers $\sin \theta \approx \theta, \cos \theta \approx 1$, and $\dot{\theta} \approx 0$ [56]. Using these assumptions, the nonlinear mathematical equations Eq. (3.4) and Eq. (3.5) are linearized around the unstable equilibrium point and therefore, the following Eq. (3.6) and Eq. (3.7) have been obtained.

$$\ddot{x}_t = \frac{1}{(M+m)} [F - ml\ddot{\theta} - b\dot{x}] \quad (3.6)$$

$$\ddot{\theta} = \frac{1}{(I-ml^2)} [ml\ddot{x}_t + mlg\theta - c\dot{\theta}] \quad (3.7)$$

By substituting Eq(3.7) into Eq(3.6):

$$\begin{aligned} \ddot{x}_t &= \frac{1}{(M+m)} [F - ml(\frac{1}{(I-ml^2)} [ml\ddot{x}_t + mlg\theta - c\dot{\theta}]) - b\dot{x}] \\ (M+m)\ddot{x}_t &= F - \frac{m^2l^2}{(I-ml^2)} \ddot{x}_t - \frac{m^2l^2g\theta}{(I-ml^2)} + \frac{mlc\dot{\theta}}{(I-ml^2)} - b\dot{x} \\ (M+m)\ddot{x}_t + \frac{m^2l^2}{(I-ml^2)} \ddot{x}_t &= F - \frac{m^2l^2g\theta}{(I-ml^2)} + \frac{mlc\dot{\theta}}{(I-ml^2)} - b\dot{x} \\ (I-ml^2)(M+m)\ddot{x}_t + m^2l^2\ddot{x}_t &= (I-ml^2)F - m^2l^2g\theta + mlc\dot{\theta} - (I-ml^2)b\dot{x} \\ [(I-ml^2)(M+m) + m^2l^2]\ddot{x}_t &= (I-ml^2)F - m^2l^2g\theta + mlc\dot{\theta} - (I-ml^2)b\dot{x} \\ [(IM + Im - Mml^2 - m^2l^2) + m^2l^2]\ddot{x}_t &= (I-ml^2)F - m^2l^2g\theta + mlc\dot{\theta} - (I-ml^2)b\dot{x} \\ (IM + Im - Mml^2)\ddot{x}_t &= (I-ml^2)F - m^2l^2g\theta + mlc\dot{\theta} - (I-ml^2)b\dot{x} \\ J &= [(IM + Im - Mml^2)] \\ J\ddot{x}_t &= (I-ml^2)F - m^2l^2g\theta + mlc\dot{\theta} - (I-ml^2)b\dot{x} \end{aligned}$$

After simplifying the steps: the final linearized equations, Eq(3.8) and Eq(3.9), are obtained.

$$\ddot{x}_t = \frac{(I-ml^2)}{J} F - \frac{m^2l^2g}{J} \theta + \frac{mlc}{J} \dot{\theta} - \frac{(I-ml^2)b}{J} \dot{x} \quad (3.8)$$

By substituting Equ(4) into Equ(5):

$$\begin{aligned} \ddot{\theta} &= \frac{1}{(I-ml^2)} [ml(\frac{1}{(M+m)} (F - ml\ddot{\theta} - b\dot{x})) + mlg\theta - c\dot{\theta}] \\ (I-ml^2)\ddot{\theta} &= \frac{mlF}{(M+m)} - \frac{m^2l^2\ddot{\theta}}{(M+m)} - \frac{mlb\dot{x}}{(M+m)} + mlg\theta - c\dot{\theta} \\ (I-ml^2)\ddot{\theta} + \frac{m^2l^2\ddot{\theta}}{(M+m)} &= \frac{mlF}{(M+m)} - \frac{mlb\dot{x}}{(M+m)} + mlg\theta - c\dot{\theta} \\ [(I-ml^2) + \frac{m^2l^2}{(M+m)}]\ddot{\theta} &= \frac{mlF}{(M+m)} - \frac{mlb\dot{x}}{(M+m)} + mlg\theta - c\dot{\theta} \\ [(M+m)(I-ml^2) + m^2l^2]\ddot{\theta} &= mlF - mlb\dot{x} + (M+m)mlg\theta - (M+m)c\dot{\theta} \end{aligned}$$

$$[(M+m)I - Mml^2]\ddot{\theta} = mlF - mlb\dot{x}_t + (M+m)m样子\theta - (M+m)c\dot{\theta}$$

$$K = (M+m)I - Mml^2$$

$$\ddot{\theta} = \frac{ml}{K}F - \frac{mlb}{K}\dot{x}_t + \frac{(M+m)m样子\theta}{K} - \frac{(M+m)c}{K}\dot{\theta} \quad (3.9)$$

In order to change to state space model, the parameters from above two linearized equations have been considered as follow.

$$x_1 = x_t, \dot{x}_1 = x_2 = \dot{x}_t, \dot{x}_2 = \ddot{x}_1 = \ddot{x}_t, x_3 = \theta, \dot{x}_3 = x_4 = \dot{\theta}, \dot{x}_4 = \ddot{x}_3 = \ddot{\theta}$$

By rewriting Equ(6)

$$\begin{aligned} \ddot{x}_t &= \frac{(I-ml^2)}{J}F - \frac{m^2l^2g}{J}\theta + \frac{mlc}{J}\dot{\theta} - \frac{(I-ml^2)b}{J}\dot{x}_t \\ \dot{x}_2 &= -\frac{(I-ml^2)b}{J}x_2 - \frac{m^2l^2g}{J}x_3 + \frac{mlc}{J}x_4 + \frac{(I-ml^2)}{J}F \end{aligned}$$

By rewriting Equ(7)

$$\begin{aligned} \ddot{\theta} &= \frac{ml}{K}F - \frac{mlb}{K}\dot{x}_t + \frac{(M+m)m样子\theta}{K} - \frac{(M+m)c}{K}\dot{\theta} \\ \dot{x}_4 &= \frac{ml}{K}F - \frac{mlb}{K}x_2 + \frac{(M+m)m样子\theta}{K}x_3 - \frac{(M+m)c}{K}x_4 \\ \dot{x}_4 &= -\frac{mlb}{K}x_2 + \frac{(M+m)m样子\theta}{K}x_3 - \frac{(M+m)c}{K}x_4 + \frac{ml}{K}F \end{aligned}$$

So, Final linerized equations are

$$\begin{aligned} \dot{x}_2 &= -\frac{(I-ml^2)b}{J}x_2 - \frac{m^2l^2g}{J}x_3 + \frac{mlc}{J}x_4 + \frac{(I-ml^2)}{J}F \\ \dot{x}_4 &= -\frac{mlb}{K}x_2 + \frac{(M+m)m样子\theta}{K}x_3 - \frac{(M+m)c}{K}x_4 + \frac{ml}{K}F \end{aligned}$$

Linerized State Space model is:

$$\dot{x} = Ax + Bu$$

$$y = Cx + Du$$

$$\begin{bmatrix} \dot{x}_1 \\ \dot{x}_2 \\ \dot{x}_3 \\ \dot{x}_4 \end{bmatrix} = \begin{bmatrix} 0 & 1 & 0 & 0 \\ 0 & -\frac{(I-ml^2)b}{J} & -\frac{m^2l^2g}{J} & \frac{mlc}{J} \\ 0 & 0 & 0 & 1 \\ 0 & -\frac{mlb}{K} & \frac{(M+m)m样子\theta}{K} & -\frac{(M+m)c}{K} \end{bmatrix} \begin{bmatrix} x_1 \\ x_2 \\ x_3 \\ x_4 \end{bmatrix} + \begin{bmatrix} 0 \\ \frac{(I-ml^2)}{J} \\ 0 \\ \frac{ml}{K} \end{bmatrix} u$$

$$y = \begin{bmatrix} 1 & 0 & 0 & 0 \\ 0 & 0 & 1 & 0 \end{bmatrix} \begin{bmatrix} x_1 \\ x_2 \\ x_3 \\ x_4 \end{bmatrix} = \begin{bmatrix} 1 & 0 & 0 & 0 \\ 0 & 0 & 1 & 0 \end{bmatrix} \begin{bmatrix} x_t \\ \dot{x}_t \\ \theta \\ \dot{\theta} \end{bmatrix}$$

$$\frac{x}{F} = \frac{0.5176 s^2 - (7.529 \times 10^{-6}) s + 5.54}{s^4 + 0.00412 s^3 + 15.23 s^2 + 0.04432 s}$$

$$\frac{\theta}{F} = \frac{-0.5647 s^2 + (2.508 \times 10^{-16}) s + 6.746}{s^4 + 0.00412 s^3 + 15.23 s^2 + 0.04432 s}$$

3.1.4 Model Excitation with simple step input

After using simple assumptions, Trolley-Payload models have been derived. This section provides general excitation in Fig. 3.2a of the system and its responses as shown in Fig. 3.2b.

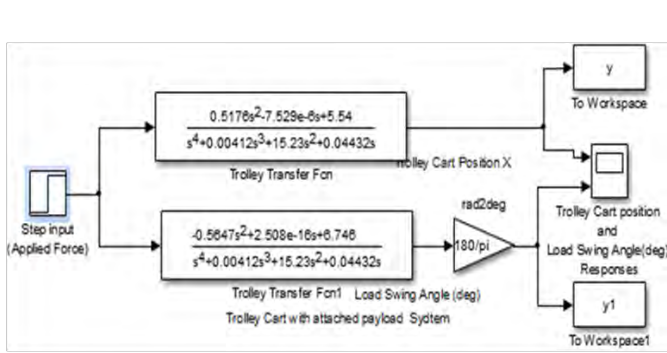


Figure3.2a Trolley-Payload Models Excitation

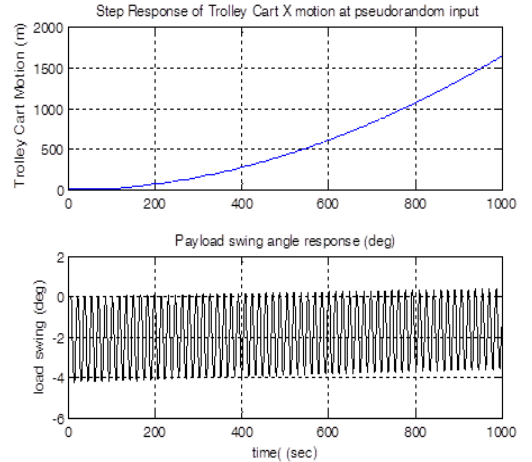


Figure3.2b Trolley-Payload System Response

3.1.5 Nonlinear Model Derivation for 2D model

This nonlinear model derivation is actual combining previously developed two nonlinear models Equations Eq.(3.4) and Eq.(3.5) from section 3.12.

$$\ddot{x}_t = \frac{1}{(M+m)} [F - ml(\ddot{\theta} \cos \theta - \dot{\theta}^2 \sin \theta) - b\dot{x}]$$

$$\ddot{\theta} = \frac{1}{(I - ml^2)} [ml(\ddot{x}_t \cos \theta + g \sin \theta) - c\dot{\theta}]$$

Substitute Eq.(3.5) into Eq.(3.4):

$$\ddot{\theta} = \left[\frac{ml\ddot{x}_t \cos \theta}{(I - ml^2)} + \frac{mlg \sin \theta}{(I - ml^2)} - \frac{c\dot{\theta}}{(I - ml^2)} \right]$$

$$\ddot{x}_t = \frac{1}{(M+m)} [F - ml \left(\left(\frac{ml\ddot{x}_t \cos \theta}{(I - ml^2)} + \frac{mlg \sin \theta}{(I - ml^2)} - \frac{c\dot{\theta}}{(I - ml^2)} \right) \cos \theta - \dot{\theta}^2 \sin \theta \right) - b\dot{x}]$$

$$(M+m)\ddot{x}_t = F - ml \left(\left(\frac{ml\ddot{x}_t \cos \theta}{(I - ml^2)} + \frac{mlg \sin \theta}{(I - ml^2)} - \frac{c\dot{\theta}}{(I - ml^2)} \right) \cos \theta - \dot{\theta}^2 \sin \theta \right) - b\dot{x}$$

$$(M+m)\ddot{x}_t = F - ml \left(\left(\frac{ml\ddot{x}_t \cos \theta \cos \theta}{(I - ml^2)} + \frac{mlg \sin \theta \cos \theta}{(I - ml^2)} - \frac{c\dot{\theta} \cos \theta}{(I - ml^2)} \right) - \dot{\theta}^2 \sin \theta \right) - b\dot{x}$$

$$(M+m)\ddot{x}_t = F - \left(\left(\frac{m^2 l^2 \ddot{x}_t \cos^2 \theta}{(I - ml^2)} + \frac{m^2 l^2 g \sin \theta \cos \theta}{(I - ml^2)} - \frac{ml c \dot{\theta} \cos \theta}{(I - ml^2)} \right) - ml \dot{\theta}^2 \sin \theta \right) - b\dot{x}$$

$$(M+m)\ddot{x}_t = F - \frac{m^2 l^2 \ddot{x}_t \cos^2 \theta}{(I - ml^2)} - \frac{m^2 l^2 g \sin \theta \cos \theta}{(I - ml^2)} + \frac{ml c \dot{\theta} \cos \theta}{(I - ml^2)} + ml \dot{\theta}^2 \sin \theta - b\dot{x}$$

$$(M+m)\ddot{x}_t + \frac{m^2 l^2 \cos^2 \theta}{(I - ml^2)} \ddot{x}_t = F - \frac{m^2 l^2 g \sin \theta \cos \theta}{(I - ml^2)} + \frac{ml c \dot{\theta} \cos \theta}{(I - ml^2)} + ml \dot{\theta}^2 \sin \theta - b\dot{x}$$

$$\begin{aligned}
 & (I - ml^2)(M + m)\ddot{x}_t + m^2l^2 \cos^2\theta \ddot{x}_t \\
 &= (I - ml^2)F - m^2l^2g \sin\theta \cos\theta + ml c \dot{\theta} \cos\theta + (I - ml^2)ml\dot{\theta}^2 \sin\theta \\
 &\quad - (I - ml^2)b\dot{x} \\
 L &= (I - ml^2)(M + m) + m^2l^2 \cos^2\theta \\
 L\ddot{x}_t &= (I - ml^2)F - m^2l^2g \sin\theta \cos\theta + ml c \dot{\theta} \cos\theta + (I - ml^2)ml\dot{\theta}^2 \sin\theta - (I - ml^2)b\dot{x} \\
 \ddot{x}_t &= \frac{(I - ml^2)}{L}F - \frac{m^2l^2g \sin\theta \cos\theta}{L} + \frac{ml c \cos\theta}{L}\dot{\theta} + \frac{(I - ml^2)ml\sin\theta}{L}\dot{\theta}^2 - \frac{(I - ml^2)b}{L}\dot{x}
 \end{aligned}$$

Substitute Eq.(3.4) into Eq.(3.5) :

$$\begin{aligned}
 \ddot{x}_t &= \left(\frac{F}{(M+m)} - \frac{ml\ddot{\theta} \cos\theta}{(M+m)} + \frac{ml\dot{\theta}^2 \sin\theta}{(M+m)} - \frac{b\dot{x}}{(M+m)} \right) \\
 \ddot{\theta} &= \frac{1}{(I - ml^2)} [ml(\ddot{x}_t \cos\theta + g \sin\theta) - c\dot{\theta}] \\
 (I - ml^2)\ddot{\theta} &= ml\ddot{x}_t \cos\theta + mlg \sin\theta - c\dot{\theta} \\
 (I - ml^2)\ddot{\theta} &= ml\left(\frac{F}{(M+m)} - \frac{ml\ddot{\theta} \cos\theta}{(M+m)} + \frac{ml\dot{\theta}^2 \sin\theta}{(M+m)} - \frac{b\dot{x}}{(M+m)}\right) \cos\theta + mlg \sin\theta - c\dot{\theta} \\
 (I - ml^2)\ddot{\theta} &= \left(\frac{mlF}{(M+m)} - \frac{m^2l^2\ddot{\theta} \cos\theta}{(M+m)} + \frac{m^2l^2\dot{\theta}^2 \sin\theta}{(M+m)} - \frac{mlb\dot{x}}{(M+m)} \right) \cos\theta + mlg \sin\theta - c\dot{\theta} \\
 (I - ml^2)\ddot{\theta} &= \left(\frac{mlFc\cos\theta}{(M+m)} - \frac{m^2l^2\ddot{\theta} \cos^2\theta}{(M+m)} + \frac{m^2l^2\dot{\theta}^2 \sin\theta \cos\theta}{(M+m)} - \frac{mlbc\cos\theta \dot{x}}{(M+m)} \right) + mlg \sin\theta - c\dot{\theta} \\
 (I - ml^2)\ddot{\theta} + \frac{m^2l^2 \cos^2\theta}{(M+m)}\ddot{\theta} &= \frac{mlFc\cos\theta}{(M+m)} + \frac{m^2l^2\dot{\theta}^2 \sin\theta \cos\theta}{(M+m)} - \frac{mlbc\cos\theta \dot{x}}{(M+m)} + mlg \sin\theta - c\dot{\theta} \\
 (M + m)(I - ml^2)\ddot{\theta} + m^2l^2 \cos^2\theta \ddot{\theta} &= mlFc\cos\theta + m^2l^2\dot{\theta}^2 \sin\theta \cos\theta - mlbc\cos\theta \dot{x} + \\
 (M + m)mlg \sin\theta - (M + m)c\dot{\theta} & \\
 P &= (M + m)(I - ml^2) + m^2l^2 \cos^2\theta \\
 P\ddot{\theta} &= mlFc\cos\theta + m^2l^2\dot{\theta}^2 \sin\theta \cos\theta - mlbc\cos\theta \dot{x} + (M + m)mlg \sin\theta - (M + m)c\dot{\theta}
 \end{aligned}$$

$$\ddot{\theta} = \frac{mlcos\theta}{P}F + \frac{m^2l^2 \sin\theta \cos\theta}{P}\dot{\theta}^2 - \frac{mlbcos\theta}{P}\dot{x} + \frac{(M+m)mlg \sin\theta}{P} - \frac{(M+m)c}{P}\dot{\theta}$$

Since $L=P$,

$$\text{So, } \ddot{\theta} = \frac{mlcos\theta}{L}F + \frac{m^2l^2 \sin\theta \cos\theta}{L}\dot{\theta}^2 - \frac{mlbcos\theta}{L}\dot{x} + \frac{(M+m)mlg \sin\theta}{L} - \frac{(M+m)c}{L}\dot{\theta}$$

Final two nonlinear equations Eq.(3.10) and Eq.(3.11) are

$$\ddot{x}_t = \frac{(I - ml^2)}{L}F - \frac{m^2l^2g \sin\theta \cos\theta}{L} + \frac{ml c \cos\theta}{L}\dot{\theta} + \frac{(I - ml^2)ml\sin\theta}{L}\dot{\theta}^2 - \frac{(I - ml^2)b}{L}\dot{x} \quad (3.10)$$

$$\ddot{\theta} = \frac{mlcos\theta}{L}F + \frac{m^2l^2 \sin\theta \cos\theta}{L}\dot{\theta}^2 - \frac{mlbcos\theta}{L}\dot{x} + \frac{(M+m)mlg \sin\theta}{L} - \frac{(M+m)c}{L}\dot{\theta} \quad (3.11)$$

3.1.6 3D Tower Crane Freebody Diagram Modelling

In this current research, jib rotation, load and trolley positions are considered using Cartesian coordinate system since polar coordinate system could produce further

complication in overall 3D tower crane model representation as shown in Fig. 3.3. The load position is also identified based on above-mentioned theoretical approach.

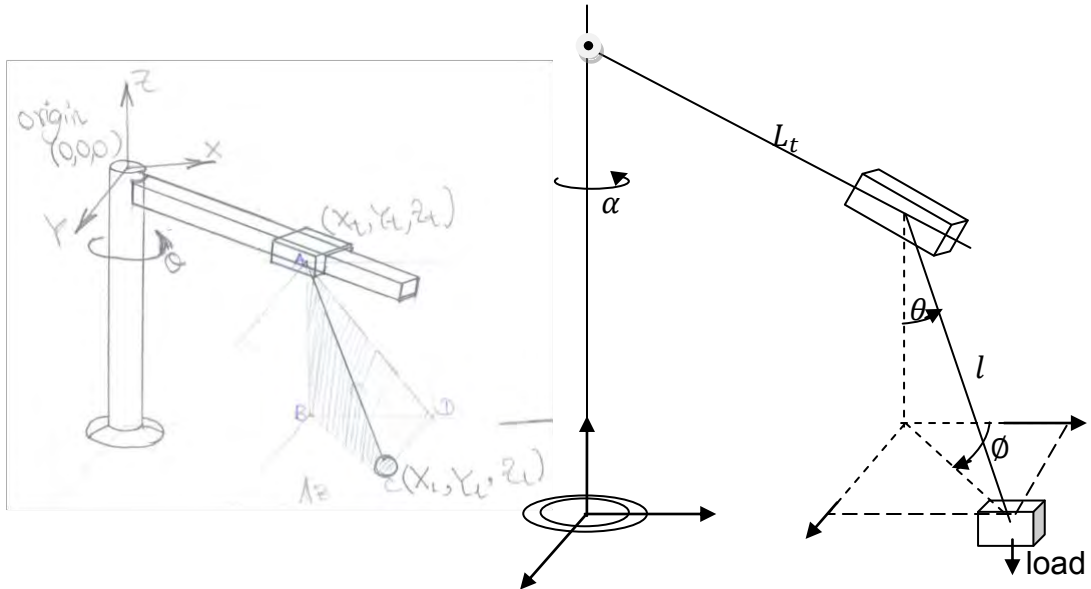


Figure 3.3 3D tower crane positions identification (Cartesian coordinate)

3.1.7 Nonlinear Model Derivation for 3D model

$$x_l = (x_t + l \cos \phi \sin \theta)$$

$$y_l = (y_t + l \sin \phi \sin \theta)$$

$$z_l = (z_t - l \cos \theta)$$

$$x_{load} = x_l = (x_l, y_l, z_l)$$

$$\dot{x}_l = \dot{x}_t + l[\dot{\theta} \cos \phi \cos \theta - \dot{\phi} \sin \phi \sin \theta] = \dot{x}_t + l[A - B], A = \dot{\theta} \cos \phi \cos \theta, B = \dot{\phi} \sin \phi \sin \theta$$

$$\dot{y}_l = \dot{y}_t + l[\dot{\theta} \sin \phi \cos \theta + \dot{\phi} \cos \phi \sin \theta] = \dot{y}_t + l[C + D],$$

$$C = \dot{\theta} \sin \phi \cos \theta, D = \dot{\phi} \cos \phi \sin \theta$$

$$\dot{z}_l = l\dot{\theta} \sin \theta$$

$$\bar{x}_l = (\dot{x}_l + \dot{y}_l + \dot{z}_l)$$

$$(\dot{x}_l)^2 = (\bar{X}_t + Al - Bl)^2 = (a + b + c)^2 = a^2 + b^2 + c^2 + 2ab + 2ac + 2bc$$

$$\bar{X}_l^2 = \bar{X}_t^2 + (Al)^2 + (-Bl)^2 + 2\bar{X}_t Al - 2\bar{X}_t Bl - 2ABl^2$$

$$= \bar{X}_t^2 + A^2 l^2 + B^2 l^2 + 2\bar{X}_t Al - 2\bar{X}_t Bl - 2ABl^2$$

$$(\dot{x}_l)^2 = (\dot{x}_t)^2 + (A^2 + B^2 - 2AB)l^2 + (A - B)2\dot{x}_t l$$

$$(\dot{y}_l)^2 = (\bar{Y}_t + Cl + Dl)^2 = (a + b + c)^2 = a^2 + b^2 + c^2 + 2ab + 2ac + 2bc$$

$$\bar{Y}_l^2 = \bar{Y}_t^2 + (Cl)^2 + (Dl)^2 + 2\bar{Y}_t Cl + 2\bar{Y}_t Dl + 2CDl^2$$

$$= \bar{Y}_t^2 + C^2 l^2 + D^2 l^2 + 2\bar{Y}_t Cl + 2\bar{Y}_t Dl + 2CDl^2$$

$$(\dot{y}_l)^2 = (\dot{y}_t)^2 + (C^2 + D^2 + 2CD)l^2 + (C + D)2\dot{y}_t l$$

$$(\dot{z}_l)^2 = l^2 \dot{\theta}^2 \sin^2 \theta$$

$$(v_l)^2 = ((\dot{x}_l)^2 + (\dot{y}_l)^2 + (\dot{z}_l)^2)$$

Velocity of load is

$$\begin{aligned}(v_l)^2 &= (\dot{x}_t)^2 + (A^2 + B^2 - 2AB)l^2 + (A - B)2\dot{x}_t l + (\dot{y}_t)^2 + (C^2 + D^2 + 2CD)l^2 \\ &\quad + (C + D)2\dot{y}_t l + l^2\dot{\theta}^2 \sin^2\theta\end{aligned}$$

Trolley translational motion along he jib tower is considered as shown in Fig. 3.4.

$$X_t = L \cos(\alpha), \quad Y_t = L \sin(\alpha)$$

Trolley moves forward/backward while Jib rotation is at equilibrium (ie. α is constat)

$$\bar{X}_t = \dot{X}_t = \dot{L} \cos(\alpha),$$

$$\bar{Y}_t = \dot{Y}_t = \dot{L} \sin(\alpha)$$

Considering Trolley translational motion,

$$\bar{X}_t^2 = \dot{X}_t^2 = \dot{L}^2 \cos^2\alpha$$

$$\bar{Y}_t^2 = \dot{Y}_t^2 = \dot{L}^2 \sin^2\alpha$$

Velocity of Trolley is

$$v_t^2 = \dot{X}_t^2 + \dot{Y}_t^2 = \dot{L}^2 \cos^2\theta + \dot{L}^2 \sin^2\theta = \dot{L}^2$$

Kinetic Energy of Jib, Trolley, and Load motion

$$K = K_{Jib} + K_{Trolley} + K_{Load}$$

$$K = \frac{1}{2}J_{jib}\dot{\alpha}^2 + \frac{1}{2}M_{trolley}v_t^2 + \frac{1}{2}m_{load}(\bar{x}_l)^2$$

$$M_{trolley} = M_t$$

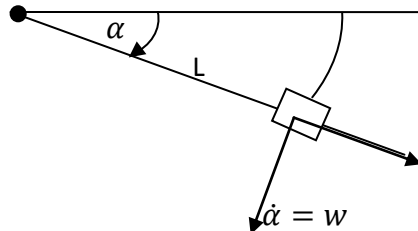


Figure3.4 Trolley translational motion along jib

$$K_{jib} = \frac{1}{2}M_j v^2 \implies v = wL = \dot{\alpha}L, \text{ where } M_j = \text{Mass of Jib}$$

$$= \frac{1}{2}M_j(wL)^2 = \frac{1}{2}(M_jL^2)w^2 = \frac{1}{2}J_j w^2$$

$J_{jib} = J_j$ (Jib moment of Inertia), $L =$ Jib length up to Trolley

$$m_{load} = m$$

Potential Energy, only hoist up/down motions appear, So,

$$P = mgZ_l \quad (\text{vertical motion})$$

$$P = -mgl \cos \theta$$

Lagrange Equation, L=K-P

$$\begin{aligned} L &= K_{jib} + K_{trolley} + K_{load} - P_{load} \\ L &= \frac{1}{2}J_j\dot{\alpha}^2 + \frac{1}{2}M_t\dot{v}_t^2 + \frac{1}{2}m(\bar{x}_l)^2 + mgl \cos \theta \\ L &= \frac{1}{2}(M_jL^2)\dot{\alpha}^2 + \frac{1}{2}M_t\dot{L}^2 + \frac{1}{2}m[\bar{X}_t^2 + (A^2 + B^2 - 2AB)l^2 + (A - B)2\bar{X}_tl + \bar{Y}_t^2 + (C^2 + D^2 \\ &\quad + 2CD)l^2 + (C + D)2\bar{Y}_tl + l^2\dot{\theta}^2 \sin^2 \theta] + mgl \cos \theta \\ \text{But, } A &= \dot{\theta} \cos \phi \cos \theta, B = \dot{\phi} \sin \phi \sin \theta \\ C &= \dot{\theta} \sin \phi \cos \theta \quad D = \dot{\phi} \cos \phi \sin \theta \\ \bar{X}_t &= \dot{X}_t = \dot{L} \cos \alpha, \\ \bar{Y}_t &= \dot{Y}_t = \dot{L} \sin \alpha \end{aligned}$$

Considering Trolley translational motion,

$$\begin{aligned} \bar{X}_t^2 &= \dot{X}_t^2 = \dot{L}^2 \cos^2 \alpha \\ \bar{Y}_t^2 &= \dot{Y}_t^2 = \dot{L}^2 \sin^2 \alpha \\ L &= \frac{1}{2}(M_jL^2)\dot{\alpha}^2 + \frac{1}{2}M_t\dot{L}^2 + \frac{1}{2}m[\bar{X}_t^2 + (A^2 + B^2 - 2AB)l^2 + (A - B)2\bar{X}_tl + \bar{Y}_t^2 + (C^2 + D^2 \\ &\quad + 2CD)l^2 + (C + D)2\bar{Y}_tl + l^2\dot{\theta}^2 \sin^2 \theta] + mgl \cos \theta \\ L &= \frac{1}{2}M_jL^2\dot{\alpha}^2 + \frac{1}{2}M_t\dot{L}^2 + \frac{1}{2}m[\dot{L}^2 \cos^2 \alpha + [(\dot{\theta} \cos \phi \cos \theta)^2 + (\dot{\phi} \sin \phi \sin \theta)^2 \\ &\quad - 2(\dot{\theta} \cos \phi \cos \theta)(\dot{\phi} \sin \phi \sin \theta)]l^2 \\ &\quad + [(\dot{\theta} \cos \phi \cos \theta) - (\dot{\phi} \sin \phi \sin \theta)]2(\dot{L} \cos \alpha)l + \dot{L}^2 \sin^2 \alpha + [(\dot{\theta} \sin \phi \cos \theta)^2 \\ &\quad + (\dot{\phi} \cos \phi \sin \theta)^2 + 2(\dot{\theta} \sin \phi \cos \theta)(\dot{\phi} \cos \phi \sin \theta)]l^2 \\ &\quad + [(\dot{\theta} \sin \phi \cos \theta) + (\dot{\phi} \cos \phi \sin \theta)]2(\dot{L} \sin \alpha)l + l^2\dot{\theta}^2 \sin^2 \theta] + mgl \cos \theta \\ L &= \frac{1}{2}M_jL^2\dot{\alpha}^2 + \frac{1}{2}M_t\dot{L}^2 + \frac{1}{2}m[\dot{L}^2 \cos^2 \alpha + l^2(\dot{\theta} \cos \phi \cos \theta)^2 + l^2(\dot{\phi} \sin \phi \sin \theta)^2 \\ &\quad - 2l^2(\dot{\theta} \cos \phi \cos \theta)(\dot{\phi} \sin \phi \sin \theta) + 2(\dot{L} \cos \alpha)l\dot{\theta} \cos \phi \cos \theta \\ &\quad - 2(\dot{L} \cos \alpha)l\dot{\phi} \sin \phi \sin \theta + \dot{L}^2 \sin^2 \alpha + l^2(\dot{\theta} \sin \phi \cos \theta)^2 + l^2(\dot{\phi} \cos \phi \sin \theta)^2 \\ &\quad + 2l^2(\dot{\theta} \sin \phi \cos \theta)(\dot{\phi} \cos \phi \sin \theta) + 2(\dot{L} \sin \alpha)l\dot{\theta} \sin \phi \cos \theta \\ &\quad + 2(\dot{L} \sin \alpha)l\dot{\phi} \cos \phi \sin \theta + l^2\dot{\theta}^2 \sin^2 \theta] + mgl \cos \theta \end{aligned}$$

Final Lagrange Equation is

$$\begin{aligned}
 L = & \frac{1}{2} M_j L^2 \dot{\alpha}^2 + \frac{1}{2} M_t \dot{L}^2 + \frac{1}{2} m [\dot{L}^2 \cos^2 \alpha + l^2 \dot{\theta}^2 \cos^2 \phi \cos^2 \theta + l^2 \dot{\phi}^2 \sin^2 \phi \sin^2 \theta \\
 & - 2l^2 \dot{\theta} \dot{\phi} \cos \phi \cos \theta \sin \phi \sin \theta + 2\dot{L}l \dot{\theta} \cos \alpha \cos \phi \cos \theta \\
 & - 2\dot{L}l \dot{\phi} \cos \alpha \sin \phi \sin \theta + \dot{L}^2 \sin^2 \alpha + l^2 \dot{\theta}^2 \sin^2 \phi \cos^2 \theta + l^2 \dot{\phi}^2 \cos^2 \phi \sin^2 \theta \\
 & + 2l^2 \dot{\theta} \dot{\phi} \sin \phi \cos \theta \cos \phi \sin \theta + 2\dot{L}l \dot{\theta} \sin \alpha \sin \phi \cos \theta \\
 & + 2\dot{L}l \dot{\phi} \sin \alpha \cos \phi \sin \theta + l^2 \dot{\theta}^2 \sin^2 \theta] + mgl \cos \theta
 \end{aligned}$$

Based on the final Lagrange Equation above for "L", four dynamic equations ($\dot{\alpha}, \dot{L}, \dot{\phi}, \dot{\theta}$) are then obtained as follow.

To make partial derivative of α , considered

$$\begin{aligned}
 L = & 0 + 0 + \frac{1}{2} m [\dot{L}^2 \cos^2 \alpha + 0 + 0 - 0 + 2\dot{L}l \dot{\theta} \cos \alpha \cos \phi \cos \theta - 2\dot{L}l \dot{\phi} \cos \alpha \sin \phi \sin \theta \\
 & + \dot{L}^2 \sin^2 \alpha + 0 + 0 + 2\dot{L}l \dot{\theta} \sin \alpha \sin \phi \cos \theta + 2\dot{L}l \dot{\phi} \sin \alpha \cos \phi \sin \theta + 0] \\
 & + 0
 \end{aligned}$$

$$\text{partial derivative of } \cos^2 \alpha = 2 \cos \alpha$$

$$\begin{aligned}
 \frac{\partial L}{\partial \alpha} = & m\dot{L}^2 \cos \alpha - m\dot{L}l \dot{\theta} \sin \alpha \cos \phi \cos \theta + m\dot{L}l \dot{\phi} \sin \alpha \sin \phi \sin \theta + m\dot{L}^2 \sin \alpha \\
 & + m\dot{L}l \dot{\theta} \cos \alpha \sin \phi \cos \theta + m\dot{L}l \dot{\phi} \cos \alpha \cos \phi \sin \theta \\
 \frac{\partial L}{\partial \dot{\alpha}} = & M_j L^2 \dot{\alpha} \\
 \frac{d}{dt} \left(\frac{\partial L}{\partial \dot{\alpha}} \right) = & M_j L^2 \ddot{\alpha}
 \end{aligned}$$

Eq.(3.12) can be obtained for Jib rotational motion: α ,

$$\frac{d}{dt} \left(\frac{\partial L}{\partial \dot{\alpha}} \right) - \frac{\partial L}{\partial \alpha} = T_{jib} - I\ddot{\alpha}$$

(T_{jib} is external driving Torque for Jib rotatioanl motion)

$$\begin{aligned}
 M_j L^2 \ddot{\alpha} - m\dot{L}^2 \cos \alpha + m\dot{L}l \dot{\theta} \sin \alpha \cos \phi \cos \theta - m\dot{L}l \dot{\phi} \sin \alpha \sin \phi \sin \theta - m\dot{L}^2 \sin \alpha - \\
 m\dot{L}l \dot{\theta} \cos \alpha \sin \phi \cos \theta - m\dot{L}l \dot{\phi} \cos \alpha \cos \phi \sin \theta = T_{jib} - I\ddot{\alpha} \quad (3.12)
 \end{aligned}$$

For Trolley translational motion: L

$$\begin{aligned}
 L_{lagrange} = & \frac{1}{2} M_j L^2 \dot{\alpha}^2 + \frac{1}{2} M_t \dot{L}^2 + \frac{1}{2} m [\dot{L}^2 \cos^2 \alpha + l^2 \dot{\theta}^2 \cos^2 \phi \cos^2 \theta + l^2 \dot{\phi}^2 \sin^2 \phi \sin^2 \theta \\
 & - 2l^2 \dot{\theta} \dot{\phi} \cos \phi \cos \theta \sin \phi \sin \theta + 2\dot{L}l \dot{\theta} \cos \alpha \cos \phi \cos \theta \\
 & - 2\dot{L}l \dot{\phi} \cos \alpha \sin \phi \sin \theta + \dot{L}^2 \sin^2 \alpha + l^2 \dot{\theta}^2 \sin^2 \phi \cos^2 \theta + l^2 \dot{\phi}^2 \cos^2 \phi \sin^2 \theta \\
 & + 2l^2 \dot{\theta} \dot{\phi} \sin \phi \cos \theta \cos \phi \sin \theta + 2\dot{L}l \dot{\theta} \sin \alpha \sin \phi \cos \theta \\
 & + 2\dot{L}l \dot{\phi} \sin \alpha \cos \phi \sin \theta + l^2 \dot{\theta}^2 \sin^2 \theta] + mgl \cos \theta
 \end{aligned}$$

$$\frac{\partial L_{lagrange}}{\partial L} = M_j L \dot{\alpha}^2$$

To make partial derivative of \dot{L} , considered

$$\begin{aligned}
 L_{lagrange} &= 0 + \frac{1}{2} M_t \dot{L}^2 + \frac{1}{2} m [\dot{L}^2 \cos^2 \alpha + 0 + 0 - 0 + 2\dot{L}l\dot{\theta} \cos \alpha \cos \phi \cos \theta \\
 &\quad - 2\dot{L}l\dot{\theta} \cos \alpha \sin \phi \sin \theta + \dot{L}^2 \sin^2 \alpha + 0 + 0 + 0 + 2\dot{L}l\dot{\theta} \sin \alpha \sin \phi \cos \theta \\
 &\quad + 2\dot{L}l\dot{\theta} \sin \alpha \cos \phi \sin \theta + 0] + 0 \\
 \frac{\partial L_{lagrange}}{\partial \dot{L}} &= M_t \dot{L} + \frac{1}{2} m [2\dot{L} \cos^2 \alpha + 2l\dot{\theta} \cos \alpha \cos \phi \cos \theta - 2l\dot{\theta} \cos \alpha \sin \phi \sin \theta + 2\dot{L} \sin^2 \alpha \\
 &\quad + 2l\dot{\theta} \sin \alpha \sin \phi \cos \theta + 2l\dot{\theta} \sin \alpha \cos \phi \sin \theta] \\
 \frac{\partial L_{lagrange}}{\partial \ddot{L}} &= M_t \ddot{L} + m \dot{L} \cos^2 \alpha + ml\dot{\theta} \cos \alpha \cos \phi \cos \theta - ml\dot{\theta} \cos \alpha \sin \phi \sin \theta + m \dot{L} \sin^2 \alpha \\
 &\quad + ml\dot{\theta} \sin \alpha \sin \phi \cos \theta + ml\dot{\theta} \sin \alpha \cos \phi \sin \theta \\
 \frac{d}{dt} \left(\frac{\partial L_{lagrange}}{\partial \dot{L}} \right) &= M_t \ddot{L} + m \ddot{L} \cos^2 \alpha + m \ddot{L} \sin^2 \alpha = M_t \ddot{L} + m \ddot{L} (\cos^2 \alpha + \sin^2 \alpha) = M_t \ddot{L} + m \ddot{L} \\
 &= (M_t + m) \ddot{L} \\
 \frac{d}{dt} \left(\frac{\partial L_{lagrange}}{\partial \dot{L}} \right) - \frac{\partial L_{lagrange}}{\partial L} &= F_t - b\dot{L} \quad (\text{external driving force for Trolley motion})
 \end{aligned}$$

$$\frac{d}{dt} \left(\frac{\partial L_{lagrange}}{\partial \dot{L}} \right) - \frac{\partial L_{lagrange}}{\partial L}$$

Eq.(3.13) can then be obtained For Trolley translational motion: L

$$(M_t + m) \ddot{L} - M_j L \dot{\alpha}^2 = F_t - b\dot{L} \quad (3.13)$$

For Load swing angle ϕ , General L equation is

$$\begin{aligned}
 L &= \frac{1}{2} M_j L^2 \dot{\alpha}^2 + \frac{1}{2} M_t \dot{L}^2 + \frac{1}{2} m [\dot{L}^2 \cos^2 \alpha + l^2 \dot{\theta}^2 \cos^2 \phi \cos^2 \theta + l^2 \dot{\phi}^2 \sin^2 \phi \sin^2 \theta \\
 &\quad - 2l^2 \dot{\theta} \dot{\phi} \cos \phi \cos \theta \sin \phi \sin \theta + 2\dot{L}l\dot{\theta} \cos \alpha \cos \phi \cos \theta \\
 &\quad - 2\dot{L}l\dot{\theta} \cos \alpha \sin \phi \sin \theta + \dot{L}^2 \sin^2 \alpha + l^2 \dot{\theta}^2 \sin^2 \phi \cos^2 \theta + l^2 \dot{\phi}^2 \cos^2 \phi \sin^2 \theta \\
 &\quad + 2l^2 \dot{\theta} \dot{\phi} \sin \phi \cos \theta \cos \phi \sin \theta + 2\dot{L}l\dot{\theta} \sin \alpha \sin \phi \cos \theta \\
 &\quad + 2\dot{L}l\dot{\theta} \sin \alpha \cos \phi \sin \theta + l^2 \dot{\theta}^2 \sin^2 \theta] + mgl \cos \theta
 \end{aligned}$$

$$\begin{aligned}
 L &= 0 + 0 + \frac{1}{2}m[0 + l^2\dot{\theta}^2 \cos^2 \phi \cos^2 \theta + l^2\dot{\phi}^2 \sin^2 \phi \sin^2 \theta - 2l^2\dot{\theta}\dot{\phi} \cos \phi \cos \theta \sin \phi \sin \theta \\
 &\quad + 2\dot{L}l\dot{\theta} \cos \alpha \cos \phi \cos \theta - 2\dot{L}l\dot{\phi} \cos \alpha \sin \phi \sin \theta + 0 + l^2\dot{\theta}^2 \sin^2 \phi \cos^2 \theta \\
 &\quad + l^2\dot{\phi}^2 \cos^2 \phi \sin^2 \theta + 2l^2\dot{\theta}\dot{\phi} \sin \phi \cos \theta \cos \phi \sin \theta + 2\dot{L}l\dot{\theta} \sin \alpha \sin \phi \cos \theta \\
 &\quad + 2\dot{L}l\dot{\phi} \sin \alpha \cos \phi \sin \theta + 0] + 0 \\
 L &= \frac{1}{2}m[l^2\dot{\theta}^2 \cos^2 \phi \cos^2 \theta + l^2\dot{\phi}^2 \sin^2 \phi \sin^2 \theta - 2l^2\dot{\theta}\dot{\phi} \cos \theta \sin \theta \cos \phi \sin \phi \\
 &\quad + 2\dot{L}l\dot{\theta} \cos \alpha \cos \phi \cos \theta - 2\dot{L}l\dot{\phi} \cos \alpha \sin \phi \sin \theta + l^2\dot{\theta}^2 \sin^2 \phi \cos^2 \theta \\
 &\quad + l^2\dot{\phi}^2 \cos^2 \phi \sin^2 \theta + 2l^2\dot{\theta}\dot{\phi} \cos \phi \sin \phi \cos \theta \sin \theta + 2\dot{L}l\dot{\theta} \sin \alpha \sin \phi \cos \theta \\
 &\quad + 2\dot{L}l\dot{\phi} \sin \alpha \cos \phi \sin \theta] \\
 \cos \phi \sin \phi &= \sin \frac{2\phi}{2} \\
 \text{partial derivative of } \sin \frac{2\phi}{2} &= \cos 2\phi \\
 \frac{\partial L}{\partial \phi} &= \frac{1}{2}m[2l^2\dot{\theta}^2 \cos \phi \cos^2 \theta + 2l^2\dot{\phi}^2 \sin \phi \sin^2 \theta - 2l^2\dot{\theta}\dot{\phi} \cos \theta \sin \theta \cos(2\phi) \\
 &\quad - 2\dot{L}l\dot{\theta} \cos \alpha \sin \phi \cos \theta - 2\dot{L}l\dot{\phi} \cos \alpha \cos \phi \sin \theta + 2l^2\dot{\theta}^2 \sin \phi \cos^2 \theta \\
 &\quad + 2l^2\dot{\phi}^2 \cos \phi \sin^2 \theta - 2l^2\dot{\theta}\dot{\phi} \cos \theta \sin \theta \cos(2\phi) + 2\dot{L}l\dot{\theta} \sin \alpha \cos \phi \cos \theta \\
 &\quad - 2\dot{L}l\dot{\phi} \sin \alpha \sin \phi \sin \theta] \\
 \frac{\partial L}{\partial \theta} &= ml^2\dot{\theta}^2 \cos \phi \cos^2 \theta + ml^2\dot{\phi}^2 \sin \phi \sin^2 \theta - ml^2\dot{\theta}\dot{\phi} \cos \theta \sin \theta \cos(2\phi) \\
 &\quad - m\dot{L}l\dot{\theta} \cos \alpha \sin \phi \cos \theta - m\dot{L}l\dot{\phi} \cos \alpha \cos \phi \sin \theta + ml^2\dot{\theta}^2 \sin \phi \cos^2 \theta \\
 &\quad + ml^2\dot{\phi}^2 \cos \phi \sin^2 \theta - ml^2\dot{\theta}\dot{\phi} \cos \theta \sin \theta \cos(2\phi) + m\dot{L}l\dot{\theta} \sin \alpha \cos \phi \cos \theta \\
 &\quad - m\dot{L}l\dot{\phi} \sin \alpha \sin \phi \sin \theta \\
 \text{for } \frac{\partial L}{\partial \dot{\phi}} &\Rightarrow \text{from original L} \\
 L &= \frac{1}{2}M_JL^2\dot{\alpha}^2 + \frac{1}{2}M_t\dot{L}^2 + \frac{1}{2}m[\dot{L}^2 \cos^2 \alpha + l^2\dot{\theta}^2 \cos^2 \phi \cos^2 \theta + l^2\dot{\phi}^2 \sin^2 \phi \sin^2 \theta \\
 &\quad - 2l^2\dot{\theta}\dot{\phi} \cos \phi \cos \theta \sin \phi \sin \theta + 2\dot{L}l\dot{\theta} \cos \alpha \cos \phi \cos \theta \\
 &\quad - 2\dot{L}l\dot{\phi} \cos \alpha \sin \phi \sin \theta + \dot{L}^2 \sin^2 \alpha + l^2\dot{\theta}^2 \sin^2 \phi \cos^2 \theta + l^2\dot{\phi}^2 \cos^2 \phi \sin^2 \theta \\
 &\quad + 2l^2\dot{\theta}\dot{\phi} \sin \phi \cos \theta \cos \phi \sin \theta + 2\dot{L}l\dot{\theta} \sin \alpha \sin \phi \cos \theta \\
 &\quad + 2\dot{L}l\dot{\phi} \sin \alpha \cos \phi \sin \theta + l^2\dot{\theta}^2 \sin^2 \theta] + mgl \cos \theta \\
 L &= 0 + 0 + \frac{1}{2}m[0 + 0 + l^2\dot{\phi}^2 \sin^2 \phi \sin^2 \theta - 2l^2\dot{\theta}\dot{\phi} \cos \phi \cos \theta \sin \phi \sin \theta + 0 \\
 &\quad - 2\dot{L}l\dot{\phi} \cos \alpha \sin \phi \sin \theta + 0 + 0 + l^2\dot{\phi}^2 \cos^2 \phi \sin^2 \theta \\
 &\quad + 2l^2\dot{\theta}\dot{\phi} \sin \phi \cos \theta \cos \phi \sin \theta + 0 + 2\dot{L}l\dot{\phi} \sin \alpha \cos \phi \sin \theta + 0] + 0
 \end{aligned}$$

$$\begin{aligned}
 \frac{\partial L}{\partial \dot{\phi}} &= \frac{1}{2} m [2l^2 \dot{\phi} \sin^2 \theta - 2l^2 \dot{\theta} \cos \theta \cos \theta \sin \theta \sin \theta - 2\dot{L}l \cos \alpha \sin \theta \sin \theta \\
 &\quad + 2l^2 \dot{\phi} \cos^2 \theta \sin^2 \theta + 2l^2 \dot{\theta} \sin \theta \cos \theta \cos \theta \sin \theta + 2\dot{L}l \sin \alpha \cos \theta \sin \theta] \\
 &= ml^2 \dot{\phi} \sin^2 \theta - ml^2 \dot{\theta} \cos \theta \cos \theta \sin \theta \sin \theta - m\dot{L}l \cos \alpha \sin \theta \sin \theta \\
 &\quad + ml^2 \dot{\phi} \cos^2 \theta \sin^2 \theta + ml^2 \dot{\theta} \sin \theta \cos \theta \cos \theta \sin \theta + m\dot{L}l \sin \alpha \cos \theta \sin \theta \\
 \frac{d}{dt} \left(\frac{\partial L}{\partial \dot{\phi}} \right) &= ml^2 \ddot{\phi} \sin^2 \theta + ml^2 \ddot{\theta} \cos^2 \theta \sin^2 \theta \\
 \frac{d}{dt} \left(\frac{\partial L}{\partial \dot{\phi}} \right) - \frac{\partial L}{\partial \phi} &= \\
 ml^2 \ddot{\phi} \sin^2 \theta + ml^2 \ddot{\theta} \cos^2 \theta - ml^2 \dot{\theta}^2 \cos \theta \cos^2 \theta - ml^2 \dot{\phi}^2 \sin \theta \sin^2 \theta + \\
 ml^2 \dot{\theta} \dot{\phi} \cos \theta \sin \theta \cos(2\theta) + m\dot{L}l \dot{\theta} \cos \alpha \sin \theta \cos \theta + m\dot{L}l \dot{\phi} \cos \alpha \cos \theta \sin \theta - \\
 ml^2 \dot{\theta}^2 \sin \theta \cos^2 \theta - ml^2 \dot{\phi}^2 \cos \theta \sin^2 \theta + ml^2 \dot{\theta} \dot{\phi} \cos \theta \sin \theta \cos(2\theta) - \\
 m\dot{L}l \dot{\theta} \sin \alpha \cos \theta \cos \theta + m\dot{L}l \dot{\phi} \sin \alpha \sin \theta \sin \theta &= I\ddot{\phi} \tag{3.14}
 \end{aligned}$$

For Load swing angle θ , General L equation is

$$\begin{aligned}
 L &= \frac{1}{2} M_j L^2 \dot{\alpha}^2 + \frac{1}{2} M_t \dot{L}^2 + \frac{1}{2} m [L^2 \cos^2 \alpha + l^2 \dot{\theta}^2 \cos^2 \theta \cos^2 \theta + l^2 \dot{\phi}^2 \sin^2 \theta \sin^2 \theta \\
 &\quad - 2l^2 \dot{\theta} \dot{\phi} \cos \theta \cos \theta \sin \theta \sin \theta + 2\dot{L}l \dot{\theta} \cos \alpha \cos \theta \cos \theta \\
 &\quad - 2\dot{L}l \dot{\phi} \cos \alpha \sin \theta \sin \theta + \dot{L}^2 \sin^2 \alpha + l^2 \dot{\theta}^2 \sin^2 \theta \cos^2 \theta + l^2 \dot{\phi}^2 \cos^2 \theta \sin^2 \theta \\
 &\quad + 2l^2 \dot{\theta} \dot{\phi} \sin \theta \cos \theta \cos \theta \sin \theta + 2\dot{L}l \dot{\theta} \sin \alpha \sin \theta \cos \theta \\
 &\quad + 2\dot{L}l \dot{\phi} \sin \alpha \cos \theta \sin \theta + l^2 \dot{\theta}^2 \sin^2 \theta] + mgl \cos \theta \\
 L &= 0 + 0 + \frac{1}{2} m [0 + l^2 \dot{\theta}^2 \cos^2 \theta \cos^2 \theta + l^2 \dot{\phi}^2 \sin^2 \theta \sin^2 \theta - 2l^2 \dot{\theta} \dot{\phi} \cos \theta \cos \theta \sin \theta \sin \theta \\
 &\quad + 2\dot{L}l \dot{\theta} \cos \alpha \cos \theta \cos \theta - 2\dot{L}l \dot{\phi} \cos \alpha \sin \theta \sin \theta + 0 + l^2 \dot{\theta}^2 \sin^2 \theta \cos^2 \theta \\
 &\quad + l^2 \dot{\phi}^2 \cos^2 \theta \sin^2 \theta + 2l^2 \dot{\theta} \dot{\phi} \sin \theta \cos \theta \cos \theta \sin \theta + 2\dot{L}l \dot{\theta} \sin \alpha \sin \theta \cos \theta \\
 &\quad + 2\dot{L}l \dot{\phi} \sin \alpha \cos \theta \sin \theta + l^2 \dot{\theta}^2 \sin^2 \theta] + mgl \cos \theta \\
 L &= \frac{1}{2} m [l^2 \dot{\theta}^2 \cos^2 \theta \cos^2 \theta + l^2 \dot{\phi}^2 \sin^2 \theta \sin^2 \theta - 2l^2 \dot{\theta} \dot{\phi} \cos \theta \cos \theta \sin \theta \sin \theta \\
 &\quad + 2\dot{L}l \dot{\theta} \cos \alpha \cos \theta \cos \theta - 2\dot{L}l \dot{\phi} \cos \alpha \sin \theta \sin \theta + l^2 \dot{\theta}^2 \sin^2 \theta \cos^2 \theta \\
 &\quad + l^2 \dot{\phi}^2 \cos^2 \theta \sin^2 \theta + 2l^2 \dot{\theta} \dot{\phi} \sin \theta \cos \theta \cos \theta \sin \theta + 2\dot{L}l \dot{\theta} \sin \alpha \sin \theta \cos \theta \\
 &\quad + 2\dot{L}l \dot{\phi} \sin \alpha \cos \theta \sin \theta + l^2 \dot{\theta}^2 \sin^2 \theta] + mgl \cos \theta \\
 \frac{\partial L}{\partial \theta} &= ml^2 \dot{\theta}^2 \cos^2 \theta \cos \theta + ml^2 \dot{\phi}^2 \sin^2 \theta \sin \theta - ml^2 \dot{\theta} \dot{\phi} \cos \theta \sin \theta \cos(2\theta) \\
 &\quad - m\dot{L}l \dot{\theta} \cos \alpha \cos \theta \sin \theta - m\dot{L}l \dot{\phi} \cos \alpha \sin \theta \cos \theta + ml^2 \dot{\theta}^2 \sin^2 \theta \cos \theta \\
 &\quad + ml^2 \dot{\phi}^2 \cos^2 \theta \sin \theta + ml^2 \dot{\theta} \dot{\phi} \cos \theta \sin \theta \cos(2\theta) - m\dot{L}l \dot{\theta} \sin \alpha \sin \theta \sin \theta \\
 &\quad + m\dot{L}l \dot{\phi} \sin \alpha \cos \theta \cos \theta + ml^2 \dot{\theta}^2 \sin^2 \theta - mgl \sin \theta
 \end{aligned}$$

for $\frac{\partial L}{\partial \dot{\theta}} \Rightarrow$ from original L

$$\begin{aligned}
 L &= \frac{1}{2} M_J L^2 \dot{\alpha}^2 + \frac{1}{2} M_t \dot{l}^2 + \frac{1}{2} m [\dot{L}^2 \cos^2 \alpha + l^2 \dot{\theta}^2 \cos^2 \phi \cos^2 \theta + l^2 \dot{\phi}^2 \sin^2 \phi \sin^2 \theta \\
 &\quad - 2l^2 \dot{\theta} \dot{\phi} \cos \phi \cos \theta \sin \phi \sin \theta + 2\dot{L}l \dot{\theta} \cos \alpha \cos \phi \cos \theta \\
 &\quad - 2\dot{L}l \dot{\phi} \cos \alpha \sin \phi \sin \theta + \dot{L}^2 \sin^2 \alpha + l^2 \dot{\theta}^2 \sin^2 \phi \cos^2 \theta + l^2 \dot{\phi}^2 \cos^2 \phi \sin^2 \theta \\
 &\quad + 2l^2 \dot{\theta} \dot{\phi} \sin \phi \cos \theta \cos \phi \sin \theta + 2\dot{L}l \dot{\theta} \sin \alpha \sin \phi \cos \theta \\
 &\quad + 2\dot{L}l \dot{\phi} \sin \alpha \cos \phi \sin \theta + l^2 \dot{\theta}^2 \sin^2 \theta] + mgl \cos \theta \\
 L &= 0 + 0 + \frac{1}{2} m [0 + l^2 \dot{\theta}^2 \cos^2 \phi \cos^2 \theta + 0 - 2l^2 \dot{\theta} \dot{\phi} \cos \phi \cos \theta \sin \phi \sin \theta \\
 &\quad + 2\dot{L}l \dot{\theta} \cos \alpha \cos \phi \cos \theta - 0 + 0 + l^2 \dot{\theta}^2 \sin^2 \phi \cos^2 \theta + 0 \\
 &\quad + 2l^2 \dot{\theta} \dot{\phi} \sin \phi \cos \theta \cos \phi \sin \theta + 2\dot{L}l \dot{\theta} \sin \alpha \sin \phi \cos \theta + 0 + l^2 \dot{\theta}^2 \sin^2 \theta] \\
 &\quad + 0 \\
 L &= \frac{1}{2} m [l^2 \dot{\theta}^2 \cos^2 \phi \cos^2 \theta - 2l^2 \dot{\theta} \dot{\phi} \cos \phi \cos \theta \sin \phi \sin \theta + 2\dot{L}l \dot{\theta} \cos \alpha \cos \phi \cos \theta \\
 &\quad + l^2 \dot{\theta}^2 \sin^2 \phi \cos^2 \theta + 2l^2 \dot{\theta} \dot{\phi} \sin \phi \cos \theta \cos \phi \sin \theta + 2\dot{L}l \dot{\theta} \sin \alpha \sin \phi \cos \theta \\
 &\quad + l^2 \dot{\theta}^2 \sin^2 \theta] \\
 \frac{\partial L}{\partial \dot{\theta}} &= \frac{1}{2} m [2l^2 \dot{\theta} \cos^2 \phi \cos^2 \theta - 2l^2 \dot{\phi} \cos \phi \cos \theta \sin \phi \sin \theta + 2\dot{L}l \cos \alpha \cos \phi \cos \theta \\
 &\quad + 2l^2 \dot{\theta} \sin^2 \phi \cos^2 \theta + 2l^2 \dot{\phi} \sin \phi \cos \theta \cos \phi \sin \theta + 2\dot{L}l \sin \alpha \sin \phi \cos \theta \\
 &\quad + 2l^2 \dot{\theta} \sin^2 \theta] \\
 \frac{\partial L}{\partial \dot{\theta}} &= ml^2 \dot{\theta} \cos^2 \phi \cos^2 \theta - ml^2 \dot{\phi} \cos \phi \cos \theta \sin \phi \sin \theta + m\dot{L}l \cos \alpha \cos \phi \cos \theta \\
 &\quad + ml^2 \dot{\theta} \sin^2 \phi \cos^2 \theta + ml^2 \dot{\phi} \sin \phi \cos \theta \cos \phi \sin \theta + m\dot{L}l \sin \alpha \sin \phi \cos \theta \\
 &\quad + m\dot{\theta} \sin^2 \theta \\
 \frac{d}{dt} \left(\frac{\partial L}{\partial \dot{\theta}} \right) &= ml^2 \ddot{\theta} \cos^2 \phi \cos^2 \theta + ml^2 \ddot{\phi} \sin^2 \phi \cos^2 \theta + m\ddot{\theta} \sin^2 \theta \\
 \frac{d}{dt} \left(\frac{\partial L}{\partial \dot{\theta}} \right) - \frac{\partial L}{\partial \theta} &= \\
 ml^2 \ddot{\theta} \cos^2 \phi \cos^2 \theta + ml^2 \ddot{\phi} \sin^2 \phi \cos^2 \theta + m\ddot{\theta} \sin^2 \theta - ml^2 \dot{\theta}^2 \cos^2 \phi \cos \theta - \\
 ml^2 \dot{\phi}^2 \sin^2 \phi \sin \theta + ml^2 \dot{\theta} \dot{\phi} \cos \phi \sin \phi \cos(2\theta) + m\dot{L}l \dot{\theta} \cos \alpha \cos \phi \sin \theta + \\
 m\dot{L}l \dot{\phi} \cos \alpha \sin \phi \cos \theta - ml^2 \dot{\theta}^2 \sin^2 \phi \cos \theta - ml^2 \dot{\phi}^2 \cos^2 \phi \sin \theta - \\
 ml^2 \dot{\theta} \dot{\phi} \cos \phi \sin \phi \cos(2\theta) + m\dot{L}l \dot{\theta} \sin \alpha \sin \phi \sin \theta - m\dot{L}l \dot{\phi} \sin \alpha \cos \phi \cos \theta - \\
 ml^2 \dot{\theta}^2 \sin \theta + mgl \sin \theta = I\ddot{\theta} \tag{3.15}
 \end{aligned}$$

3.1.8 Trolley-Payload Nonlinear Equations of motion

In order to gain a better understanding of trolley-payload dynamics and to derive the simulation model, the following nonlinear dynamics models are then obtained. Referring to the dynamic equations: Eq.(3.12), Eq.(3.13),Eq.(3.14), and Eq.(3.15), equations are then simplified as Eq.(3.16), Eq.(3.17),Eq.(3.18), and Eq.(3.19)

$$M_j L^2 \ddot{\alpha} - m \dot{L}^2 \cos \alpha + m \dot{L} l \dot{\theta} \sin \alpha \cos \phi \cos \theta - m \dot{L} l \dot{\phi} \sin \alpha \sin \phi \sin \theta - m \dot{L}^2 \sin \alpha - m \dot{L} l \dot{\theta} \cos \alpha \sin \phi \cos \theta - m \dot{L} l \dot{\phi} \cos \alpha \cos \phi \sin \theta = T_{jib} - I \ddot{\alpha} \quad (3.16)$$

$$(M_t + m) \ddot{L} - M_j L \dot{\alpha}^2 = F_t - b \dot{L} \quad (3.17)$$

$$\begin{aligned} ml^2 \ddot{\phi} \sin^2 \phi \sin^2 \theta + ml^2 \ddot{\phi} \cos^2 \phi \sin^2 \theta - ml^2 \dot{\theta}^2 \cos \phi \cos^2 \theta - ml^2 \dot{\phi}^2 \sin \phi \sin^2 \theta + \\ ml^2 \dot{\theta} \dot{\phi} \cos \theta \sin \theta \cos(2\phi) + m \dot{L} l \dot{\theta} \cos \alpha \sin \phi \cos \theta + m \dot{L} l \dot{\phi} \cos \alpha \cos \phi \sin \theta - \\ ml^2 \dot{\theta}^2 \sin \phi \cos^2 \theta - ml^2 \dot{\phi}^2 \cos \phi \sin^2 \theta + ml^2 \dot{\theta} \dot{\phi} \cos \theta \sin \theta \cos(2\phi) - \\ m \dot{L} l \dot{\theta} \sin \alpha \cos \phi \cos \theta + m \dot{L} l \dot{\phi} \sin \alpha \sin \phi \sin \theta = I \ddot{\phi} \end{aligned} \quad (3.18)$$

$$\begin{aligned} ml^2 \ddot{\theta} \cos^2 \phi \cos^2 \theta + ml^2 \ddot{\theta} \sin^2 \phi \cos^2 \theta + m \ddot{\theta} \sin^2 \theta - ml^2 \dot{\theta}^2 \cos^2 \phi \cos \theta - \\ ml^2 \dot{\theta}^2 \sin^2 \phi \sin \theta + ml^2 \dot{\theta} \dot{\phi} \cos \phi \sin \phi \cos(2\theta) + m \dot{L} l \dot{\theta} \cos \alpha \cos \phi \sin \theta + \\ m \dot{L} l \dot{\phi} \cos \alpha \sin \phi \cos \theta - ml^2 \dot{\theta}^2 \sin^2 \phi \cos \theta - ml^2 \dot{\phi}^2 \cos^2 \phi \sin \theta - \\ ml^2 \dot{\theta} \dot{\phi} \cos \phi \sin \phi \cos(2\theta) + m \dot{L} l \dot{\theta} \sin \alpha \sin \phi \sin \theta - m \dot{L} l \dot{\phi} \sin \alpha \cos \phi \cos \theta - \\ ml^2 \dot{\theta}^2 \sin \theta + mg l \sin \theta = I \ddot{\theta} \end{aligned} \quad (3.19)$$

Rewriting the Eq. (3.16) for Jib rotational motion: α

$$\begin{aligned} \ddot{\alpha} = \frac{1}{(M_j L^2 + I)} [T_{jib} + m \dot{L}^2 \cos \alpha - m \dot{L} l \dot{\theta} \sin \alpha \cos \phi \cos \theta + m \dot{L} l \dot{\phi} \sin \alpha \sin \phi \sin \theta + \\ + m \dot{L}^2 \sin \alpha + m \dot{L} l \dot{\theta} \cos \alpha \sin \phi \cos \theta + \\ + m \dot{L} l \dot{\phi} \cos \alpha \cos \phi \sin \theta] \end{aligned}$$

Rewriting the Eq. (3.17) for Trolley translational motion: L

$$\ddot{L} = \frac{1}{(M_t + m)} [F_t + M_j L \dot{\alpha}^2 - b \dot{L}]$$

Rewriting the Eq. (3.18) for Load swing angle ϕ ,

$$\begin{aligned} \ddot{\phi} = \frac{1}{(ml^2 \sin^2 \phi \sin^2 \theta + ml^2 \cos^2 \phi \sin^2 \theta - I)} [ml^2 \dot{\theta}^2 \cos \phi \cos^2 \theta + ml^2 \dot{\phi}^2 \sin \phi \sin^2 \theta - \\ ml^2 \theta \dot{\phi} \cos \phi \sin \theta \cos 2\theta - m \dot{L} l \dot{\theta} \cos \alpha \sin \phi \cos \theta - m \dot{L} l \dot{\phi} \cos \alpha \cos \phi \sin \theta + ml^2 \theta^2 \sin \phi \cos 2\theta + \\ + ml^2 \theta^2 \cos \phi \sin 2\theta - ml^2 \theta \dot{\phi} \cos \theta \sin \phi \cos 2\theta + m \dot{L} l \dot{\theta} \sin \alpha \cos \phi \cos \theta - m \dot{L} l \dot{\phi} \sin \alpha \sin \phi \sin \theta] \end{aligned}$$

Rewriting the Eq. (3.19) for Load swing angle θ ,

$$\ddot{\theta} = \frac{1}{(ml^2 \cos^2 \phi \cos^2 \theta + ml^2 \sin^2 \phi \cos^2 \theta + m \sin^2 \theta - I)} [ml^2 \dot{\theta}^2 \cos^2 \phi \cos \theta + ml^2 \dot{\phi}^2 \sin^2 \phi \sin \theta - ml^2 \dot{\theta} \dot{\phi} \cos \phi \sin \phi \cos(2\theta) - m \dot{L} l \dot{\theta} \cos \alpha \cos \phi \sin \theta - m \dot{L} l \dot{\phi} \cos \alpha \sin \phi \cos \theta + ml^2 \dot{\theta}^2 \sin^2 \phi \cos \theta + ml^2 \dot{\phi}^2 \cos^2 \phi \sin \theta + ml^2 \dot{\theta} \dot{\phi} \cos \phi \sin \phi \cos(2\theta) - m \dot{L} l \dot{\theta} \sin \alpha \sin \phi \sin \theta + m \dot{L} l \dot{\phi} \sin \alpha \cos \phi \cos \theta + ml^2 \dot{\theta}^2 \sin \theta - mgl \sin \theta]$$

3.1.9 3D Model Simplification using parameters assumption

In the case of the system at an equilibrium point, load swing angles (θ, ϕ, α) and their velocities ($\dot{\theta}, \dot{\phi}, \dot{\alpha}$) can be assumed as small. Therefore, $\sin \theta \approx \theta, \sin \alpha \approx \alpha, \sin \phi \approx \phi, \cos \theta \approx \cos \alpha \approx \cos \phi \approx 1, \dot{\theta} \theta \approx 0, \dot{L} L \approx 0, \dot{\alpha} \alpha \approx 0$, and $\dot{\phi} \phi \approx 0$ are assumed. Using these approximations, simplified equations of motions Eq.(3.20), Eq.(3.21), Eq.(3.22), and Eq.(3.23) are then obtained as follow.

$$\ddot{\alpha} = \frac{1}{(M_j L^2 + I)} [T_{jib} + m \dot{L}^2 - m \dot{L} l \dot{\theta} \alpha + 0 + m \dot{L}^2 \alpha + m \dot{L} l \dot{\theta} \phi + m \dot{L} l \dot{\phi} \theta] \quad (3.20)$$

$$\ddot{L} = \frac{1}{(M_t + m)} [F_t + M_j L \dot{\alpha}^2 - b \dot{L}] \quad (3.21)$$

$$\begin{aligned} \ddot{\phi} &= \frac{1}{(ml^2 \theta^2 \phi^2 + ml^2 \theta^2 - I)} [ml^2 \dot{\theta}^2 + ml^2 \dot{\phi}^2 \phi \theta^2 - ml^2 \dot{\theta} \dot{\phi} \theta - m \dot{L} l \dot{\theta} \phi - m \dot{L} l \dot{\phi} \theta + ml^2 \dot{\theta}^2 \phi + \\ &\quad ml^2 \theta^2 \phi^2 - ml^2 \theta \phi \theta + m \dot{L} l \theta \alpha \phi - m \dot{L} l \phi \alpha \phi \theta \\ \ddot{\theta} &= \frac{1}{(ml^2 \theta^2 \phi^2 + ml^2 \theta^2 - I)} [ml^2 \dot{\theta}^2 + 0 - 0 - m \dot{L} l \dot{\theta} \phi - m \dot{L} l \dot{\phi} \theta + ml^2 \dot{\theta}^2 \phi + ml^2 \dot{\phi}^2 \theta^2 - 0 + \\ &\quad m \dot{L} l \theta \alpha - 0] \end{aligned} \quad (3.22)$$

$$\begin{aligned} \ddot{\theta} &= \frac{1}{(ml^2 + ml^2 \phi^2 + m \theta^2 - I)} [ml^2 \dot{\theta}^2 + ml^2 \dot{\phi}^2 \phi^2 \theta - ml^2 \dot{\theta} \dot{\phi} \phi - m \dot{L} l \dot{\theta} \theta - m \dot{L} l \dot{\phi} \phi + ml^2 \dot{\theta}^2 \phi^2 + \\ &\quad ml^2 \dot{\phi}^2 \theta + ml^2 \dot{\theta} \dot{\phi} \phi - m \dot{L} l \dot{\theta} \alpha \phi \theta + m \dot{L} l \dot{\phi} \alpha + ml^2 \dot{\theta}^2 \theta - mgl \theta] \end{aligned} \quad (3.23)$$

3.2 SimMechanics-Visualized Crane model Development

Currently, most of the researches on different types of cranes are based on mathematical assumed Modelling and simulations. Since the proposed controllers were designed based on those above- mentioned factors, it would only provide surface idea about how the crane load swing is produced and controller responds. Besides, most variables have been assumed mathematically while avoiding some important factors such as: load length change, frictions, disturbances on actuators and sensors, etc. Those proposed controllers appear to be impractical in real time operations.

Therefore, most of current crane operators still use manual joy stick in dealing with very tedious crane operations work. The major platform of this research is, model visualization of the crane system has been developed based on real crane parts, which includes trolley cart, rail jib, steel cable, actual load, sensors and actuators, actual mass-moment of inertia-densities calculations, and 2D and 3D operations. Therefore, the simulation of this visualization would provide real time load swing response as well as other factors which affect crane operation and based on that, the most reliable controller would be proposed in order to let the controller do the job while reducing further burdens on crane operators. The following sections provide further details of real crane model design, simulation, and analyses.

3.2.1 2D Overhead Crane Design

This SimMechanics-based experimental model is based on Physical Modelling blocks which represent physical components, geometric, and kinematic relationships directly. This is not only more intuitive, it also saves the time and effort to derive the equations of motion. In this research, simple 2D Overhead crane mechanical model is designed using MATLAB SimMechanics visualization [57]-[58]-[59]. First of all, 5 meter long jib bar frame was mounted above the ground using two fixed revolute joints. Trolley cart with certain measurement has been mounted on top of jib fram. At this stage, low friction prismatic joint is considered in order to minimize constraints. A steel cable type body with payload was attached to the trolley using revolute joint. Certain measurements were assigned to appear 2D crane model as shown in Fig. 3.5. Signal builder produces applied force (step input signal) which actuates the trolley cart, Fig (2), for X-directional motion.

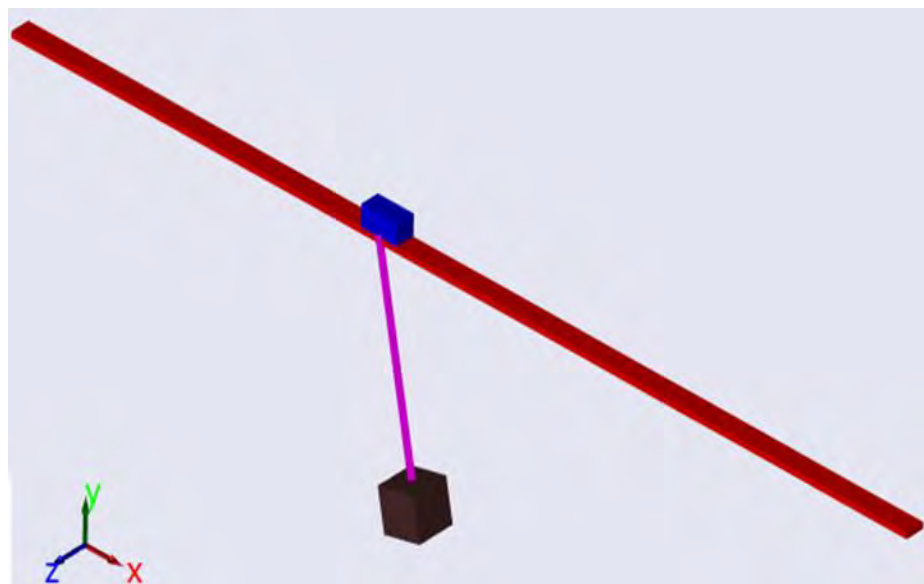


Figure 3.5 2D SimMechanics Visualized Overhead

3.2.2 Mass and Moment of Inertia tensor calculation

In order to get the correct virtual response of the simulation, moment of inertia tensors for each body part were calculated and assigned in the matrix form. Assumptions have been used to represent scaled-model crane structure at this stage, it can further be transformed into any other large crane model structure later.

Trolley Cart

Trolley cart is considered as a rectangular form below Fig. 3.6 and then suitable moment of inertia tensors were calculated based on its dimensions. By assuming Mass: $m= 2 \text{ Kg}$, Width: $w=0.2 \text{ m}$, Height: $h=0.1 \text{ m}$, and Depth: $d=0.1 \text{ m}$.

Therefore, Moment of Inertia tensor:

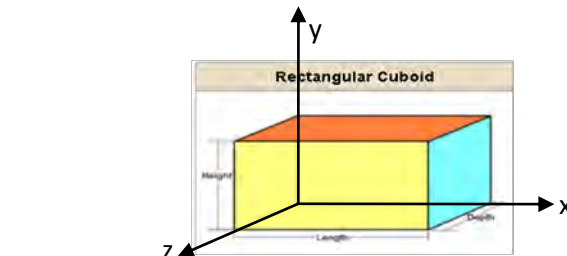


Figure 3.6 Measurements and Moment of Inertia for Rectangle

$$I_w = \frac{1}{12}m(h^2 + d^2), I_h = \frac{1}{12}m(w^2 + d^2), I_d = \frac{1}{12}m(h^2 + w^2), \\ (x, y, z) = (w, h, d)$$

$$I_w = \frac{1}{12}m(h^2 + d^2) = \frac{1}{12} \times 2 (0.1^2 + 0.1^2) = 0.00333 \text{ Kgm}^2$$

$$I_h = \frac{1}{12}m(w^2 + d^2) = \frac{1}{12} \times 2 (0.2^2 + 0.1^2) = 0.00833 \text{ Kgm}^2$$

$$I_d = \frac{1}{12}m(h^2 + w^2) = \frac{1}{12} \times 2 (0.1^2 + 0.2^2) = 0.00833 \text{ Kgm}^2$$

The inertia tensor of the trolley,

$$\begin{bmatrix} I_{ww} & 0 & 0 \\ 0 & I_{hh} & 0 \\ 0 & 0 & I_{dd} \end{bmatrix} = \begin{bmatrix} 0.00333 & 0 & 0 \\ 0 & 0.00833 & 0 \\ 0 & 0 & 0.00833 \end{bmatrix}$$

Jib (Rail)

The calculation of moment of inertia for the jib, Fig. 3.7 is similar to the trolley cart but the following parameters were assumed first: $m= 2 \text{ Kg}$, Width: $w=5 \text{ m}$, Height: $h=0.03 \text{ m}$, Depth: $d=0.1 \text{ m}$. Therefore, Moment of Inertia tensor:

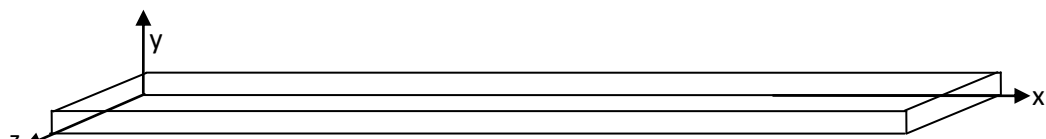


Figure 3.7 Measurement and Moment of Inertia for Rectangle form Jib

$$I_{ww} = \frac{1}{12}m(h^2 + d^2), I_{hh} = \frac{1}{12}m(w^2 + d^2), I_{dd} = \frac{1}{12}m(h^2 + w^2), (x, y, z) = (w, h, d)$$

The inertia tensor of the trolley,

$$\begin{bmatrix} I_{ww} & 0 & 0 \\ 0 & I_{hh} & 0 \\ 0 & 0 & I_{dd} \end{bmatrix} = \begin{bmatrix} 0.00182 & 0 & 0 \\ 0 & 4.1683 & 0 \\ 0 & 0 & 4.1668 \end{bmatrix}$$

Steel cable

Inflexible steel cable to attach the payload is assumed to be of cylindrical form Fig. 3.8 and based on the structure moment of inertia tensors were calculated. The following section shows the detail of those calculations. By assuming Length: L=h=1 m, Diameter: d=0.25 cm, Radius: r=0.125 cm, and Density: $\rho = 7.93 \text{ gm/cc}$. Therefore, Cylinder type:

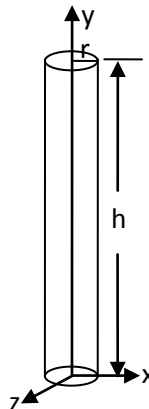


Figure 3.8 Measurements and Moment of Inertia for Cylindrical shape steel cable

$$\text{Mass } m = \rho\pi r^2 L = 7.93 \frac{\text{gm}}{\text{cm}^3} \times \pi \times (0.125)^2 \text{cm}^2 \times 100 \text{ cm} = 0.03891 \text{ kg}$$

$$\text{Radius: } r = 0.125 \text{ cm} = 0.125 * 10^{-2} \text{ m},$$

$$r^2 = (0.125)^2 * 10^{-4} \text{ m}^2 = 0.015625 * 10^{-4} \text{ m}^2$$

$$I_{xx} = I_{yy} = \frac{m(3r^2 + h^2)}{12} = \frac{0.03891 * (3 * 0.015625 * 10^{-4} + 1^2)}{12} = 0.0032425 \text{ kgm}^2$$

$$I_{zz} = \frac{mr^2}{2} = \frac{0.03891 * 0.015625 * 10^{-4}}{2} = 0.3e - 7$$

The inertia tensor of the steel cable

$$\begin{bmatrix} I_{xx} & 0 & 0 \\ 0 & I_{yy} & 0 \\ 0 & 0 & I_{zz} \end{bmatrix} = \begin{bmatrix} 0.0032425 & 0 & 0 \\ 0 & 0.0032425 & 0 \\ 0 & 0 & 0.3e - 7 \end{bmatrix}$$

Payload (rectangular container)

Payload container box is considered as a rectangular form and then suitable moment of inertia tensors were calculated based on its dimensions. By assuming Mass: m=0.75 Kg, Width: w=0.2 m, Height: h=0.2 m, Depth: d=0.2 m.

Therefore, Moment of Inertia tensor:

$$I_w = \frac{1}{12}m(h^2 + d^2), I_h = \frac{1}{12}m(w^2 + d^2), I_d = \frac{1}{12}m(h^2 + w^2),$$

$$I_w = \frac{1}{12}m(h^2 + d^2) = \frac{1}{12} \times 0.75(0.2^2 + 0.2^2) = 0.005 \text{ Kgm}^2$$

$$I_h = \frac{1}{12}m(w^2 + d^2) = \frac{1}{12} \times 0.75 (0.2^2 + 0.2^2) = 0.005 \text{ Kgm}^2$$

$$I_d = \frac{1}{12}m(h^2 + w^2) = \frac{1}{12} \times 0.75 (0.2^2 + 0.2^2) = 0.005 \text{ Kgm}^2$$

$$\text{The inertia tensor of the payload, } \begin{bmatrix} I_{ww} & 0 & 0 \\ 0 & I_{hh} & 0 \\ 0 & 0 & I_{dd} \end{bmatrix} = \begin{bmatrix} 0.005 & 0 & 0 \\ 0 & 0.005 & 0 \\ 0 & 0 & 0.005 \end{bmatrix}$$

3.2.3 Actuators, sensors and connectors used in the model

Body actuator which uses step input signal (Force) drives trolley cart mounted on the jib (rail object). Simple prismatic joint is connected between trolley and jib rail to move forward/backward along the jib. Both ends of the Jib rail are fixed at certain point above the ground level. So that, jib rail can be adjusted to move Z direction later on. Another revolute joint is connected to the trolley cart followed by the body (steel cable). Then, the payload is attached on the other end of the body (steel cable). Two sensors are attached in this model: one for payload swing angle detection and another for payload position trajectory. Since this SimMechanics MATLAB model represents actual body parts, each part calculated data (mass, moment of inertia, and so on) has to be correctly assigned.

3.2.4 The SimMechanics visualization of the crane model

The simple 2D crane as shown in Fig. 3.9 becomes feasible after assigning parameters in each part of the crane and assembling them correctly. In order to observe the system performance, several simulations using different applied forces, load and load length changes have been conducted. The detail simulation process would be discussed in next section.

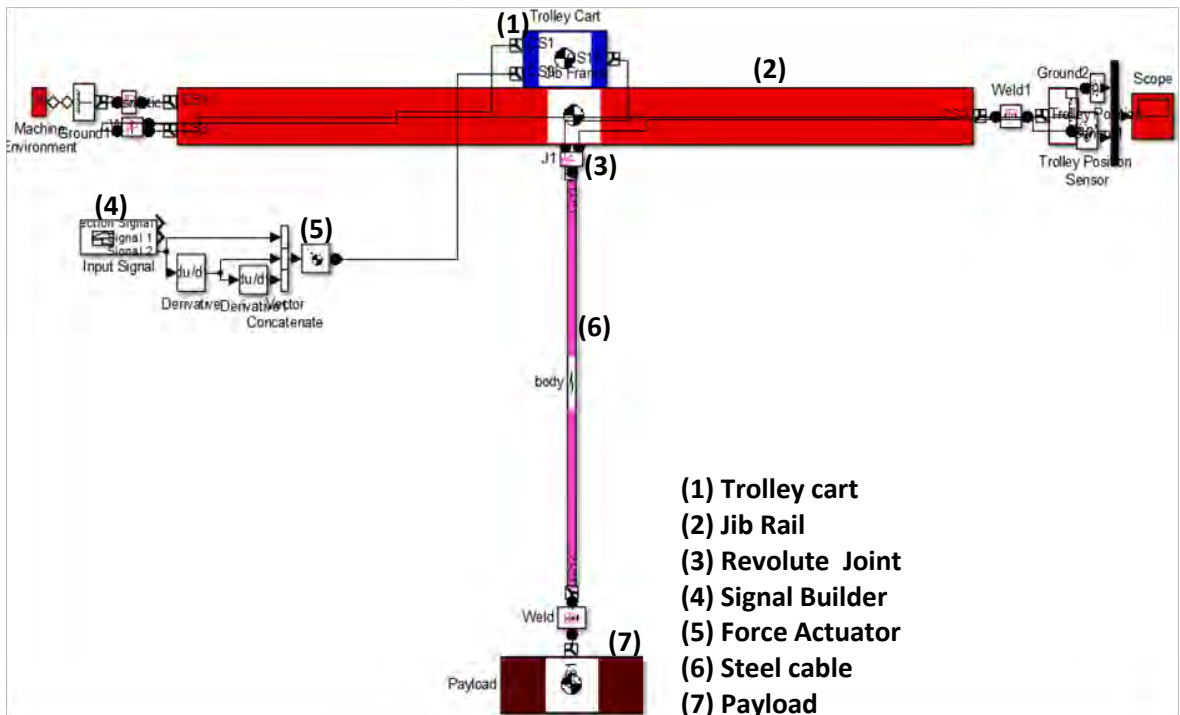


Figure 3.9 SimMechanics model visualization of the crane system with payload

3.2.5 Force Input Signal

For x, y, and z motions, the system uses 3-different motors and therefore, pseudo-random binary inputs have been used to simulation the system. Initially, other higher frequencies between (20 Hz to 100 Hz) were tested however each simulation does not have enough time to respond to changes in the input. In results, the response produced averaging effect. Using the specially designed pseudo-random inputs with sampling frequency 10-Hz as shown in Fig. 3.10, the load output movement in the X direction was obtained for the trolley translational motion. By varying the input signal and adjust longer pulse, it will enhance the statistics of the data, optimize the effectiveness of system identification as well as have visual respond to each input state.

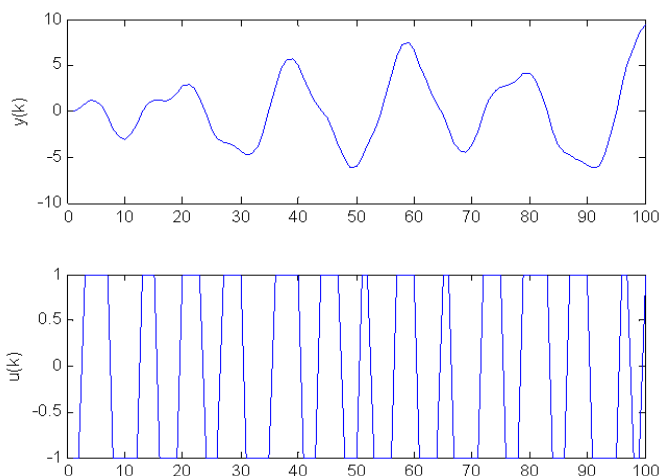


Figure 3.10 Pseudo-Random Input Signal at Frequency 10, range -1 to 1

3.2.6 Simulation of Trolley Cart forward/Reverse motion in X-direction

Though people usually develop mathematical model from sketch or lab scale prototype, this 2D Trolley-Payload model using SimMechanics visualization platform provides flexibility. It is easy to change measurements, design, parameters according to real crane, and most of all to visualize system motion. Using this random force signal actuation of (-2N to 2 N), trolley translation and payload swing motion has been obtained, driving trolley back-and-forth between (0 to 2.5 m) while payload swing angle (-10 to 15) degree in Fig. 3.11. Changing the force actuation pattern would create different working profiles. To achieve reference trajectory tracking for both trolley and loadswing, further suitable controllers can be designed.

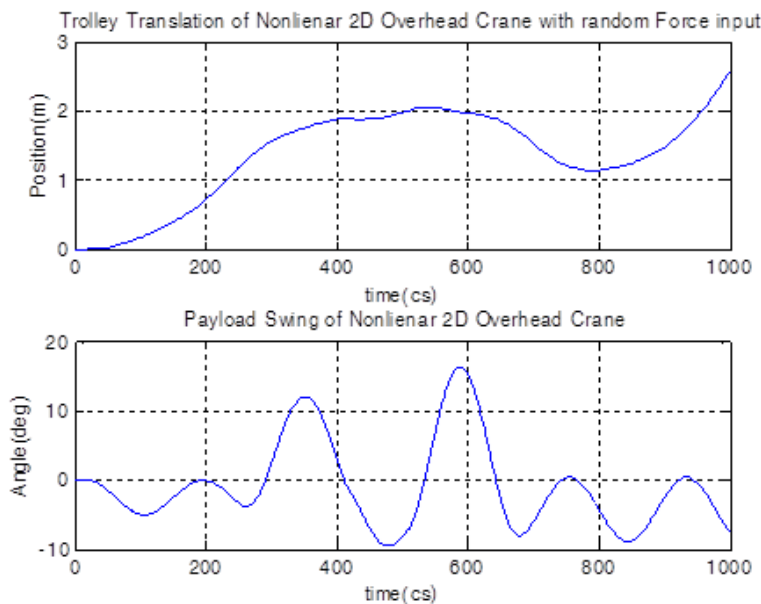


Figure 3.11 2D Overhead Crane Model excitation and Trolley-Payload

As this research aims to develop reliable 3D crane model later, creating 2D and 3D different crane models have been necessary. After 2D trolley-payload system has been established, the next step is to continue to 3D crane design. This time, it is aimed to develop 3D Overhead gantry crane used in shipyard and industries.

3.2.7 3D Overhead Crane Design

In this 3D visualization, trolley cart, jib rail, steel cable, payload, actuators and sensors from previous 2D design have been reapplied. But additionally, Gantry crane base frame was designed in order to mount jib rail and trolley cart on top to appear as a 3D feature. In this session, detail design, spherical joint connector consideration, input signal, simulation and analysis of gantry crane operations are discussed.

Detail Design of 3D gantry crane

First of all, 5 m Width, 2.825 m Height, and 7 m Depth gantry body was built by using grounded links and welded joints of Matlab SimMechanics structure. Then, previous trolley cart with jib rail attached was mounted on the crane frame. Therefore, the whole appearance not only like a real crane but also each item represents an actual crane body part. Since it is the 3D structure, trolley cart has two connected joints, prismatic joint is between trolley and jib rail while another gimbal joint is between trolley and the steel cable. So that, the payload can be able to swing in all three X-Y-Z directions while trolley moves. Jib rail is also mounted on top of the crane frame using two prismatic joints. The following figure Fig. 3.12 shows the complete 3D structure of gantry crane.

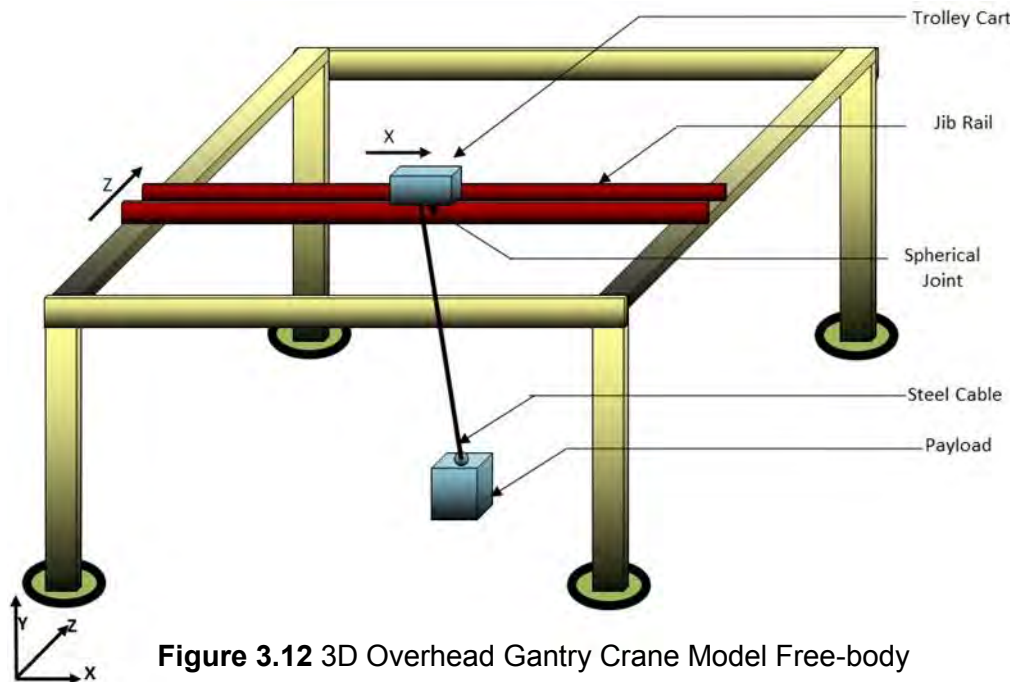


Figure 3.12 3D Overhead Gantry Crane Model Free-body Diagram

Spherical joint connector

Payload In 3D working space, trolley will move along X-Z axes while payload will swing in all X-Y-Z directions. Therefore, the system needs spherical joint connection in the reaction joint between trolley and steel cable which carries payload. The Spherical block represents in Fig. 3.13a three rotational degrees of freedom (DoFs) at a single pivot point, a "ball-in-socket" joint as shown in Fig. 3.13b. Two rotational DoFs specify a directional axis, and a third rotational DoF specifies rotation about that directional axis. Sensor measurement provides, a quaternion form, which mathematically represents a three-dimensional spherical rotation as a four-component row vector of unit length. Three rotational angles are derived from the quaternion form

in simulink. The following diagrams show the details of each angle measurement in 3D motion. The detailed calculation of each rotational angle is shown below.

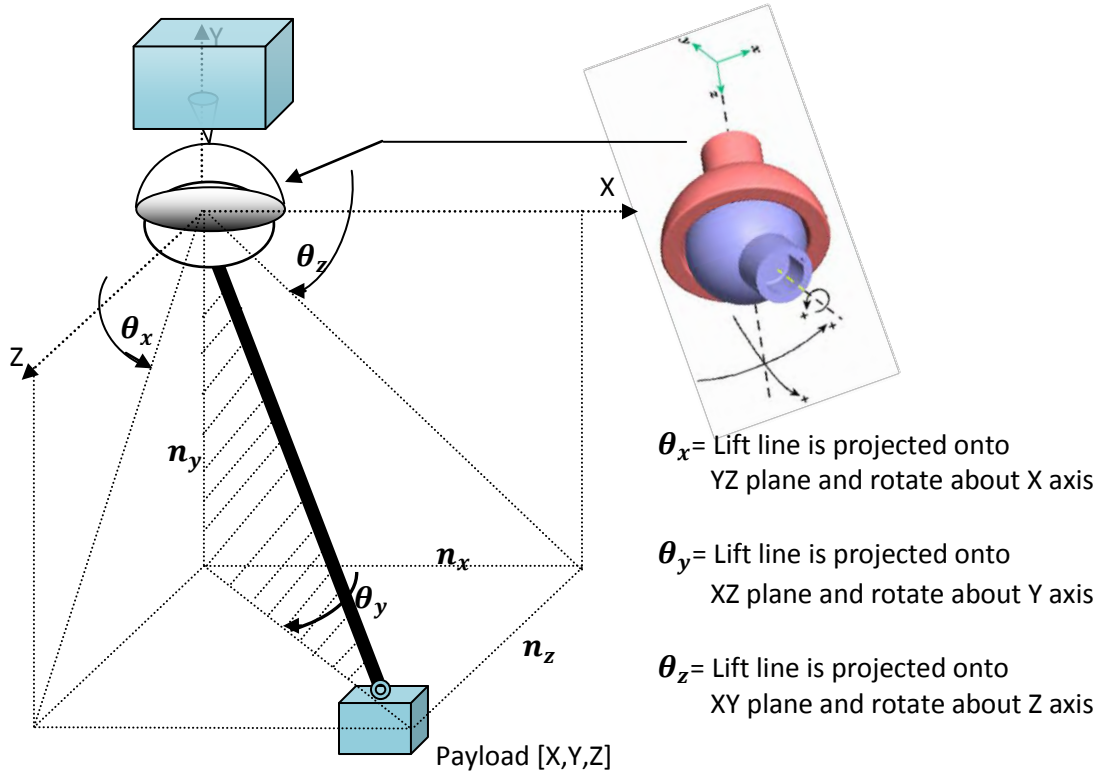


Figure 3.13a Spherical joint used between trolley and steel cable

Figure 3.13b Spherical joint and its specifications

The Spherical Joint allows three rotational degrees of freedom. The follower (steel cable-payload) and base (trolley) origins always coincide. The follower frame can rotate freely in three dimensions around the pivot of this common origin. The joint direction is defined by rotation of the follower frame relative to the base frame.

State of Motion and Degrees of Freedom

The Spherical Joint has one spherical primitive and adds three rotational components to the mechanical state of the model shown below in Fig. 3.14. The spherical degrees of freedom are represented by a quaternion, which is equivalent to an axis-angle rotation. Start with the axis-angle rotation $[n_x, n_y, n_z, \theta_x, \theta_y, \theta_z]$: unit vector axis n first, then (signed) right-handed rotation angle θ around that axis. $n = (n_x, n_y, n_z)$ satisfies $.n = n_x^2 + n_y^2 + n_z^2 = 1$. The axis-angle rotation has three independent components, and four components in total.

$$n_x = n \sin \left(\frac{\theta_z}{2} \right) \hat{k}, n_y = n \sin \left(\frac{\theta_x}{2} \right) \hat{i}, n_z = n \sin \left(\frac{\theta_y}{2} \right) \hat{j}$$

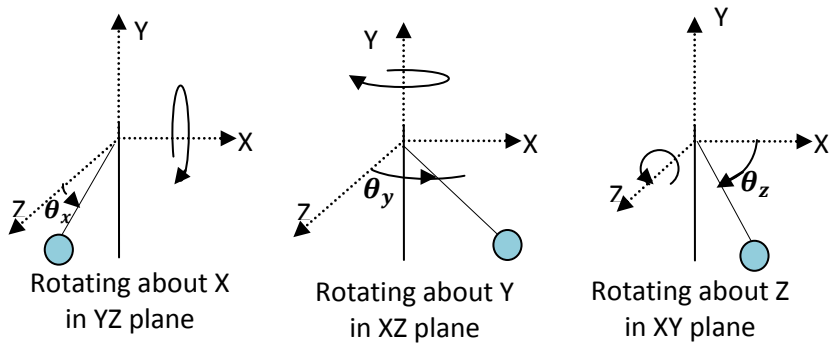


Figure 3.14 Spherical joint sensor outputs in 3D load swing angles

A spherical primitive is more complex than a revolute primitive as it has three rotational degrees of freedom instead of just one. The equivalent quaternion Q represents a three-dimensional rotation as a four-component row vector of unit length: $q = [n_x, n_y, n_z \text{ with } 3 \text{ independent rotational angles } (\theta_x, \theta_y, \theta_z)]$. From 3-rotational quaternion outputs, actual angles can then be computed as follow, that is actual sensor output would need to be multiplied by $(2 * 180/\pi)$ in order to get real output.

$$q = [n \sin\left(\frac{\theta_x}{2}\right) \hat{i}, \quad n \sin\left(\frac{\theta_y}{2}\right) \hat{j}, \quad n \sin\left(\frac{\theta_z}{2}\right) \hat{k}]$$

$$\left(\frac{\theta_x}{2}\right) = A \text{ rad} \quad (\text{Joint sensor output}), \text{So} \Rightarrow \theta_x = 2 * (A \text{ rad} * \frac{180^\circ}{\pi})$$

$$\left(\frac{\theta_y}{2}\right) = B \text{ rad} \quad (\text{Joint sensor output}), \text{So} \Rightarrow \theta_y = 2 * (B \text{ rad} * \frac{180^\circ}{\pi})$$

$$\left(\frac{\theta_z}{2}\right) = C \text{ rad} \quad (\text{Joint sensor output}), \text{So} \Rightarrow \theta_z = 2 * (C \text{ rad} * \frac{180^\circ}{\pi})$$

Force Input Signal

The two body actuators used for trolley cart and jib rail motion needs two separate applied forces and therefore, the following input signal Fig. 3.15 is designed. For simulation purpose, applied forces (2N to -2 N) are assigned to run in both X and Z directions. Different types of applied forces would be given in future for further simulations.

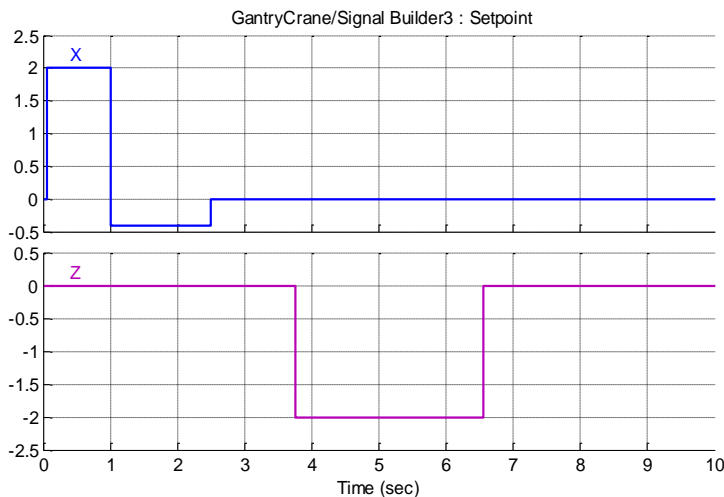


Figure 3.15 Force Signals for Trolley-Jib X-Y Run

3.2.8 SimMechanics visualization of Overhead Gantry Crane

The detail crane structure including trolley cart, steel cable, base frame, payload, sensors and actuators, and joints were discussed above. The figure Fig. 3.16 below uses spherical joint connection between trolley and steel cable with payload in order to view each rotational angle/axis representation.

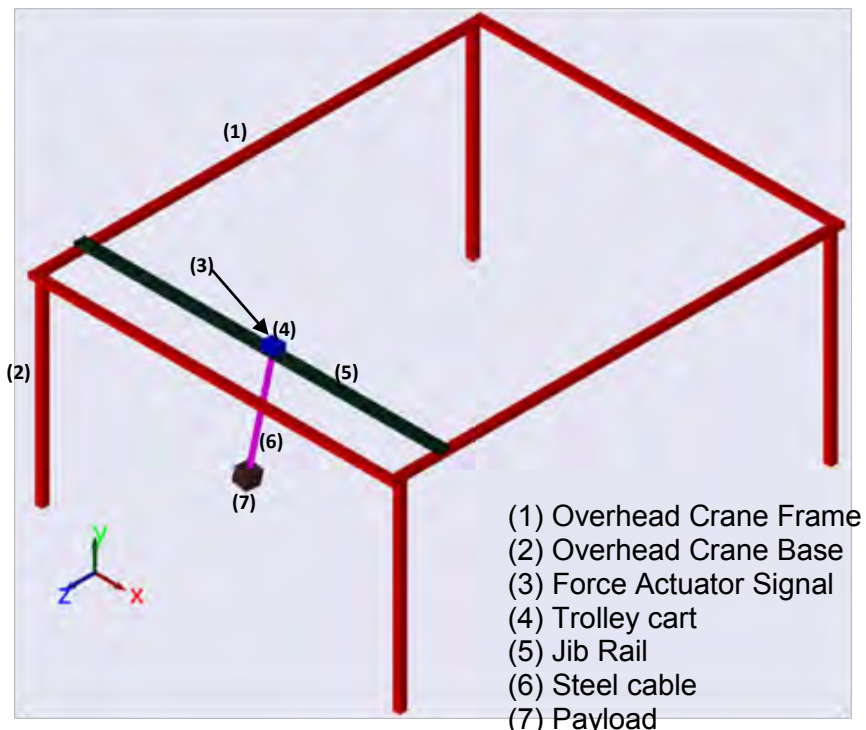


Figure 3.16 3D Overhead Crane Visualized Model

In this SimMechanics system below Fig. 3.17, the same parameters from previous simulations have been applied such as: force= 2N, steel cable = 1.5 m, and both trolley cart and payload values are unchanged. Previous 2D crane is mounted on top of overhead frame. Assume that, the height of frame legs are 2.75 m and frame

length is 5 m. Consider a pendulum of mass m and length ℓ , which is attached to a support with Trolley mass M which can move along a Jib line in the x -direction. Let x be the coordinate along the line of the support, and let us denote the position of the pendulum by the angle θ from the vertical.

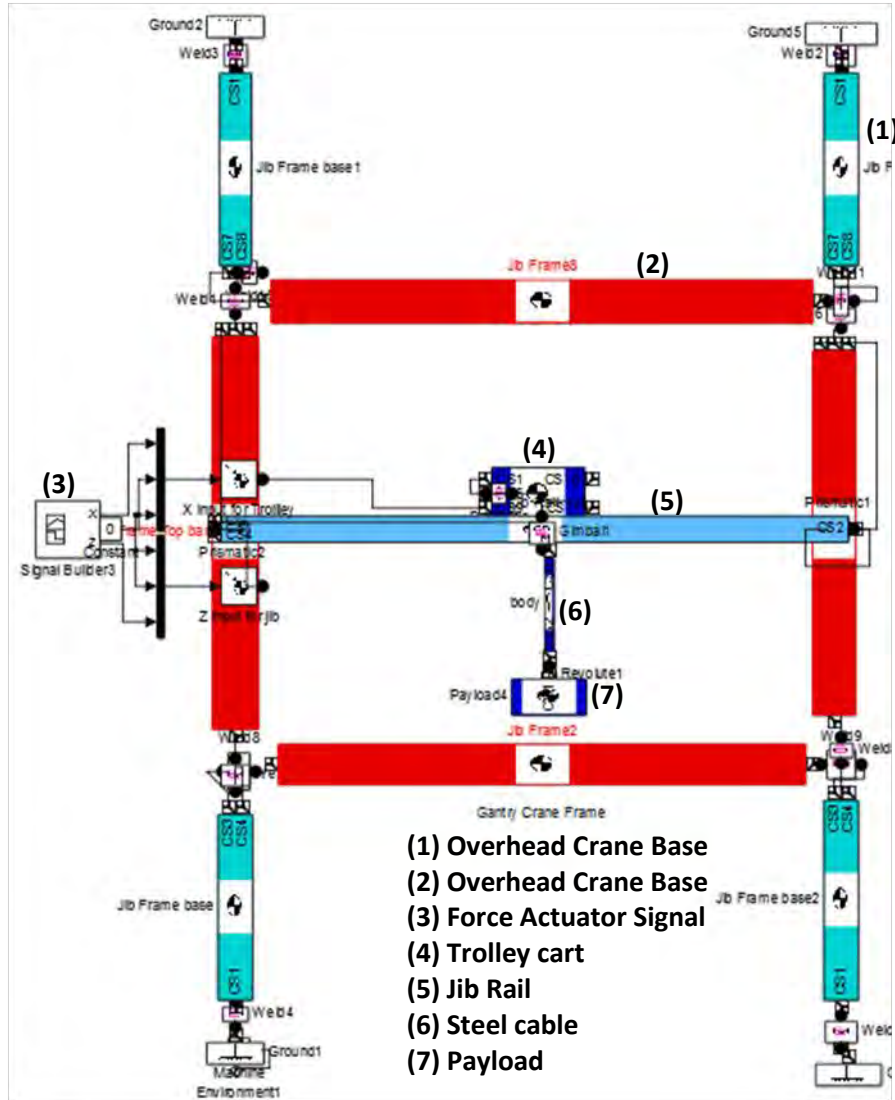


Figure 3.17 3D Overhead Crane SimMechanics Model to generate Visualization

3.2.9 Simulation of Jib-Trolley motion in Overhead Crane

After certain actuation signals are excited through signal builder, trolley runs in X-Z direction while swing angles produce all three X-Y-Z values. The simulation shows that $\theta_z = \text{between } (-10^\circ \text{ to } 10^\circ)$ throughout trolley cart motion in X-Z direction. However, during 0 to 4-seconds of trolley's X directional motion (X-Y plane) which is rotation about Z axis \hat{k} , only θ_z provides swing angle while both other θ_x and θ_y are zero. Then, all three rotational angles appear as soon as it changes direction from X to

Z in 3D in Fig. 3.18a. Swing behaviour and load moving trajectory through X-Y-Z planes can also be viewed as a Lissajous curve in Fig. 3.18b.

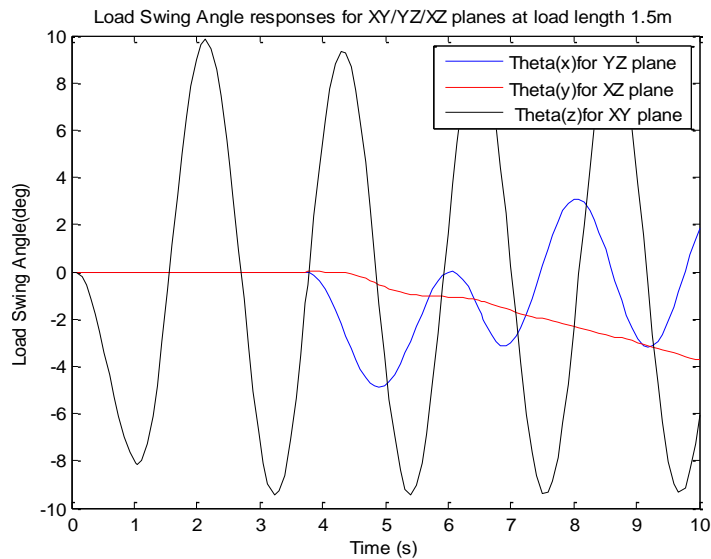


Figure 3.18a Load-swing in X-Y-Z Directions

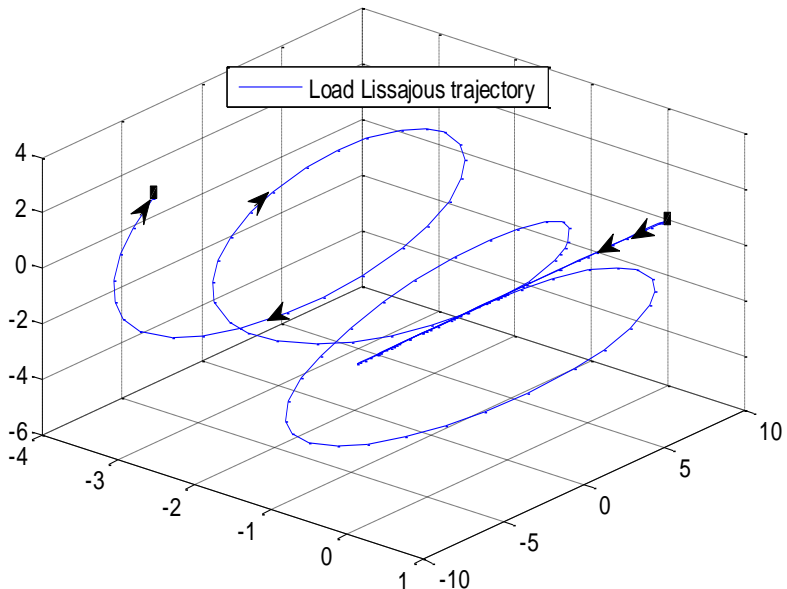


Figure 3.18b Lissajous Graph for X-Y-Z Load-swings

3.3 Linearization of 2D Overhead Crane using Linear Least Square Approach

To linearize the model, adaptive perturbation approach with “linmod” command is used in Matlab simulink. That command will search for an equilibrium point (operating point) of the system where the net force is zero. Then, it generates linear time-invariant (LTI) state-space models. However, a simple step of creating model using “linmod” command without the details would make difficulty in analyzing the

model. Therefore, instead of direct linearizing by MatLab, the mathematical model would be developed from collected dataset. The following steps have taken: model the input signal, collect the data set, and determine denominator/numerators using Least Square System Identification. Once the input/outputs dataset is collected, Least Square System Identification is applied to determine the number of parameters required for the plant model dynamics and find those parameters (b_1, b_2, \dots, b_m and a_1, a_2, \dots, a_n), Eq.(3.24) [60].

$$\Delta y(k) = \frac{b_1 z^{-1} + b_2 z^{-2} + \dots + b_m z^{-m}}{1 + a_1 z^{-1} + a_2 z^{-2} + \dots + a_n z^{-n}} \Delta u(k) \quad (3.24)$$

The output of the system represents the linear combination of past inputs and outputs, where, $\theta_1, \dots, \theta_m, \theta_{m+1}, \dots, \theta_{m+n}$ are the states of the system, Eq.(3.25).

$$y(k) = -\theta_1 y(k-1) - \dots - \theta_m y(k-m) + \theta_{m+1} u(k-1) + \dots + \theta_{m+n} u(k-n) \quad (3.25)$$

$$y \begin{bmatrix} y(k) \\ y(k+1) \\ \vdots \\ y(k+N) \end{bmatrix} = \begin{bmatrix} -y(k-1) & \dots & -y(k-m) & u(k-1) & \dots & u(k-n) \\ -y(k) & \dots & -y(k-m+1) & u(k) & \dots & u(k-n+1) \\ \vdots & \ddots & \vdots & \vdots & \ddots & \vdots \\ -y(k-1+N) & \dots & -y(k-m+N) & u(k-1+N) & \dots & u(k-1+N) \end{bmatrix} \begin{bmatrix} \theta_1 \\ \vdots \\ \theta_m \\ \theta_{m+1} \\ \vdots \\ \theta_{m+n} \end{bmatrix}$$

$$y(k) = [-y(k-1) \dots -y(k-m) u(k-1) \dots u(k-n)]$$

$$y(k) = X\theta \quad (X \text{ is } m \times n \text{ with } m > n)$$

3.3.1 Denominator and Numerator Coefficients consideration

Current least square approach computes 2-Denominator and 2-Numerator Coefficients for 100-datalines and uses two simultaneous past inputs/outputs data to form X Matrix and therefore the following matrix would be formed.

$$\begin{bmatrix} y(3) \\ y(4) \\ \vdots \\ y(100) \end{bmatrix} = \begin{bmatrix} -y(2) & -y(1) & u(2) & u(1) \\ -y(3) & -y(2) & u(3) & u(2) \\ \vdots & \vdots & \vdots & \vdots \\ -y(99) & -y(98) & u(99) & u(98) \end{bmatrix} \theta$$

3.3.2 Training and Checking Model

Initially, the collected data set is divided into two parts, training and checking as shown in Fig. 3.19a. The reason is, the developed model from the training part would be tested against checking output in order to verify how well the model matches. In this system, first half training data set, y_{tr}, u_{tr} and X_{tr} are developed to calculate Denominator and Numerator Coefficients, θ and produce Model Transfer Function.

$$\begin{array}{c}
 \text{Training} \\
 \text{Data Set}
 \end{array}
 \left\{
 \begin{array}{l}
 \left[\begin{array}{l} y_{tr} \\ \vdots \\ y_{ch} \end{array} \right] = \left[\begin{array}{l} X_{tr} \\ \vdots \\ X_{ch} \end{array} \right] \left[\begin{array}{l} u_{tr} \\ \vdots \\ u_{ch} \end{array} \right]
 \end{array} \right.$$

Figure 3.19a Training and Checking Model

Considering 2 Denominator and 2 Numerator Coefficients case, X_{tr} Matrix is identified and θ is computed using Equ.(3). The coefficients are estimated $\theta = x_{est} = [a_1, a_2, b_1, b_2]$ to form the following Model Transfer Function [33].

$$\begin{aligned}
 X_{tr}^T * y_{tr} &= (X_{tr}^T * X_{tr}) * x_{est} \\
 x_{est} &= [X_{tr}^T * X_{tr}]^{-1} * X_{tr}^T * y_{tr} \\
 y_{Model_tr} &= \frac{b_1 q^{-1} + b_2 q^{-2}}{1 + a_1 q^{-1} + a_2 q^{-2}}
 \end{aligned}$$

3.3.3 Root Mean Square Error Calculation

Root-mean-square error (RMSE) in Eq.(3.26) is used to measure the differences between estimated values by the developed model, and actual outputs such as: y_{Model_tr} VS y_{tr} and y_{Model_ch} VS y_{ch} . Minimizing RMSE could produce better fit of the model and enhance approximation. RMSE in Eq.(3.27) is calculated in the following form in Fig. 3.19b Least Square General Form [6]:

$$\|Ax - y\| = \left(\sum_{i=1}^m (\sum_{j=1}^n a_{ij} x_j - y_i)^2 \right)^{1/2} \quad (3.26)$$

$$\|X * x_{est} - y_{tr}\| = \|y_{Model_{tr}} - y_{tr}\| = \text{norm}(y_{tr} - y_{Model_{tr}})$$

$$RMSE = \frac{\text{norm}(y_{tr} - y_{Model_{tr}})}{\sqrt{\text{length of } (y_{tr})}} \quad (3.27)$$

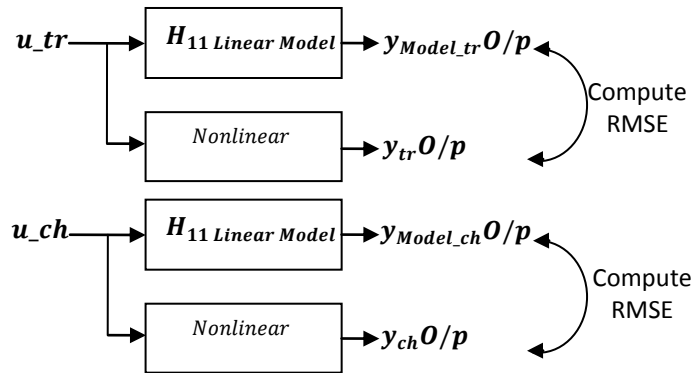


Figure 3.19b RMSE Comparison between actual and predicted

Using Least Square System Identification: Den2Num2, Den3Num3, Den4Num4, Den2Num3, Den3Num2, Den4Num3, and Den3Num4 models are computed followed by their respective RMSE. After comparing all RMSE, lowest RMSE and its respective model would be picked up as the best linearly approximated model of the system. The following table shows, each model adjustment and calculated RMSE for both Training and Checking parts. Least Square System Identification with past consecutive inputs-outputs, Table (3.1):

[Den Num]	Data Start from	Past data start from
[2 2]	y_3	$[y_2 \ -y_1 \ u_2 \ u_1]$
[3 3]	y_4	$[-y_3 \ -y_2 \ -y_1 \ u_3 \ u_2 \ u_1]$
[4 4]	y_5	$[-y_4 \ -y_3 \ -y_2 \ -y_1 \ u_4 \ u_3 \ u_2 \ u_1]$
[2 3]	y_3	$[-y_2 \ -y_1 \ u_3 \ u_2 \ u_1]$
[3 2]	y_4	$[-y_3 \ -y_2 \ -y_1 \ u_2 \ u_1]$
[4 3]	y_5	$[-y_4 \ -y_3 \ -y_2 \ -y_1 \ u_3 \ u_2 \ u_1]$
[3 4]	y_4	$[-y_3 \ -y_2 \ -y_1 \ u_4 \ u_3 \ u_2 \ u_1]$

Table 3.1 Linear Least Square System Identified Models

Since 1D overhead crane has Trolley cart's translational motion and load's swing angle outputs, the Least Square calculation produce two models for Trolley and load swing while each model has training RMSE and checking RMSE. After generating all RMSEs, lowest RMSE would be picked up from Trolley model and load swing model considering the best linear approximation. The following Table (3.2a) and Table (3.3a) show each computed RMSE(Training), RMSE(Checking), as well as its total RMSE for models (22,33,44,23,32,43,34) while Table (3.2b) and Table (3.3b) show lowest to

highest computed RMSE in which Den 2 Num 2 model appears to have lowest RMSE not only in Trolley model but also in Load Swing model.

TrolleyCartRMSEDenNum				
RMSEs(Tr)	RMSEs(Ch)	RMSE	Den	Num
0.12645	0.13602	0.13123	2	2
0.090981	0.09955	0.095266	3	3
0.12587	0.13558	0.13073	2	3
0.1246	0.13457	0.12959	3	2
0.092136	0.099108	0.095622	4	3
0.092508	0.098946	0.095727	3	4
7.5184e+10	9.4161e+10	NaN	4	4

Table 3.2a RMSE(Training) and RMSE (Checking) for Trolley Model

LoadSwingRMSEDenNum				
RMSEs(Tr)	RMSEs(Ch)	RMSE	Den	Num
0.82772	2.4455	1.6366	2	2
3.7683	3.3389	3.5536	3	3
0.82772	2.4455	1.6366	2	3
0.82773	2.4455	1.6366	3	2
1.3679	2.5621	1.965	4	3
0.8683	2.4819	1.6751	3	4
7.5184e+10	9.4161e+10	NaN	4	4

Table 3.3a RMSE(Training) and RMSE (Checking) for Loadswing Model

RMSEs(Trolley)	Den	Num
0.095266	3	3
0.095622	4	3
0.095727	3	4
0.12959	3	2
0.13073	2	3
0.13123	2	2
NaN	4	4

Table 3.2b from lowest to highest RMSE for Trolley Model

RMSEs(LS)	Den	Num
1.6366	2	3
1.6366	2	2
1.6366	3	2
1.6751	3	4
1.965	4	3
3.5536	3	3
NaN	4	4

Table 3.3b from lowest to highest RMSE for Load Swing Model

The following figure, Fig (5,a) from lowest RMSE model Den3 Num3 show how well the linear approximation match the actual outputs. For the Trolley model: residuals are less than 0.08 and RMSE is only 0.095499 in Fig. 3.20a and for the load swing model Den3 Num2: residuals are between (-0.4 to 0.4) and RMSE is only 1.6366 in Fig. 3.20b.

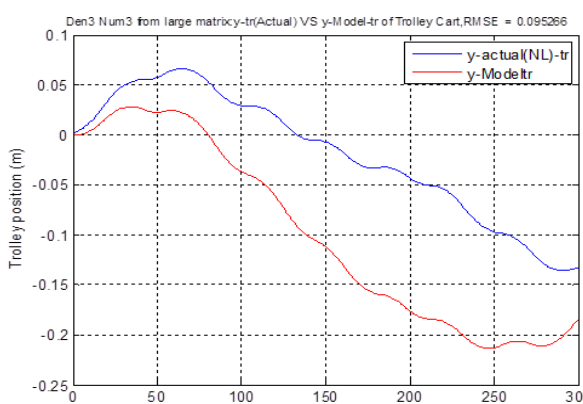


Figure 3.20a Den 3 Num 3 Trolley model

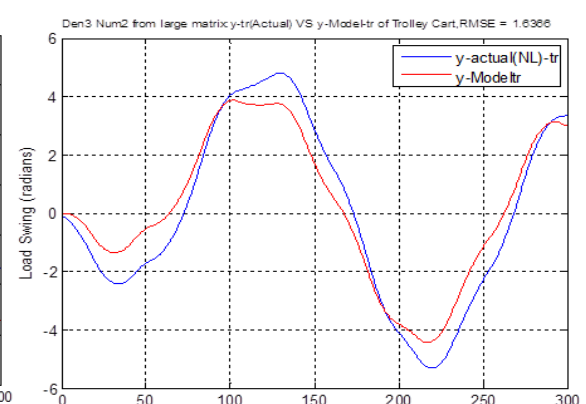


Figure 3.20b Den 3 Num 2 Load Swing model

3.3.4 Linearization using Improved Least Square with 7 past inputs-outputs

To represent the X-translational motion of the load-attached trolley cart, the collected data are used to develop linear least square form. Currently, Linear Least

Square approach uses a linear combination of the past data $[y3] = [-y2 \ -y1 \ u2 \ u1]$ and it can achieve only one Root Mean Square Error (RMSE). And it would be hard to analyze whether the model provides better approximation within the processed past 4 data. Therefore, up to 7 past inputs/outputs data are used to maximize the X Matrix with more inputs/outputs and to enhance the effectiveness of experimental model [7]. For instance, if $N=100$, then where N is the last output data.

$$\begin{bmatrix} y(8) \\ y(9) \\ \vdots \\ y(100) \end{bmatrix} = \begin{bmatrix} 1 & \dots & 7 & 8 & \dots & 14 \\ -y(7) & \dots & -y(1) & u(7) & \dots & u(1) \\ -y(8) & \dots & -y(2) & u(8) & \dots & u(2) \\ \vdots & \ddots & \vdots & \vdots & \ddots & \vdots \\ -y(99) & \dots & -y(93) & u(99) & \dots & u(93) \end{bmatrix} \theta$$

Den and Num Coefficients consideration using Least Square modified approach

Selecting every possible combination of the columns from a large matrix with 14 past inputs/outputs according to the model needs and forming X matrix to compute estimated states, are some of the essential tasks to look for better approximated model. For instance, to get Den 2 Num 2 model, X matrix with 2 outputs columns and 2 inputs columns are required.

$$\begin{bmatrix} y(8) \\ \vdots \\ y(N) \end{bmatrix} = \begin{bmatrix} -y(7) & -y(6) & u(7) & u(6) \\ \vdots & \vdots & \vdots & \vdots \\ -y(?+N) & -y(?) & u(?+N) & u(?+N) \end{bmatrix} \theta,$$

$$y(k) = X\theta$$

From available 7 outputs columns, every possible 2 columns are picked at each time and same as every possible 2 from 7 inputs columns. That is, all possible 21 pairs of outputs/inputs columns can be picked to form 21 possible models. In previous section, $y3 = [-y2 \ -y1 \ u2 \ u1]$ with only one model could be formed while in this case there would be 21-models with Den2 Num2 coefficients which may produce better approximation.

$$\begin{bmatrix} X_1 \\ X_2 \\ \vdots \\ X_{21} \end{bmatrix} = \begin{bmatrix} Column & Column & Column & Column \\ 1 & 2 & 8 & 9 \\ 1 & 3 & 8 & 10 \\ \vdots & \vdots & \vdots & \vdots \\ 6 & 7 & 13 & 14 \end{bmatrix}$$

For each X_1, X_2, \dots, X_{21} , each estimated states are calculated to form estimated Model which would be compared against actual output. From X_1 matrix:

$$X_1 = \begin{bmatrix} Column & Column & Column & Column \\ 1 & 2 & 8 & 9 \\ -y(7) & -y(6) & u(7) & u(6) \\ \vdots & \vdots & \vdots & \vdots \\ -y(7+N) & -y(6+N) & u(7+N) & u(6+N) \end{bmatrix},$$

$$\theta_1 = X_1^T * Y_1 ==> RMSE_1$$

3.3.5 Improved LLS Algorithm

Overall steps from selecting pairs, calculating estimated states and rmse for each case to computing lowest RMSE among 21 rmse are shown in the following algorithm figure in Fig. 3.21. For the Den2Num2 Model, the Algorithm could generate 21 RMSE and respective models. After comparing all RMSE, the lowest RMSE and its related model would be picked up for further analysis. Figure Fig. 3.21 shows improved version of Linear Least Square algorithm [7] with all highest to lowest RMSEs and their columns combinations.

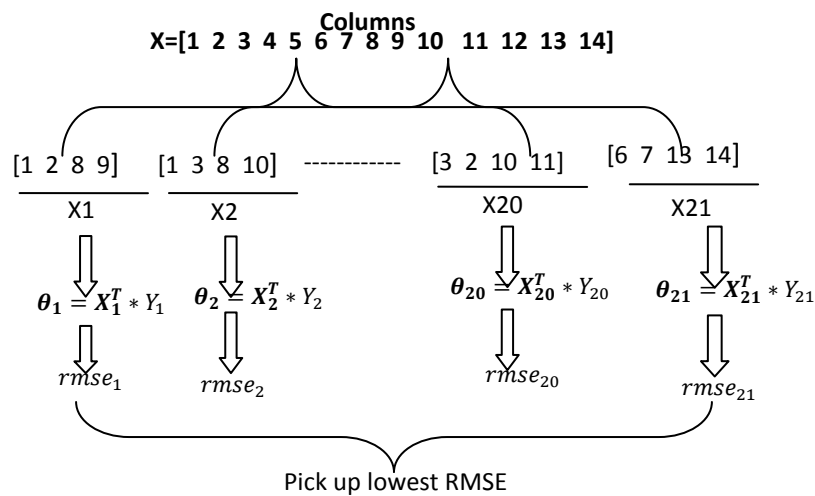


Figure 3.21 Improved LLS Algorithm to compute lowest RMSE

In the case of generating Den2 Num2 Model, the algorithm would create a total of 21 models from the main X matrix since there are 14 columns of the past 7 outputs and 7 inputs. Table (3.4a) displays each model pick up columns and the calculated RMSE then those RMSEs are rearranged from high to low values as in Table (3.4b). The comparison graph based on Table (3.4b) with each generated model columns could also be viewed in Fig. 3.22.

Models	{Columns of each model}														RMSE
	1	2	3	4	5	6	7	8	9	10	11	12	13	14	
1	1	2						8	9						0.1312
2	1		3					8		10					0.1145
3	1			4				8		11					0.1145
4	1				5			8			12				0.1142
5	1					6		8				13			0.1138
6	1						7	8					14		0.1133
7		2	3						9	10					3+
8		2		4					9		11				0.9096
9		2			5				9		12				0.1027
10		2				6			9			13			0.1057
11		2					7		9				14		0.1062
12			3	4						10	11				3+
13			3		5					10		12			3+
14			3			6				10			13		2.6933
15			3				7			10				14	0.0901
16				4	5					11	12				3+
17				4		6				11			13		3+
18					4		7			11				14	3+
19						5	6				12	13			3+
20						5		7			12			14	3+
21							6	7				13	14		3+

Table 3.4a Generated Models and respective RMSEs

Models	{Columns of each model}														RMSE (high to low)	
	1	2	3	4	5	6	7	8	9	10	11	12	13	14		
1						6	7					13	14	3+		
2					5		7				12		14	3+		
3					5	6					12	13			3+	
4				4			7			11			14		3+	
5				4		6				11			13		3+	
6				4	5					11	12				3+	
7			3		5					10		12			3+	
8			3	4						10	11				3+	
9		2	3						9	10					3+	
10			3			6				10			13		2.6933	
11		2		4					9		11				0.9096	
12	1	2						8	9						0.1312	
13	1			4				8			11				0.1145	
14	1		3					8		10					0.1145	
15	1			5				8			12				0.1142	
16	1				6			8				13			0.1138	
17	1					7	8						14		0.1133	
18		2					7		9					14	0.1062	
19		2				6			9			13			0.1027	
20		2			5		7			10						0.1027
21			3											14		0.0901

Table 3.4b RMSEs from high to low and respective models

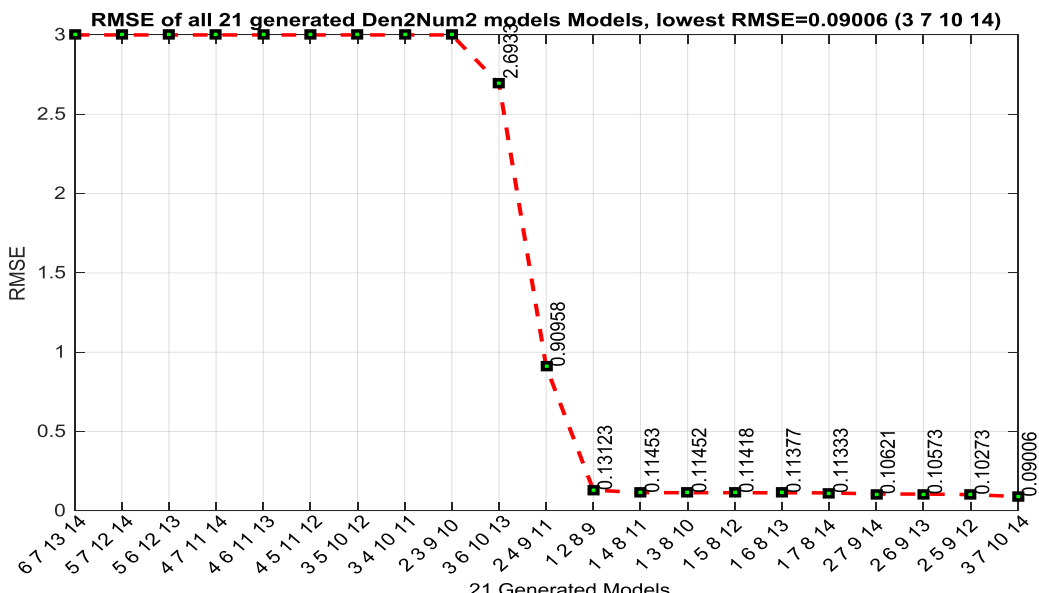


Figure 3.22 RMSEs from high to low with respective models

This improved LLS Algorithm is quite effective as it can allow the user to select numbers of Den-Num. Having Den 2-Num 2 alone, the algorithm could create 21 models and combination of different Num-Den has different number of models can be generated. Since the algorithm considers past 7 outputs-7 inputs in the main matrix, there could be more than 200 generated models throughout Den2-Num2 to Den7-Num7 combinations. This research has tried up to Den4-Num4 models development and their RMSEs comparisons are discussed below.

3.3.6 Den2-Num2 to Den4-Num4 Models Development using Improved LLS

For the other Modelling cases such as: (Den 3 Num 3, Den 2 Num 3, Den 3Num 2, Den 4Num 3, Den 3 Num 4, Den 4 Num 4), the above-mentioned Algorithm is applied in which, all possible combination of columns pairs are first established then calculate estimated sates, generate Model Transfer Functions and compute RMSEs for all. The following Table (3.5a) and Table (3.6a) provide details of RMSE (Training part), RMSE (Checking part), and total RMSE each model for both Trolley and Load Swing simulations. Table (3.5b) and Table (3.6b) show the lowest RMSEs such as: RMSE=0.014485 for Trolley model Den 4 Num 4, and RMSE=1.6161 for Load Swing Model Den 3 Num 4, Table (3.6b).

TrolleyCartRMSEDenNum				
RMSEs(Tr)	RMSEs(Ch)	RMSE	Den	Num
0.062355	0.11777	0.09006	2	2
0.062837	0.16689	0.036442	3	3
0.063118	0.11684	0.089978	2	3
0.058021	0.1539	0.10596	3	2
0.055614	0.10507	0.080342	4	3
0.092217	0.099155	0.095686	3	4
0.046732	0.13316	0.014485	4	4
0.06305	0.11571	0.08938	2	4
0.042649	0.11697	0.079812	4	2

Table 3.5a RMSE(Training) and RMSE(Checking) for Trolley Model

LoadSwingRMSEDenNum				
RMSEs(Tr)	RMSEs(Ch)	RMSE	Den	Num
0.82772	2.4455	1.6366	2	2
0.82523	2.444	1.6346	3	3
0.82772	2.4455	1.6366	2	3
0.82771	2.4455	1.6366	3	2
0.81693	2.4393	1.6281	4	3
0.8021	2.43	1.616	3	4
0.82509	2.444	1.6345	4	4
0.82772	2.4455	1.6366	2	4
0.82751	2.4454	1.6364	4	2

Table 3.6a RMSE(Training) and RMSE(Checking) for Loadswing Model

RMSEs (Trolley)	Den	Num
0.014485	4	4
0.036442	3	3
0.079812	4	2
0.080342	4	3
0.08938	2	4
0.089978	2	3
0.09006	2	2
0.095686	3	4
0.10596	3	2

Table 3.5b from lowest to highest RMSE for Trolley Model

RMSEs (LS)	Den	Num
1.616	3	4
1.6281	4	3
1.6345	4	4
1.6346	3	3
1.6364	4	2
1.6366	3	2
1.6366	2	4
1.6366	2	3
1.6366	2	2

Table 3.6b from lowest to highest RMSE for Loadswing Model

Using Linear Least Square with 7 past inputs/outputs data, Den 4 Num 4 trolley model provides lowest RMSE 0.046732 Fig. 3.23a and while load swing model Den3 Num4 appeared to have better approximation with RMSE 1.6161, Fig. 3.23b

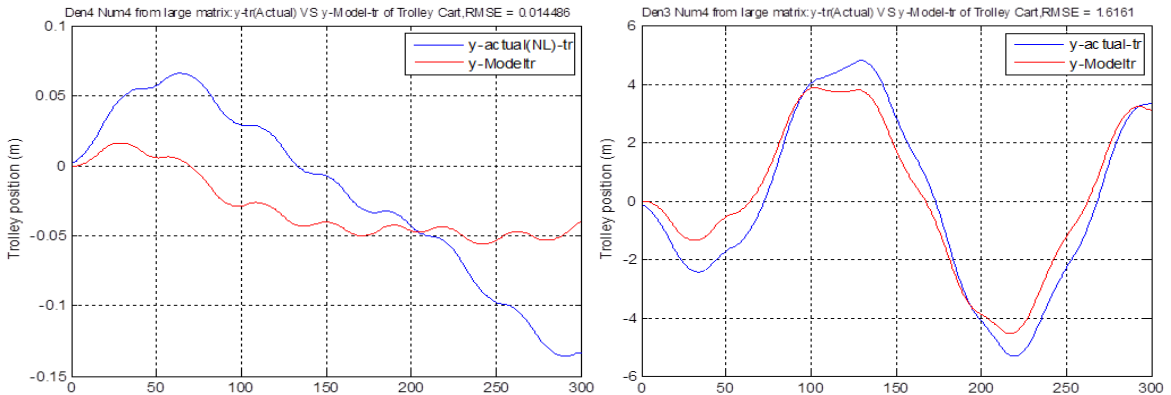


Figure 3.23a Den 4 Num 4 Trolley model

Figure 3.23b Den 3 Num 4 Load Swing model

3.3.7 RMSE comparison and Linear Models selection

Simple Linear Least Square (LLS) approach produced lowest RMSE=0.0.095495 for trolley model structure with 3 Denominator 3 Numerator Coefficients while improved version of Linear Least Square (ILLS) generated lowest RMSE=0.014485 with 4 Denominator 4 Numerator Coefficients. In the case of payload swing model, LLS has RMSE= 1.6366 with (3 Denominator 2 Numerator Coefficients) and ILLS has 1.616 with (3 Denominator 4 Numerator Coefficients), as shown in Table (3.7). Those developed models from both approaches would be transformed into continuous state-space for control and performance comparison purposes. In both trolley and loadswing cases, ILLS made significantly generating perfect linear models with lower RMSEs compared to current normal LLS approach, Fig (10a,10b).

"Trolley_RMSE Comparison"		"Loadswing_RMSE Comparison"	
Normal_LLS	Improved_LLS	Normal_LLS	Improved_LLS
0.14527	0.10596	4.5197	1.6366
0.14431	0.095727	3.9874	1.6366
0.14398	0.09006	3.5642	1.6366
0.13123	0.089978	3.5536	1.6366
0.13073	0.08938	1.965	1.6366
0.12959	0.080342	1.6751	1.6346
0.095727	0.079812	1.6366	1.6345
0.095622	0.036442	1.6366	1.6282
0.095266	0.014486	1.6366	1.6161

Table 3.7 RMSE Comparison for Normal LLS and Improved LLS

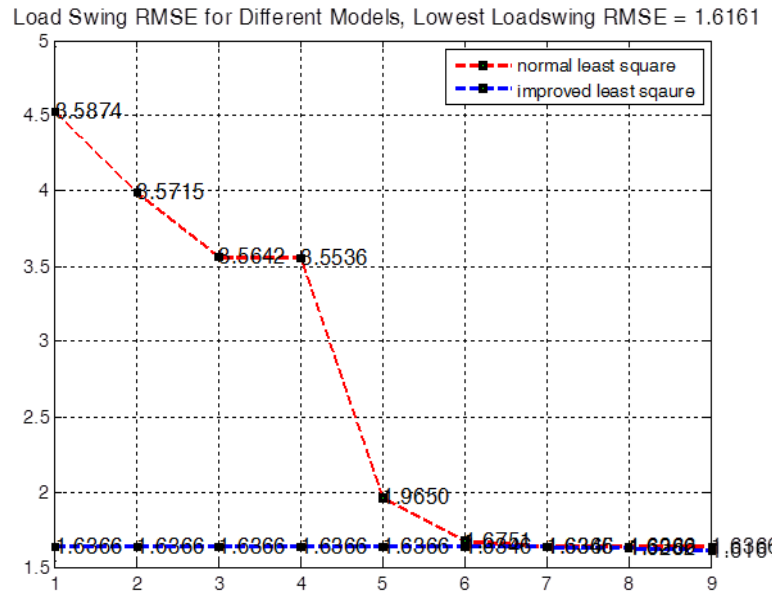


Figure 3.24a RMSE Comparison for Normal LLS and Improved LLS for Loadswing Case

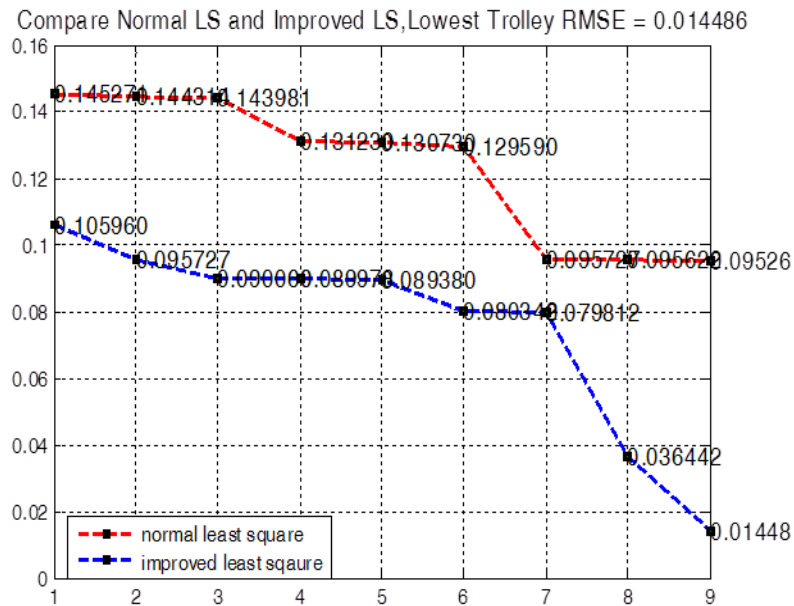


Figure 3.24b RMSE Comparison for Normal LLS and Improved LLS for Trolley Case

This section discussed about getting raw data from the developed 2D overhead crane, applied simple LLS approach and improved to generate models with lower RMSE. Furthermore, improved version of LLS (ILLS) algorithm was then developed in order to seek better fit linear model with significantly lower RMSE. The RMSE comparison table and figures clearly shown that ILLS approach of models development could improve not only the better fit linear models but also the control performance. Both LLS and ILLS models for trolley-payload swing are mentioned below, Table (3.8).

	Den	Num	Model		RMSE
Least Square	3	3	Trolley	$\frac{4.924e - 005q^{-1} + 4.964e - 010q^{-2} - 4.924e - 005q^{-3}}{1 - 3q^{-1} + 3q^{-2} - q^{-3}}$	0.095499
Least Square	3	2	Load Swing	$\frac{-0.002723q^{-1} - 0.002722q^{-2}}{1 - 1.999q^{-1} + q^{-2} - 7.993e - 005q^{-3}}$	1.6366
Least Square with 7 past IOs	4	4	Trolley	$\frac{8.07e - 005q^{-1} + 1.321e - 005q^{-2} + 3.682e - 005q^{-3} - 2.993e - 005q^{-4}}{1 - 1.703q^{-1} + 1.026q^{-2} - 0.8826q^{-3} + 0.5598q^{-4}}$	0.014485
Least Square with 7 past IOs	3	4	Load Swing	$\frac{-0.002723q^{-1} - 0.002721q^{-2} + 2.736e - 006q^{-3} + 1.992e - 007q^{-4}}{1 - 2q^{-1} + 1.001q^{-2} - 0.0002781q^{-3}}$	1.616

Table 3.8 Linear Trolley-Loadswing Models based on LLS and ILLS

3.3.8 Linear Quadratic Regulator (LQR) Design

Linear quadratic (LQ) optimal control can be used to resolve the trade-offs issues between robustness, performance, and control effort by specifying some kind of performance objective function to be optimized. This optimal state-space method requires knowledge of the plant model to compute feedback control gain K that minimizes the quadratic cost function "J". The plant state equations can be written as follow:

$$\dot{x}(t) = Ax(t) + B_u u(t), \text{ and } y = Cx(t) + Du(t)$$

Linear quadratic regulation method is implemented for this overhead crane to determine the state-feedback control gain matrix K. LQR needs two parameters, Q and R weighting matrices which will balance the relative importance of the control effort (u) and error (deviation from 0), respectively, in the cost function J. Initially, $Q = \rho C^T C$ with $\rho = 1$ and $R = 1$ were assumed,[2]. The cost function corresponding to this and Q and R places equal importance on the control and the state variables outputs (cart's position x , and the pendulum's angle θ).

Q, R weighting matrices and Cost function J

Q and R matrices are considered as diagonal, $q \times q$ Matrix is positive-definite ($x' Q x > 0$ for every nonzero vector, x) and were adjusted by hit and trial method to obtain the desired responses. The element in the (2, 2) position of Q represents the weight on the cart's position and the element in the (5,5) position represents the weight on the pendulum's angle. The input weighting R will remain at 0.001. In order to reach

faster stabilization, it has been put more weights on the states as: $x = 30$, and $\theta = 20$ while $R=0.001$ to produce good controller gain K matrix. The following cost function J , Eq.(3.28) [61], is minimized to define the trade-off between regulation performance and control effort of x-directional motion with the states $x, \dot{x}, \theta, \dot{\theta}$:

$$J = \int_0^\infty [x^T Q_x x + \theta^T Q_\theta \theta + u^T R u] dt \quad (3.28)$$

where (Q_x, Q_θ and R) are symmetric positive matrices. The control goal generally is to keep $x(t)$ close to 0, especially, at the final time (t), using control effort u . To wit, observe in the cost function (3.28)

- $x^T Q_x x$ penalizes the transient state deviation, and
- $u^T R u$ penalizes control effort.

This formulation can accommodate regulating an output $y(t) = C(t)x(t)$. As the system is highly nonlinear time invariant, and states are infinite, this research has considered using infinite-time horizon approach.

After Q and R weighting matrices are established and the controller gain (K) values are computed, the system with step reference as shown in Fig.3.25, is controlled by LQR Controller, Eq.(3.29). Initially, the system use the weighting matrices: $Q(2,2)=Q(5,5)=1$ and $R=1$ and it showed the plot was not satisfactory. Both cart and pendulum responses overshoot. To improve their settling times and reduce rise time, $Q(2,2)=30$, $Q(5,5)=20$ and $R=0.001$ are selected after several trials.

$$\begin{aligned} \dot{x} &= Ax + B(-Kx), \text{ and } Y = Cx + D(-Kx), \\ u &= -R^{-1}B_u^T P(t)x(t) = -Kx \\ \dot{x} &= (A - BK)x, \quad Y = (C - DK)x \end{aligned} \quad (3.29)$$

Whereby, the optimal feedback gain is, $K = -R^{-1}B_u^T P(t)$. In the following Riccati Equation in which P is the steady state solution that yields a unique optimal control to minimize the cost function, J , [62].

$$\dot{P}(t) = -P(t)A - A^T P(t) - Q + P(t)B_u R^{-1} B_u^T P(t)$$

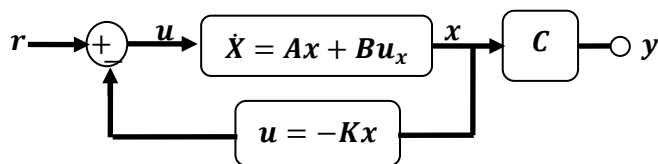


Figure 3.25 LQR Controller Design

In this overhead crane system, LQR performance of Trolley cart models, Den3 Num3 and Den4 Num4, are compared. The following figure Fig. 3.26 shows, Den4 Num4 model of modified Linear Least Square using 7past inputs/outputs dataset appeared to have shorter rise time and reach stability before 3 seconds while Den3 Num3 model of simple Least Square approach still fluctuating with longer rise time though the same Q and R weighting matrices have been applied.

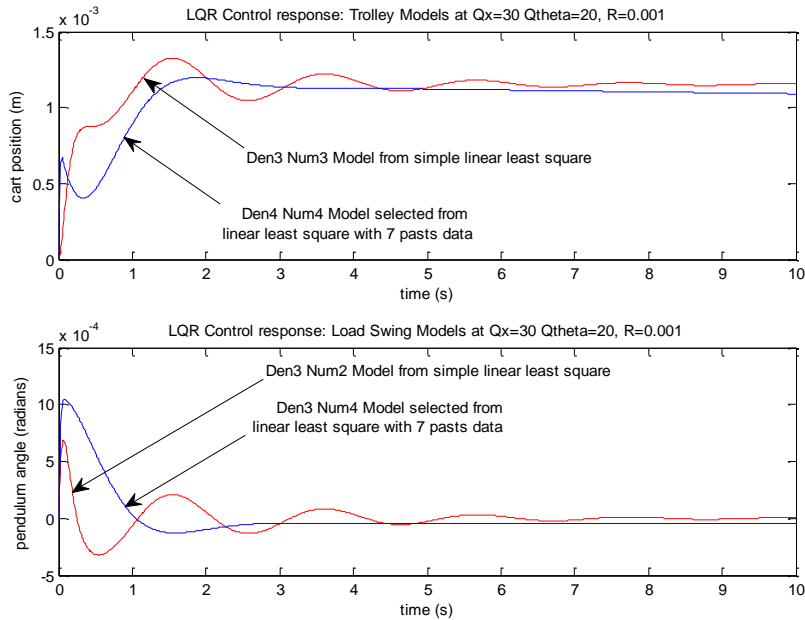


Figure 3.26 LQR-Controlled models response comparison

For Load swing performance, again Den3 Num4 from Linear Least Square using 7past inputs/outputs data appeared to reach zero swing angle in less than 3 seconds with less rise time and shorter settling time compared to Den3 Num2 model from simple least square. Besides, Linear Least Square using 7past inputs/outputs data produce more models, in this case up to 35 models have been analyzed before selecting the best fit model for control purpose. In this specific case of up to 600 data points, Den4 Num4 and Den3 Num4 models with lowest RMSEs have been picked for further reference tracking performance analysis. Though the controller response is better, steady-state errors still appear and therefore reference input tracking has been implemented to achieve desired inputs.

3.3.9 Full state feedback-LQR Reference Tracking control

Adding the reference input to the system, $u=-Kx+r$ can lead to steady state errors. Pre-multiply r by carefully chosen matrix N . In order to create pre-compensation \bar{N} , there are two possible methods such as: full-state feedback, and full-state feedback with full-order observer [63]. In this case, full-state feedback reference input tracking

would be used. The following equations, Eq.(3.30) and Eq.(3.31), and figures, Fig. 3.27a and Fig.3.27b explain the pre-compensation \bar{N} calculation. Full-state feedback controller form

$$u = -Kx + \bar{N}r \text{ where } \bar{N} = N_u + KN_x \quad (3.30)$$

And therefore, full-state regulating input is: $u = -Kx + (N_u + KN_x)r$

$$u = N_u r - K(x - N_x r) \quad (3.31)$$

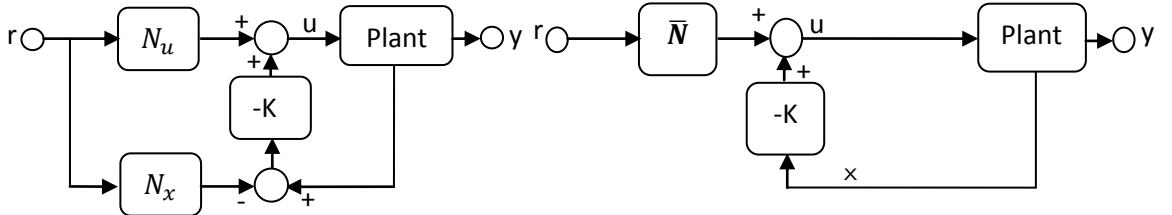


Figure 3.27a Full state feedback-LQR
Reference Tracking Control

Figure 3.27b Full state feedback-LQR
with pre-compensator \bar{N}

Full-state feedback would regulate steady-state output y_{ss} to desired steady-state value r_{ss} . In this trolley cart X directional motion, to track a constant desired position, x_{ss} (ss=steady-state) with control, u_{ss} , the control equation

$$0 = Ax_{ss} + Bu_{ss} \quad \{ \text{for steady state, } \dot{x} = 0 \}$$

$$y_{ss} = Cx_{ss} + Du_{ss}$$

By substituting

$$x_{ss} = N_x r_{ss}, \text{ and } u_{ss} = N_u r_{ss},$$

$$0 = AN_x r_{ss} + BN_u r_{ss}$$

$$y_{ss} = CN_x r_{ss} + DN_u r_{ss}$$

When $y_{ss} = r_{ss}$ in the steady-state

$$0 = AN_x r_{ss} + BN_u r_{ss},$$

$$r_{ss} = CN_x r_{ss} + DN_u r_{ss}$$

The above equations can be formed as state-space:

$$\begin{bmatrix} 0 \\ 1 \end{bmatrix} r_{ss} = \begin{bmatrix} A & B \\ C & D \end{bmatrix} \begin{bmatrix} N_x \\ N_u \end{bmatrix} r_{ss} \quad (\text{or}) \quad \begin{bmatrix} N_x \\ N_u \end{bmatrix} = \begin{bmatrix} A & B \\ C & D \end{bmatrix}^{-1} \begin{bmatrix} 0 \\ 1 \end{bmatrix}$$

However, when computing the large matrices inverse, $\begin{bmatrix} A & B \\ C & D \end{bmatrix}^{-1}$, it gives error. To be able to solve for larger matrices, this research applies the following way, Eq. (3.32).

$$F = \begin{bmatrix} A & B \\ C & D \end{bmatrix}, Z = \begin{bmatrix} 0 \\ 1 \end{bmatrix}$$

$$N = \text{inv} [(F^T F)(F^T Z^T)] \quad (3.32)$$

$$N = [N_x \ N_{u1} \ N_{u1} \ \dots \ N_{un}]^T$$

$$N_u = N_{u1} + N_{u2} + \dots + N_{un}$$

$$\bar{N} = N_u + KN_x, \text{ where } K \text{ is the controller gain.}$$

The established full-state feedback pre-compensators N_u and N_x are then applied in LQR-control, Fig (13), to achieve the desired input. The robustness of reference tracking produces perfect control stability on both trolley motion and pendulum load swing. Each Trolley desired position has been achieved in less than 3 seconds while load swing could be suppressed in 2 seconds time compared to nonlinear high fluctuating pendulum output as shown in Fig. 3.28. It shows that, the developed trolley and load swing linear models using modified linear least square with 7 past inputs/outputs are more reliable and LQR with pre-compensator just make the whole system perfect.

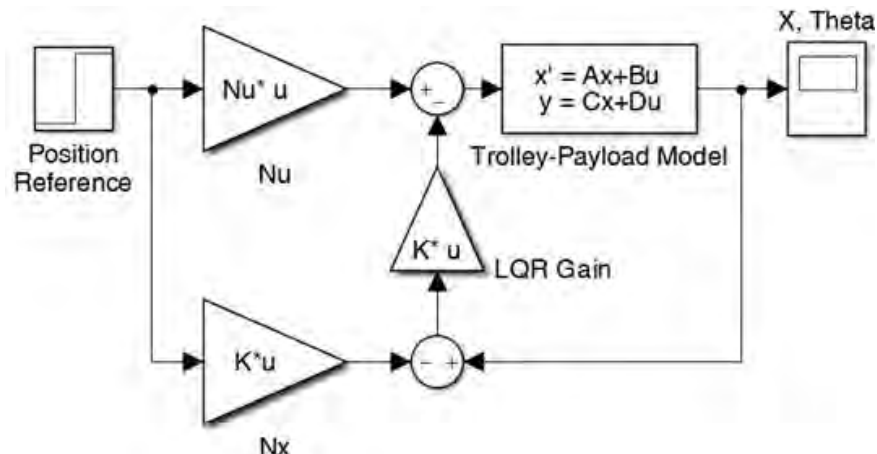


Figure 3.28 Full-state feedback-LQR Reference Tracking Control

3.3.10 Results and Discussion

According to the simulation result explained in section 3.3.8, the models developed by improved linear least square (Den4-Num4 for Trolley and Den3-Num4 for Payload) with LQR control could easily track the set point with less fluctuation. To achieve further robust reference tracking, full state feedback-LQR Control was then implemented. In each case of trial, different Q and R weighting matrices were applied to fine tune the pattern of robustness. Using different patterns of state gains (Q_x) in Q weighting matrix in the case of trolley model control clearly shows that the tracking performances vary according to the state gains Q_x . Fig. 3.29a shows, that, having the

state gains low to high would result in a bit of overshoot yet it achieves steady state in shorter time. However, it contradicts with the payload model control cases in which state gains Q_{θ} needs lower value in order to maintain lesser oscillation, Fig. 3.29b. In both control cases, the input state R is considered as 0.05 because assigning higher input value on the input weight has resulted in larger system overshoot.

2D Crane Trolley positions using Fullstate feedback-LQR,different Q&R,at Reference 3-m

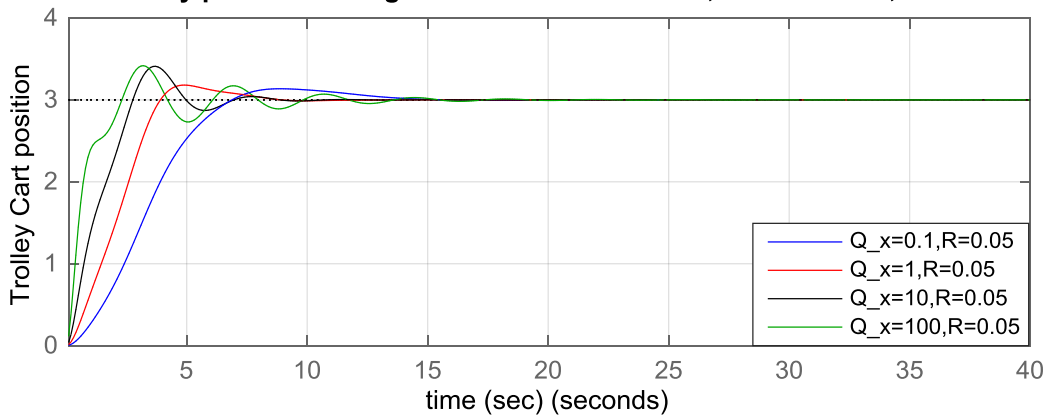


Figure 3.29a Full-state feedback-LQR Control Responses

Trolley Models with different QR

2D Crane Payload Swing using Fullstate feedback-LQR,different Q&R,at Reference 3-m

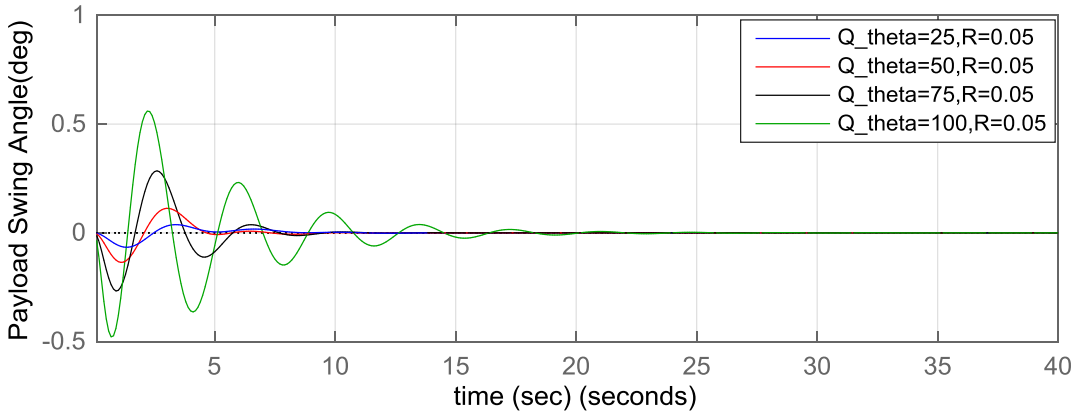


Figure 3.29b Full-state feedback-LQR Control Responses

Payload Models with different QR

The main objective of this work is to design Overhead Crane experimental model using SimMechanics Visualization aiming not only to achieve real crane-like model feature but also to implement robust, fast and practical controller. Furthermore, it would also be a major milestone to deliver better crane Modelling and control for the real operation instead of relying on lab-scaled model work. This development would close the gap between pure mathematical sketch with real time operation. Throughout this work, trolley translational motion with attached pendulum is designed which represents exact lab model measurements and features. Practical considerations, such

as: joints actuation, moment of inertia, and the gravity, are taken into account. In addition, friction effects are included in the design using a friction-compensation technique.

To accomplish the objective, collected simulation data are then used in linear least square system identification to produce predicted models. To have better estimated model, 7 past outputs and 7 past inputs dataset matrix Algorithm was designed to produce more models. Root Mean Square Errors checking has then been implemented to compare predicted models against the actual output.

Once the best fit linearized models have been established, those were implemented in reference input tracking-LQR controller design. The simulation result shows proposed control scheme guarantees both rapid damping of load swing and accurate control of crane position. Since the major milestone of physical Modelling using SimMechanics visualization was achieved, the future step is to design 3D Tower Crane physical model which would have Trolley translation, Jib rotation, and Hoist up/down motion. Furthermore, jib oscillation would be thoroughly analyzed to suppress payload swing during the operation.

3.4 3D Tower Crane Modelling using SimMechanics-Visualization

3D SimMechanics-Visualized Ideal model tower crane development is presented for future robust anti-sway control. First of all, actual tower crane data from Morrow (Liebherr 71 EC) was referred in designing computer-based ideal crane model and moment of inertia for each and every part of the crane structure were calculated to represent as a real crane. Secondly, wind disturbance model is designed in order to apply on the standing tall tower crane. Thirdly, payload swing instability due to Jib Tower/Hub Oscillations was analyzed by means of inertia moment derivation at pivot (Hub shoulder point), as well as by applying wind disturbance model. Finally, simulation results of higher payload swings (vs) jib oscillation due to wind disturbance are discussed as well as recommended for future nonlinear controller with oscillation compensation.

3.4.1 SimMechanics-Visualization Development

SimMechanics Visualization in Matlab comes with multi model features and it can navigate 3D design. In this Matlab mathematical computing, mechanical parts such as: sensors, actuators, bodies, joints, and signals inputs are available and flexible to design according to the system needs. In this research, tower crane model consists of

Hub, trolley cart, jib tower, steel cable, counterweight, and payload have been designed. The detail crane structure (Standing Hub : 22.2 m, Counter balance:10.3 m, and Tower Jib extension: 27.6 m) is based on, Liebherr 71 EC Morrow tower crane data. This computer based model exactly appears like real operating crane, can run for all three X-Y-Z directions (translation, rotation, and hoist up/down), most of all the simulations results are much reliable. Details design of tower crane are discussed in the following sections.

3.4.2 Liebherr 71 EC Morrow Crane Data Sheet

In order to realize the 3D visualization of the crane, Liebherr 71 EC Morrow crane, data was referred in Fig. 3.30 [64]. According to the crane fact sheet, it has got 4 levels of crane from small to large can be seen. However, this simmechanics mode development would only refer to the first stage crane level (22m Hub, 38m Jib). Details of the crane structure measurements such as: hook and load weight charts, rotation and translation drives info, and component list are available.

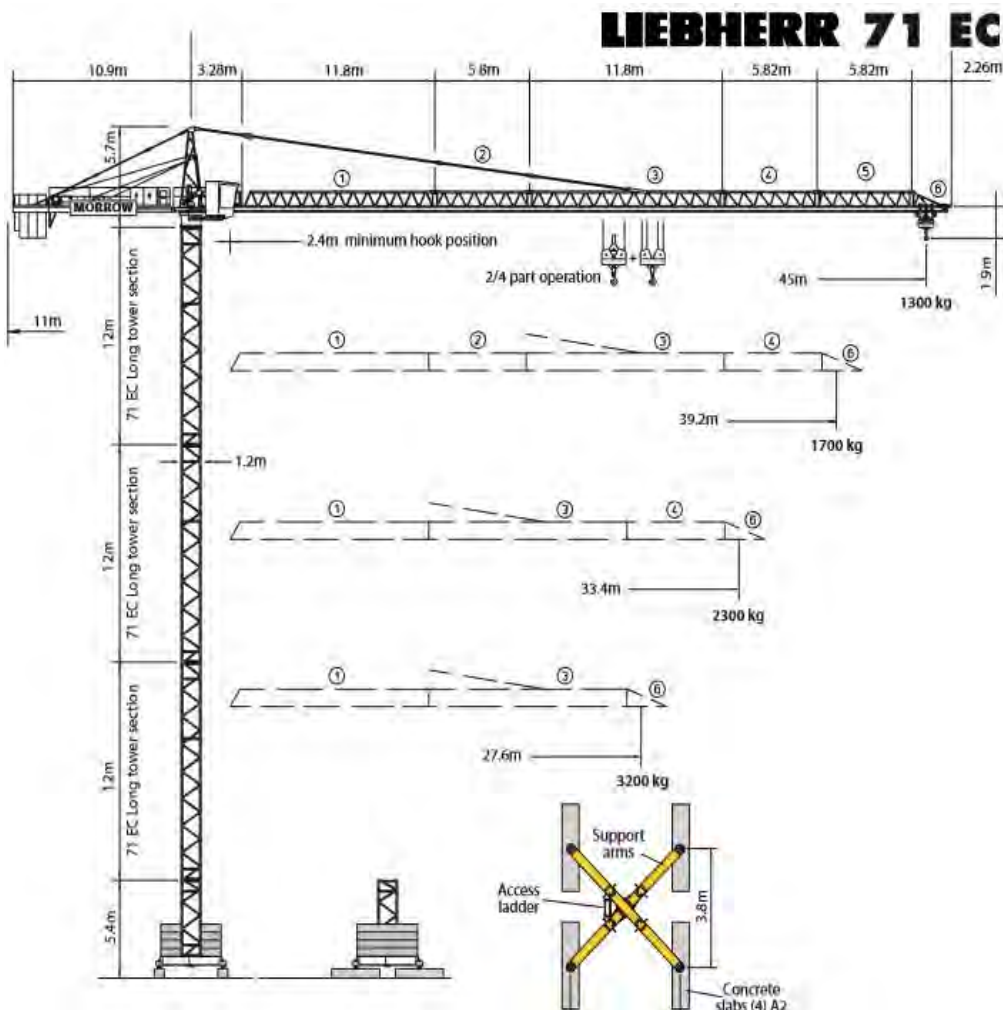


Figure 3.30 Libherr 71-EC Morrow Tower Crane Datasheet

3.4.3 Base Concrete Footing

For Tower crane base which consist of 4 concrete bases, 2 cross supports and main iron metal sheet, Fig. 3.31a and Fig. 3.31b. Four large concrete blocks with each 100 Kg have been firmly lock with cement ground and two metal cross links are then mounted on top of those blocks in order to stand still. Cement foundation details can be seen in (Appendix: Liebherr 71 EC). The metal sheet with 16-square meter is then fit on top of cross links so that the whole crane hub can be built further.

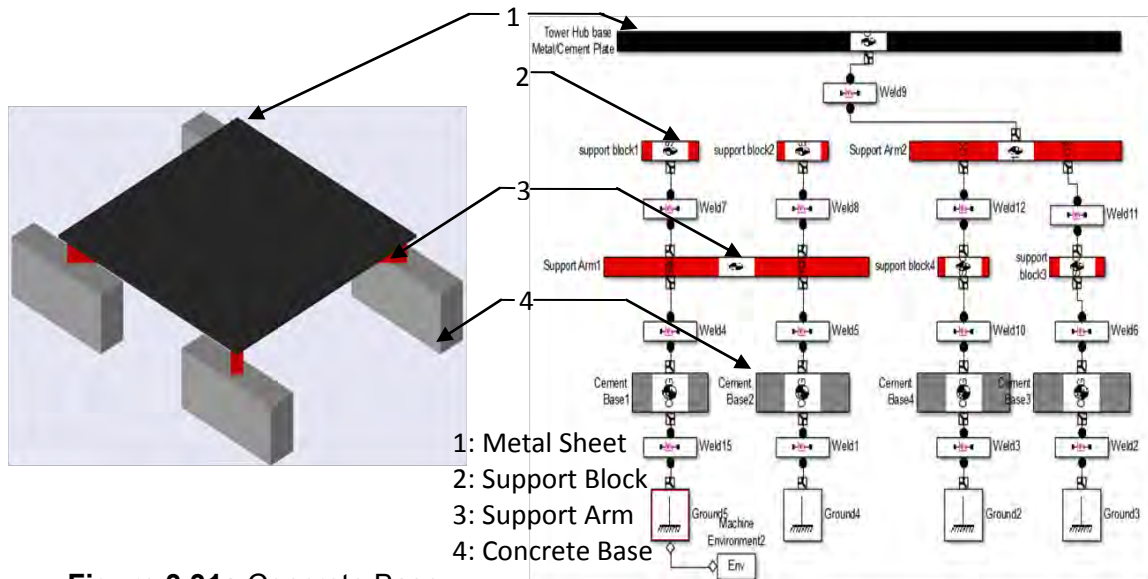


Figure 3.31a Concrete Base Visualization

Figure 3.31b Concrete Base SimMechanics

Mass, Measurements, and Moment of Inertia

To reflect the real representation of tower crane, actual parameters (dimension, mass, and moment of inertia) from Liebherr-71EC Morrow tower crane data has been applied in Fig. 3.32a. As the structures in concrete blocks are all rectangle form, Fig. 3.32b, rectangle-based moment of inertia calculation [$I_{xx} = \frac{1}{12}M(w^2 + h^2)$, $I_{yy} = \frac{1}{12}M(l^2 + h^2)$, $I_{zz} = \frac{1}{12}M(l^2 + w^2)$] is introduced. Details of each part mass-measurements-moment of inertia are presented in the Table (3.9) below.

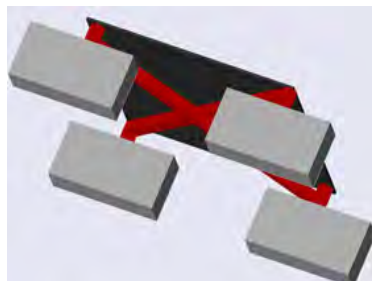


Figure 3.32a Concrete Footing in angle view

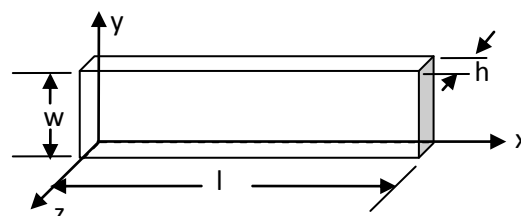


Figure 3.32b Measure style for Rectangle block

Parts	Mass (Kg)	Measurements (m)			Moment of Inertia (Kg m ²)		
		Length	Width	Height	I _{xx}	I _{yy}	I _{zz}
1	100	4	0.05	4.005	133.6877	267.0002	133.3542
2	2	0.2	0.2	0.2	0.0133	0.0133	0.0133
3	2	0.2	0.2	5.37	4.82	4.82	0.0133
4	100	2	1	0.5	10.417	35.417	41.667

Table 3.9 Concrete Footing in mass-measurements-moment of inertia

3.4.4 Base Section 4 m

After 1.4 m height of concrete footing is built up, the base frame 4 m needs to be mounted which would top up maximum of 5.4 m height long base section with 1.44 m². According to Morrow crane datasheet, the load of base is 2610 Kg to stand strong.

One Side of base Section 4 m

The following one side of base frame with 4 m long metal structure consists of right and left metal bar which are connected by top/bottom links as well as zigzag struts in Fig. 3.33a to be able to stand strong. Each block in figure Fig. 3.33b contains Mass, 3-D Measurements, and Moment of Inertia based-on Liebherr crane data. From total weight of 2610 Kg, distributed weight of each has been calculated as $\frac{2610}{4} = 609.86 \text{ Kg}$.

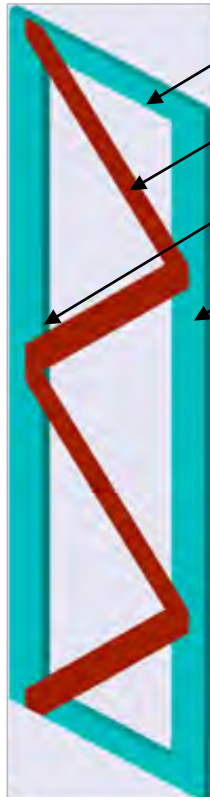


Figure 3.33a One side of Base Frame
4-m Visualization

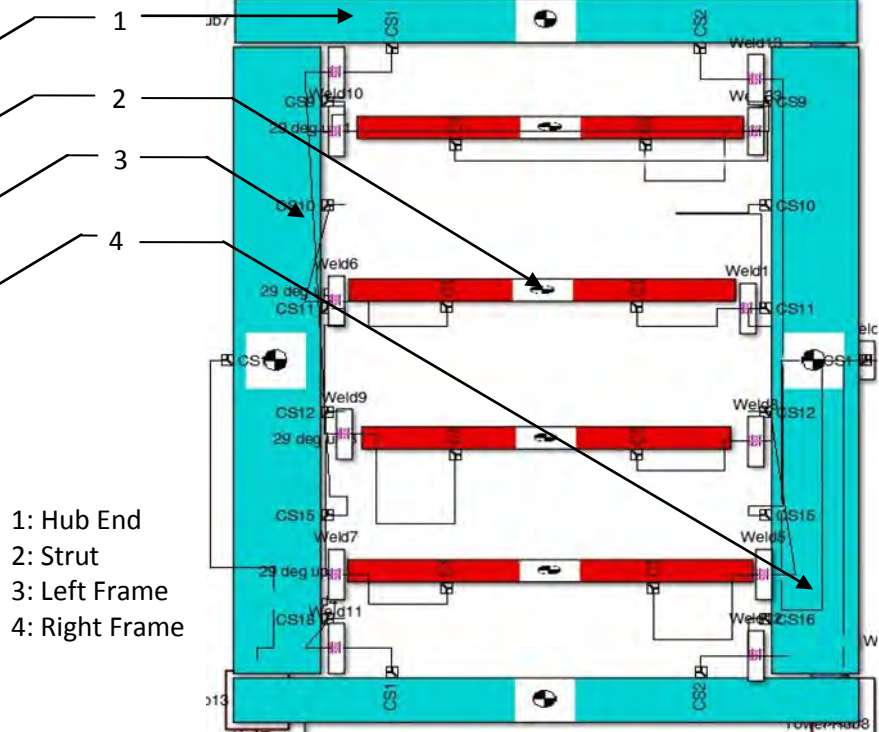


Figure 3.33b One side of Base Frame
4-m SimMechanics

Mass, Measurements, and Moment of Inertia

As this one side of the frame consists of 4 sub-structures with two Hub-ends, four Struts, one Left frame and one Right frame, mass of each part has been assigned accordingly. Details of each part mass-measurements-moment of inertia are presented in the Table (3.10) below.

$$M_t = [(2 \times M_1) + M_3 + (4 \times M_2) + M_4] = 609.86$$

Where

$$A = \frac{609.86}{4} - [(2 \times M_1) + (4 \times M_2)]$$

Let $M_1 = 15 \text{ Kg}, M_2 = 3.16 \text{ Kg}, M_3 = (65\% \text{ of } A)\text{Kg}, M_4 = (35\% \text{ of } A)\text{Kg}$

Parts	Mass (Kg)	Measaurements (m)			Moment of Inertia (Kg m^2)		
		Length	Width	Height	I_{xx}	I_{yy}	I_{zz}
1	15	0.8	0.15	0.05	0.0313	0.8031	0.8281
2	3.16	1.45	0.15	0.005	0.0059	0.5537	0.5596
3	396.4090	4	0.2	0.05	1.4039	528.6279	529.866
4	213.4510	4	0.15	0.05	0.4447	284.6458	285.0016

Table 3.10 one side of 4-m frame in mass-measurements-moment of inertia

Complete Design of Base Section 4 m

By combining 4 sides of simmechanics structure, Fig. 3.34b, the following Base section with final visualization Fig. 3.34a was achieved. This complete structure is 2610 Kg weight in total and its measurement is 1.44 m^2 .

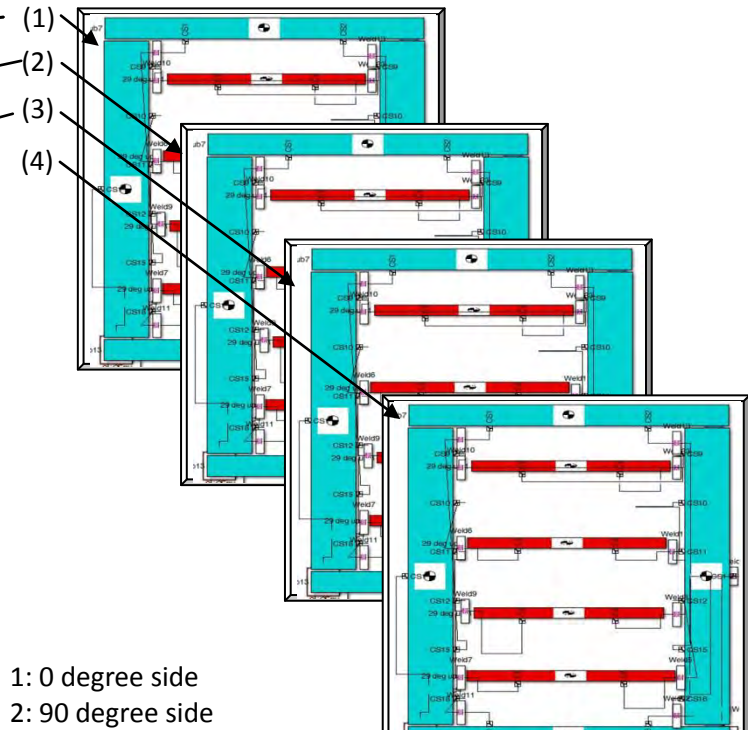
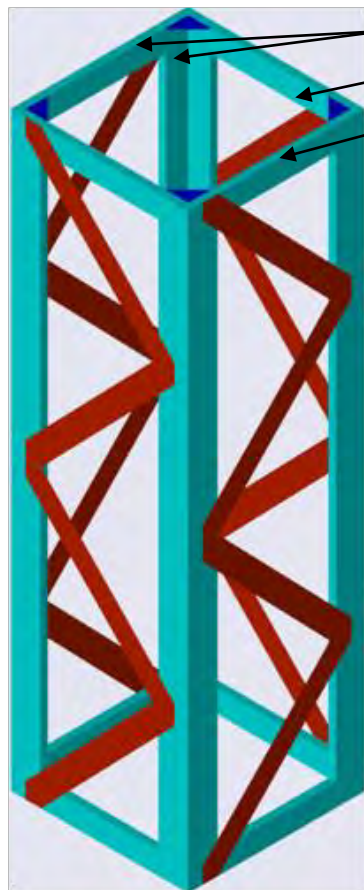


Figure 3.34a Base Frame Visualization

Figure 3.34b Base Frame SimMechanics

3.4.5 Hub Section 12 m

This Hub section has 12 m height with 1.44 m^2 . According to Morrow crane datasheet, this base would weigh 2610 Kg to stand the crane strong.

One Side of Hub Section 12 m

The following one side of base frame with 12 m long metal structure consists of right and left metal bar which are connected by top/bottom links as well as zigzag struts in Fig. 3.35a to be able to stand strong. Each block in figure Fig. 3.35b contains Mass, 3-D Measurements, and Moment of Inertia based-on Liebherr crane data. From total weight of 2610 Kg, distributed weight of each has been calculated as $\frac{2610}{4} = 609.86\text{ Kg}$.

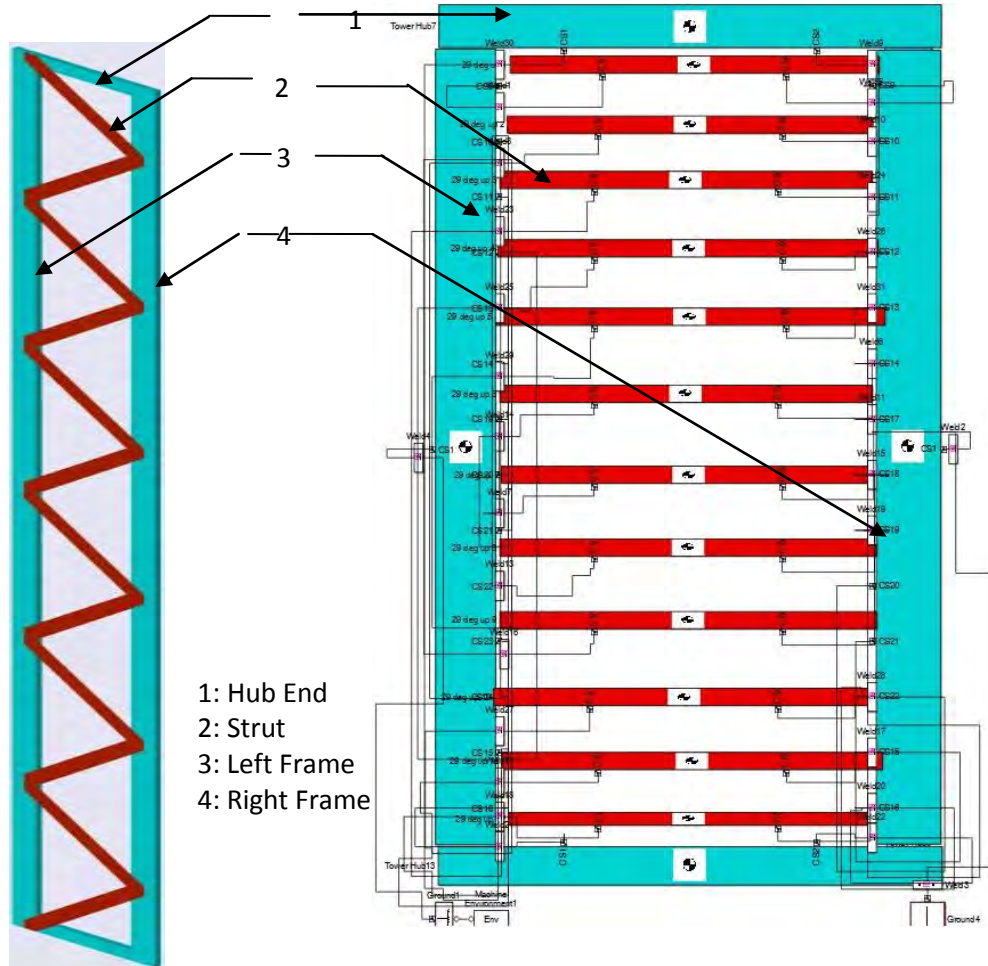


Figure 3.35b One side of Hub Frame 12-m SimMechanics

Mass, Measurements, and Moment of Inertia

As this one side of the frame consists of 4 sub-structures with two Hub-ends, twelve Struts, one Left frame and one Right frame, mass of each part has been assigned accordingly. Details of each part mass-measurements-moment of inertia are presented in the Table (3.11) below.

$$M_t = [(2 \times M_1) + M_3 + (12 \times M_2) + M_4] = 609.86$$

Where

$$A = \frac{609.86}{4} - [(2 \times M_1) + (12 \times M_2)]$$

Let $M_1 = 15 \text{ Kg}, M_2 = 3.16 \text{ Kg}, M_3 = (65\% \text{ of } A)\text{Kg}, M_4 = (35\% \text{ of } A)\text{Kg}$

Parts	Mass (Kg)	Measurements (m)			Moment of Inertia (Kg m^2)		
		Length	Width	Height	I_{xx}	I_{yy}	I_{zz}
1	15	0.8	0.15	0.05	0.0313	0.8031	0.8281
2	3.16	1.45	0.15	0.005	0.0059	0.5537	0.5596
3	355.3290	12	0.2	0.05	1.2585	4264.0	4265.1
4	191.3310	12	0.15	0.05	0.3986	2296.0	2296.3

Table 3.11 one side of 12-m frame in mass-measurements-moment of inertia

Complete Design of Hub Section 12 m

By combining 4 sides of simmechanics structure, Fig. 3.36b, the following Base section with final visualization Fig. 3.36a was achieved. This complete structure is 2610 Kg weight in total and its measurement is 1.44 m^2 .

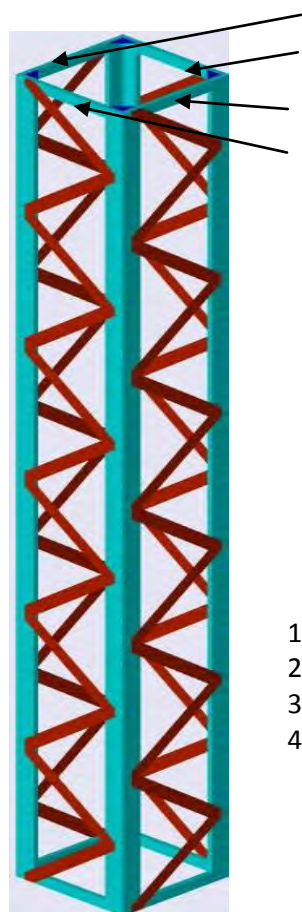


Figure 3.36a Hub Frame
12-m Visualization

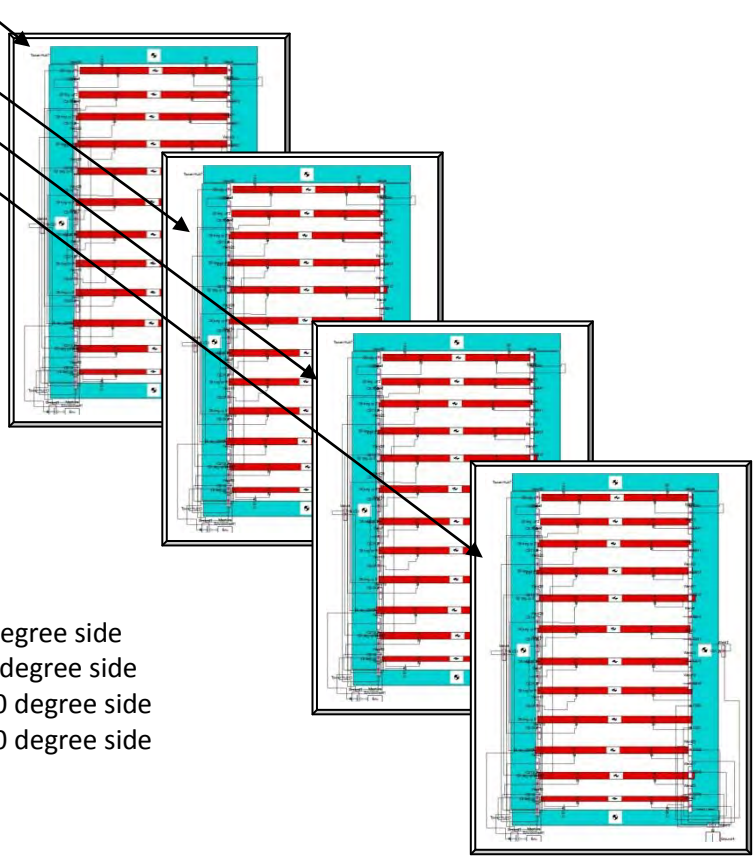


Figure 3.36b Hub Frame
12-m SimMechanics

3.4.6 Hub Section 6 m

This Hub section has 6 m height with 1.44 m^2 . According to Morrow crane datasheet, this base would weigh 1480 Kg to stand strong.

One Side of Hub Section 6 m

The following one side of base frame with 6 m long metal structure consists of right and left metal bar which are connected by top/bottom links as well as zigzag struts in Fig. 3.37a to be able to stand strong. Each block in figure Fig 3.37b contains Mass, 3-D Measurements, and Moment of Inertia based-on Liebherr crane data. From total weight of 1480 Kg, distributed weight of each has been calculated as $\frac{1480}{4} = 370\text{ Kg}$.

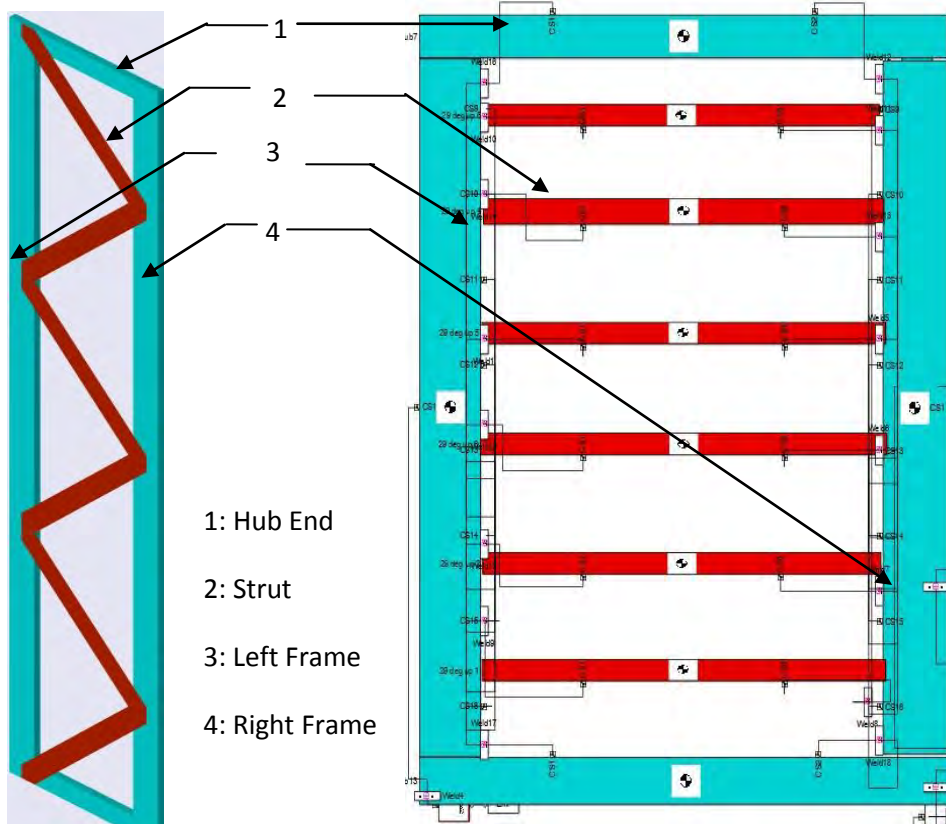


Figure 3.37a Hub Frame
6-m Visualization

Figure 3.37b Hub Frame
12-m SimMechanics

Mass, Measurements, and Moment of Inertia

As this one side of the frame consists of 4 sub-structures with two Hub-ends, six Struts, one Left frame and one Right frame, mass of each part has been assigned accordingly. Details of each part mass-measurements-moment of inertia are presented in the Table (3.12) below.

$$M_t = [(2 \times M_1) + M_3 + (6 \times M_2) + M_4] = 370$$

Where

$$A = \frac{370}{4} - [(2 \times M_1) + (6 \times M_2)]$$

Let $M_1 = 15 \text{ Kg}, M_2 = 3.16 \text{ Kg}, M_3 = (65\% \text{ of } A) \text{ Kg}, M_4 = (35\% \text{ of } A) \text{ Kg}$

Parts	Mass (Kg)	Measurements (m)			Moment of Inertia (Kg m^2)		
		Length	Width	Height	I_{xx}	I_{yy}	I_{zz}
1	15	0.8	0.15	0.05	0.0313	0.8031	0.8281
2	3.16	1.45	0.15	0.005	0.0059	0.5537	0.5596
3	208.676	6	0.2	0.05	0.7391	626.0715	626.7236
4	112.364	6	0.15	0.05	0.2341	337.1154	337.3027

Table 3.12 one side of 6-m frame in mass-measurements-moment of inertia

Complete Design of Hub Section 6 m

By combining 4 sides of SimMechanics structure, Fig. 3.38b, the following Base section with final visualization Fig. 3.38a was achieved. This complete structure is 1480 Kg weight in total and its measurement is 1.44 m^2 .

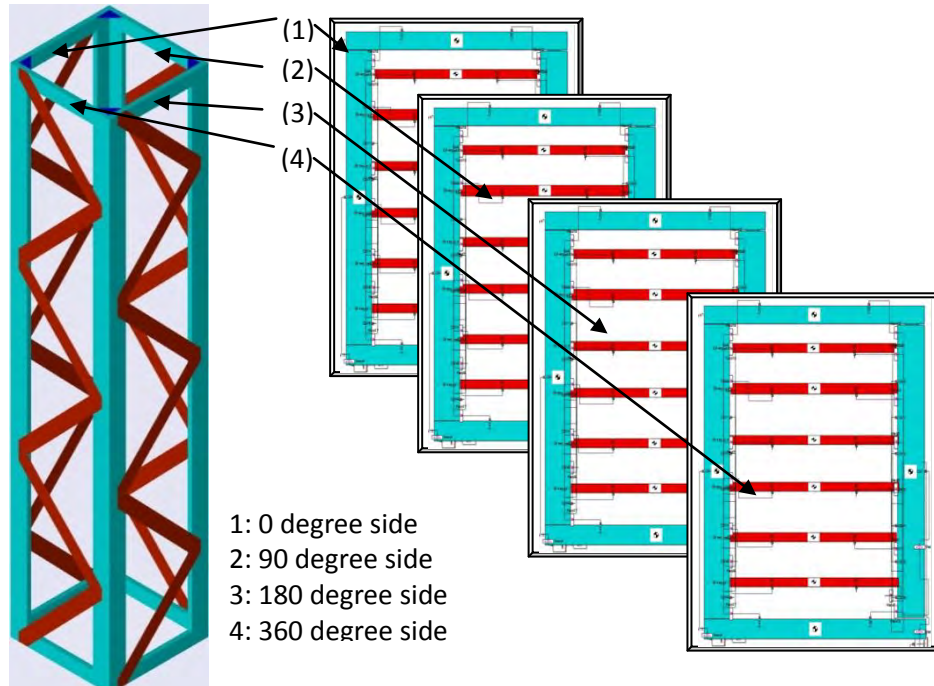


Figure 3.38a Hub Frame
6-m Visualization

Figure 3.38b Hub Frame
6-m SimMechanics

3.4.7 Tower Crane Hub with Concrete Base

According to Libherr (Morrow) crane data, the crane hub can be up to 41.4 m tall while crane tower jib can be extended up to (10.9 m counter length and 46.58m jib).

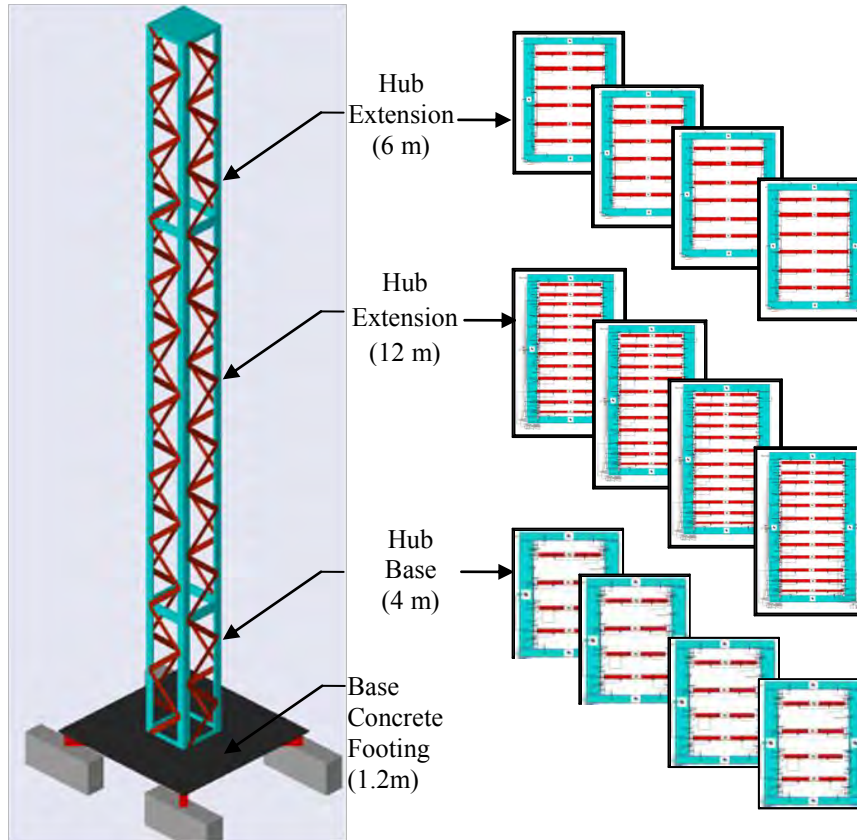


Figure 3.39a Visualized Tower Crane Hub 22.2 m

Figure 3.39b SimMechanics Tower Crane Hub 22.2 m

However, the crane can also be formed as (1) smaller design (Hub:22.2m, Tower:29.14m), (2) medium design (Hub:28.2, Tower:34.94m), (3) higher medium design (Hub:34.2, Tower:40.74m), and (4) highest design (Hub:41.4, Tower:46.58m). In this research, stage (1) implementation Fig. 3.39b has been established which comprises base frame 4.2-m, base section 12-m, and hub section 6-m. Final simmechanis design and visualized model as shown in Fig. 3.39a.

3.4.8 Slew Assembly

Slew Assembly consists of Tower Top with 4 steel frames, cab with platform, and complete slewing assembly. Each part mass and measurements from Morrow datasheet has been displayed below in Fig. 3.40.

		Length	Width	Height	Kg
Cab with platform		3.1	1.3	2.2	610
Slewing assembly complete		4.2	1.8	1.97	3280
Tower top		4.55	1.0	1.35	575

Figure 3.40 Slewing Assembly from Morrow data sheet

According to the real crane, tower top is sitting on top of the whole slewing assembly in Fig. 3.41a which is at the hub top where cabin operator handles the crane operation. The following section shows the detail structure of each part, in Fig. 3.41b.

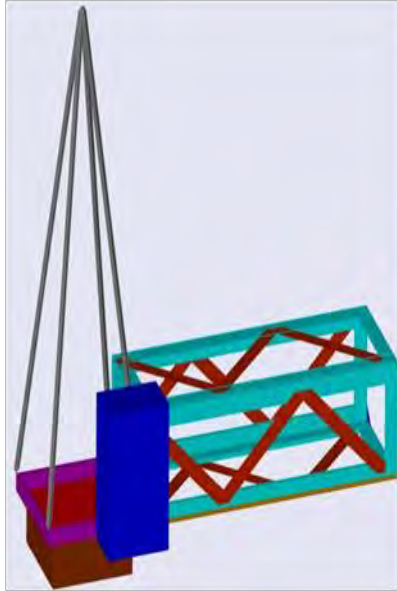


Figure 3.41a Visualized Slewing Assembly

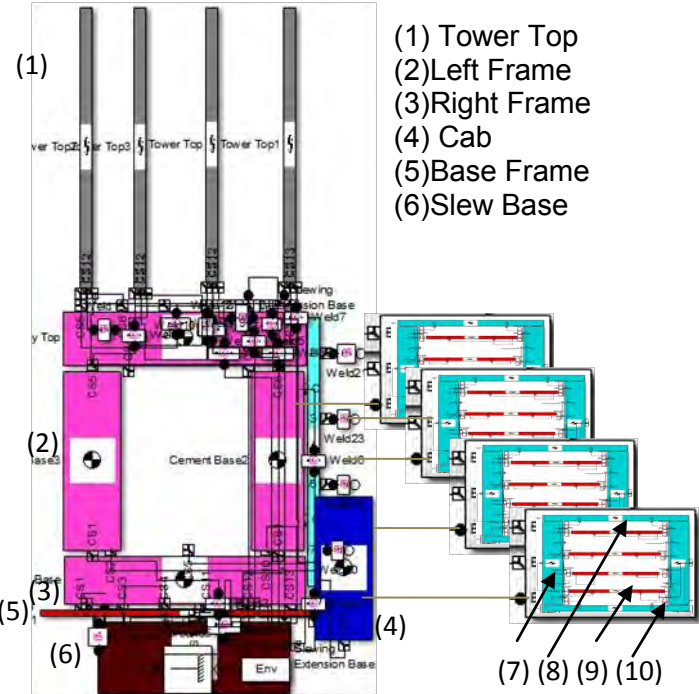


Figure 3.41b SimMechanics Slewing Assembly

Mass, Measurements, and Moment of Inertia

Each part of Slew Assembly mass-measurements-moment of inertia are assigned based on Morrow and the detail is in the Table (3.13) below where

$$\text{Slew Assembly} = \text{Tower Top} + \text{Cab with platform} + \text{Slew Base}$$

$$= 575 + 610 + (3280 - 696) \text{ Kg}$$

$$\text{Each steel frame} = \frac{575}{4} = 143.75 \text{ Kg}$$

$$\text{Cab with platform} = \text{Short platform} * 2 + \text{Long platform} * 2 + \text{Cab}$$

$$= 112 * 2 + 112 * 2 + 112$$

$$\text{Slewing Assembly} = \text{Slew Base} + \text{Right Extension} = 2584 + 696 = 3280 \text{ Kg}$$

Parts	Mass (Kg)	Measaurements (m)			Moment of Inertia (Kg m^2)		
		Length	Width	Height	I_{xx}	I_{yy}	I_{zz}
1	143.75	0.05	5	0.05	299.5091	0.0599	299.5091
2	112	0.17	1.2	0.0250	13.4458	0.2756	13.7097
3	112	1.2	1.2	0.0050	13.4402	13.4402	26.8800
4	50	1.9	1.3	2.2	27.2083	35.2083	22.083
5	112	1.2	1.2	0.0050	13.4402	13.4402	26.8800
6	2584	1.00	0.500	1.00	269.200	430.00	269.200

Table 3.13 Slew Assembly in mass-measurements-moment of inertia

Slew Right extension 3.2 m

Slew right extension is part of complete slew assembly and it has 696 Kg mass. One side of the extension consists of 4 sub-structures with two Hub-ends, three Struts, one Left frame and one Right frame, mass of each part has been assigned accordingly. Details of each part mass-measurements-moment of inertia are presented in the Table (3.14) below.

$$M_t = [(2 \times M_1) + M_2 + (3 \times M_3) + M_4] = 696 \text{ Kg}$$

Where

$$A = \frac{696}{4} - [(2 \times M_1) + (3 \times M_3)]$$

Let

$$M_1 = 15 \text{ Kg}, M_3 = 3.16 \text{ Kg}, M_2 = (65\% \text{ of } A) \text{ Kg}, M_4 = (35\% \text{ of } A) \text{ Kg}$$

Parts	Mass (Kg)	Measurements (m)			Moment of Inertia (Kg m^2)		
		Length	Width	Height	I_{xx}	I_{yy}	I_{zz}
7	15	0.8	0.15	0.05	0.0313	0.8031	0.8281
8	87.438	3.2	0.2	0.05	0.3097	74.6320	74.9052
9	3.16	1.45	0.15	0.005	0.0059	0.5537	0.5596
10	47.082	3.2	0.12	0.05	0.0981	40.1864	40.2649

Table 3.14 Slew right extension in mass-measurements-moment of inertia

3.4.9 Combined Counterjib

Counter Jib plays vital role in stabilizing tower crane operation. According to the moment calculation at pivot (joint between tower and hub), counter load tops were initially added to achieve equilibrium. Since Libherr Morrow crane uses maximum allowable load of 3000 Kg, additional counter load bottoms were attached in order to counter balance the crane. Initial calculation shows, by adding counter load bottoms would produce reasonable jib's oscillation. Counter Jib consists of slewing assembly with cabin, counter jib frame with loads top/bottom, adaptors, and Jib right attached as shown in Morrow data sheet Fig. 3.42. Each part parameters mass, measurements and moment of inertia have also been provided in the table Table (3.15) below.

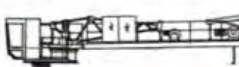
		Length	Width	Height	Kg
Combined tower top, cab and counterjib		12.0	2.44	2.38	9000
Counterjib complete L1		10.2	1.9	2.32	4070
Counterjib complete L2		8.0	1.9	2.32	3490

Figure 3.42 Complete Counter Jib shown in Morrow data sheet

Mass, Measurements, and Moment of Inertia

The whole SimMechanics design of combined counterjib mass is 9000 Kg which includes cab with platform, tower top, two adapters, three counterload top, and counterload bottom are presented in Fig. 3.43a.

$$\begin{aligned}
 M_{\text{combined_counterjib}} &= \text{cab with platform} + \text{tower top} + \text{counterjib} + (\text{Adapter} * 2) \\
 9000 &= 610 + 575 + 4070 + \text{Adapter} \\
 \text{Adapters} &= 3745, \\
 \text{Each Adapter} &= \frac{3745}{2} = 1872.5 \text{ Kg}
 \end{aligned}$$

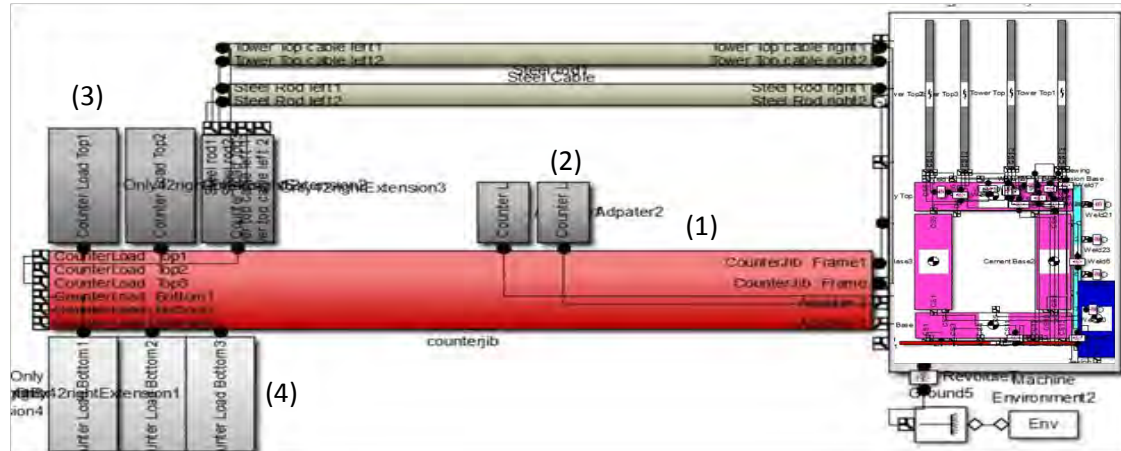


Figure 3.43a Combined Counter-jib SimMechanics design

To reach equilibrium of the crane, counterload bottom is assigned 3000 Kg mass to balance maximum allowable carrying load however the crane still needs to add counterload (1789 Kg) on top of the jib in order to stabilize standalone crane. The combined counter-jib visualized form can be viewed in Fig. 3.43b. Counterload top value has been obtained from crane equilibrium calculation in the next chapter, vibration impact analysis.

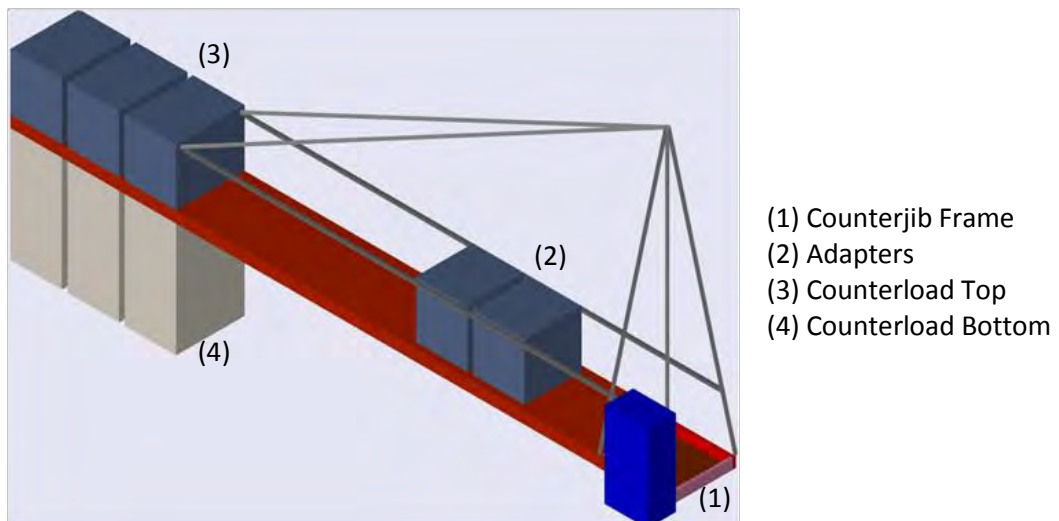


Figure 3.43b Combined Counter-jib visualized-view

Based on available masses and measurements from Morrow table, Table (3.15) provides details as follow:

Parts	Mass (Kg)	Measuarements (m)			Moment of Inertia (Kg m^2)		
		Length	Width	Height	I_{xx}	I_{yy}	I_{zz}
1	4070	0.2	10.3	1.2	36471	501.9667	35996
2	1872.5	1	1	1	312.0833	312.0833	312.0833
3	596.333	1	1	1.2	121.2544	121.2544	99.3889
4	1000	2	1	1.2	203.3	453.3	416.7

Table 3.15 Combined Counter-jib mass-measurements-moment of inertia

3.4.10 Tower Jib Butt Extension

Tower Jib extension is a combination of 12 tower section1, 12 m tower section2, and Jib tip(end: 2.26m). The following section would explain the detail structure from one side of 12m tower section to complete design of 12m tower section followed by the whole 12+12+2.26 m long extension.

One side of Tower Jib Extension (12m)

In this 1 side of tower section 12m, there are 2 ends, 2 metal frames, and 24 struts in Fig. 3.44a and Fig. 3.44b as mentioned below.

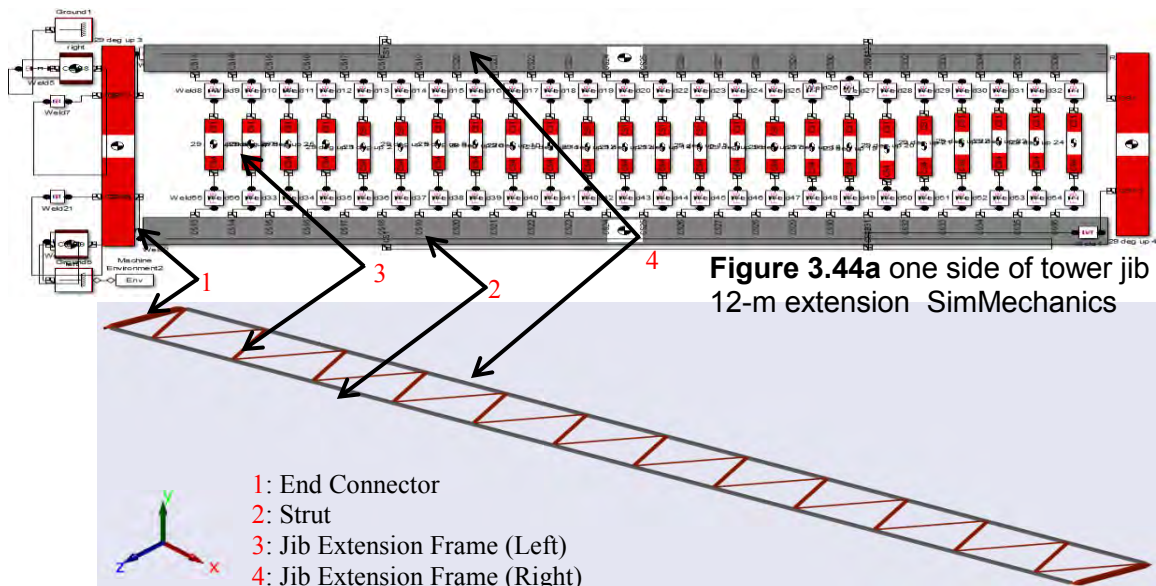


Figure 3.44b one side of tower jib 12-m extension Visualization

Mass, Measurements, and Moment of Inertia

$$M_{Jib_butt} = (Jib\ Extension\ Frame * 2) + (End\ Connector * 2) + (Strut * 24)$$

$$A = \frac{1300}{3} - [(2 \times M_1) + (24 \times M_2)]$$

$$\text{Let } M_1 = 15 \text{ Kg}, M_2 = 3.16 \text{ Kg}, M_3 = \frac{A}{2} \text{ Kg}, M_4 = \frac{A}{2} \text{ Kg}$$

Parts	Mass (Kg)	Measurements (m)			Moment of Inertia (Kg m^2)		
		Length	Width	Height	I_{xx}	I_{yy}	I_{zz}
1	15	0.05	0.97	0.05	1.1792	0.0063	1.1792
2	3.16	0.05	1.05	0.0005	0.2903	0.0007	0.2910
3	163.7	0.05	12	0.05	1965.0	0.0682	1965.0
4	163.7	0.05	12	0.05	1965.0	0.0682	1965.0

Table 3.16 tower jib 12-m extension mass-measurements-moment of inertia

3.4.11 Complete Tower Jib Extension (12m+12m+2.31m)

Each of one side jib is placed at 0 degree, 60 degree and -60 degree, and interconnecting each other to make the jib strong so that it can be able to hold the trolley run and load swing. The following complete tower jib includes two 12m long jib extensions and 2.31 m long jip tip at the end as shown in Fig. 3.45. After that, trolley rail would be attached right under the complete long jib extension and mount the trolley cart with pendulum attached.

$$\begin{aligned} M_{Jib_butt_complete} &= Jib\ Extension\ Frame1 + Jib\ Extension\ Frame2 + Jib\ End \\ &= 1300 + 1300 + 125 \text{ Kg} \end{aligned}$$

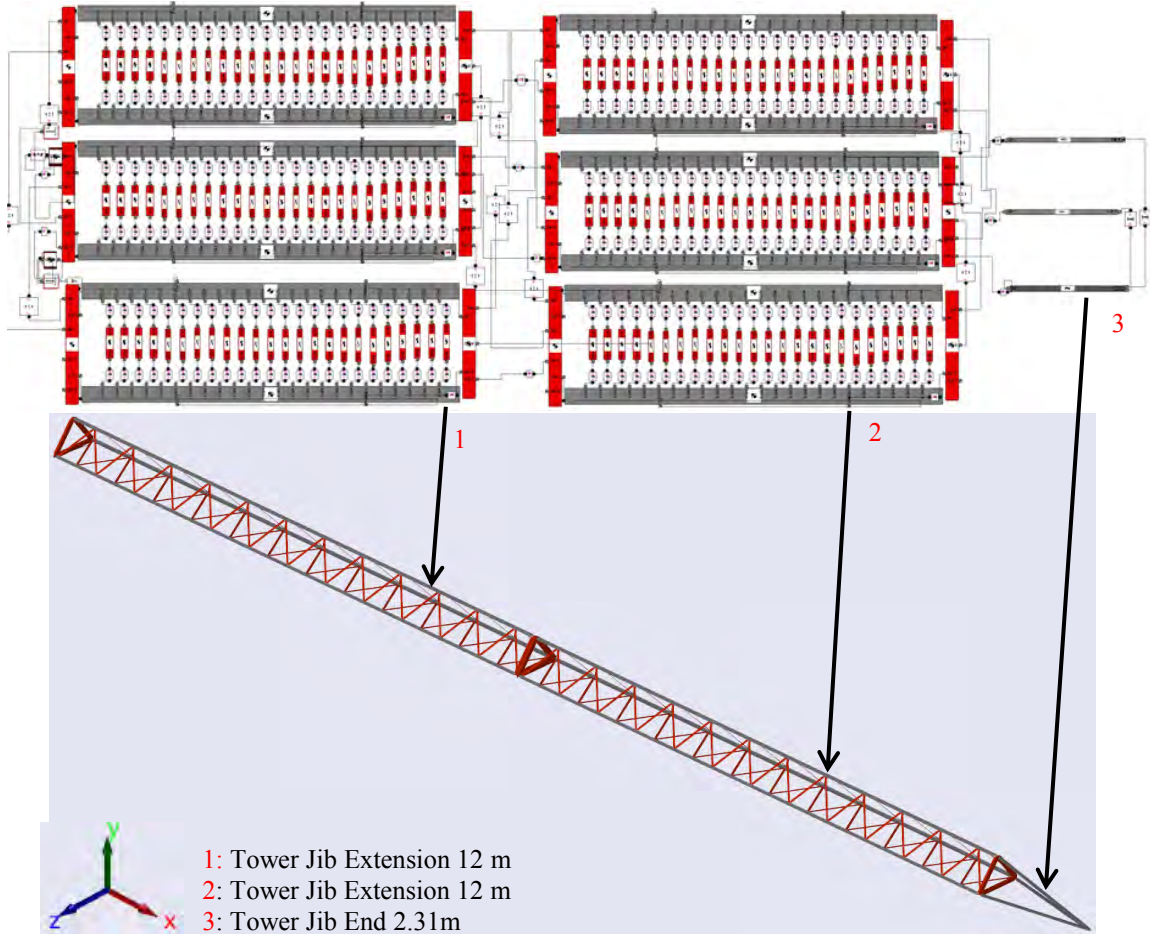


Figure 3.45 SimMechanics Visualized tower jib extension (12+12+2.31m)

3.4.12 Trolley Rail-Cart-attached Load

Trolley rail-cart-attached load design, there are 4 support rail ends with 24 m long rails attached which are mounted right below the long tower jib. On top of the rails, trolley cart ($0.96 \times 0.05 \times 0.3$ measurements and 5 Kg weight) has been mounted. Two flexible steel cables with specific moment of inertia were then attached under the trolley cart while the 340 Kg hook was attached at the other end of the cable followed by the load. The following SimMechanics structure in Fig. 3.46a is designed base-on real tower crane data and the visualized model in Fig. 3.46b was then obtained upon running the system. Steel cable is considered as cylindrical form and so the detail of mass, measurements and moment of inertia Table (3.17) can be predicted as follow.

$$M2 = 10 \text{ Kg}, l = 0. w = 18\text{m}, h = 0, I_{xx} = I_{zz} = I_{yy} = \frac{1}{12} mw^2 = 1.1792$$

Moment of Inertia for tube box: $M = 1000 \text{ Kg}, b = 2 \text{ m}, b = 2 \text{ m}, b = 2\text{m}$

$$I_{xx} = I_{yy} = I_{zz} = \frac{2}{3} Mb^2$$

$$I_{xy} = I_{yx} = I_{zy} = I_{yz} = I_{zx} = I_{xz} = \frac{1}{4} Mb^2$$

$$I = \begin{bmatrix} I_{xx} & -I_{xy} & -I_{xz} \\ -I_{yx} & I_{yy} & -I_{yz} \\ -I_{zx} & -I_{zy} & I_{zz} \end{bmatrix} = \begin{bmatrix} \frac{2}{3}Mb^2 & -\frac{1}{4}Mb^2 & -\frac{1}{4}Mb^2 \\ -\frac{1}{4}Mb^2 & \frac{2}{3}Mb^2 & -\frac{1}{4}Mb^2 \\ -\frac{1}{4}Mb^2 & -\frac{1}{4}Mb^2 & \frac{2}{3}Mb^2 \end{bmatrix}$$

Parts	Mass (Kg)	Measaurements (m)			Moment of Inertia (Kg m^2)		
		Length	Width	Height	I_{xx}	I_{yy}	I_{zz}
1	None						
2	15	0.05	0.97	0.05	1.1792	0.0063	1.1792
3	163.7462	0.05	24	0.05	15720	0.1365	15720
4	5	0.5	0.97	0.01	0.3921	0.1042	0.4962
5	10	0	18	0	1.1792	1.1792	1.1792
6	340	0.5	0.3	0.05	2.6208	7.1542	9.63

Table 3.17 Trolley rail-cart mass-measurements-moment of inertia

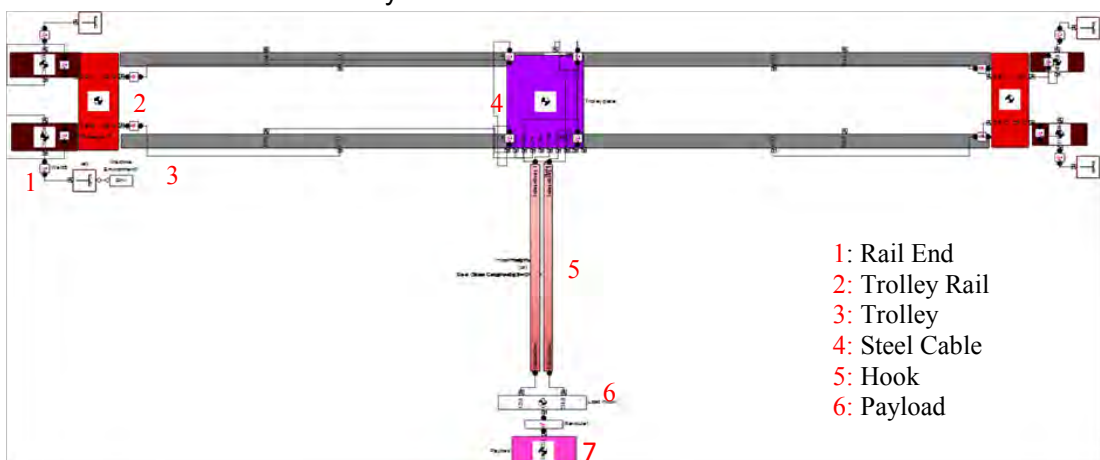


Figure 3.46a SimMechanics trolley rail cart-attached load

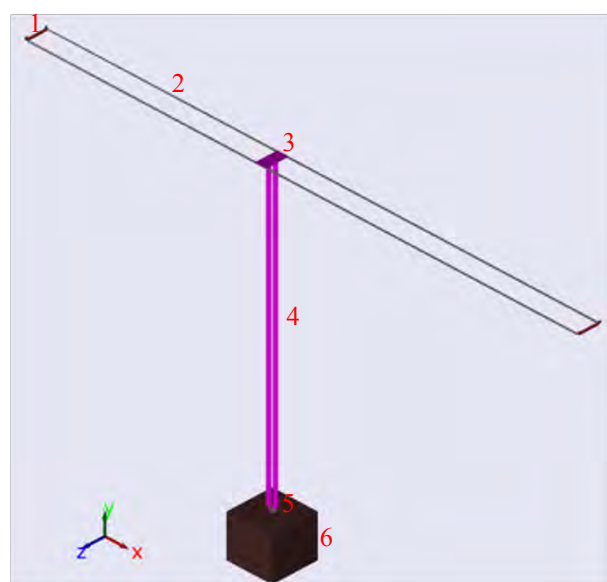


Figure 3.46b Visualised trolley rail cart-attached load

3.4.13 Complete Ideal Tower Crane SimMechanics Visualized Model

After designing the above-mentioned steps starting from Concrete footing, base, Hubs, Counter Jib, Slewing Assembly, Tower Jib Extensions, and Trolley cart with attached load, the following SimMechanics visualized Ideal Tower crane model has been achieved. Using technical computing software Matlab SimMechanics, designing with detail parameters, and applying each part mass/moment of inertia, would produce reliable crane operating data through which suitable controller can be designed. Adding the sensors where ever necessary in this flexible ideal model provides not only the running data but also the operating defects which can be taken into account for further improvement. Currently, sensors for (trolley position, Tower rotation, Tower oscillation, load swing, load position, and Hub top oscillation) have been mounted and the details are in Fig. 3.47 Fig. 3.48.

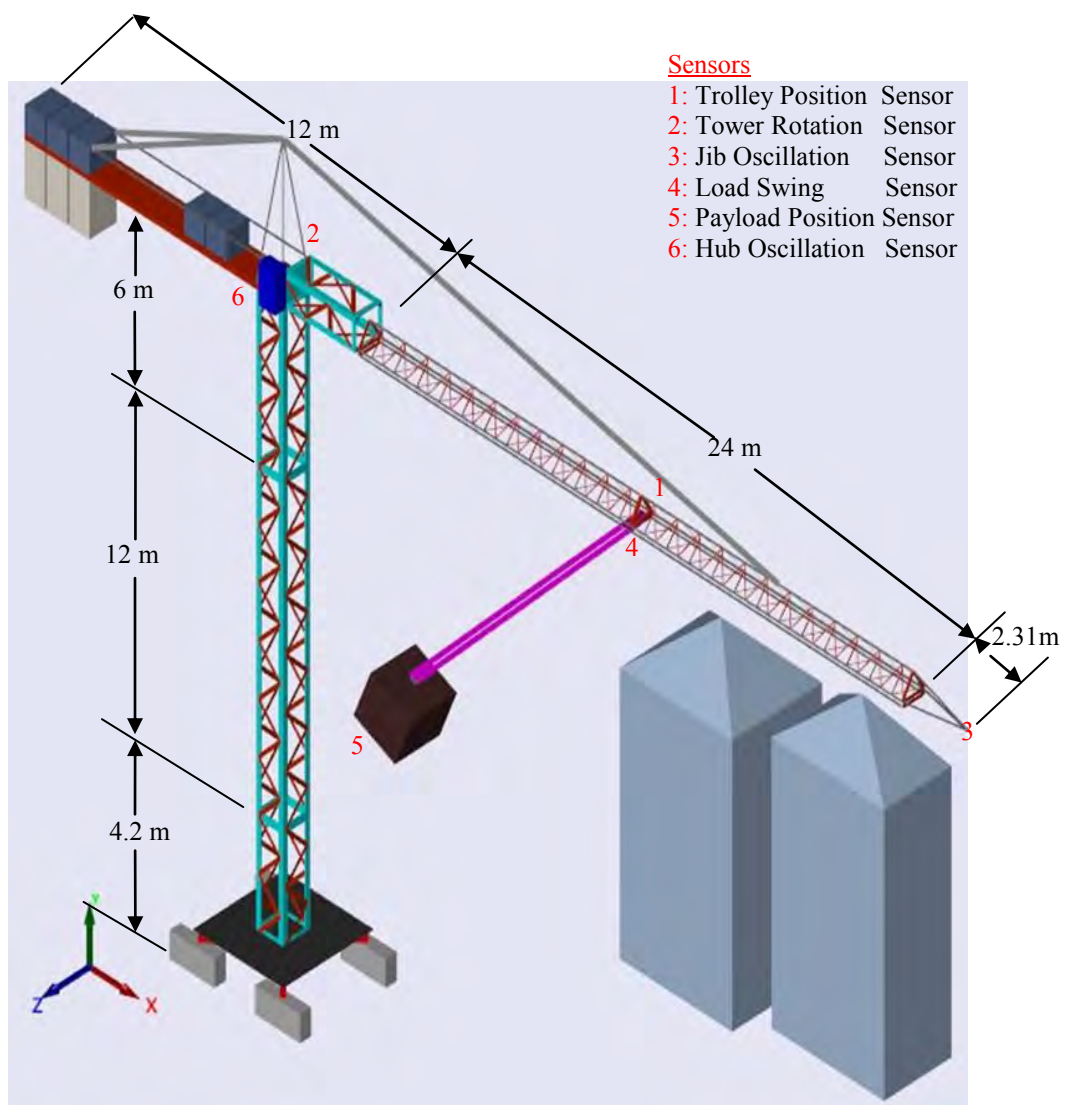


Figure 3.47 Visualized Tower Crane Model

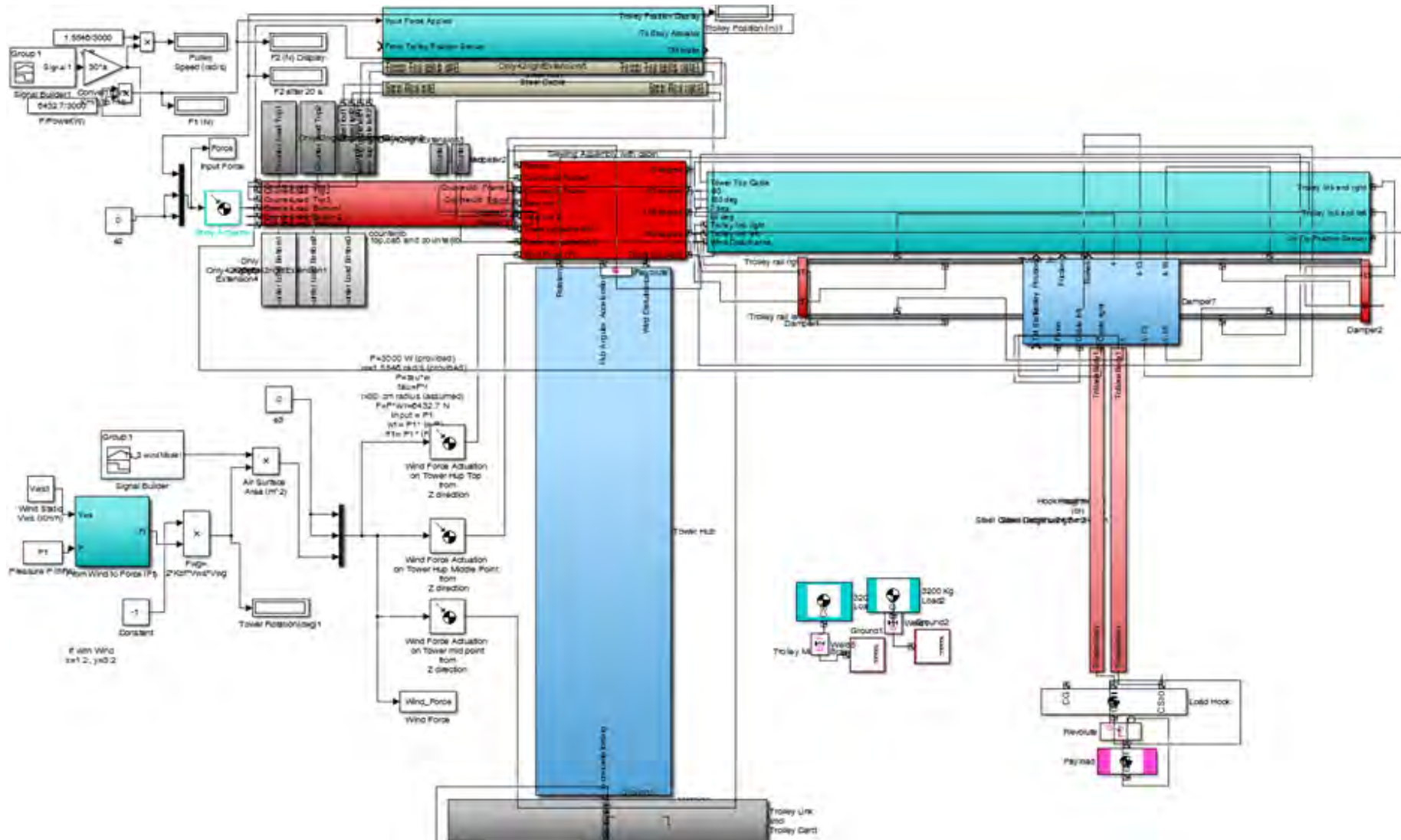


Figure 3.48 Visualized Tower Crane Model
93

3.4.14 Input Trolley Drive for Translational Motion

In order to run trolley cart back and forth translation, the certain force has to be applied on the cart. According to Liebherr 71 EC Morrow crane data sheet, 14.875 rpm and maximum 3 kW are used for the crane as shown in Fig. 3.49. Therefore, using those data, the following derivation has been carried out to develop Power-Speed-Force relationship in Fig. 3.49. Radius of driving pulley connected to the motor is considered as 30 cm.



Figure 3.49 Libherr Crane Drive Info and its motor with pulley attached

$$\text{For Translation: Pulling Force, } F = \frac{P}{r \cdot \omega} = \frac{3000 \text{ W}}{0.3 \cdot 14.845 \text{ rpm}} = 6432.7 \text{ N (Maximum)}$$

$$F_1 = P_1 * \frac{F}{P}$$

From provided parameters: 14.845 rpm, maximum Power 3000 W, and assumed pulley radius 30 cm, maximum Force is calculated as 6432.7 N. By varying input power, pulley speeds would change and so does applied force. In this research, range of input power such as: 1000 W, 2000W and 3000W have been used in all simulations for comparison purpose.

3.4.15 Trolley Brake and Friction Design

In real tower crane operation, the operator uses manual joy stick to run the trolley and hold the brake to stop around desired positions. For this ideal model, the brake is designed from modified damper without spring. Initial parameters such as: damping force and desired trolley stop position are required for the brake system to compare instantly and apply the force upon reaching the position. Four frictional dampers are added as constrain actuators and two brakes are placed in between trolley and jib rail while 3N friction forces are also applied in trolley's corners in Fig.

3.50. For 20 m translational motion, trolley stops around desired location however the positions may elapse due to open loop system without control.

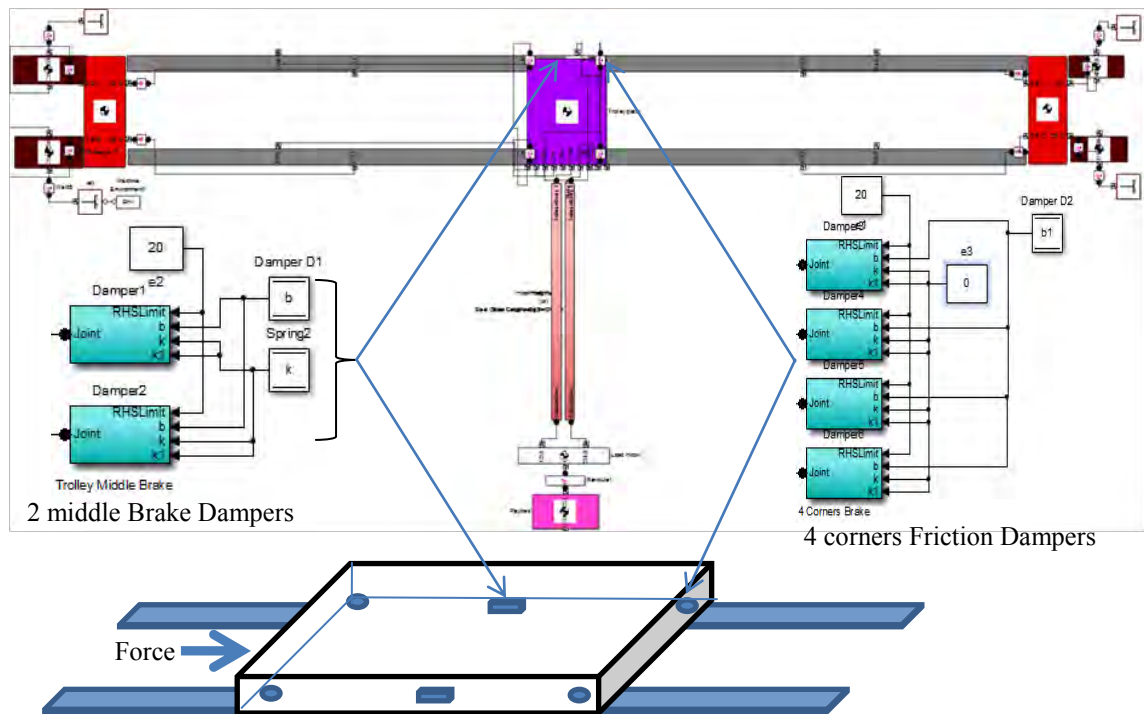


Figure 3.50 Frictions and Brakes Dampers Design

3.4.16 Input Tower Rotation Drive and Constrain Actuator

For Tower rotation, Liebherr 71 EC Morrow crane data sheet provides 0.85 rpm with maximum 6.3 kW for input power in Fig. 3.51. Therefore, using those data, the following derivation has been carried out to develop Power-Speed-Force relationship. Again, driving pulley radius is considered as 50 cm. From provided parameters: 0.85 rpm, maximum Power 6300 W, and assumed pulley radius 50 cm, maximum Force is calculated as 141,573 N (141.573 kN). By varying input power from 1000 W-6300W, Tower rotation speeds would change and so does applied force. A constrain actuator has also been added to the rotation actuator to limit the tower rotation over reference input. Though maximum power requirement for this crane is not more 7 kW, the power drive used in this system uses 20 kW, 40 kVA, 3-Phase, and 50 Hz. For Rotation: rotational torque is:

$$\tau = \frac{P}{\omega} = \frac{6300}{0.089} = 70786.5 \text{ Nm (Maximum)}, \quad \tau_1 = P_1 * \frac{\tau}{P} \text{ rad/s}$$

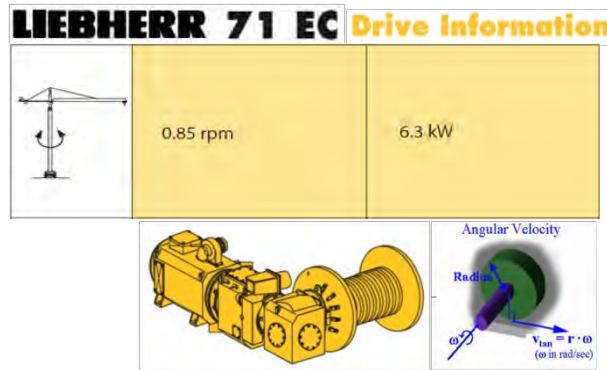


Figure 3.51 Libherr Crane Drive Info and its motor with pulley attached

3.5 Conclusion

This chapter discusses about the detail design of 3D SimMechanics-visualized modelling based-on Liebherr-71EC Morrow crane specifications. Starting from the concrete base footing, hub-base 4-m, hub-section 12-m, hub-section 6-m, slew assembly, combined counter-jib, slew right extension, jib tower 24-m, and trolley rail with payload attached are all presented above. All the necessary input power drives have been derived as well. The complete visualized crane model is presented in Fig. 3.47. The next chapter would discuss about the linear modelling of this developed tower crane.

Chapter (4)

Tower Vibration Impact on Payload Swing Analysis

4.0 Crane Vibration Analysis

Normally, researchers have to develop Mathematical Model from the sketch/prototype and develop controllers since it would be hard to access real operating crane. Therefore, those developed controllers would have been impractical in real time. Modelling of the system plays vital role In order to have practical controller. This research developed ideal tower crane model which is based-on real crane “Leibherr 71 Morrow Crane” [64]. The flexibility of this modelling approach appears to become major milestone for the crane research area such as such as, tower rotation, trolley translation, load swing control, and safety issues. The following tower/jib oscillation analysis based-on the developed ideal crane model, shows provides the clues of why and how jib oscillations appear especially in the standing tall tower crane. Obtaining the essential jib oscillation analysis, the future best suited controller development could be designed to maximize the crane operating capabilities such as: rotation, translation, hoist up/down in maximum speed, keep load swing minimum, operate in a shortest time, and run in a safest way. To compare jib oscillations, rigid structure model has also been developed and carried out the following analysis: Moment of Inertia Calculation, SimMechanics Rigid Model Translation, SimMechanics Ideal Model Translation, SimMechanics Ideal Model Rotation, and Applied Wind Disturbance.

4.1 Jib Moment Calculation

Before calculating jib moment at pivot joint a, crane equilibrium needs to be established by taking the moment at pivot point a. The reason is to make the crane stand still before adding any payload.

4.1.1 Equilibrium Establishment

In this study, crane equilibrium would be established first before adding load and counter weight [65]. To achieve equilibrium, Moment at pivot A in Fig. 4.1 has to be

zero so that tower jib can stand still. After obtaining crane's parameters such as: mass, weight, force, and measurements, then counter weight is identified at equilibrium position. It is very much essential to establish Equilibrium, otherwise there is a higher chance of crane collapse even before carrying the load or operating. After calculating all required forces, Weight of Jib F_{jib} is placed at the point of attached tower top cable. From derivation, the weight and mass of counter jib are then established eventually achieving equilibrium in Fig. 4.2. On the jib tower side, Mass of jib consists of operator cab, jib's extensions, half of slewing machine, and slew right extension. On counter jib side, Mass of counter jib consists of adapters, counterweight, counter jib, and half of slewing machine. Initially, Mass of counterweight has been unknown. By taking the moment M_a while placing F_{jib} at 21.6m of the jib side and $F_{counterjib}$ at the end of counterjib, $F_{counterjib}$ was then established followed by Mass of counter weight, $M_{counterweight}$ (1789 Kg), which needs to be added at counter jib to achieve crane's equilibrium.

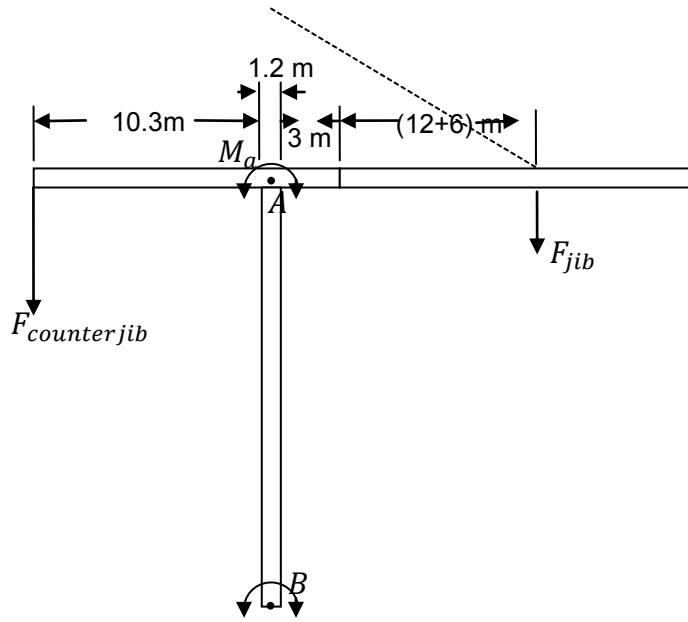


Figure 4.1 Identify Counter weight at Crane's equilibrium position

Left Side

$$\begin{aligned}
 M_{combined_counterjib} &= 9000, \\
 M_{combined_counterjib} &= cap + tower\ top + counterjib + adapter \\
 9000 &= 610 + 575 + 4070 + adapter \\
 adapter &= 3745 \\
 M_{slew} &= 3280 \\
 M_{slew} &= M_{slewcentre} + M_{slewrightextension} \\
 M_{slew} &= 2540 + 740 \\
 \frac{M_{slewcentre}}{2} &= 2540/2, \frac{M_{towertop}}{2} = 575/2
 \end{aligned}$$

$$M_{counterweight} = ?$$

Right Side

$$\frac{M_{slewcentre}}{2} = 2540/2, \frac{M_{towertop}}{2} = 575/2$$

$$M_{slewrightextension} = 740$$

$$M_{cab} = 610, M_{jib(12m)} = 1300, M_{jibtip} = 125$$

Right Side

$$M_{jib} = \frac{M_{slewcentre}}{2} + \frac{M_{towertop}}{2} + M_{slewrightextension} + M_{cab} + M_{jib(12m)} + M_{jib(12m)}$$

$$+ M_{jibtip}$$

$$M_{jib} = \frac{2540}{2} + \frac{575}{2} + 740 + 610 + 1300 + 1300 + 125 = 5632.5 \text{ Kg}$$

Left Side

$$M_{counterjib} = \frac{M_{slewcentre}}{2} + \frac{M_{towertop}}{2} + M_{counterjib} + M_{adapter} + M_{counterweight}$$

$$M_{counterjib} = \frac{2540}{2} + \frac{575}{2} + 4070 + 3745 + M_{counterweight} = ?$$

$$Torque = mass * gravity * length$$

$$F_{counterjib} = M_{counterjib} * gravity$$

$$F_{jib} = M_{jib} * gravity = 55254.825 \text{ N}$$

$$(F_{counterjib} * d_{cj}) = (F_{jib} * d_j)$$

$$d_{cj} = 10.3 + \frac{1.2}{2} = 10.9 \text{ m}$$

$$d_j = \frac{1.2}{2} + 3 + 12 + 6 \{ \text{the point where tower tope cable is connected on the jib}\}$$

$$d_j = 21.6 \text{ m}$$

$$F_{counterjib} = \frac{F_{jib} * d_j}{d_{cj}} = \frac{5632.5 * 9.81 * 21.6}{10.9} = 109495.8 \text{ N}$$

$$F_{counterjib} = M_{counterjib} * g$$

$$M_{counterjib} = \frac{109495.8 \text{ N}}{9.81} = 11161.65 \text{ Kg}$$

$$M_{counterjib} = \frac{2540}{2} + \frac{575}{2} + 4070 + 3745 + M_{counterweight} = 11161.65 \text{ Kg}$$

$$M_{counterweight} = 11161.65 - \frac{2540}{2} - \frac{575}{2} - 4070 - 3745 = 1789 \text{ Kg}$$

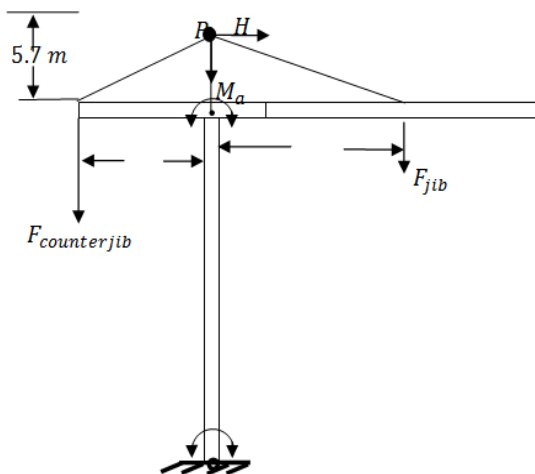


Figure 4.2 Establish equilibrium position

$$\begin{aligned} \sum M_a (CCW+) &= 0 \\ +(F_{counterjib} * d_{cj}) + (H * 5.7) - (F_{jib} * d_j) &= 0 \\ +(109495.8 * 10.9) + (H * 5.7) - (55254.825 * 21.6) &= 0 \end{aligned}$$

Equilibrium is achieved.

$$H = \frac{(55254.825 * 21.6) - (109495.8 * 10.9)}{5.7} = 0$$

4.1.2 Jib Moment at pivot A

Liebherr crane data sheet for tower hub (4.2+12+6)m and tower jib (3.6+12+12+2.31)m provides maximum applicable load as 3000 Kg. Therefore, after equilibrium is achieved in this system, additional counter load 3000 Kg has been mounted. In order to identify the significant moment changes at pivot point A, different payloads, M_l (from 1000 Kg to 3000 Kg) have been applied as shown in Fig. 4.3.

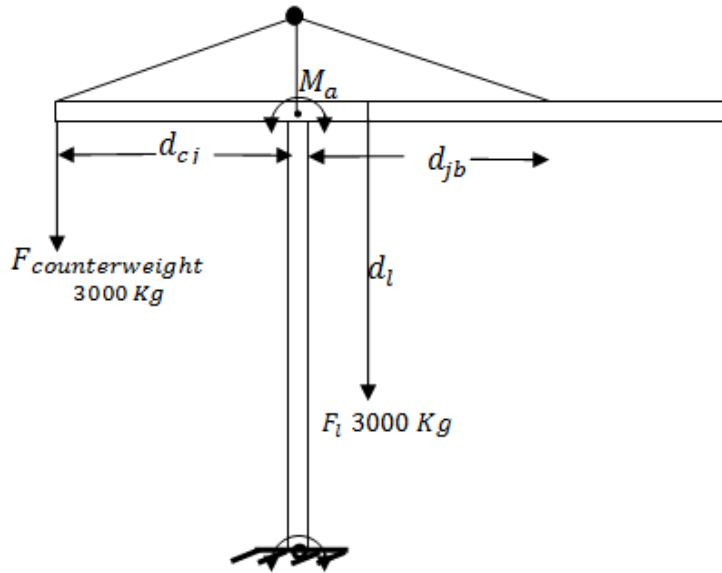


Figure 4.3 Jib Moment M_a at Pivot A

$$F_l = M_l * g = 3000 \text{ Kg} * 9.81$$

$$M_a = +(F_{counterweight} * d_{cj}) - (F_{load} * d_l)$$

$$\begin{aligned} M_a &= +(3000 \text{ Kg} * 9.81 * (\frac{1.2}{2} + 10.3)) - (3000 \text{ Kg} * 9.81 * (\frac{1.2}{2} + 3)) \\ &= 214.839 \text{ kNm} \end{aligned}$$

$$\begin{aligned} M_a &= +(3000 \text{ Kg} * 9.81 * (\frac{1.2}{2} + 10.3)) - (3000 \text{ Kg} * 9.81 * (\frac{1.2}{2} + 3 + 12 + 12)) \\ &= -491.481 \text{ kNm} \end{aligned}$$

Trolley is moved along the jib which starts from 3.6-m of jib tower and end the trolley motion at the end of jib (27.6-m). Along this jib of 24-m, trolley travels with carrying payload (from 1000 Kg to maximum 3000 Kg). The jib moment calculations all respective trolley position and loads have been presented in the Table (4.1) below.

x (3.6-27.6 m)	Ma1 (1000Kg)	Ma2 (1500Kg)	Ma3 (2000Kg)	Ma4 (2500Kg)	Ma5 (3000Kg)
3.6	285.47	267.81	250.16	232.5	214.84
4.6	275.66	253.1	230.54	207.97	185.41
5.6	265.85	238.38	210.91	183.45	155.98
6.6	256.04	223.67	191.29	158.92	126.55
7.6	246.23	208.95	171.68	134.4	97.119
8.6	236.42	194.24	152.06	109.87	67.689
9.6	226.61	179.52	132.44	85.347	38.259
10.6	216.8	164.81	112.82	60.822	8.829
11.6	206.99	150.09	93.195	36.297	-20.601
12.6	197.18	135.38	73.575	11.772	-50.031
13.6	187.37	120.66	53.955	-12.753	-79.461
14.6	177.56	105.95	34.335	-37.278	-108.89
15.6	167.75	91.233	14.715	-61.803	-138.32
16.6	157.94	76.518	-4.905	-86.328	-167.75
17.6	148.13	61.803	-24.525	-110.85	-197.18
18.6	138.32	47.088	-44.145	-135.38	-226.61
19.6	128.51	32.373	-63.765	-159.9	-256.04
20.6	118.7	17.658	-83.385	-184.43	-285.47
21.6	108.89	2.943	-103.01	-208.95	-314.9
22.6	99.081	-11.772	-122.63	-233.48	-344.33
23.6	89.271	-26.487	-142.25	-258	-373.76
24.6	79.461	-41.202	-161.87	-282.53	-403.19
25.6	69.651	-55.917	-181.49	-307.05	-432.62
26.6	59.841	-70.632	-201.1	-331.58	-462.05
27.6	50.031	-85.347	-220.72	-356.1	-491.48

Table 4.1 Load positions VS Moments at pivot A

Applying payload 1000 Kg on the jib and varying the load positions from 3.6-m to the jib end 27.6-m, simulation produced moment at pivot A still positive(CCW+) moments. However, gradually increasing the payload from 1000 Kg to 3000 Kg, simulations at each step, Table (4.1) and Fig. 4.4, show moments at pivot A change from CCW (+) to CW (-) direction. First trial shows the projection of calculated moments, green dotted line in Fig. 4.4 appeared to be having CCW(+) moments and it does not even reach equilibrium at any point. Second trial of applying 1500 Kg load, red dotted line in Fig. 4.4, and varies again from 3.6 m to 27.6 m translational motion reached to equilibrium around 22 m of trolley position and continue to CW(-) moments. Referring to Fig. 4.4, 2000 Kg (blue dotted line) reached equilibrium around 16m of trolley position, 2500 Kg (brown dotted line) reached equilibrium around 13-m of trolley position, and 3000 Kg (yellow dotted line) reached equilibrium around 11m trolley position.

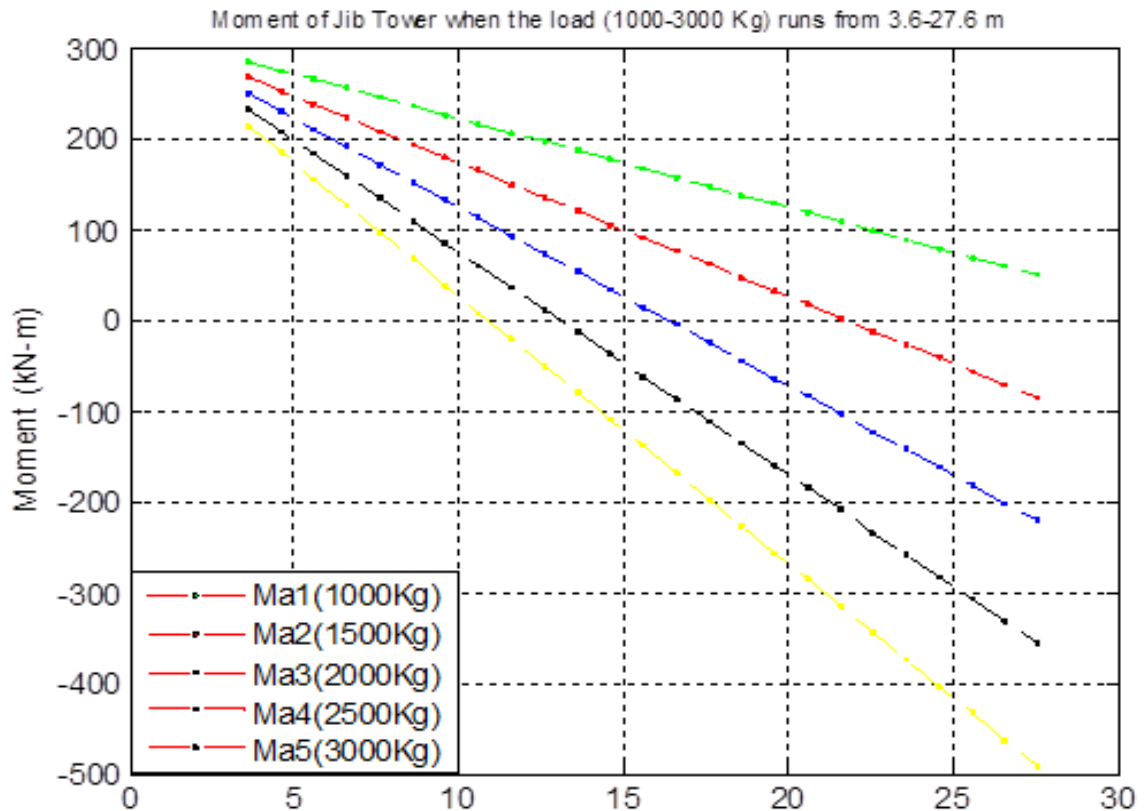


Figure 4.4 Moment of Inertia at pivot A using different payloads

The calculated data set has been transformed into jib's moment rotation at pivot A in Fig. 4.5a and Fig 4.5b. Fig. 4.5a shows even though the load 1000 Kg varies its position from 3.6 (initial position) to 27.6 (final position), the moment at pivot A gradually less but still positive moments. However, once 3000 Kg load is applied to the system, the moment at pivot A changes from (+) to (-) in Fig. 4.5b. Therefore, the initial calculation and data projection proved that there are moments at pivot A which changes the way loads and loads positions change.

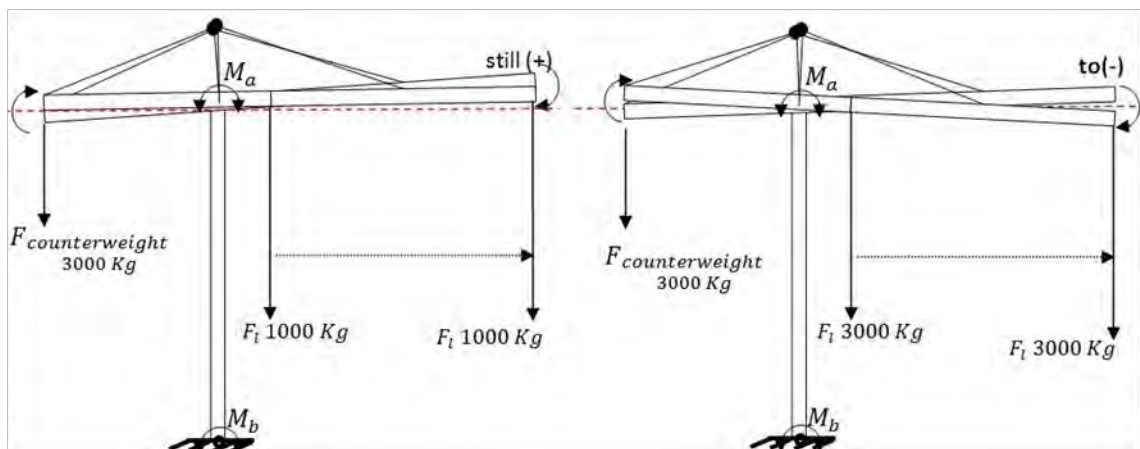


Figure 4.5a Moments at pivot A for payload 1000 Kg

Figure 4.5b Moments at pivot A for payload 3000 Kg

4.2 Vibration Analysis on Rigid Model Translation without wind Disturbance

For jib oscillation analysis purpose, rigid crane has also been developed which is similar to ideal one except having rigid bodies for hub and tower jib as shown in Fig 4.6. Each rigid body used in this model has: only one mass, three x-y-z measurements, and three moment of inertia (I_{xx} - I_{yy} - I_{zz}) from ideal model which hub has more than 100 parts and parameters [5]. Therefore, jib oscillations between rigid structure and ideal model would definitely be different. Based-on this facts-finding, suitable and more realistic model could be recommended for future modeling and simulation. Details parameters, (Mass, Measurements, and Inertia Tensors) of each part of rigid crane has been mentioned below, Table (2).

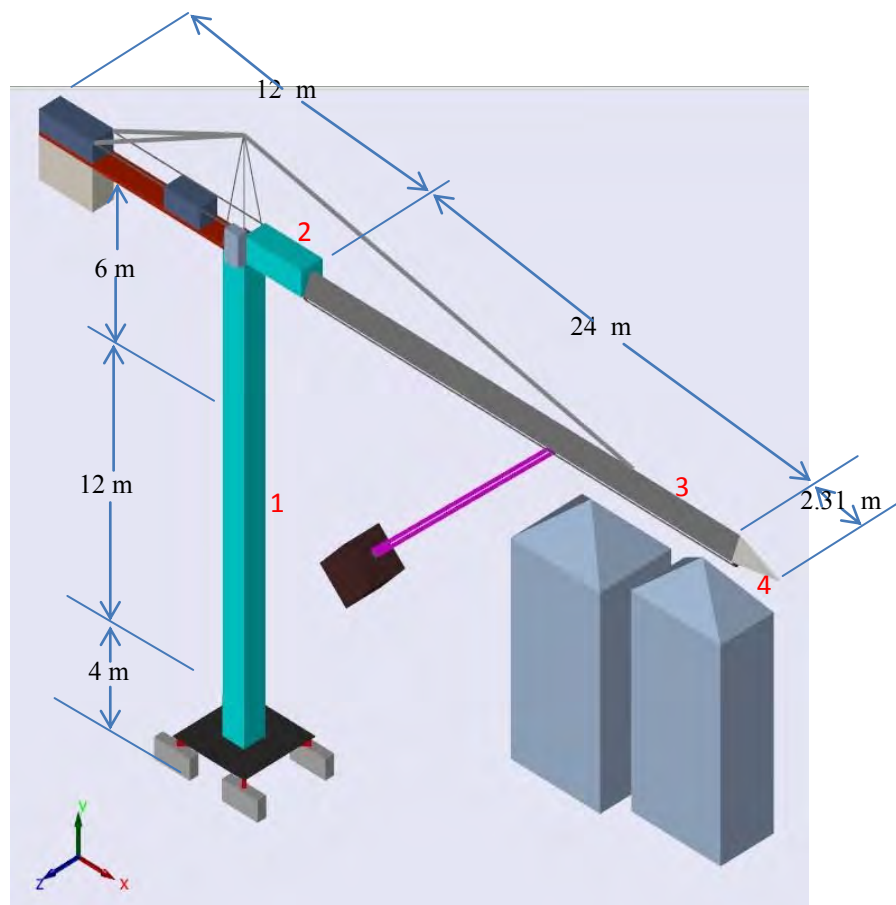


Figure 4.6 Rigid Crane Model with Trolley Translational Motion

4.2.1 Mass, Measurements, and Moment of Inertia for rigid structure

Before analyzing the crane vibration of ideal model, hub and jib tower structure are transformed into rigid forms while other parts of ideal crane model remain unchanged. Mass, Measurements, and Moment of Inertia in Table (4.2) for rigid structure are

Parts	Mass (Kg)	Measurements (m)			Moment of Inertia (Kg m^2)		
		Length	Width	Height	I_{xx}	I_{yy}	I_{zz}
1, hub 22 m	6700	1.2	22	1.2	271040	1608	271040
2, tower right extention 3.2 m	789	3.2	1.2	1.2	189.36	767.96	767.96
3, tower 24 m	2600	24	1.2	1.2	624	125112	125112
4, jib tip 2.31m	125	2.31	0.6	1.2	18.75	70.5844	59.3344

Table 4.2 Mass, Measurements and Moment of Inertia for Rigid Structure

At this stage, simulation is all about applying power input on trolley with attached payload, and getting data of load swing, jib/hub top oscillations. No other input disturbance has been taken into account so far.

Simulation of this rigid model which uses power inputs (1000W-3000W) with attached (1000Kg-3000Kg) payload produced Trolley positions, load swing angles, Jib tip and hub top oscillations. The maximum values for each simulation from 1000W_1000Kg to 3000W_3000Kg: has been shown in Table (4.3). The reason of developing rigid model is to compare with ideal model outputs and analyze which model would be more reliable and realistic. The following figure, Fig. 4.7, of rigid simulation shows: applying 2000W on the trolley with attached 1000 Kg payload has dramatic rise in load swing (deg) and Jib tip angular acceleration. This pattern continues for power input 3000W with 1000 Kg load in Fig. 4.8, as well appeared to be worst case scenario among all 9 simulations. The figure also shows that, jib oscillation continuously pounding up and down between -30 to 30 deg/sec^2 during the operation. Even though there has been no such rigid high tower crane due to its loaded oscillation, this research has intentionally developed rigid model in order to significantly identify the differences between rigid model and ideal model.

Power Input Vs Maximum values of Trolley Position, Load Swing, Jib Tip, and Hub Top =				
	TP (m)	LS (deg)	JT (deg/s^2)	HT (deg/s^2)
1kW_1000Kg	20.17400	7.79920	0.88987	2.58430e-14
1kW_2000Kg	20.07900	2.33620	0.31412	3.37570e-14
1kW_3000Kg	20.17300	3.14820	0.34076	3.57310e-14
2kW_1000Kg	20.44300	21.58100	10.24400	9.14060e-14
2kW_2000Kg	20.44700	12.09700	3.48400	1.27030e-13
2kW_3000Kg	20.23200	3.95120	1.14910	1.11150e-13
3kW_1000Kg	20.78600	36.31100	18.43500	1.75010e-13
3kW_2000Kg	20.70600	19.60500	10.06200	8.72620e-14
3kW_3000Kg	20.80700	13.73200	3.75100	2.69810e-13

Table 4.3 Rigid Crane Model Simulations results

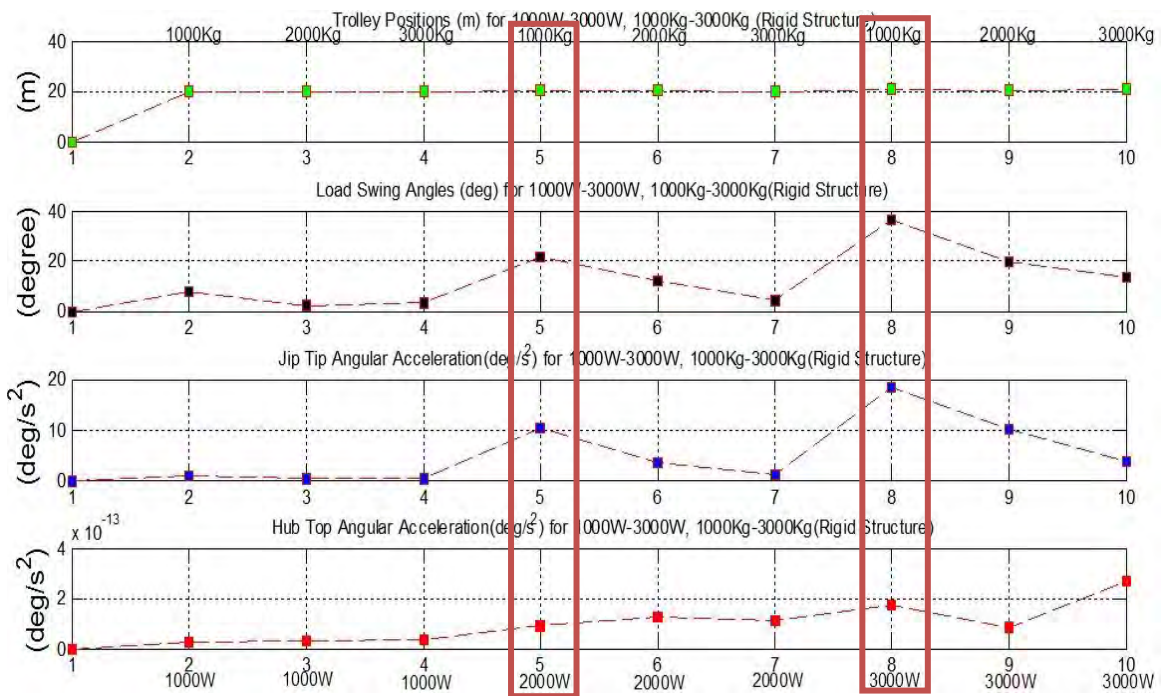


Figure 4.7 Rigid Crane Model Simulations results

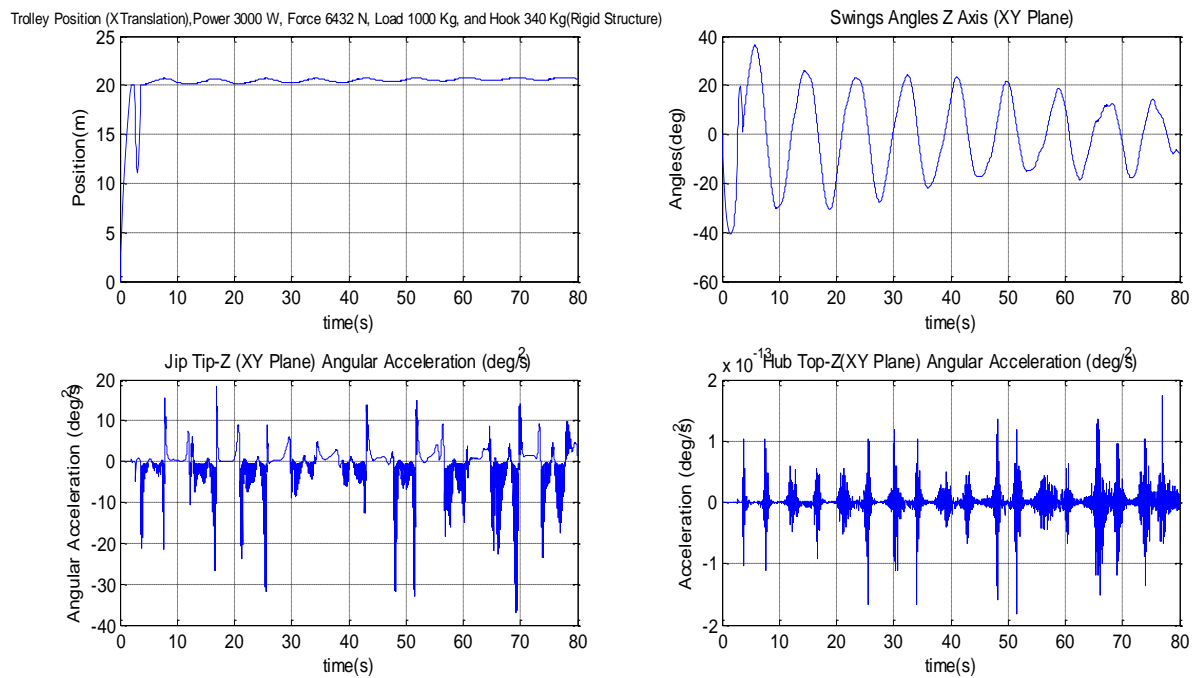


Figure 4.8 Worst Case results for (3000W_1000Kg) in Rigid Crane Model Simulations

4.3 Vibration Analysis on Ideal Model Translation without wind Disturbance

The ideal model Fig. 4.9 also runs all 9 simulations from 1000W-1000Kg to 3000W_3000Kg and those data has been shown in the table blow, Table (4). Details of

ideal model design has been discussed in earlier section. Obviously, this ideal model has structurally-built crane hub, and tower extensions according to real operating crane. Based on the simulations results, this model would be analyzed whether it produces more reliable/realistic data for further modeling and control or the simulated outputs considered to be very close to rigid model.

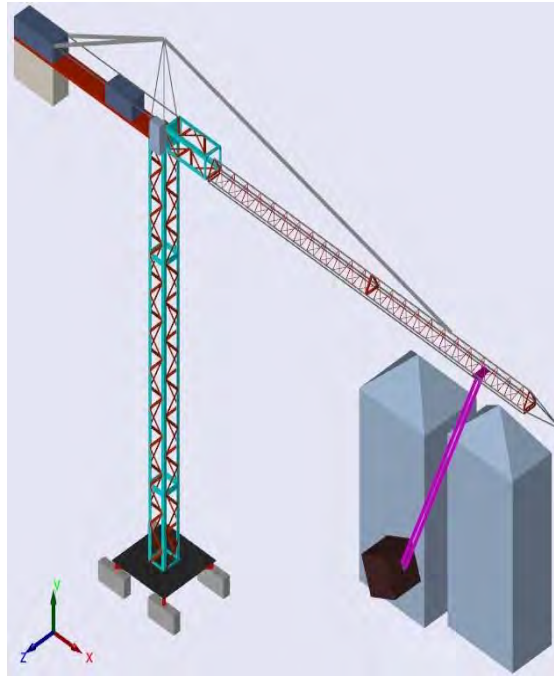


Figure 4.9 Ideal Crane Model with Trolley Translational Motion

The ideal model simulations provide very much realistic results as shown in Table(4.4), with load swing appeared to become highest (47.478 degree) for power input 3000W_1000 Kg load while second highest (27 deg) for 2000W_1000Kg as shown in Fig. 4.10. Even though jib oscillation has been less than 1 deg/sec² throughout simulation, this realistic data proves that the current crane companies prefer to use ideal model looks-alike real crane in order to have less oscillation.

Ideal Model: Power Input Vs Maximum values of Trolley Position, Load Swing, Jib Tip, and Hub Top =					
	None	TP (m)	LS (deg)	JT (deg/s ²)	HT (deg/s ²)
1kW_1000Kg	0	20.28600	14.02600	1.52450e-13	1.52450e-13
1kW_2000Kg	0	20.06800	1.88900	5.68030e-14	5.68030e-14
1kW_3000Kg	0	20.45600	10.19400	4.10500e-09	1.78390e-13
2kW_1000Kg	0	20.79400	27.10900	3.26740e-09	2.72880e-12
2kW_2000Kg	0	20.43100	11.34700	2.42790e-09	3.24540e-13
2kW_3000Kg	0	20.20500	10.51500	2.42610e-09	1.13540e-13
3kW_1000Kg	0	21.26000	47.47800	1.29640e-09	7.38900e-13
3kW_2000Kg	0	20.66600	18.27200	2.80810e-09	2.27260e-12
3kW_3000Kg	0	20.73200	13.04900	5.82210e-09	8.75640e-13

Table 4.4 Ideal Crane Model Trolley Translation with results

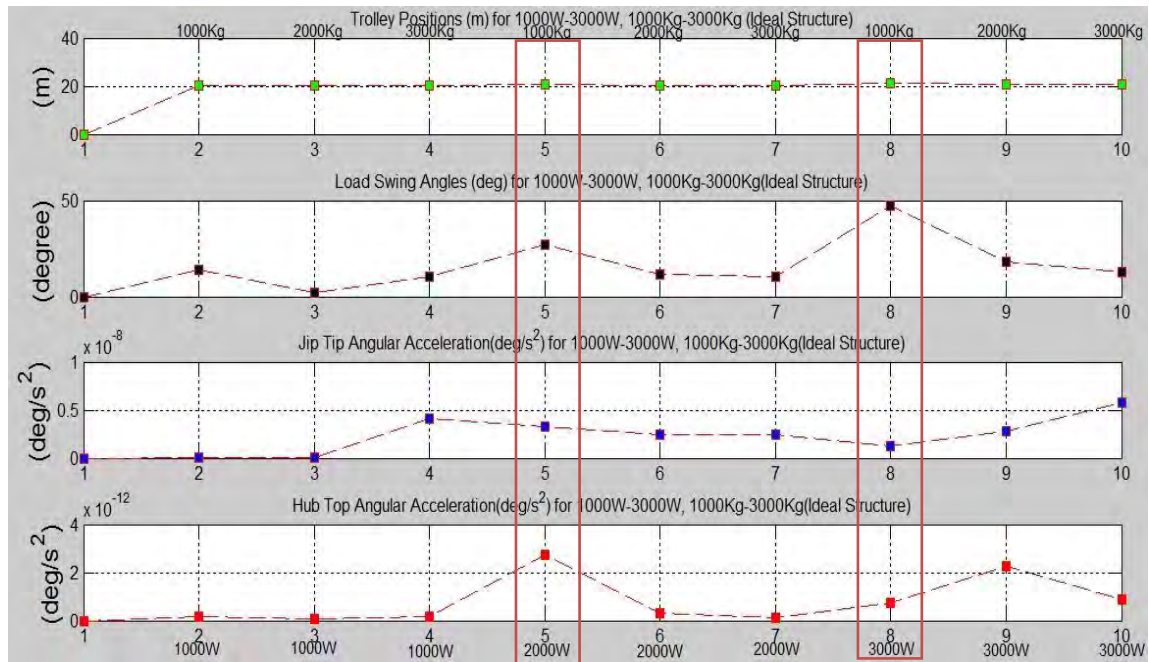


Figure 4.10 Ideal Crane Model Trolley Translation with results

Worst case scenario among all 9 ideal-based model simulations is again 3000W_1000Kg for having highest load swing followed by 2000W_1000Kg. Simulations prove that, having unstable load swing is because of input power vs payload changes as well as jib/hub oscillations, Fig. 4.11. Internally connected cycle would jeopardize the whole crane operation because power input strikes the trolley, and load swing appears which makes jib/hub oscillates, then trolley would be shaky and consequently causing more unstable load swing, which goes on to the certain time.

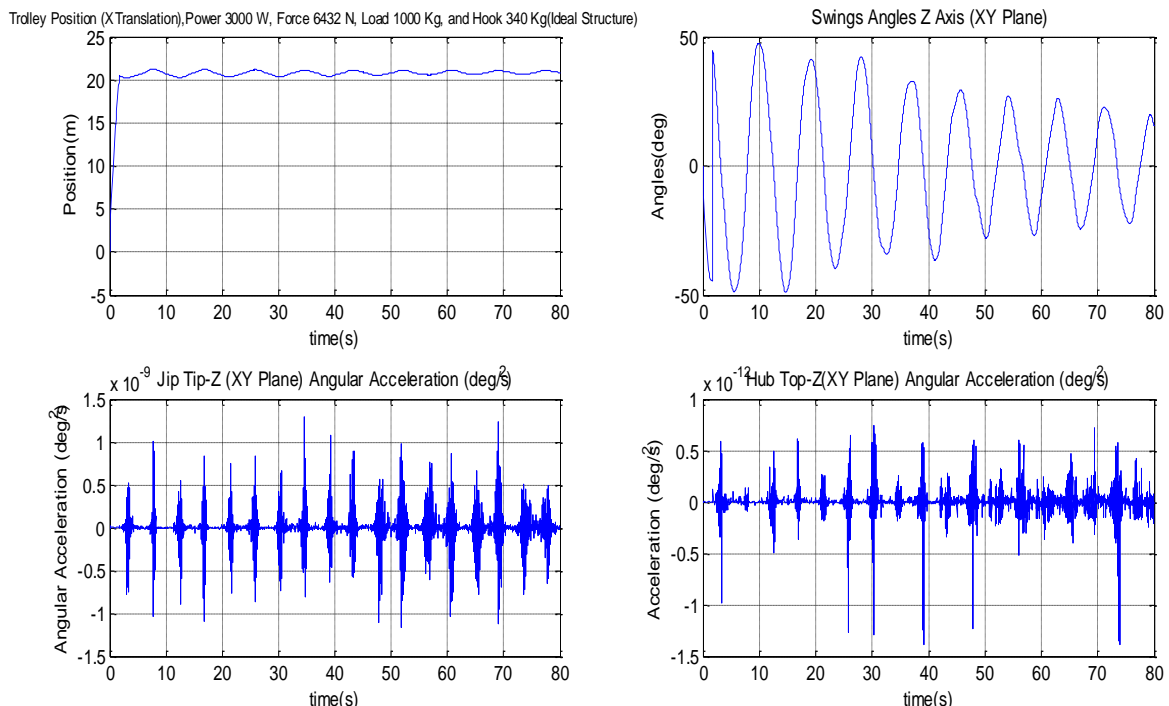


Figure 4.11 Ideal Crane Model Trolley Translation with results for 3000W_1000Kg

Ideal crane model without any other disturbance still produces higher load swing and jib/oscillations. As a standing tall tower crane, wind disturbance could be another obstacle which can cause trouble to inter-connected crane operation cycle.

However, this research has developed SimMechanics model tower crane and sensors have been mounted at specific positions to monitor jib-hub vibration and analyze their impacts on payload swing. In this jib vibration analysis, manual jib moment calculation, Fig. 4.3, SimMechanics Rigid-Model trolley translation Fig. 4.6, and SimMechanics ideal-Model trolley translation, Fig. 4.9, are tested by applying without Wind Disturbance. Simulations results show there have been significant impact of crane vibration on payload swing. The next section would develop wind disturbance model and applied on the crane in order to make further analysis of vibration impact on the crane.

4.4 Wind Disturbance Model Development

High winds can be very destructive and considered as another source of disturbance which loads the tower crane structure and causes Jib Tower/Hub oscillation problems. The total wind load is actually a combination of static wind (mean) and gusts wind (variable), Equ (4.1). Calculating wind load is necessary to have safer tower crane operation. Wind impact is one of the major loads affecting buildings and other constructions, among which the most affected is large-standing construction tower crane which can be seriously damaged by wind, resulting in serious collateral damage in its surrounding environments, as in [35]. The destructive irregular wind disturbance would also be the reason for tower vibration causing higher unstable payload swing during the operation. In order to design a controller with wind disturbance rejection properties, wind disturbance should be known at the input to the crane model. Therefore, Gawronski approach, as in [35], proposed a “wind force acting on the dish” model for the large standing tall antenna at 34-m height. However, instead of deriving gusts wind speed $\Delta_{v_0}(t)$ through Davenport Spectrum as mentioned in the article, this research considers available input from Sydney Metrological Weather Office. Wind load is represented as a combination of static wind (static) and gusts wind (variable), Eq.(4.1) in [66]- [16].

$$v_t = v_{ws} + v_{wg} \quad (4.1)$$

4.4.1 Obtaining Wind Static Force from Wind Static Velocity

To obtain Wind-static Force, F_{ws} , quadratic law is applied which relates its velocity and force, as in [35]. The Dragging Force Coefficient, K_{df} , depends on the scaling of air surface terrain. Usually, static wind, gusts wind and wind pressure could be obtained from the sensor mounted on the crane. Currently, those parameters are according to Sydney Metrological Weather Focus and then converted to disturbance wind force and torque. For instance, wind data of 16th April 2014 Sydney weather forecast, [66], provides wind (static) speed, $v_{ws} = 22 \text{ km/h}$, gusts wind speed, $v_{wg} = 43 \text{ km/h}$, and wind pressure, $P=1017.4 \text{ hPa}$. By varying wind surface area $A = x * y$, (see Fig. 4.12), static wind, Force (F_{ws}), and dragging force coefficient (K_{df}) can be derived as follow. Total Wind Force is also a combination of Wind-static Force and Wind-gusts Force in Eq.(4.2). To obtain Wind-static Force, F_{ws} , quadratic law which relates its velocity and force is applied Eq.(4.3) [35]. The Dragging Force Coefficient, K_{df} in Eq.(4.4) depends on the scaling of air surface terrain.

$$F_t = F_{ws} + F_{wg} = ? \quad (4.2)$$

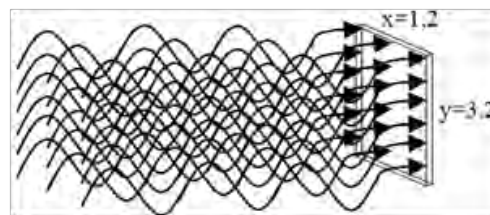


Figure 4.12 Wind surface terrain ($x=0.12\text{m}$, $y=0.12\text{m}$)

$$F_{ws} = PA \quad (4.3)$$

$$F_{ws} = K_{df} v_{ws}^2$$

$$K_{df} = \frac{F_{ws}}{v_{ws}^2} \quad (4.4)$$

4.4.2 Dragging Force Coefficient Derivation

Based on Sydney weather focus Sydney, Velocity of wind-static, Velocity of wind-gusts, and Pressure can be obtained. To establish Wind-static Force F_{ws} from provided Pressure, initially wind surface terrain area is assumed as ($x=0.12m$, $y=0.12m$) which is 10% of actual crane width, Fig. 4.12. Wind surface area can be varied based of windy or unwind situation. From known parameter P and derived parameter A, Wind-static Force F_{ws} is then achieved. Finally, Dragging Force Coefficient, K_{df} has been established in Eq.(4.4).

Known parameters Wind data for the date 16 April 2014 are

$$\text{Wind (static) Speed, } v_{ws} = 22 \text{ km/h}$$

$$\text{Wind (gusts) Speed, } v_g \text{ is } 43 \text{ km/h, and}$$

$$\text{Wind Pressure, } P=1017.4 \text{ hPa}$$

$$\text{Assume the Air Surface Area as, } A = x * y, P = \frac{F_{ws}}{A}, F_{ws} = K_{df} v_{ws}^2$$

$$\text{Dragging Force Coefficient } K_{df} = \frac{F_{ws}}{v_{ws}^2}$$

4.4.3 Wind-gusts Force

The Wind-gusts Force variations, F_{wg} , are related to wind-gusts velocity variations, Δv [35]. According to Taylor series, F_{wg} is derived from the derivative of F_{ws} as followed:

$$F_{wg} = \left[\frac{\partial F_{ws}}{\partial v} \right]_{v=v_{ws}} = \frac{\partial (K_{df} v_{ws}^2)}{\partial v}$$

Wind-gusts Force:

$$F_{wg} = 2K_{df} v_{ws} \Delta v \text{ where } \Delta v = \Delta_{v_0} * \sigma_v$$

$$\Delta_{v_0} = v_{wg}(\text{known}),$$

where σ_v is the standard deviation of Δv . However, the standard deviation of the gusts wind is proportional to the mean wind static speed. According to Gawrongska's approach, $\Delta_{v_0} = \frac{\Delta v(t)}{\sigma_v}$, $\Delta_{v_0(t)}$ was obtained by applying a white noise input of unit standard deviation to a filter that approximates the Davenport filter.

$$\Delta v(t) = \Delta_{v_0}(t) * \sigma_v$$

$$\sigma_v = \alpha v_{ws}, \Delta v = \alpha v_{ws} \Delta_{v_0}, \alpha = \sqrt{6K}, \Delta v = \sqrt{6K} * v_{ws} * \Delta_{v_0} \text{ where } (\Delta_{v_0} = v_{wg})$$

$$\Delta v = \sqrt{6K} * v_{ws} * v_{wg}$$

$$K \text{ is the surface terrain roughness } K = \frac{1}{\left(2.5 \ln \left(\frac{z}{z_0} \right) \right)^2}$$

z is the distance from the ground to the Hub top, z_0 is the height of terrain roughness

$$F_{wg} = 2K_{df} v_{ws} \Delta v, F_{wg} = 2K_{df} v_{ws} * \alpha v_{ws} v_{wg}$$

Final applied force

$$F_t = F_{ws} + F_{wg}$$

4.5 Vibration Impact Analysis on Trolley Translation with wind Disturbance

Due to the unpredicted weather condition, usually wind might strike on standing tall crane with low terrain roughness and sometimes high terrain. In order to analyze the jib oscillation vs load swing, the developed wind disturbance model, Fig(13), has been added to ideal model with trolley translation as well as tower rotation. In the simulation, wind with $(0.12 * 0.12)$ surface area is applied on 3 spots (mid of hub, slew assemble, and mid of jib tower) on the crane, Fig. 4.13. Wind surface area, wind speed, striking spots and time, amount of gusts wind would change time to time. But at this initial analyzing stage, wind disturbance model has been developed based on Sydney weather focus of (16 April 2014) and wind surface area was considered as $(0.12*0.12 \text{ m}^2)$ which would have a one notch (1 second) strike on 3 spots of the crane model as follow.

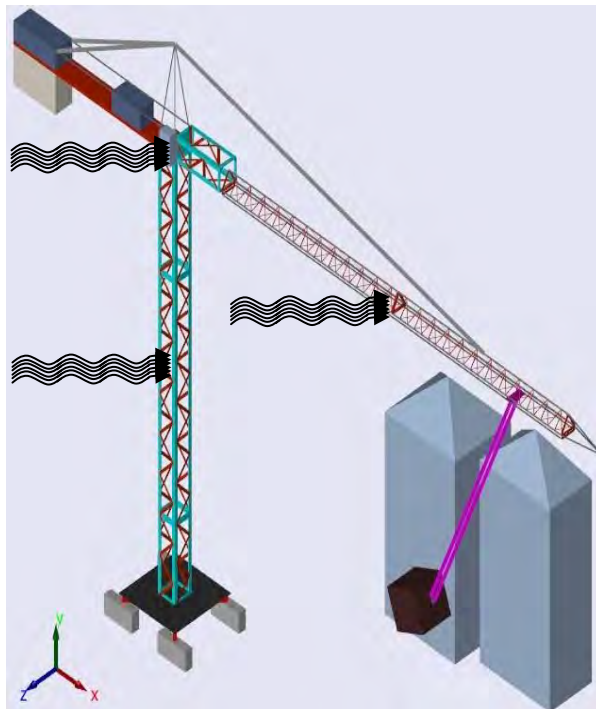


Figure 4.13 Apply Wind Disturbance Model on Ideal Model

Wind disturbance pattern would always be irregular time to time due to wind-static, wind-gusts, wind-pressure, wind-surface area, wind-strike duration, and terrain-roughness. In order to analyze jib vibration and its impact on load swing, wind-surface area ($x=1.2\text{m}$, $y = 3.2 \text{ m}$, wind-strike duration (1 second-pattern 3-times separate strikes) and terrain-roughness ($z_0=0.71$) have been assumed while the other parameters are variable.

In the second and third trials, 3 wind strike(1-s notch each) area surfaces ($x=1.2, y=1.2$) and ($x=1.2, y=3.2$), Fig. 4.14, have been applied on tower crane hub and jib/tower. The reason of those trials is to identify jib/hub oscillation upon applied wind model changes. Obviously, three different trials produced different simulation results which are discussed below.

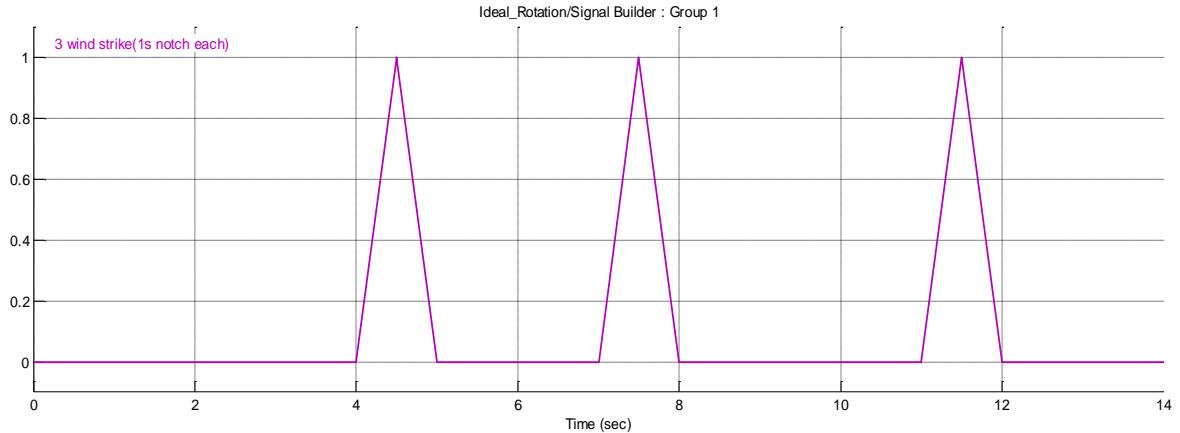


Figure 4.14 Wind Model Surface Area ($x=0.12\text{m}, y=0.12\text{m}$), 1-s notch wind strike

4.5.1 Vibration impact Analysis with Different Wind Surface Area

Again, input power 1000W-3000W produced 2144N-6433N of trolley driving force and one notch of applied force signal (applies 1s only), is generated to ensure the trolley does not run overboard. In this case, Trolley friction coefficient of 10 N and brake friction is $(75^*\alpha)$ N are assumed as before, and initial wind disturbance model with one notch of applied force signal (applies 1 s only), is added. It means, wind disturbance of (Wind static Speed, $v_{ws} = 22 \text{ km/h}$, gusts wind Speed, $v_{wg} = 43 \text{ km/h}$, and Wind Pressure, $P=1017.4 \text{ hPa}$) which produces Wind Force of 4931.8 N would strike the Hub top position and middle of Jib tower for 1 second while trolley is running. In the first trial, wind model striking surface is assumed as ($x = 0.12 \text{ m}, y = 0.12 \text{ m}$) making the wind surface area small would produce less striking force on the tower crane.

Real operating Tower crane may oscillate during trolley translation or tower rotation and many reasons could play the role in oscillation. Different power inputs have been tried to indentify oscillation in previous section which showed maximum load swing (47 deg) and Jib tip oscillation $5.822\text{e-}10 \text{ deg/s}^2$ occurred at 3000W input. However, in real environment, wind disturbance plays vital role in destabilizing standing tall tower crane operation. And therefore, at this stage, 3 different types of wind models have been applied on the crane such as: surface area (case1-red line: $(x = 0.12 \text{ m} * y = 0.12 \text{ m}):1\text{s_1 notch}$), (case2-blue line: $x = 1.2 \text{ m} * y = 1.2 \text{ m}):1\text{s_3 notch}$) and (case3-green line: $x = 1.2 \text{ m} * y = 3.2 \text{ m}:1\text{s_3 notch}$). Load swing results of three trials

show, Fig. 4.15, case1 could reach maximum 36.225 deg, while case 2 could reach maximum 50.313 deg, and case3 has 54.163 deg. It proves that having higher wind pattern means higher load swing could occur. Further jib tip/hub top oscillation analysis would be discussed in the next section.

	LS	JT	HT						
	1W(0.12*0.12)	3W(1.2*1.2)	3W(1.2*3.2)	1W(0.12*0.12)	3W(1.2*1.2)	3W(1.2*3.2)	1W(0.12*0.12)	3W(1.2*1.2)	3W(1.2*3.2)
1kW_1000Kg	9.26050	9.71430	9.71430	7.86690e-10	1.37030e-09	3.45950e-09	7.79700e-13	1.05030e-10	2.21350e-10
1kW_3000Kg	3.59370	3.57070	3.62280	7.48410e-10	1.30720e-09	3.18310e-09	6.54700e-13	6.12860e-11	1.31960e-10
2kW_1000Kg	21.98400	50.31300	21.60100	1.31010e-09	6.27590e-09	5.09920e-09	6.71310e-12	1.12880e-10	3.99880e-10
2kW_3000Kg	7.66500	15.49200	6.19170	1.80290e-09	2.88140e-09	4.37540e-09	8.34900e-13	1.14130e-10	3.40070e-10
3kW_1000Kg	36.22500	33.09400	54.16300	2.92010e-09	3.40310e-09	3.55570e-09	1.35900e-11	1.09600e-10	4.04060e-10
3kW_3000Kg	13.85200	14.56400	14.54500	3.81660e-09	4.53970e-09	4.02870e-09	4.83570e-12	1.12200e-10	3.02510e-10

Figure 4.15 Load swing , Jip Tip, Hub Top Oscillations changes due to different wind model strikes

Lower wind model (case1) strikes give certain nature of jib oscillation as appeared in the figure, Fig. 4.16. Furthermore, case 2 and case3 produced reasonable amount of jib oscillations. For case 2, jib tip oscillation appeared to be highest ($6.2759e-9$) at 2kW_1000Kg trolley runs while case3 was closely following with ($5.0992e-9$). However, case3 turned up to produce highest jip oscillation for 2kW_3000Kg and 3kW_1000Kg trolley runs. Again, Hub top oscillations were always at high in case 3 simulations, Fig. 4.16.

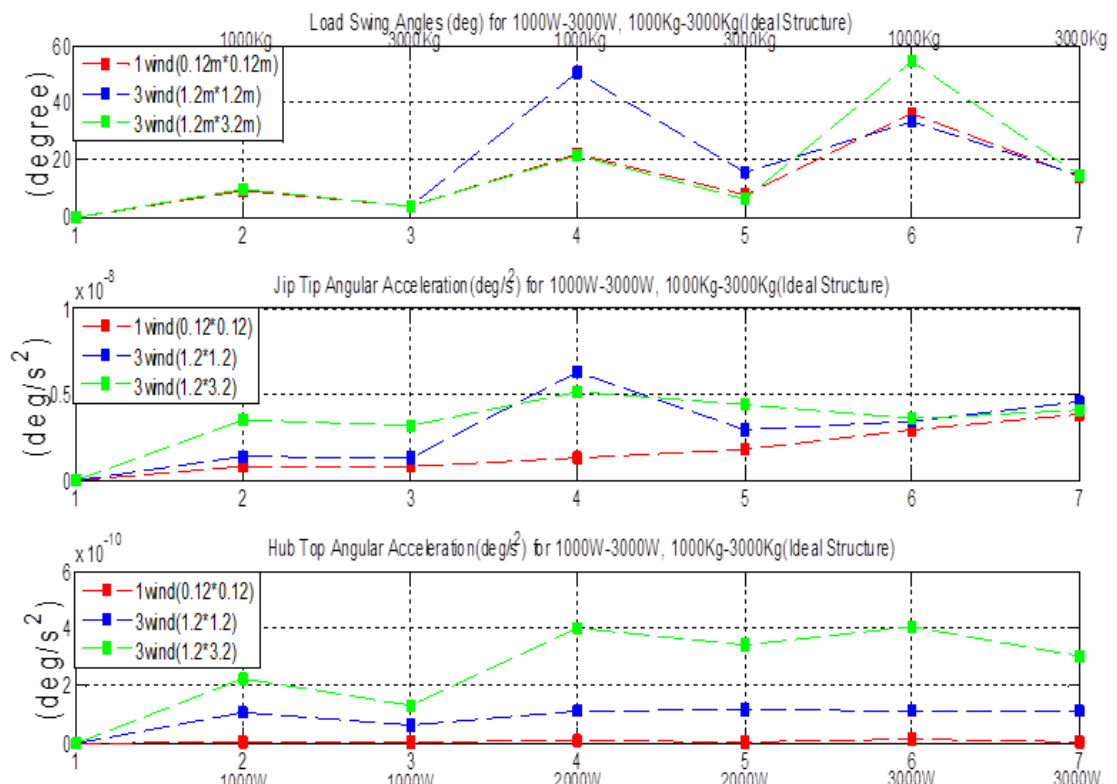


Figure 4.16 Load Swing-Jib tip-Hub top relationship due to different wind models strikes

In this wind disturbance applied trolley translation case study, both trolley speed and wind play certain roles in producing tower vibration and unstable load swing. Several different combinations of trolley speed vs load swing have been analyzed. However, wind disturbance makes significant impact on vibration and load swing. In the case of (3kW power, 1000Kg load, 18m load length) system, it has been analyzed by “without wind and applied wind (static-gusts-pressure: 22-43-1017)”, where swing error is $E=1649.8$ in Fig. 4.17a. while Jib tip angular acceleration error is $E=1.547e-9$ in Fig. 4.17b. In another case of “without wind and applied wind (static-gusts-pressure: 41-86-1010)”, where large swing error appeared as $E = 5747.1$ as shown in Fig. 4.17c while Jib tip angular acceleration error is $E=2.408e-9$ in Fig. 4.17d. Due to changes in wind static-gusts-pressure pattern, jib vibration becomes reasonably higher and causes substantial impact on the load swing.

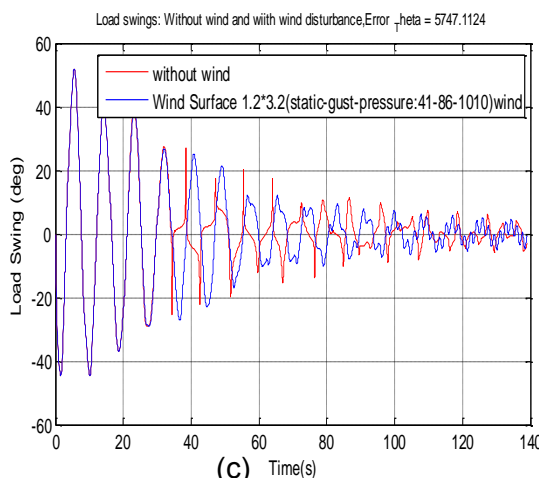
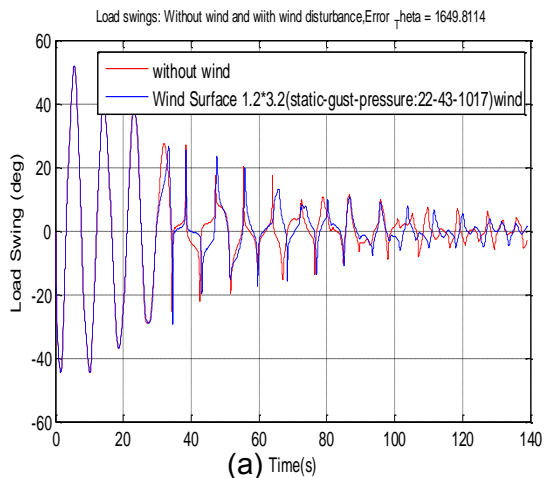


Figure 4.17a Load Swings of without Wind and with Wind Pattern (22-43-017) in Trolley Translation Case

Figure 4.17c Load Swings of without Wind and with Wind Pattern (41-86-1010) in Trolley Translation Case

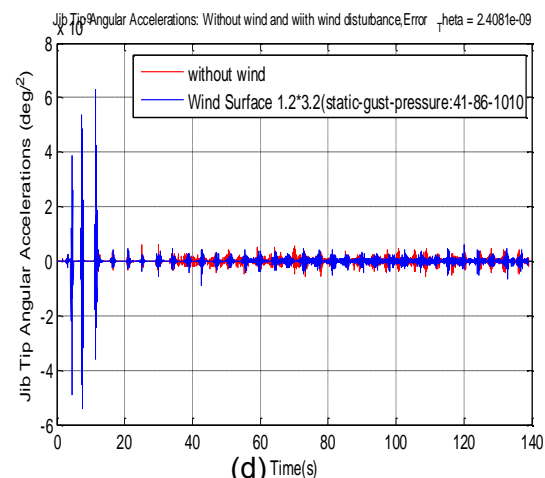
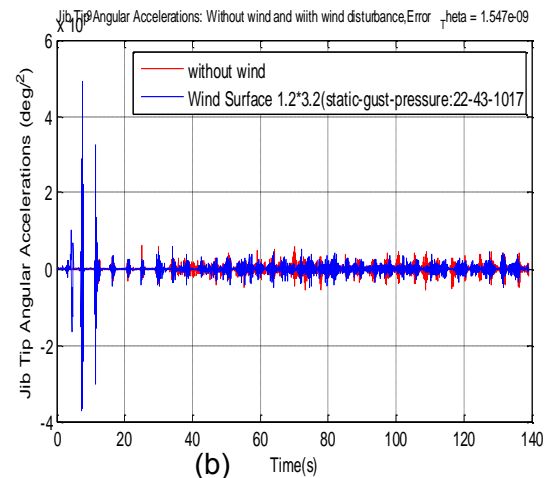


Figure 4.17b Jib Oscillation of without Wind and with Wind Pattern (22-43-017) in Trolley Translation Case

Figure 4.17d Jib Oscillation of without Wind and with Wind Pattern (41-86-1010) in Trolley Translation Case

4.6 Vibration Impact Analysis on Tower Rotation without Wind Disturbance

After Trolley translation with wind strike was proven to have jib/hub oscillations, ideal tower rotation in Fig. 4.18 was tested without wind model by placing trolley-payload at the beginning of jib tower as well as at the end of jib tower.

4.6.1 Oscillation Analysis while trolley-payload is at the beginning of jib tower

This research had initially tested ideal model with and without wind disturbance while the trolley cart is placed stationary at 3.6 m jib tower. In all cases, tower rotation power inputs are considered from (1000 W to 6300 W) with payload ranging from (1000 Kg to maximum allowable 3000 Kg). However, simulation results show that there have been little changes in both payload swing and less significant oscillations of jib and hub. Therefore, it is noted jib-hub oscillation changes would become obvious along with trolley cart-payload travel towards the jib end. The next section would discuss about jib-hub oscillation impact on payload swing when trolley is placed at near the jib end.

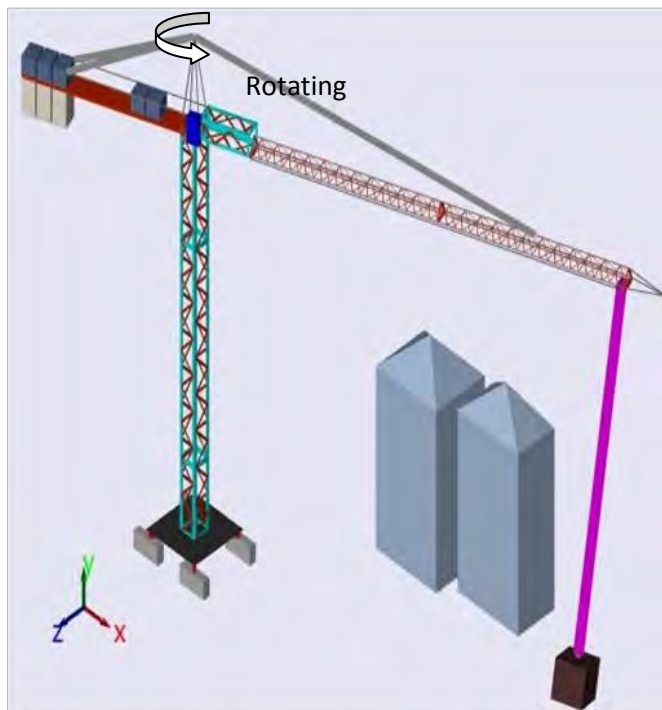


Figure 4.18 Jib/Hub Oscillation of Tower rotation with/without wind model

4.6.2 Oscillation Analysis while trolley-payload is at the end of jib tower

Since placing trolley-payload at the beginning of jib tower (3.6 m from slew assembly) has made little changes in oscillations, trolley-payload is then placed stationary at the end of jib tower (3.6+24 m from slew assembly). Power input vs payload are paired as in Table (4.5) to prove swings and oscillations. As there is been no wind

disturbance consideration, all the results are due to tower rotation power input with assigned payloads. Though there were little swing with less oscillation throughout different input-load combinations, 6 kW_3000 Kg eventually produced (-4 to 4) with 2.27154 deg/s^2 ib tip oscillation) as shown in Fig. 4.19.

	None	TR(deg)	LS(deg)	JT(deg/s^2)	HT(deg/s^2)
1kW_1000Kg	0	15.74097	0.13481	0.36770	1.51307e-15
1kW_3000Kg	0	15.74502	0.10866	0.36644	1.74725e-15
2kW_1000Kg	0	16.75205	0.27366	0.73539	1.44158e-15
2kW_3000Kg	0	16.75929	0.23996	0.73289	2.11475e-15
3kW_1000Kg	0	17.75551	0.34947	1.10309	1.46183e-15
3kW_3000Kg	0	17.77635	0.32086	1.09933	2.34204e-15
4kW_1000Kg	0	18.76565	0.61883	1.47079	1.21428e-15
4kW_3000Kg	0	18.82532	0.61798	1.46578	1.73437e-15
5kW_1000Kg	0	19.77185	0.53175	1.83848	1.15407e-15
5kW_3000Kg	0	19.82346	0.52131	1.83222	1.32703e-15
6kW_1000Kg	0	21.06901	0.66228	2.31649	1.05358e-15
6kW_3000Kg	0	14.16059	3.71562	2.27154	4.40069e-15

Table 4.5 Ideal Tower Rotation without Wind Disturbance and Stationary Trolley at 24 m

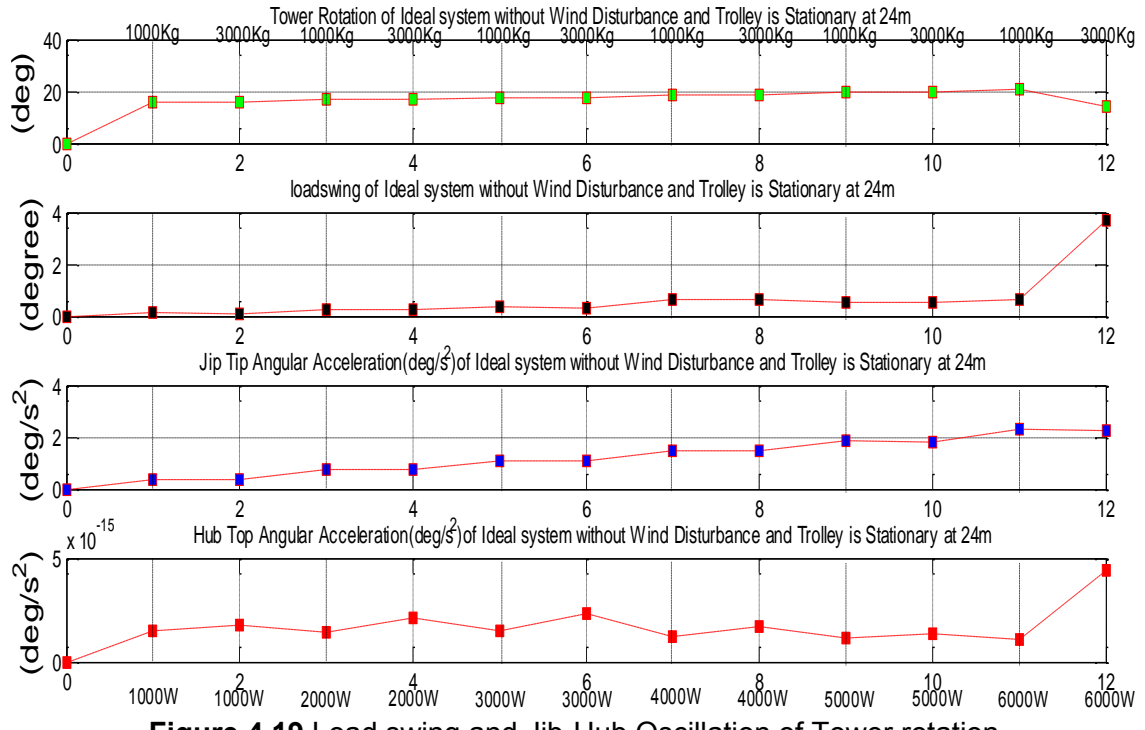


Figure 4.19 Load swing and Jib-Hub Oscillation of Tower rotation without Wind Disturbance

In this simulation, maximum allowable power input 6300 W has been applied, Trolley is stationary at 24m (end of the jib), maximum pay load 3000 Kg was attached, and run the tower rotation without Wind model strike.

Simulation of tower rotation without wind model disturbance shows, tower settled at near the target input 15 while payload swings ($\theta_x, \theta_y, \theta_z$) in respective X-Y-Z directions appeared to be within (-4 to 4), Fig. 4.20a. Even though this simulation

uses applied maximum power (6300W) with payload (3000Kg) attached at the jib's end, Jib tip and Hub top have very less oscillations which does not seem to make impact on the load swing in Fig. 4.20b. Due to that, payload position 3D trajectory appeared to have a few swings then settled down at even highest tower rotation speed. The next section is to analyze oscillation, swings and load trajectory by applying wind disturbance.

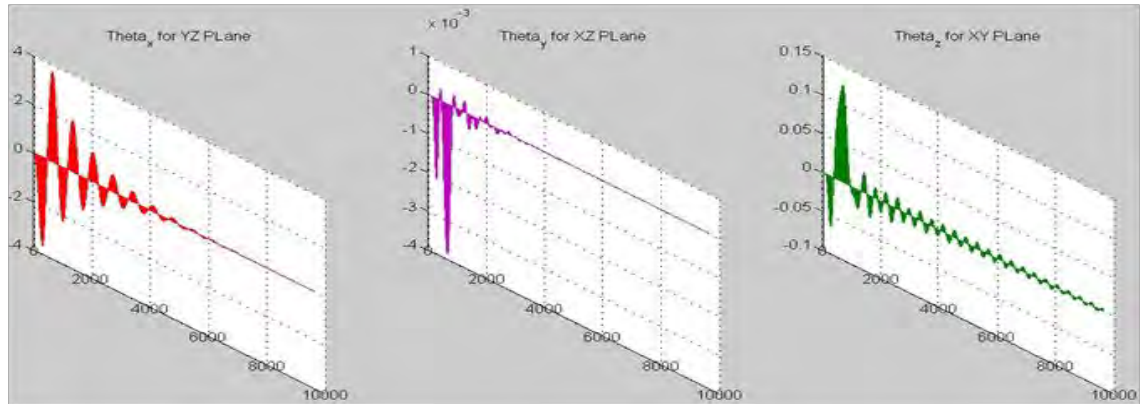


Figure 4.20a Load Swing X-Y-Z responses for 6.3kW_3000Kg without wind

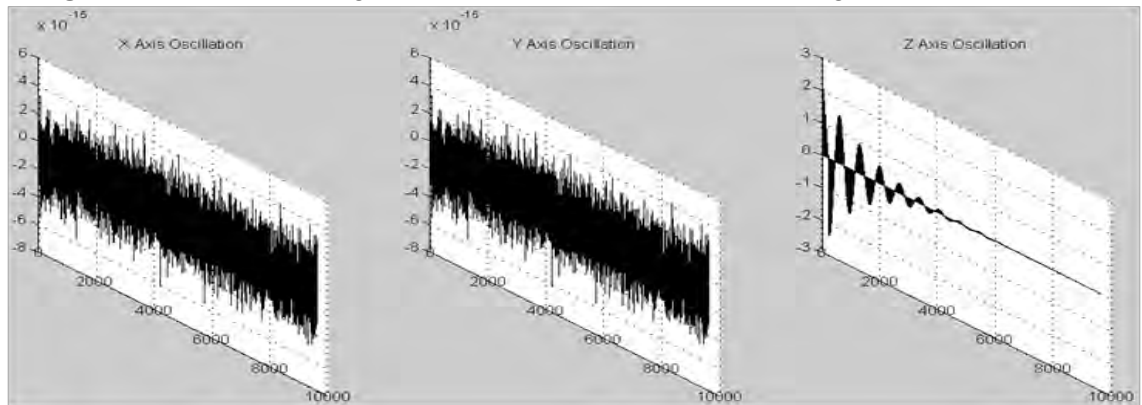


Figure 4.20b Jib tip-Hub top Oscillations for 6.3kW_3000Kg without wind

4.7 Vibration Impact Analysis on Tower Rotation with Wind Disturbance

In this section, wind model disturbance has been applied on rotating tower crane which uses the same setting as: power 1000W-6300W, load 1000Kg-3000Kg, trolley is stationary at 24m (jib end). Wind model (1s notch) is reapplied to strike 3 times at certain time and spots. As stand tall tower crane, it has to face wind disturbance more frequently and it is hard to identify what the actual impacts are. Using this visualized 3D ideal model, the main aim is to easily pin points the facts and to develop suitable control strategy.

As stated above, trials of applying different power-load pairs on the crane with wind disturbance produce significant changes in all payload swing, jib tip oscillation, and hub top oscillation, Table (4.6). Though it shows less swing angle during (1kW-

1000kG to 6kW-1000Kg), jib tip oscillation is having higher amount of fluctuation and that reminds how unstable the crane would be and the operational risk it might cause on the crane and its surrounding. The worst case is at 6kW-3000 Kg which causes large swing (-30 to 30) with 379 deg/s^2 jib oscillation in Fig. 4.21. This case reminds that, having a 1s wind disturbance notch on the crane while the higher payload is at the end of jib could cause the crane tragedy unless the payload swing is suppressed in time. As discussed earlier, operator has to juggle back-and-forth the trolley to minimize swing manually causing fatigue in long run, the operation can be out of control at any time which can cause the crane collapse. Therefore, this research aims to initially identify those dreadful situations so that further suitable control can be designed.

Tower Rotation with Wind Disturbance and Trolley is Stationary at 24m =				
	None	TR(deg)	LS(deg)	JT(deg/s ²)
1kW_1000Kg	0	20.03642	6.04991	32.57941
1kW_3000Kg	0	19.32866	5.62581	30.28098
2kW_1000Kg	0	16.04339	4.19598	22.27253
2kW_3000Kg	0	15.64711	3.90155	20.86583
3kW_1000Kg	0	10.59529	2.56004	12.56190
3kW_3000Kg	0	10.36667	2.45389	11.25387
4kW_1000Kg	0	7.30947	1.42774	6.61928
4kW_3000Kg	0	7.40113	1.43044	6.69448
5kW_1000Kg	0	4.21481	0.53703	1.83848
5kW_3000Kg	0	4.55268	0.57319	2.32571
6kW_1000Kg	0	4.29530	1.39683	3.06241
6kW_3000Kg	0	49.47872	24.34930	379.73047

Table 4.6 Ideal Tower Rotation with Wind Disturbance and Stationary Trolley at 24m

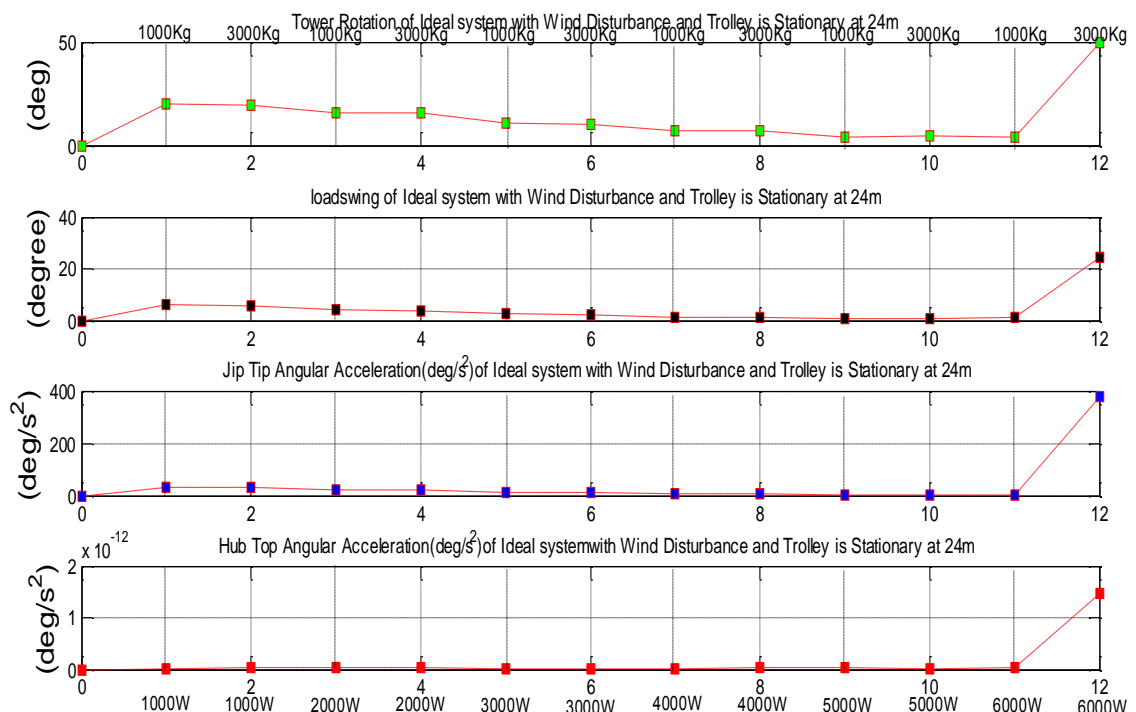


Figure 4.21 Ideal Tower Rotation with Wind Disturbance and Trolley at 24 m

Rotating tower crane with 3 times (1s notch) wind disturbances simulation results provides significant load swings, payload trajectory, jib tip, and hub top oscillations such as: tower rotation appeared to reach further beyond the target, having large unsettled load swings (-30 to 30), higher range of jib angular accelerations $379 \frac{\text{deg}}{\text{s}^2}$ and $1.48e^{-12} \frac{\text{deg}}{\text{s}^2}$, reasonable amount of Hub top oscillations, and large swings payload trajectory in Fig. 4.22a and Fig. 4.22b. Therefore it proves that, maximum applicable power input and load alone could not produce higher load trajectory however even a small amount of wind disturbance could make major impact on the whole crane operation.

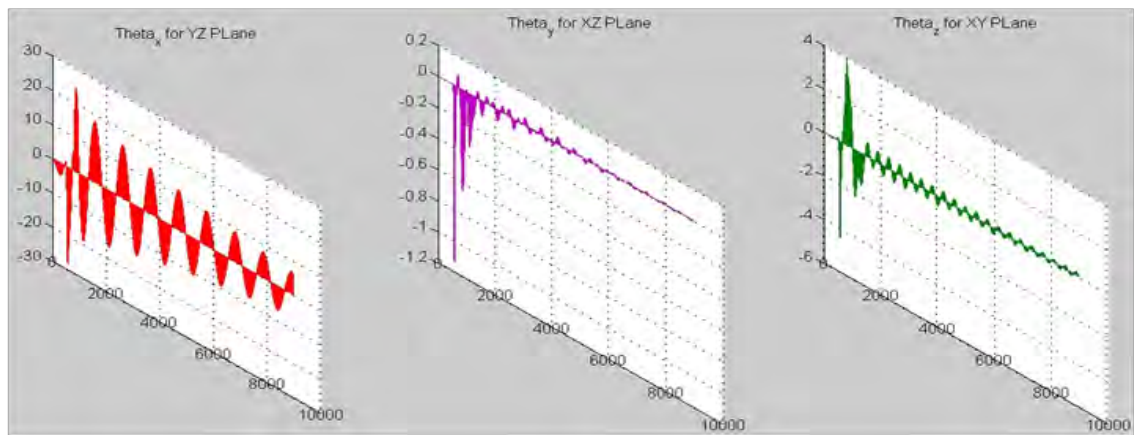


Figure 4.22a Load Swing X-Y-Z responses for 6.3kW and 3000Kg with wind disturbance

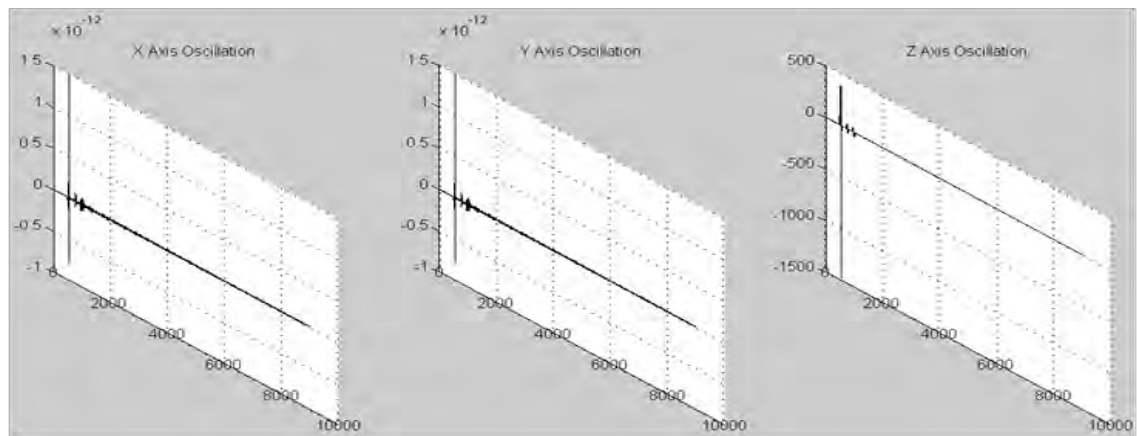


Figure 4.22b Jib tip-Hub top Oscillations for 6.3kW and 3000Kg with wind disturbance

To further analyse the vibration impact on the load swing, Tower rotation with trolley-attached payload has been simulated using different combinations of power input (0~6.3kW) vs load (0~3000 Kg) while applying wind disturbance. Simulations results show that there are significant load-swing changes due to different wind patterns affecting tower vibration. For instance, the extreme case of (maximum allowable 6.3kW-power input to tower rotation, maximum allowable 3000Kg-payload,

18m-load length, trolley is stationary at 23m) system applied by wind (static-gusts-pressure: 22-43-1017) shows swing output error is $E=2323.7$ in Fig. 4.23a, while Jib tip angular acceleration error is $E=1.29e-12$ in Fig. 4.23b, and applied wind (static-gusts-pressure: 41-86-1010) shows swing output error is $E=3074.2$ in Fig. 4.23c, while Jib tip angular acceleration error is $E=2.86e-10$ in Fig. 4.23d. Simulation shows that: changes in wind static-gusts-pressure on tower rotation turn out to have higher tower vibration which causes large unsettled load swing.

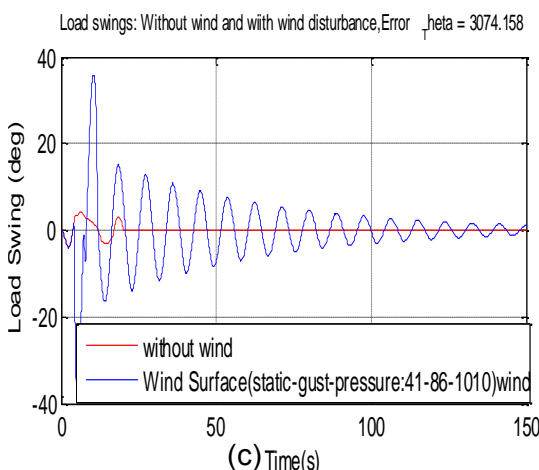
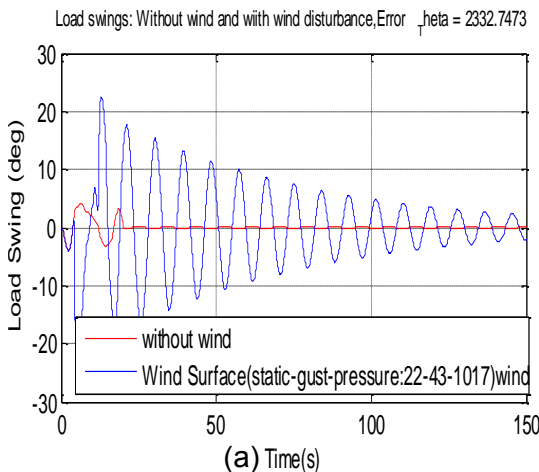


Figure 4.23a Load Swings without Wind and with Wind Pattern (22-43-1017) in Tower Rotation Case

Figure 4.23c Load Swings without Wind and with Wind Pattern (41-86-1010) in Tower Rotation Case

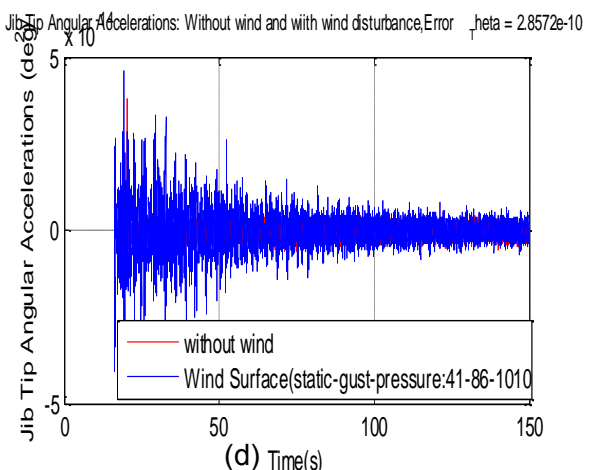
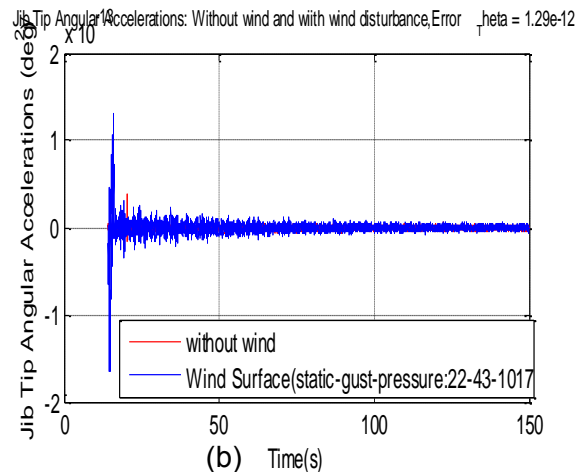


Figure 4.23b Jib Oscillation of without Wind and with Wind Pattern (22-43-1017) in Tower Rotation Case

Figure 4.23d. Jib Oscillation of without Wind and with Wind Pattern (41-86-1010) in Tower Rotation Case

4.7.1 Vibration Impact Analysis on Tower Rotation-Trolley Translation with Wind Disturbance

In this section, wind model disturbance has been applied on rotating tower crane while trolley translation throughout the jib tower. This simulation uses power

input 6300W for tower to rotate (0 to 60 degree, maximum load 3000Kg, and the power input 3kW for trolley translation (0 to 20m). Wind model (1s notch) is reapplied to strike 3 times at certain time and spots. It is intended to identify vibration impact of the crane due to the dynamical interactions of tower rotation while trolley is translating. Interestingly, the simulation results contain vital information about the vibration impact of the crane in this scenario. The following Fig. 4.24a shows Tower rotation while Trolley translation is in process. During the operation, Wind pattern (static-gusts-pressure: 22-43-1017) is applied the same as before. However, due to the parallel tower-trolley run, swings angles fluctuations , Fig. 4.24b, and jibtip-hubtop oscillations are high. Fig. 4.24c obviously shows high oscillation reaching (-7 to 7 deg/se²) while reasonable amount of Hub-top oscillation appeared, Fig. 4.24d, which can cause the crane collapse. Therefore, this preliminary simulations results show running tower-trolley parallel operation is not recommended in real time.

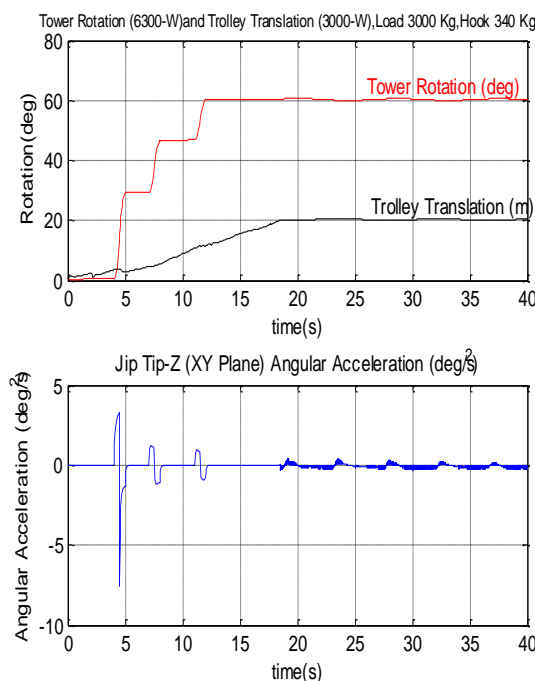


Figure 4.24a Parallel Operation of Tower Rotation and Trolley Translation

Figure 4.24c Jib-Tip Oscillation with Wind Pattern (22-43-1017)

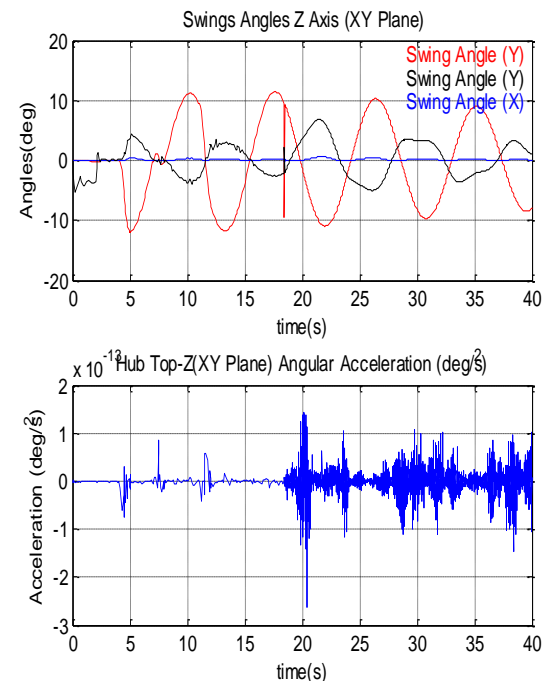


Figure 4.24b Swing angles in (X-Y-Z) directions

Figure 4.24d Hub-Top Oscillation with Wind Pattern (22-43-1017)

4.9 Discussion and Analysis

In previous sections, the model developments and simulations of rigid model, and Ideal model have been discussed. Initially, Rigid model tower crane with rigid hub and jib shows higher jip tip angular acceleration throughout simulation. Even though, it seems to be simple model for simulation purpose however continuous high oscillation

contradicts real operating crane and it cannot be used as research model. Then, ideal model has been focused as the most suitable and reliable model which was then tested with and without wind disturbance. Applying $x=1.2\text{m}$ (width) and $y=3.2\text{m}$ (height) of wind surface which simply notches for 1 second proves significant impact on tower crane. Firstly, the models with (3kW maximum power input with 1000Kg and 3000Kg attached payload) were tested separately and it shows Jib tip and Hub Top oscillations are reasonably higher than the model without wind disturbance. Secondly, ideal model tower rotation with (maximum power 6300W, 3000Kg load attached at the jib's end) was tested and again the simulations shows that all load swing, jib tip, and hub top angular acceleration values are much higher than the tower rotation without wind disturbance, Table (4.7).

Overall, this research clearly proves that, "if the stronger wind with larger wind surface area strikes, the higher jib tip/hub top oscillations would be, and it makes not only the higher load swing but also longer swing settling time".

Oscillation ~ Load Swing Analysis of Tower Crane Translation/Rotation

Models	Power ~ Load	Load Swings (deg)		Jib Tip Angular Acceleration		Hub Top Angular Acceleration	
Rigid Model Translation (No Wind Disturbance)	3kW-1000Kg	36.3°	76.7°	18.4	55.3	$2.7e^{-13}$	$5.6e^{-13}$
		-40.4°		-36.9		$-2.9e^{-13}$	
Ideal Model Translation (No Wind Disturbance)	3kW-1000Kg	47.4°	96.5°	$1.3e^{-9}$	$3e^{-9}$	$7.4e^{-13}$	$8.8e^{-13}$
		49.1°		$-1.7e^{-9}$		$-1.4e^{-13}$	
Ideal Model Translation (with 1.2_3.2 Width wind disturbance)	3kW-3000Kg	13.1°	32.3°	$5.8e^{-9}$	$10.6e^{-9}$	$8.8e^{-13}$	$14.0e^{-13}$
		19.2°		$-4.8e^{-9}$		$-5.2e^{-13}$	
Ideal Model Rotation (No Wind Disturbance)	6.3kW-3000Kg	54.2°	95.3°	$3.6e^{-9}$	$7.3e^{-9}$	$4.0e^{-10}$	$6.3e^{-10}$
		-41.1°		$-3.7e^{-9}$		$-2.2e^{-10}$	
Ideal Model Rotation (with 1.2_3.2 Width wind disturbance)	6.3kW-3000Kg	14.6°	33.1°	$4.03e^{-9}$	$8.0e^{-9}$	$3.0e^{-10}$	$7.1e^{-9}$
		-18.5°		$-3.2e^{-9}$		$-4.1e^{-10}$	

Table 4.7 Oscillation VS Load Swing comparison Case Analysis

4.10 Linearized System Identification and Optimization of 6kW-3000Kg case

The SimMechanics-Visualized tower crane model with wind disturbance discussed above is shown as schematic diagram representation in which, the control input is the torque (T) that rotates around Y-axis and the outputs are angular positions

of Tower(θ_y) and Load Swing (θ_x). As a 3D model, both outputs produce X-Y-Z axes values however θ_y for tower and θ_x for load swing are always highest during tower rotation. Necessary interaction forces, F_z , and F_y between the cart and attached payload are also considered to fully model the system's dynamics in Fig. 4.25. Applying Newton's second law of motion ($F=ma$), the differential equations, as in (6) and (7), are generated as follow.

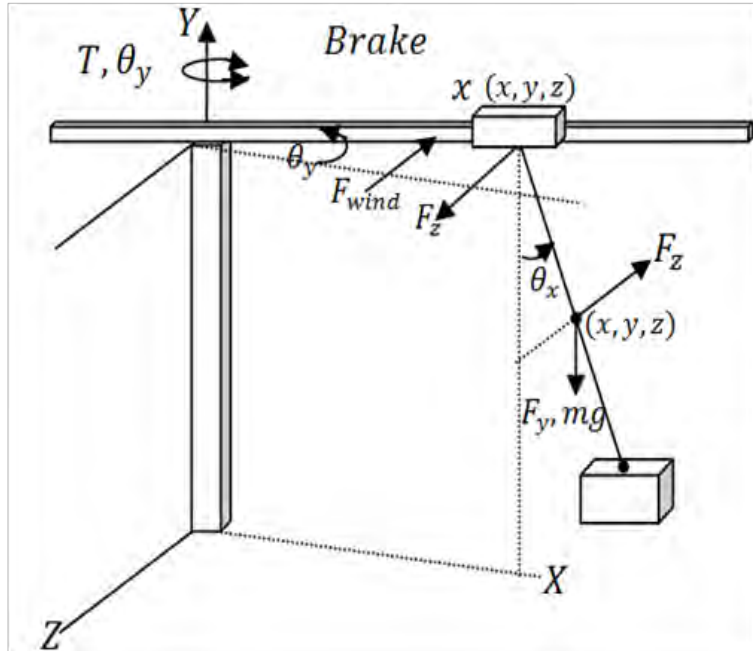


Figure 4.25 Wind Disturbance strikes on Tower Crane

For Tower Rotation θ_y in Eq.(4.5) is

$$\sum \tau = I\ddot{\theta}_y = T - (F_{wind} * 1) - (F_z * x) + B\dot{x}_t \\ \ddot{\theta}_y = \frac{1}{I}[T - (F_{wind} * 1) - (F_z * x) + B\dot{x}_t] \quad (4.5)$$

For Load Swing θ_x in Eq.(4.6) is

$$\sum \tau = I\ddot{\theta}_x = (F_z * y) + ((F_z + mg) * z) \\ \ddot{\theta}_x = \frac{1}{I}[(F_z * x) + ((F_y + mg) * z)] \quad (4.6)$$

where F_{wind} is wind disturbance, F_z and F_y are interaction forces between trolley and load cable, and B is Brake friction.

4.10.1 System Identification and Model Optimization

This research discussed ILLS algorithm in earlier section. Once the models are generated from the identified states, $\theta_1 \dots \theta_M$, one such common criterion is the minimization of sum of the squared differences between the actual data and the predicted data due to the least squares line [6]. The error (E), in Eq.(4.7), where $i = 1, 2, 3, \dots, N$ is the number of data points, and y_{ls} is the approximating curve's predicted y at the point θ_i .

$$E = \sum_{i=1}^N [y_i - y_{ls}(\theta_i)]^2 \quad (4.7)$$

To identify the system and optimize the best fit, this research picked the worse case scenario of "6300 W power input_3000 Kg load" tower rotation with wind disturbance since the values of loadswing angle and jib tip-hub top acceleration are at peak. The ILLS algorithm [5] in Eq.(4.8), has been reapplied to pick up lowest RMSE of individual case from (Den2-Num2 to Den-6-Num6) then compare again to filter for the best fit model. In the case of Tower rotation, the following Table, Table (4.8), shows RMSE 16.515 which is lowest in the case of Den6-Num6 however the best fit model appears to be Den4-Num4 with RMSE 4.7876 among the lowest in Fig 4.26a. Likewise, load swing best fit model appears to be Den6-Num6 with RMSE 7.5094 in Fig 4.26b. where M is total number of generated models.

$$\theta_1 = X_1^T * Y_1, \theta_2 = X_2^T * Y_2, \theta_3 = X_3^T * Y_3, \dots, \theta_M = X_M^T * Y_M \quad (4.8)$$

RMSEs (Tower)	Den	Num	RMSEs (LS)	Den	Num
4.7876	4	4	7.5094	6	6
11.878	4	2	7.8129	5	5
12.151	5	5	7.9132	3	3
12.834	4	3	7.915	3	2
13.89	3	4	7.9325	3	4
13.927	2	4	7.9756	2	4
13.958	2	3	7.998	2	3
14.877	3	3	8.0359	2	2
15.885	3	2	8.2527	4	2
16.192	2	2	8.3405	4	4
16.515	6	6	8.3609	4	3

Table 4.8 Tower Rotation with Wind Disturbance 6.3kW_3000Kg case using improved Linear Least Square Algorithm

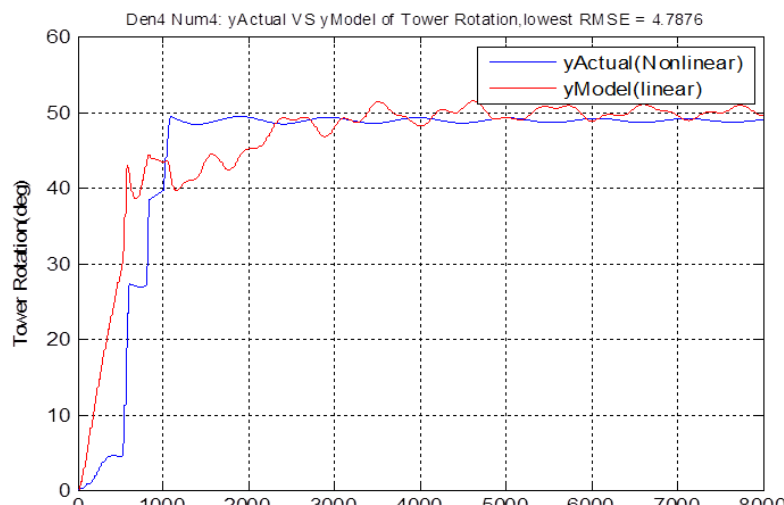


Figure 4.26a The Best Fit Tower Angular Rotational Linear Model vs Nonlinear Actual Output

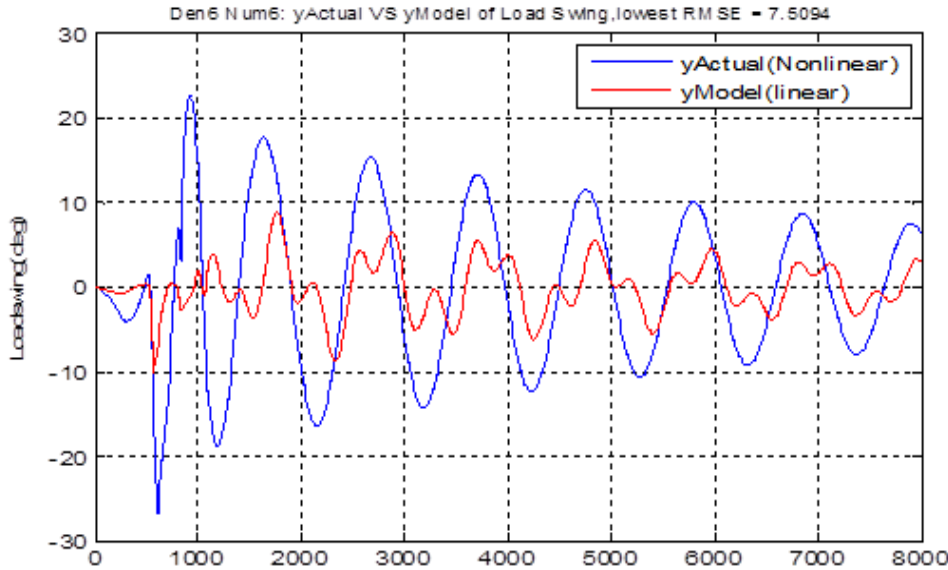


Figure 4.26b The Best Fit Paylaod swing Linear Model vs Nonlinear Actual Output

From the generated best fit models of both Den4-Num4 in Eq.(4.9)and Den6-Num6,in Eq.(4.10), transfer functions are developed.

Tower Rotation ~ Torque Model:

$$\frac{\theta_{yt}}{T_t} = \frac{(-2.72 \times 10^{-9})s^4 + (2.59 \times 10^{-7})s^3 - (4.104 \times 10^{-6})s^2 + (6.87 \times 10^{-6})s - (1.304 \times 10^{-4})}{s^4 + 31.34 s^3 + 588.9 s^2 + 109.3 s + 1.32} \quad (4.9)$$

Load Swing ~ Torque Model

$$\frac{\theta_{xl}}{T_l} = \frac{(-2.76 \times 10^{-11})s^6 + (1.52 \times 10^{-9})s^5 - (1.67 \times 10^{-7})s^4 + (3.254 \times 10^{-6})s^3 - (1.95 \times 10^{-5})s^2 + (2.5 \times 10^{-4})s + (4.17 \times 10^{-4})}{s^6 + 92.1 s^5 + 3206 s^4 + 3.4e4 s^3 + 3.997e5 s^2 + 3.44e4 s + 4084} \quad (4.10)$$

where θ_{yt} represents Y-axis tower rotation angle, T_t is tower drive torque, θ_{xl} is X-axis load swing angle, and T_l is load drive torque. Differential equation in Eq.(4.11) with input (u) output (y) and state (x), is used to convert the model transfer functions into final state space format, A and B.

$$\ddot{x} + a_1\ddot{x} + a_2\dot{x} + a_3x + a_4u = b_0u \quad (4.11)$$

$$\begin{aligned} q_1 &= x, q_2 = \dot{q}_1 = \dot{x}, q_3 = \dot{q}_2 = \ddot{x}, \\ q_4 &= \dot{q}_3 = \ddot{x}, \dot{q}_4 = \dddot{x} \end{aligned}$$

So $\dot{q}_4 + a_1q_4 + a_2q_3 + a_3q_2 + a_4q_1 = b_0u$

Then $\dot{q}_4 = -a_1q_4 - a_2q_3 - a_3q_2 - a_4q_1 + b_0u$

$$\dot{q} = Aq + Bu, y = Cq + Du$$

$$\begin{bmatrix} \dot{q}_4 \\ \dot{q}_3 \\ \dot{q}_2 \\ \dot{q}_1 \end{bmatrix} = \begin{bmatrix} -a_1 & -a_2 & -a_3 & -a_4 \\ 1 & 0 & 0 & 0 \\ 0 & 1 & 0 & 0 \\ 0 & 0 & 1 & 0 \end{bmatrix} \begin{bmatrix} q_4 \\ q_3 \\ q_2 \\ q_1 \end{bmatrix} + \begin{bmatrix} b_0 \\ 0 \\ 0 \\ 0 \end{bmatrix} u$$

$$\text{State space format for } \frac{\theta_{yt}}{T_t}, \quad A = \begin{bmatrix} -a_1 & -a_2 & -a_3 & -a_4 \\ 1 & 0 & 0 & 0 \\ 0 & 1 & 0 & 0 \\ 0 & 0 & 1 & 0 \end{bmatrix}, \quad B = \begin{bmatrix} b_0 \\ 0 \\ 0 \\ 0 \end{bmatrix}$$

State space format for $\frac{\theta_{xl}}{T_l}$,

$$q_5 = \theta, q_6 = \dot{q}_5 = \dot{\theta}, q_7 = \dot{q}_6 = \ddot{\theta}, q_8 = \dot{q}_7 = \ddot{\theta}, q_9 = \dot{q}_8 = \ddot{\theta}, \dots, q_{10} = \dot{q}_9 = \ddot{\theta}$$

$$\begin{bmatrix} \dot{q}_{10} \\ \dot{q}_9 \\ \dot{q}_8 \\ \dot{q}_7 \\ \dot{q}_6 \\ \dot{q}_5 \end{bmatrix} = \begin{bmatrix} -a_5 & -a_6 & -a_7 & -a_8 & -a_9 & -a_{10} \\ 1 & 0 & 0 & 0 & 0 & 0 \\ 0 & 1 & 0 & 0 & 0 & 0 \\ 0 & 0 & 1 & 0 & 0 & 0 \\ 0 & 0 & 0 & 1 & 0 & 0 \\ 0 & 0 & 0 & 0 & 1 & 0 \end{bmatrix} \begin{bmatrix} q_{10} \\ q_9 \\ q_8 \\ q_7 \\ q_6 \\ q_5 \end{bmatrix} + \begin{bmatrix} b_1 \\ 0 \\ 0 \\ 0 \\ 0 \\ 0 \end{bmatrix} u$$

By combining for $\frac{\theta_{yt}}{T_t}$, and $\frac{\theta_{xl}}{T_l}$ in Stat Space format, the matrices A and B are

$$\begin{bmatrix} -a_1 & -a_2 & -a_3 & -a_4 & 0 & 0 & 0 & 0 & 0 & 0 \\ 1 & 0 & 0 & 0 & 0 & 0 & 0 & 0 & 0 & 0 \\ 0 & 1 & 0 & 0 & 0 & 0 & 0 & 0 & 0 & 0 \\ 0 & 0 & 1 & 0 & 0 & 0 & 0 & 0 & 0 & 0 \\ 0 & 0 & 0 & 0 & -a_5 & -a_6 & -a_7 & -a_8 & -a_9 & -a_{10} \\ 0 & 0 & 0 & 0 & 1 & 0 & 0 & 0 & 0 & 0 \\ 0 & 0 & 0 & 0 & 0 & 1 & 0 & 0 & 0 & 0 \\ 0 & 0 & 0 & 0 & 0 & 0 & 1 & 0 & 0 & 0 \\ 0 & 0 & 0 & 0 & 0 & 0 & 0 & 1 & 0 & 0 \\ 0 & 0 & 0 & 0 & 0 & 0 & 0 & 0 & 1 & 0 \end{bmatrix}, \quad \begin{bmatrix} b_0 \\ 0 \\ 0 \\ 0 \\ 0 \\ b_1 \\ 0 \\ 0 \\ 0 \\ 0 \end{bmatrix}$$

4.11 LQR Full State Feedback Controller With Reference Tracking

Researchers propose a full-order friction disturbance observer with sensor-delay correction for a lab scale 1D overhead crane prototype to eliminate swing caused by vibration-affected nonlinear friction [8]. Though nonlinear friction is considered due to vibration, the analysis of vibration was not discussed. Time Delay Filtering method for cancelling vibration has also been proposed [9]. Likewise, Ref. [44] considered vibration in rotary crane system (which is similar to tower jib rotation) and proposed three-layered neural network Generic Algorithm (GA-based) training controller.

4.11.1 Tower Crane Rotation and LQR Swing Control

In this research, Linear quadratic regulation (LQR) method in Fig. 4.27 is applied for the tower crane model aiming to achieve robust control in minimizing the

load swing. The plant is written in the state space form, $\dot{x} = Ax + Bu$, and the optimal feedback gain (K) is implemented as $u = -K(x - x_{desired})$, as in [67].

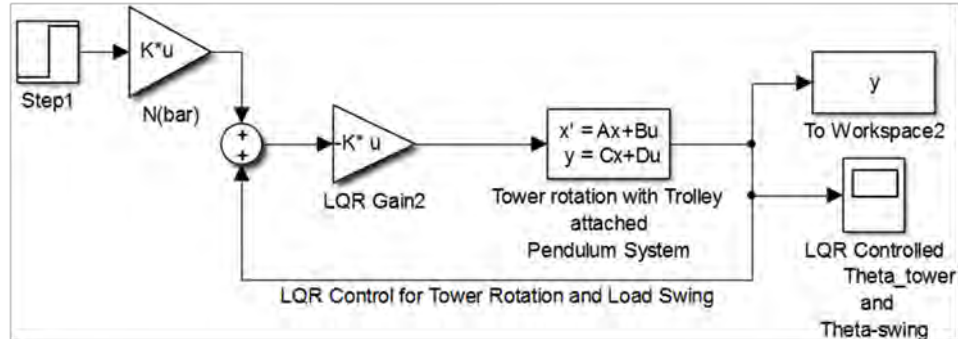


Figure 4.27 Full state feedback-LQR Control for Tower rotation and loadswing

For the particular 6300W input tower drive with payload 3000Kg system: Tower vibration impact due to wind effect causing longer unsettled load swing has also been discussed above. LQR implementation with Q and R weighting matrices brings both tower rotation and load swing under control. Since the system still needs to track the desired reference, full state feedback is then implemented. The simulation results show, desired reference tower rotation smoothly achieves within 50- second in Fig. 4.28a, while payload swing up to maximum 5 degree with no fluctuation and bring back to 0 degree in 40 seconds time in Fig 4.28b.

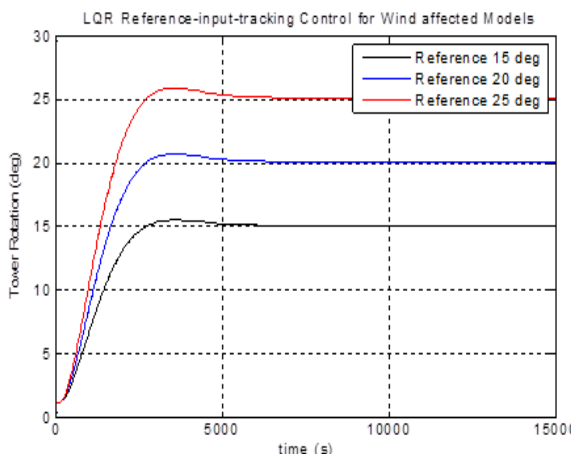


Figure 4.28a LQR Full State Feedback Control for Tower Rotation

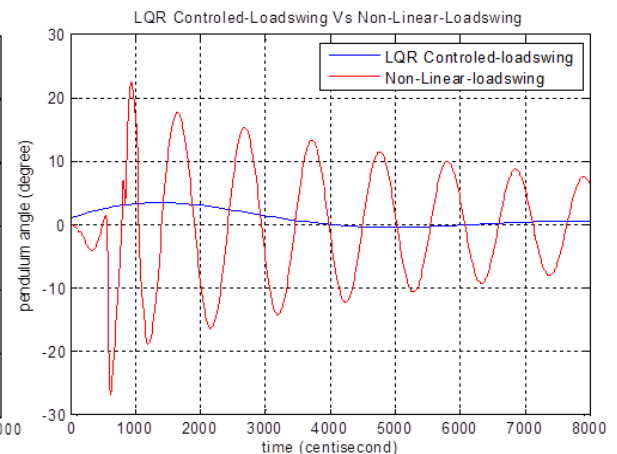


Figure 4.28b Comparison of LQR Full-State Feedback Controlled Load Swing and Nonlinear Load Swing

4.11.2 Simulations and Results Comparison with PID

This section contains performance evaluations of the proposed LQR Full state feedback strategy and results from the SimMechanics-Visualized tower crane model introduced in Section 2. In addition, robustness investigations and a comparison with simple Proportional-Integral-Derivative (PID) Control are carried out. LQR full state feedback applies ($Q_{\theta_{yt}} = 1, Q_{\theta_{xt}} = 1, R = 0.00001$) for states and input weighting

values while simple PID in Fig. 4.29 needs larger parameters ($P = -600000, I = -7000, D = 50000$) to stabilize the system. In tower rotation, LQR smoothly brings the tower to desired angular position and reaches to stability in less than 50 seconds while PID uses large gains yet there are fluctuations and overshoots in both Tower rotation in Fig. 4.30a and payload swing in Fig. 4.30b. It is very much crucial to have steady tower rotation with very low load swing in every operation. Again, LQR controlled-load swing appeared to have just one overshoot reaching maximum 3 degree before gradually goes to zero while PID controlled-response has continuous swings. Therefore, the proposed LQR full state feedback controller proves to be reliable.

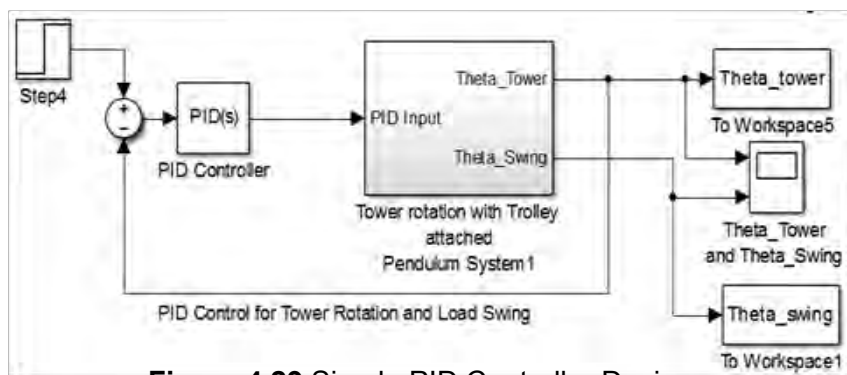


Figure 4.29 Simple PID Controller Design

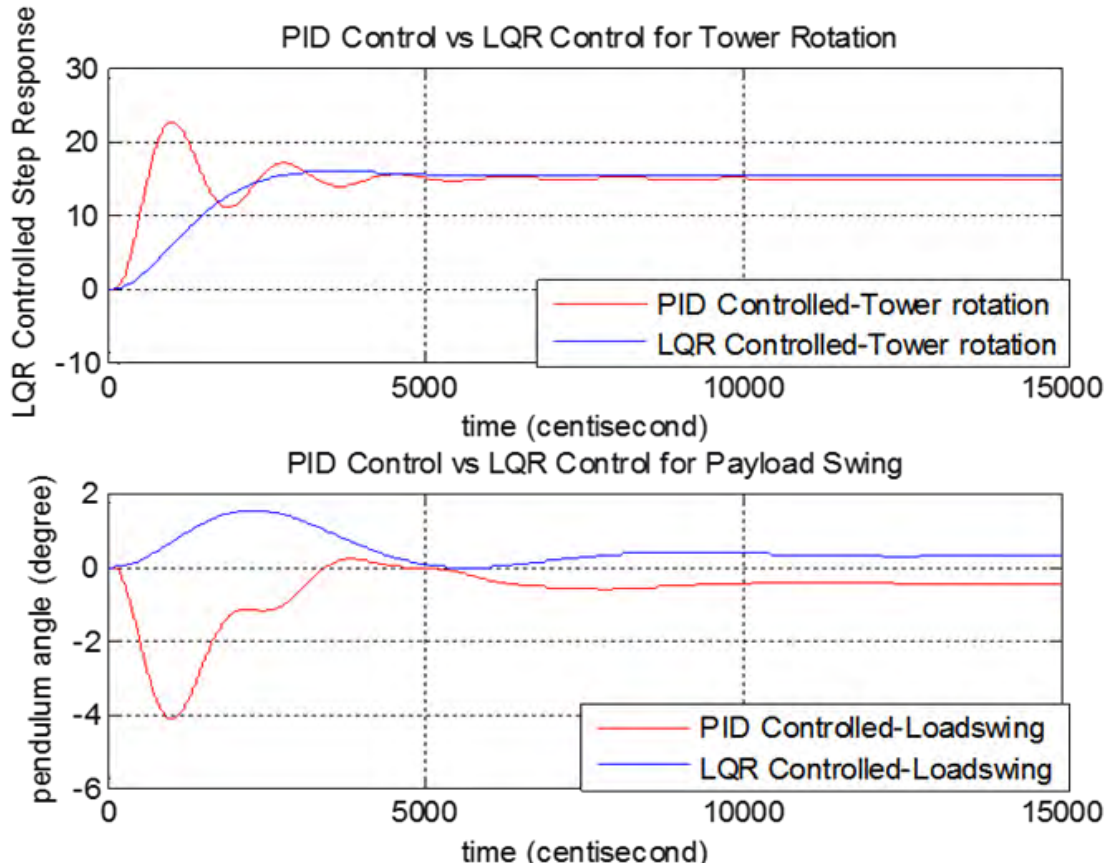


Figure 4.30a Full state feedback-LQR Control for Tower rotation

Figure 4.30b Full state feedback-LQR Control for Payload swing

4.12 Conclusion

In short, 3D Tower Crane SimMechanics visualized model based on real crane (Morrow:Liebherr71EC) was successfully built. It is a major landmark for crane researchers who do not need to rely on real crane in the future to do more credible research since this model could be the reliable research platform. From this flexible model, many other types of crane such as gantry crane, ship crane, and mobile crane could be easily transformed for future research. Initial calculation shows crane is having moment at the joint (between hub top and jib tower) which means jib oscillation could happen at any time during operation which results in more load swing. Therefore, wind disturbance came to attention since it is the major factor for the stand alone large tower crane. Wind disturbance model was then developed. Ideal crane and rigid crane were then tested separately with/without wind disturbance. Once jib tip/hub top oscillations appeared in ideal crane model (real crane looks alike), different types of wind models were again introduced to thoroughly check how load swing/jib tip/hub top responses. Then, the analysis of Ideal tower rotation with/without wind disturbance again proved that the trend of load swing/jib oscillation was lower for the system without wind strike however those load swing/jib oscillation trends became significantly higher once the wind disturbance is applied.

Obviously, the simulations show the more wind strikes/the bigger wind surface/the rougher wind terrain is, jib tip/hub top oscillation becomes high to elevate load swing and apparently causes crane's instability. At this stage, this research is believed to have provided clear view for crane researchers who likes to go further control process. This research would also come up with nonlinear modeling and non-linear controller design to run real time crane control in near future.

Chapter 5

Linear Controllers Development

5.0 Controllers Implementation

Construction tower crane load swing control is a diverse field that can be presented in many different ways. Inferring models from mathematical derivations (or) lab-scale prototypes and designing the strategy to minimize the effects of variables which would increase the reliability is really what load swing control is about. Specifically, Payload swing control deals with the surrounding problems of swing uncertainties, cable nonlinearities, and trolley dynamical systems. Though the extensive research has indeed been done, some of the basic dynamical issues such as wind disturbance, vibration, lab-scale models, factor assumptions based on real parameters are sometimes abundant in the crane load-swing controls. The subject is thus part of swing control methodology, and since it is difficult to access real time crane operation for research purpose, the techniques of load-swing control have continued becoming a wide application area of interest.

This research had developed a new modeling scheme "SimMechanics-visualized crane model for 3D tower crane" in Fig. 5.1 analyzed wind disturbance affected-tower vibration impact on the load swing, improved version of linear least square system identification algorithm, and then proposed reference point tracking with full state feedback Linear Quadratic Regulator (LQR) control, [5]. However, to cancel out the disturbance which affects the system, minimize payload swing, as well as achieve robust reference tracking, methods such as: LQR-Disturbance Rejection Observer, LQR-Estimator-Integral Controls for linear trolley-loadswing models are presented in this section.

Simulations prove that, LQR-DRO implementation actively rejects the disturbance while in the absence of a detailed mathematical model of the plant or the disturbance itself. Likewise, the combined LQR-Estimator-Integral Control (LEIC) that

presents internal model principle (error space approach) with full-order estimator performs robust reference tracking.

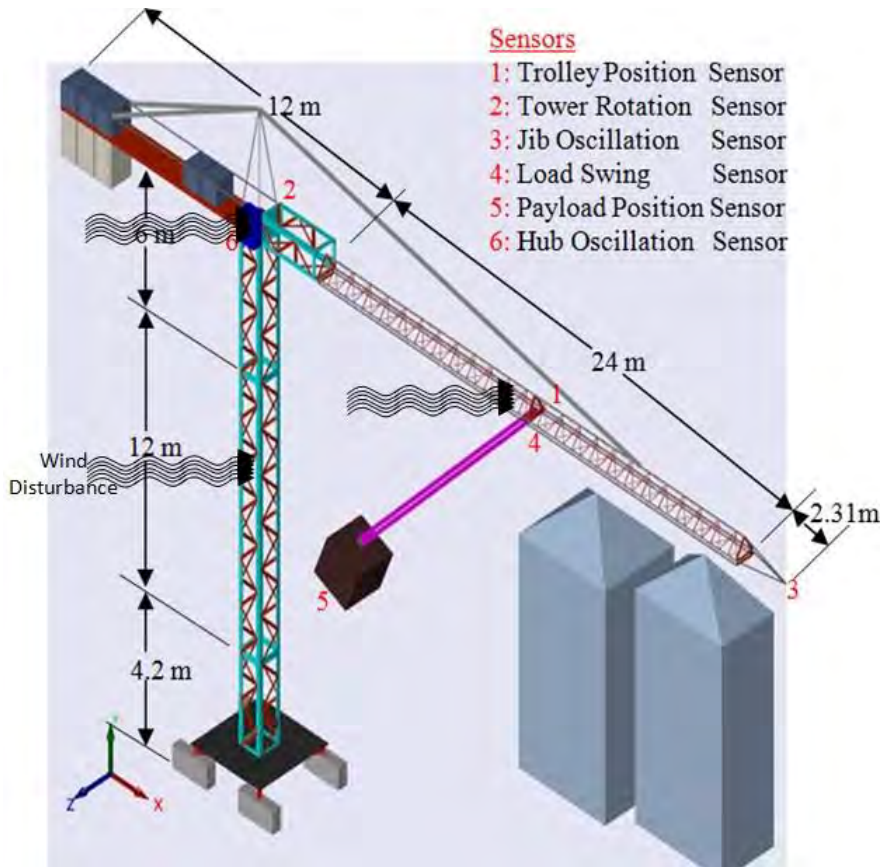


Figure 5.1 Tower Crane SimMechanics-Visualized 3D Model
based on (Liebheer 71 EC: Morrow Crane data sheet)

5.1 LQR-Disturbance Rejection Observer Control

The majority of tower crane manipulators are designed and used for handling known loads under limited perturbations. Control methods for the crane manipulators have therefore focused mainly on modeling and control of the dynamics of the trolley-jib, tower-loadswing, rather than on counteracting external disturbances. In an industrial scenario, cranes work in highly structured environments where disturbances are minimized and tasks are repetitive. However, torque disturbances generate velocity and position errors. Likewise, load currents can also act as a disturbance to a power supply by pulling the output voltage away from the target. That is, an undesired source of power is added to the power converter output and fed to the plants (trolley translation with payload attached, tower rotation) the result is that the plant states are disturbed. Although feed-forward action is used to achieve high tracking performance in such crane manipulators, disturbance rejection usually relies on high-reduction gearing in the drive train and high-gain feedback, as in [3]-[4].

5.1.1 Disturbance Rejection Observer (DRO)

Disturbance rejection observer can estimate unknown dynamic and compensate to make control more robust and less dependent on the detailed mathematical model of the physical process, as in [5]. This research implements a disturbance rejection observer as an adaptive alternative to integral action to increase the disturbance rejection of the feedback LQR controller. Assuming that frictional and interaction forces between trolley and payload cable can be represented as varying disturbances which are then canceled by the control input once the disturbance observer has estimated the values in order to achieve desired trajectory. By considering controllable and observable system with uncertainty disturbance, the state representation Eq.(5.1) can then be formed, as in [63]

$$\dot{x} = f(x, w, u, t), y = Cx \quad (5.1)$$

whereby f is the function vector of state equations involving variables such as state ($x \in R^n$), external disturbance (w), control input (u), and time (t). Furthermore, the measurement (y) is the linear function (C) of the state variables. Since the system is regarded as controllable, the state representation is then transformed into canonical controllable form as follow.

5.1.2 Trolley Model in Control Canonical Form

There are special canonical forms of the state-variable equations where the algebra for finding the gains is simple. Once such canonical form useful in control law design is the control canonical form and this research refers to the following Differential equation, Eq.(4.11), discussed in section 4.10.1.

$$\ddot{x} + a_1\ddot{x} + a_2\dot{x} + a_3x + a_4u = b_0u$$

Let, $q_1 = x, q_2 = \dot{x}, \dots$ etc.: the state space representation can then be expressed by

$$q_1 = x$$

$$q_2 = \dot{q}_1 = \dot{x}$$

$$q_3 = \dot{q}_2 = \ddot{x}$$

$$q_4 = \dot{q}_3 = \ddot{x}$$

$$q_5 = \dot{q}_4 = \dddot{x}$$

$$\dot{q} = Aq + Bu$$

$$\dot{q}_4 + a_1q_4 + a_2q_3 + a_3q_2 + a_4q_1 = b_0u$$

$$\begin{aligned}\dot{q}_4 &= -a_1 q_4 - a_2 q_3 - a_3 q_2 - a_4 q_1 + b_0 u \\ y &= b_1 \ddot{x} + b_2 \dot{x} + b_3 x + b_4 q_1\end{aligned}$$

All the feedback loops return to the point of the application of the input, or control variable, and hence the form is referred to as the control canonical in Fig. 5.2 [63].

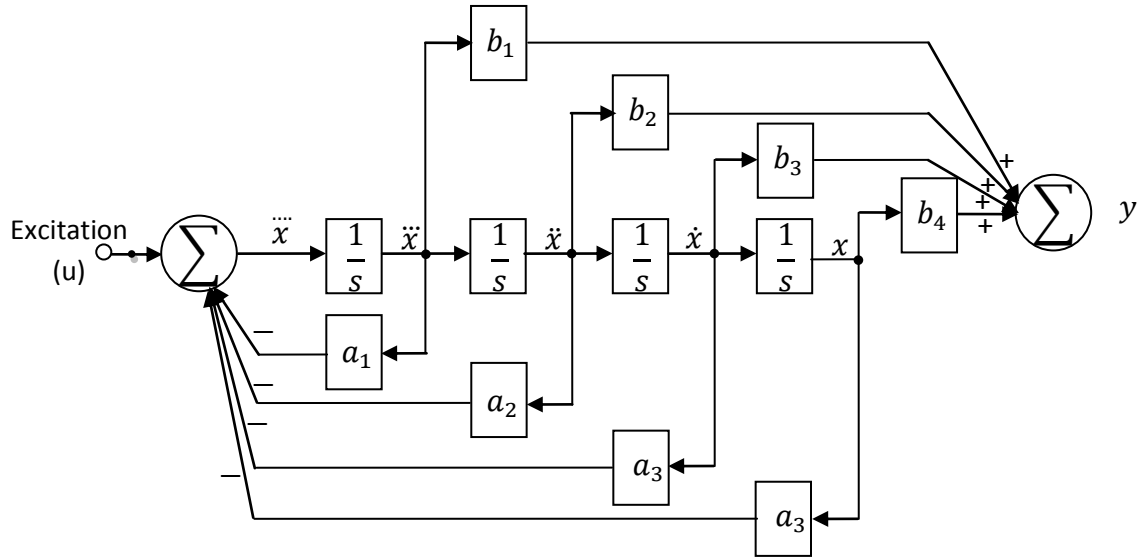


Figure 5.2 Trolley Translation in Control Canonical Form

The matrices describing the control canonical form in general are

$$\begin{bmatrix} \ddot{x} \\ \dot{x} \\ x \end{bmatrix} = \begin{bmatrix} -a_1 & -a_2 & -a_3 & -a_4 \\ 1 & 0 & 0 & 0 \\ 0 & 1 & 0 & 0 \\ 0 & 0 & 1 & 0 \end{bmatrix} \begin{bmatrix} \ddot{x} \\ \dot{x} \\ x \end{bmatrix} + \begin{bmatrix} b_0 \\ 0 \\ 0 \\ 0 \end{bmatrix} u$$

$$\begin{bmatrix} \dot{q}_4 \\ \dot{q}_3 \\ \dot{q}_2 \\ \dot{q}_1 \end{bmatrix} = \begin{bmatrix} -a_1 & -a_2 & -a_3 & -a_4 \\ 1 & 0 & 0 & 0 \\ 0 & 1 & 0 & 0 \\ 0 & 0 & 1 & 0 \end{bmatrix} \begin{bmatrix} q_4 \\ q_3 \\ q_2 \\ q_1 \end{bmatrix} + \begin{bmatrix} b_0 \\ 0 \\ 0 \\ 0 \end{bmatrix} u, \quad y = [0 \ 0 \ 0 \ 1] \begin{bmatrix} q_4 \\ q_3 \\ q_2 \\ q_1 \end{bmatrix}$$

$$\dot{x} = Ax + Bu \tag{5.2}$$

$$y = C_x p_{est}$$

State space, Eq.(5.2), of Trolley Translation System without Disturbance and its states $p_{est}(q, w, u, t)$ are presented where q is states, u is input.

5.1.3 Disturbance Realisation

In order to implement DRO in the system, the system is initially required to convert to an augmented state space model that includes f , short for $f(\ddot{x}, \dot{x}, \dot{x}, x, w, u, t)$, as an additional state, as in [10]. In particular, the augmented state space form of Eq.(5.3) is

$$\dot{q} = A_a q + B_a u + E d, \quad (5.3)$$

$$y_a = C_a q_{est}$$

where the disturbance, nonlinearities and uncertainties have been translated into the last state variable. To represent disturbance, let $q_{n+1} = p_{est}(q, w, u, t)$, and new state variables has been defined as follow:

$$\begin{aligned} q_{1+1} &= q_2 = x \\ q_{2+1} &= q_3 = \dot{x} \\ q_{3+1} &= q_4 = \ddot{x} \\ q_{4+1} &= q_5 = \dddot{x} \\ q_{5+1} &= q_6 = \ddot{\ddot{x}} \end{aligned}$$

By taking derivative of new state variables, Disturbance(d) is realized as, $d = \dot{p}$ which means

$$\begin{aligned} q_2 &= \dot{x} \\ q_3 &= \ddot{x} \\ q_4 &= \dddot{x} \\ q_5 &= \ddot{\ddot{x}} \\ q_6 &= \ddot{\ddot{\ddot{x}}} \end{aligned}$$

The augmented State-space form with Disturbance is,

$$= \begin{bmatrix} -a_1 & -a_2 & -a_3 & -a_4 & 0 \\ 1 & 0 & 0 & 0 & 0 \\ 0 & 1 & 0 & 0 & 0 \\ 0 & 0 & 1 & 0 & 0 \\ 0 & 0 & 0 & 0 & 0 \end{bmatrix} \begin{bmatrix} \ddot{x} \\ \dot{x} \\ \ddot{x} \\ x \\ \dot{d} \end{bmatrix} + \begin{bmatrix} b_0 \\ 0 \\ 0 \\ 0 \\ 0 \end{bmatrix} u + \begin{bmatrix} 0 \\ 0 \\ 0 \\ 0 \\ 1 \end{bmatrix} d$$

Then

$$= \begin{bmatrix} -a_1 & -a_2 & -a_3 & -a_4 & 0 \\ 1 & 0 & 0 & 0 & 0 \\ 0 & 1 & 0 & 0 & 0 \\ 0 & 0 & 1 & 0 & 0 \\ 0 & 0 & 0 & 0 & 0 \end{bmatrix} \begin{bmatrix} q_4 \\ q_3 \\ q_2 \\ q_1 \\ \dot{d} \end{bmatrix} + \begin{bmatrix} b_0 \\ 0 \\ 0 \\ 0 \\ 0 \end{bmatrix} u + \begin{bmatrix} 0 \\ 0 \\ 0 \\ 0 \\ 1 \end{bmatrix} \begin{bmatrix} q_6 \\ q_5 \\ q_4 \\ q_3 \\ q_2 \end{bmatrix}$$

$$= \begin{bmatrix} -a_1 & -a_2 & -a_3 & -a_4 & 0 \\ 1 & 0 & 0 & 0 & 0 \\ 0 & 1 & 0 & 0 & 0 \\ 0 & 0 & 1 & 0 & 0 \\ 0 & 0 & 0 & 0 & 0 \end{bmatrix} \begin{bmatrix} q_4 \\ q_3 \\ q_2 \\ q_1 \\ d \end{bmatrix} + \begin{bmatrix} b_0 \\ 0 \\ 0 \\ 0 \\ 0 \end{bmatrix} u + \begin{bmatrix} 0 \\ 0 \\ 1 \\ 0 \\ 0 \end{bmatrix} \begin{bmatrix} q_4 \\ q_3 \\ q_2 \\ q_5 \\ q_6 \end{bmatrix}$$

$$\dot{q} = A_a q + B_a u + E d,$$

$$A_a = \begin{bmatrix} -a_1 & -a_2 & -a_3 & -a_4 & 0 \\ 1 & 0 & 0 & 0 & 0 \\ 0 & 1 & 0 & 0 & 0 \\ 0 & 0 & 1 & 0 & 0 \\ 0 & 0 & 0 & 0 & 0 \end{bmatrix}, B_a = \begin{bmatrix} b_0 \\ 0 \\ 0 \\ 0 \\ 0 \end{bmatrix}, E = \begin{bmatrix} 0 \\ 0 \\ 1 \\ 0 \\ 0 \end{bmatrix}$$

$$C_a = \begin{bmatrix} 1 & 0 & 0 & 0 & 0 \\ 0 & 1 & 0 & 0 & 0 \\ 0 & 0 & 1 & 0 & 0 \\ 0 & 0 & 0 & 1 & 0 \\ 0 & 0 & 0 & 0 & 1 \end{bmatrix}, D_a = [0; 0; 0; 0; 0]$$

$$y_a = C_a q_{est}$$

5.1.4 Extended State Observer (ESO) Design

There are also many observers proposed in the literature, including the unknown input observer, the disturbance observer, the perturbation observer, and the extended state observer (ESO). The ESO design was originally proposed by J. Han [68]. The plant model is represented by the state matrix A and the input matrix B , with measurement given by the output matrix C . The model of the augmented process given as A_a, B_a, C_a, D_a contains an extra state representing the disturbance d . The ESO model runs in parallel with the augmented plant generating predictions $[\hat{x}_1, \hat{x}_2, \dots, \hat{x}_n, \hat{d}]^T$. Since the disturbance is not part of the input of the observer model, the predicted and observe variables y and y_o will differ. This error in prediction is corrected by the use of the gains L to control the observer dynamics back to the true dynamics in Fig. 5.3. Under perfect model assumptions, the amount of correction needed is the estimated value of the disturbance at the plant input \hat{d} . Mathematically, such an equivalent disturbance is “observable” from the input-output data from the process and the observer can be easily constructed as shown below.

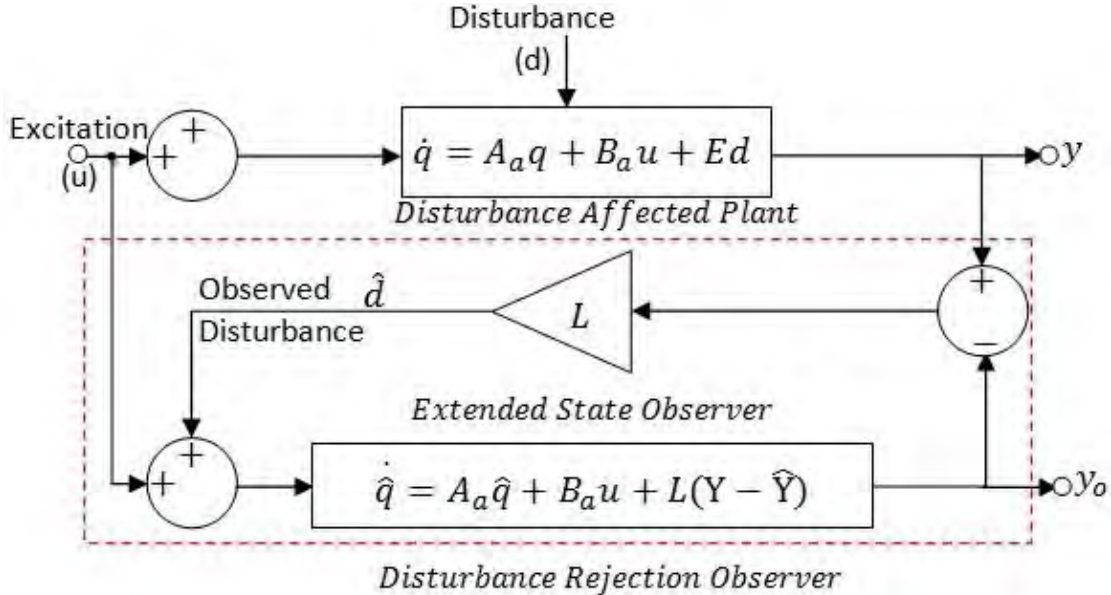


Figure 5.3 Disturbance Rejection Observer Implementation

Most require a nominal mathematical model. The main idea is to estimate the disturbance, q_{n+1} and a Luenberger observer, as in [10], for the system described in Eq.(5.4) can be designed as

$$\dot{\hat{q}} = A_a \hat{q} + B_a u + L(Y - \hat{Y}) \quad (5.4)$$

$$y = C_a q_{est}$$

$$\dot{y} = derivative(y)$$

$$q = [y, \dot{y}, p_{est}]^T$$

$$Y = [y, \dot{y}]^T$$

$$C_o = \begin{bmatrix} 1 & 0 & 0 \\ 0 & 1 & 0 \\ 0 & 0 & 1 \end{bmatrix}$$

$$\hat{Y} = C_o q = \begin{bmatrix} 1 & 0 & 0 \\ 0 & 1 & 0 \\ 0 & 0 & 1 \end{bmatrix} \begin{bmatrix} y \\ \dot{y} \\ p_{est} \end{bmatrix}$$

5.1.5 Extended State Observer Gains

The ESO in its original form employs nonlinear observer gains. Here, with the use of linear gains, this observer is denoted as the linear extended state observer (LESO). The estimator is stable if the observer gains $L = [l_1, l_2, \dots, l_N]^T$ are selected so that the eigenvalues of $(A_a - LC_a)$ lie on the left side of the s plane where the observer bandwidth, w_0 , is the only tuning parameter, as in [10]-[68]. Existing method as follow is to tune the matrix L using only one parameter, the bandwidth of the observer w_0 .

$$L = [nw_0^1 \quad nw_0^2 \quad nw_0^3 \quad \dots \quad nw_0^{m-1} \quad w_0^m]$$

$$m = 1, 2, 3, \dots$$

n = number of states including error

$$L = [5w_0^1 \quad 5w_0^2 \quad 5w_0^3 \quad 5w_0^4 \quad w_0^5]$$

As observer bandwidth is the only tuning parameter in the existing method, the ESO might create instability if the parameter bandwidth is not adjusted correctly while time consuming. An alternative method can also be computed using Ackermann's formula in estimator form, which is $L = \alpha_e(F)O^{-1}[0 \quad 0 \quad \dots \quad 1]^T$ where observability matrix O is $O = [H \quad HF \quad \dots \quad HF^{n-1}]^T$, as in [10]-[63]. However, the observability matrix has to be square, nonsingular, and nonzero determinant to transform to observer canonical form which can cause unnecessary complication. Therefore, the observer gains in Eq.(5.5) from the augmented matrix, $A_a = [A + E]$, to simplify the tuning process can be generated, [3], as

$$L = A_a^{-1}y \quad (5.5)$$

$$L = \text{inv}(A_a' * A_a) * (A_a' * y)$$

It is very useful to have intuitive parameters and as few as possible. Let us denote by l_{ij} the entries of the matrix L . In order to provide an on-line tuning of the observer, the following structure of the matrix L is proposed in [11]. Each column of observer gain L can then be applied for trial-error in the system. With the well-tuned DRO, total disturbance is estimated and rejected by control LQR, $u = -Kx$. To achieve the stable estimator, the observer gains are selected as follow.

$$L = \begin{bmatrix} l_{11} & l_{12} & l_{13} & l_{14} \\ l_{21} & l_{22} & l_{23} & l_{24} \\ l_{31} & l_{32} & l_{33} & l_{34} \\ l_{41} & l_{42} & l_{43} & l_{44} \\ l_{51} & l_{52} & l_{53} & l_{54} \end{bmatrix} = \begin{bmatrix} l_{ij} & l_{i(j+1)} & \dots & l_{i(j+m)} \\ l_{(i+1)j} & l_{(i+1)(j+1)} & \dots & l_{(i+1)(j+m)} \\ \vdots & \vdots & \dots & \vdots \\ \vdots & \vdots & \dots & \vdots \\ l_{(i+n)j} & l_{(i+n)(j+1)} & \dots & l_{(i+n)(j+m)} \end{bmatrix}$$

where

$$i, j, m, n = 1, 2, 3, \dots$$

$$L_j = \begin{bmatrix} l_{(i+0)j} \\ l_{(i+1)j} \\ \vdots \\ l_{(i+n)j} \end{bmatrix}, L_{j+1} = \begin{bmatrix} l_{(i+0)(j+1)} \\ l_{(i+1)(j+1)} \\ \vdots \\ l_{(i+n)(j+1)} \end{bmatrix}, L_{j+2} = \begin{bmatrix} l_{(i+0)(j+2)} \\ l_{(i+1)(j+2)} \\ \vdots \\ l_{(i+n)(j+2)} \end{bmatrix}, L_{j+3} = \begin{bmatrix} l_{(i+0)(j+3)} \\ l_{(i+1)(j+4)} \\ \vdots \\ l_{(i+n)(j+4)} \end{bmatrix}$$

5.1.6 LQR-DRO Trolley Model Control

Assuming that, the ESO produces an accurate estimation of the unknown dynamics. The following control law, $u = -Kq$, will ensure the tracking of the reference input. For a continuous time system, the state-feedback law is expected to minimize the quadratic cost function, $J = \int_0^\infty \{q^T Q q + u^T R u\} dt$, which is subject to the system dynamics, $\dot{q} = Aq + Bu$, [5]-[7]. The associated Riccati equation is Eq.(5.6) and K is derived in Eq.(5.7).

$$A^T S + S A - (S B + N) R^{-1} (B^T S + N^T) + Q = 0 \quad (5.6)$$

K is derived from using

$$K = R^{-1} (B^T S + N^T) \quad (5.7)$$

One reasonable method to start LQR design iteration, Eq.(9), is suggested by Bryson's rule. In practice, an appropriate choice to obtain acceptable values of x and u is to initially choose diagonal matrices Q and R such that

$$Q_{ii} = \frac{1}{\text{maximum acceptable value of } [x_i^2]}$$

$$R_{ii} = \frac{1}{\text{maximum acceptable value of } [u_i^2]}$$

The weighting matrices (Q and R) are then modified during subsequent iterations to achieve an acceptable tradeoff between performance and control effort. The direct solution for the optimal control gain, K, in the MATLAB statement Eq.(5.8) is

$$Q = \rho H^T H$$

$$Q = \begin{bmatrix} 0 & 0 & 0 & 0 \\ 0 & 0 & 0 & 0 \\ 0 & 0 & 0 & 0 \\ 0 & 0 & 0 & 1e5 \end{bmatrix}, R = 0.1$$

$$K = lqr(A_a, B_a, Q, R) \quad (5.8)$$

Referring to the Luenberger observer, as in (5), and the control rule, $u = -Kq$, LQR design iteration can be defined in Eq.(5.9).

$$\dot{\hat{q}} = (A_a - (B_a * K))\hat{q} + L(Y - \hat{Y}) \quad (5.9)$$

The central aim of DRO implementation in this trolley translation model is to actively reject the disturbance in the absence of a detailed mathematical model of the plant or the disturbance itself. For that purpose, the controller is designed based on ideal, disturbance free, process where any discrepancies between the actual process and the ideal one is considered as disturbance, being estimated and, afterwards, canceled. Even though applying simple LQR follows the reference trajectory, reasonable amount of overshoot and undershoot cause the controller unreliable.

However the inclusion of a disturbance observer improved the performance of the LQR-DRO controller in Fig. 5.4, it is significantly reducing overshoot and undershoot. The effectiveness of the compensation depends on how fast the state estimates, as in [10], converge to the true values.

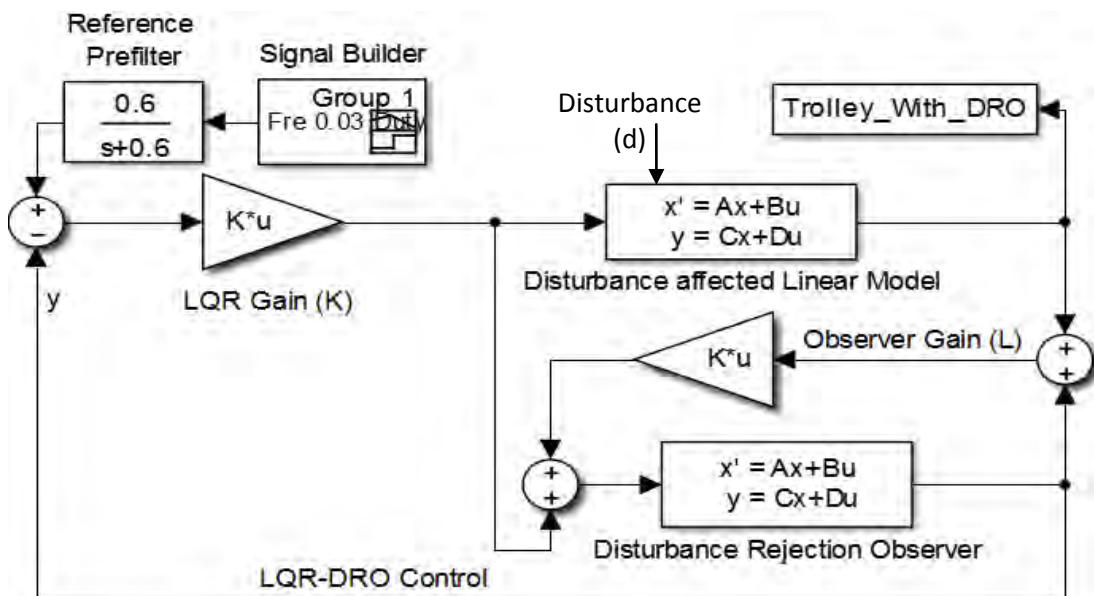


Figure 5.4 LQR-DRO Control

Trolley model simulations using different columns of observer gains are carried out to test the tracking and disturbance rejection performance LQR-DRO. Each observer gains column (Column 1 to 4 in the trolley model case) has been implemented in the DRO model with applied LQR control. Even though LQR-DRO using observer gains columns (1,2,3) create overshoots/undershoots comparable to the results without DRO, column 4 (L_{j+3}) presents better result by tracking the reference input without overshoot in Fig. 5.5..

Trolley model simulations using different columns of observer gains are carried out to test the tracking and disturbance rejection performance LQR-DRO. Control performance would vary based on each observer gains column and the best simulation results have been obtained after trials-and-errors. Using observer gains column-1, $l_{ij} \dots l_{(i+n)j}$, the system produces robust tracking of the reference input with reasonably less overshoot in Fig. 5.5.

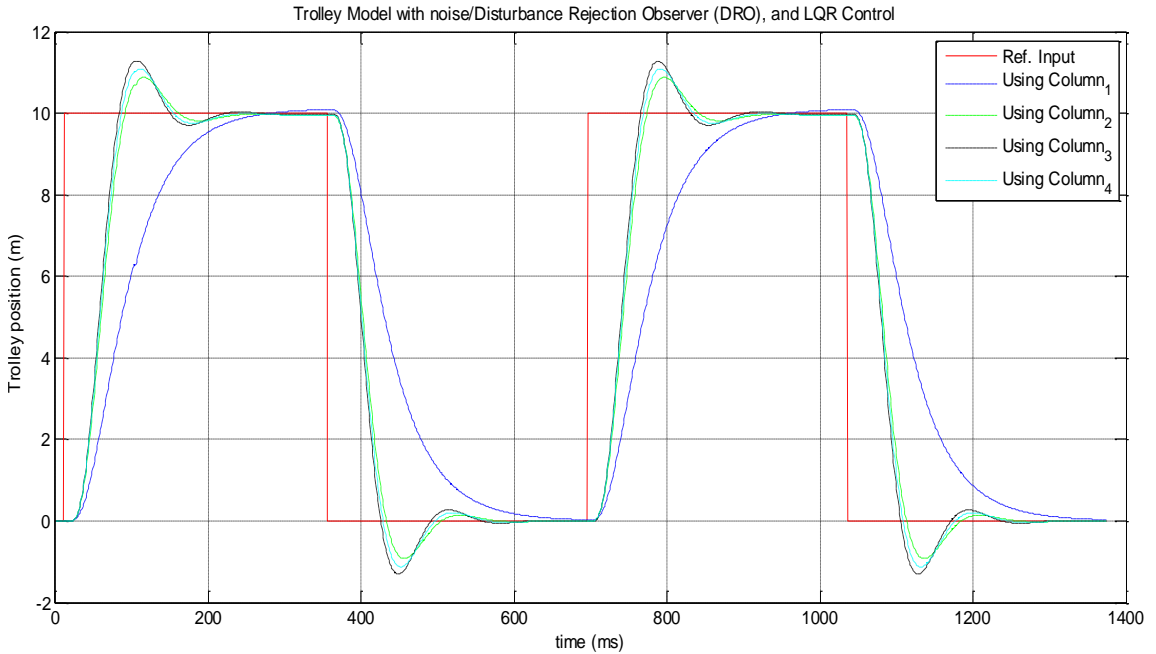


Figure 5.5 LQR-DRO Controller performance with different Observer columns

5.1.7 LQR-DRO Trolley and Loadswing controls

Robustness and the adaptive ability of this method makes it an interesting solution in scenarios where the full knowledge of the system is not available. The central aim of DRO implementation in this Trolley translation model is to actively reject the disturbance, in the absence of a detailed mathematical model of the plant or the disturbance itself. For that purpose, the controller is designed based on the ideal, disturbance free, process where any discrepancies between the actual process and the ideal one is considered as disturbance, being estimated and, afterwards, canceled. In result, the system performance is better than the system without disturbance rejection observer (DRO). Control performance would vary based on each observers gains column and the best simulation results can then be obtained after trials-and-errors. In this case, using observer gains column 1, $l_{ij} \dots l_{(i+n)j}$, produced robust tracking of the reference input with reasonably less overshoot in Fig. 5.6.

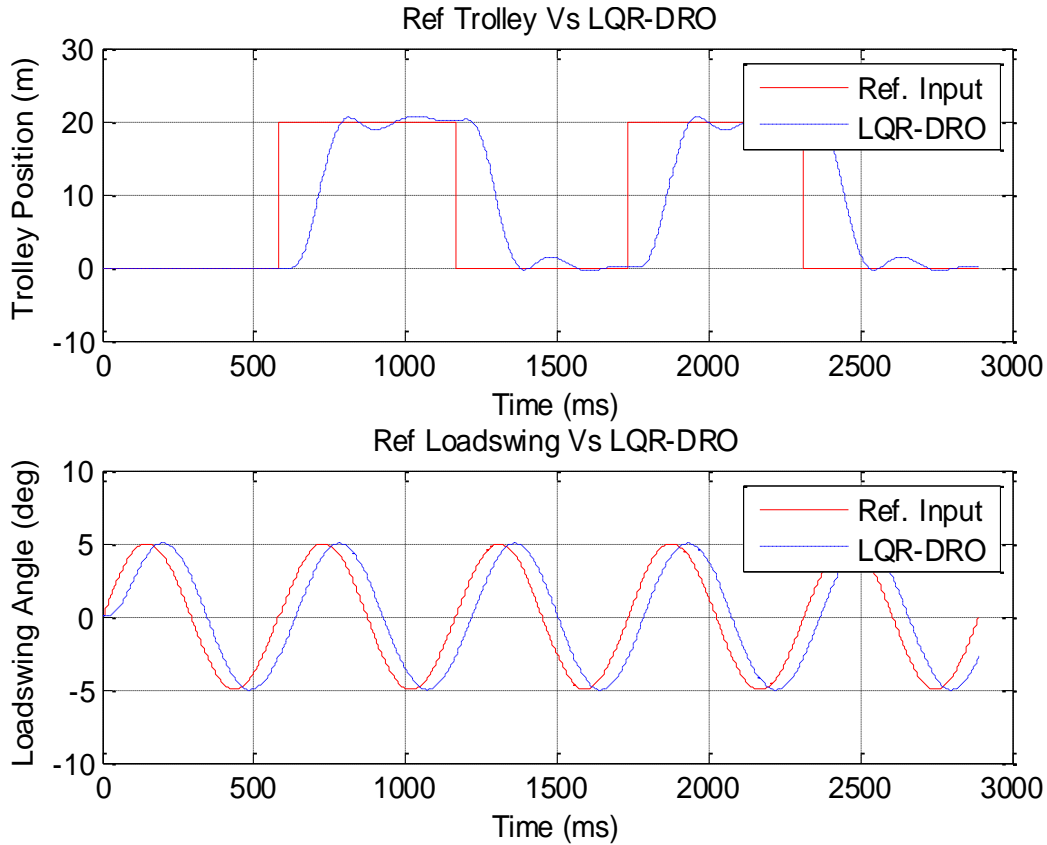


Figure 5.6 LQR-DRO Controlled Trolley-Loadswing

Despite the improvement in LQR-DRO method with smooth trajectory tracking, tracking error problem still exists in the control scheme and seriously limits its practical application in the crane trolley control. Slow convergence would also mean that the DRO presents long transients when tracking the true disturbance values, during which time disturbance has not been correctly compensated. To achieve robust tracking, the next section would discuss about the implementation of internal model integral control with estimator which uses the augmented model, as in [4].

5.2 LQR-Estimator-Integral Control (LEIC) Development

The Robotic Tower Crane model simulation produced nonlinear data including trolley translational positions($X_{x,y,z}$), payload swing angles($\theta_{x,y,z}$), and tower rotational positions($\phi_{x,y,z}$) respectively. The details of simple LQR and LQR-DRO designs discussed in section 5.1 produced significant amount of steady-state error to a reference input and were less robust. To achieve robust tracking, integral control that presents the internal model principle is introduced by a direct method of adding the integral of the system error to the equations of motion. Since the system needs to

reject the disturbance from the augmented model, estimator model has also been included in this optimal LQR-Estimator-Integral Control design in Fig. 5.7.

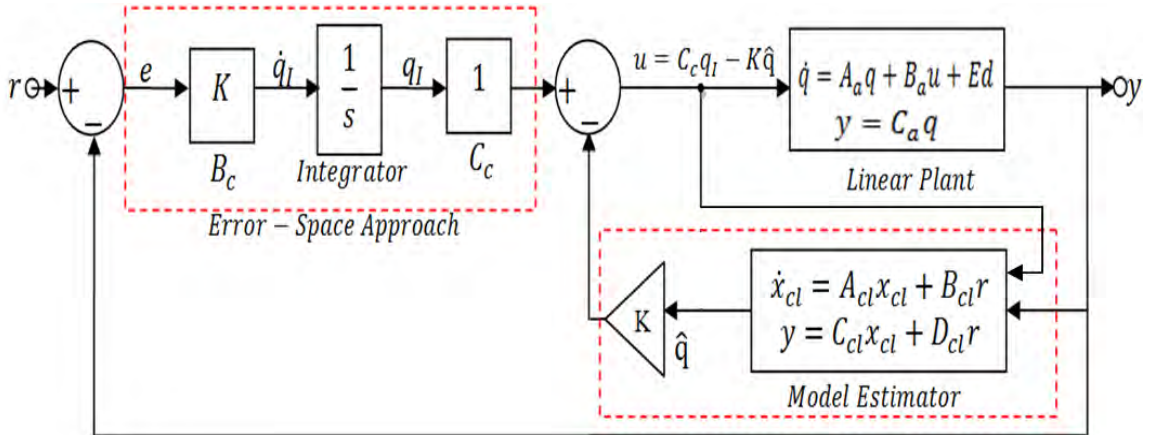


Figure 5.7 LQR-Estimator-Integral Control (LEIC) for Linear Model

This control layout consists of disturbance affected trolley translational model (augmented) position control and estimator-integral control loop for tackling disturbances and uncertainties at the surrounding issues. The disturbance affected plant used in section 5.13 is referred in which A_a, B_a , and C_a , are considered. Consequently, the control goals are to achieve the trolley position and payload swing suppression that track a prespecified desired reference trajectory (X_r) and (θ_r).

5.2.1 Error Space Approach

The choice of LQR-DRO control resulted in a reference input response with a less steady-state error. But the result is not robust because any change in the parameters caused the error higher. Integral control is then introduced to obtain robust tracking of square and sinusoid inputs for both trolley and payload swing. However, integral control has a limitation to square response tracking, and therefore error-space approach is considered a more analytical approach which has the ability to track a non-decaying inputs (square or sinusoid), as in [69]. As the reference signal is generated by a dynamic system, it is considered as part of the formulation and solving the control problem in an error-space to make the error approaches zero. Given the reference dynamic(r) and the augmented plant dynamics from Section 5.1.3, Eq.(5.3)

$$\begin{aligned}\dot{q} &= A_a q + B_a u + E d, \\ y &= C_a q + D_a u\end{aligned}$$

where the parameters A_a, B_a, C_a , and D_a are the matrices from section II.3. Then the tracking error is defined as,

$$e = y - r,$$

This integral control system feeds back the integral of the error, e , with the state of the plant, q , then followed by augmenting the plant state with the extra (integral) state x_I which obeys the differential equation Eq.(5.10).

$$\dot{q}_I = C_a q - r = K e \quad (5.10)$$

which leads to

$$x_I = K \int_0^t e dt$$

One way to formulate the tracking problem is to differentiate the error equation and introduce the error as a state. Thus, the error system Eq.(5.11) is

$$\begin{bmatrix} \dot{e} \\ \dot{q} \end{bmatrix} = \begin{bmatrix} 0 & C_a \\ 0 & A_a \end{bmatrix} \begin{bmatrix} e \\ q \end{bmatrix} + \begin{bmatrix} 0 \\ B_a \end{bmatrix} u - \begin{bmatrix} 1 \\ 0 \end{bmatrix} r + \begin{bmatrix} 0 \\ E \end{bmatrix} d \quad (5.11)$$

Using the augmented state equation, as in [11], then the state representation is

$$A = \begin{bmatrix} 0 & C_a \\ 0 & A_a \end{bmatrix}, B = \begin{bmatrix} 0 \\ B_a \end{bmatrix}$$

Existing Integral control of the form, $\dot{x}_I = B_c e$, which considers $B_c = -K_1$, the associated feedback gain of error state, as in [16]. However, implementing this existing approach could not produce better reference tracking. In contrast to the consideration, as in [63], this paper then applies $B_c = K$, see Fig. 5.7, of all feedback gains (controller gain K = error state and plant states) in error-space implementation. The controller gains K derivation is discussed in the next section.

5.2.2 LQR Gains

Details LQR Control design has been presented in earlier section in which the need of quadratic cost function, $J = \int_0^\infty \{q^T Q q + u^T R u\} dt$, to penalize the tracking error (e) and the control (u), the state and control weighting matrices (Q and R) design as well as LQR gains derivation were covered. Since the augmented system includes error state, the factor of " 1 " was determined as the relative weighting for error state while other plant states weighting were determined by trial and error. The state and control weighting matrices are then

$$Q = \begin{bmatrix} 1 & 0 & 0 & 0 \\ 0 & 0 & 0 & 0 \\ 0 & 0 & 0 & 0 \\ 0 & 0 & 0 & 1e5 \end{bmatrix}, R = 0.1$$

The resulting feedback gain (K) computed from MATLAB ($K = \text{lqr}(A, B, Q, R)$) is formed as $K = [K_1 \ K_2 \ K_3 \ K_4 \ K_5]$ or $K = [K_1 \ : \ K_0]$. The combination of error space approach and LQR gains is then called internal model controller of the form Eq.(5.12)

$$u = C_c q_I - K \hat{q} \quad (5.12)$$

where x_I denotes as the controller state and the value of $C_c = 1$, as in [63].

5.2.3 Full-order Estimator

The controller which combines the control law with the estimator is essentially a regulator design. One method of estimating all the state variables that one may consider is to construct a model Eq.(5.13) of the plant dynamics, as in [13].

$$\dot{q} = A_a q + B_a u, \quad y = C_a q \quad (5.13)$$

where q is the estimate of all the actual states, ($q = [y, \dot{y}, p_{est}]^T$), discussed in section II.4, and A_a and C_a are augmented plants referred from section 5.1.3. The full-order estimator is driven by three inputs such as: control term input (u), correction term derived from the actual output of the plant, and the predicted term derived from the estimator, as in [70]. In order to speed up the process and provide a useful state estimate, the system applies the following the full-order estimator equation Eq.(5.14)

$$\dot{\hat{q}} = A_a \hat{q} + B_a u + L(Y - C_a \hat{q}) \quad (5.14)$$

5.2.4 Estimator Gains

The estimator ESO gain (L) in Eq.(5.15) which minimizes the covariance for a linear system in continuous time can be obtained based on Kalman-Bucy filter, as in [70].

$$L = P C^T R_v^{-1} \quad (5.15)$$

where $P(t)$ represents covariance matrix, C is a linear function output, and R_v is the process sensor noise intensity. This paper considers $R_v = 0.001$. Suitable L values can be chosen to stabilize the dynamics of $P(t)$ so that the estimator gain can converge to a constant and satisfies the algebraic Riccati equation, as in [70].

This research then examines estimator gain (L) matrix for using "lqe" command in MATLAB: $L = lqe(A_a, B_a, C_a, R_v, R_w)$. Having the suitable estimator gains (L) to compute estimator, and the feedback controller gains (K), the internal model controller equation can further be improved. The overall system equations are obtained by substituting ($y = C_a q$, $\dot{q}_I = Ke$, and $u = C_c q_I - K\hat{q}$) in Eq.(5.1), Eq.(5.13), and Eq.(5.14). New derived version becomes as in (10)

$$\begin{aligned} \dot{q}_I &= Ke = B_c(y - r) = B_c y - B_c r \\ \dot{q}_I &= B_c C_a q - B_c r \end{aligned} \quad (5.10)'$$

As in (13):

$$\begin{aligned} \dot{q} &= A_a q + B_a u = A_a q + B_a(C_c q_I - K\hat{q}) \\ \dot{q} &= A_a q + B_a C_c q_I - B_a K\hat{q} \end{aligned} \quad (5.13)'$$

As in (14),

$$\begin{aligned}
 \dot{\hat{q}} &= A_a \hat{q} + B_a u + L(Y - C_a \hat{q}) \\
 &= A_a \hat{q} + B_a(C_c q_I - K \hat{q}) + L(C_a q - C_a \hat{q}) \\
 &= A_a \hat{q} + B_a C_c q_I - B_a K \hat{q} + L C_a q - L C_a \hat{q} \\
 \dot{\hat{q}} &= L C_a q + B_a C_c q_I + (A_a - B_a K - L C_a) \hat{q}
 \end{aligned} \tag{5.14}'$$

The closed loop system equations are then given by

$$\dot{x}_{cl} = A_{cl} x_{cl} + B_{cl} r$$

$$y = C_{cl} x_{cl} + D_{cl} r$$

where r is the reference input trajectory, and the closed loop state vector is $x_{cl} = [q \quad q_I \quad \dot{q}]^T$, and therefore combining those three equations (13)', (10)', and (14)' equations in the matrix notation and form the complete estimator design, as in [franklin 63].

$$\begin{aligned}
 A_{cl} &= \begin{bmatrix} A_a & B_a C_c & -B_a K \\ B_c C_a & 0 & 0 \\ L C_a & B_a C_c & (A_a - B_a K - L C_a) \end{bmatrix}, B_{cl} = \begin{bmatrix} 0 \\ -B_c \\ 0 \end{bmatrix} \\
 C_{cl} &= [C_a \quad 0 \quad 0], \quad D_{cl} = [0]
 \end{aligned}$$

5.2.5 LQR-LEIC for Trolley Model

This simulink control layout consists of augmented trolley translational model, and estimator-integral feedback. This robust LQR-Estimator-Integral controller is designed in the sense that regulation of "e" to zero in the steady-state occurs in the presence of perturbation system parameters in Fig. 5.8.

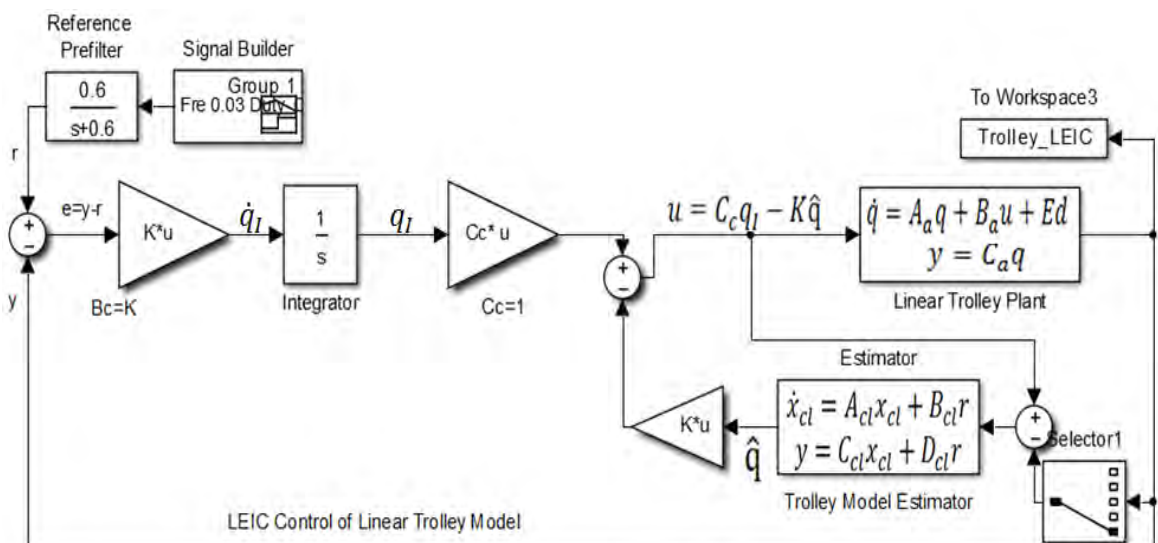


Figure 5.8 LQR-Estimator-Integral Control (LEIC) in Simulink

5.2.6 LQR, LQR-DRO, and LEIC Performance Comparison for Trolley-Loadswing

Trolley translational model system runs on 20-m jib length with having multiple reference position changes at different times setting. The MATLAB-Simulink is used for the simulation of simple LQR, LQR-DRO, and LEIC for linear model. The disturbance rejection observer and error-space method with inclusion of estimator-integral control are implemented, as in [9]-[1]-[14] respectively. Several simulations have been carried out to test the disturbance rejection performance and tracking of the LQR-DRO and LEIC.

The commanded trolley position trajectory with (0-20 m) duty cycles were fed to the controller and one can see the systems track the input and attenuates the disturbance with minor tracking errors. The simulation results in Fig. 5.9, shows the system output with LQR control has overshoot and undershoot. On the other hand, LQR-DRO control effectively rejects the disturbance, tracks the commanded position trajectory with around 10-milliseconds time delay for the ramp with no overshoot. Nevertheless, the settling time in every reference duty cycle is reasonably large. The LQR-Estimator-Integral Control is then developed in which internal model controller of the form produces better reference tracking while full-order estimator clearly rejects the disturbance. Based-on the findings of all three methods, the LEIC approach has proven to perform better robust tracking compare to the other two.

Since the LEIC performance executes smooth robust tracking on reference trajectory, the next section would discuss about the linear development from Nonlinear Autoregressive exogenous (NARX) structure and LEIC-Antiwindup controller implementation.

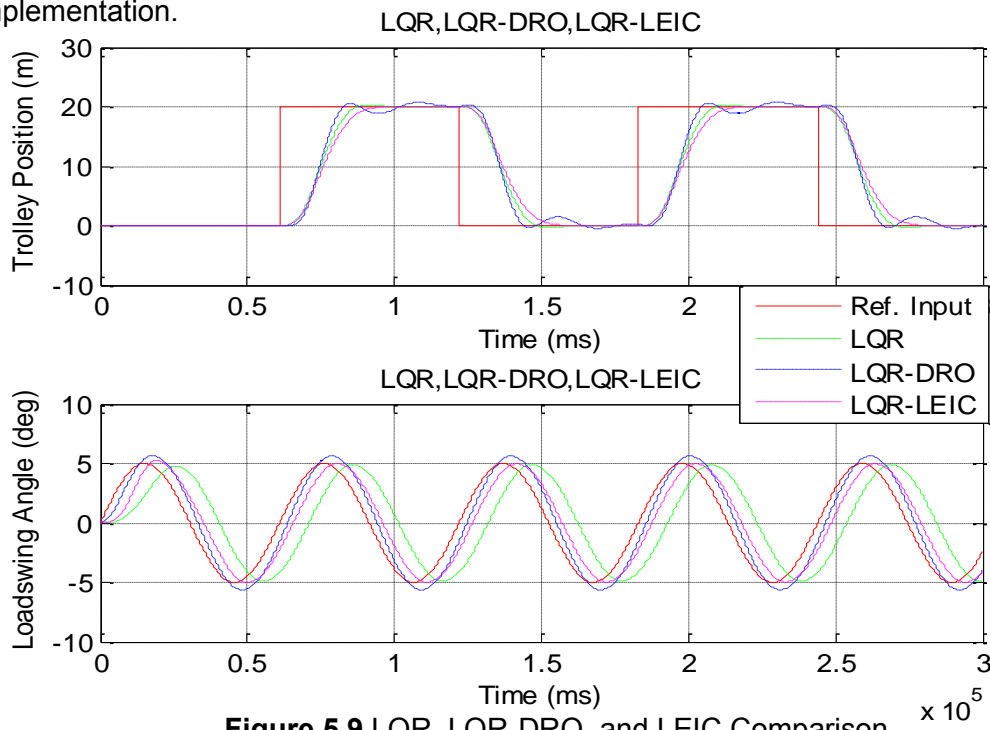


Figure 5.9 LQR, LQR-DRO, and LEIC Comparison

Reference input of (5 to -5 degree) sinusoidal range has been set which changes at different times within 100 seconds for load swing control principle. For the simple LQR model without disturbance consideration, simulation result has been obtained that tracks the reference steadily and has tracking errors in Fig. 5.10a. To make the actual swing output equilibrium of the reference dynamics, disturbance rejection had to be employed on the controller as LQR-DRO in Fig. 5.10b. Motivated by LEIC for linear trolley model control response introduced earlier, the same control approach has been applied for the load swing model. The Figure in Fig. 5.10c, shows the significant reduction of tracking error has been achieved.

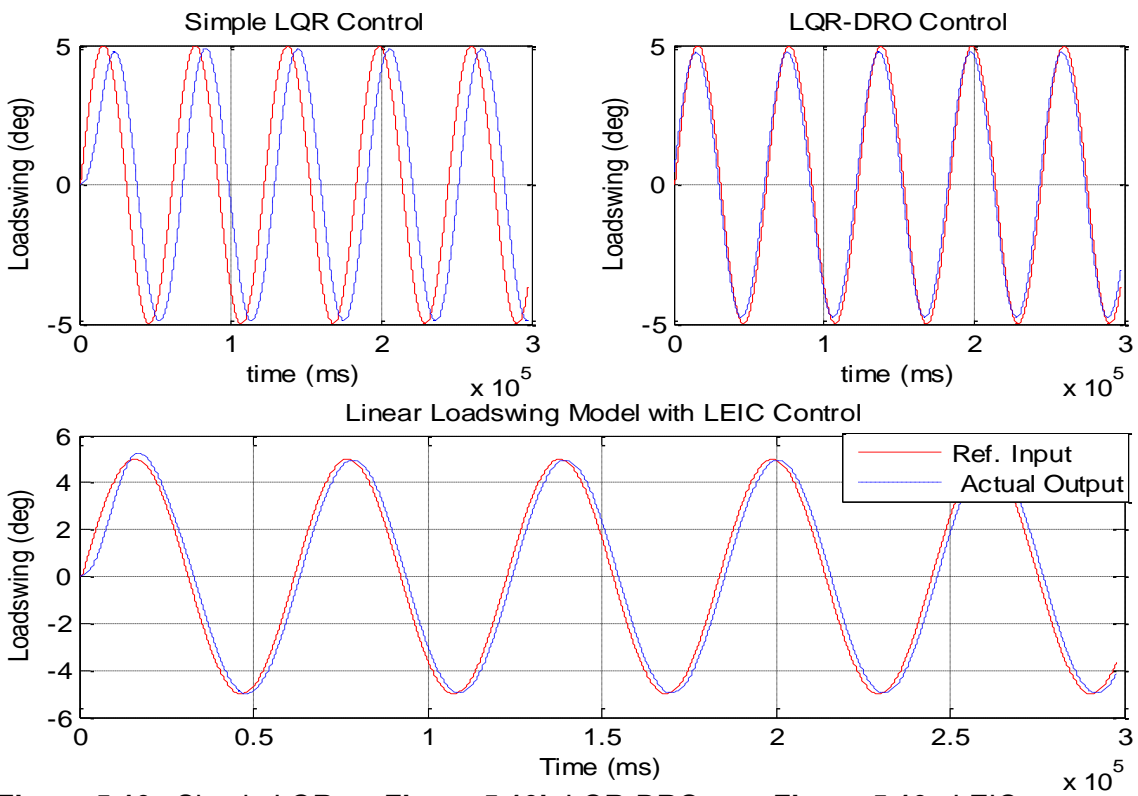


Figure 5.10a Simple LQR
Controlled Loadswing output

Figure 5.10b LQR-DRO
Controlled Loadswing output

Figure 5.10c LEIC-
Controlled Loadswing output

As LEIC performance smooth robust tracking of reference trajectory, the extraction of linear model from NARX structure would be considered in the next approach while antiwindup to be integrated into LEIC.

5.3 LEIC- Antiwindup Control for Linear Models

This section has twofold, one: linear model development using NARX structure and, two: antiwindup implementation in LEIC. The dynamic range of practical controller is usually limited. For instance, the control surfaces in an aircraft can be deflected only to a certain angle from their nominal positions, as in [71]. Using such actuators in the system might have phenomenon like "integrator windup". The integrator output may

become quite large if saturation lasts longer time which eventually triggers to produce large commands. If this happens, the integrator builds up a large value which results in large overshoots and errors. To overcome this problem, "antiwindup" is implemented to "turn off" the integral action as soon as the actuator saturates.

Regarding the linear model development, the NARX model provides a powerful representation modeling and prediction due to its strength in accommodating the dynamic, complex and nonlinear nature of real time series applications, as in [72]. Therefore, instead of applying traditional way of linear modeling techniques, this paper introduced the linear model derivation from Nonlinear Autoregressive exogenous (NARX) structure to further explore robust control.

5.3.1 Linear System Identification from NARX Structure

Initial construction tower crane system simulation produces a bunch of nonlinear data which includes trolley translation, payload swing, tower rotation, etc.. Since it is essential to keep the payload swing low while trolley is in motion, this research further develops trolley-payload linear models. Trolley-payload free body diagram in Fig. 5.11 provides the details of trolley cart mass (M), payload mass (m), load length (l), swing angle (θ). Since the external force (F) applies on trolley to move back-and-forth along X -direction, large swing angle (θ) appears. The input ($u(k)$: derived force from power drive) and the output ($y(k)$: the trolley translational position) are then obtained from the SimMechanics-visualized tower crane model simulation.

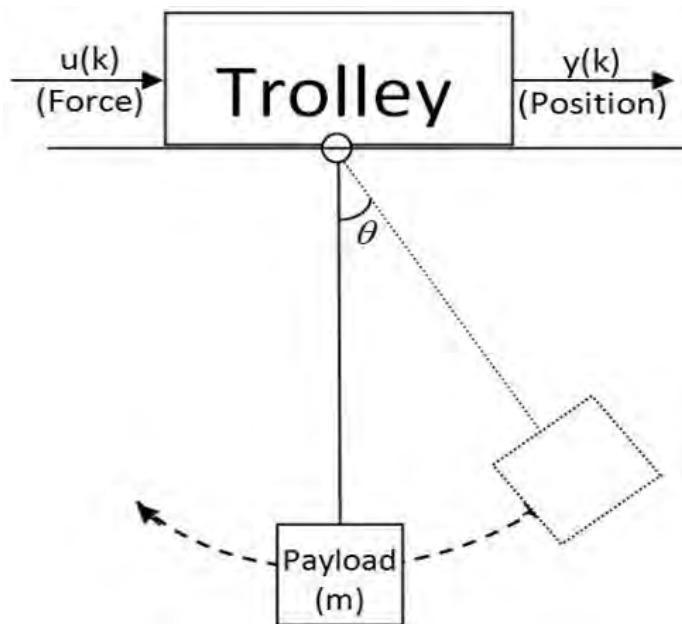


Figure 5.11 Trolley-Payload Free Body Diagram

The field of process-parameter identification and estimation has developed rapidly during the past decade. There are plenty of nonlinear-based system identification methods such as: the online and real-time nonlinear identification based on least square approach were discussed, as in [Astrom 73]. Nonlinear Autoregressive exogenous model (NARX), as in [57]-[58]-[59]-[74], adaptive neuro-fuzzy inference system (ANFIS), as in [75], non-linear formulation that is linear in parameters using recursive least square method (RSLM), as in [76], nonlinear Hammerstein-Wiener (NLHW), as in [58]-[59], etc. This paper aims to derive linear models (for trolley and payload) from NARX structure, and analyze the LEIC-Antiwindup control performance to achieve robust trajectory tracking.

However, in regards to (trolley and payload) linear modelling, this research aims to discuss about NARX approach as to achieve better fit linear model with robust LQR control. Initially, More than twenty thousand input-output data points were collected from the simulation process as the input $u(k)$ was chosen to be a pseudorandom signal shifting between (0 W: 0 N) and (3000 W:6432.7 N). The below plots in Fig. 5.12 show the output trolley translational position $y(k)$ and input force $u(t)$ for the first 80 time steps.

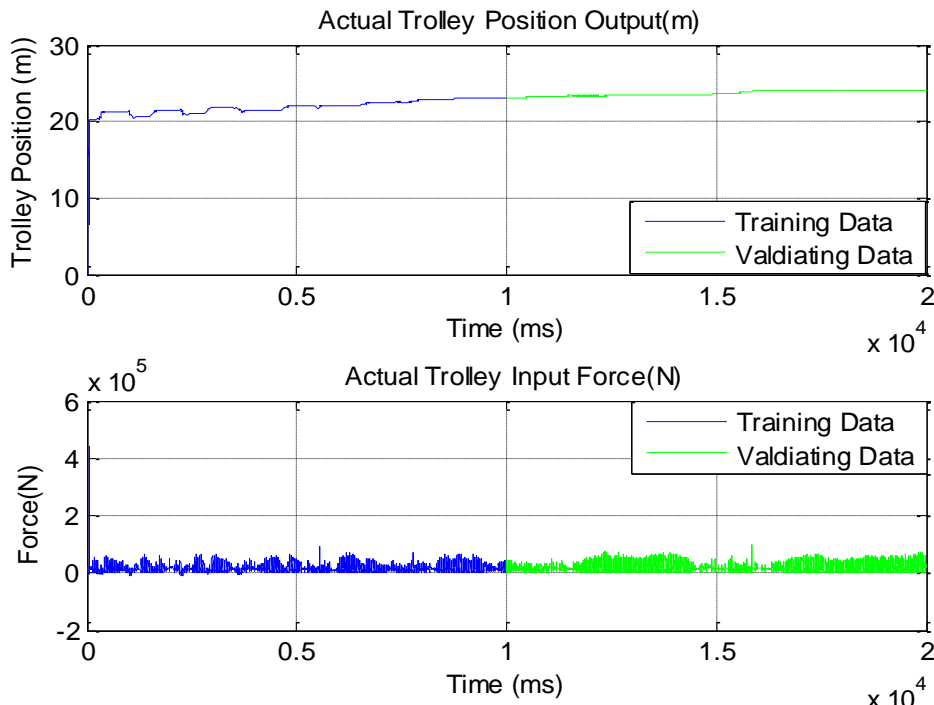


Figure 5.12 Training and Validating Trolley Model using NARX

5.3.2 Linear ARX Model Development

The function of nonlinear ARX model is to predict future values of a time series $y(t)$ from past values of that time series and past values of a second time series $x(t)$ in

Eq.(5.16). It computes in two stages. Firstly, the next value of the dependent output signal $y(t)$ is regressed on previous values of the output signal and previous values of an independent (exogenous) input signal. And secondly, the nonlinearity estimator maps the regressors to the model output using a combination of nonlinear and linear functions. The following structure represents the nonlinear ARX model in Fig. 5.13.

$$y(t) = f[y(t-1), y(t-2), \dots, u(t-1), u(t-2), \dots] + e(t) \quad (5.16)$$

where $u(t)$ represents the inputs, $y(t)$ represents the outputs of the model at time (t) and $e(t)$ is the error term.

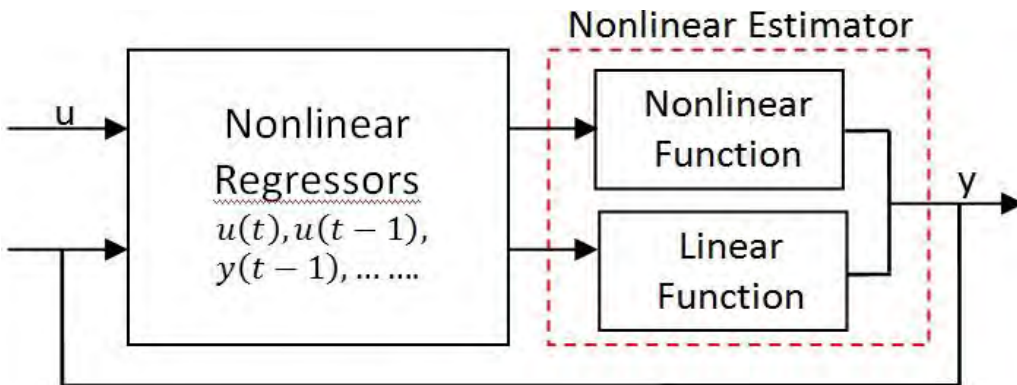


Figure 5.13 Nonlinear Autoregressive exogenous (NARX) Structure

In this work, the system identification is developed using "nlarx" and "sigmoidnet" as nonlinear estimator function in the MATLAB. Different combinations of regressors $[y(t-1), \dots, y(t-6), u(t-1), \dots, u(t-6)]$ are assigned in "nlarx" algorithm "sigmident" nonlinear estimator in search of better fit model output, as in [68]-[69]. Extracting nonlinear and linear parameters from the model, both y_{Linear} and $y_{Nonlinear}$ in Eq.(5.17) and Eq.(5.18) respectively can be derived as follow.

$$\begin{aligned} \hat{y} &= y_{Linear}(x) + y_{Nonlinear}(x) \\ y_{Linear}(x) &= (x - r) * P * L + d \\ f(s) &= (e^s + 1)^{-1} \end{aligned} \quad (5.17)$$

$$\begin{aligned} f_{Input}(k) &= Q * (x - r) * bMat(:, k) * cVec(k) \\ y_{Nonlinear}(x) &= \sum_{k=1}^n [aVec(k) * f * f_{Input}(k)] \end{aligned} \quad (5.18)$$

whereby, " x " is a vector of the regressors, " r " is the mean of regressors, " P " is the linear subspace, " L " is the linear coefficient, " d " is the output offset, " f " is sigmoid function, " Q " is the nonlinear subspace, $bMat$ is the dilation, " $cVec$ " is the translation, and " $aVec$ " is nonlinear output coefficient, as in [59].

Using the linear coefficients extracted from NARX model, the transfer function and state-space representation be formed as

$$\frac{x(k)}{F(k)} = \frac{-1.725 s^3 + 37.71 s^2 + 459 s - 1.047e04}{s^3 + 72.53 s^2 + 1620 s + 1.138e04}$$

$$\begin{bmatrix} \ddot{x} \\ \dot{x} \\ x \end{bmatrix} = \begin{bmatrix} -72.5264 & -50.6155 & -22.2331 \\ 32.0000 & 0 & 0 \\ 0 & 16.0000 & 0 \end{bmatrix} \begin{bmatrix} \ddot{x} \\ \dot{x} \\ x \end{bmatrix} + \begin{bmatrix} 16 \\ 0 \\ 0 \end{bmatrix} u$$

$$y = [10.1751 \quad 6.3526 \quad 1.1187] \begin{bmatrix} \ddot{x} \\ \dot{x} \\ x \end{bmatrix}, D = [-1.7247]$$

5.3.3 LEIC-Antiwindup Control for Linear ARX Trolley Model

In previous section, LQR-Estimator-Integral Control (LEIC) of Linear Model had been discussed. The simulations were also proved that LEIC performs better than simple LQR and LQR-Disturbance Rejection Observer (LQR-DRO). However, actual plant in real time is nonlinear, and therefore it is necessary to prove that this developed LEIC Controller can perform well for nonlinear model as well. In this LEIC control of nonlinear model consists of integral control, full-order estimator, and other features such as Integrator anti-windup, Saturation Nonlinearity, Trolley uncertainty parameter, prefilter to smoothen the sharp corners of output, and feedback loop gain. Similar nonlinear closed-loop control for Rapid Thermal Processing was discussed in Feedback Control of Dynamics Systems in [63]. However, controller gains and features implementations in this research work are according to the nonlinear trolley plant's needs. The details are clarified below.

5.3.4 Weighting Matrices Q, and R

Q and R weighting matrices were fine-tuned till LEIC achieves robust performance and generated LQR gains, $[K_1 \ K_2 \ K_3 \ K_4 \ K_5]$, are then used in integral control, integrator anti-windup, full-order estimator, and linear plant output feedback. Internal model controller of the form (integral control) considers $\dot{x}_I = [K_1 \ 0 \ 0 \ K_5] e$ where K_1 is error state feedback gain and K_5 is trolley position output feedback gain. Saturation is included for the trolley as well as integrator anti-windup logic gain, K_1 , to deal with trolley saturation while the full-order estimator remains the same structure as used in LEIC control of linear model. This LEIC Anti-Windup approach is based-on LEIC structure with additional features (Saturation and integrator anti-windup). Anti-windup features are highlighted with red-dotted line in Fig. 5.14. Saturation values range are selected upon trial-and-errors to achieve the best control response.

To achieve the robust tracking performance of the LEIC with Anti-Windup control, in Fig. 5.14 as in [10], for developed linear ARX model, a series of simulation cases were performed by adjusting: weights in Q and R matrices, different LQR gains in integral control and estimator, saturation, prefilter, and trolley uncertainty parameters. At saturation (1,50) range, $Q_x = 5e5$, and $R_u = 0.008$, the trajectory tracking follows closely to the reference signal.

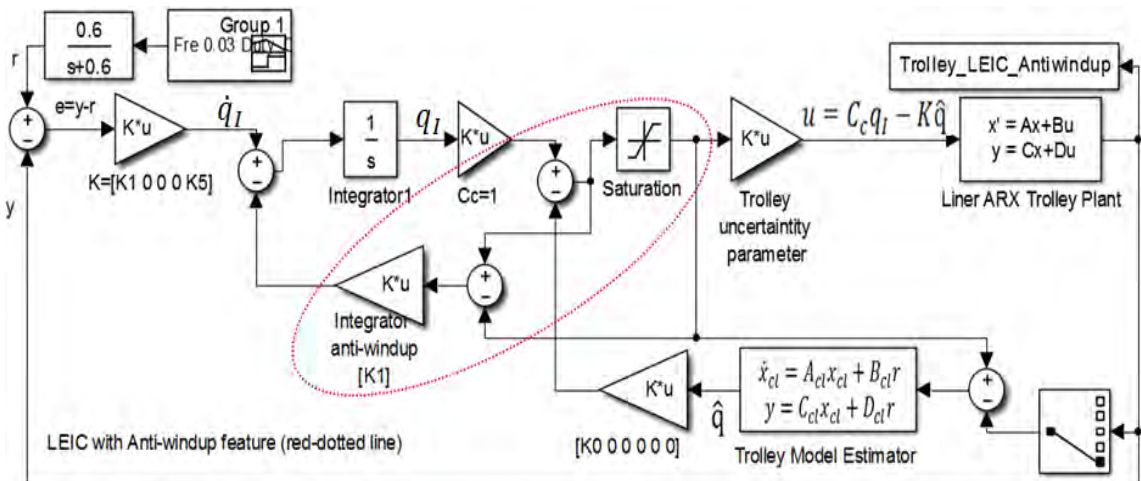


Figure 5.14 LEIC-Antiwindup Controller Design for Linear ARX Trolley Model

5.3.5 Result and Discussion

To access the performance of the Linear trolley model with LQR-Estimator-Integral Control (LEIC) controller, a series of simulation cases were performance by adjusting: weights in Q and R matrices, different LQR gains in integral control and estimator, saturation, prefilter, and trolley uncertainty parameters. At saturation (1,30) range, $Q_x = 5e5$, and $R_u = 0.008$, the trajectory tracking follows closely to the reference signal which appers to performs very well in Fig. 5.15.

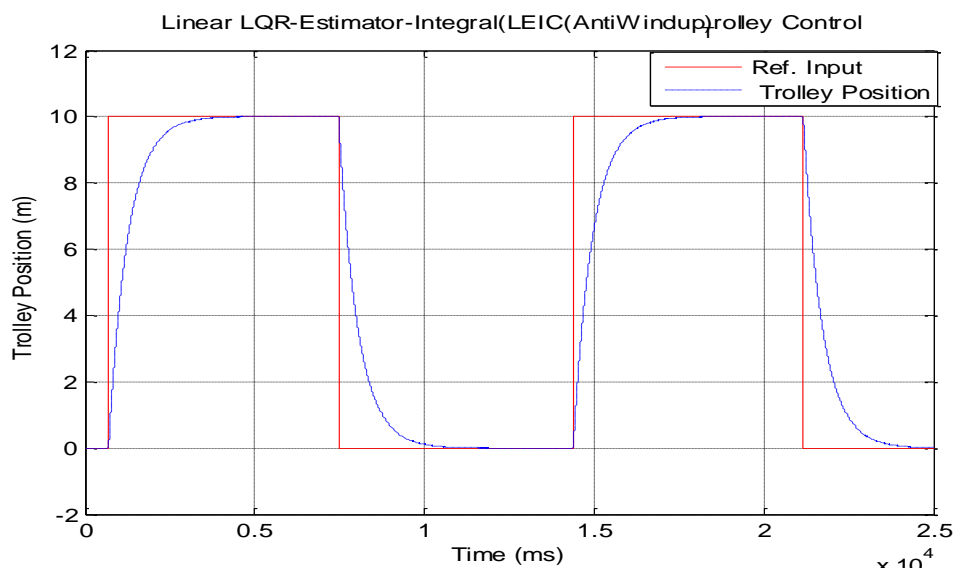


Figure 5.15 Trolley position Tracking using LEIC-antiwindup Control
152

5.3.6 DRO, LEIC, LEIC-Antiwindup performance Comparison for Trolley

This research has developed four controllers (Simple LQR, LQR-DRO, LEIC for Linear model, and LEIC-Antiwindup) and analysed their performances separately to control trolley translational motion followed by loadswing minimization. All four controllers combination in one simulation with same reference has been presented in figure in Fig. 5.16 Simulation shows, simple LQR control without DRO or Estimator had resulted in higher overshoots with settling time of about 10 seconds. LQR-DRO has larger steady-state error as compared to others reached the set-point after about 18 seconds. In contrast, both LEIC and LEIC-Antiwindup results show that the controllers had driven the process output to the desired set-point with response time approximately (less than 10 seconds) and no overshoot or oscillatory response. Since LEIC-Antiwindup has taken actuator saturation into consideration apart from integral control and estimator, the performance has exceptionally improved compared to others. These results would provide more efficient intelligent tower crane control strategies and may lead to practical significance in the analysis of safety issues.

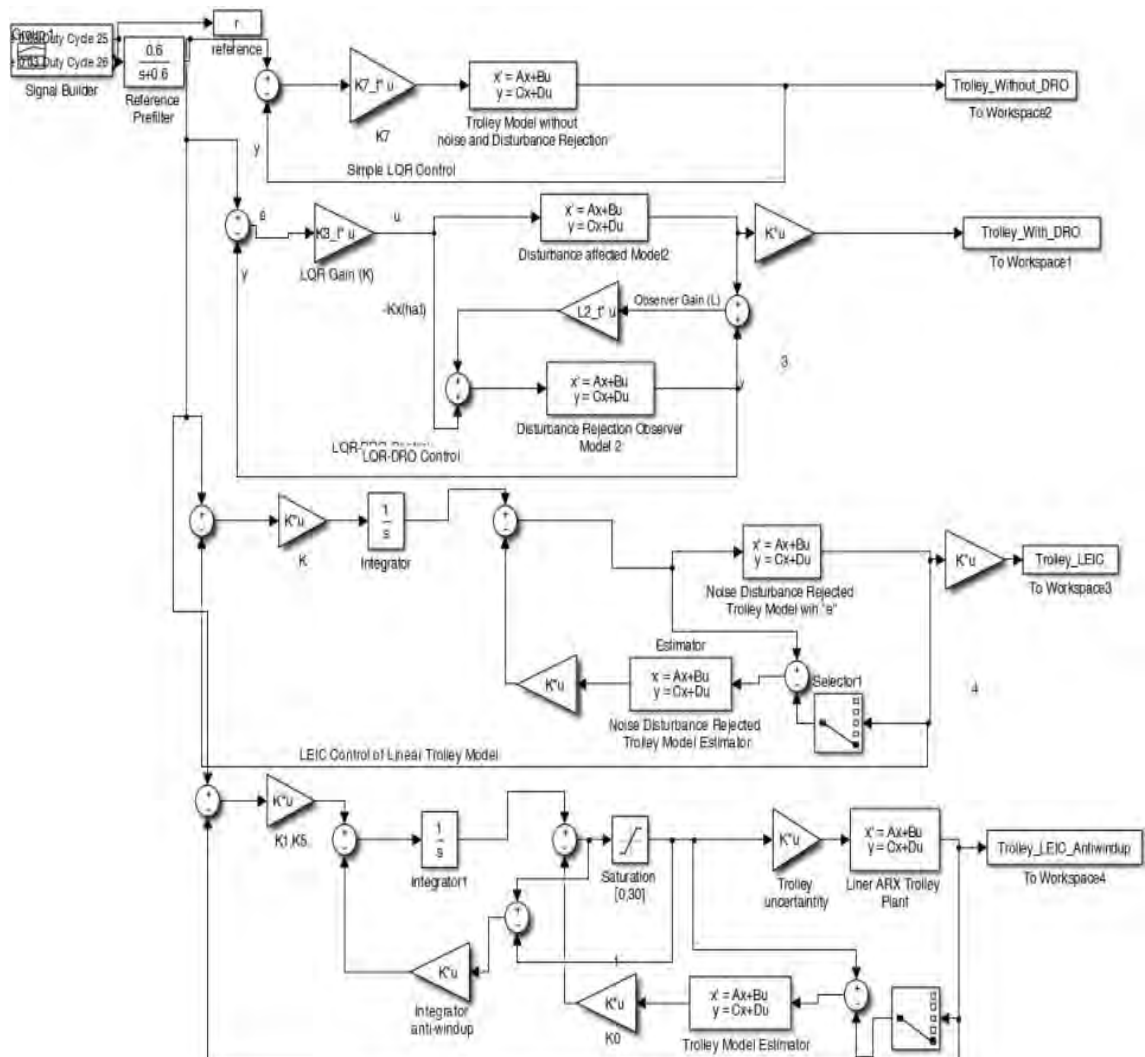


Figure 5.16 LQR, LQR-DRO, LQR-LEIC, LQR-LEIC Antiwindup Controllers
153

Each control performance for the trolley translation model has been presented below in Fig. 5.17a. Comparing all four developed controllers LQR, LQR-DRO, and LEIC, LEIC Antiwindup appears to achieve more or less robust reference tracking. LQR-DRO output has slight overshoot compare to others however troubleshooting observer gains would fix the issue. All those 4 outputs have been put together in one figure, as well in Fig. 5.17b.

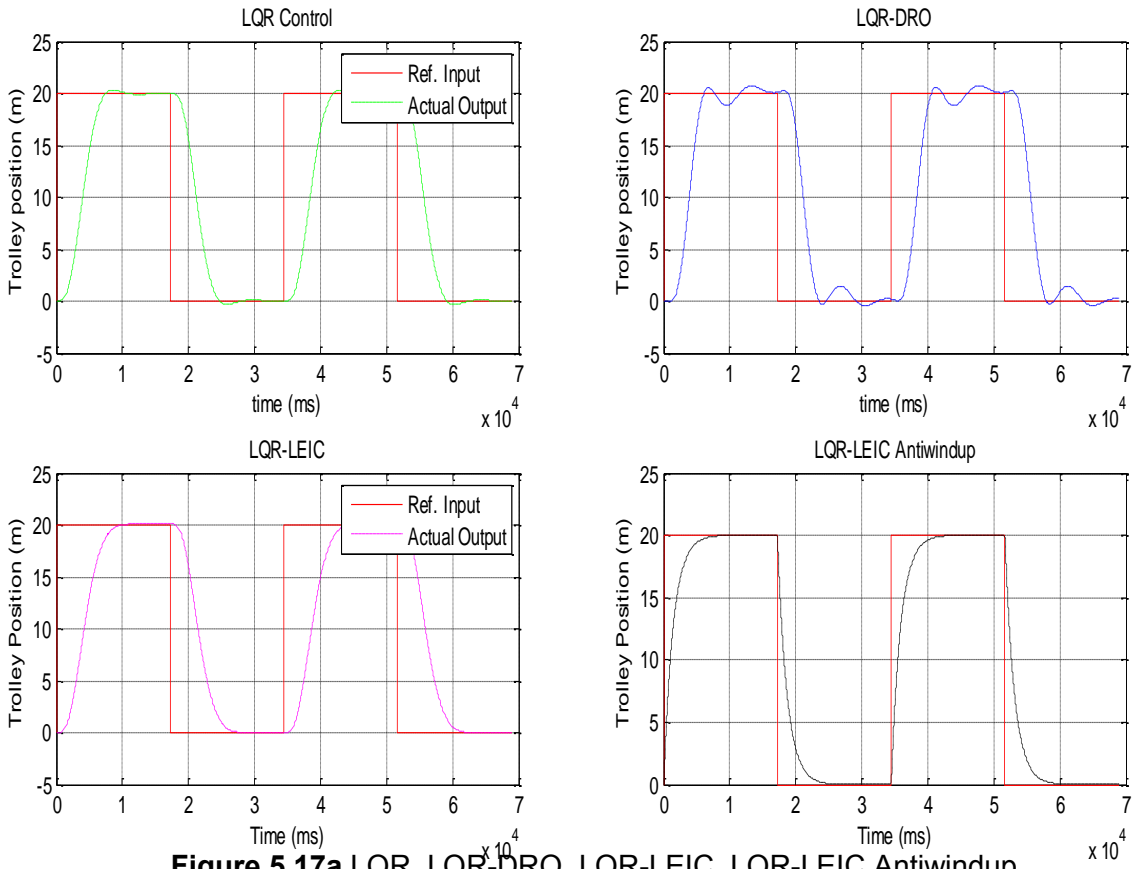


Figure 5.17a LQR, LQR-DRO, LQR-LEIC, LQR-LEIC Antiwindup
Performance Comparison for Trolley Model

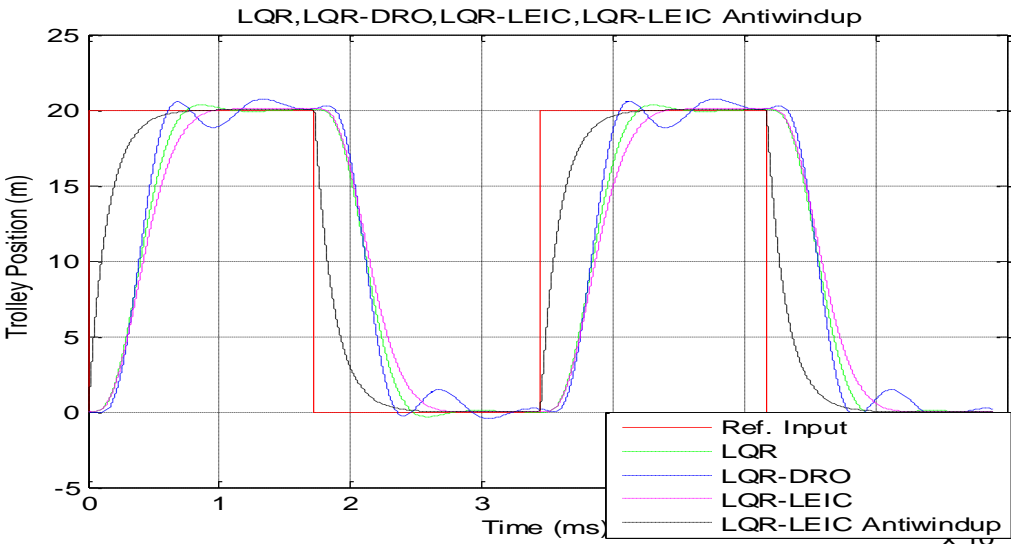


Figure 5.17b LQR, LQR-DRO, LQR-LEIC, LQR-LEIC Antiwindup
Performance Comparison for Trolley Model

5.3.7 Control Efforts Comparison

This research further checks the control efforts of all developed linear controllers running in Trolley Translation controls. In order to do so, control signal from each design is squared-sum-integrate to analyze how good the control efforts are compared to each other. The following figures Fig. 5.18a provides the control effort of LQR with its peak value reaching $5.5131e^{11}$ while DRO control effort, Fig. 5.18b, takes largest control effort compared to others with its peak value $2.5448e^{15}$. Even though control effort in LEIC, Fig. 5.18c, further reduces to peak value with $1.0267e^{10}$, the significant changes happened in LEIC Anti-windup, Fig. 5.18d, with control effort takes up to $1.7358e^4$ only. Further simulations, improvements, and comparison would be made in payload swing control in the next section.

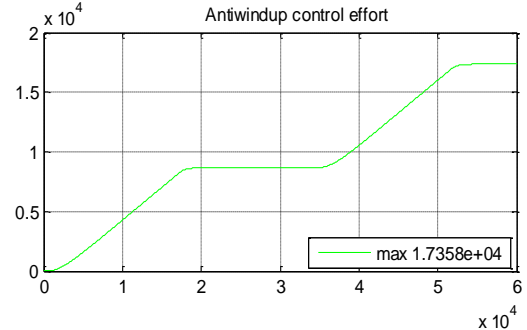
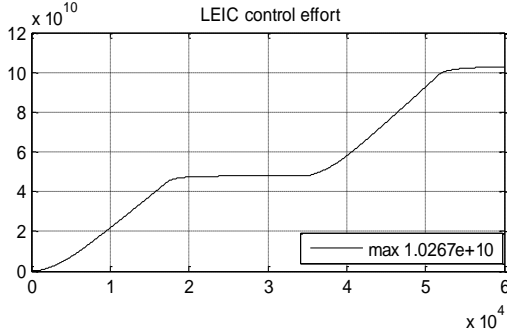
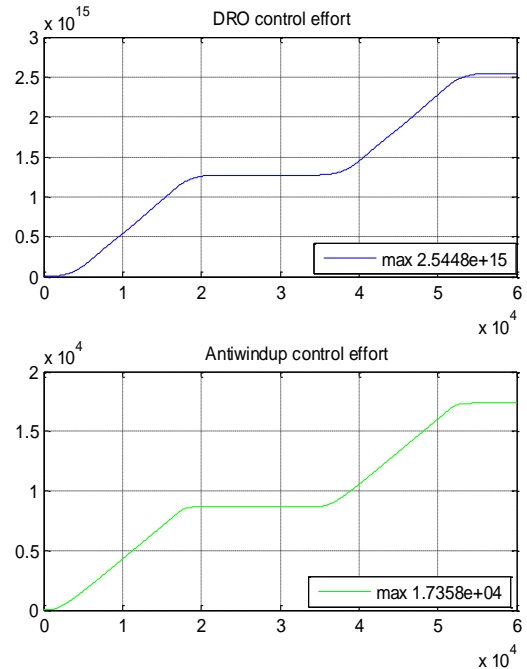
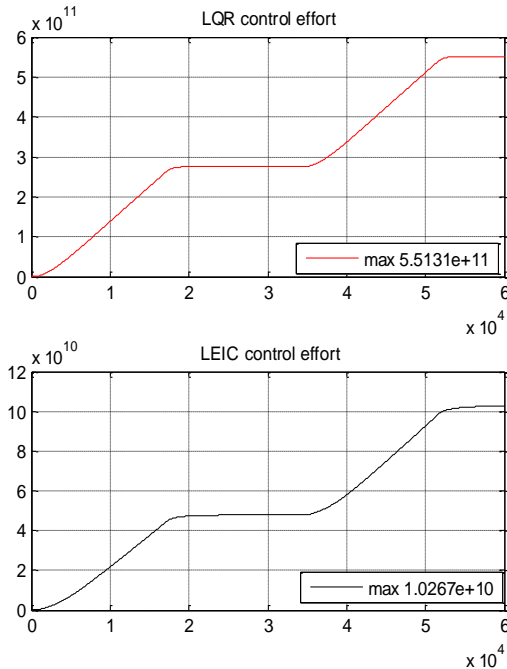


Figure 5.18a LQR Control Effort

Figure 5.18b DRO Control Effort

Figure 5.18c LEIC Control Effort

Figure 5.18d LEIC-Antiwindup Control Effort

5.3.8 Linear ARX Payload Plant

This section identifies the loadswing model using same NARX approach. Several combinations of nonlinear regressors with different model orders [na nb nk: 1 1 1 to 4 4 1] were applied in order to get better fit model. The estimation and validation figures in Fig. 5.19 are presented below. Among the several model orders, the simulation shows model order [2 4 1] achieves estimation fit (Narx8e:19.33%) while validation fit (Narx8e:21.91%). Though the suitable model with certain fit has been achieved, further optimization approach can further be used to have better fit model. The current selected linear loadswing model is

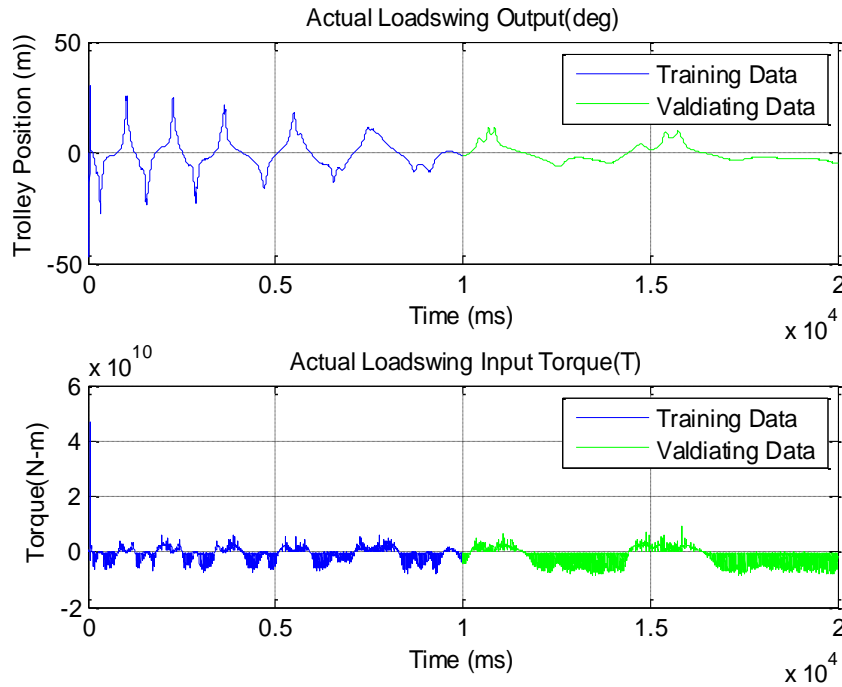


Figure 5.19 Training and Validating Payload Model using NARX

The coefficients of linear ARX model which contribute to the dynamic equation can then be written as “`x_est11=m1{i,j}`. Nonlinearity.Parameters.LinearCoef”:

$$\begin{aligned}\dot{x} &= Ax + Bu \\ y &= Cx + Du \\ \frac{y(k)}{u(k)} &= \frac{b_1 q^{-1} + \dots + b_m q^{-m}}{1 + a_1 q^{-1} + \dots + a_n q^{-n}} = \frac{B(q^{-1})}{1 + A(q^{-1})}\end{aligned}$$

The selected linear Trolley model and its Linear state-space forms are

$$\text{Discrete Model: } \frac{0.3807 q^{-1} + 0.1885 q^{-2} - 6.7373 q^{-3} - 0.4033 q^{-4}}{1 - 3.435 q^{-1} - 0.1156 q^{-2}}$$

$$Z - \text{transformed Model: } \frac{0.3807 z^3 + 0.1885 z^2 - 6.7373 z - 0.4033}{z^4 - 3.435 z^3 - 0.1156 z^2}$$

$$\text{Continuous Model: } \frac{1.422 s^4 - 58.48 s^3 - 259 s^2 + 2.936 e^{04} s - 2.434 e^{05}}{s^4 + 50.33 s^3 + 577.1 s^2 - 5315 s - 9.448 e^{04}}$$

$$\dot{x} = Ax + Bu, \quad y = Cx + Du$$

In minimizing loadswing linear model with LEIC was initially unachievable because of the input concerns. Since there is only one input force directly applying on the trolley whereby payload cable is attached underneath via pulley. During the operation, interaction torque between the trolley and payload appears at pulley. To cancel out that torque and achieve robust control, torque-to-power conversion, $P_3 =$

$T_2 \begin{bmatrix} 3000 \text{ W} \\ 6876 \text{ Nm} \end{bmatrix}$ in Fig. 5.20 is then introduced. Trials-and errors were necessary by adjusting such as: weights in Q and R matrices, different LQR gains in integral control and estimator, saturation, prefilter, and trolley uncertainty parameters. At saturation (0,1.75) range, $Q_x = 1$, and $R_u = 0.0001$, the robustness of LEIC for nonlinear control has been extraordinary, and follows the reference trajectory perfectly. After several trials-and-errors, suitable prefilter, $G_{pf}(s) = \frac{0.185}{s+0.185}$, saturation range (upper limit 1.44 and lower limit 0), and loadswing uncertainty parameters have been achieved.

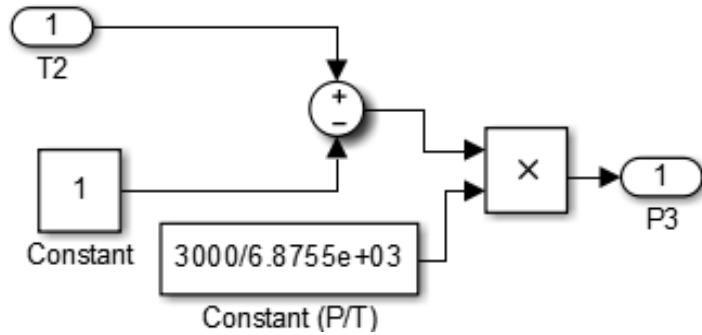


Figure 5.20 Torque to Power Conversion

5.3.9 DRO, LEIC, LEIC-Antiwindup performance Comparison for Payload

The goal of the controller development is to achieve loadswing minimization so that tower crane can perform faster in a reasonable amount of time while safe working environment is preserved. To this end, a number of techniques have been developed right from the simechanics-visualized modeling, modified least square linearization to four controllers, as discussed earlier. This section combines all four controllers (simple LQR, LQR-DRO, and LEIC for linear and nonlinear models in Fig. 5.21 in one to compare swing trajectory performances. All those developed controllers turn out to have satisfactory performance in tracking reference loadswing trajectory except simple LQR which produces slight delay and steady-state error compared to others.

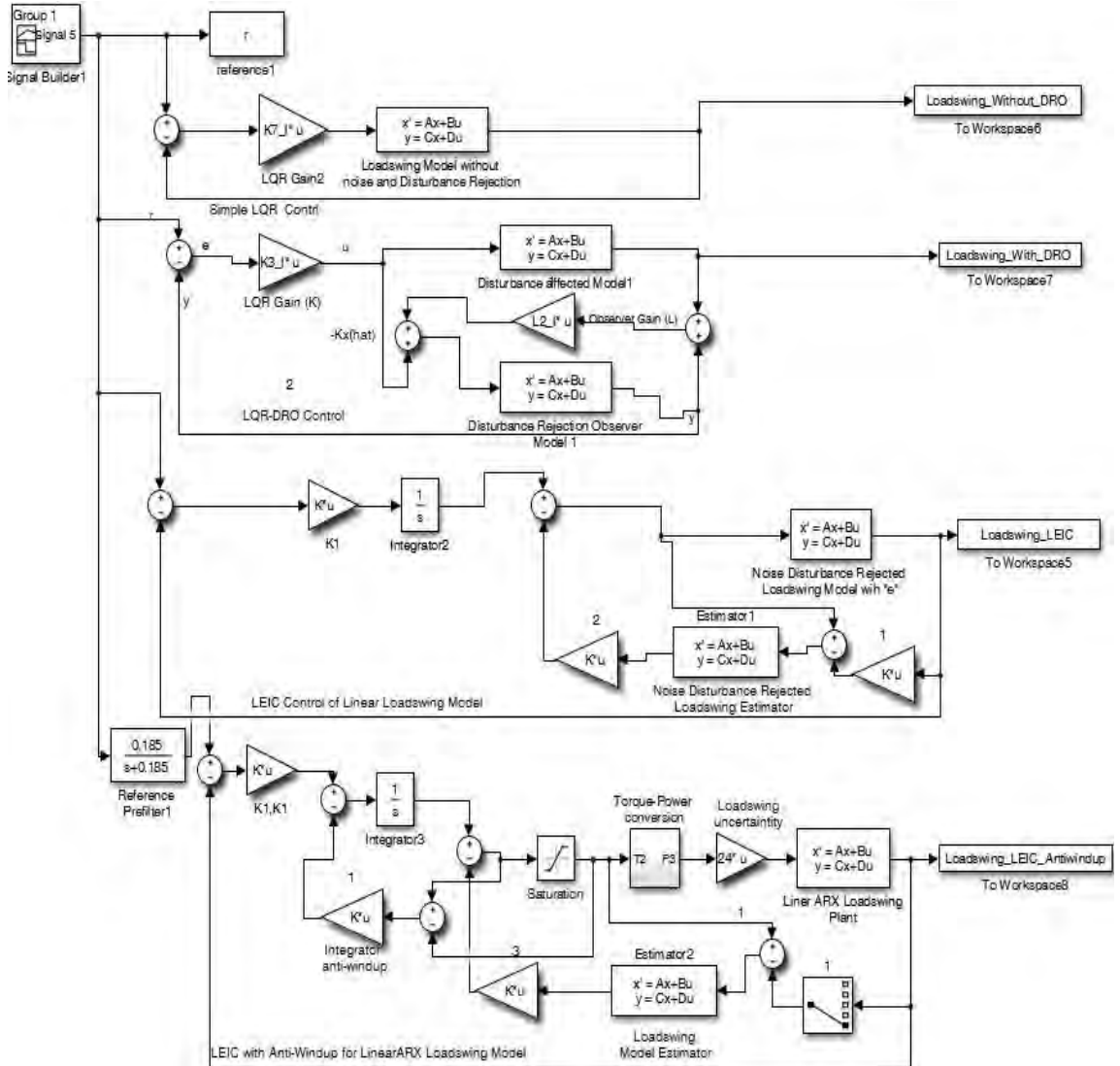


Figure 5.21 LQR, LQR-DRO, LQR-LEIC, LQR-LEIC Antiwindup Controls for Payload Swing Models

From NARX loadswing model system identification, linear ARX model was generated, as in (19). Reference tracking of loadswing linear model using LEIC Anti-Windup control was initially unachievable because of the input concern. Trials-and-errors were necessary by adjusting such as: weights in Q and R matrices, different LQR gains in integral control and estimator, saturation, prefilter, and loadswing uncertainty parameters. All control performances from LQR, LQR-DRO, LEIC, and LEIC Antiwindup produce perfect reference trajectory tracking in Fig. 5.22a and Fig. 5.22b.

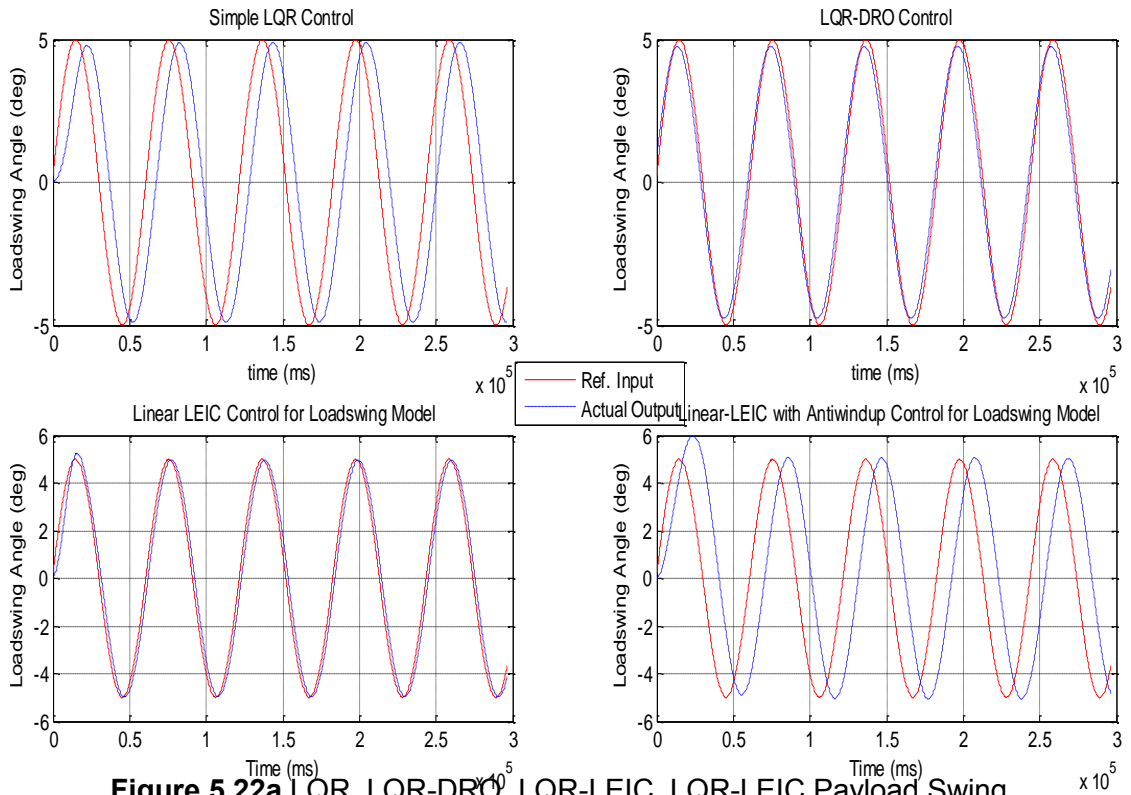


Figure 5.22a LQR, LQR-DRO, LQR-LEIC, LQR-LEIC Payload Swing responses

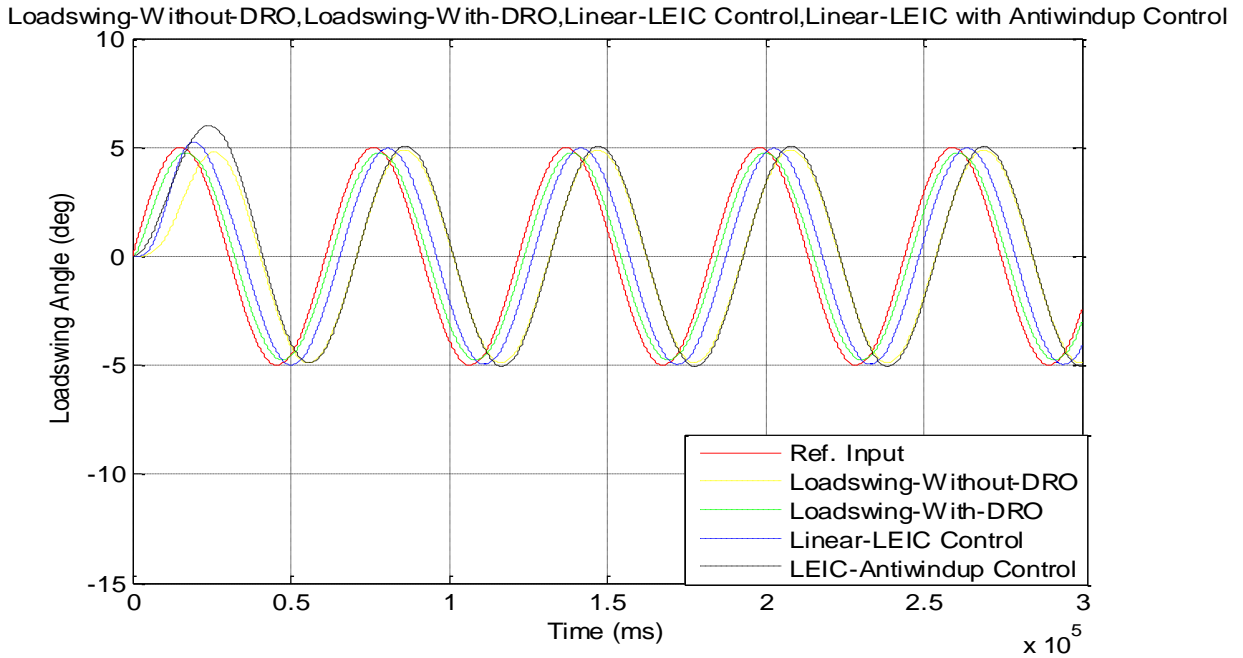


Figure 5.22b LQR, LQR-DRO, LQR-LEIC, LQR-LEIC Antiwindup Performance Comparison for Payload Swing

5.4 Summary

This research has made great contribution towards 3D modeling. Firstly, 3D Tower Crane SimMechanics-Visualized model was developed based-on real crane (Morrow: Liebherr71EC). Secondly, designed wind disturbance model was using

Gawronski approach and applied on the crane. Thirdly, this research analyzed tower vibration impact on the crane operation and load swing. Fourthly, linearized the system and optimized for the better fit using improved version of linear least square approach. And finally, this research developed (i) simple LQR, (ii) LQR-DRO and (iii) LQR-Estimator-Integral (LEIC) Controllers for linear model to achieve trolley position and payload swing suppression, and (iv) LQR-Estimator-Integral (LEIC) Controllers for non-linear models that track a predefined desired reference trajectory (X_r) and (θ_r). Simple LQR control was first established for the trolley and loadswing systems without noise disturbance. Having overshoot/undershoot in the tracking response makes the control unreliable. Besides, almost every system is affected by noise disturbance and therefore achieving noise rejected control is indeed essential.

As to implement Disturbance Rejection Observer (DRO) based-on Luenberger observer approach, the matrices describing the control canonical form was initially established in which the disturbance, nonlinearities and uncertainties have been translated into the last state variable. Generating observer gains are based-on the inverse of augmented matrix so that the unknown dynamics and disturbance can be actively estimated and compensated in real time while achieving the stable estimator. Well-tuned DRO would optimize the tracking performance, and reject the disturbance making LQR-DRO feedback control more robust. It not only simplifies the process of design but also makes the tracking trajectory smoother.

Despite the improvement of LQR-DRO method, slow convergence still exists in the control scheme and seriously limits its practical application in trolley translational control. Through the estimator with error space approach, LEIC for linear models goes one step further. It consists of disturbance affected trolley translational model (augmented) position control and estimator-integral control loop for tackling disturbances and uncertainties at the surrounding issues. Integral control that presents the internal model principle to achieve robust tracking is introduced by a direct method of adding the integral of the system error to the equations of motion. Since the system needs to reject the disturbance from the augmented model, Estimator has also been included in this optimal control. Although the existing method employs error state gain (K_1) for internal model controller while states gains (K_0) for estimator separately, [4], this research has applied K directly on both internal model controller and estimator. The estimator gain, L , is then derived using Kalman-Bucy filter. LEIC has a much smaller tracking error and a much steadier error curve than the proposed LQR-DRO method. The ability to filter and tracking system states also enhance the robustness

and practical application of the control method. By connecting the error space method and estimator method, a complete control scheme is established.

Those developed controllers are considered to be robust for the crane system with all applicable sensors working condition. In the case of sensor failure during the operation, the robust controller is still usable but may have a slower response or become less effective to achieve the desire actuation and therefore, Fault Tolerant Control (FTC) is needed to be able to produce the desired effect, as in [77]. Since FTC is a combination of robust control and reconfigurable control, and further complexity in nature, it is recommended to implement in real crane operation though it has not been included in this stage of research.

Linear Models were then generated from Nonlinear Autoregressive exogenous model (NARX) Structure. LEIC-Antiwindup control was then designed and applied on developed models better to achieve better robust control. This method includes not only integral control with full-order estimator like before but also additional features such as Integrator anti-windup, Saturation Nonlinearity, Trolley uncertainty parameter, prefilter to smoothen the sharp corners of output, and feedback loop gain. Bringing the saturation function into the controller exactly decreases the degree of buffeting, but it also weakens the convergence performance of the system. Methods used to track the reference have been relatively mature and robustness of all those developed controllers have been presented.

These remarkable research developments from the SimMechanics-visualized model to the LQR-DRO, LEIC, and LEIC-Antiwindup controls are the significant milestone for all the crane research disciplines in which modeling and simulations, linearization and optimization, vibration analysis due to wind disturbance, position and swing controls developments could essentially be carried out without necessarily relying on the real time operating cranes or the lab prototypes.

Chapter 6

Nonlinear Robotic Tower Crane Modeling Control (RTCMC)

6.0 Robotic Tower Crane Modeling

As previously proposed controllers from chapter (5) have proven to achieve robust tracking on crane linear models, this paper applies LQR-DRO controller with feedback torque actuator compensation on actual nonlinear SimMechanics-visualized tower crane model discussed in chapter (3). The reason of naming as "Robotic Tower Crane Modeling Control" is because it covers the whole aspects of: the recently developed nonlinear simmechanics-visualized model, optimized the best fit linear model, and the proposed trajectory tracking controllers of this work. This approach is motivated by two reasons. First, the controller is relatively simpler compare to other proposed ones and it only needs trials-and-errors for oberserver gains. Second, if LQR-DRO implemenetation is found to achieve robust tracking for nonlinear RTC, it proves that other controllers would definetly execute more or less similar performance. Though initial LQR-DRO implementation on nonlinear RTCMC could neither track trolley trjectory nor supress the payload swing, a number of step-by-step trials were necessary to bring the system under control. Three considerations have been taken into accounts such as; LQR-DRO controller parameters tuning, feedback forces and torques investigations, and mechanical structure adjustments.

6.1 Nonlinear RTCMC Flowchart

The following RTCMC flowchar in Fig. 6.1 shows three main features. Firstly, it is all about designing simmechanics-visualized crane model based on real tower Morrow crane. Secondly, developed wind disturbance model and analyzed vibration impact on the crane and more specifically towards payload swing instability. Thirdly, complete nonlinear simulation data collection, system identification using Linear Least Square(LLS) approach, and optimization by proposed version of LLS algorithm to obtain the best fit linear model. Finally, extended state observer (ESO)

with disturbance rejection implementation, and tuning Q-R weighting matrices for better system's tracking performance.

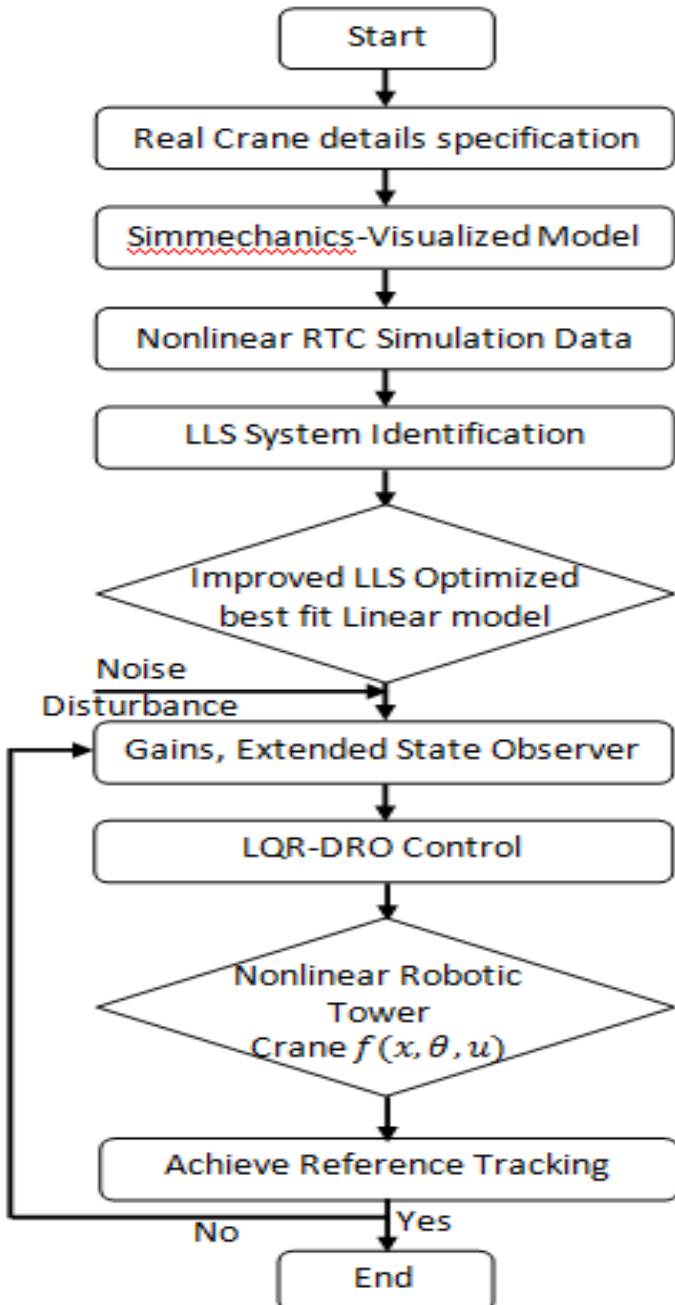


Figure 6.1 Nonlinear Robotic Tower Crane Modeling Control (RTCMC) operation Flowchart

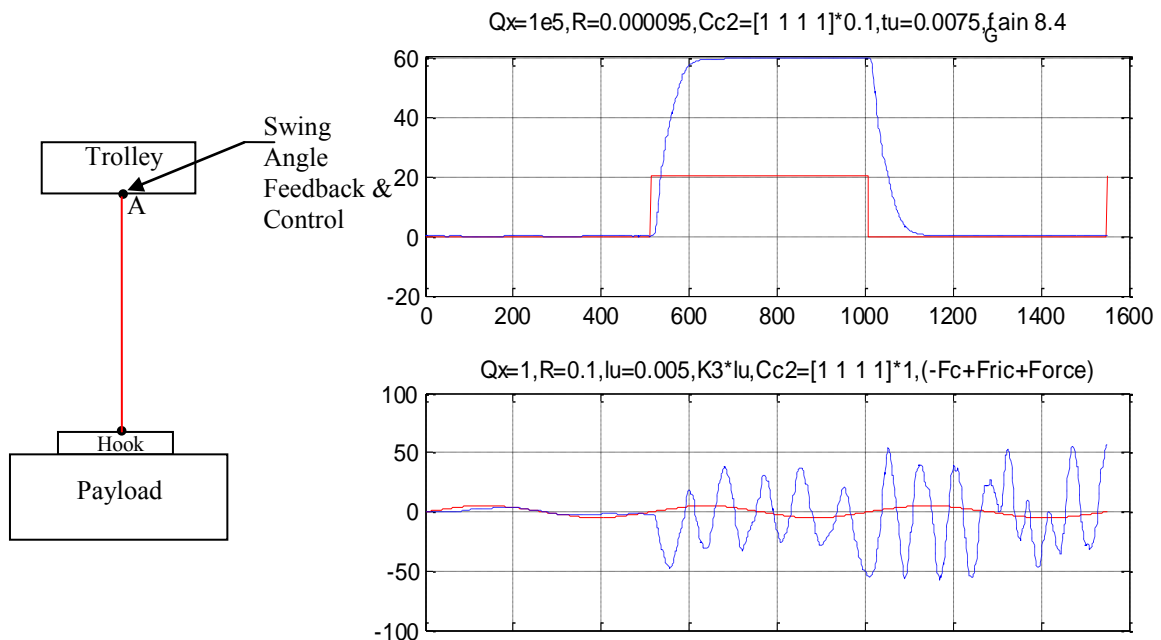
6.2 Cable structure impact on Payload Swing Minimization

To date, crane industries around the globe use two-cables payload attached to trolley. The reasons could be to avoid having much unsettled payload shake in any move during the operation. As this research has developed the very first SimMechanics visualized based-RTC Model in the world using real crane data, it takes initiative to try

switching to one-cable payload attached to trolley approach. As this RTC Model represents actual crane, its simulation and visualization would explain the trolley-payload swing issues. In this case, this research started the trials with one cable type. Initially, trolley without any payload attached simulation shows this nonlinear system with LQR-DRO control approach achieve perfect reference tracking. Likewise, trolley is placed stationary at any position on the jib tower whereby payload swing operation has also been under perfectly controlled using LQR-DRO. Though separate simulations of trolley and payload swing achieve reference tracking, combining in one as trolley-payload simulation was unable to achieve stable trajectory tracking since it is highly nonlinear.

6.2.1 Applying One-link Payload Swing Cable

In this one cable approach, swing angle feedback force via only interaction point A in Fig. 6.2a is taken back to trolley translational control while payload swing control actuation is implemented at the same point A. Though all necessary feedback forces and torques were taken into consideration in this trial, only trolley control could achieve reference tracking while payload remains unsettled according to the simulations results as shown in Fig. 6.2b.



6.2.2 Applying Cross-link Payload Swing Cable

Since one cable approach could not produce expected results, another approach which uses two additional cross cables attached to the existing two cables was put on trial. The idea is to suppress higher payload swing during trolley back-and-

forth operation. Interestingly, these two cross cables appear to create internal constraints during operation, and due to that the payload swing angles reached to almost zero (-2e-13 to 2e-13) degree. However, drawing both swing feedback forces from points A and B in Fig. 6.3a to trolley control could have become obstacles which resulted trolley control out of reference tracking as shown in Fig. 6.3b.

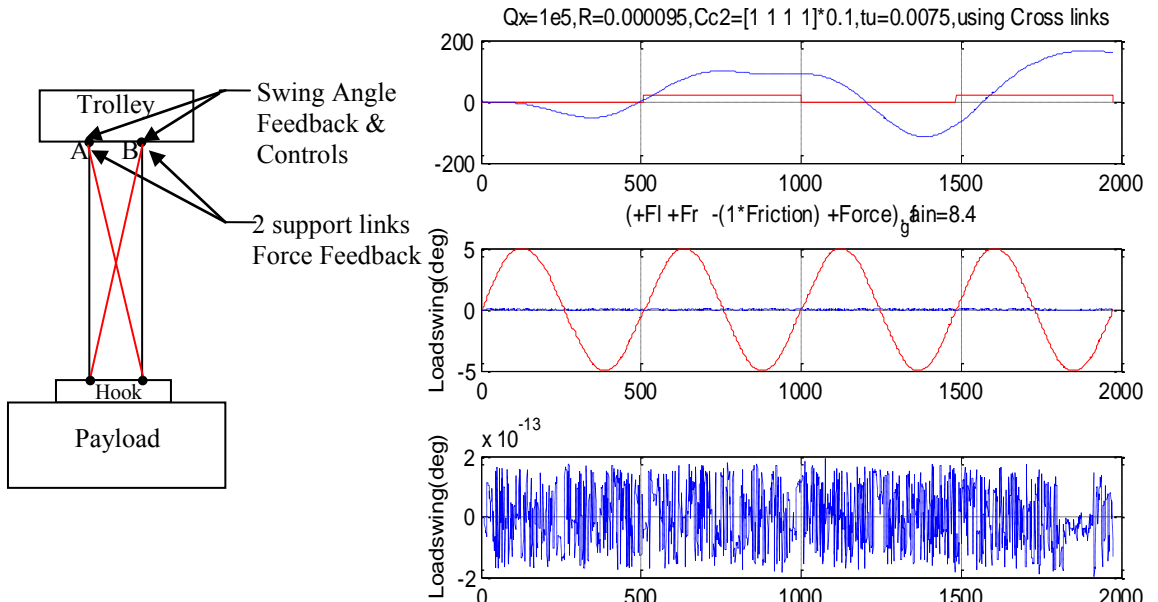


Figure 6.3a Using Cross-link Payload Swing

Figure 6.3b Trolley-Payload results from Cross-link cable

6.2.3 Applying W-link Payload Swing Cable

Since the second approach could not produce fruitful results, this research went on to W-link payload cable to be attached underneath the trolley. Using this W-link, three different approaches were taken into consideration. Case(1) considers drawing all three interaction feedback forces from points (a,b,c) for trolley control while only two swing actuators are placed at points (a,c) as shown in Fig. 6.4a. Case(2) considers drawing only two interaction feedback forces from points (a,c) for trolley control while placing two swing actuators at points (a,c) as shown in Fig. 6.4b. That means, point (b) is just a support to stabilize the cables on both sides in minimizing the swing. Case(3) this time is similar to Case(1) by drawing all three feedback forces from interactions points (a,b,c) however swing actuation is implemented at only point (b) as shown in Fig. 6.4c. All those three cases (1,2,3) resulted in trolley out of control though payload could be suppressed to nearly zero degree.

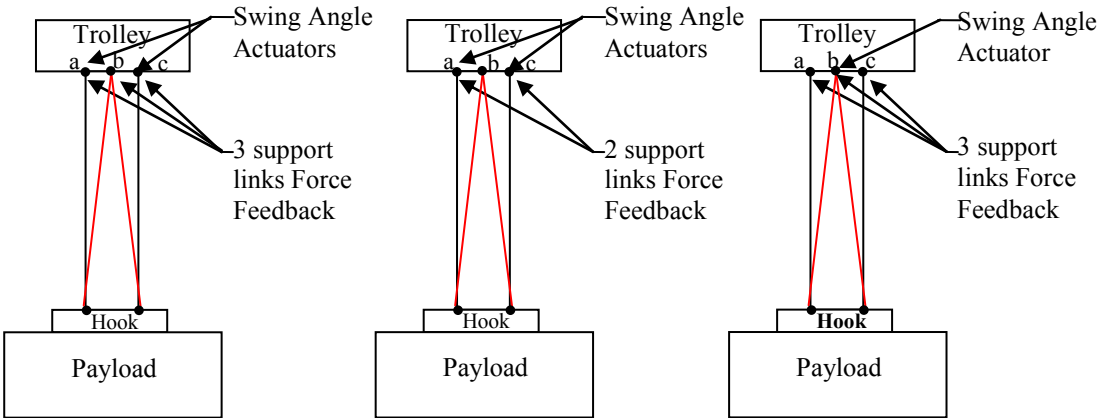


Figure 6.4a Case 1 W-link **Figure 6.4b** Case 2 W-link **Figure 6.4c** Case 3 W-link

6.2.4 Applying Connector-link Payload Swing Cable

Since both cross-links and W-links approaches do not provide better trolley reference tracking, one link connector has been added to the two-cable link as below. The first case in Fig. 6.5a has taken feedback from points (a,b) to trolley control while the second case in Fig. 6.5b considered payload force (that is; $F = \text{payload mass} * \text{payload acceleration}$). Even though payload swing could be brought under control, trolley control still could not be achieved after trials-and-errors in Fig. 6.5c.

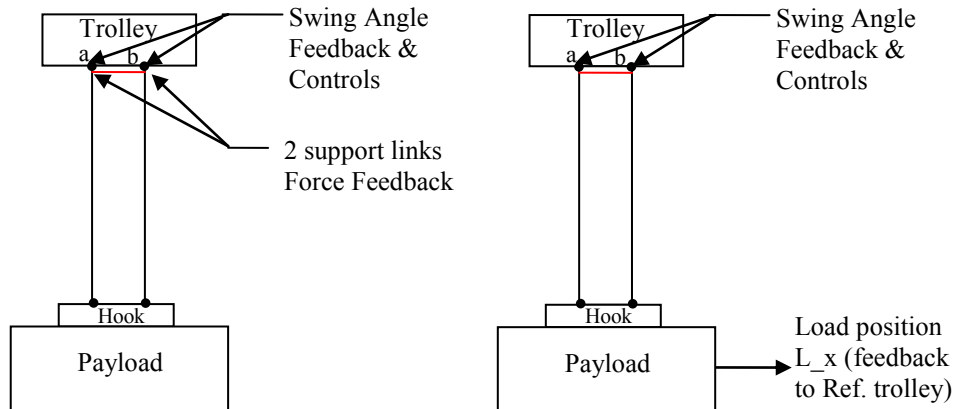


Figure 6.5a Case 1 Connector-link **Figure 6.5b** Case 2 Connector-link

$Q_x=1e5, R=0.000095, Cc2=[1 1 1 1]*0.1, tu=0.0001, fain=8.4$, Added payload position feedback

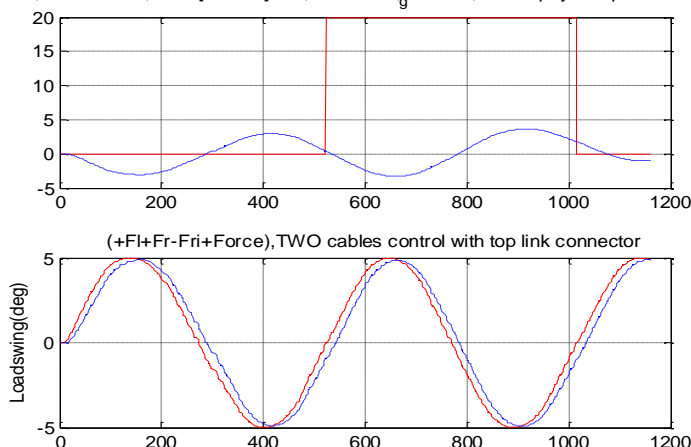


Figure 6.5c Trolley-Payload responses from Connector-link trial

6.2.5 Applying T-link Payload Swing Cable

After the connector-link trial mentioned-above, reverse T-link in the two cables is used to control both trolley translation and payload swing minimization. All the joints used in the design have been mentioned as shown in Fig. 6.6a. Similar to W-link case, this trial takes points (a,c) feedback forces and only control point (b). Interestingly, trolley translation control becomes feasible and payload swing suppression has maintained around zero-angle throughout trolley motion in Fig. 6.6b. Reference swing tracking is not applicable in this case since reverse T-link has locked the cable swing. If any crane industry wants to keep the swing stationary during the operation, this type of invention is recommended. Since this research wants to achieve swing reference tracking control, other types of trials would further be analyzed.

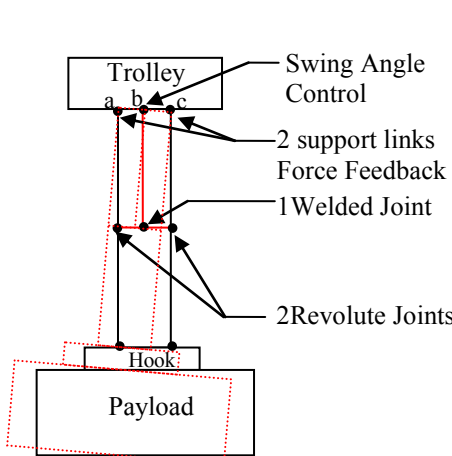


Figure 6.6a Using Reverse T-link Payload Swing

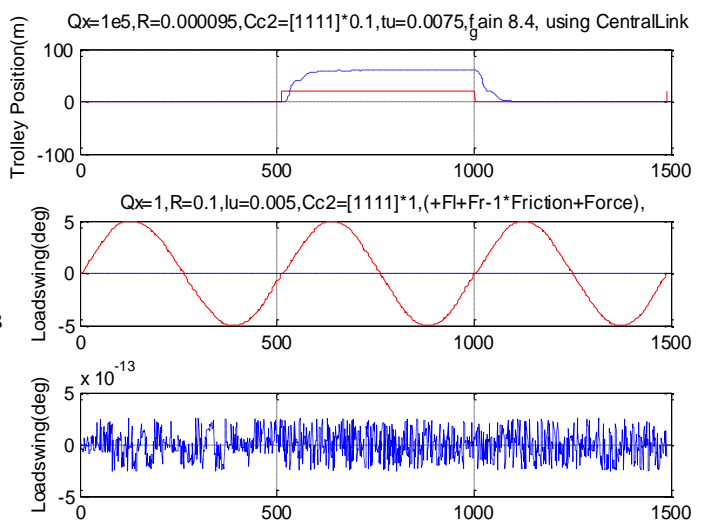


Figure 6.6b Trolley-Payload results from Reverse T-link cable

6.2.6 Applying Two-link Payload Swing Cable

After ways of different analysis on cable structures, this case uses existing two-cable structure without any other combination as shown in Fig. 6.7a. In this scenario, tuning control parameters such as: Q-R weighting matrices, trolley uncertainty, swing uncertainty, and adjusting necessary feedback forces-torques were essential to achieve both nonlinear trolley-payload robust tracking. Details of those parameters tuning, analyzing feedback forces-torques, and designing swing compensation actuator would be discussed in the next section. After trial-and-errors, trolley translational motion is seen smoothly tracking without significant overshoot while payload swing has slight fluctuation as shown in Fig. 6.7b.

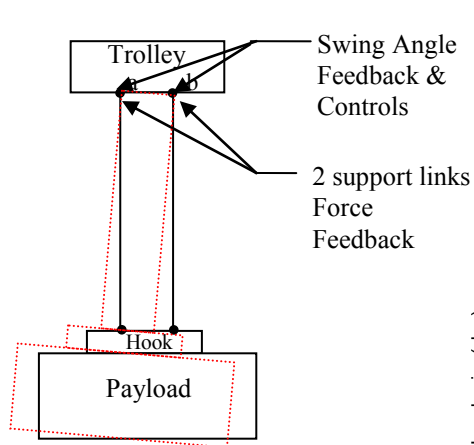


Figure 6.7a Using two cable-link

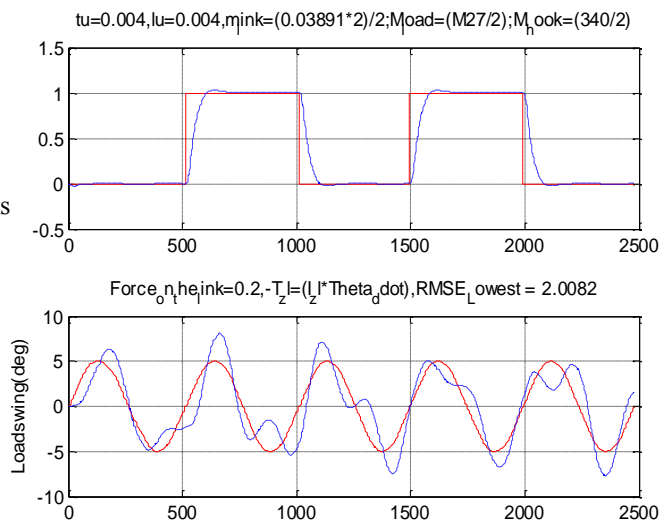


Figure 6.7b Trolley-Payload results from two cable-link

6.3 Reaction Forces and Torques Investigation

This research thoroughly investigated the concerns of reaction forces and reaction torques on highly nonlinear trolley-payload motion environment in RTCMC. H. Sano in [8] proposed friction disturbance observer based on time correction in order to eliminate trolley-to-rail friction. A. Elharfi in [13], analyzed the flexible cable vibration which destabilizes the trolley motion and therefore he proposed a boundary feedback law to achieve desired zero equilibrium. Inverted pendulum with frictionless trolley motion has been tested whereby a thrust force effect on reaction joint was a concern in [45]. Sliding mode control is then applied to overcome external disturbances and uncertainties. In [78], the authors discuss about the multiple-point payload suspension control approach for gantry crane. Because, This approach allows for enhanced stiffness of the cable-payload system and thus more resistance to pendulations. However, due to the wind gusts or initial disturbances inducing payload pendulations, this control approach is not effective in disturbance rejection, which can destabilize the system. Similarly, Beznos in [79] proposed the implementation of an electric motor with a flywheel at the end of payload pendulum. This paper aims to steer the motion of pendulum from initial position to the unstable upper equilibrium point so that the control law can take action in stabilizing the payload.

In this work, initial investigations on both "trolley translation without payload attached" and "payload swing without trolley motion" with external driving force and translational frictions were taken into account. Though the trolley translational motion could track the reference without setback, payload swing control case needs to draw reaction torque in minimizing the swing. Next, the combined nonlinear trolley-payload

system with having total load of 3340 Kg for both load and hook, the cable length-18 m, and square reference signal to drive trolley back-and-forth along the tower jib are the preset scenario. However, applying LQR-DRO control on this highly nonlinear system could hardly reach a stable reference tracking due to the lack of correct reaction forces-torques consideration. The simulation results show that, trolley-payload reference tracking is only achievable for (0m~2m) run trials. In order to run for higher trolley reference positions (2m~20m), torque compensation actuator is introduced to attenuate reaction torque at trolley-payload connection joint as shown in Fig. 6.8.

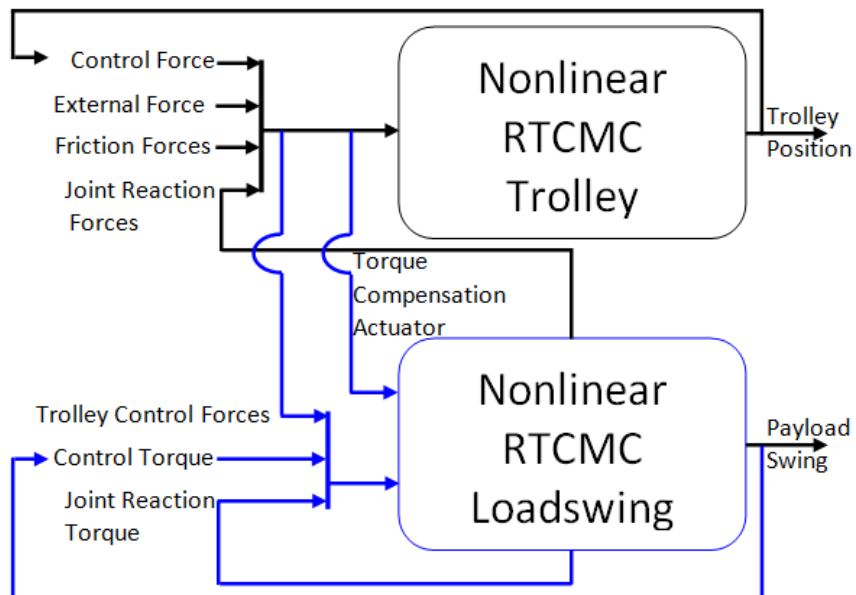


Figure 6.8 Feedback Forces and Torques consideration on nonlinear Trolley-Payload System

6.4 Joints, Sensors, and Actuators, implementation

The mechanisms of mounting a trolley on the rail-jib (tower) and the payload cable underneath may differ in crane to crane throughout the world. Some of the tower crane and overhead gantry crane mount the trolley on top of the rail-jib while the other mounts underneath the rail-jib. No matter those mechanical systems differ one another, feedback frictions and reaction forces-torques would be the same. Let's have a look on the past works of sensors and actuators implementation on the crane.

Tower crane lab-prototype developed by Quanser has the crane model with a mounted trolley on the rotary arm. The suspended cable is also attached underneath using gimble joint to produce pendulum deflection angle in [19]. Another crane model developer, Inteco, designed an overhead 3D gantry crane with jib-trolley-pendulum system. The measurement encoders are then employed to detect trolley motion and pendulum swing in [20]. However, most of the payload swing models in literature apply

only one swing cable while actual live crane has two. Moreover, proper sensors-actuators implementation in regards to swing minimization is also in question.

To properly analyze the need of suitable joints-sensors-actuators, this paper thoroughly attempted several ways of joints-sensors-actuators implementations. On the other hand, different combinations of reaction forces-torques are taken as feedback to control upon any changes. After a number of trials, the following consideration of: joints, spherical joints, revolute joints, and sensors are confirmed to be reliable arrangement as shown in Fig. 6.9.

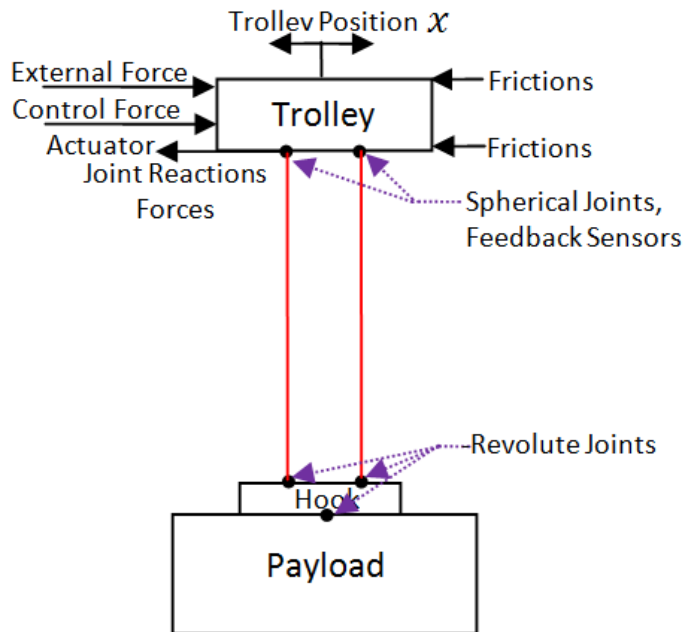


Figure 6.9 Joints, Sensors, and Actuators for Nonlinear Trolley-Payload Control

6.5 Torque Compensation in Swing Minimization

In the situation of highly nonlinear tower crane operation with wind disturbance and vibration impact, swing suppression is in fact impracticable. Looking at the shipyard gantry cranes and giant construction tower cranes in which, operators act in the form of compensation actuator by manually juggling trolley back-and-forth to minimize payload swing since no practical approach of torque compensation in swing minimization has been available to date. Global swing minimization researches have largely focused on reference tracking in some ways yet little known about torque compensation actuator with feedback implementation. For instance, H.M.Omar introduced anti-swing tracking control with friction-compensator in [18]. The quasi time optimal control with feedforward and feedbackward terms were proposed in [80]. However, since the controller consists of discontinuous function of time with several

switching time instants, this approach causes unstable payload sway and undesirable vibrations of the crane.

Similarly, Chwa D. proposed feedback linearization tracking control based on swing angular rate as well as the swing angle in [49]. Moreover, torque compensation actuators are mounted upon each changed-structure to suppress the swing to achieve reference tracking control. Even though adding extra T-link in existing two cable-structure proved to minimize the swing angle to nearly zero according to the simulation results, this paper still proposes swing compensation actuators be implemented at joint reaction points (a and b) of existing two cable-structure to avoid extra cost and complication as shown in Fig. 6.10.

Each actuator has two actions parts, one is torque compensation and the other is torque control. Torque compensation draws the driving power from trolley force control while the other one torque control is driven by LQR-DRO swing control. Details electrical structure of feedback forces-torques has been discussed above.

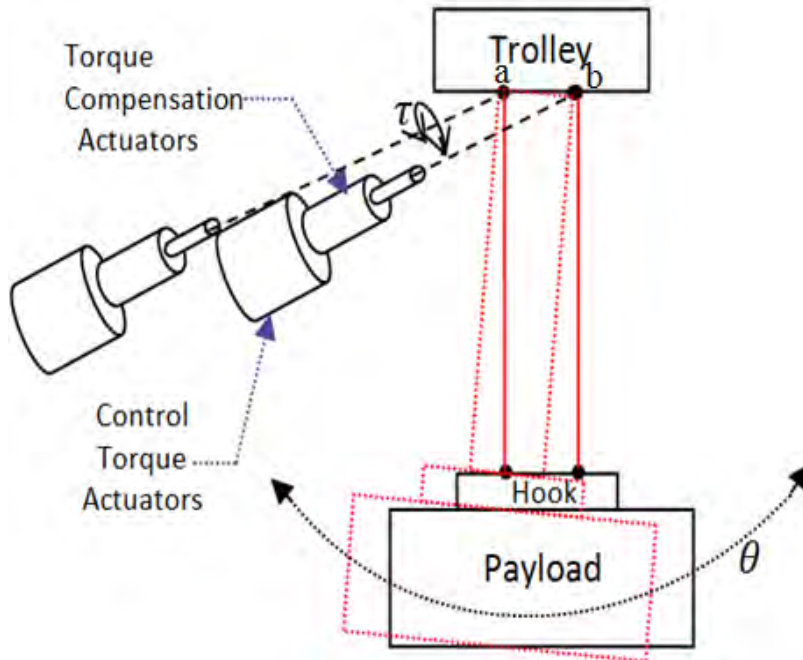


Figure 6.10 Torque Compensation Actuators Implementation. τ is Torque

6.6 Nonlinear RTCMC

The above-mentioned Nonlinear Robotic Tower Crane Model Control (RTCMC) design in Fig. 6.11 is based on the flowchart discussed in section 6.1. It has two control parts; one LQR-DRO for nonlinear Trolley translation, and the other LQR-DRO is for nonlinear loadswing. The proposed controller has the nonlinear uncertainty properties to improve the disturbance rejection accuracy of LQR-DRO as well as to achieve robust tracking.

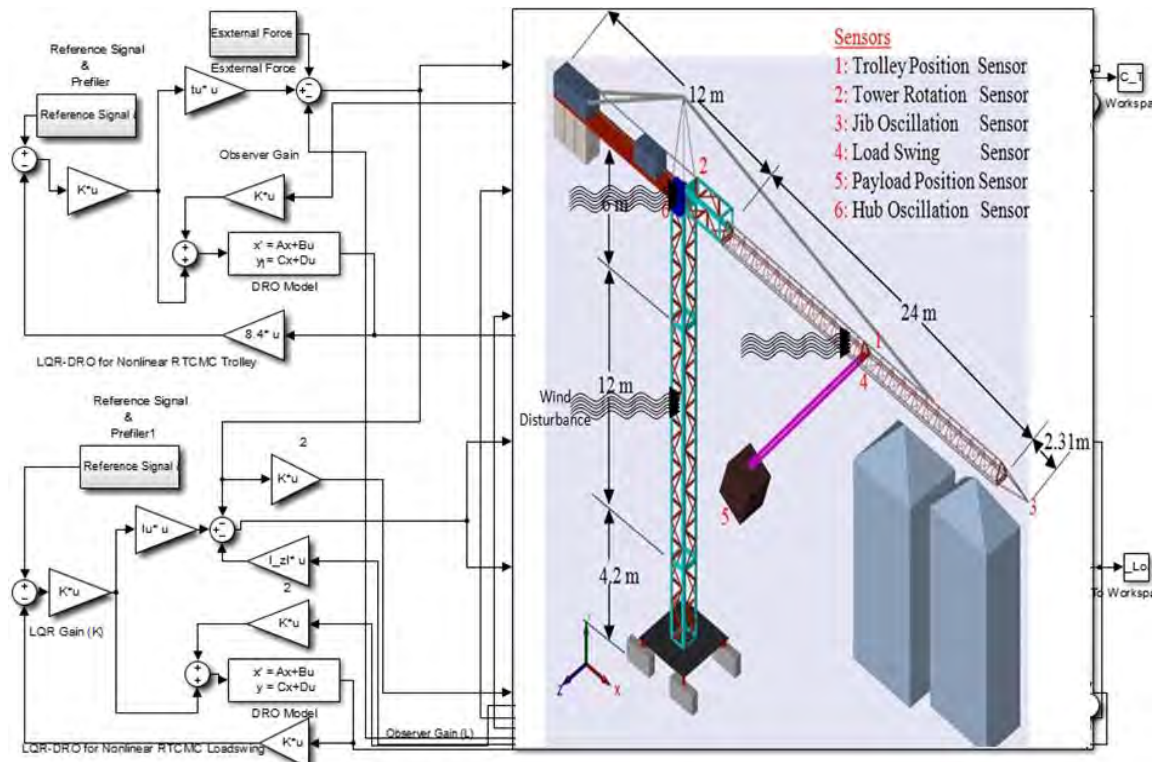


Figure 6.11 Nonlinear RTCMC with LQR-DRO for Trolley Loadswing Operation

6.7 Comparison of Square Reference and Semi-Hexagonal Reference

A number of case studies have been done on trolley-payload controls. Initially, Square- Reference input for trolley was considered in seeking robust tracking. During the trials from Square-Reference inputs (1m-to-20m), trolley control variables and payload control variables such as: Position output state (Q_t), Trolley input state (R_t), Trolley uncertainty gain, Trolley position feedback gain, Swing angle output state (Q_l), Swing angle input state (R_l), Payload swing uncertainty gain, Torque compensation actuator gain, and Payload swing feedback gain have been taken into considerations. Throughout those trials, trolley reference tracking has been achieved however payload swing tracking error became larger. As the nonlinear trolley system which carries maximum 3340 kg payload, it is found to be impractical to track the reference in a matter of one-second. Therefore, Semi-Hexagonal Reference input with 5-seconds ram time is introduced for trolley.

The following specific case studies compare both trolley translational motion and payload swing tracking control outputs using two reference inputs: Square-reference and Semi-Hexagonal reference. The control variables for trolley includes: Position output state $Q_t=9700$, Trolley input state $R_t=0.000095$, Trolley uncertainty gain=0.004, and Trolley position feedback gain=7.8. And the control variables for payload includes: Swing angle output state $Q_l=1$, Swing angle input state $R_l=0.1$,

Payload swing uncertainty gain=0.004, and Payload swing feedback gain=1. These parameters are then considered to be suitable based on trials-and-errors while torque compensation actuator gains are gradually increased from by 0.42 from 1-m to 20-m. The following figure as shown in Fig. 6.12 show trials based on square reference input produce higher root mean square error (RMSEs) while using semi-hexagonal reference inputs turn outs to have lower RMSEs. These comparison trials proved that semi-hexagonal reference is more suitable in this nonlinear control as in Table (6.1).

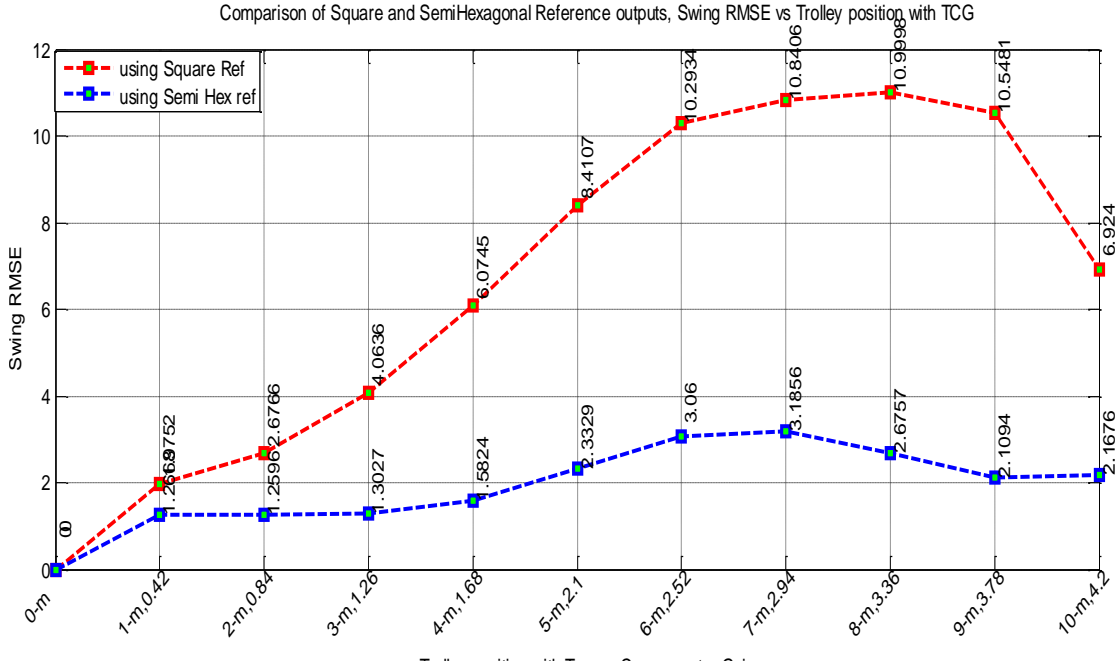


Figure 6.12 RMSE Comparison of Square Reference and Semi-Hexagonal Reference

Reference Trolley (m)	Torque Compensation Gain	Swing RMSE for Square Ref	Swing RMSE for Semi-Hex Ref
1-m	0.42	1.9752	1.2668
2-m	0.84	2.6766	1.2596
3-m	1.26	4.0636	1.3027
4-m	1.68	6.0745	1.5824
5-m	2.1	8.4107	2.3329
6-m	2.52	10.2934	3.06
7-m	2.94	10.8406	3.1856
8-m	3.36	10.9998	2.6757
9-m	3.78	10.5481	2.1094
10-m	4.2	6.924	2.1676

Table 6.1 RMSE Comparison in both Squre_Ref and Semi-Hex_Ref inputs

6.8 Results and Discussion of Square-Reference Input applications

After comparing between square reference and semi-hexagonal reference inputs trials, 1-m and 20-m cases with further tuning on torque compensator gains are discussed in this section. The simulations initially apply square-reference (1-m) with trolley back-and-forth run. After trial-and-error, the following values: trolley

uncertainty=0.004, Payload uncertainty=0.004, and torque compensation=0.5 are set to produce perfect trolley translation runs. In which, the swing achieves within the reference range of (5 to -5 deg) and its Root Mean Square Error (RMSE) is 1.9626 as shown in Fig. 6.13a.

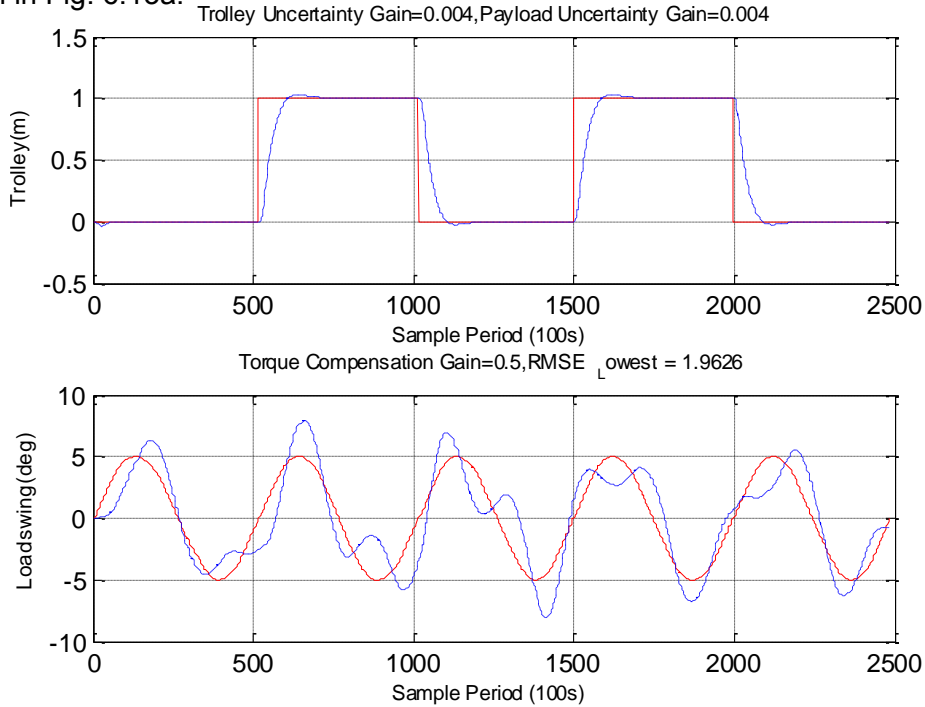


Figure 6.13a Nonlinear Trolley-Loadswing result at Square Reference 1m

Since actual jib tower is 24-m length, the next reference is set to be 20-m trolley with back-and-forth run. In this situation, trolley translation output has larger settling time but the payload swing still runs on the right with having its RMSE as low as 1.588 at the values of trolley uncertainty=0.0008, Payload uncertainty=0.004, and torque compensation=7.8 as shown in Fig. 6.13b.

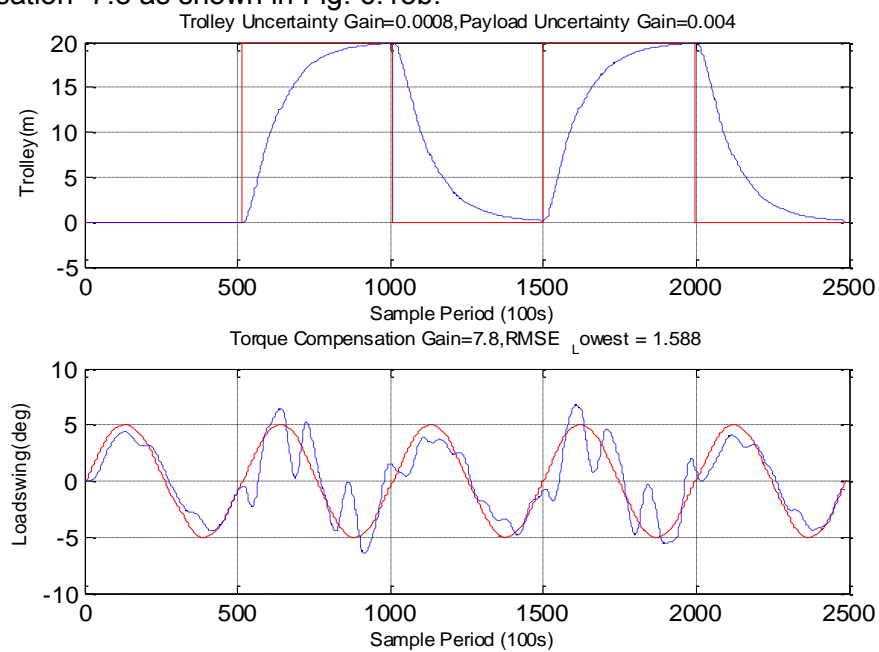


Figure 6.13b Nonlinear Trolley-Loadswing result for Square Reference 20m

In reality, trolley carrying payload (3340 Kg) to run along 20-m reference track in one second is impractical which makes the settling time large. Therefore, this paper further investigates the robust tracking performance using Semi-Hexagonal Reference. In the case of Semi-Hexagonal Reference 1-m, trolley translation tracks the reference with rise time 5-s. And, it has the reasonable setpoint tracking error, no overshoot, and allow trolley to reach steady state in about two seconds time. In contrast to the previous square reference 1-m simulation, the payload swing control achieves robust tracking with RMSE 1.2844 which is even lower than the previous trial as shown in Fig. 6.14.

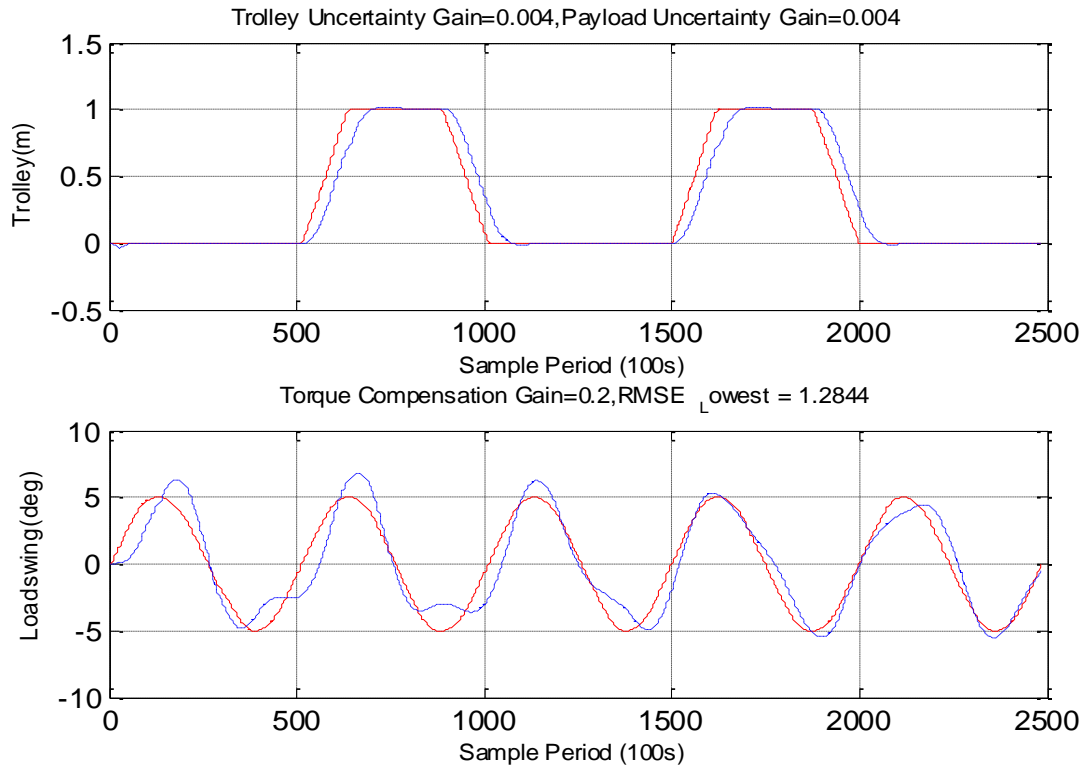


Figure 6.14 Nonlinear Trolley-Loadswing result
For Semi-Hexagonal Reference 1-m

Likewise, increasing the Semi-Hexagonal Reference to 20-m still remains both trolley and payload swing reference tracking robust as shown in Fig. 6.15. Trials parameters in both reference tracking cases are also presented below, see Table (6.2).

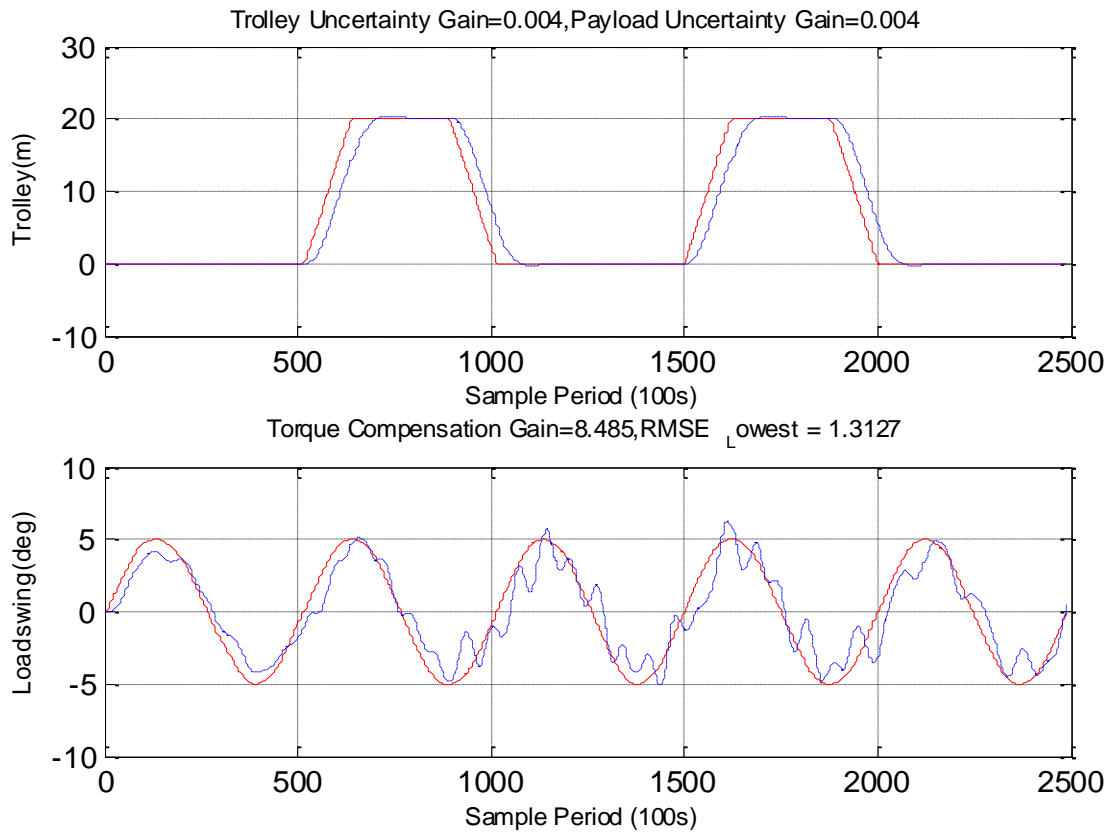


Figure 6.15 Nonlinear Trolley-Loadswing result for Semi-Hexagonal Reference 20-m

	(m)	Trolley Uncertainty Gain	Payload Uncertainty Gain	Torque Compensation Actuator Gain	Swing Lowest RMSE
Trolley Square Reference	1-m	0.004	0.004	0.5	1.9626
	20-m	0.004	0.004	4	15.642
	20-m	0.0008	0.004	7.8	1.588
Trolley Semi Hex Reference	1-m	0.004	0.004	0.2	1.2844
	20-m	0.004	0.004	8.485	1.3127
	20-m	0.0008	0.004	7.8	1.078

Table 6.2 Comparison of swing RMSEs for both Square-Reference and Semi-Hexagonal Reference inputs cases

6.9 Sudden Trolley Velocity Change and RTCMC Response

In real time operation, trolley translational position and tower angular rotation are the main trajectory concerns. The crane operator needs to control the joy-stick to carry the payload based-on trolley position and tower rotation trajectories. Therefore, this research initially set reference trolley position and the payload swing reference

constraints. The developed LQR-DRO control with actuator compensation will then perform the tracking process to achieve desire trolley position trajectory while keeping the payload swing within the reference constraints (5 to -5 degree). Even though the trolley velocity occurred sudden changes during the nonlinear RTCMC operations, trolley position control with payload swing suppression remains unaffected, Fig. 6.16. It is therefore proven that, the developed controller design is robust and reliable for the real time application.

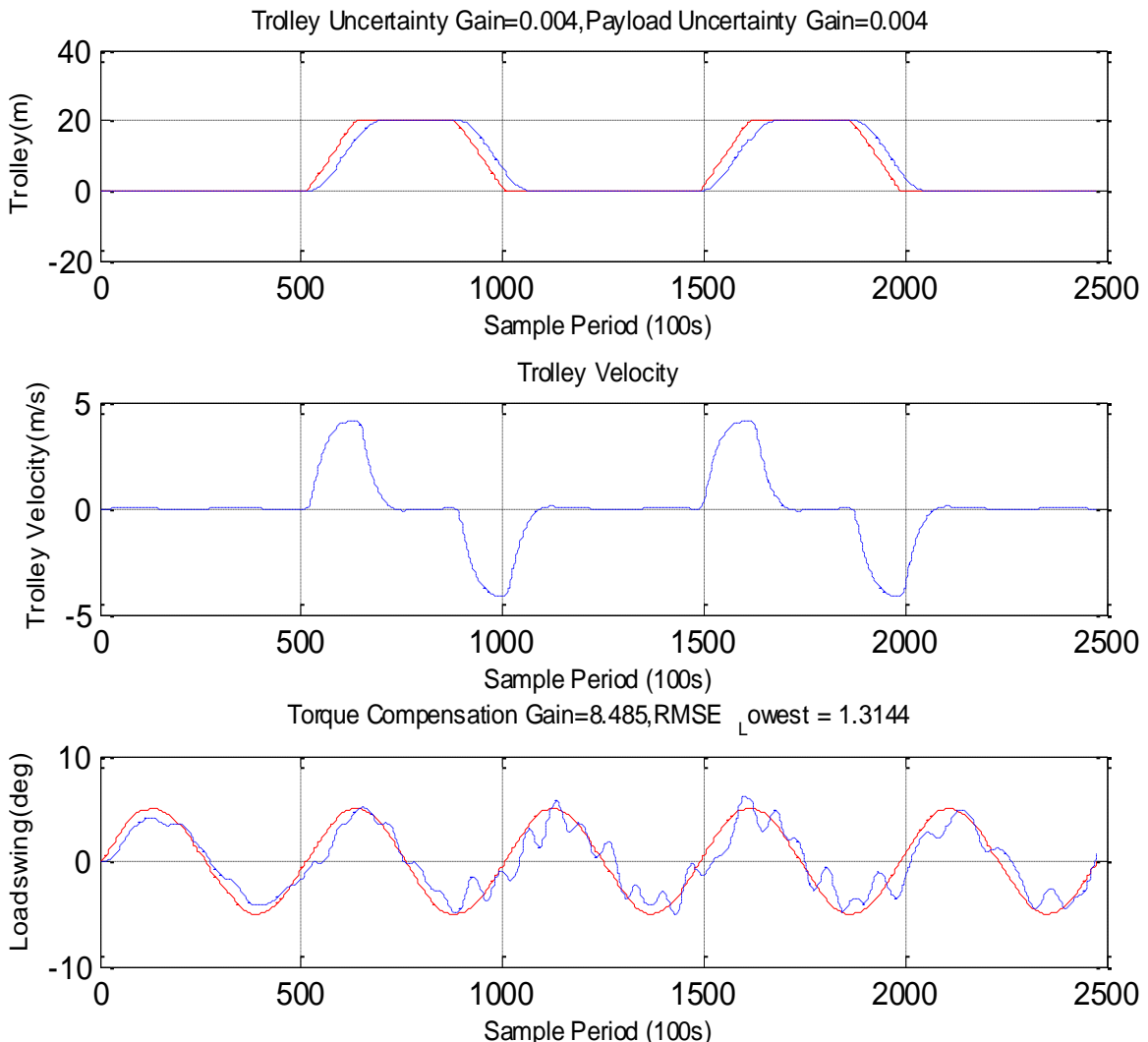


Figure 6.16 Sudden trolley velocity change and Response of Nonlinear RTCMC

6.10 Conclusion

This paper discussed in twofold, one: tower crane linear model controls and, two: nonlinear model control. Firstly, 3D Tower Crane SimMechanics-Visualized model and its optimized the best fit linear models from recent work were referred. Secondly, linear controller developments of LQR-DRO, LQR-Estimator-Integral (LEIC), and LEIC-

Antiwindup designs were discussed. Considering the disturbance in the system, Luenberger-based LQR-Disturbance Rejection Observer was introduced. LQR-Estimator-Integral Control which consists of error-space approach and full-order estimator is further discussed. LEIC is then reconstructed by adding antiwindup and saturation. Linear model derived from Nonlinear Autoregressive exogenous (NARX) has then been applied in LEIC-Antiwindup control.

Finally, LQR-DRO controller is considered suitable for nonlinear crane model as it is proven to be robust in the case of linear model control. Overall research covers; nonlinear SimMechanics-visualized model based on actual crane, applied wind disturbance and analysed vibration impact on the crane, optimized the best fit linearized model based on improved version of linear least square approach, then all the aspects of linear and nonlinear model controls discussed in this paper.

Having the complete package of such works, it is then named as Robotic Tower Crane Modeling Control (RTCMC). To operate safe and fast trolley-payload nonlinear system in such a three-dimensional working environment, it needs perfect modeling, correct choice of joints-sensor-actuators, feedback forces and torques, and on top of that having the best robust tracking control is essential. This RTCMC nonlinear design representing the real crane Morrow has made a great initiative in the fields of cranes industries and global cranes research at large. As this nonlinear model control has proven to be practical, this research future aim is to test the controller on large standing tall operating crane on site.

Chapter 7

Thesis Conclusion and Future work

7.1 Thesis Conclusion

Cranes are an integral part of our society. Nonlinear Robotic Tower Crane Model with LQR-DRO Control development has already been shown the improvement of the overall operating efficiency and safety of the cranes. The inclusive goal of this thesis contribution achieved in five areas:

7.1.1 Tower Crane Modeling

The modeling of tower crane is essential to develop practical controller. This part presents in threefold:

- **Mathematical Model:** Initial consideration of the crane modeling was to make mathematical model for control purpose. Two-dimensional overhead free-body diagram and 3-dimensional tower crane free-body diagram were designed. And then, their mathematical models were developed.
- **2D Overhead Crane SimMechanics model:** SimMechanics-Visualization tool from Matlab software was considered the suitable platform to build 2D overhead crane model. Since the model is developed based-on dynamics and kinematic of physical modeling framework, it is not only easy to visualize the crane operation but also analyze trolley motion and payload swing behaviors.
- **3D Tower Crane SimMechanics model:** After successfully developed 2D overhead crane, model optimization, and full-state feedback LQR control, this research focus is on 3D tower crane model. As this research very aim is to have practical model rather mathematical sketch or lab-scale prototype, Liebherr-71EC Morrow actual crane specifications have been considered in building this 3D tower crane model. The crane operations include: trolley translation with attached payload, tower rotation, and payload hoist up/down motion. The payload swing behavior, trolley translational motion, tower rotation, and crane's

vibration can easily be viewed and analyzed. It is a great milestone for the crane researchers around the globe who mostly rely on mathematical or lab-scale prototype models. Based-on this developed model, other types of cranes such as: shipyard gantry crane and mobile crane can be designed in future.

7.1.2 Linearization and Optimization: The part discussed in twofold:

- **Linear Least Square (LLS):** Existing linear least square system identification approach was applied to define linearized trolley and payload models from 3D tower crane.
- **Improved LLS for optimization:** Though the existing LLS model produced linearized models in the combination of (Denominators:2,3,4,... and Numerators:2,3,4,...), those predicted models were not perfect fit. This research then developed an algorithm which combine (7 past outputs and 7 past inputs dataset) and pick the random columns in generating each model. The best fit model with lowest RMSE is then considered after Root Mean Square Errors checking.

7.1.3 Vibration Impact Analysis

Large tall operating tower crane shoulders counterweight in one side and payload-attached trolley on the other side. Standing on its only hub support while payload-attached trolley runs or tower rotation situations, would certainly cause vibration. Moreover, variable trolley speeds, different weight of payloads, and load lengths changes make Hugh impact on the crane operational vibration which cannot be easily identified by human naked eyes. Therefore, this research investigated the vibration impact in five categories.

- **Jib Tower Mathematical Moment Calculation:** 2D free-body diagram in which the crane measurements and loads are in accordance with Libherr-71EC crane. Then, crane equilibrium was established to choose required counterweight. Jib moment calculations are done by gradually increasing the payload (from 1000Kg to 3000Kg) and changing trolley positions (from 0-m to the end of jib 24-m), jib moment. Analysis proved that there are jib-hub vibrations and significantly large payload oscillation.

Chapter 7: Thesis Conclusion and Future Work

- **3D Simmechancis rigid-structure model simulation:** This rigid-structure crane model has hub-counterweight-jib in rigid forms which uses the same mass and measurements according to Liebherr-71EC. Having tested using different combinations of trolley-payload, the simulation results proved that neither this rigid model should be used for control purpose nor the real crane should be built in rigid structure due to higher vibration and longer unsettled payload swing.
- **3D Simmechancis crane model tower rotation:** A number of simulations on ideal tower rotation were tested considering no wind disturbance effect on the crane. In all cases of different driving power (from 0W to 6300W) and payload (from 0Kg to maximum applicable load 3000Kg), Jib tip and Hub top have very less vibrations while the payload swings vary within (-4° to 4°) which does not seem to make impact on the load swing. Since the simulations are in the context of no wind disturbance consideration, it is impractical in nature.
- **Wind Disturbance Model development:** To prove the crane vibration, wind disturbance model which consists of Wind-gust Force and Wind-static Force is the developed based-on Gawronski approach. The velocities of wind-gust and wind-static are obtained from Sydney weather report in generating the wind model. Different amount of wind force and wind surface area have been applied in the simulations to view the vibration impact.
- **3D Simmechancis tower crane model with Wind Disturbance:** Since the nature of wind disturbance pattern has varying low terrain roughness and sometimes high terrain time-to-time, this research applies a number of wind patterns on the crane model to verify its impact on payload swing. In both cases of trolley translation and tower rotation, the simulations proved that there are significant changes in jib-hub vibrations and payload swing. Based-on the worst case simulation scenarios, this research proves that, "the stronger wind with larger wind surface area strikes, the higher jip tip/hub top vibrations and the higher load swing would be" and it can even lead to the crane collapse.

7.1.4 Controllers for Linear Models

- **LQR with Full-State Feedback:** After obtaining the best fit linearized models using linear least square approach, simple LQR control ($u = -Kx$) was initially introduced. Though the controller response is better, steady-state errors still appear and therefore reference input tracking has been implemented to achieve desired inputs. However, adding the reference input, ($u = -Kx + r$) to the system can lead to steady state errors. Full-state feedback controller with pre-compensation (\bar{N}) is then proposed. The simulation result shows robustness in proposed control scheme having rapid damping of load swing and achieving trolley trajectory.
- **LQR-Disturbance Rejection Observer (LQR-DRO):** Cranes work in highly structured environments where many forms of disturbances can add to the driving power actuator and measurement sensors as undesired source of power. As a result, all the plant states in trolley translation, payload swing, and tower rotation are disturbed. This research then implements a disturbance rejection observer as an adaptive alternative to full-state feedback action to increase the disturbance rejection of the feedback LQR controller. Luenberger-based Disturbance Rejection Observer was then introduced. The complete step consists of combining the control law LQR and DRO, which covers plant control canonical form, disturbance realisation, Extended State Observer design, ESO gains calculation, Q-R weighting matrices, and LQR Control.
- **LQR-Estimator-Integral Control (LEIC):** To deal with slow convergence as previous LQR-DRO presents long transients when tracking the true disturbance values, the error-space approach is introduced by a direct method of adding the integral of the system error as a state to the equations of motion. In this combination of control law with full-order estimator approach, the control law calculations are based on the estimated state variables rather than the actual state. The proposed LQR-Estimator-Integral Control produces better reference tracking according to the simulation results.
- **LQR-Estimator-Integral-Antiwindup (LEIC-Antiwindup):** LEIC control actuator in the system might have integrator windup phenomenon in practical application. Since the saturation lasts longer time triggering to produce large commands, the integrator output may become quite large. If this happens, the

integrator builds up a large value which results in large overshoots and errors. In order to overcome this problem, anti-windup is implemented in LEIC to turn off the integral action as soon as the actuator saturates. This section also introduced trolley-payload linear models development from Nonlinear Autoregressive exogenous (NARX) structure which provides a powerful representation modeling and prediction. This combination of new approach (LEIC-Antiwindup control on linear model from NARX) proved to have robust tracking on reference trajectory.

7.1.5 Nonlinear Robotic Tower Crane Modeling Control (RTCMC)

Overall of this research covers: nonlinear SimMechanics-visualized model based on actual crane, applied wind disturbance and analysed vibration impact on the crane, optimized the best fit linearized model based on improved version of linear least square approach, then all the aspects of linear and nonlinear model controls have been presented in section 5 and section 6. Having the whole complete package of such works, it is then named as Robotic Tower Crane Modeling Control (RTCMC). This nonlinear RTCMC discussed the following issues:

- **Feedback reaction forces and Torques investigation:** After a number of thorough investigations regarding the reaction forces and torques in this highly nonlinear trolley-payload motion environment, the most suitable configuration has been confirmed in section 6.3.
- **Joints-Sensors-Actuators Implementation:** The mechanisms of mounting a trolley on the rail-jib (tower) and the payload cable underneath may differ in crane to crane throughout the world. This research thoroughly attempted several ways (joints, sensors, and actuators) implementations in this Robotic Tower Crane Model. And based-on the simulations trials, this research proposed the most relevant joints-sensors-actuators as discussed in section 6.4.
- **Payload Cable structure Design:** Different types of payload cable-structures have been analysed in this research in swing minimization control process. Though LQR-DRO has proven to achieve robust control in section 5.1, it is found that the cable-structure design and torque compensator actuation plays

equal role to bring the payload swing under control. This exploration includes other cable structures such as having: extra T-link, Cross-link, and W-link in this existing two-cable structure. Interestingly, the simulation proved that adding extra T-link in existing two-cable structure could minimize the swing angle to nearly zero. However to avoid extra cost and complication, this research implements swing compensation actuators in existing two cable-structure.

- **Torque Compensation in Swing Minimization:** It is a very new approach in swing minimization. To date, tower crane operators has to act like compensation actuator by manually juggling trolley back-and-forth to minimize payload swing and there has been no practical approach of torque compensation available. To solve this mystery, this research implemented torque compensation actuators in the reaction joints between trolley and payload cables. Each actuator has two actions parts, one is torque compensation and the other is torque control. Torque compensation draws the driving power from trolley force control while the other one torque control is driven by LQR-DRO swing control. Details discussion can be seen in section 6.5.
- **LQR-Disturbance Rejection Observer (LQR-DRO):** Finally, LQR-DRO controller is considered suitable for this nonlinear RTCMC crane model as it is proven to be robust in the case of linear model control.

To operate safe and fast trolley-payload nonlinear system in such a three-dimensional working environment, it needs perfect modeling, correct choice of joints-sensor-actuators, feedback forces and torques, and on top of that having the best robust tracking control is essential. This RTCMC nonlinear design representing the real crane Morrow has made a great initiative in the fields of cranes industries and global cranes research at large.

7.2 Future Work

As this nonlinear model control has proven to be practical, this research future aim is to test the controller on large standing tall operating crane on site.

Bibliography

- [1] Health and Safety Executive (HSE), Tower Crane Incidents Worldwide, (Crown Press, 2010, pp. 1-62).
- [2] F. Ju, Y.S. Choo, F.S. Cui, Dynamic response of tower crane induced by the pendulum motion of the payload, International Journal of Solids and Structures, Volume 43, Issue 2, January 2006, Pages 376-389, ISSN 0020-7683, <http://dx.doi.org/10.1016/j.ijsolstr.2005.03.078>.
- [3] Lagerev, A., Lagerev, I., Milto, A., Tool for Preliminary Dynamics and Stress Analysis of Articulating Cranes, (2014) International Review on Modelling and Simulations (IREMOS), 7(4), pp. 644-652. doi:<http://dx.doi.org/10.15866/iremos.v7i4.2045>
- [4] Lagerev, A., Lagerev, I., Milto, A., Preliminary Dynamics and Stress Analysis of Articulating Non-Telescoping Boom Cranes Using Finite Element Method, (2015) International Review on Modelling and Simulations (IREMOS), 8(2),pp.223-226.doi:<http://dx.doi.org/10.15866/iremos.v8i2.5713>
- [5] Thein Moe Win, Tim Hesketh, and Ray Eaton. Construction Tower Crane SimMechanics-Visualized Modelling Tower Vibration Impact on Payload Swing Analysis and LQR Swing Control, *International Review on Modeling and Simulations (IREMOS)*, Volume 7 (Issue 6):979-994, December 2014.
- [6] Ilse C. F. Ipsen, Numerical Matrix Analysis (Philadelphia Society for Industrial and Applied Mathematics, 2009, pp. 43-76).
- [7] Thein Moe Win, Tim Hesketh, and Ray Eaton. SimMechanics Visualization of Experimental Model Overhead Crane, Its Linearization And Reference Tracking-LQR Control, *AIRCC International Journal of Chaos, Control, Modeling and Simulation (IJCCMS)*, Volume 2 (Issue 3):1-16, September 2013.
- [8] H. Sano, K. Sato, K Ohishi, and T. Miyazaki. Robust Design of Vibration Suppression Control System for Crane Using Say Angle Observer Considering Friction Disturbance, *Electrical Engineering Conference in Japan*, Vol. 184, No. 3, pp. 36–46, Nagoya, Japan, Jan. 2013.
- [9] G. Pelaez, J. Doval-Gandoy, N. Caparrini, and J.C.Garcia-Prada. The Time Delay filtering Method for cancelling vibration overhead transportation systems modeled as a physical pendulum, Spain, *Shock and Vibration Journal of IOS Press*. Volume 14 (Issue 1): 53-64, February. 2007.
- [10] Zhiqiang Gao, Active Disturbance Rejection Control: A Paradigm Shift in Feedback Control System Design Center for Advanced Control Technologies, *Proceeding of the 2006 American Control Conference, Minneapolis*, Volume 9 (Issue 2): 2399-2405, June 14-16, 2006
- [11] Manuel Olivares a, Pedro Albertos, Linear control of the flywheel inverted pendulum, ELSEVIER Journal of ISA Transactions, Volume 53 (Issue 1): 1396-1403, January 2014.
- [12] Lal B. Prasad, B. Tyagi, and Hari O. Gupta, Optimal Control of Nonlinear Inverted Pendulum System Using PID Controller and LQR: Performance Analysis Without and With Disturbance Input, *International Journal of Automation and Computing*, Volume 11 (Issue 6): 661-670, December 2014.
- [13] Abdelhadi Elharfi, Feedback Controller Stabilizing Vibrations of a Flexible Cable Related to an Overhead Crane, Mathematical Problems in Engineering Research, *Hindawi*, Volume 1, 1-12, August 2010.
- [14] Martin Böck and Andreas Kugi, Real-time Nonlinear Model Predictive Path-Following Control of a Laboratory Tower Crane, *IEEE Transactions on the Control Systems Technology Journal*, Volume 22 (Issue 4): 1461-1473, July 2014.
- [15] Dongkyoung Chwa, Real Nonlinear Tracking Control of 3-D Overhead Cranes Against the Initial Swing Angle and the Variation of Payload Weight, *IEEE Transactions on the Control Systems Technology Journal*, Volume 17 (Issue 4): 876-883, July 2009.
- [16] Renuka V. S. & Abraham T Mathew. Precise Modelling of a Gantry Crane System Including Friction, 3D Angular Swing and Hoisting Cable Flexibility, *International Journal on Theoretical and Applied Research in Mechanical Engineering (IJTARME)* ,Volume 2 (Issue-1):2319-3182, December 2013

- [17] Naif B. Almutairi and Mohamed Zribi. Sliding Mode Control of a Three-dimensional Overhead Crane, *Journal of Vibration and Control*, Volume 15 (Issue-11):1679-1730, July 2009,<http://jvc.sagepub.com/content/15/11/1679>
- [18] H.M. Omar, A.H. Nayfeh. Anti-swing control of gantry and tower cranes using fuzzy and time-delayed feedback with friction compensation, *Shock and Vibration Journal of Hindawi*, Volume 12 (Issue 2): 73-89, March 2005.
- [19] Quanser (2010). "3 Degrees of Freedom Crane User Manual", Quanser Ltd. (Quanser User Manual)
- [20] Inteco (2010). "Tower Crane Control User Manual", Inteco Ltd. (Inteco User Manual, Version 1.4.)
- [21] Ismail G, Serpil K, Finite Element Analysis of the Tower Crane, International Research/Expert Conference, pp. 561-561, Mediterranean Cruise, September 2010.
- [22] Getting Started with SimMechanics User Guide
<http://au.mathworks.com/help/physmod/sm/gs/product-description.html> (Accessed 15 February 2012).
- [23] Sahan S. Hiniduma Udugama Gamage and Patrick R. Palmer. Hybrid System Modeling, simulation and visualization; A crane system, Geo-Spatial and Temporal Image and Data Exploitation III Proceedings of (SPIE), Volume 5097 (Issue 3):1-10, July 2003. University of Cambridge, UK.
- [24] Raul G. Longoria. Modeling of Mechanical System for Mechatronics Applications (CRC Press 2002, chap. 9).
- [25] Schlotter Michael. Multi Body System Simulation with SimMechanics, *Dynamic Seminar*. pp. 1-23, May 2003.
- [26] Viliam Fedák, František Ďurovský and Robert Üveges. Analysis of Robotic System Motion in SimMechanics and MATLAB GUI Environment, INTECH Open Science Journal of MATLAB Applications for the Practical Engineer, Volume 1 (Chapter 20):565-581, August 2014.
- [27] M. Al-Hussein, M. A. Niaz, H Yu, H Kim. Integrating 3D visualization and simulation for tower crane operations on construction sites, *ELSEVIER Journal of Automation in Construction*, Volume 15 (Issue 1):554-561, January 2006.
- [28] Liebherr 71 EC Tower Crane datasheet, Morrow Equipment, USA, www.morrow.com. (MORROW, 2009, pp. 1-6)
- [29] Ho-Hoon Lee. Modeling and Control of a Three-Dimensional Overhead Crane, *Journal of Dynamic Systems, Measurement, and Control*, Volume 120 (Issue 1):471-476, December 1998
- [30] Sien K. Shyang (2006). "Command shaping control of a crane system". A thesis submitted in fulfilment of the Master of Engineering. Universiti Teknologi Malaysia
- [31] Vaughan, J., W. Singhose. "Initial experiments on the control of a mobile tower crane". *ASME International Mechanical Engineering Congress and Exposition*, IMECE 2007, November 11, 2007 - November 15, 2007, Seattle, WA, United states, American Society of Mechanical Engineers.
- [32] Juraj Vörös*, Ján Mikleš, Ľuboš Čirka. Parameter Estimation of Nonlinear Systems, *Acta Chimica Slovaca Journl*, Vol. 1, No. 1, 2008, 309 – 320
- [33] Hesketh Timothy. Real time Computing & Control. ELEC9403 Linear Systems - Modelling - Revision Lecture Notes, March 2010.
- [34] C. Alex Simpkins. Real time Computing & Control. Linear and Nonlinear Least Squares Regression, October 25, 2006
- [35] W. Gawronski. Wind Disturbance Models, Modeling and Control of Antennas and Telescopes (Springer, 2008, pp. 51-70)
- [36] Avila, J. J. R., R. Alcantara-Ramirez, et al. (2008). "Design of a self-balancing tower crane". *Circuits, Systems, Signal, & Communications*. 2nd WSEAS International Conference on Circuits, Systems, Signal and Telecommunications (CISST'08), Athens, Greece, WSEAS.

Bibliography for Robotic Tower Crane Modelling Control (RTCMC)

- [37] Lawrence, J., W. Singhose, et al. (2006). "Closure to "discussion of 'friction-compensating command shaping for vibration reduction'" (2006, ASME J. Vib. Acoust., 128, p. 540)." *Journal of Vibration and Acoustics, Transactions of the ASME* 128(Compendex): 541-541.
- [38] Yu, Y., J. Ou, et al. (2008). "Wireless inclinometer acquisition system for reducing swing movement control module experiment of hook model". Sensors and Smart Structures Technologies for Civil, Mechanical, and Aerospace Systems 2008, San Diego, CA, United states
- [39] Trabia, M. B., J. M. Renno, et al. (2008). "Generalized design of an anti-swing fuzzy logic controller for an overhead crane with hoist." *JVC/Journal of Vibration and Control* 14(3): 319-346.
- [40] Baicu, Cathalin. F., C. D. Rahn, et al. (1998). "Backstepping boundary control of flexible-link electrically driven gantry robots". *IEEE/ASME Transactions on Mechatronics* 3: 60-66.
- [41] Uchiyama, N. (2009). "Robust control for overhead cranes by partial state feedback." Proceedings of the Institution of Mechanical Engineers. Part I: *Journal of Systems and Control Engineering* 223(4): 575-580.
- [42] Neupert, J., E. Arnold, et al. (2010). "Tracking and anti-sway control for boom cranes." *Control Engineering Practice* Chapter 18: 31-44.
- [43] Park, Mun.-Soo., D. Chwa, et al. (2008). "Antisway tracking control of overhead cranes with system uncertainty and actuator nonlinearity using an adaptive fuzzy sliding-mode control." *IEEE Transactions on Industrial Electronics* 55(11): 3972-3984.
- [44] K. Nakano, K. Ohishi, H. Kinjo, and T. Yamamoto. Vibration control of load for rotary crane system using neural network with GA-based training. *International Conference on Artificial Life and Robotics (ISAROB), Vol. 3, pp.98-101, Oita, Japan, February 2008*
- [45] Ailane Abdellah, Aitelmahjoub Abdelhafid, Rachik Mostafa, Combining Sliding Mode and Linear Quadratic Regulator to Control the Inverted Pendulum, *International Review on Automatic Control (IREACO), Volume 6 (Issue 1): 69-76, February 2013*
- [46] Chen, W.-T., Q. Wu, et al. (2008). "Actuator fault diagnosis using High-Order Sliding Mode Differentiator (HOSMD) and its application to." *IFAC Proceedings Volumes (IFAC-PapersOnline)* 17(1).
- [47] Garrido, S., M. Abderrahim, et al. (2008). "Anti-swinging input shaping control of an automatic construction crane." *IEEE Transactions on Automation Science and Engineering* 5(Copyright 2008, The Institution of Engineering and Technology): 549-557.
- [48] Liu, G. and I. Mareels (2008). "Advantages of smooth trajectory tracking as crane anti-swing schemes". 2008, *IEEE International Conference on Robotics and Biomimetics*, ROBIO 2008, February 21, 2009 - February 26, 2009, Bangkok, Thailand, IEEE Computer Society.
- [49] Chwa, D. (2009). "Nonlinear tracking control of 3-D overhead cranes against the initial swing angle and the variation of payload weight." *IEEE Transactions on Control Systems Technology* 17(4): 876-883.
- [50] Su, S. W., H. Nguyen, et al. (2009). "Model predictive control of gantry crane with input nonlinearity compensation." *Proceedings of World Academy of Science, Engineering and Technology* 38: 312-316.
- [51] Kim, J.-Y., D.-H. Kim, et al. (2007). On-line minimum-time trajectory planning for industrial manipulators. *International Conference on Control, Automation and Systems*, ICCAS 2007, October 17, 2007 - October 20, 2007, Seoul, Korea, Republic of, Inst. of Elec. and Elec. Eng. Computer Society.
- [52] Giam, T. S., K. K. Tan, et al. (2007). "Precision coordinated control of multi-axis gantry stages." *International Standard for Automation (ISA) Transactions* 46(3): 399-409.
- [53] Chen Chih Peng, K. and W. Singhose (2009). "Crane control using machine vision and wand following". 2009 *IEEE International Conference on Mechatronics*, Piscataway, NJ, USA, IEEE
- [54] Lee, U.-K., K.-I. Kang, et al. (2006). "Improving tower crane productivity using wireless technology." *Computer-Aided Civil and Infrastructure Engineering* 21(Compendex): 594-604.
- [55] Donghyun, Kim. and R. B. Langley (2003). "On ultrahigh-precision GPS positioning and navigation." *Navigation. Journal of the Institute of Navigation* 50, IEE: 103-116.

Bibliography for Robotic Tower Crane Modelling Control (RTCMC)

- [56] Shebel Asad, Maazouz Salahat, Design of fuzzy PD-controlled overhead crane system with anti-swing compensation, *Journal of Engineering and Computer Innovation*, Vol.2(3), pp. 51-58 , March 2011
- [57] Lennart Ljung and Qinghua Zhang, An integrated System Identification tool- box for linear and non-linear models, *IFAC Symposium on System Identification*, Vol. 1, No. 3, pp. 1–9, Newcastle, Australia, June 2007
- [58] Lennart Ljung, *System Identification* , Theory for the User, (Prentice Hall, 1999, 2nd Edition, Chapter 17)
- [59] Lennart Ljung and Qinghua Zhang, System Identification Toolbox 7 User's Guide MATLAB SIMULINK, (The MathWorks USA, 2008)
- [60] Bei Na Wei, (2008). "An Innovative Approach to Overhead Crane Control". The University of New, South Wales, Sydney, Australia.
- [61] Marcel Dekker, Linear Quadratic Regulator, (Prentice Hall, 2003, Chapter 12)
- [62] Oishi Meeko. (2012). "State Space Reference Tracking and other control problems" (Lecture Notes:EECE360). Electrical and Computer Engineering, The University of British Columbia.
- [63] G. F. Franklin and J.D. Powell, Feedback Control of Dynamics Systems, (Prentice Hall, 2002, Chapter 7: State-Space Design, Chapter 9: Control System Design)
- [64] Liebherr 71 EC Tower Crane datasheet, Morrow Equipment, USA, www.morrow.com. (MORROW, 2009, pp. 1-6)
- [65] Mechanical Engineering, Carlos III University, Transportation and Crane, Madrid, Spain, 2008. <http://www.euni.de/tools/jobpopup.php?lang=en&option=showJobs&jobid=137260&jobtyp=5&jtyp=0&university=Universidad+Carlos+III+de+Madrid&country=ES&sid=5093&name=Course%3A+Transport+Engineering>.
- [66] Sydney Weather Office, WeatherZone. <http://www.weatherzone.com.au/nsw/sydney/Sydney>
- [67] Martin J. Corless and Arthur E. Frazho, *Linear Systems and Control* (CRC Press, 2003, chap. 12).
- [68] J.Han, Active Disturbance Rejection Control, *IEEE Transactions on Industrial Electronics*, Volume 56 (Issue 3), 900-906, August 2006
- [69] Magdi S. Mahmoud and Yuanqing Xia, Applied Control System Design, Chapter 7: (7.8: Integral Control and Robust Tracking) Springer, 2012, pg: 440-446
- [70] Richard M. Murray, Optimization-Based Control, Control and Dynamical Systems, (California Institute of Technology Press, 2010, Chapter 5: Kalman Filtering).
- [71] G. F. Franklin and J.D. Powell, Feedback Control of Dynamics Systems, (Prentice Hall, 1991, Chapter 3: Basic Principles of Feedback.
- [72] Harris, T.J. and Yu, W, Controller assessment for a class of nonlinear systems, *ELSEVIER Journal of Process Control*, Volume 17 (Issue 7): 607-619, August 2007.
- [73] K. J. Astrom and P. Eykhoff , System Identification-Survey, *Automatica Journal*, Volume 7 (Issue 1): pp. 123-162, January 1971
- [74] Zulkeflee, S.A. & Aziz, N., Nonlinear Autoregressive with Exogenous Inputs Based Model Predictive Control for Batch Citronellyl Laurate Esterification Reactor, *INTECHOPEN Journal*, Volume 1 (Issue 13): 268-290, June. 2011.
- [75] Heikki Koivo , Adaptive Neuro-Fuzzy Inference System ,(ANFIS, 2000, Japan)
- [76] Ivan Taufer and Oldrich Drabek Identification of nonlinear systems based on mathematical – physical analysis and least square method, *Acta Montanistica Slovaca Conference*, Volume 8 (Issue 4): 188-190, Nov 2003

Bibliography for Robotic Tower Crane Modelling Control (RTCMC)

- [77] Alwi, H.; Edwards, C; Pin Tan C. Fault Detection and Fault-Tolerant Control Using Sliding Modes, (Springer, 20011, Chapter 2: Fault Tolerant Control and Fault Detection and Isolation).
- [78] Abdel-Rahman, E.M., Nayfeh, A.H., Masoud, Z.N , Dynamics and control of cranes: A review, *Journal of Vibration Control (JVC)*, Volume 9 (Issue 7): pp. 863-908, July 2003
- [79] Beznos, A.V., Grishin, A.A., Lensky, A.V., Okhotsimsky, D.E., Formal'sky, A.M , A flywheel use-based control for a pendulum with a fixed suspension point, *Journal of Computer and Systems Sciences International*, Volume 43 (Issue 1): pp. 22-33, January 2004
- [80] Aoustin, Y., Formal'sky, A, Simple anti-swing feedback control for a gantry crane, *Journal of Robotica*, Volume 21 (Issue 6): pp. 655-666, November 2003

Appendix A

Award (iTof 2015)

Certificate of Publication

(Commended Paper): Robotic Tower Crane Modeling and Control (RTCMC) with LQR-DRO and LQR-LEIC for Linear and Nonlinear Payload Swing Minimization,
International Review of Automatic Control (IREACO), Volume 9 (Issue 2):72-87, March 2016

Appreciation

Graduate Research Newsletter (June-2016 Issue)

Participations & Competitions

(iTof 2013)

(iTof 2014)

(iTof 2015)

(2016 Postgraduate Research Symposium, UNSW)



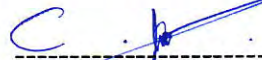
IEEE Student Branch
University of New South Wales

IEEE TECHNOLOGIES of THE FUTURE
iToF 2015

WINNER OF
CATEGORY 2: "MODELLING AND SIMULATIONS "

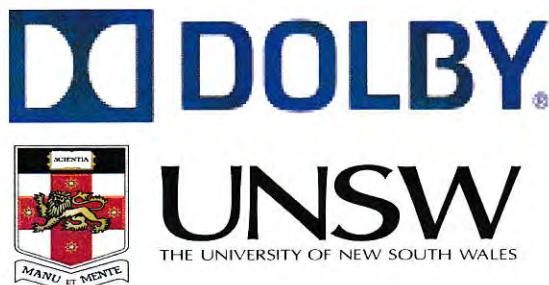
**Thein Moe Win, Timothy Hesketh and
Raymond Eaton**

**Simmechanics-Visualized Tower Crane
Modeling and Nonlinear Swing Minimization
Control using LQR-Disturbance Rejection**



Wael Y. Alghamdi

Chair of IEEE Student Branch 2015



Faculty of Engineering



Tower Crane Simmechanics-Visualized Modeling, Vibration Impact Analysis, and Linear/Nonlinear Trolley-Loadswing Control using LQR-DRO

Author: Thein Moe WIN, Supervisors: Timothy HESKETH & Raymond EATON

Background and Motivation

- Manual Operator Fatigue, Wind Disturbance, Vibration, Unstable Loadswing, Crane Incidents, Environmental damages, Uneasy access, Impractical Models-Controller



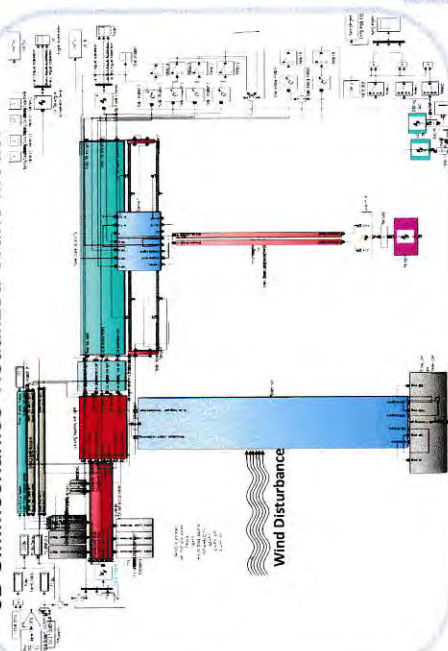
The Dreams

- Develop Practical Model-Controller, Minimize Load swing, Crane Operation under Control.
- Achieve Crane & Environmental Safety

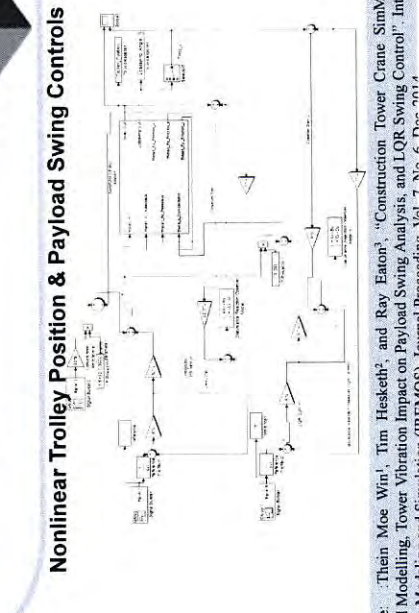
Research Development

- Build 3D Simmechanics-Visualized Crane Model
- Wind Disturbance Model, Vibration impact Analysis
- Linearize & optimize the best fit Mathematical model
- Linear Controllers:
 - LQR-Disturbance Rejection Observer,
 - Linear Estimator Integral Control (LEIC)
 - Nonlinear Controller: Reference Tracking LQR-DRO

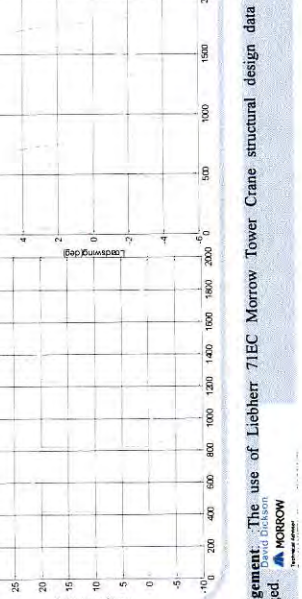
3D Simmechanics-Visualized Crane Model



Nonlinear Trolley Position & Payload Swing Controls



Nonlinear Trolley Position & Payload Swing Controls



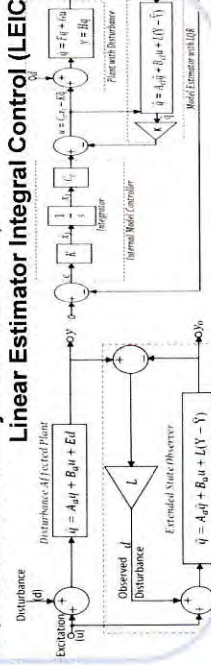
Reference: Thein Moe Win, Tim Hesketh, and Ray Eaton, "Construction Tower Crane SimMechanics-Visualized Modelling, Tower Vibration Impact on Payload Swing Analysis, and LQR Swing Control" International Conference on Advanced Computing and Communications, Vol. 1, pp. 7 - 11, 2015.

Keywords: SimMechanics-Visualized crane modeling, System Optimization, Vibration-Impact Analysis, System Optimization, DRO-Nonlinear swing minimization Control

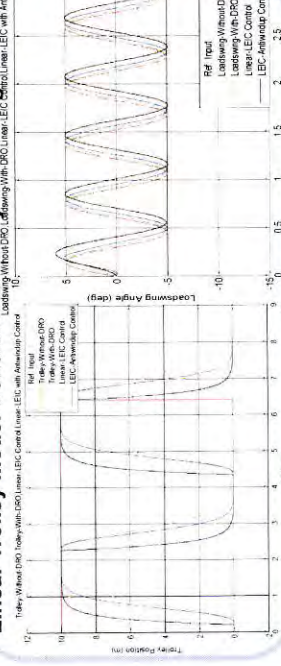
System Identification & Optimization by LS

$$\begin{aligned} X = [1 & 2 & 3 & 4 & 5 & 6 & 7 & 8 & 9 & 10 & 11 & 12 & 13 & 14] \\ \text{Columns} \\ [1 & 2 & 3 & 4 & 5 & 6] & [7 & 8 & 9 & 10] \\ [1 & 3 & 5 & 10] & [1 & 2 & 10 & 11] \\ [1 & 1] & [6 & 7 & 13 & 14] \\ Y_1 & Y_2 \\ \theta_1 = X_1^T * Y_1 & \theta_2 = X_2^T * Y_2 \\ \theta_{20} = X_{20}^T * Y_{20} & \theta_{21} = X_{21}^T * Y_{21} \\ rmse_{10} & rmse_{20} \\ rmse_{21} & rmse_{21} \end{aligned}$$

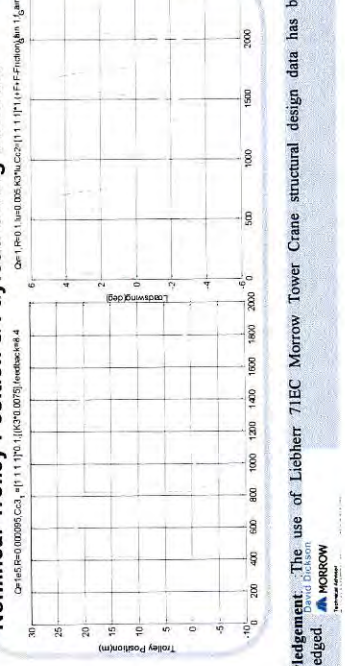
LQR-Disturbance Rejection Observer, Linear Estimator Integral Control (LEIC)



Linear Trolley Model Control Linear Payload Swing Control



Nonlinear Trolley Position & Payload Swing Controls



Acknowledgement: The use of Liebherr 71EC Morrow Tower Crane structural design data has been acknowledged.

Reference: David Bickson, "Construction Tower Crane SimMechanics-Visualized Modelling, Tower Vibration Impact on Payload Swing Analysis, and LQR Swing Control" International Conference on Advanced Computing and Communications, Vol. 1, pp. 7 - 11, 2015.

Certificate of publication

We certificate that the paper titled:

“Robotic Tower Crane Modeling and Control (RTCMC) with LQR-DRO and LQR-LEIC for Linear and Nonlinear Payload Swing Minimization”

Authors:

WIN, Thein Moe, Timothy Hesketh, Raymond Eaton

has been published as **commended paper**

in:

**Volume 9 (2), 2016, Pages 72-87
DOI: 10.15866/ireaco.v9i2.8431**



Engineer Win!

Congratulations to Thein Moe Win, a PhD candidate from the System & Control group (School of Electrical Engineering & Telecommunication) for receiving IEEE-iToF 2015 Best award in the "Modelling and Simulation" category. Under the supervision of Assoc. Prof. Timothy Hesketh and Dr. Raymond Eaton, his research has developed robotic tower crane model control (RTCMC) using Simmechanics-Visualization and proposed nonlinear payload swing minimization based-on LQR-DRO compensation actuator.

This Morrow tower crane based-RTCMC has aimed to address the concerns of reference tracking, swing minimization, faster operation time, cost effectiveness, and environment safety. As RTCMC provides flexibility in analysing the crane performance, it has so much to offer for both crane industries and global crane research. This remarkable achievement has also earned "Commended Paper" status in IREACO Journal's March issue.



[3-5 June 2016](#)

Starting a conversation about your research with impact

Produce and practise a concise statement about your research that will engage listeners.

[15 June 2016](#)

Volunteer for InSPiRE Conference

We want you! We are looking for two volunteers to assist with various aspects of this conference. Volunteers will attend the conference free of charge in return for their service. For more information and to register your interest, please use this [link](#).

[4 – 6 July 2016](#)



Postgraduate Research Symposium

26-29 Sep, 2016

Abstract Submission

Never Stand Still

Engineering

ME 102	DIGITAL FUTURE Chair: Yu Wang
19:00	DF01: Sustainability and adaptable/flexible infrastructure <i>Reza Taheraltar, Civil & Environmental Engineering</i>
19:20	DF02: Robotic tower crane modelling control (RTCMC) <i>Thein Moe WIN, Electrical Engineering & Telecommunications</i>
19:40	DF03: A dynamically configurable architecture for multi-GNSS receiver <i>Tuan Vinh Tran, Electrical Engineering & Telecommunications</i>
19:00	DF04: Detection and prediction of emotion changes from speech <i>Zhaocheng Huang, Electrical Engineering & Telecommunications</i>
19:00	DF05: Personalize air pollution exposure using wireless sensor network <i>Ke Hu, Electrical Engineering & Telecommunications</i>
19:00	DF06: Collision free navigation of multiple robots in search tasks <i>Xiaolian Yang, Electrical Engineering & Telecommunications</i>
15:00	

Thein Moe Win

Civil & Environmental Engineering

DF02 | Digital Future

Robotic Tower Crane Modelling Control (RTCMC)

Fast and accurate positioning and swing minimization of payloads in large standing tall tower crane operation are challenging as well as conflicting tasks. Juggling the trolley back-and-forth manually by crane operator to suppress payload swing can make time consuming and cause fatigue and subsequently cause the crane collapse as well risk the whole working environment. Motivated by Robotic Tower Crane Modelling Control (RTCMC), this work investigates solutions where swing suppression is critical for highly nonlinear trolley-tower-payload crane operation and therefore this work proposes a range of issues in implementing RTCMC. Firstly, SimMechanics-visualized RTC model development using real tower crane Morrow datasheet is considered. Secondly, wind disturbance model is designed based on Gawronski approach, and analyses the vibration impact on the payload swing. Thirdly, the best optimized mathematical linear model is derived using improved-linear least square algorithm. Fourthly, to actively reject the disturbances caused by undesired source of inputs or unknown dynamics, LQR-Disturbance Rejection Observer (DRO) Control with Luenberger-based Extended State Observer is introduced. This research further examines the combination of error space approach with estimator, from which it is argued that the LQR-Estimator-Integral Control (LEIC) for linear model is necessary to achieve robust tracking. Finally, in order to achieve robust tracking control of highly nonlinear trolley translation-payload swing working environment fuelled by wind disturbance, LQR-DRO control with torque compensator actuation is implemented on the interaction joints between trolley and payload cables. Proposed RTCMC demonstrated the ability to iteratively achieve a desired trolley translation-loadswing geometry. Evidence of improvements in LQR-DRO, LQR-LEIC, LEIC-Antiwindup, and LQR-DRO for nonlinear RTCMC are presented. Control solutions in this research focused on simplicity of implementation: general and straightforward reference-tracking control methods were preferred over Tower crane-tailored formulations. The benefit is that, the proposed RTCMC has potential applications to other types of crane operations and global crane research.



IEEE Student Branch

University of New South Wales

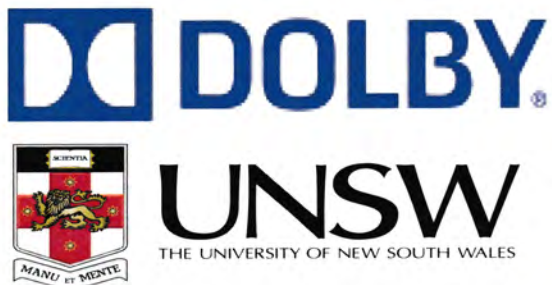
IEEE TECHNOLOGIES of THE FUTURE iTof 2015

CERTIFICATE of PARTICIPATION

Thein Moe Win, Timothy Hesketh and
Raymond Eaton
UNSW

Simmechanics-Visualized Tower Crane Modeling and
Nonlinear Swing Minimization Control using LQR-
Disturbance Rejection Observer

Wael Y. Alghamdi
Chair of IEEE Student Branch 2015



Faculty of Engineering





iToF
14



IEEE TECHNOLOGIES OF THE FUTURE COMPETITION & EXHIBITION

iToF 2014

Certificate of Participation

Thein Moe Win, Timothy Hesketh and Raymond Eaton

Construction Tower Crane Simmechanics- Visualized Modeling, Tower Vibration Impact on Payload Swing Analysis, and LQR Swing Control

Elias Aboutanios

Nov 5th, 2014

Dr. Elias Aboutanios

IEEE UNSW Student Branch

Proudly organized by the *IEEE UNSW Student Branch 2014*

Construction Tower Crane Simmechanics-Visualized Modeling, Tower Vibration Impact on Payload Swing Analysis, and LQR Swing Control

Author: Thein Moe WIN

Supervisors: Timothy HESKETH & Raymond EATON,

Research Theme: Automation and Adaptation (Poster: Physical Modeling & Simulation Category)

Background and Motivation

- Load Swing appears during Construction Tower Crane operation. Since, it is a standing tall-large crane, **wind disturbance strikes and causes more unstable load swing**. Swing is usually controlled manually and if it is out, then the crane collapse and environmental disaster. World statistic shows **23% of crane accidents are due to wind disturbance**.

2) Since it is **difficult to identify the vibration on the actual crane**, researchers make assumptions base on the lab-scale model.

3) So, most of the proposed controllers are **impractical and impossible to minimize the load swing** due to wind-affected vibration.

Aims

- To minimize the load swing, to identify the actual vibration, there is a **need to develop the crane model** which represents actual crane.
- Reliable simulation results are necessary to develop the **best suitable controller** in minimizing the load swing to reduce environmental disasters.



Fig. 1. World-wide tower crane accidents and its statistics

Research Methodology

- Build Simmechanics-Visualized 3D construction tower crane Model which complies "Kinematics , Dynamics, and Measurements" of actual MORROW Tower crane dataset.
- Analyze crane vibration impact on payload swing due to wind disturbance
- Linearize and optimize the best fit model ("Better fit model is essential for Better control")
- Full state-Feedback Reference Tracking LQR control to minimize the load swing and reduce environmental disasters

Algorithm



Fig 2: Research Methodology

2. Simmechanics Design

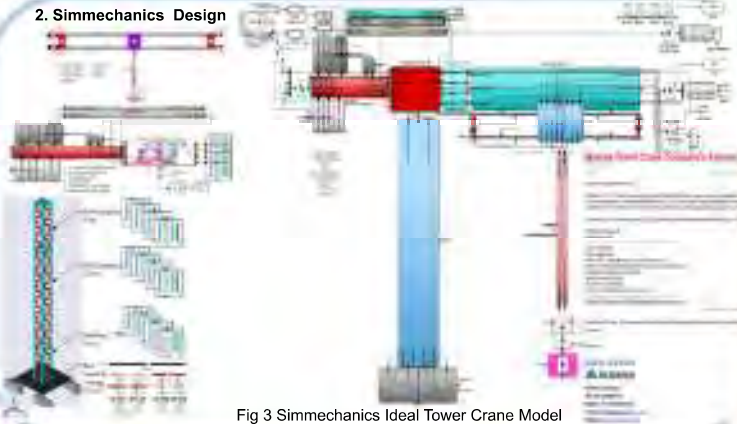


Fig 3 Simmechanics Ideal Tower Crane Model

2. Ideal Model Visualization

- To be exact, LIEBHERR 71 EC (Morrow Tower Crane) specification details have been used to design this simmechanic experimental model.

- Physical modeling blocks** represents actual components parameters such as; measurement, Mass, Moment of Inertia, Components axes, Centre of Gravity.

- Preliminary Simulation Tests** show, applying the pulling force (similar to manual joystick input) on the Trolley motion/Tower Rotation will have direct impact on load swing and Jib oscillation.

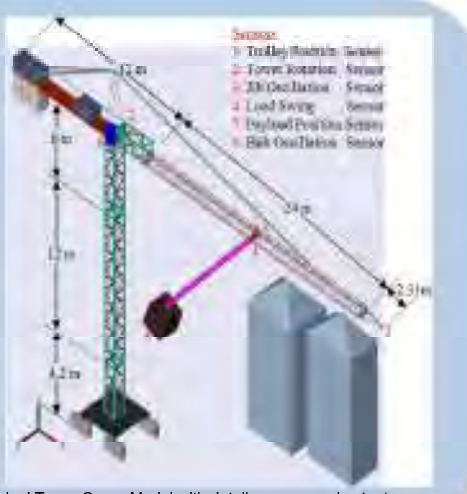


Fig 4: Visualized Ideal Tower Crane Model with detail sensors and actuators

Wind Disturbance & Jib Vibration Impact on Load Swing Wind Disturbance Model Development

-Wind disturbance can be very destructive for tower crane structure and it causes jib and hub vibrations problems as well as payload swing consequently:

$$\begin{aligned} F_{WS} &= P \cdot A \\ F_{WS} &= K_{df} v_{ws}^2, \quad K_{df} = \frac{F_{ws}}{v_{ws}^2} \\ F_{wg} &= 2K_{df} v_{ws} + \alpha v_{ws} v_{wg} \\ F_t &= F_{ws} + F_{wg} \end{aligned}$$

-Usually, wind strikes on standing tall tower crane with low terrain roughness and sometimes high terrain.

-To analyze jib vibration and its impact on load swing, the developed wind disturbance model has been added to ideal model during tower crane operation

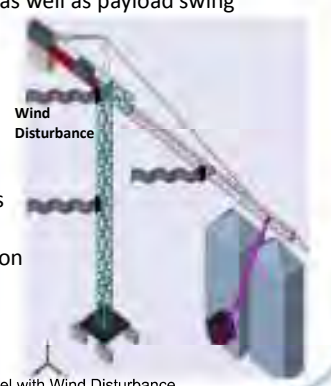


Fig 5: Ideal crane model with Wind Disturbance

Jib Vibration Impact on Load Swing due to Wind Disturbance

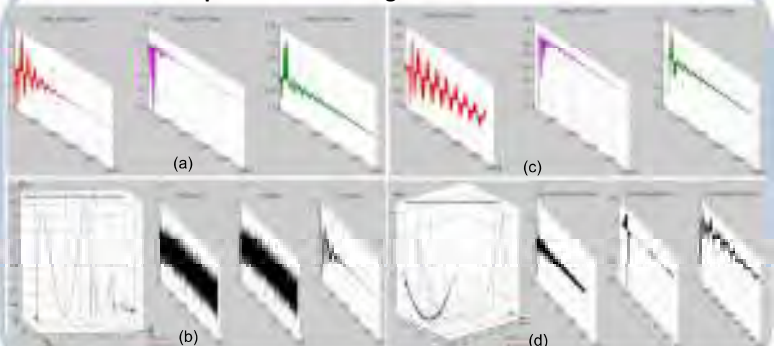


Fig 6 : Ideal model tower rotation without wind disturbance:
(a) Load swings;(b)Payload Trajectory and Jib vibrations Fig 6 : Ideal model tower rotation with wind disturbance:
(c) load swings,(d) Payload Trajectory and Jib vibrations

Linearized System Identification and Model Optimization

-Linear Least Square Approach (Modified to optimize for the better fit)

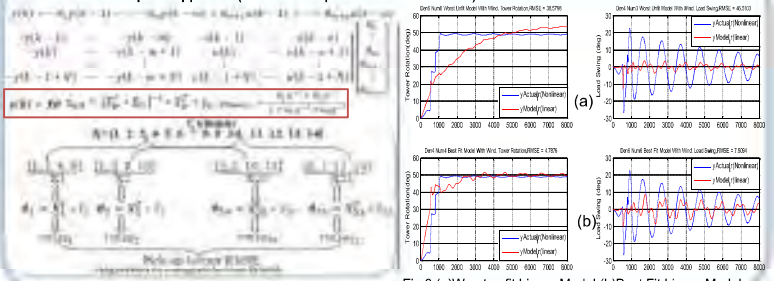


Fig 7: Modified Linear Least Square Algorithm
(a)Worst unfit Linear Model,(b)Best Fit Linear Model

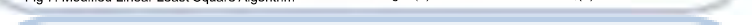


Fig 8:(a)Worst unfit Linear Model,(b)Best Fit Linear Model

LQR-Vibration Compensator Control for Load swing

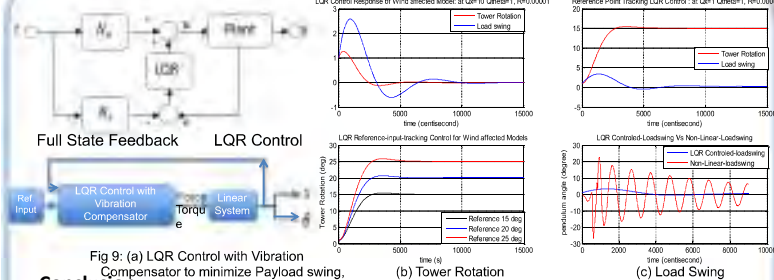


Fig 9: (a) LQR Control with Vibration Compensator to minimize Payload swing,

Conclusion

- Robust LQR-Vibration Compensator Control could minimize the load swing and achieve desired Inputs.
- Achieve the research aim "maximal load transit speed with minimal swing".
- Avoid Environmental Disaster, Has Productive operation, Less running cost.

Reference

- [1] Thein Moe Win¹, Tim Hesketh², and Ray Eaton³, "3D Simmechanics-Visualized Ideal Tower Crane Modeling and Analysis of Jib Vibration Impact on Payload Swing", IEEE Transactions on Mechatronics Journal (IJCCMS), Journal Proceeding, Aug 2014.

IEEE TECHNOLOGIES OF THE FUTURE
COMPETITION & EXHIBITION
iToF 2013

Certificate of Participation

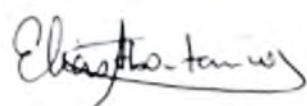
This is to certify that

Thein Moe Win

Has participated in the event

iToF 2013

at University of New South Wales



Dr Elias Aboutanios

IEEE Student Branch Counselor @ UNSW

6th November 2013

Proudly organized by the **IEEE UNSW Student Branch**

University of New South Wales

Experimental Model Tower Crane Using Simmechanics Visualization and Load Swing Control with Reference Tracking Compensation

Author: Thein Moe Win

Supervisors: Tim Hesketh & Ray Eaton,

Research Theme: Automation and Adaptation

Background and Motivation

Large and tall Tower cranes are widely used for the heavy loads transfer. Usually, load swing appears during back and forth load transfer, and therefore, skilled operators use manual joysticks and apply mental map to minimize the load swing.



Fig 1: Crane Incident

Human fatigue or manual joysticks lost control can make unstable load swing which eventually cause operational/environmental damages.

Safe and efficient Tower Crane operation requires maximal load transit speed with minimal swing. To achieve these two goals in every aspect of crane operation presents a real challenging control problem.

Since, conducting research on real operating crane in the field is usually hard and therefore, pre-existing tower crane control systems have appeared to be based on either mathematically derived models or lab-scaled models with several assumptions, which do not address issues of real crane's factors and are difficult to implement in practice.

Aims and Objectives

- To improve the mathematical model by introducing Simmechanics Visualized-3D Physical Model
- To develop reference tracking LQR control for the linearized model
- To develop practical Nonlinear Controller on 3D Physical Model

Research Methodology

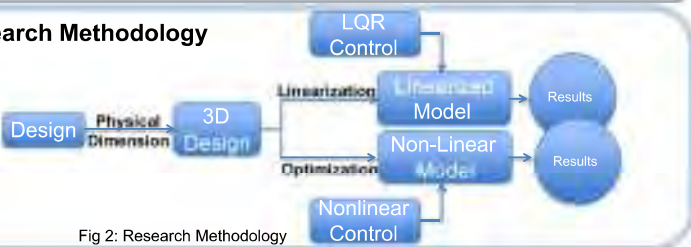
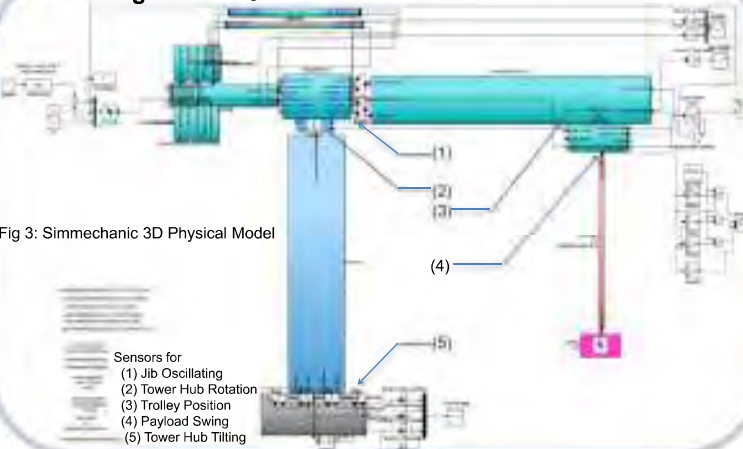


Fig 2: Research Methodology

3D Design 1. Modelling

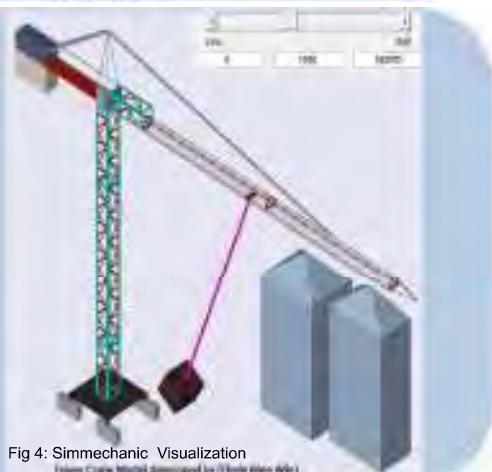


2. Simmechanics Visualization

❖ To be exact, LIEBHERR 71 EC (Morrow Tower Crane) specification details have been used to design this simmechanic experimental model.

❖ Physical modeling blocks represents actual components parameters such as; measurement, Mass, Moment of Inertia, Components axes, Centre of Gravity.

❖ Preliminary Simulation Tests show, applying the pulling force (similar to manual joystick input) on the Trolley motion/Tower Rotation will have direct impact on load swing and jib oscillation.



Linearized Modelling for Trolley Translation

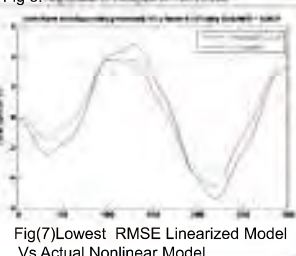
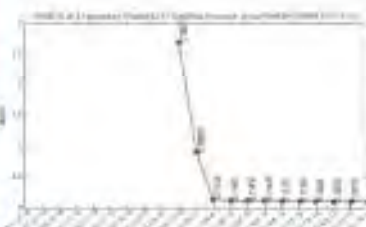
1. Modified Linear Least Square System Identification

The collected data set is divided into two parts, training and checking. Then, Least Square System Identification is applied to determine the number of parameters required for the system transfer function.

$$\begin{aligned}
 \text{Data} &= \frac{\text{Data}}{1 + \alpha_1 z^{-1} + \alpha_2 z^{-2} + \dots + \alpha_n z^{-n}} \\
 \text{Column 1} &= [1 \quad 2 \quad 8 \quad 9 \quad 10] \\
 \text{Column 2} &= [-\gamma(T) \quad -\gamma(\theta) \quad u(T) \quad u(\theta)] \\
 Y_1 &= \begin{bmatrix} 1 \\ -\gamma(T) \\ -\gamma(\theta) \\ u(T) \\ u(\theta) \end{bmatrix} \\
 X_{11} &= \begin{bmatrix} 1 & 1 & 1 & 1 & 1 \\ -\gamma(T) & -\gamma(T) & -\gamma(T) & -\gamma(T) & -\gamma(T) \\ u(T) & u(T) & u(T) & u(T) & u(T) \\ u(\theta) & u(\theta) & u(\theta) & u(\theta) & u(\theta) \end{bmatrix} \\
 \end{aligned}$$

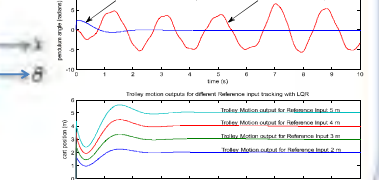
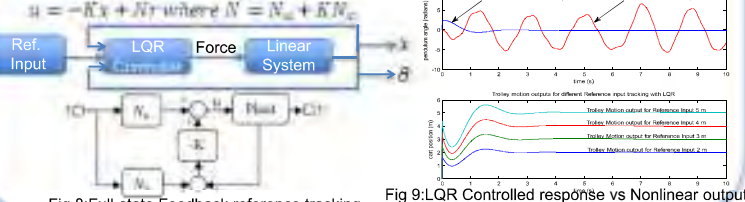
2. Root Mean Square Error Calculation

Root-mean-square error (RMSE) is used to measure the differences between estimated values by the developed model.



Reference Tracking Linear Quadratic Regulator (LQR) Control

- Linear quadratic regulation method is implemented for this overhead crane to determine the state-feedback control gain matrix K.
- Q and R weighting matrices** which will balance the relative importance of the control effort (u) and error (deviation from 0).
- Reference input tracking with Full-state feedback** has been implemented to achieve desired inputs and eliminate steady-state errors.



Simulations Analysis

Why Load Swing appears? A number of factors those can cause unstable load swing, such as;

- ✓ Imbalance between counterweight and (Tower jib + payload) produces moment of inertia on Tower Hub
- ✓ Jib's oscillation due to the wind disturbance
- ✓ High speed trolley translation
- ✓ High speed tower rotation
- ✓ Higher Friction in translational/rotational joints might cause load swing

Conclusion

3D Tower Crane physical model was developed based on Liebherr 71 EC Morrow Tower Crane, linearized Trolley Translation and applied Reference Tracking LQR Control on linear model. The simulation results show, robust LQR Controller could minimize the load swing and achieve desired reference trolley positions.

Simulations analysis show several contributing factors which cause unstable load swing and therefore Nonlinear Controller with compensators would be developed to suppress the disturbances and achieve this research aim "maximal load transit speed with minimal swing".

Future Work

- Optimize better parameter estimations of nonlinear system identification
- Apply compensator to overcome disturbance
- Develop Practical Nonlinear Controller



Reference

- [1] Thein Moe Win¹, Tim Hesketh², and Ray Eaton³, "Simmechanics Visualization of Experimental Model Overhead Crane, Its Linearization and Reference Tracking-LQR Control", International Journal of Chaos, Control, Modeling and Simulation (IJCCMS), Vol (2) No. (3). Sep 2013.

The University of New South Wales, Sydney, Australia.

<http://airccse.org/journal/ijccms/current2013.html>

Appendix B

“Robotic Tower Crane Modeling and Control (RTCMC)
with LQR-DRO and LQR-LEIC for Linear and
Nonlinear Payload Swing Minimization”

Robotic Tower Crane Modeling and Control (RTCMC) with LQR-DRO and LQR-LEIC for Linear and Nonlinear Payload Swing Minimization

Thein Moe Win, Timothy Hesketh, Raymond Eaton

Abstract – Fast and accurate positioning and swing minimization of payloads in large standing tall tower crane operation are challenging as well as conflicting tasks. Juggling the trolley back-and-forth manually by crane operator to suppress payload swing can make time consuming and cause fatigue and subsequently cause the crane collapse as well risk the whole working environment. Motivated by Robotic Tower Crane Modelling Control (RTCMC), this work investigates solutions where swing suppression is critical for highly nonlinear trolley-tower-payload crane operation and therefore this work proposes a range of issues in implementing RTCMC. Firstly, recent work of SimMechanics-visualized RTC model and its optimized mathematical linear model are briefly introduced for further controller designs. Secondly, to actively reject the disturbances caused by undesired source of inputs or unknown dynamics, LQR-Disturbance Rejection Observer (DRO) Control with Luenberger-based Extended State Observer is introduced. This research further examines the combination of error space approach with estimator, from which it is argued that the LQR-Estimator-Integral Control (LEIC) and LEIC-Antiwindup for linear model are necessary to achieve robust tracking. Finally, in order to achieve robust tracking control of highly nonlinear trolley translation-payload swing working environment fueled by wind disturbance, LQR-DRO control with torque compensator actuation is implemented on the interaction joints between trolley and payload cables. Proposed RTCMC demonstrated the ability to iteratively achieve desired trolley translation-loadswing geometry. Under this iterative method, all weighting Q-R matrices, Observer gains (L) matrix, and uncertainties gains have adapted to different input conditions until pre-specified trajectories of trolley-loadswing are achieved. Evidence of improvements in linear model controls using (LQR-DRO, LQR-LEIC, and LEIC-Antiwindup), and in nonlinear RTCMC using (LQR-DRO) are presented. Control solutions in this research focused on simplicity of implementation: general and straightforward reference-tracking control methods are preferred over Tower crane-tailored formulation. The benefit is that, the proposed RTCMC has potential applications to other types of crane operations and global crane research. Copyright © 2016 Praise Worthy Prize S.r.l. - All rights reserved.

Keywords: Robotic Tower Crane Modeling Control, Disturbance Rejection Observer, LQR-Estimator-Integral Control, Linear, Nonlinear

Nomenclature

RTC	Robotic Tower Crane
autoCAD	Computer-Aided-Design software
SimMechanics	Set of block libraries with mechanical modeling and simulation tools
LLS	Linear Least Square

I. Introduction

Large and tall Tower cranes are widely used for the heavy loads transfer. In each crane operation like; hoist up-down motion, trolley forward-backward motion, and flat-top rotation, the level of payload swing uncertainty eventually develops. To stabilize payload swing, skilled operators apply mental map and use manual joysticks to juggle the trolley back-and-forth so that the operation can be brought under control. However in busy working environments such as construction sites and shipyard docks, meeting the customers demand/deadline are

crucial. And therefore, employer concern is to complete the tasks in shorter time with low operational cost whereby operator concern is to perform the operation without environmental risk. Unfortunately, that workplace pressure might have caused operator's fatigue which may lead to operational failure. To ease the burden on operator while having safe and efficient tower crane operation, practical controller automation becomes necessary. Nevertheless, the major obstacle is, the researchers around the globe find it hard to on large standing tall live operating tower crane on site which forces them to rely on mathematically derived models or lab-scaled models with several assumptions. Since majority of those models do not represent real crane's factors, the credibility of

proposed swing minimization controllers to sort out challenging control problem is in question. This research initially indentifies the significant role of having the ideal model which represents actual crane followed by the consideration of suitable linear-nonlinear controller implementations to further improve safe and sound working environment.

A number of crane modeling strategies from a set of mathematical equations, lab-scale prototype, solid works, autoCAD, to finite elements approaches have been proposed in the past. F. Ju, as in [1], presented the tower crane model which was built on finite element approach and demonstrated the payload oscillation effect on the crane structure deformation due to pendulum-induced vibration. Several approaches on dynamics and stress analysis of articulating cranes also exist in the literature. From modeling point of view, crane's dynamics and structural analysis can be tackled by a set of algorithms; Recursive Newton-Euler Algorithm (RNEA), Composite Rigid Body Algorithm (CRBA), and finite element method to analyze structural members of a complex shape, as in [2]-[3] and references given therein.

Considering the real crane facts and visualization, this research recently developed Tower crane model based on SimMechanics-visualized modelling approach, as in [4], see Fig. 1. Simmechanics provides a multi-body simulation environment for 3-Dimensional (3D) mechanical system which contains joints, constraints, actuator elements, and sensors. Another reason using this approach was; it can deal with the equations of motion for the complete mechanical system and integrate the controller implementation.

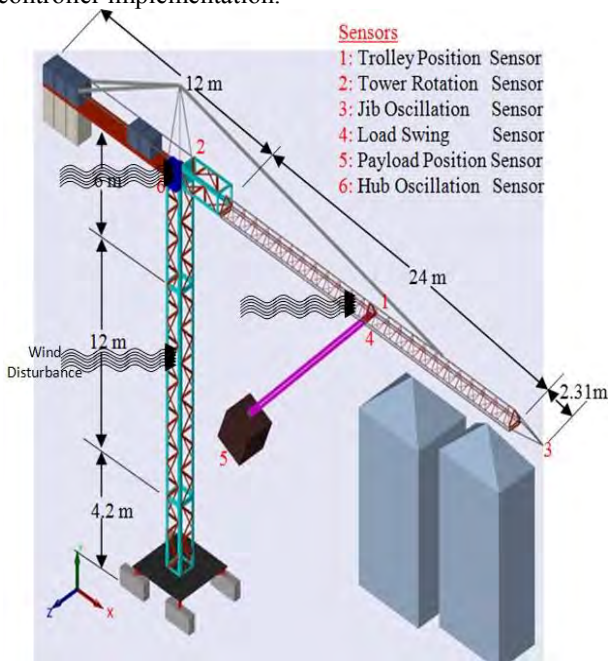


Fig. 1. Robotic Tower Crane (RTC) Model using Morrow crane data

In the case of construction tower crane load swing control, diverse field of swing minimization can be presented in many different ways. To date, the extensive researches have taken considerations on swing

uncertainties problem due to wind or frictional disturbances, vibrations, cable nonlinearities, and trolley-tower (jib) dynamical systems, etc.. Z. Gao, as in [5], discussed about the Active Disturbance Rejection Control which included stability analysis and the characteristics of new significance paradigm to reduce from complex nonlinear to the simple problem using active estimation and rejection. H. Sano, as in [6], emphasized on nonlinear friction disturbance of trolley and delay time from vision sensor response would deteriorate the control performance. Frictional force between trolley-rail was also considered as disturbance and time correction observer was further implemented to eliminate disturbance, as in [6]. Since the dynamics of a trolley-payload system is similar to inverted pendulum dynamical system, another important method of compensating measurement disturbances using PID (Proportional-Integral-Derivative) control was proposed to nonlinear flywheel inverted pendulum model, as in [7]. Furthermore, M. Olivares introduced full state feedback control with state estimator/observer to overcome an unstable open-loop pole and a zero at the origin, as in [7]. Likewise, Both PID-LQR and 2PID-LQR control techniques have been implemented on the nonlinear inverted pendulum-cart system with continuous disturbance input, as in [8]. The cause of flexible cable vibration is the major concern for unstable overhead crane operation and therefore, A. Elharfi came up with boundary feedback law implementation to bring the cable vibrations to the desired zero equilibrium, as in [9]. Some literatures proposed payload trajectory controls using model predictive control and feedback linearization methods. Model Predictive Control scheme based on direct method with path-following was introduced, as in [10]. D. Chwa, as in [11], proposed the feedback linearization control using swing angle and angular rate to eliminate the nonlinear characteristics of the system as well as achieve payload swing suppression. Regarding those unmeasured states such as; trolley and swing angular rate, numerical backward difference technique and low-pass filtering were also applied, as in [11].

In contrast to the approaches described, as in [1]-[2]-[3], this paper presents a practical solutions to the modeling and control of 3D construction tower crane where the trolley motion, tower rotation, and payload swing are all together in the modeling and control. First, recently developed 3D Simmechanics-Visualized crane model and its linearized model, as in [4]-[12], are briefly recalled. To reject disturbance, minimize payload swing, and achieve robust reference tracking, this paper further discussed the combination of LQR-Disturbance Rejection Observer (LQR-DRO), LQR-Estimator-Integral Control (LEIC), and LQR-Estimator-Integral-Antiwindup control (LEIC-Antiwindup).

The remainder of this paper is organized as follow. In section 2, LQR-Disturbance Rejection Observer controller is designed which includes disturbance rejection observer gain and extended state observer. In section 3, errors-space approach and full-order estimator are integrated to

form LQR-Estimator-Integral control. In section 4, the linear model derivation using Nonlinear Autoregressive exogenous (NARX) approach is introduced. Then, LEIC-Antiwindup with saturation is further analyzed to accomplish better robust control. In section 5, complete nonlinear robotic tower crane control with LQR-DRO controller implementation are designed. The comparison of those controllers performance is also discussed after each section. Finally in section 6, conclusion is drawn for this study.

II. LQR-Disturbance Rejection Observer Control

The majority of tower crane manipulators are designed and used for handling known loads under limited perturbations. Control methods for the crane manipulators have therefore focused mainly on modeling and control of the dynamics of the trolley-jib, tower-loadswing, rather than on counteracting external disturbances. In an industrial scenario, cranes work in highly structured environments where disturbances are minimized and tasks are repetitive. However, torque disturbances generate velocity and position errors. Likewise, load currents can also act as a disturbance to a power supply by pulling the output voltage away from the target. That is, an undesired source of power is added to the power converter output and fed to the plants (trolley translation with payload attached, tower rotation) the result is that the plant states are disturbed. Although feed-forward action is used to achieve high tracking performance in such crane manipulators, disturbance rejection usually relies on high-reduction gearing in the drive train and high-gain feedback, as in [3].

II.1. Disturbance Rejection

Disturbance rejection observer can estimate unknown dynamic and compensate to make control more robust and less dependent on the detailed mathematical model of the physical process, as in [5]. This research implements a disturbance rejection observer as an adaptive alternative to integral action to increase the disturbance rejection of the feedback LQR controller. Assuming that frictional and interaction forces between trolley and payload cable can be represented as varying disturbances which are then canceled by the control input once the disturbance observer has estimated the values in order to achieve desired trajectory. By considering controllable and observable system with uncertainty disturbance, the state representation can then be formed, as in [13]

$$\dot{x} = f(x, w, u, t); y = Cx \quad (1)$$

whereby f is the function vector of state variables, w is uncertainty disturbance, u is input control, y is the system output, C is the linear function, and t is time. Since the system is regarded as controllable, the state representation

is then transformed into canonical controllable form as follow.

II.2. Trolley Model in Control Canonical Form

There are special canonical forms of the state-variable equations where the algebra for finding the gains is simple. Once such canonical form useful in control law design is the control canonical form, consider the 4th-order Trolley Translation linear system derived from nonlinear model using linearized system identification in [4]-[12];

$$\begin{aligned} \frac{y}{u} &= \frac{(x, \dot{x}, \ddot{x}, \ddot{\ddot{x}})}{F} \\ &= \frac{-1.172e^{-7}s^4 - 4.761e^{-6}s^3 + 4.331e^{-6}s^2 + 0.002011s^1 + 0.01488}{s^4 + 54.86s^3 + 628s^2 + 586.2s^1 + 9.631} \\ \frac{x}{F} &= \frac{0.01563}{s^4 + 54.86s^3 + 19.63s^2 + 4.58s^1 + 0.301} \end{aligned}$$

$$p_{est} = [54.86; 19.63; 4.58; 0.301]$$

Let, $q_1 = x$, $q_2 = \dot{x}$, ... etc. the state space representation, as in (2), can be expressed by

$$\begin{aligned} \ddot{x} &= f(\ddot{x}, \dot{x}, x, t) + b_0u & (2) \\ \ddot{x} + a_1\ddot{x} + a_2\dot{x} + a_3\dot{x} + a_4x &= b_0u \\ q_1 &= x \\ q_2 &= \dot{q}_1 = \dot{x} \\ q_3 &= \dot{q}_2 = \ddot{x} \\ q_4 &= \dot{q}_3 = \ddot{\ddot{x}} \\ q_5 &= \dot{q}_4 = \ddot{\ddot{\ddot{x}}} \\ \dot{q} &= Aq + Bu \\ \dot{q}_4 + a_1q_4 + a_2q_3 + a_3q_2 + a_4q_1 &= b_0u \\ \dot{q}_4 = -a_1q_4 - a_2q_3 - a_3q_2 - a_4q_1 + b_0u \\ y &= b_1\ddot{x} + b_2\dot{x} + b_3\dot{x} + b_4x \\ y &= b_1q_4 + b_2q_3 + b_3\dot{x}q_2 + b_4q_1 \end{aligned}$$

All the feedback loops return to the point of the application of the input or the control variable, and hence the following form, see Fig. 2, is referred to as the control canonical form, as in [13].

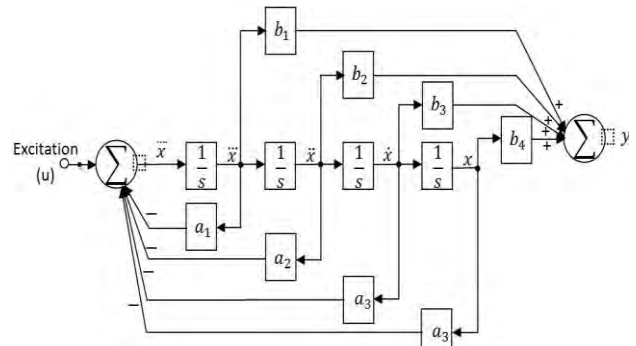


Fig. 2: Trolley Translation in Control Canonical Form. The blocks (a_1, a_2, a_3, a_4) are the coefficients of the states, and the blocks (b_1, b_2, b_3, b_4) are the coefficients of outputs.

The matrices describing the control canonical form in general are;

$$\begin{bmatrix} \ddot{x} \\ \ddot{\dot{x}} \\ \ddot{\ddot{x}} \\ \ddot{\ddot{\dot{x}}} \end{bmatrix} = \begin{bmatrix} -a_1 & -a_2 & -a_3 & -a_4 \\ 1 & 0 & 0 & 0 \\ 0 & 1 & 0 & 0 \\ 0 & 0 & 1 & 0 \end{bmatrix} \begin{bmatrix} \ddot{x} \\ \ddot{\dot{x}} \\ \ddot{\ddot{x}} \\ \ddot{\ddot{\dot{x}}} \end{bmatrix} + \begin{bmatrix} b_0 \\ 0 \\ 0 \\ 0 \end{bmatrix} u$$

$$\begin{bmatrix} \ddot{q}_4 \\ \ddot{q}_3 \\ \ddot{q}_2 \\ \ddot{q}_1 \end{bmatrix} = \begin{bmatrix} -a_1 & -a_2 & -a_3 & -a_4 \\ 1 & 0 & 0 & 0 \\ 0 & 1 & 0 & 0 \\ 0 & 0 & 1 & 0 \end{bmatrix} \begin{bmatrix} q_4 \\ q_3 \\ q_2 \\ q_1 \end{bmatrix} + \begin{bmatrix} b_0 \\ 0 \\ 0 \\ 0 \end{bmatrix} u,$$

$$y = [0 \ 0 \ 0 \ 1] \begin{bmatrix} q_4 \\ q_3 \\ q_2 \\ q_1 \end{bmatrix}$$

State space representation without Disturbance is

$$\begin{aligned} \dot{x} &= Ax + Bu \\ y &= Cp_{est} \end{aligned}$$

where the output (y) is a linear function (C) of the state variables, $p_{est}(q, u, t)$.

II.3. Disturbance Realisation

In order to implement DRO in the system, the system is initially required to convert to an augmented state space model that includes f , short for $f(\ddot{x}, \ddot{\dot{x}}, \ddot{\ddot{x}}, \ddot{\ddot{\dot{x}}}, w, u, t)$, as an additional state, as in [5]. In particular, the augmented state space form, as in (3), is

$$\begin{aligned} \dot{q} &= A_a q + B_a u + E d, \\ y_a &= C_a q_{est} \end{aligned} \quad (3)$$

where the disturbance, nonlinearities and uncertainties have been translated into the new state variable, d . To represent as the disturbance, consider $q_{n+1} = p_{est}(q, w, u, t)$, and new state variables (q_{est}) can then be defined as follow;

$$\begin{aligned} q_{1+1} &= q_2 = x \\ q_{2+1} &= q_3 = \dot{x} \\ q_{3+1} &= q_4 = \ddot{x} \\ q_{4+1} &= q_5 = \ddot{\dot{x}} \\ q_{5+1} &= q_6 = \ddot{\ddot{x}} \end{aligned}$$

By taking derivative of new state variables, Disturbance (d) is realized as, $d = \dot{p}$ which means;

$$\begin{aligned} q_2 &= \dot{x} \\ q_3 &= \ddot{x} \\ q_4 &= \ddot{\dot{x}} \\ q_5 &= \ddot{\ddot{x}} \\ q_6 &= \ddot{\ddot{\dot{x}}} \end{aligned}$$

The augmented State-space form with Disturbance is,

$$= \begin{bmatrix} -a_1 & -a_2 & -a_3 & -a_4 & 0 \\ 1 & 0 & 0 & 0 & 0 \\ 0 & 1 & 0 & 0 & 0 \\ 0 & 0 & 1 & 0 & 0 \\ 0 & 0 & 0 & 0 & 0 \end{bmatrix} \begin{bmatrix} \ddot{x} \\ \ddot{\dot{x}} \\ \ddot{\ddot{x}} \\ \ddot{\ddot{\dot{x}}} \\ d \end{bmatrix} + \begin{bmatrix} b_0 \\ 0 \\ 0 \\ 0 \\ 0 \end{bmatrix} u + \begin{bmatrix} 0 \\ 0 \\ 0 \\ 0 \\ 1 \end{bmatrix} d$$

Then

$$= \begin{bmatrix} -a_1 & -a_2 & -a_3 & -a_4 & 0 \\ 1 & 0 & 0 & 0 & 0 \\ 0 & 1 & 0 & 0 & 0 \\ 0 & 0 & 1 & 0 & 0 \\ 0 & 0 & 0 & 0 & 0 \end{bmatrix} \begin{bmatrix} q_4 \\ q_3 \\ q_2 \\ q_1 \\ d \end{bmatrix} + \begin{bmatrix} b_0 \\ 0 \\ 0 \\ 0 \\ 0 \end{bmatrix} u + \begin{bmatrix} 0 \\ 0 \\ 0 \\ 0 \\ 1 \end{bmatrix} q_2$$

$$= \begin{bmatrix} -a_1 & -a_2 & -a_3 & -a_4 & 0 \\ 1 & 0 & 0 & 0 & 0 \\ 0 & 1 & 0 & 0 & 0 \\ 0 & 0 & 1 & 0 & 0 \\ 0 & 0 & 0 & 0 & 0 \end{bmatrix} \begin{bmatrix} q_4 \\ q_3 \\ q_2 \\ q_1 \\ d \end{bmatrix} + \begin{bmatrix} b_0 \\ 0 \\ 0 \\ 0 \\ 0 \end{bmatrix} u + \begin{bmatrix} 0 \\ 0 \\ 0 \\ 0 \\ 1 \end{bmatrix} q_2$$

Referring to Equation (4);

$$A_a = \begin{bmatrix} -a_1 & -a_2 & -a_3 & -a_4 & 0 \\ 1 & 0 & 0 & 0 & 0 \\ 0 & 1 & 0 & 0 & 0 \\ 0 & 0 & 1 & 0 & 0 \\ 0 & 0 & 0 & 0 & 0 \end{bmatrix}, B_a = \begin{bmatrix} b_0 \\ 0 \\ 0 \\ 0 \\ 0 \end{bmatrix}, E = \begin{bmatrix} 0 \\ 0 \\ 0 \\ 0 \\ 1 \end{bmatrix}$$

$$C_a = \begin{bmatrix} 1 & 0 & 0 & 0 & 0 \\ 0 & 1 & 0 & 0 & 0 \\ 0 & 0 & 1 & 0 & 0 \\ 0 & 0 & 0 & 1 & 0 \\ 0 & 0 & 0 & 0 & 1 \end{bmatrix}, D_a = [0; \ 0; \ 0; \ 0; \ 0]$$

II.4. Extended State Observer (ESO) Design

There are also many observers proposed in the literature, including the unknown input observer, the disturbance observer, the perturbation observer, and the extended state observer (ESO). The ESO design was originally proposed by J. Han, as in [14]. The plant model is represented by the state matrix A and the input matrix B , with measurement given by the output matrix C . The model of the augmented process given as A_a, B_a, C_a, D_a contains an extra state representing the disturbance (d). The ESO model runs in parallel with the augmented plant generating predictions $[\hat{x}_1, \hat{x}_2, \dots, \hat{x}_n, \hat{d}]^T$. Since the disturbance is not part of the input of the observer model, the predicted and observe variables y and y_o will differ. This error in prediction is corrected by the use of the gains (L) to control the observer dynamics back to the true dynamics, see Fig. 3. Under perfect model assumptions, the amount of correction needed is the estimated value of the disturbance at the plant input (\hat{d}). Mathematically, such an equivalent disturbance is “observable” from the input-output data from the process and the observer can be easily constructed as shown below.

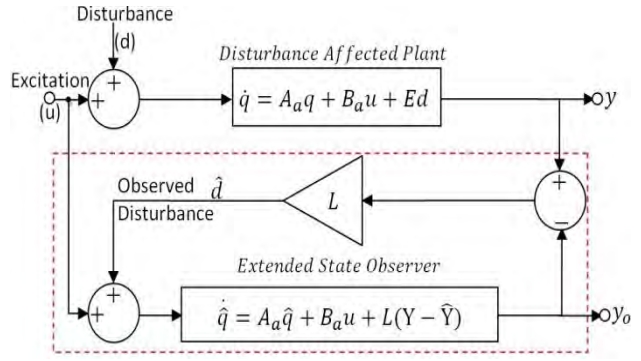


Fig. 3. Disturbance Rejection Observer Implementation

Most require a nominal mathematical model. The main idea is to estimate the disturbance, q_{n+1} and a Luenberger

observer, as in [5], for the system described, as in (4), can be designed as

$$\begin{aligned}\dot{\hat{q}} &= A_a \hat{q} + B_a u + L(Y - \hat{Y}) \\ y &= C_a q_{est} \\ \dot{y} &= derivative(y) \\ q &= [y, \dot{y}, p_{est}]^T \\ Y &= [y, \dot{y}]^T \\ C_o &= \begin{bmatrix} 1 & 0 & 0 \\ 0 & 1 & 0 \\ 0 & 0 & 1 \end{bmatrix}, \hat{Y} = C_o q = \begin{bmatrix} 1 & 0 & 0 \\ 0 & 1 & 0 \\ 0 & 0 & 1 \end{bmatrix} \begin{bmatrix} y \\ \dot{y} \\ p_{est} \end{bmatrix}\end{aligned}\quad (4)$$

II.5. ESO Gains

The ESO in its original form employs nonlinear observer gains. With the use of linear gains, this observer is denoted as the linear extended state observer (LESO). The estimator is stable if the observer gains $L = [l_1, l_2, \dots, l_N]^T$ are selected accordingly so that the eigenvalues of $(A_a - LC_a)$ lie on the left side of the s-plane where the observer bandwidth (w_0) is the only tuning parameter, as in [5]-[14]. The following existing method is to tune the matrix (L) using only one parameter, the bandwidth of the observer (w_0).

$$\begin{aligned}L &= [nw_0^1 \ nw_0^2 \ nw_0^3 \ \dots \ nw_0^{m-1} \ w_0^m] \\ m &= 1, 2, 3, \dots \\ n &= number\ of\ states\ including\ error \\ L &= [5w_0^1 \ 5w_0^2 \ 5w_0^3 \ 5w_0^4 \ w_0^5]\end{aligned}$$

As observer bandwidth is the only tuning parameter in the existing method, the ESO might create instability if the parameter bandwidth is not adjusted correctly. An alternative method can also be computed using Ackermann's formula in estimator form, which is $L = \alpha_e(F)O^{-1}[0 \ 0 \ \dots \ 1]^T$ where observability matrix is, $O = [H \ HF \ \dots \ HF^{n-1}]^T$, as in [5]-[13]. However, the Observability matrix has to be square, nonsingular, and nonzero determinant to transform to observer canonical form which can cause unnecessary complication. Therefore, the observer gains, as in (5), from the augmented matrix, $A_a = [A + E]$, to simplify the tuning process can be generated, as in [3], as

$$\begin{aligned}L &= A_a^{-1}y \\ L &= inv(A_a * A_a) * (A_a * y)\end{aligned}\quad (5)$$

It is very useful to have intuitive parameters and as few as possible. In order to provide an on-line tuning of the observer, the following structure of the matrix L is proposed, as in [7]. Let us denote by l_{ij} the entries of the matrix (L). Each column of observer gain (L) can then be applied for trial-error in the system. With the well-tuned DRO, total disturbance is estimated and rejected by LQR

control, $u = -Kq$. To achieve the stable estimator, the observer gains are selected as follow.

$$L = \begin{bmatrix} l_{ij} & l_{i(j+1)} & \dots & l_{i(j+m)} \\ l_{(i+1)j} & l_{(i+1)(j+1)} & \dots & l_{(i+1)(j+m)} \\ \vdots & \vdots & \ddots & \vdots \\ \vdots & \vdots & \dots & \vdots \\ l_{(i+n)j} & l_{(i+n)(j+1)} & \dots & l_{(i+n)(j+m)} \end{bmatrix}$$

where $i, j, m, n = 1, 2, 3, \dots$

II.6. LQR-DRO Control

Assuming that, the ESO produces an accurate estimation of the unknown dynamics. The following control law, $u = -Kq$, will ensure the tracking of the reference input. For a continuous time system, the state-feedback law is expected to minimize the quadratic cost function, $J = \int_0^\infty \{q^T Q q + u^T R u\} dt$, which is subject to the system dynamics, $\dot{q} = Aq + Bu$, as in [4]-[12]. The associated Riccati equation, as in (6), and controller gain (K) are derived, as in (7).

$$A^T S + SA - (SB + N)R^{-1}(B^T S + N^T) + Q = 0 \quad (6)$$

$$K = R^{-1}(B^T S + N^T) \quad (7)$$

In practice, an appropriate choice to obtain acceptable values of x and u is to initially choose diagonal matrices Q and R such that

$$\begin{aligned}Q_{ii} &= \frac{1}{maximum\ acceptable\ value\ of\ [x_i^2]} \\ R_{ii} &= \frac{1}{maximum\ acceptable\ value\ of\ [u_i^2]}\end{aligned}$$

The weighting matrices (Q and R) are then modified during subsequent iterations to achieve an acceptable tradeoff between performance and control effort. The direct solution for the optimal control gain, K , in the MATLAB statement, as in (8), is

$$Q = \rho H^T H \\ Q = \begin{bmatrix} 0 & 0 & 0 & 0 \\ 0 & 0 & 0 & 0 \\ 0 & 0 & 0 & 0 \\ 0 & 0 & 0 & 1e5 \end{bmatrix}, R = 0.1 \\ K = lqr(A_a, B_a, Q, R) \quad (8)$$

Referring to the Luenberger observer, as in (5), and the control rule, $u = -Kq$, LQR design iteration can be defined, as in (9).

$$\dot{\hat{q}} = (A_a - (B_a * K))\hat{q} + L(Y - \hat{Y}) \quad (9)$$

The central aim of DRO implementation in this trolley translation model is to actively reject the disturbance in the absence of a detailed mathematical model of the plant or the disturbance itself. For that purpose, the controller is designed based on ideal, disturbance free, process where

any discrepancies between the actual process and the ideal one is considered as disturbance, being estimated and, afterwards, canceled. Even though applying simple LQR follows the reference trajectory, reasonable amount of overshoot and undershoot cause the controller unreliable. However, the inclusion of a disturbance observer improved the performance of the LQR-DRO controller, see Fig. 4, significantly by reducing overshoot and undershoot, the effectiveness of the compensation depends on how fast the state estimates, as in (10), converge to the true values.

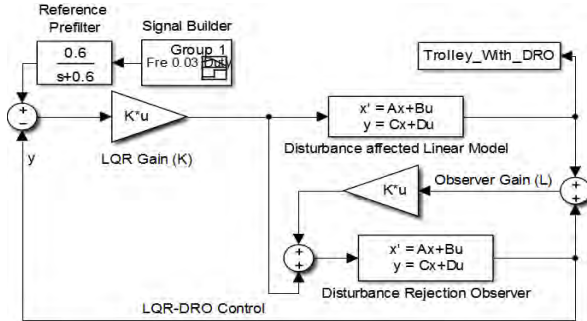


Fig. 4. LQR-DRO Control

Trolley model simulations using different columns of observer gains are carried out to test the tracking and disturbance rejection performance LQR-DRO. Control performance would vary based on each observer gains column and the best simulation results have been obtained after trials-and-errors. Using observer gains column-1, $l_{ij} \dots l_{(i+n)j}$, the system produces robust tracking of the reference input with reasonably less overshoot, see Fig. 5.

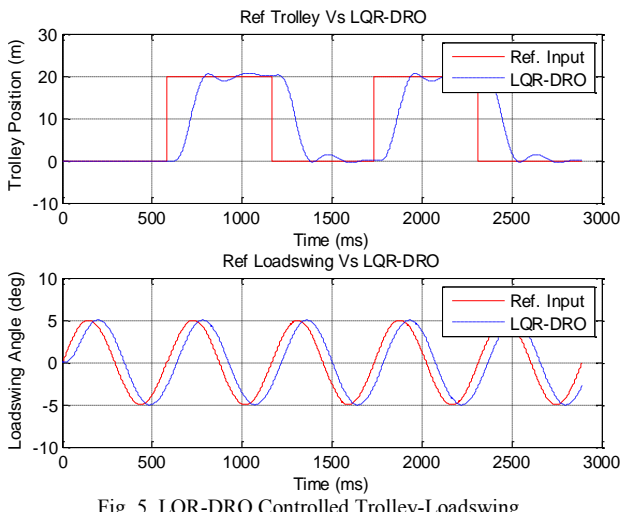


Fig. 5. LQR-DRO Controlled Trolley-Loadswing

Despite the improvement in LQR-DRO method with smooth trajectory tracking, tracking error problem still exists in the control scheme and seriously limits its practical application in the crane trolley control. Slow convergence would also mean that the DRO presents long transients when tracking the true disturbance values, during which time disturbance has not been correctly compensated. To achieve robust tracking, the next section would discuss about the implementation of internal model

integral control with estimator which uses the augmented model, as in (4).

III. LQR-Estimator-Integral Control (LEIC) for Linear Model

The Robotic Tower Crane model simulation produced nonlinear data including trolley translational positions($X_{x,y,z}$), payload swing angles($\theta_{x,y,z}$), and tower rotational positions($\phi_{x,y,z}$) respectively. The details of simple LQR and LQR-DRO designs discussed in sections-II produced significant amount of steady-state error to a reference input and were less robust. To achieve robust tracking, integral control that presents the internal model principle is introduced by a direct method of adding the integral of the system error to the equations of motion. Since the system needs to reject the disturbance from the augmented model, estimator model has also been included in this optimal LQR-Estimator-Integral Control design, see Fig. 6.

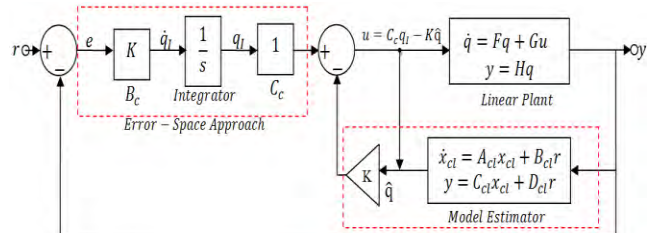


Fig. 6. LQR-Estimator-Integral Control (LEIC) for Linear Model

III.1. Error-Space Approach

The choice of LQR-DRO control resulted in a reference input response with a less steady-state error. But the result is not robust because any change in the parameters caused the error higher. Integral control is then introduced to obtain robust tracking of square and sinusoid inputs for both trolley and payload swing. However, integral control has a limitation to square response tracking, and therefore error-space approach is considered a more analytical approach which has the ability to track a non-decaying inputs (square or sinusoid), as in [15]. As the reference signal is generated by a dynamic system, it is considered as part of the formulation and solving the control problem in an error-space to make the error approaches zero. Given the reference dynamic(r) and the augmented plant dynamics from Section II.3, as in (4);

$$\begin{aligned}\dot{q} &= A_a q + B_a u + E_d, \\ y &= C_a q + D_a u\end{aligned}$$

where the parameters A_a , B_a , C_a , and D_a are the matrices from section II.3. Then the tracking error is defined as,

$$e = y - r,$$

This integral control system feeds back the integral of the error, e , with the state of the plant, q , then followed by augmenting the plant state with the extra (integral) state x_l which obeys the differential equation, as in (10),

$$\dot{x}_l = C_a q - r = Ke \quad (10)$$

which leads to $x_I = K \int_0^t e dt$

One way to formulate the tracking problem is to differentiate the error equation and introduce the error as a state. Thus, the error system, as in (11), is

$$\begin{bmatrix} \dot{e} \\ \dot{q} \end{bmatrix} = \begin{bmatrix} 0 & C_a \\ 0 & A_a \end{bmatrix} \begin{bmatrix} e \\ q \end{bmatrix} + \begin{bmatrix} 0 \\ B_a \end{bmatrix} u - \begin{bmatrix} 1 \\ 0 \end{bmatrix} r + \begin{bmatrix} 0 \\ E \end{bmatrix} d \quad (11)$$

Using the augmented state equation, as in (11), then the state representation is

$$A = \begin{bmatrix} 0 & C_a \\ 0 & A_a \end{bmatrix}, B = \begin{bmatrix} 0 \\ B_a \end{bmatrix}$$

Existing Integral control of the form, $\dot{x}_I = B_c e$, which considers $B_c = -K_1$, the associated feedback gain of error state, as in [16]. However, implementing this existing approach could not produce better reference tracking. In contrast to the consideration, as in [16], this paper then applies $B_c = K$, see Fig. 7, of all feedback gains (controller gain K= error state and plant states) in error-space implementation. The controller gains K derivation is discussed in the next section.

III.2. LQR Gains

Details LQR Control design has been presented in earlier section in which; the need of quadratic cost function, $J = \int_0^T \{q^T Q q + u^T R u\} dt$, to penalize the tracking error (e) and the control (u), the state and control weighting matrices (Q and R) design as well as LQR gains derivation were covered. Since the augmented system includes error state, the factor of "1" was determined as the relative weighting for error state while other plant states weighting were determined by trial and error. The state and control weighting matrices are then

$$Q = \begin{bmatrix} 1 & 0 & 0 & 0 \\ 0 & 0 & 0 & 0 \\ 0 & 0 & 0 & 0 \\ 0 & 0 & 0 & 1e5 \end{bmatrix}, R = 0.1$$

The resulting feedback gain (K) computed from MATLAB ($K = \text{lqr}(A, B, Q, R)$) is formed as $K = [K_1 \ K_2 \ K_3 \ K_4 \ K_5]$ or $K = [K_1 \ \vdots \ K_0]$. The combination of error space approach and LQR gains is then called internal model controller of the form, as in (12)

$$u = C_c q_I - K \hat{q} \quad (12)$$

where x_I denotes as the controller state and the value of $C_c = 1$, as in [13].

III.3. Full-Order Estimator

The controller which combines the control law with the estimator is essentially a regulator design. One method of estimating all the state variables that one may consider is to construct a model, as in (13), of the plant dynamics, as in [13].

$$\dot{q} = A_a q + B_a u, \quad y = C_a q \quad (13)$$

where q is the estimate of all the actual states, ($q = [y, \dot{y}, p_{est}]^T$), discussed in section II.4, and A_a and A_a are augmented plants referred from II.3. The full-order estimator is driven by three inputs such as; control term input (u), correction term derived from the actual output of the plant, and the predicted term derived from the estimator, as in [17]. In order to speed up the process and provide a useful state estimate, the system applies the following the full-order estimator equation, as in (14),

$$\dot{\hat{q}} = A_a \hat{q} + B_a u + L(Y - C_a \hat{q}) \quad (14)$$

III.4. Estimator Gains

The estimator ESO gain (L), as in (15), which minimizes the covariance for a linear system in continuous time can be obtained based on Kalman-Bucy filter, as in [17].

$$L = P C^T R_v^{-1} \quad (15)$$

where $P(t)$ represents covariance matrix, C is a linear function output, and R_v is the process sensor noise intensity. This paper considers $R_v = 0.001$. Suitable L values can be chosen to stabilize the dynamics of $P(t)$ so that the estimator gain can converge to a constant and satisfies the algebraic Riccati equation, as in [17].

This paper then examines estimator gain (L) matrix for using "lqe" command in MATLAB; $L = lqe(A_a, B_a, C_a, R_v, R_w)$. Having the suitable estimator gains (L) to compute estimator, and the feedback controller gains (K), the internal model controller equation can further be improved. The overall system equations are obtained by substituting ($y = C_a q$, $\dot{q}_I = Ke$, and $u = C_c q_I - K \hat{q}$) in (10)-(13)-(14). New derived version becomes;

As in (10),

$$\begin{aligned} \dot{q}_I &= Ke = B_c(y - r) = B_c y - B_c r \\ \dot{q}_I &= B_c C_a q - B_c r \end{aligned} \quad (10)'$$

As in (13):

$$\begin{aligned} \dot{q} &= A_a q + B_a u = A_a q + B_a(C_c q_I - K \hat{q}) \\ \dot{q} &= A_a q + B_a C_c q_I - B_a K \hat{q} \end{aligned} \quad (13)'$$

As in (14),

$$\begin{aligned} \dot{\hat{q}} &= A_a \hat{q} + B_a u + L(Y - C_a \hat{q}) \\ &= A_a \hat{q} + B_a(C_c q_I - K \hat{q}) + L(C_a q - C_a \hat{q}) \\ &= A_a \hat{q} + B_a C_c q_I - B_a K \hat{q} + L C_a q - L C_a \hat{q} \\ \dot{\hat{q}} &= L C_a q + B_a C_c q_I + (A_a - B_a K - L C_a) \hat{q} \end{aligned} \quad (14)'$$

The closed loop system equations are then given by

$$\begin{aligned} \dot{x}_{cl} &= A_{cl} x_{cl} + B_{cl} r \\ y &= C_{cl} x_{cl} + D_{cl} r \end{aligned}$$

where r is the reference input trajectory, and the closed loop state vector is $x_{cl} = [q \ q_I \ \hat{q}]^T$, and therefore combining those three equations (13)', (10)', and (14)' equations in the matric notation and form the complete estimator design, as in [16].

$$A_{cl} = \begin{bmatrix} A_a & B_a C_c & -B_a K \\ B_c C_a & 0 & 0 \\ LC_a & B_a C_c & (A_a - B_a K - LC_a) \end{bmatrix}, B_{cl} = \begin{bmatrix} 0 \\ -B_c \\ 0 \end{bmatrix}$$

$$C_{cl} = [C_a \ 0 \ 0], \ D_{cl} = [0]$$

III.5. LQR-LEIC

This simulink control layout consists of augmented trolley translational model, and estimator-integral feedback. This robust LQR-Estimator-Integral controller is designed in the sense that regulation of "e" to zero in the steady-state occurs in the presence of perturbation system parameters, see Fig. 7.

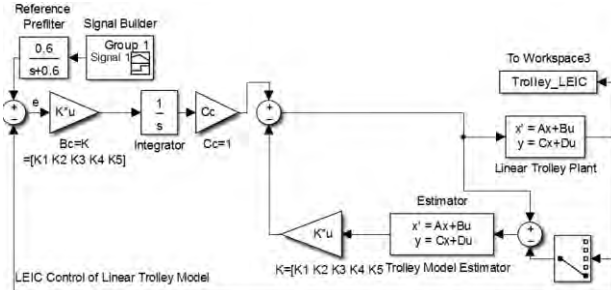


Fig. 7. LQR-LEIC Design for Linear Plant

III.6. LQR, LQR-DRO, and LEIC performance Comparison

Trolley translational model system runs on 20-m jib length with having multiple reference position changes at different times setting. The MATLAB-Simulink is used for the simulation of simple LQR, LQR-DRO, and LEIC for linear model. The disturbance rejection observer, error-space method with inclusion of estimator-integral control are implemented, as in (9)-(13)-(14) respectively. Several simulations have been carried out to test the disturbance rejection performance and tracking of the LQR-DRO and LEIC.

The commanded trolley position trajectory with (0-20 m) duty cycles were fed to the controller and one can see the systems track the input and attenuates the disturbance with minor tracking errors. The simulation result, see Fig. 8, shows the system output with LQR control has overshoot and undershoot. On the other hand, LQR-DRO control effectively rejects the disturbance, tracks the commanded position trajectory with around 10-milliseconds time delay for the ramp with no overshoot. Nevertheless, the settling time in every reference duty cycle is reasonably large. The LQR-Estimator-Integral Control is then developed in which internal model controller of the form produces better reference tracking while full-order estimator clearly rejects the disturbance. Based-on the findings of all three methods, the LEIC approach has proven to perform better robust tracking compare to the other two.

Since the LEIC performance executes smooth robust tracking on reference trajectory, the next section would discuss about the linear development from Nonlinear Autoregressive exogenous (NARX) structure and LEIC-Antiwindup controller implementation.

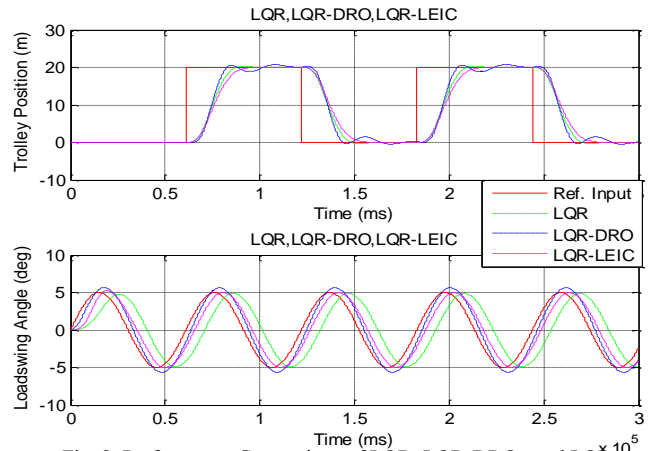


Fig. 8. Performance Comparison of LQR, LQR-DRO, and LQR-LEIC controllers for both Trolley and Loadswing linear models

IV. LEIC-Antiwindup for Linear Model

This section has twofold, one: linear model development using NARX structure and, two: antiwindup implementation in LEIC.

The dynamic range of practical controller is usually limited. For instance, the control surfaces in an aircraft can be deflected only to a certain angle from their nominal positions, as in [18]. Using such actuators in the system might have phenomenon like "integrator windup". The integrator output may become quite large if saturation lasts longer time which eventually triggers to produce large commands. If this happens, the integrator builds up a large value which results in large overshoots and errors. To overcome this problem, "antiwindup" is implemented to "turn off" the integral action as soon as the actuator saturates.

Regarding the linear model development, the NARX model provides a powerful representation modeling and prediction due to its strength in accommodating the dynamic, complex and nonlinear nature of real time series applications, as in [19]. Therefore, instead of applying traditional way of linear modeling techniques, this paper introduced the linear model derivation from Nonlinear Autoregressive exogenous (NARX) structure to further explore robust control.

IV.1. Linear System Identification from NARX Structure

Initial construction tower crane system simulation produces a bunch of nonlinear data which includes trolley translation, payload swing, tower rotation, etc.. Since it is essential to keep the payload swing low while trolley is in motion, this research further develops trolley-payload linear models. Trolley-payload free body diagram, see Fig. 9, provides the details of trolley cart mass (M), payload mass (m), load length (l), swing angle (θ). Since the external force (F) applies on trolley to move back-and-forth along X -direction, large swing angle (θ) appears. The input ($u(k)$): derived force from power drive) and the output ($y(k)$: the trolley translational

position) are then obtained from the simmechanics-visualized tower crane model simulation.

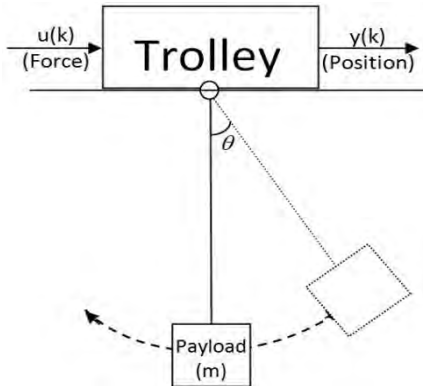


Fig. 9. Trolley-Payload Free Body Diagram

The field of process-parameter identification and estimation has developed rapidly during the past decade. There are plenty of nonlinear-based system identification methods such as; the online and real-time nonlinear identification based on least square approach were discussed, as in [20]. Nonlinear Autoregressive exogenous model (NARX), as in [21]-[22]-[23]-[24], adaptive neuro-fuzzy inference system (ANFIS), as in [25], non-linear formulation that is linear in parameters using recursive least square method (RSLM), as in [26], nonlinear Hammerstein-Wiener (NLHW), as in [21]-[22], etc. This paper aims to derive linear models (for trolley and payload) from NARX structure, and analyze the LEIC-Antiwindup control performance to achieve robust trajectory tracking.

IV.2. Linear ARX Model development

The function of nonlinear ARX model is to predict future values of a time series $y(t)$ from past values of that time series and past values of a second time series $x(t)$. It computes in two stages. Firstly, the next value of the dependent output signal $y(t)$ is regressed on previous values of the output signal and previous values of an independent (exogenous) input signal. And secondly, the nonlinearity estimator maps the regressors to the model output using a combination of nonlinear and linear functions. The following structure represents the nonlinear ARX model, see Fig. 10.

$$y(t) = f[y(t-1), y(t-2), \dots, u(t-1), u(t-2), \dots] + e(t) \quad (16)$$

where $u(t)$ represents the inputs, $y(t)$ represents the outputs of the model at time (t) and $e(t)$ is the error term.

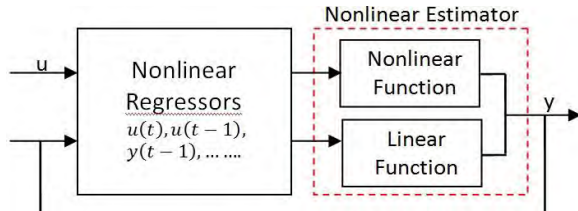


Fig. 10. Nonlinear Autoregressive exogenous (NARX) Structure

In this work, the system identification is developed using "nlarx" and "sigmoidnet" as nonlinear estimator function in the MATLAB. Different combinations of regressors $[y(t-1), \dots, y(t-6), u(t-1), \dots, u(t-6)]$ are assigned in "nlarx" algorithm "sigmoidident" nonlinear estimator in search of better fit model output, as in [14]-[15]. Extracting nonlinear and linear parameters from the model, both y_{Linear} and $y_{Nonlinear}$, as in (17) and (18), can be derived as follow.

$$\hat{y} = y_{Linear}(x) + y_{Nonlinear}(x)$$

$$y_{Linear}(x) = (x - r) * P * L + d \quad (17)$$

$$f(s) = (e^s + 1)^{-1}$$

$$f_{Input}(k) = Q * (x - r) * bMat(:, k) * cVec(k)$$

$$y_{Nonlinear}(x) = \sum_{k=1}^n [aVec(k) * f * f_{Input}(k)] \quad (18)$$

whereby, " x " is a vector of the regressors, " r " is the mean of regressors, " P " is the linear subspace, " L " is the linear coefficient, " d " is the output offset, " f " is sigmoid function, " Q " is the nonlinear subspace, $bMat$ is the dilation, " $cVec$ " is the translation, and " $aVec$ " is nonlinear output coefficient, as in [23].

Using the linear coefficients extracted from NARX model, the transfer function and state-space representation be formed as

$$\frac{x(k)}{F(k)} = \frac{-1.725 s^3 + 37.71 s^2 + 459 s - 1.047e04}{s^3 + 72.53 s^2 + 1620 s + 1.138e04}$$

$$\begin{bmatrix} \ddot{x} \\ \dot{x} \\ x \end{bmatrix} = \begin{bmatrix} -72.5264 & -50.6155 & -22.2331 \\ 32.0000 & 0 & 0 \\ 0 & 16.0000 & 0 \end{bmatrix} \begin{bmatrix} \ddot{x} \\ \dot{x} \\ x \end{bmatrix} + \begin{bmatrix} 16 \\ 0 \\ 0 \end{bmatrix} u$$

$$y = [10.1751 \ 6.3526 \ 1.1187] \begin{bmatrix} \ddot{x} \\ \dot{x} \\ x \end{bmatrix}, D = [-1.7247]$$

IV.3. LEIC Anti-Windup Control with Linear ARX

To achieve the robust tracking performance of the LEIC with Anti-Windup control, as in [5], see Fig. 11, for developed linear ARX model, a series of simulation cases were performed by adjusting; weights in Q and R matrices, different LQR gains in integral control and estimator, saturation, prefilter, and trolley uncertainty parameters.

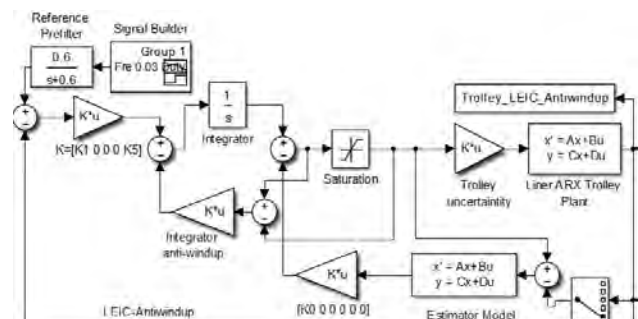


Fig. 11. LEIC-Antiwindup Control with Linear ARX Model

IV.4. LQR-DRO, LEIC, LEIC-Antiwindup Control Performances Comparison for Trolley Model

Performance comparison of (LQR, LQR-DRO, and LEIC, and LEIC-Antiwindup) in regards to the trolley translation model control has been presented below. As it is seen in the simulation results, increasing the weighting of the state vector (Q), and decreasing the weighting of the input (R) leads to decreasing the maximum of the trolley cart position and increasing of the maximum values of the input controller. Therefore, one can choose appropriate values of (Q) and (R) to obtain desired results. After trials-and-errors in this LEIC-Antiwindup approach, the saturation range (upper limit:50, lower limit:1), $Q = 5e5$, and $R = 0.008$ have been set to achieve better robust reference tracking. LQR-DRO output, see Fig. 12(b), has slight overshoot compare to others, see Fig. 12(a,b,c,d). The effect of using Antiwindup has significantly reduced both the error overshoot and the control effort in this LEIC-Antiwindup design, see Fig. 13.

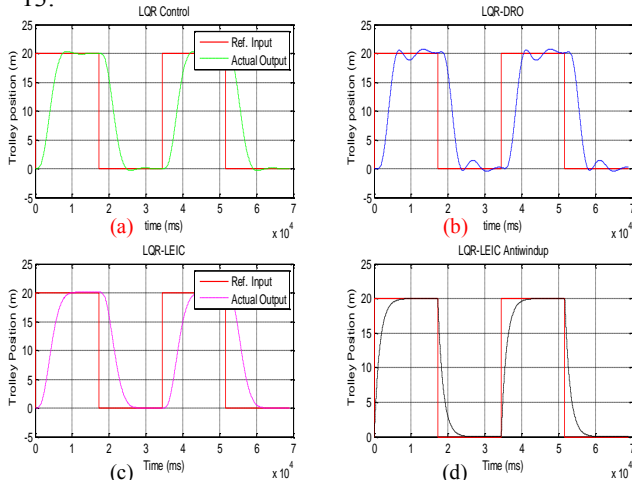


Fig. 12 . Performance Comparison for Trolley Model. Simulated results with (a) LQR, (b) LQR-DRO, (c) LQR-LEIC, (d) LQR-LEIC Antiwindup

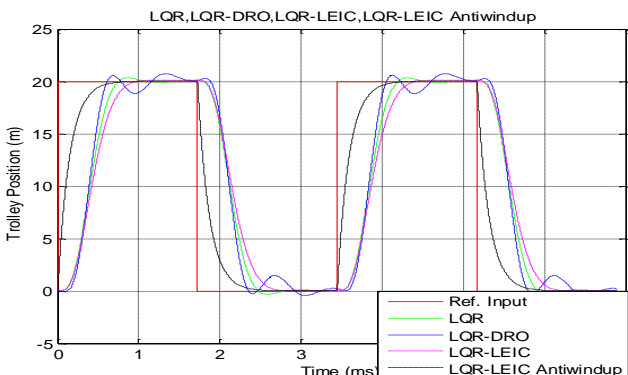


Fig. 13 . LQR, LQR-DRO, LQR-LEIC, LQR-LEIC Antiwindup Performance Comparison for Trolley Model in one plot

IV.5. LQR-DRO, LEIC, LEIC Antiwindup Control Performances Comparison for Payload Swing Model

Agin, linear ARX loadswing model, as in (19), was generated using NARX system identification. Initial simulation results show LEIC-Antiwindup approach could not achieve reference tracking of loadswing due to

the external applied force on trolley cart with interaction forces/torques uncertainties. Trials-and errors were required on essential parameters such as; weighting matrices(Q , R), controller gains (K) in integral control, estimator, saturation, prefilter, and loadswing uncertainty parameters. The performances from LQR, LQR-DRO, LEIC, and LEIC Antiwindup, see Fig. 14(a,b,c,d), produce perfect reference trajectory tracking. All four outputs have been plot in one, see Fig. 15.

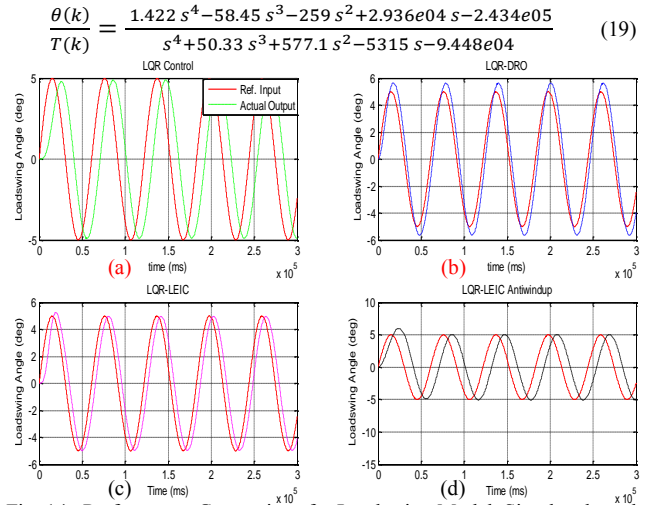


Fig. 14 . Performance Comparison for Loadswing Model. Simulated results with (a) LQR, (b) LQR-DRO, (c) LQR-LEIC, (d) LQR-LEIC Antiwindup

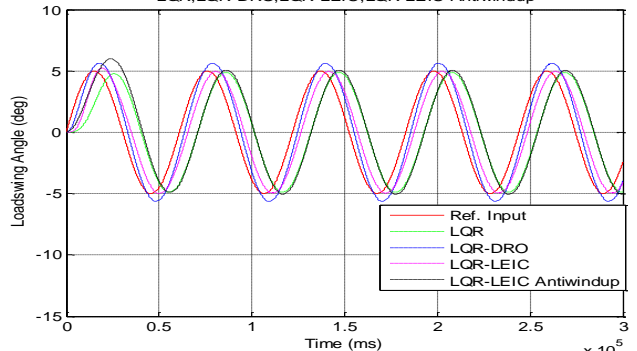


Fig. 15 . LQR, LQR-DRO, LQR-LEIC, LQR-LEIC Antiwindup Performance Comparison for Payload swing Model in one plot

V. Nonlinear Robotic Tower Crane Modeling Control (RTCMC)

As previously proposed controllers from sections (II, III, and IV) have proven to achieve robust tracking on crane linear models, this paper applies LQR-DRO controller with feedback torque actuator compensation on actual nonlinear simmechanics-visualized tower crane model discussed in section I. The reason of naming as "Robotic Tower Crane Modeling Control" is because it covers the whole aspects (from the recently developed nonlinear simmechanics-visualized model, optimized the best fit linear model, to the proposed trajectory tracking controllers of this work). This approach is motivated by two reasons. First, the controller is relatively simpler compare to other proposed ones and it only needs trials-and-errors for observer gains. Second, if LQR-DRO implemenetation is found to achieve robust tracking for

nonlinear RTC, it proves that other controllers would definitely execute more or less similar performance. Though initial LQR-DRO implementation on nonlinear RTCMC could neither track trolley trajectory nor suppress the payload swing, a number of step-by-step trials were necessary to bring the system under control. Three considerations have been taken into accounts such as; LQR-DRO controller parameters tuning, feedback forces and torques investigations, and mechanical structure adjustments.

V.I. Nonlinear RTCMC Flowchart

The following RTCMC flowchart, see Fig. 16, shows three main features. Firstly, it is all about designing simmechanics-visualized crane model based on real tower Morrow crane. Secondly, developed wind disturbance model and analyzed vibration impact on the crane and more specifically towards payload swing instability. Thirdly, complete nonlinear simulation data collection, system identification using Linear Least Square(LLS) approach, and optimization by proposed version of LLS algorithm to obtain the best fit linear model. Finally, extended state observer (ESO) with disturbance rejection implementation, and tuning Q-R weighting matrices for better system's tracking performance.

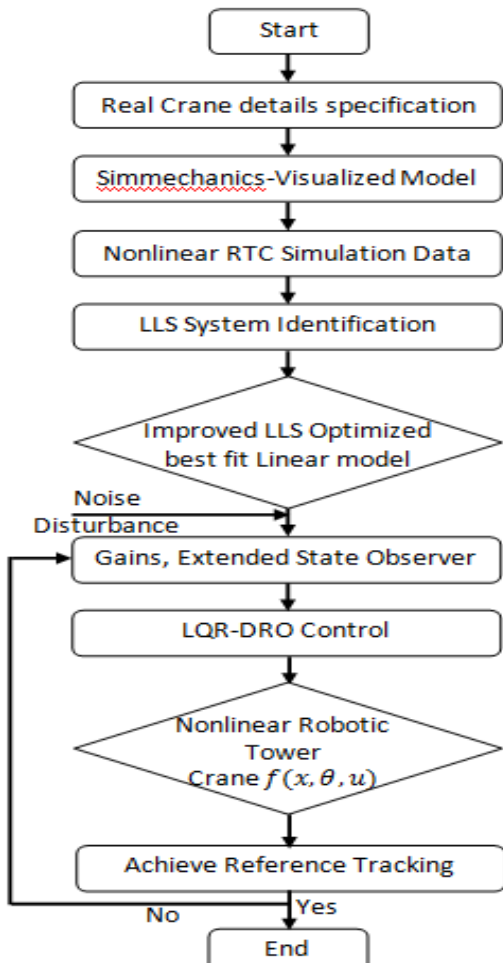


Fig. 16 .Nonlinear Robotic Tower Crane Modeling Control (RTCMC) operation Flowchart

V.2. Reaction Forces and Torques Investigation

This paper thoroughly investigated the concerns of reaction forces and reaction torques on highly nonlinear trolley-payload motion environment in RTCMC.

H. Sano, as in [6], proposed friction disturbance observer based on time correction in order to eliminate trolley-to-rail friction. A. Elharfi, as in [9], analyzed the flexible cable vibration which destabilizes the trolley motion and therefore he proposed a boundary feedback law to achieve desired zero equilibrium. Inverted pendulum with frictionless trolley motion has been tested whereby a thrust force affect on reaction joint was a concern, as in [27]. Sliding model control is then applied to overcome external disturbances and uncertainties.

In this work, initial investigations on both "trolley translation without payload attached" and "payload swing without trolley motion" with external driving force and translational frictions were taken into account. Though the trolley translational motion could track the reference without setback, payload swing control case needs to draw reaction torque in minimizing the swing.

Next, the combined nonlinear trolley-payload system with having; total load of 3340 Kg (for both load and hook), the cable length-18 m, and square reference signal to drive trolley back-and-forth along the tower jib are the preset scenario. However, applying LQR-DRO control on this highly nonlinear system could hardly reach a stable reference tracking due to the lack of correct reaction forces-torques consideration. The simulation results show that, trolley-payload reference tracking is only achievable for (0m~2m) run trials. In order to run for higher trolley reference positions (2m~20m), torque compensation actuator is introduced to attenuate reaction torque at trolley-payload connection joint, see Fig. 17.

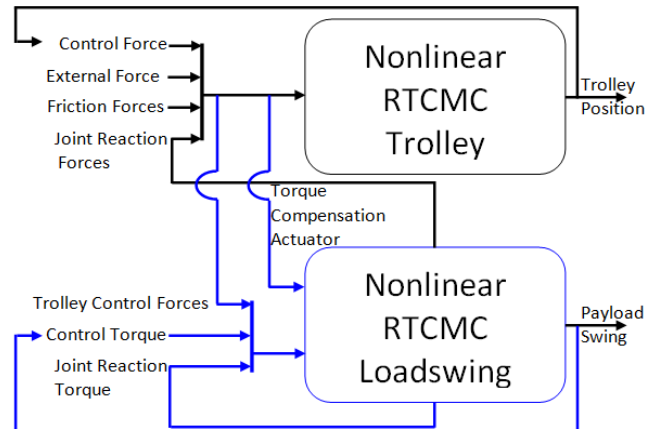


Fig. 17. Feedback Forces and Torques consideration on nonlinear Trolley-Payload System

V.3. Joints, Sensors, and Actuators implementation

The mechanisms of mounting a trolley on the rail-jib (tower) and the payload cable underneath may differ in crane to crane throughout the world. Some of the tower crane and overhead gantry crane mount the trolley on top of the rail-jib while the other mount underneath the rail-jib. No matter those mechanical systems differ one

another, feedback frictions and reaction forces-torques would be the same. Let's have a look on the past works of sensors and actuators implementation on the crane.

Tower crane lab-prototype developed by Quanser has the crane model with a mounted trolley on the rotary arm. The suspended cable is also attached underneath using gimble joint to produce pendulum deflection angle, as in [28]. Another crane model developer, Inteco, designed an overhead 3D gantry crane with jib-trolley-pendulum system. The measurement encoders are then employed to detect trolley motion and pendulum swing, as in [29]. However, most of the payload swing models in literature apply only one swing cable while actual live crane has two. Moreover, proper sensors-actuators implementation in regards to swing minimization are also in question.

To properly analyze the need of suitable (joints, sensors, and actuators), this paper thoroughly attempted several ways of (joints, sensors, actuators) implementations. On the other hand, different combinations of reaction forces-torques are taken as feedback to control upon any changes. After a number of trials, the following consideration of (joints, spherical joints, revolute joints, and sensors) are confirmed to be reliable arrangement, see Fig. 18.

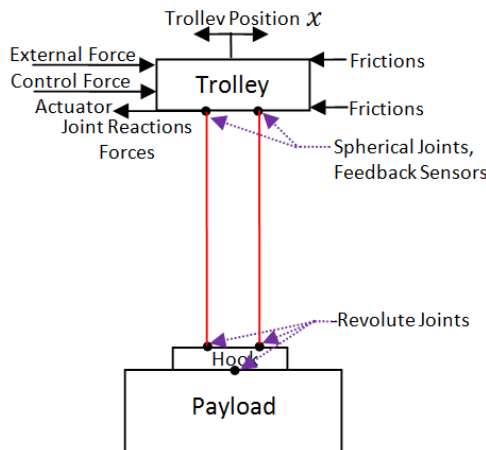


Fig. 18. Joints, Sensors, and Actuators for Nonlinear Trolley Control

V.4. Torque Compensation in Swing Minimization

In the situation of highly nonlinear tower crane operation with wind disturbance and vibration impact, swing suppression is in fact impracticable. Looking at the shipyard gantry cranes and giant construction tower cranes, whereby operators act in the form of compensation actuator by manually juggling trolley back-and-forth to minimize payload swing since no practical approach of torque compensation in swing minimization has been available to date.

Global swing minimization researches have largely focused on reference tracking in some ways. Yet, little known about torque compensation actuator with feedback implementation. For instance, H.M.Omar introduced anti-swing tracking control with friction-compensator, as in [30].

Similarly, D Chwa proposed feedback linearization tracking control based on swing angular rate as well as the swing angle, as in [11].

Instead of relying on traditional swing tracking approaches, this paper has come up with the idea of designing different payload cable structures such as; extra T-link, Cross-link, and W-link in between the two cables, see Fig. 19. It is the beauty of simmechanics-visualization MATLAB software on which the crane structures and its dynamics are easily adjustable according to needs. Moreover, torque compensation actuators are mounted upon each changed-structure to suppress the swing to achieve reference tracking control. Even though adding extra T-link in existing two cable-structure proved to minimize the swing angle to nearly zero according to the simulation results, this paper still proposes swing compensation actuators be implemented at joint reaction points (a and b) of existing two cable-structure to avoid extra cost and complication, see Fig. 20.

Each actuator has two actions parts, one is torque compensation and the other is torque control. Torque compensation draws the driving power from trolley force control while the other one torque control is driven by LQR-DRO swing control. Details electrical structure of feedback forces-torques have been discussed above.

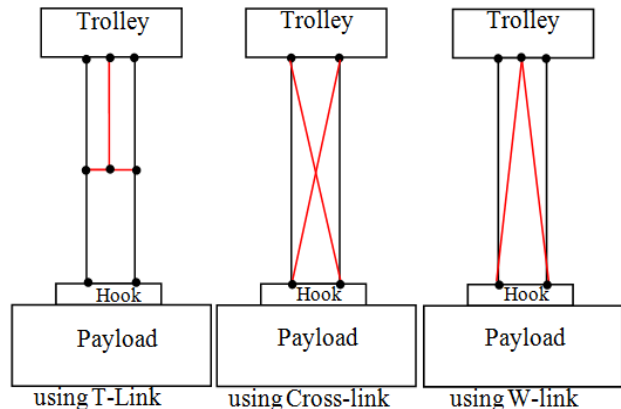


Fig. 19. Payload Cable structures with; T-link, Cross-link, and W-link

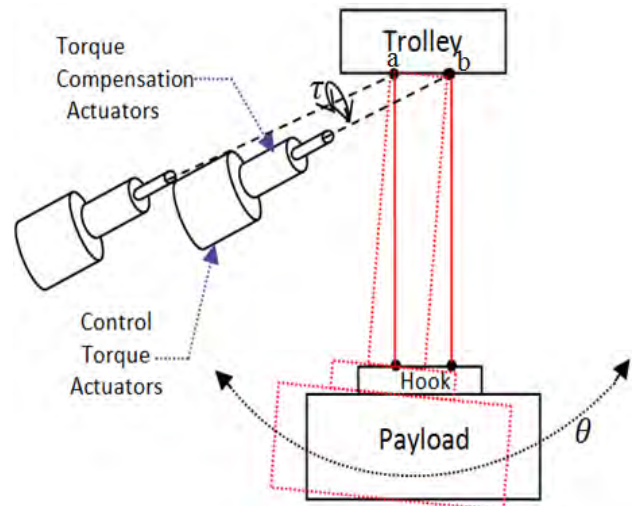


Fig. 20. Torque Compensation Actuators Implementation. τ is Torque.

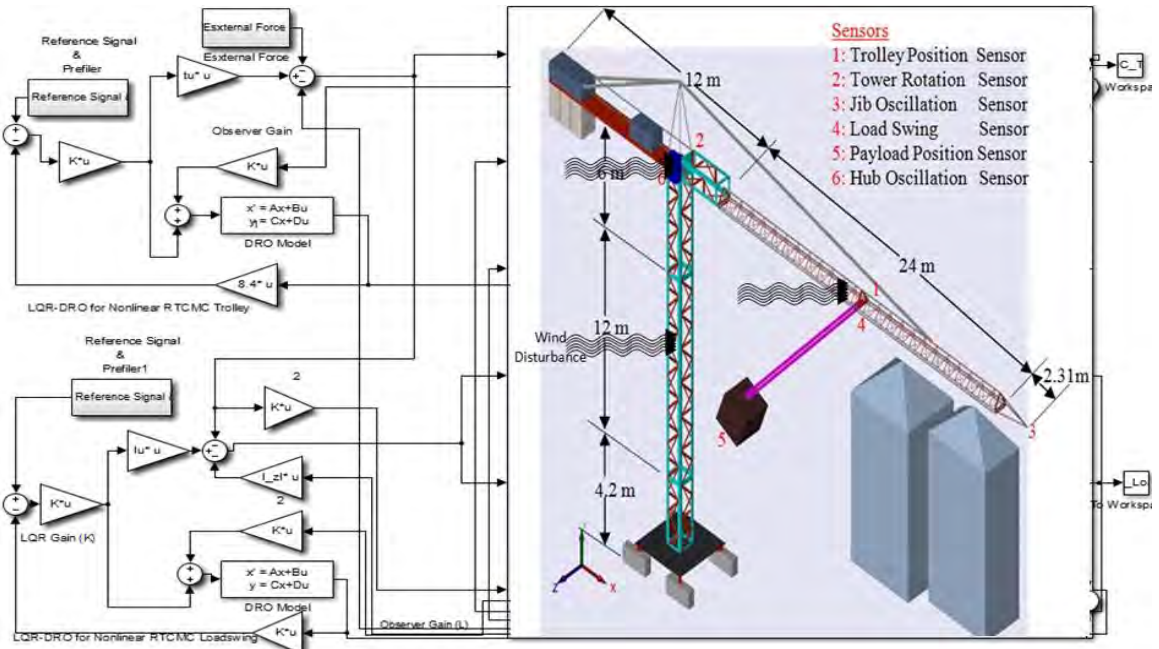


Fig. 21 Nonlinear RTCMC with LQR-DRO for Trolley Loadswing Operation

V.5. Nonlinear RTCMC

The above-mentioned Nonlinear Robotic Tower Crane Model Control (RTC MC) design, see Fig. 21, is based on the flowchart discussed in section V.1. It has two control parts; one LQR-DRO for nonlinear Trolley translation, and the other LQR-DRO is for nonlinear loadswing. The proposed controller has the nonlinear uncertainty properties to improve the disturbance rejection accuracy of LQR-DRO as well as to achieve robust tracking.

V.6. Results and Discussion

The simulations initially apply square-reference (1-m) with trolley back-and-forth run. After trial-and-error, the following values (trolley uncertainty=0.004, Payload uncertainty=0.004, and torque compensation=0.5) are set to produce perfect trolley translation runs, while the swing achieves within the reference range of (5 to -5 deg) and its Root Mean Square Error (RMSE) is 1.9626, see Fig. 22(a).

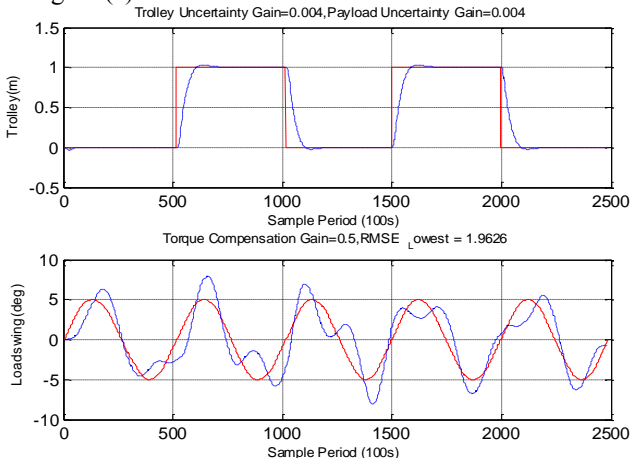


Fig. 22 (a). Nonlinear Trolley-Loadswing result at Square Reference 1m

Since actual jib tower is 24-m length, the next reference is set to be 20-m trolley with back-and-forth run. In this situation, trolley translation output has larger settling time but the payload swing still runs on the right with having its RMSE as low as 1.588 at the values of (trolley uncertainty=0.0008, Payload uncertainty=0.004, and torque compensation=7.8), see Fig. 22(b).

In reality, trolley carrying payload (3340 Kg) to run along 20-m reference track in one second is impractical which makes the settling time large. Therefore, this paper further investigates the robust tracking performance using Semi-Hexagonal Reference.

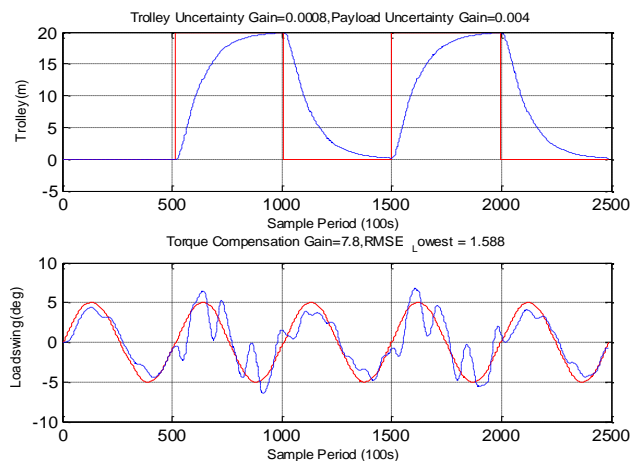


Fig. 22 (b). Nonlinear Trolley-Loadswing result for Square Reference 20m

In the case of Semi-Hexagonal Reference 1-m, trolley translation tracks the reference with rise time 5-s. And, it has the reasonable setpoint tracking error, no overshoot, and allow trolley to reach steady state in about two seconds time. In contrast to the previous square reference 1-m simulation, the payload swing control achieves robust tracking with RMSE 1.2844 which is even lower than the

previous trial, see Fig. 23(a). Likewise, increasing the Semi-Hexagonal Reference to 20-m still remains both trolley and payload swing reference tracking robust. Trials parameters in both reference tracking cases are also presented below, see Table (1).

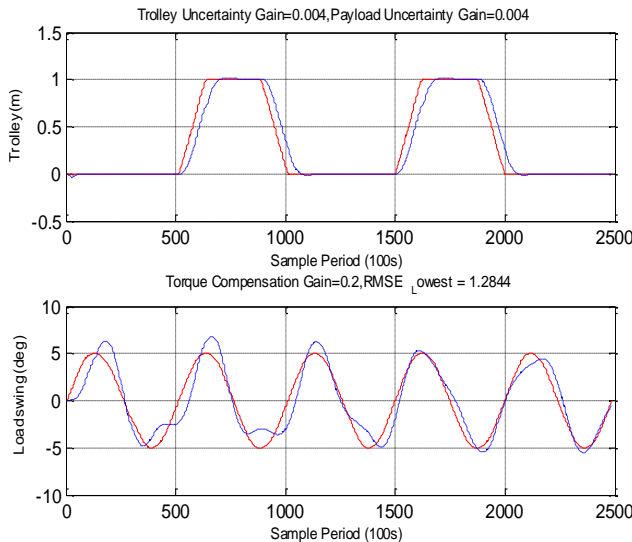


Fig. 21 (a) Nonlinear Trolley-Loadswing result at Semi-Hexagonal Reference 1-m

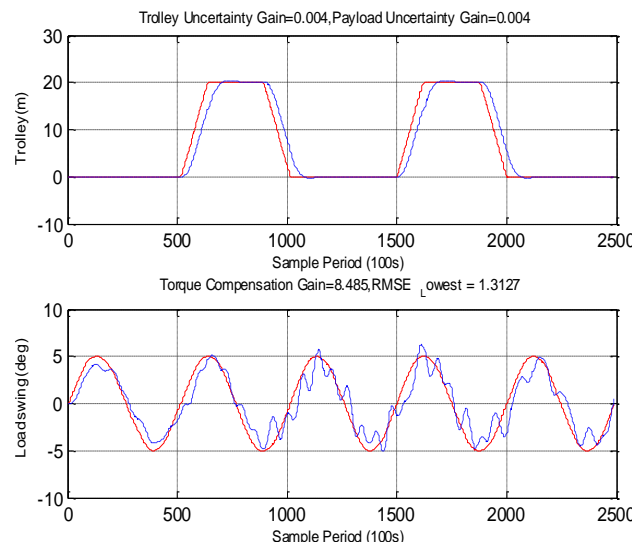


Fig. 21 (b) Nonlinear Trolley-Loadswing result at Semi-Hexagonal Reference 20-m

TABLE I
SWING RMSE COMPARISON OF DIFFERENT TROLLEY
REFERENCE

	(m)	Trolley Uncertainty Gain	Payload Uncertainty Gain	Torque Compensation Actuator	Swing RMSE
Trolley Square Reference	1	0.004	0.004	0.5	1.9626
	20	0.0008	0.004	7.8	15.642
	20	0.004	0.004	4	1.588
Trolley Semi Hex Reference	1	0.004	0.004	0.2	1.2844
	20	0.0008	0.004	7.8	1.078
	20	0.004	0.004	8.485	1.3127

VI. Conclusion

This paper discussed in twofold, one: tower crane linear model controls and, two: nonlinear model control. Firstly, 3D Tower Crane SimMechanics-Visualized model and its optimized the best fit linear models from recent work were referred. Secondly, linear controller developments of (LQR-DRO, LQR-Estimator-Integral (LEIC), and LEIC-Antiwindup) designs were discussed. Considering the disturbance in the system, Luenberger-based LQR-Disturbance Rejection Observer was introduced. LQR-Estimator-Integral Control which consists of error-space approach and full-order estimator is further discussed. LEIC is then reconstructed by adding antiwindup and saturation. Linear model derived from Nonlinear Autoregressive exogenous (NARX) has then been applied in LEIC-Antiwindup control.

Finally, LQR-DRO controller is considered suitable for nonlinear crane model as it is proven to be robust in the case of linear model control. Overall research covers; nonlinear simmechanics-visualized model based on actual crane, applied wind disturbance and analysed vibration impact on the crane, optimized the best fit linearized model based on improved version of linear least square approach, then all the aspects of linear and nonlinear model controls discussed in this paper.

Having the complete package of such works, it is then named as Robotic Tower Crane Modeling Control (RTCMC). To operate safe and fast trolley-payload nonlinear system in such a three-dimensional working environment, it needs perfect modeling, correct choice of joints-sensor-actuators, feedback forces and torques, and on top of that having the best robust tracking control is essential. This RTCMC nonlinear design representing the real crane Morrow has made a great initiative in the fields of cranes industries and global cranes research at large. As this nonlinear model control has proven to be practical, this research future aim is to test the controller on large standing tall operating crane on site.

Acknowledgements

Construction Tower Crane SimMechanics-Visualized Model was developed based on MORROW crane (Liebherr 71EC) datasheet and has been approved by MORROW Tower Crane (NSW, Australia).

References

- [1] F. Ju, Y.S. Choo, F.S. Cui, Dynamic response of tower crane induced by the pendulum motion of the payload, International Journal of Solids and Structures, Volume 43, Issue 2, January 2006, Pages 376-389, ISSN 0020-7683, <http://dx.doi.org/10.1016/j.ijsolstr.2005.03.078>.
- [2] Lagerev, A., Lagerev, I., Milton, A., Tool for Preliminary Dynamics and Stress Analysis of Articulating Cranes, (2014) International Review on Modelling and Simulations (IREMOS), 7(4), pp. 644-652. doi:<http://dx.doi.org/10.15866/iremos.v7i4.2045>

- [3] Lagerev, A., Lagerev, I., Milto, A., Preliminary Dynamics and Stress Analysis of Articulating Non-Telescoping Boom Cranes Using Finite Element Method, (2015) International Review on Modelling and Simulations (IREMOS), 8(2), pp. 223-226. doi:<http://dx.doi.org/10.15866/iremos.v8i2.5713>
- [4] Thein Moe Win, Tim Hesketh, and Ray Eaton. Construction Tower Crane SimMechanics-Visualized Modelling Tower Vibration Impact on Payload Swing Analysis and LQR Swing Control, *International Review on Modeling and Simulations (IREMOS)*, Volume 7 (Issue 6):979-994, December 2014.
- [5] Zhiqiang Gao, Active Disturbance Rejection Control: A Paradigm Shift in Feedback Control System Design Center for Advanced Control Technologies, *Proceeding of the 2006 American Control Conference, Minneapolis, Volume 9* (Issue 2): 2399-2405, June 14-16, 2006
- [6] H. Sano, K. Sato, K Ohishi, and T. Miyazaki. Robust Design of Vibration Suppression Control System for Crane Using Say Angle Observer Considering Friction Disturbance, *Electrical Engineering Conference in Japan, Vol. 184, No. 3, pp. 36–46, Nagoya, Japan, Jan. 2013.*
- [7] Manuel Olivares a, Pedro Albertos, Linear control of the flywheel inverted pendulum, *ELSEVIER Journal of ISA Transactions*, Volume 53 (Issue 1): 1396-1403, January 2014.
- [8] Lal B. Prasad, B. Tyagi, and Hari O. Gupta, Optimal Control of Nonlinear Inverted Pendulum System Using PID Controller and LQR: Performance Analysis Without and With Disturbance Input, *International Journal of Automation and Computing*, Volume 11 (Issue 6): 661-670, December 2014.
- [9] Abdelhadi Elharfi, Feedback Controller Stabilizing Vibrations of a Flexible Cable Related to an Overhead Crane, *Mathematical Problems in Engineering Research, Hindawi*, Volume 1, 1-12, August 2010.
- [10] J Martin Böck and Andreas Kugi, Real-time Nonlinear Model Predictive Path-Following Control of a Laboratory Tower Crane, *IEEE Transactions on the Control Systems Technology Journal*, Volume 22 (Issue 4): 1461-1473, July 2014.
- [11] Dongkyoung Chwa, Real Nonlinear Tracking Control of 3-D Overhead Cranes Against the Initial Swing Angle and the Variation of Payload Weight, *IEEE Transactions on the Control Systems Technology Journal*, Volume 17 (Issue 4): 876-883, July 2009.
- [12] Thein Moe Win, Tim Hesketh, and Ray Eaton. SimMechanics Visualization of Experimental Model Overhead Crane, Its Linearization And Reference Tracking-LQR Control, *AIRCC International Journal of Chaos, Control, Modeling and Simulation (IJCCMS)*, Volume 2 (Issue 3):1-16, September 2013.
- [13] G. F. Franklin and J.D. Powell, Feedback Control of Dynamics Systems, (Prentice Hall, 2002, Chapter 7: State-Space Design
- [14] J.Han, Active Disturbance Rejection Control, *IEEE Transactions on Industrial Eletronics*, Volume 56 (Issue 3), 900-906, August 2006
- [15] Magdi S. Mahmoud and Yuanqing Xia, Applied Control System Design, Chapter 7: (7.8: Integral Control and Robust Tracking) Springer, 2012, pg: 440-446
- [16] G. F. Franklin and J.D. Powell, Feedback Control of Dynamics Systems, (Prentice Hall, 2002, Chapter 9: Control System Design.
- [17] Richard M. Murray, Optimization-Based Control, Control and Dynamical Systems, (California Institute of Technology Press, 2010, Chapter 5: Kalman Filtering).
- [18] G. F. Franklin and J.D. Powell, Feedback Control of Dynamics Systems, (Prentice Hall, 1991, Chapter 3: Basic Principles of Feedback.
- [19] Harris, T.J. and Yu, W, Controller assessment for a class of nonlinear systems, *ELSEVIER Journal of Process Control*, Volume 17 (Issue 7): 607-619, August 2007.
- [20] K. J. Astrom and P. Eykhoff , System Identification-Survey, *Automatica Journal, Volume 7* (Issue 1): pp. 123-162, January 1971
- [21] Lennart Ljung and Qinghua Zhang, An integrated System Identification tool- box for linear and non-linear models, *IFAC Symposium on System Identification, Vol. 1, No. 3, pp. 1-9*, Newcastle, Australia, June 2007
- [22] Lennart Ljung, System Identification , Theory for the User, (Prentice Hall, 1999, 2nd Edition, Chapter 17)
- [23] Lennart Ljung and Qinghua Zhang, System Identification Toolbox 7 User's Guide MATLAB SIMULINK, (The MathWorks USA, 2008)
- [24] Zulkeflee, S.A. & Aziz, N., Nonlinear Autoregressive with Exogenous Inputs Based Model Predictive Control for Batch Citronellyl Laurate Esterification Reactor, *INTECHOPEN Journal, Volume 1* (Issue 13): 268-290, June. 2011.
- [25] Heikki Koivo , Adaptive Neuro-Fuzzy Inference System ,(ANFIS, 2000, Japan)
- [26] Ivan Taufer and Oldrich Drabek, Identification of nonlinear systems based on mathematical – physical analysis and least square method, *Acta Montanistica Slovaca Conference, Volume 8* (Issue 4): 188-190, Nov 2003
- [27] Ailane Abdellah, Aitelmahjoub Abdelhafid, Rachik Mostafa, Combining Sliding Mode and Linear Quadratic Regulator to Control the Inverted Pendulum, *International Review on Automatic Control (IREACO)*, Volume 6 (Issue 1): 69-76, February 2013.
[http://www.praiseworthyprize.org/jsm/index.php?journal=ireaco&page=article&op=view&path\[\]](http://www.praiseworthyprize.org/jsm/index.php?journal=ireaco&page=article&op=view&path[])=11286
- [28] Quanser (2010). “3 Degrees of Freedom Tower Crane User Manual”, Quanser Ltd. (Quanser User Manual)
- [29] Inteco (2010). “Tower Crane Control User Manual”, Inteco Ltd. (Inteco User Manual, Version 1.4.)
- [30] H.M. Omar, A.H. Nayfeh. Anti-swing control of gantry and tower cranes using fuzzy and time-delayed feedback with friction compensation, *Shock and Vibration Journal of Hindawi*, Volume 12 (Issue 2): 73-89, March 2005.

Authors' information

¹Thein Moe WIN

School of Electrical Engineering & Telecommunication, University of New South Wales, Sydney, Australia.
(e-mail: t.win@student.unsw.edu.au)

²Timothy HESKETH

School of Electrical Engineering & Telecommunication, University of New South Wales, Sydney, Australia.
(e-mail: t.hesketh@exemail.com.au)

³Raymond EATON

School of Electrical Engineering & Telecommunication, University of New South Wales, Sydney, Australia.
(e-mail: r.eaton@unsw.edu.au)



Thein Moe Win studied third year Mechanical Engineering degree at Yangon Institute of Technology (YIT), Yangon, Myanmar (Burma), in 1996. He received the B.Sc.(Hons) and M.Sc. (Hons) degrees with a major in Mechatronics engineering from International Islamic University Malaysia (IIUM), Kuala Lumpur, Malaysia, in 2003 and 2007, respectively. He had worked as a Project Engineer at ControleZ Technology (subsidiary of SIEMENS Automation and Drive), 2003-2004. He was a Tutor at IIUM between (2000-2007) before holding full time Lecturer position at the Department of Mechatronics Engineering, The University of Selangor (UNISEL), Kuala Lumpur, Malaysia, 2007-2009. He is also a Bronze Medal award winner Malaysia National Research Symposium for his outstanding MSc. Research project. He also received Ph.D. merit scholarship from The Islamic Development Bank (I.D.B) and currently he is working toward the Ph.D. degree in the School of Electrical and Telecommunication System and Control Group, The University of New South Wales, Sydney, Australia. He had published some research articles and journals in regards to RFID, Fuzzy Control, Simmechanics-Visualized Modeling, and LQR control. His research work on "Tower Crane Modeling and Swing Minimization" has earned the best Award at IEEE-iToF 2015 Modelling-Simulation Competition. His research interests include Nonlinear and Linear Modeling, Simmechanics Visualization, Linear and nonlinear Control, Robotics, and Automation. He is also a Graduate student Member of IEEE.



Tim Hesketh received the B.Sc.(Hons) and M.Sc. degrees in Electrical Engineering from Cape Town University in 1969 and 1971, respectively, and the Ph.D. degree from Massey University, New Zealand. He had worked as Systems Engineer and Senior Lecturer in various places and universities, 1971-1987. He also held Visiting Fellow and Visiting Professor positions during 1983-1992. He has been with the School of Electrical and Telecommunication Engineering, The University of New South Wales, Sydney, Australia, since 1987, and head of School of Electrical and Telecommunication Engineering, UNSW, 2006-2009. He is currently a Conjoint Associate Professor (System and Control). His teaching areas are; Control Theory, Robust Control, Adaptive Control, Non-linear systems, Applications of Control, and Computer Control and Real-Time Systems. His research interests include Computer Aided Design and Real Time Control, Control Algorithms, Control Applications, Industrial Consulting. He has published many research articles and journals. He is also a Committee Member of IEAust, Process Control Society.



Raymond Eaton received the B.E. and Ph.D. degrees in Electrical Engineering from the University of New South Wales, Sydney, Australia, in 1992 and 2002, respectively. He is a member of the Institute of Electrical and Electronics Engineers. He has been with the School of Electrical and Telecommunication Engineering, The University of New South Wales, Sydney, Australia, since 1993. He was a Director of Academic Studies, 2009-2014, and currently he is Associate Dean (Education) in the Faculty Engineering, The University of New South Wales. His teaching areas are; Control System, Embedded Systems, Real Time Control, and Digital Circuits. His research interests include; Nonlinear and Robust Control, Control of Autonomous Vehicles, Real-time Control Implementation, and Automation for Precision Farming. He has published many research articles and journals in regards to System and Control.

Appendix C

“Construction Tower Crane SimMechanics-Visualized
Modelling Tower Vibration Impact on Payload Swing Analysis and
LQR Swing Control”

Construction Tower Crane SimMechanics-Visualized Modelling, Tower Vibration Impact on Payload Swing Analysis and LQR Swing Control

Thein Moe Win¹, Timothy Hesketh², Raymond Eaton³

Abstract – Fast and accurate positioning and swing minimization of payloads in tower crane operation are challenging as well as conflicting tasks. Minimizing the load swing is primarily limited by the existence of wind disturbance effect triggering higher tower vibration, especially in the high speed course and load is in the end of tower region. In this paper, the authors propose a new modeling scheme for 3D tower crane, analyze wind disturbance affected-tower vibration impact on the load swing and develop LQR swing control. Firstly, SimMechanics-visualized crane model has been developed using actual tower crane Morrow (Liebherr 71EC) datasheet. Secondly, wind disturbance model was designed based on Gawronski approach and applies different wind patterns on the model for vibration impact analysis. Thirdly, improved version of linear least square system identification algorithm using 7 past inputs-outputs data has been developed to create better fit model. And finally, propose a new control scheme for 3D tower crane that consists of a reference point tracking with full state feedback Linear Quadratic Regulator (LQR). The simulations results show the robust controller performs well in minimizing the load swing due to wind-affected tower vibration and high speed region. Copyright © 2014 Praise Worthy PrizeS.r.l.
- All rights reserved.

Keywords: Visualization, Tower Crane Modelling, Vibration, Wind, LQR Swing Control

Nomenclature

HSE	Health and Safety Executive
AutoCAD	Autodesk Computer-Aided Design
SimMechanics	Set of block libraries with mechanical modeling and simulation tools for use with Simulink
RMSE	Root Mean Square Error
LLS	Linear Least Square

I. Introduction

Large and tall Tower cranes are widely used for the heavy loads transfer.

The crane operates hoist up-down motion, trolley forward-backward motion and flat-top rotation causes certain amount of load swing. Due to the large-standing operating crane (see Fig. 1(a)).wind disturbance would strike the crane time to time which causes crane vibration and affect unstable load swing. If this happen, crane operator runs the trolley back-and-forth manually in order to gradually minimize the swing. Depending on the swing fluctuation, it takes sometimes for skilled-operator to bring the load into stability, as in [1]. However, if the operator cannot minimize the load swing properly, the crane might collapse and environmental safety is at risk (see Fig. 1(b)).



Fig. 1(a). Large Standing-tall Tower Crane



Fig. 1(b). Tower Crane Accident

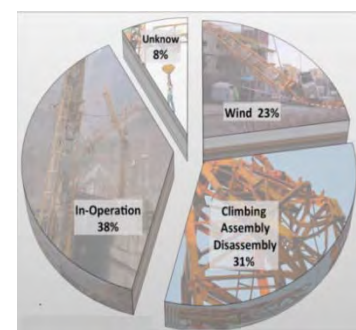


Fig. 1(c). Tower Crane Incidents World statistic

Tower Crane Incidents World statistic by HSE shows 23% of crane accidents are due to wind disturbance, as in [2], (see Fig. 1(c)).

Since it is difficult to draw wind-affected crane vibration data from the operating crane, researchers make assumptions base on the lab-scale model or mathematical sketch which do not represent actual “kinematic, dynamic, and measurements” issues. Therefore, most of the proposed controllers become impractical and impossible to minimize the load swing due to wind-affected vibration.

In order to accumulate vibration from the actual crane and develop controller for the load swing, it is essential to develop a crane model which represents actual crane’s “kinematic, dynamic, and measurements”. Therefore, this research aims to build a computer-based model using MORROW Tower Crane (22m-Hub & 45m-Jib Tower) datasheet. Reliable simulation results would then be used to develop the best suitable controller in minimizing the load swing as well as reducing environmental risks.

Visualized-ideal model of tower crane has been developed based on MORROWTOWER (Liebherr 71EC) crane datasheet, as in [3], which includes trolley cart, rail jib, steel cable, load, sensors and actuators, actual mass-moment of inertia-densities, and frictions. This Ideal model is a milestone development for the crane research since wide range of crane research can be done using this model such as, tower rotation, trolley translation, load swing control, and safety issues. It is the landmark for researchers to do real time research without having trouble in dealing with real cranes at working site.

To further analyse the crane vibration, wind disturbance model was designed and applied at separate locations on the crane in order to differentiate system response. After identifying the significant swing changes due to wind-affected vibration, linearize and optimize the models in search of the best fit one. Full state-Feedback Reference Tracking LQR control was then developed to minimize the load swing and reduce environmental disasters.

The simulation results show, the best fit models (Trolley: Denominator 4 Numerator 4, Tower: Denominator 4 Numerator 4, and Load Swing: Denominator 6 Numerator 6) have been achieved and LQR Control could successfully control the system and minimize the load swing within 50 seconds while nonlinear swing continue fluctuating format.

II. SimMechanics-Visualization of Tower Crane

Some researchers came up with free-body diagrams to develop mathematical model and propose controllers based on several assumptions.

For instance in [4], the mathematical model was developed using free body sketch by ignoring interaction forces between the swing and trolley, actual measurements, location of load cable, joint between hub and tower, friction during trolley stop, etc.

In [5], the mathematical model was developed based on labs-scale prototype which has no counter weight, jib tower is only one link, not referring to any specific tower crane mechanisms, and so on. Moreover in [6], the researcher incorporated AutoCAD predesigned model on the SimMechanics platform which plays merely as a graphic display and does not contain actual “Mass, Inertia, and Measurements”.

In order to analyze the wind disturbance effect on tower vibration causing certain impact on the payload swing, there is a real need to have the model which reflects actual crane in terms of detail mechanisms. This research uses SimMechanics-Visualization tool which is a block diagram modeling environment with ability of dynamic multi-body machines simulation, [7].

Furthermore, the SimMechanics uses the standard Newtonian dynamics of forces and torques in motions, [8]. Based on Physical Principles, it allows modeling and simulating mechanical systems with a suite of tools to specify bodies and their mass properties, their possible motions, kinematic constraints, and coordinate systems, and to initiate and measure body motions, [9]-[10].

Since SimMechanics offers that the industrial proved features and reliable simulation results, this research designs tower crane model which consists of hub, trolley cart, jib tower, steel cable, counterweight, and payload in SimMechanics platform using actual crane factors (Liebherr 71EC Morrow). The features include; Hub-22.2 m, Counter Jib-10.3 m, Tower Jib extension-27.6 m and detail designs are cussed below.

And, each property of the crane model has been encompassed with necessary mass, motions, kinematic constraints, coordinates, and measurements, see Appendix. The visualized-tower crane model runs all three X-Y-Z directions (translation, rotation, and hoist up/down), [10].

II.I. Base Concrete Footing

In order to realize the 3D visualization of the crane, crane structure details, as in [3], such as; measurements, hook and load weight charts, rotation and translation drives info, and component list are referred. For Tower crane base, which consist of four concrete bases, two cross supports and main iron metal sheet, (see Fig. 2).

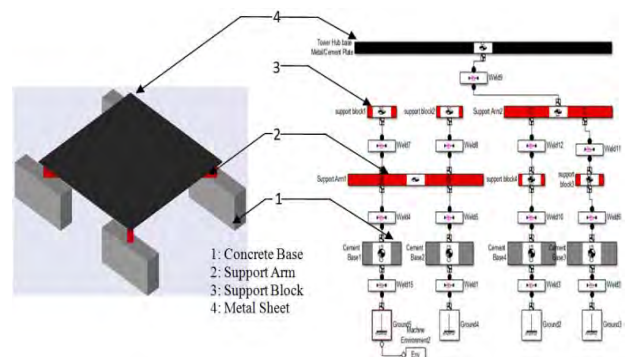


Fig. 2. Base Concrete Footing Visualization and SimMechanics Design

II.2. Base Frame (4-m)

In this base frame 4 m long metal structure consists of right and left metal bars which are connected by top/bottom hub ends as well as zigzag struts to be able to stand strong (see Fig. 3(a)).

Each block in figure contains Mass, 3-D Measurements, and Moment of Inertia based-on Liebherr crane data.

Running this SimMechanics structure would provide graphic visual form. Connecting four sides of the SimMechanics structure becomes a base hub frame (see Fig. 3(b)).

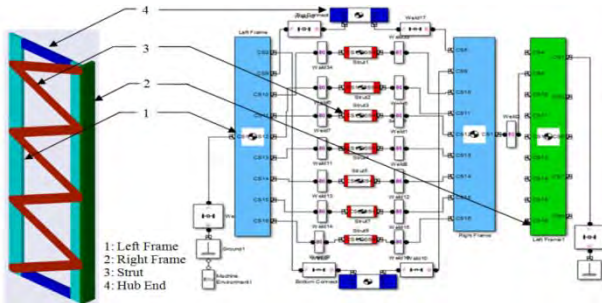


Fig. 3(a). Base Frame 4-m Visualization and SimMechanics Design

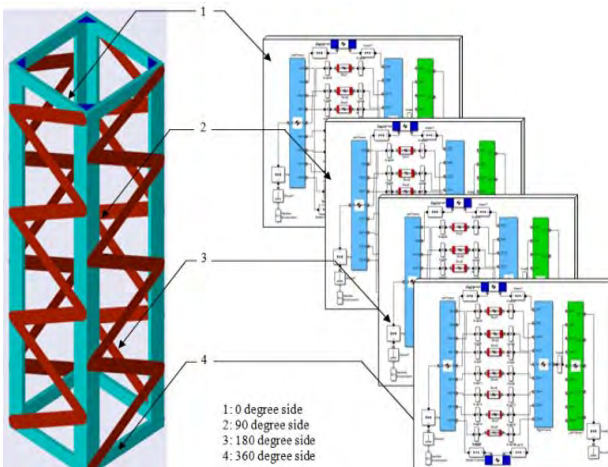


Fig. 3(b). Completed Base Frame Visualization and SimMechanics Design

II.3. Tower Crane 22.2-m(4.2m+12m+6m) tall Hub

As in[3], the crane hub can be up to 41.4 m tall while crane tower jib can be extended up to (10.9 m counter length and 46.58m jib).

However, the crane can also be formed as; smaller design (Hub:22.2m, Tower:29.14m), medium design (Hub:28.2, Tower:34.94m), higher medium design (Hub:34.2, Tower:40.74m), and highest design (Hub:41.4, Tower:46.58m).

In this research, stage1, crane hub 22.2m tall has been established which comprises base frame 4.2 m, base section1-12 m, and base section2-6 m, (see Fig. 4). Details of Mass, Measurements, and Inertia Tensors were assigned according to [3].

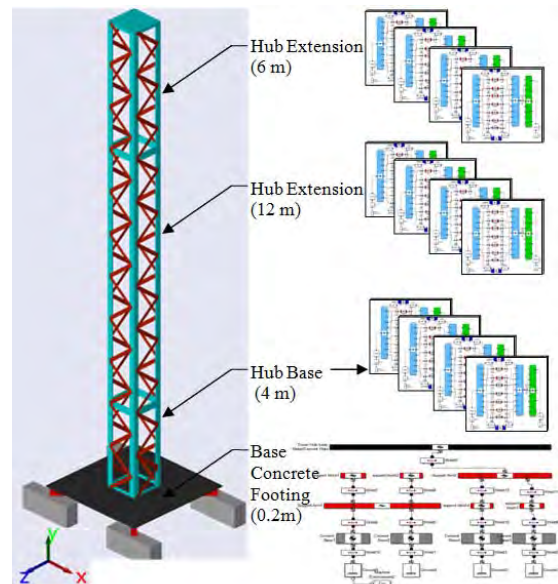


Fig. 4. Completed Crane Hub Visualization, and SimMechanics Design

II.4. Counter-jib and Slew Assembly

Counter Jib plays vital role in stabilizing tower crane operation. According to the moment calculation at pivot (joint between tower and hub), counter load tops were initially added to achieve equilibrium.

Since Libherr Morrow crane uses maximum allowable load of 3000 kg, additional counter load bottoms were attached in order to counter balance the crane. Initial calculation shows, by adding counter load bottoms would produce reasonable jib's vibration. Counter Jib consists of slewing assembly with cabin, counter jib frame with loads top/bottom, adaptors, and Jib right attached, whereas mass, measurements and moment of inertia are assigned, (see Fig. 5(a) and Fig. 5(b)).

II.5. Tower Jib Extension

Tower Jib extension is a combination of two 12m tower sections and Jib tip(2.26-m). The following session would explain the detail structure from one side of 12m tower section to complete design of 12-m tower section followed by the whole 12+12+2.26 m long extension. One side of Tower Jib Extension (12-m)side of tower section 12-m, there are 2 ends, 2 metal frames, and 24 struts, (see Fig. 6).

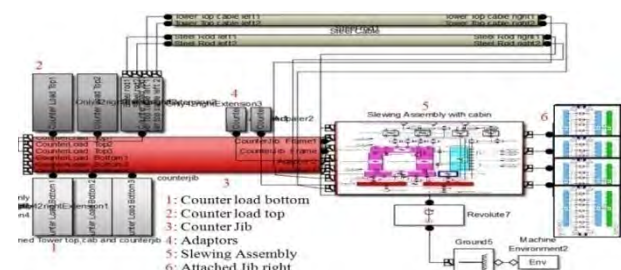


Fig. 5(a). Counter-Jib SimMechanics Design

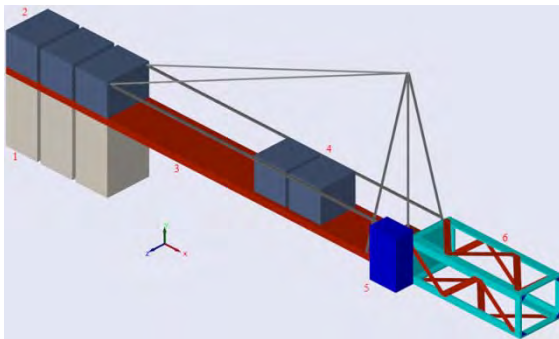


Fig. 5(b). Counter-Jib Visualization

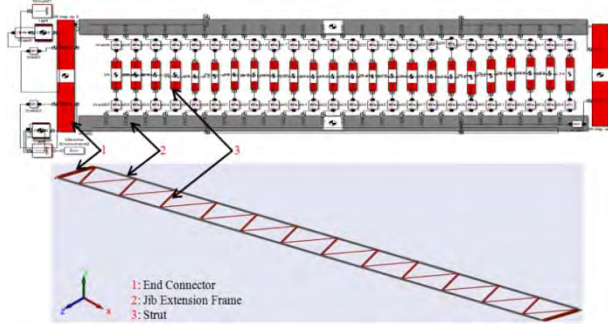


Fig. 6. Tower SimMechanics Design (top) and Visualization (bottom)

Combining the 3 of one side jib extension would appear the triangle tower jib. Each of one side jib is placed at 0 degree, 60 degree and -60 degree, and interconnecting each other to make the jib strong so that it can be able to hold the trolley run and load swing.

The following complete tower jib includes two 12m long jib extensions and 2.31 m long jip tip at the end, (see Fig. 7). After that, trolley rail would be attached right under the complete long jib extension and mount the trolley cart with pendulum attached.

II.6. Trolley Rail-Cart-Attached Payload

Trolley rail-cart-attached load design, there are 4 support rail ends with 24 m long rails attached which are mounted right below the long tower jib.

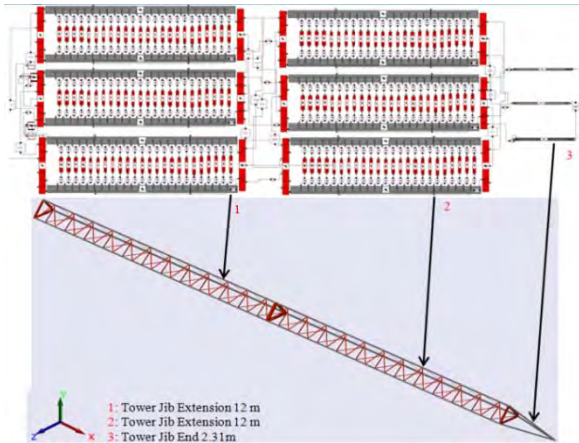


Fig. 7. Tower SimMechanics Design (top) and Visualization (bottom)

On top of the rails, trolley cart ($0.96 \times 0.05 \times 0.3$ measurements and 5 kg weight) has been mounted. Two flexible steel cables with specific moment of inertia were then attached under the trolley cart while the 340 Kg hook was attached at the other end of the cable followed by the load.

The following simmechanics structure (see Fig. 8(a)), is designed base-on real tower crane data and the visualized model, (see Fig. 8(b)), was then obtained upon running the system.

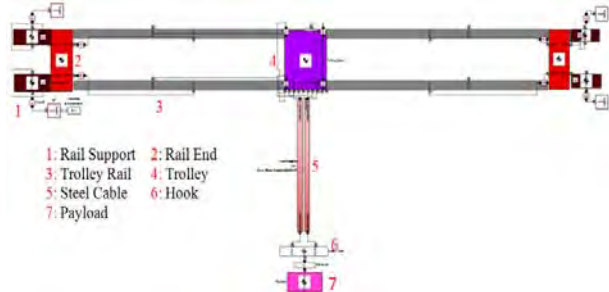


Fig. 8(a). Trolley Rail-Cart-Attached Payload SimMechanic Design

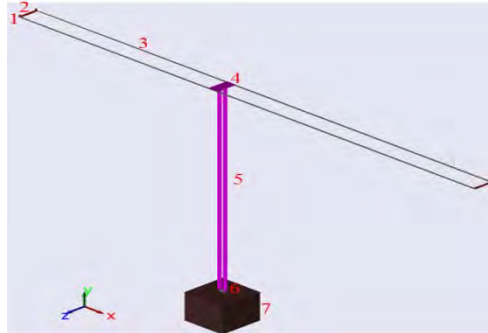


Fig. 8(b). Trolley Rail-Cart-Attached Payload Visualization

II.7. SimMechanics-Visualized View of Tower Crane

From the combination of the above-mentioned simmechanics structures such as; concrete footing, base, hubs, counter jib, slewing assembly, jib extensions, and trolley cart with attached load, the following simmechanics tower crane model has been achieved, (see Fig. 9(a)).

Designing with detail parameters, and applying each part mass/moment of inertia, would produce reliable crane operating data through which suitable controller can be achieved, [11]. Currently, sensors for (trolley position, Tower rotation, Tower vibration, load swing, load position, and Hub top vibration) have been mounted and the details (see Fig. 9(b)).

II.8. Power Drive and Brake for Trolley Translation

As in [3], maximum applicable Power (P) 3kW with angular speed, ω , 14.875 rpm can be used for the crane trolley cart back and forth translational drive while 6.3kW with 0.85 rpm are considered for jib tower rotation.

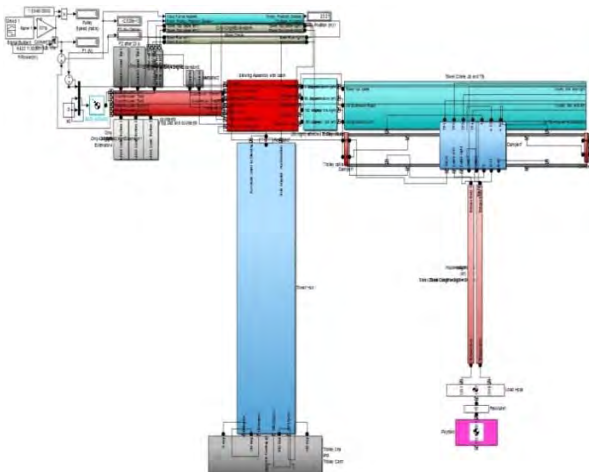


Fig. 9(a). Complete Tower Crane SimMechanic Surface Design

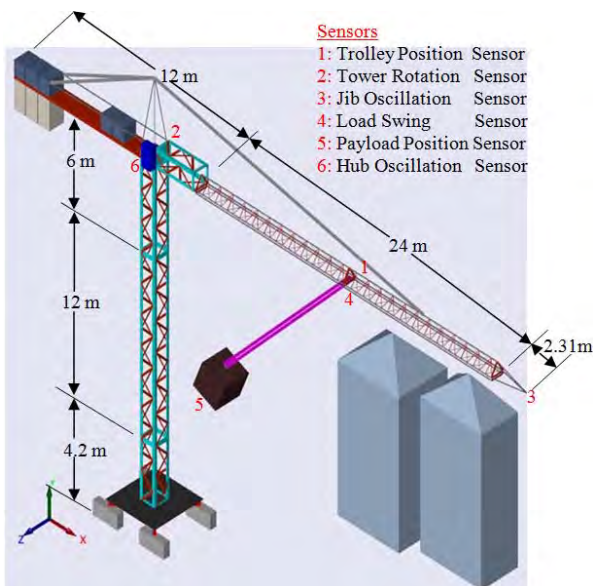


Fig. 9(b). Complete Tower Crane Visualization

Input Power-Speed-driving Force relationship has also been derived, as in (1).

Pulley connected to the driving motor is assumed as 30 cm. Based on input power changes from 1W to 3000W, output applied force, as in (2), drives the trolley translation back and forth.

In real tower crane operation, the operator uses manual joy stick to run the trolley and hold the brake to stop around desired positions.

For this SimMechanics model, the brake is designed from modified damper without spring. Initial parameters such as damping force and desired trolley stop position are required for the brake system to compare instantly and apply the force upon reaching the position.

Two brakes are placed in between trolley and jib rail while friction forces (F) 3N are also applied in trolley's corners, (see Fig. 10). For 20m translational motion, trolley stops around desired location however the positions may elapse due to open loop system without control. For Translation: Pulling Force, F :

$$F = \frac{P}{r \cdot \omega} \quad (1)$$

$$F_1 = P_1 \cdot \frac{F}{P} \quad (2)$$

II.9. Power Drive and Brake for Tower Rotation

For Tower rotation, 0.85 rpm with maximum 6.3 kW for input power, P , is assigned, as in [3]. Therefore, using those data, the following derivation has been carried out to develop Power (P)-Speed (ω)-Torque(τ) relationship, as in (3). Again, driving pulley radius is considered as 50 cm. From provided parameters; 0.85 rpm, maximum Power 6300 W, and assumed pulley radius 50 cm, maximum Force is calculated as 141.573 kN.

By varying input power from 1000W to 6300W, tower rotation speed and applied torque, as in (4), would be changed. For Rotation: rotational torque:

$$\tau = \frac{P}{\omega} \quad (3)$$

$$\tau_1 = P_1 \cdot \frac{\tau}{P} \quad (4)$$

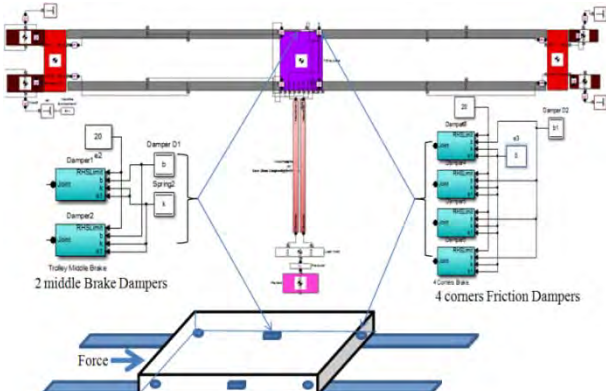


Fig. 10. Power Drive and Brake for Trolley Translation

III. Jib Vibration Impact on Payload Swing Analysis

As a standing tall construction tower crane with only hub support, shouldering counterweight in one side and payload-attached trolley runs on the other side of the jib could eventually cause jib-hub vibration making huge impact on load swing instability. Not only it is difficult to view jib vibration by naked eyes but also hard to do much research work on operating crane.

Therefore, researchers have to rely on small model crane prototype to develop anti-sway control strategies. Ref. [12] envisages that, residual vibration would occur on completion of a trolley traverse due to the operator's manual control, different containers size and load lengths causing more friction and unstable load swing.

In [13], transient sway and residual oscillation appear for certain types of payload and riggings, the payload

mass is comparable to the cable mass, or the mass hangs from a hook without a cable in which the dynamics can become slightly different from a single pendulum due to the effects of inertia.

However, this research has developed SimMechanics model tower crane and sensors have been mounted at specific positions to monitor jib-hub vibration and analyze their impacts on payload swing.

In this jib vibration analysis, manual jib moment calculation, SimMechanics Model trolley translation, and SimMechanics Model tower rotation are tested by applying with and without Wind Disturbance. Simulations results are really fruitful.

III.1. Jib Moment Calculation

Before calculating jib moment at pivot joint a, crane equilibrium was first established by taking the moment at pivot point a, [14]. The reason is to make the crane stand still before adding any payload (see Fig. 11).

Firstly, calculate all required forces, place Force of jib, F_{jib} , along the jib at the point of attached tower top cable (consistent with Morrow crane data), and Force of counter-jib, $F_{counterjib}$, at the end of counter-jib, establish equilibrium, as in (5), and calculate the required Mass of counterweight, $M_{counterweight}$, in (6). Moment at pivot point a is:

$$F_{counterjib} \cdot d_{cj} = F_{jib} \cdot d_j \quad (5)$$

$$M_{counterjib} = \frac{F_{counterjib}}{g} \quad (6)$$

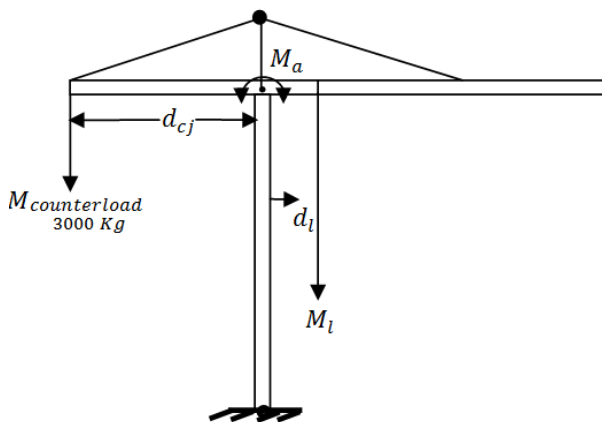


Fig. 11. Free Body Diagram of Tower Crane

Once the equilibrium is established, the next stage is to add maximum applicable payload 3000 kg on the jib and therefore additional 3000 kg counter-load is added to balance the jib stand on top of the hub to avoid crane's collapse.

However, the situations such as; variable trolley speeds, different weight of payloads, and load lengths changes could all add to the jib vibration which can cause more trouble to payload swing.

In this moment of inertia calculation analysis, as in (7), different payloads, M_{load} , (weighing from 1000 kg to 3000 kg) have been used to identify the significant moment changes at pivot point a, (see Fig. 12).

Right side of Tower:

$$M_{jib} = \frac{M_{slewcentre}}{2} + \frac{M_{towertop}}{2} + M_{slewrightextension} + M_{cab} + M_{jib(12m)} + M_{jib(12m)} + M_{jibtip}$$

Left side of Tower:

$$M_{counterjib} = \frac{M_{slewcentre}}{2} + \frac{M_{towertop}}{2} + M_{counterjib} + M_{adapter} + M_{counterweight}$$

$$F_{load} = M_{load} \cdot g \\ M_a = (F_{counterload} \cdot d_{cj}) - (F_{load} \cdot d_l) \quad (7)$$

Moment calculation results show that; 1000Kg payload with 18m load length moves along 24-m jib still provides counter-clockwise (positive direction) jib moment.

However, gradually increasing the payload from 1000 kg to 3000 kg appeared to change counter-clockwise (CCW) to clockwise (CW) direction jib moment and it could make significant impact on the payload swing in reality.

III.2. Wind Disturbance Model Development

Wind impact is one of the major loads affecting buildings and other constructions, among which the most affected is large-standing construction tower crane which can be seriously damaged by wind, resulting in serious collateral damage in its surrounding environments, as in [15].

The destructive irregular wind disturbance would also be the reason for tower vibration causing higher unstable payload swing during the operation.

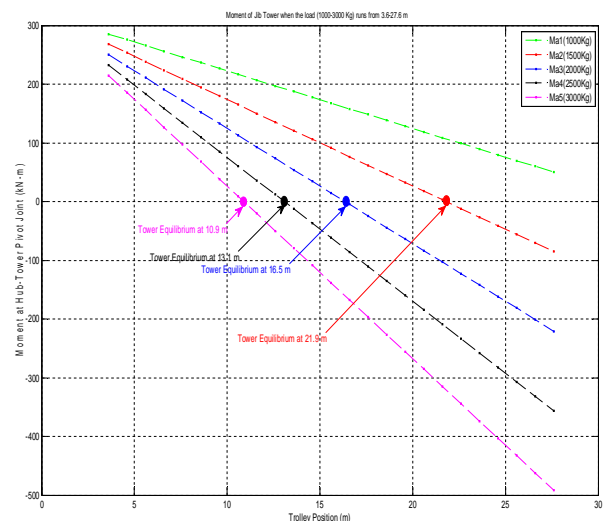


Fig. 12. Moment Changes at Pivot point

In order to design a controller with wind disturbance rejection properties, wind disturbance should be known at the input to the crane model.

Therefore, Gawronski approach, as in [15], proposed a “wind force acting on the dish” model for the large standing tall antenna at 34-m height. However, instead of deriving wind gust speed $\Delta v_0(t)$ through Davenport Spectrum as mentioned in the article, this research considers available input from Sydney Metrological Weather Focus.

Wind load is represented as a combination of static wind(static) and wind gust (variable), as in [16], as in (8):

$$v_t = v_{ws} + v_{wg} \quad (8)$$

III.2.1. Obtaining Wind Static Force From Wind Static Velocity

To obtain Wind-static Force, F_{ws} , quadratic law is applied which relates its velocity and force, as in [15].

The Dragging Force Coefficient, K_{df} , depends on the scaling of air surface terrain. Usually, wind (static), wind (gust) and wind pressure could be obtained from the sensor mounted on the crane.

Currently, those parameters are according to Sydney Metrological Weather Focus and then converted to disturbance wind force and torque. For instance, wind data of 16th April 2014 Sydney weather forecast, [16], provides wind (static) speed, $v_{ws} = 22 \text{ km/h}$, wind (gust) speed, $v_{wg} = 43 \text{ km/h}$, and wind pressure, $P=1017.4 \text{ hPa}$.

By varying wind surface area $A = x \cdot y$, (see Fig. 13), wind (static) Force (F_{ws}), as in (9), and dragging force coefficient (K_{df}), as in (10), can be derived as follow:

$$\begin{aligned} F_{ws} &= P \cdot A \\ F_{ws} &= K_{df} v_{ws}^2 \end{aligned} \quad (9)$$

$$K_{df} = \frac{F_{ws}}{v_{ws}^2} \quad (10)$$

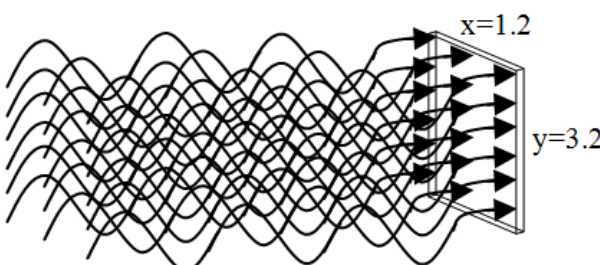


Fig. 13. Wind Disturbance Model

III.2.2. Obtaining Wind Gust Force From Wind Gust Velocity

Wind (gust) Force variation, F_{wg} , is related to wind (gust) velocity variation, Δv , [15]. Using Taylor series, F_{wg} is derived from the derivative of F_{ws} , as in (11):

$$\begin{aligned} F_{wg} &= \left[\frac{\partial F_{ws}}{\partial v} \right]_{v=v_{ws}} = \frac{\partial (K_{df} v_{ws}^2)}{\partial v} \\ F_{wg} &= 2K_{df} v_{ws} \Delta v \end{aligned} \quad (11)$$

According to Gawronski's approach:

$$\Delta v_0 = \frac{\Delta v(t)}{\sigma_v}$$

$$\Delta v(t) = \Delta v_0(t) \cdot \sigma_v$$

where σ_v is the standard deviation of Δv . However, the standard deviation of the wind gust is proportional to the mean wind static speed:

$$\sigma_v = \alpha v_{ws}$$

$$\Delta v = \alpha v_{ws} \Delta v_0, \quad \alpha = \sqrt{6}K$$

$$\Delta v = \sqrt{6K} \cdot v_{ws} \cdot \Delta v_0 \quad \text{where } (\Delta v_0 = v_{wg})$$

$$\Delta v = \sqrt{6K} \cdot v_{ws} \cdot v_{wg}$$

$$K = \frac{1}{\left(2.5 \ln \left(\frac{z}{z_0} \right) \right)^2}$$

where, K is the surface drag coefficient, obtained from the roughness of the terrain. In this equation, z is the distance from the ground to the point where wind force strikes ($z = 22\text{m}$ at hub-tower joint), and z_0 is the height of the terrain roughness.

Terrain roughness can be categorized into four, as in [17], but at this stage it has been assumed as category 1 (i.e. $z_0 = 0.71$). Then, the total wind force, as in (12), could be obtained as follow:

$$\begin{aligned} F_{wg} &= 2K_{df} v_{ws} \cdot \alpha v_{ws} v_{wg} \\ F_t &= F_{ws} + F_{wg} \end{aligned} \quad (12)$$

III.3. Wind Disturbance Affected-Vibration Analysis on Trolley Translation

Wind disturbance pattern would always be irregular time to time due to wind-static, wind-gust, wind-pressure, wind-surface area, wind-strike duration, and terrain-roughness.

In order to analyze jib vibration and its impact on load swing, wind-surface area ($x=1.2\text{m}$, $y = 3.2 \text{ m}$, wind-strike duration (1second-pattern 3-times separate strikes) and terrain-roughness ($z_0=0.71$) have been assumed while the other parameters are variable (see Fig. 14).

In this wind disturbance applied trolley translation case study, both trolley speed and wind play certain roles in producing tower vibration and unstable load swing.

Several different combinations of trolley speed vs load swing have been analyzed.

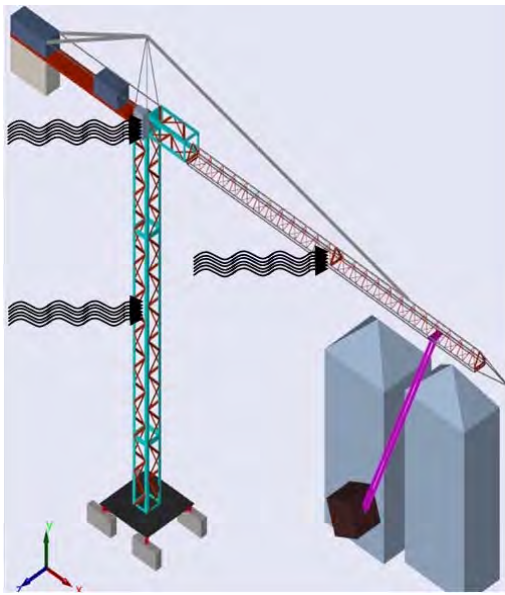


Fig. 14. Wind Disturbance strikes on Tower Crane

However, wind disturbance makes significant impact on vibration and load swing. In the case of (3kW power, 1000 kg load, 18m load length) system, it has been analyzed by “without wind and applied wind (static-gust-pressure: 22-43-1017)”, where swing error is $E=1649.8$, (see Fig. 15(a)) while Jib tip angular acceleration error is $E=1.547e-9$ (see Fig. 15(b)).

In another case of “without wind and applied wind (static-gust-pressure: 41-86-1010)”, where large swing error appeared as $E = 5747.1$, (see Fig. 15(c)), while Jib

tip angular acceleration error is $E=2.408e-9$ (see Fig. 15(d)). Due to changes in wind static-gust-pressure pattern, jib vibration becomes reasonably higher and causes substantial impact on the load swing.

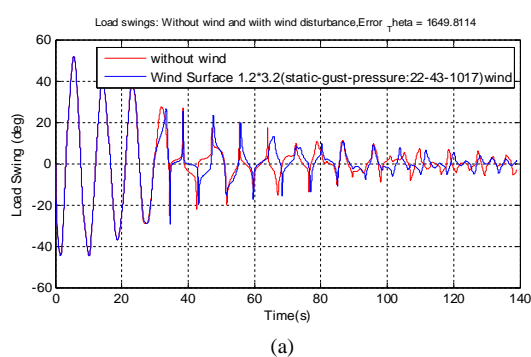
III.4. Wind Disturbance Affected-Vibration Analysis On Tower Rotation

To further analyse the vibration impact on the load swing, Tower rotation with trolley-attached payload has been simulated using different combinations of power input (0~6.3kW) vs load (0~3000 Kg) while applying wind disturbance.

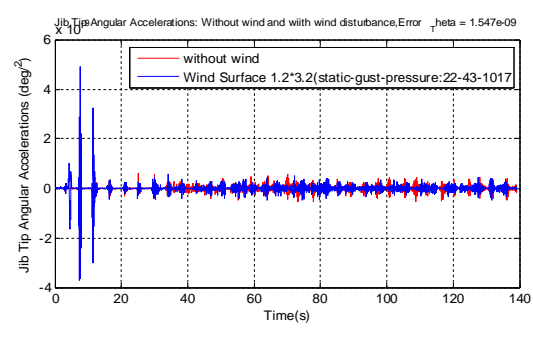
Simulations results show that there are significant load-swing changes due to different wind patterns affecting tower vibration.

For instance, the extreme case of (maximum allowable 6.3kW-power input to tower rotation, maximum allowable 3000 kg-payload, 18m-load length, trolley is stationary at 23m) system applied by wind (static-gust-pressure: 22-43-1017) shows swing output error is $E=2323.7$ (see Fig. 16(a)), while Jib tip angular acceleration error is $E=1.29e-12$ (see Fig. 16(b)), and applied wind (static-gust-pressure: 41-86-1010) shows swing output error is $E=3074.2$ (see Fig. 16(c)), while Jib tip angular acceleration error is $E=2.86e-10$, (see Fig. 16(d)).

Simulation shows that; changes in wind static-gust-pressure on tower rotation turn out to have higher tower vibration which causes large unsettled load swing.

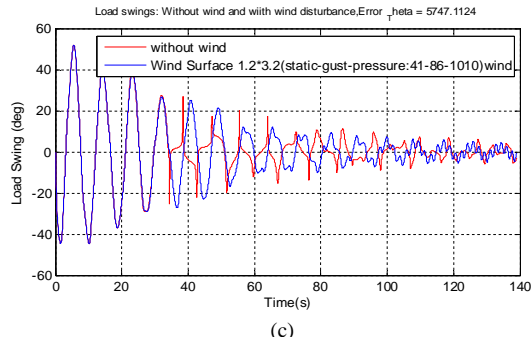


(a)

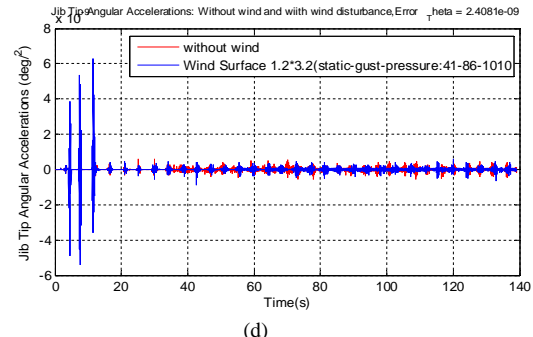


(b)

Figs. 15(a)-(b). Load Swings and Jib Oscillation of without Wind and with Wind Pattern (22-43-017) in Trolley Translation Case

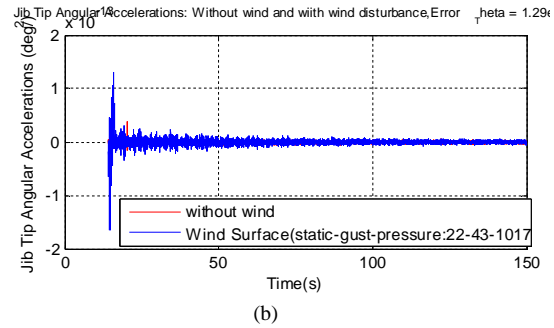
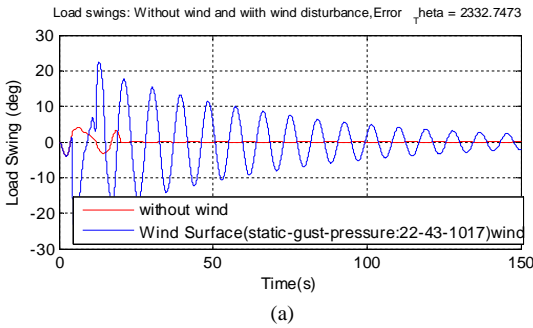


(c)

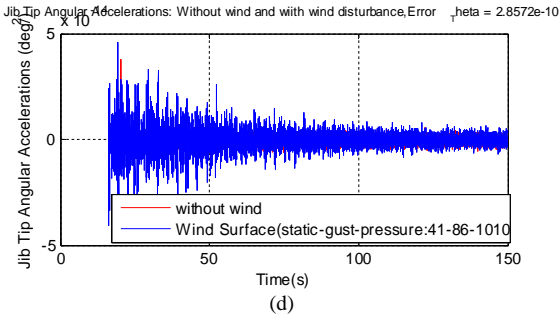
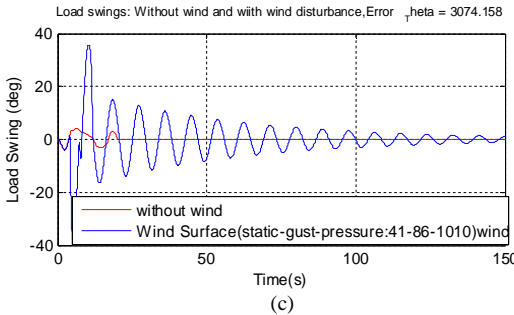


(d)

Figs. 15(c)-(d). Load Swings and Jib Oscillation of without Wind and with Wind Pattern (41-86-1010)in Trolley Translation Case



Figs. 16(a)-(b). Load Swings and Jib Oscillation of without Wind and with Wind Pattern (22-43-017) in Tower Rotation Case



Figs. 16(c)-(d). Load Swings and Jib Oscillation of without Wind and with Wind Pattern (41-86-1010) in Tower Rotation Case

IV. Linearized System Identification and Model Optimization

The SimMechanics-Visualized tower crane model with wind disturbance discussed above is shown as schematic diagram representation in which, the control input is the torque (T) that rotates around Y-axis and the outputs are angular positions of Tower (θ_y) and Load Swing (θ_x).

As a 3D model, both outputs produce X-Y-Z axes values however θ_y for tower and θ_x for load swing are always highest during tower rotation. Necessary interaction forces, F_z , and F_y between the cart and attached payload are also considered to fully model the system's dynamics (see Fig. 17).

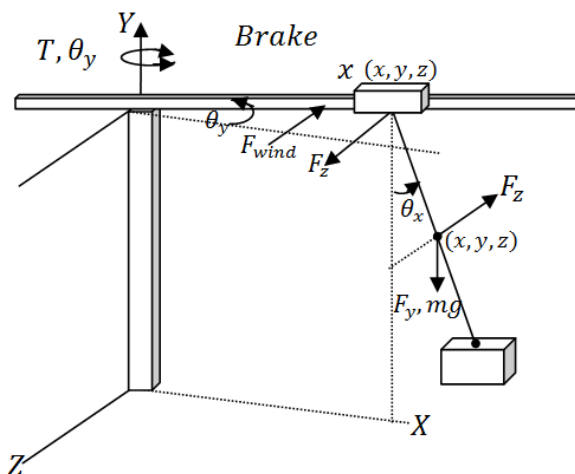


Fig. 17. Wind Disturbance strikes on Tower Crane

Applying Newton's second law of motion ($F=ma$), the differential equations, as in (13) and (14), are generated as follow.

For Tower Rotation θ_y :

$$\sum \tau = I\ddot{\theta}_y = T - (F_{wind} * 1) - (F_z * x) + B\dot{x}_t \quad (13)$$

$$\ddot{\theta}_y = \frac{1}{I} [T - (F_{wind} * 1) - (F_z * x) + B\dot{x}_t]$$

For Load Swing θ_x :

$$\sum \tau = I\ddot{\theta}_x = (F_z * y) + ((F_z + mg) * z) \quad (14)$$

$$\ddot{\theta}_x = \frac{1}{I} [(F_z * x) + ((F_y + mg) * z)]$$

where F_{wind} is wind disturbance, F_z and F_y are interaction forces between trolley and load cable, and B is Brake friction.

IV.I. System Identification By Linear Least Square

Linear least square (LLS) is one useful way to develop linear model from the simulated nonlinear result. Existing LLS uses past consecutive data to compute the states, as in [18].

However this research designs an algorithm which would pick 7 past data randomly in order to maximize the better fit while minimizing the error. By selecting every possible combination of the columns from a large matrix with 7 past inputs and 7 past outputs according to the model needs, the matrix, X , is formed to compute estimated states, as in (15):

$$\begin{bmatrix} y(8) \\ y(9) \\ \vdots \\ y(N) \end{bmatrix} = \begin{bmatrix} \text{Column 1} & \text{Column 2} & \text{Column 8} & \text{Column 9} \\ -y(7) & -y(6) & u(7) & u(6) \\ \vdots & \vdots & \vdots & \vdots \\ -y(7+N) & -y(6+N) & u(7+N) & u(6+N) \end{bmatrix} \theta \quad (15)$$

$$\theta = X^T * Y$$

IV.2. Model Optimization by Fitting

The following algorithm, (see Fig. 18), select every possible pair, compute estimated states, as in (16), compare root-mean-square error (RMSE) for each case, and finally picks up the lowest RMSE-related model, as in [1].

This algorithm generates 21 RMSEs and respective models for the Denominator 2-Numerator 2 (Den2-Num2) case alone, and likewise respective RMSEs for the others (Den3-Num3), (Den4-Num4), (Den5-Num5), (Den6-Num6), (Den3-Num2), (Den2-Num3), (Den3-Num4), (Den4-Num3), (Den2-Num4), and (Den4-Num2):

$$\begin{bmatrix} X_1 \\ X_2 \\ \vdots \\ X_M \end{bmatrix} = \begin{bmatrix} \text{Column 1} & \text{Column 2} & \text{Column 8} & \text{Column 9} \\ 1 & 2 & 8 & 9 \\ 1 & 3 & 8 & 10 \\ \vdots & \vdots & \vdots & \vdots \\ 6 & 7 & 13 & 14 \end{bmatrix}$$

where M is total number of generated models:

$$\theta_1 = X_1^T * Y_1, \theta_2 = X_2^T * Y_2, \theta_3 = X_3^T * Y_3, \dots, \theta_M = X_M^T * Y_M \quad (16)$$

Once the models are generated from the identified states, $\theta_1 \dots \theta_M$, one such common criterion is the minimization of sum of the squared differences between the actual data and the predicted data due to the least squares line.

The error (E), as in (17), where $i = 1, 2, 3, \dots, N$ is the number of data points, and y_{ls} is the approximating curve's predicted y at the point θ_i :

$$E = \sum_{i=1}^N [y_i - y_{ls}(\theta_i)]^2 \quad (17)$$

This algorithm first picks up lowest RMSE of individual case from (Den2-Num2 to Den-6-Num6) then compare again to filter for the best fit model.

In the case of Tower rotation, the following Table, Table I, shows RMSE 16.515 which is lowest in the case of Den6-Num6 however the best fit model appears to be Den4-Num4 with RMSE 4.7876 among the lowest, (see Fig. 19(a)).

Likewise, load swing best fit model appears to be Den6-Num6 with RMSE 7.5094 (see Fig. 19b).

From the generated best fit models of both Den4-Num4, as in (18), and Den6-Num6, as in (19), transfer functions are developed.

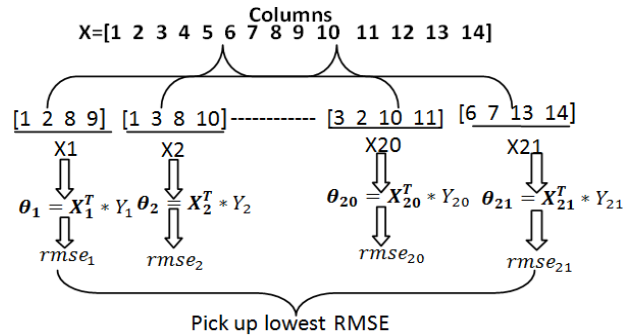


Fig. 18. Improved Version of Linear Least Square Algorithm

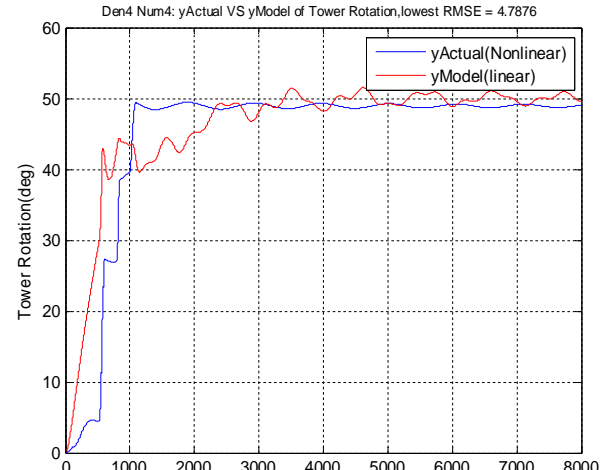


Fig. 19(a). Nonlinear Vs the Best Fit Linear Model Outputs (Tower)

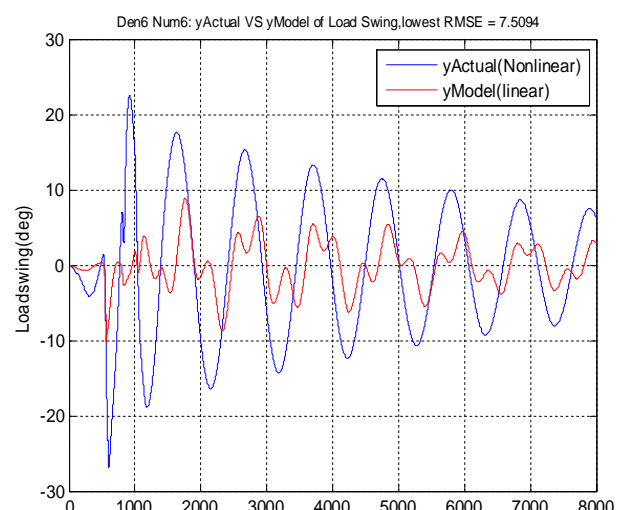


Fig. 19(b). Nonlinear Vs the Best Fit Linear Model Outputs (Swing)

TABLE I
RMSE COMPARISON FOR EACH DEN-NUM PAIR

RMSEs (Tower)	Den	Num
4.7876	4	4
11.878	4	2
12.151	5	5
12.834	4	3
13.89	3	4
13.927	2	4
13.958	2	3
14.877	3	3
15.885	3	2
16.192	2	2
16.515	6	6
7.5094	6	6
7.8129	75	5
7.9132	3	3
7.915	3	2
7.9325	3	4
7.9756	2	4
7.998	2	3
8.0359	2	2
8.2527	4	2
8.3405	4	4
3.3609	4	3

Tower Rotation ~ Torque Model:

$$\frac{\theta_{yt}}{T_t} = \frac{-2.72e^{-9}s^4 + 2.59e^{-7}s^3 - 4.104e^{-6}s^2 + 6.87e^{-6}s^1 - 0.0001304}{s^4 + 31.34s^3 + 588.9s^2 + 109.3s^1 + 1.32} \quad (18)$$

Load Swing ~ Torque Model:

$$\frac{\theta_{xl}}{T_l} = \frac{-2.76e^{-11}s^6 + 1.52e^{-9}s^5 - 1.67e^{-7}s^4 + 3.254e^{-6}s^3 - 1.95e^{-5}s^2 + 0.00025s^1 + 0.000417}{s^6 + 92.1s^5 + 3206s^4 + 3.4e^{04}s^3 + 3.997e^{05}s^2 + 3.44e^{04}s^1 + 4084} \quad (19)$$

where θ_{yt} represents Y-axis tower rotation angle, T_t is tower drive torque, θ_{xl} is X-axis load swing angle, and T_l is load drive torque. Differential equation, as in (20), with input (u) output (y) and state (x), is used to convert the model transfer functions into final state space format, A and B :

$$\ddot{x} + a_1\ddot{x} + a_2\dot{x} + a_3x + a_4x = b_0u \quad (20)$$

$$\begin{aligned} q_1 &= x, q_2 = \dot{q}_1 = \dot{x}, q_3 = \dot{q}_2 = \ddot{x}, \\ q_4 &= \dot{q}_3 = \ddot{x}, \dot{q}_4 = \ddot{x} \end{aligned}$$

so:

$$\dot{q}_4 + a_1q_4 + a_2q_3 + a_3q_2 + a_4q_1 = b_0u$$

then:

$$\dot{q}_4 = -a_1q_4 - a_2q_3 - a_3q_2 - a_4q_1 + b_0u$$

$$\dot{q} = Aq + Bu, y = Cq + Du$$

$$\begin{bmatrix} \dot{q}_4 \\ \dot{q}_3 \\ \dot{q}_2 \\ \dot{q}_1 \end{bmatrix} = \begin{bmatrix} -a_1 & -a_2 & -a_3 & -a_4 \\ 1 & 0 & 0 & 0 \\ 0 & 1 & 0 & 0 \\ 0 & 0 & 1 & 0 \end{bmatrix} \begin{bmatrix} q_4 \\ q_3 \\ q_2 \\ q_1 \end{bmatrix} + \begin{bmatrix} b_0 \\ 0 \\ 0 \\ 0 \end{bmatrix} u$$

State space format for $\frac{\theta_{yt}}{T_t}$:

$$A = \begin{bmatrix} -a_1 & -a_2 & -a_3 & -a_4 \\ 1 & 0 & 0 & 0 \\ 0 & 1 & 0 & 0 \\ 0 & 0 & 1 & 0 \end{bmatrix}, B = \begin{bmatrix} b_0 \\ 0 \\ 0 \\ 0 \end{bmatrix}$$

State space format for $\frac{\theta_{xl}}{T_l}$:

$$q_5 = \theta, q_6 = \dot{q}_5 = \dot{\theta}, q_7 = \dot{q}_6 = \ddot{\theta}, q_8 = \dot{q}_7 = \ddot{\theta},$$

$$q_9 = \dot{q}_8 = \ddot{\theta}, q_{10} = \dot{q}_9 = \ddot{\theta}$$

$$\begin{bmatrix} \dot{q}_{10} \\ \dot{q}_9 \\ \dot{q}_8 \\ \dot{q}_7 \\ \dot{q}_6 \\ \dot{q}_5 \end{bmatrix} = \begin{bmatrix} -a_5 & -a_6 & -a_7 & -a_8 & -a_9 & -a_{10} \\ 1 & 0 & 0 & 0 & 0 & 0 \\ 0 & 1 & 0 & 0 & 0 & 0 \\ 0 & 0 & 1 & 0 & 0 & 0 \\ 0 & 0 & 0 & 1 & 0 & 0 \\ 0 & 0 & 0 & 0 & 1 & 0 \end{bmatrix} \begin{bmatrix} q_{10} \\ q_9 \\ q_8 \\ q_7 \\ q_6 \\ q_5 \end{bmatrix} + \begin{bmatrix} b_1 \\ 0 \\ 0 \\ 0 \\ 0 \\ 0 \end{bmatrix} u$$

By combining for $\frac{\theta_{yt}}{T_t}$, and $\frac{\theta_{xl}}{T_l}$ in Stat Space format, the matrices A and B are:

$$\begin{bmatrix} -a_1 & -a_2 & -a_3 & -a_4 & 0 & 0 & 0 & 0 & 0 & 0 \\ 1 & 0 & 0 & 0 & 0 & 0 & 0 & 0 & 0 & 0 \\ 0 & 1 & 0 & 0 & 0 & 0 & 0 & 0 & 0 & 0 \\ 0 & 0 & 1 & 0 & 0 & 0 & 0 & 0 & 0 & 0 \\ 0 & 0 & 0 & 0 & -a_5 & -a_6 & -a_7 & -a_8 & -a_9 & -a_{10} \\ 0 & 0 & 0 & 0 & 1 & 0 & 0 & 0 & 0 & 0 \\ 0 & 0 & 0 & 0 & 0 & 1 & 0 & 0 & 0 & 0 \\ 0 & 0 & 0 & 0 & 0 & 0 & 1 & 0 & 0 & 0 \\ 0 & 0 & 0 & 0 & 0 & 0 & 0 & 1 & 0 & 0 \\ 0 & 0 & 0 & 0 & 0 & 0 & 0 & 0 & 1 & 0 \end{bmatrix}, \begin{bmatrix} b_0 \\ b_1 \end{bmatrix}$$

V. LQR Full State Feedback Controller with Reference Tracking

In [12], researchers propose a full-order friction disturbance observer with sensor-delay correction for a lab scale 1D overhead crane prototype to eliminate swing caused by vibration-affected nonlinear friction. Though nonlinear friction is considered due to vibration, the analysis of vibration was not discussed. Time Delay Filtering method for cancelling vibration has also been proposed, as in [13]. Likewise, Ref. [19] considered vibration in rotary crane system (which is similar to tower jib rotation) and proposed three-layered neural network Generic Algorithm (GA-based) training controller. In this research, Linear quadratic regulation (LQR) method ([23], [24]) (see Fig. 20), is applied for the tower crane model aiming to achieve robust control in minimizing the load swing. The plant is written in the state space form, $\dot{x} = Ax + Bu$, and the optimal feedback gain (K) is implemented as $u = -K(x - x_{desired})$, as in [20].

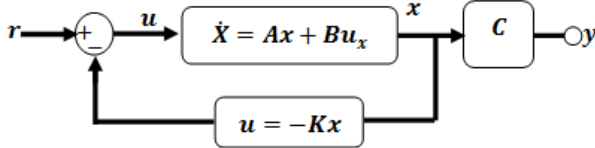


Fig. 20. LQR Controller Design

V.I. Q,R Weighting Matrices and Cost Function J

Respective Q and R weighting matrices plays vital role in stabilizing control effort between input (u) and error (deviation from 0). The element in the (4, 4) position of Q represents the weight on the tower rotation angle position and the element in the (10, 10) position of Q represents the weight on the pendulum's angle. In order to achieve robust control, it has been put more weights on the states Q matrix as; $x = 1$, and $\theta = 1$ while input $R=0.00001$.

The following cost function J , as in (21), is considered to define the trade-off between regulation performance and control effort of the states; tower rotation angular position θ_{yt} , and the pendulum's angle, θ_{xl} . In the following matrix Riccati Equation as in (22), in which P is the steady state solution that yields a unique optimal control to minimize the cost function (J) and compute the optimal feedback gain, K , as in (23), as in [20]:

$$J = \int_0^\infty [\theta_{yt}^T Q_{\theta_{yt}} \theta_{yt} + \theta_{xl}^T Q_{\theta_{xl}} \theta_{xl} + u^T R u] dt \quad (21)$$

$$\dot{P} = A^T P - PA - C^T C + PBR^{-1}B^T P \quad (22)$$

$$K = R^{-1}B^T P \quad (23)$$

V.2. Full State Feedback Reference Point Tracking

Ref. [21] applies sliding mode control (SMC)-LQR control strategy on called Inverted pendulum with and without disturbances. Since wind disturbance effect on tower vibration impact creates higher unstable load swing, this research designs reference input tracking with full state feedback-LQR control approach (see Fig. 21), is implemented to achieve the desired input while bringing the swing under control. However, adding the reference (r) to the system, $u = -Kx + r$, would lead to steady state errors, as in [1], and therefore, pre-compensation \bar{N} is multiplied as follow, as in (24):

$$u = -Kx + (\bar{N} * r) \quad (24)$$

Full-state feedback would regulate steady-state output y_{ss} to desired steady-state value, r_{ss} . In this trolley cart X directional motion, to track a constant desired position, x_{ss} (ss: steady-state) with control, u_{ss} , the control equation is:

$$0 = Ax_{ss} + Bu_{ss}, y_{ss} = Cx_{ss} + Du_{ss}$$

By substituting $x_{ss} = N_x r_{ss}$, and $u_{ss} = N_u r_{ss}$:

$$0 = AN_x r_{ss} + BN_u r_{ss}, y_{ss} = CN_x r_{ss} + DN_u r_{ss}$$

when $y_{ss} = r_{ss}$ in the steady-state:

$$0 = AN_x r_{ss} + BN_u r_{ss}, r_{ss} = CN_x r_{ss} + DN_u r_{ss}$$

The above equations can be formed as state-space:

$$\begin{bmatrix} 0 \\ 1 \end{bmatrix} r_{ss} = \begin{bmatrix} A & B \\ C & D \end{bmatrix} \begin{bmatrix} N_x \\ N_u \end{bmatrix} r_{ss}$$

$$\begin{bmatrix} N_x \\ N_u \end{bmatrix} = \begin{bmatrix} A & B \\ C & D \end{bmatrix}^{-1} \begin{bmatrix} 0 \\ 1 \end{bmatrix}$$

and finally, pre-compensation \bar{N} can be formed, as in (25):

$$\bar{N} = N_u + K N_x \quad (25)$$

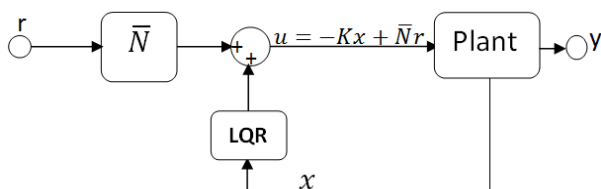


Fig. 21. LQR Full State Feedback Controller Design

V.3. Tower Crane Rotation and LQR Swing Control

For the particular 6300W input tower drive with payload 3000 kg system; Tower vibration impact due to wind effect causing longer unsettled load swing has also been discussed above.

LQR implementation with Q and R weighting matrices brings both tower rotation and load swing under control. Since the system still needs to track the desired reference, full state feedback is then implemented.

The simulation results show, desired reference tower rotation smoothly achieves within 50 seconds, (see Fig. 22(a)), while payload swing up to maximum 5 degree with no fluctuation and bring back to 0 degree in 40 seconds time (see Fig. 22(b)).

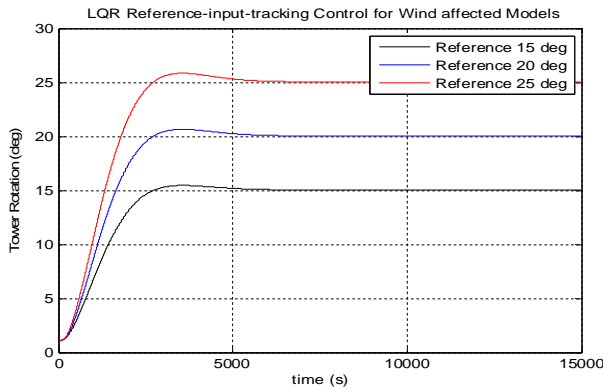


Fig. 22(a). LQR Full State Feedback Control for Tower Rotation

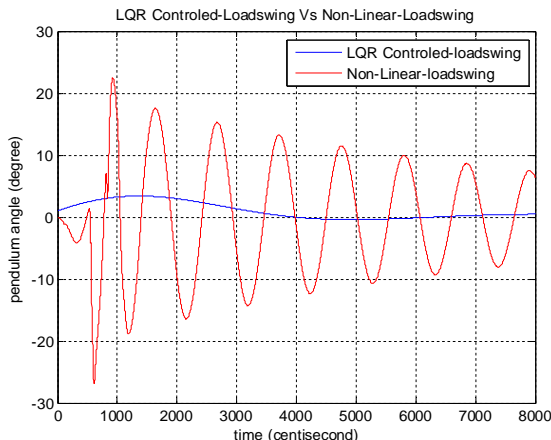


Fig. 22(b). LQR Full State Feedback Controlled Load Swing VS Nonlinear Load Swing

V.4. Simulations and Results Comparison with PID

This section contains performance evaluations of the proposed LQR Full state feedback strategy and results from the SimMechanics-Visualized tower crane model introduced in Section II.

In addition, robustness investigations and a comparison with simple Proportional-Integral-Derivative (PID) Control are carried out. LQR full state feedback applies ($Q_{\theta_{yt}} = 1, Q_{\theta_{xl}} = 1, R = 0.00001$) for states and input weighting values while simple PID, (see Fig. 23), needs larger parameters ($P = -60000, I = -700, D = 500000$) to stabilize the system. In tower rotation, LQR smoothly brings the tower to desired angular position and reaches to stability in less than 50 seconds while PID uses large gains yet there are fluctuations and overshoots (see Fig. 24(a)). It is very much crucial to have steady tower rotation with very low load swing in every operation.

Again, LQR controlled-load swing appeared to have just one overshoot reaching maximum 3 degree before gradually goes to zero while PID controlled-response has continuous swings (see Fig. 24b). Therefore, the proposed LQR full state feedback controller proves to be reliable.

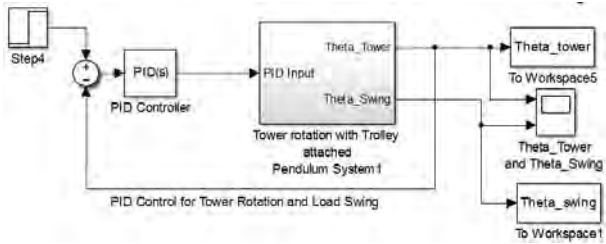
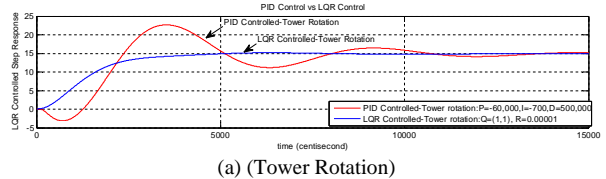
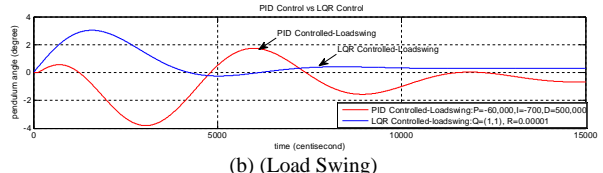


Fig. 23. Simple PID Controller Design



(a) (Tower Rotation)



(b) (Load Swing)

Figs. 24. LQR VS PID Controlled Outputs Comparison

VI. Conclusion

In short, 3D Tower Crane SimMechanics-Visualized model based on real crane (Morrow:Liebherr71EC) was presented. Initial moment calculation shows jib tower has moments at the pivot (shoulder point between hub and jib). Different combination of input drives and payloads were then tested in both trolley translation and tower

rotation operations. The simulations show there are tower vibrations and load swings fluctuating up to certain extents.

Since standing tall large tower crane would normally face windy weather, wind disturbance model was designed using Gawronski approach. Wind pattern is initially assumed as; surface area ($x=1.2m^*y=3.2m$) with 1 second wind strike while wind (static), win(gusts), and wind pressure parameters are drawn from Sydney metrological focus data. Applying wind disturbance on the trolley translation and tower rotation, simulations show that tower vibrations as well as load swings appeared to become much higher than the outputs without wind. To identify the linearized system and optimize the better fit, improved version of linear least square approach with 7 past inputs-outputs data has been developed.

In each trolley translation and tower rotation cases, the proposed LQR full state feedback controller aims at minimizing the load swing due to wind disturbance affected-tower vibration. Results from simulations of the developed SimMechanics-Visualized model are promising, and emphasize the usefulness of the proposed research. Robustness investigations underline the validity of the proposed model and control approach. The comparison with PID reveals the advantages of the LQR. Current work is dedicated to the tower crane model development, wind affected-vibration impact on load swing analysis , and swing minimization using LQR full state feedback control scheme.

Appendix

Mass-Measurement-Inertia Tensors for the crane parts are.

Mass, Measurements and Inertia Tensors of Tower Jib 12+12+2.31m Parts =							
	Mass (Kg)	x (m)	y (m)	z (m)	Ixx (Nm)	Iyy (Nm)	Izz (Nm)
Rail_End	100.00000	2.00000	1.00000	0.50000	10.41667	35.41667	41.66667
Jib_Rail	2.00000	0.20000	0.20000	5.37901	4.82000	4.82000	0.01333
Strut	2.00000	0.20000	0.20000	0.01333	0.01333	0.01333	0.01333
Jib_Tip_Righ	2.00000	4.00000	0.05000	4.00500	2.67375	5.34000	2.66700
Slewing_Cent	2584.00000	1.00000	0.50000	1.00000	269.16667	430.66667	269.16667
Slewing_Exte	40.66670	1.20000	0.05000	1.20000	4.88000	9.76001	4.88000
Slewing_Exte	40.66670	1.20000	0.17000	0.05000	0.10641	4.88448	4.97794
Slewing_Asse	2.00000	0.05000	0.17000	1.10000	0.20658	0.20208	0.00523
Slewing_Exte	40.66670	0.05000	1.20000	1.20000	9.76001	4.88000	4.88000
Tower_Top	4.14286	8.10000	0.05000	0.05000	0.00173	8.98051	8.98051
Counter_jbs	4070.00000	10.30000	0.02000	1.20000	501.96667	36470.59167	35995.75833
Adaptor	1872.50000	0.80000	1.00000	0.10000	312.03333	282.43542	282.43542
Counter_Load	596.33330	0.30000	1.00000	1.20000	121.25444	111.81249	89.94694
Counter_Load	1000.00000	0.90000	2.00000	1.20000	453.59333	187.50000	400.63533
Steel_Rod	4.14286	8.30000	0.05000	0.05000	0.00173	23.78431	23.78431
Tower_Top_Ca	10.00000	8.30000	0.05000	0.05000	0.00417	57.41042	57.41042
Rail_support	4.14286	0.10000	0.01500	0.12000	0.00505	0.00842	0.00353
rail_end	15.00000	0.97000	0.02500	0.05000	0.00391	1.17925	1.17691
rail_right	327.94930	24.05000	0.05000	0.05000	0.13696	15785.36172	15785.36172
Trolley	5.00000	0.50000	0.01000	0.97000	0.39206	0.49621	0.10421
Steel_Cable	5.00000	0.50000	0.01000	0.97000	0.35000	0.135.00000	0.135.00000
Hook	340.00000	0.30000	0.15000	0.05000	0.70853	2.62093	3.18750
Load	3000.00000	2.00000	2.00000	2.00000	8000.00000	8000.00000	8000.00000
Left_Frame	396.49090	0.20000	4.00000	0.05000	528.62792	1.40395	529.86670
Right_Frame	213.45100	0.05000	4.00000	0.15000	285.00155	0.44469	284.86580
Strut	3.16000	1.45000	0.07500	0.05000	0.00148	0.55366	0.55514
Hub_end	15.00000	0.80000	0.15000	0.05000	0.03125	0.80313	0.82813
Left_Frame	196.35200	0.20000	6.00000	0.05000	589.09691	0.69541	589.71051
Right_Frame	105.72800	0.05000	6.00000	0.15000	317.59224	0.22027	317.20603
Strut	3.16000	1.45000	0.07500	0.00050	0.00148	0.55366	0.55514
Hub_end	15.00000	0.80000	0.15000	0.05000	0.03125	0.80313	0.82813
Left_Frame	203.33330	1.20000	0.05000	1.20000	24.40042	45.79999	24.40042
Right_Frame	87.63800	0.20000	3.20000	0.05000	74.63198	0.30968	79.90522
Strut	47.08200	0.05000	3.20000	0.15000	40.26492	0.09809	40.18645
Hub_end	3.16000	1.45000	0.07500	0.00050	0.00148	0.55366	0.55514
Hub_Plat	15.00000	0.80000	0.15000	0.05000	0.03125	0.80313	0.82813
Left_Frame	15.00000	0.97000	0.02500	0.05000	0.00391	1.17925	1.17691
Right_Frame	163.74670	12.00000	0.05000	0.05000	0.06823	1964.99451	1964.99451
Strut	3.16000	1.05000	0.02500	0.00050	0.00016	0.29033	0.29049
Hub_end	41.66670	2.31000	0.05000	0.05000	0.01736	18.53682	18.53682

Acknowledgements

SimMechanics-Visualized Tower Crane Model is developed based on MORROW (Liebherr 71EC) datasheet and has been approved by MORROW Tower Crane (NSW, Australia).

References

- [1] Thein Moe Win, Tim Hesketh, and Ray Eaton. SimMechanics Visualization of Experimental Model Overhead Crane, Its Linearization And Reference Tracking-LQR Control, *AIRCC International Journal of Chaos, Control, Modeling and Simulation (IJCCMS)*, Volume 2(Issue 3):1-16, September 2013.
- [2] Health and Safety Executive (HSE), Tower Crane Incidents Worldwide, (Crown Press, 2010, pp. 1-62).
- [3] Liebherr 71 EC Tower Crane datasheet, Morrow Equipment, USA, www.morrow.com. (MORROW, 2009, pp. 1-6)
- [4] H.M. Omar, A.H. Nayfeh. Anti-swing control of gantry and tower cranes using fuzzy and time-delayed feedback with friction compensation, *Shock and Vibration Journal of Hindawi*, Volume 12 (Issue 2): 73-89, March 2005.
- [5] Martin Böck, Andreas Kugi. Real-time Nonlinear ModelPredictive Path-Following Control of a Laboratory Tower Crane, *IEEE Transaction on Control System Technology Journal*, Volume 22 (Issue 4): 1461-1473, July 2014.
- [6] M. Al-Hussein, M. A. Niaz, H Yu, H Kim. Integrating 3D visualization and simulation for tower crane operations on construction sites, *ELSEVIER Journal of Automation in Construction*, Volume 15(Issue 1):554-561, January 2006.
- [7] Getting Started with SimMechanics User Guide.<http://au.mathworks.com/help/physmod/sm/gs/product-description.html> (Accessed 15 February 2012).
- [8] Sahan S. HinidumaUdugamaGamage and Patrick R. Palmer. Hybrid System Modeling, simulation and visualization; A crane system, Geo-Spatial and Temporal Image and Data Exploitation III Proceedings of (SPIE), Volume 5097(Issue 3):1-10, July 2003. University of Cambridge, UK.
- [9] Raul G. Longoria. Modeling of Mechanical System for Mechatronics Applications (CRC Press 2002, chap. 9).
- [10] Schlotter Michael. Multi Body System Simulation with SimMechanics, *Dynamic Seminar*. pp. 1-23, May 2003.
- [11] ViliamFedák, FrantišekDúrovský and Robert Uveges. Analysis of Robotic System Motion in SimMechanics and MATLAB GUI Environment, *INTECH Open Science Journal of MATLAB Applications for the Practical Engineer*, Volume 1 (Chapter 20):565-581, August 2014.
- [12] H. Sano, K. Sato, K Ohishi, and T. Miyazaki. Robust Design of Vibration Suppression Control System for Crane Using Say Angle Observer Considering Friction Disturbance, *Electrical Engineering Conference in Japan*, Vol. 184, No. 3, pp. 36-46, Nagoya, Japan, Jan. 2013.
- [13] G. Pelaez, J. Doval-Gandoy, N. Caparrini, and J.C.Garcia-Prada. The Time Delay filtering Method for cancelling vibration overhead transportation systems modeled as a physical pendulum, Spain, *Shock and Vibration Journal of IOS Press*. Volume 14 (Issue 1): 53-64, February. 2007.
- [14] Mechanical Engineering, Carlos III University, Transportation and Crane, Madrid, Spain, 2008. <http://www.euni.de/tools/jobpopup.php?lang=en&option=showJob&jobid=137260&jobtyp=5&jtyp=0&university=Universidad+C+arlos+III+de+Madrid&country=ES&sid=5093&name=Course%3+A+Transport+Engineering>.
- [15] W. Gawronski. Wind Disturbance Models, Modeling and Control of Antennas and Telescopes (Springer, 2008, pp. 51-70)
- [16] Sydney Weather Forecast, WeatherZone, <http://www.weatherzone.com.au/nsw/sydney/sydney>
- [17] Tracy Gowen, Peter Karantonis, and Tony Rofail. Converting Bureau of Meteorology Wind Speed and Data to Local Wind Speeds at 1.5-m above Ground Level, *ACOUSTICS Conference*, Vol. 1, pp. 57-62, Gold Coast, Australia, November 2004.

- [18] Ilse C. F. Ipsen, Numerical Matrix Analysis(Philadelphia Society for Industrial and Applied Mathematics, 2009, pp. 43-76).
- [19] K. Nakano, K. Ohishi, H. Kinjo, and T. Yamamoto.Vibration control of load for rotary crane system using neural network with GA-based training.*International Conference on Artificial Life and Robotics (ISAROB)*, Vol. 3, pp.98-101, Oita, Japan, February 2008
- [20] Martin J. Corless and Arthur E. Frazho, Linear Systems and Control (CRC Press, 2003, chap. 12).
- [21] Abdellah, A., Abdelhafid, A., Mostafa, R., Combining sliding mode and linear quadratic regulator to control the inverted pendulum, (2013) *International Review of Automatic Control (IREACO)*, 6 (1), pp. 69-76.
- [22] Moutchou, M., Abbou, A., Mahmoudi, H., Induction machine speed and flux control, using vector-sliding mode control, with rotor resistance adaptation, (2012) *International Review of Automatic Control (IREACO)*, 5 (6), pp. 804-814.
- [23] Muhammad, M., Buyamin, S., Ahmad, M.N., Nawawi, S.W., Ibrahim, Z., Velocity tracking control of a Two-Wheeled Inverted Pendulum robot: A comparative assessment between partial feedback linearization and LQR control schemes, (2012) *International Review on Modelling and Simulations (IREMOS)*, 5 (2), pp. 1038-1048.
- [24] El Majdoub, K., Ouadi, H., Touati, A., LQR control for semi-active quarter vehicle suspension with magnetorheological damper and bouc-wen model, (2014) *International Review on Modelling and Simulations (IREMOS)*, 7 (4), pp. 703-711.

Authors' information

¹School of Electrical Engineering & Telecommunication, University of New South Wales, Sydney, Australia.
E-mail: t.win@student.unsw.edu.au

²School of Electrical Engineering & Telecommunication, University of New South Wales, Sydney, Australia.
E-mail: t.hesketh@exemail.com.au

³School of Electrical Engineering & Telecommunication, University of New South Wales, Sydney, Australia.
E-mail: r.eaton@unsw.edu.au



Thein Moe Win studied 1st-3rd year Mechanical Engineering degree at Yangon Institute of Technology (YIT), Yangon, Myanmar (Burma), in 1995-96. He received the B.Sc.(Hons) and M.Sc.(Hons) degrees with a major in Mechatronics engineering from the International Islamic University Malaysia (IIUM), Kuala Lumpur, Malaysia, in 2003 and 2007, respectively. He had worked as a Project Engineer at ControleZ Technology (subsidiary of SIEMENS Automation and Drive), 2003-2004. He held Lecturer position at the Department of Mechatronics Engineering, The University of Selangor (UNISEL), Kuala Lumpur, Malaysia, in 2007-2009. He also received Ph.D. merit scholarship from The Islamic Development Bank (I.D.B) and currently he is working toward the Ph.D. degree in the School of Electrical and Telecommunication System and Control Group, The University of New South Wales, Sydney, Australia. He had published some research articles and journals in regards to RFID, Fuzzy Control, and SimMechanics-Visualized Modeling. His research interests include Nonlinear and Linear Modeling, SimMechanics-Visualization, Linear and nonlinear Control, Robotics, and Automation. He is also a Graduate student Member of IEEE.

Appendix D

“SimMechanics Visualization of
Experimental Model Overhead Crane, Its Linearization And
Reference Tracking-LQR Control”

SIMMECHANICS VISUALIZATION OF EXPERIMENTAL MODEL OVERHEAD CRANE, ITS LINEARIZATION AND REFERENCE TRACKING-LQR CONTROL

Thein Moe Win¹ Tim Hesketh² Ray Eaton³

School of Electrical Engineering & Telecommunication
The University of New South Wales, High St, Kensington, NSW 2052, Australia

ABSTRACT

Overhead Crane experimental model using Simmechanic Visualization is presented for the robust antisway LQR control. First, 1D translational motion of overhead crane is designed with exact lab model measurements and features. Second, linear least square system identification with 7 past inputs/outputs is applied on collected simulation data to produce more predicted models. Third, minimize root mean square error and identified the best fit model with lowest RMSE. Finally, Linear Quadratic Regulator (LQR) and Reference tracking with pre-compensator have been implemented to minimize load swing and perform fast track on trolley positioning.

KEYWORDS

Simmechanic Visualization, linear least square system identification, Linear Quadratic Regulator (LQR), Reference tracking with pre-compensator, Overhead Crane.

1. INTRODUCTION

In modern industrial system, shipyard, warehouse, and construction, tower cranes are widely used for the heavy loads transfer. The crane operates hoist up-down motion, trolley forward-backward motion, and flat-top rotation causing unexpected load swing. In those working aspects, transferring load at a shorter time, perfect safety with no load swing or damage, and low operational cost are the main concerns. The cranes use open loop system to control position while anti-swing control is done manually by skilled operators using joysticks with analog control, [6]. Since, skilled operator always needs to focus on the operational trajectory map back and forth to carry the load, it creates fatigue problem and eventually affect the whole operation. Higher running costs, operational delay, and environmental damages have to be taken into account. Therefore, minimizing the load swing with proper control action during operation would be essential to avoid several risks. Even though researchers worldwide have been proposing many forms of anisway approaches, yet using manual joy stick with human operators are inevitable.

2. PROBLEM STATEMENT

Conducting live research on the real operating crane on site is usually impossible and therefore, most of the researches derived mathematically assumed crane model for simulations purpose. Furthermore, to simplify the crane modeling, assumptions were sometimes taken on the factors such as; (frictions, noises and disturbances, actuators, and sensors, etc.). Linearization also plays vital role in getting better accurate model however considering certain range of small load swing angle to be zero would have impact on linear approximation of the model and subsequently the controller design.

Therefore in this research, having a reliable model to represent real crane is the initial focus followed by linearization and suitable controller development. Experimental model visualization of the crane system has been developed based on real crane parts/parameters, which include trolley cart, rail jib, steel cable, load, sensors and actuators, actual mass-moment of inertia-densities, and frictions. Visual appearance of this crane design would not only feature the real crane but also be flexible enough to assemble parts and assign real time parameters. It is the landmark for researchers to do real time research without having trouble in dealing with real cranes on site. The raw data collected from model simulation are used by linear least square approach to maximize better approximation model for further LQR with reference tracking. In order to compare the performances, normal mathematical model derivation is first developed in the following session.

3. FREE BODY DIAGRAM OF 2D X-MOTION

Simple free body diagram, Fig (1), below is developed to represent 2D crane model. A trolley cart is mounted on a jib (rail) along x direction, [9]. Trolley cart mass (M), payload mass (m), and load length (l) are assigned certain values while (θ) is considered load swing angle in XY plane. For 2 dimensional (2D) simple motion, payload length is initially considered unchanged and frictionless between trolley and jib. Since certain amount of applied force F pushes trolley to move along X direction, large swing angle θ appears which needs to be minimized to as small as possible. In order to get mathematical model of the crane, kinetic energy, potential energy, Lagrange equation are derived to form equations of motions (nonlinear).

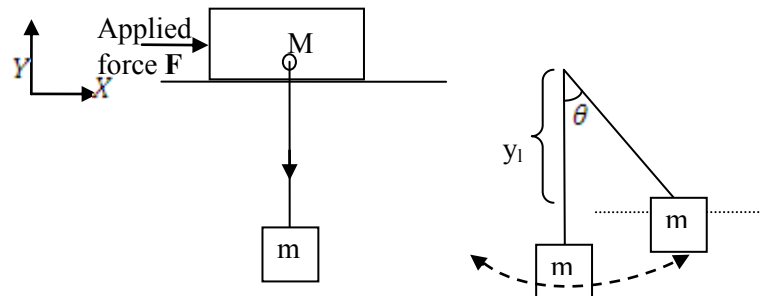


Figure (1): Simple 1D free body diagram

3.1 Mathematical Modeling of Trolley cart and load swing

From free body diagram of the system, nonlinear equations, Equ.(1) and Equ.(2), have been derived as follow;

$$\ddot{x}_t = \frac{1}{(M+m)} [F - ml(\ddot{\theta} \cos \theta - \dot{\theta}^2 \sin \theta) - b\dot{x}] \quad (1)$$

$$\ddot{\theta} = \frac{1}{(I+ml^2)} [ml(\ddot{x}_t \cos \theta + g \sin \theta) - c\dot{\theta}] \quad (2)$$

3.2 Linearization using simple assumption

Several assumptions such as; ($\sin \theta \approx 0, \cos \theta \approx 1$ (OR) $\sin \theta = \tan \theta = \theta, \cos \theta = 1$ ect.) have been made from nonlinear model by the researchers in the past to linearize nonlinear equations of crane model. Even though that assumption makes a model simpler, the linearized model could not be close enough to actual crane model, [5]. In this research, at equilibrium point of load swing, both θ and $\dot{\theta}$ are considered as small and assumed as $\sin \theta \approx \theta, \cos \theta \approx 1$, and $\dot{\theta}\theta \approx 0$, [12]. Using these approximations, the mathematical model

linearized around the unstable equilibrium point of load swing has been obtained, Equ.(3) and Equ.(4). Final linerized equations and state-space form of the overhead crane free body diagram are;

$$\dot{x}_2 = -\frac{(I-ml^2)b}{J}x_2 - \frac{m^2l^2g}{J}x_3 + \frac{mlc}{J}x_4 + \frac{(I-ml^2)}{J}F \quad (3)$$

$$\dot{x}_4 = -\frac{mlb}{K}x_2 + \frac{(M+m)mlg}{K}x_3 - \frac{(M+m)c}{K}x_4 + \frac{ml}{K}F \quad (4)$$

Linearized State Space model is; $\dot{x} = Ax + Bu$, $y = Cx + Du$

$$\begin{bmatrix} \dot{x}_1 \\ \dot{x}_2 \\ \dot{x}_3 \\ \dot{x}_4 \end{bmatrix} = \begin{bmatrix} 0 & 1 & 0 & 0 \\ 0 & -\frac{(I-ml^2)b}{J} & -\frac{m^2l^2g}{J} & \frac{mlc}{J} \\ 0 & 0 & 0 & 1 \\ 0 & -\frac{mlb}{K} & \frac{(M+m)mlg}{K} & -\frac{(M+m)c}{K} \end{bmatrix} \begin{bmatrix} x_1 \\ x_2 \\ x_3 \\ x_4 \end{bmatrix} + \begin{bmatrix} \frac{(I-ml^2)}{J} \\ 0 \\ 0 \\ \frac{ml}{K} \end{bmatrix} u, y \\ = \begin{bmatrix} 1 & 0 & 0 & 0 \\ 0 & 0 & 1 & 0 \end{bmatrix} \begin{bmatrix} \dot{x}_1 \\ \dot{x}_2 \\ \dot{x}_3 \\ \dot{x}_4 \end{bmatrix}$$

4. SIMMECHANIC VISUALIZATION OF OVERHEAD CRANE

This simmechanic-based experimental model is based on Physical Modeling blocks which represents physical components, geometric, and kinematic relationships directly. This is not only more intuitive, it also saves the time and effort to derive the equations of motion. In this research, simple 2D Overhead crane mechanical model is designed using MATLAB Simmechanic visualization. First of all, 5 meter long jib bar frame was mounted above the ground using two fixed revolute joints. Trolley cart with certain measurement has been mounted on top of jib frame,[4],[8]. At this stage, low friction prismatic joint is considered in order to minimize constraints. A steel cable type body with payload was attached to the trolley using revolute joint,[11],[13]. Certain measurements were assigned to appear 2D crane model, Fig (2). Signal builder produces applied force (step input signal) which actuates the trolley cart, Fig (2), for X-directional motion.

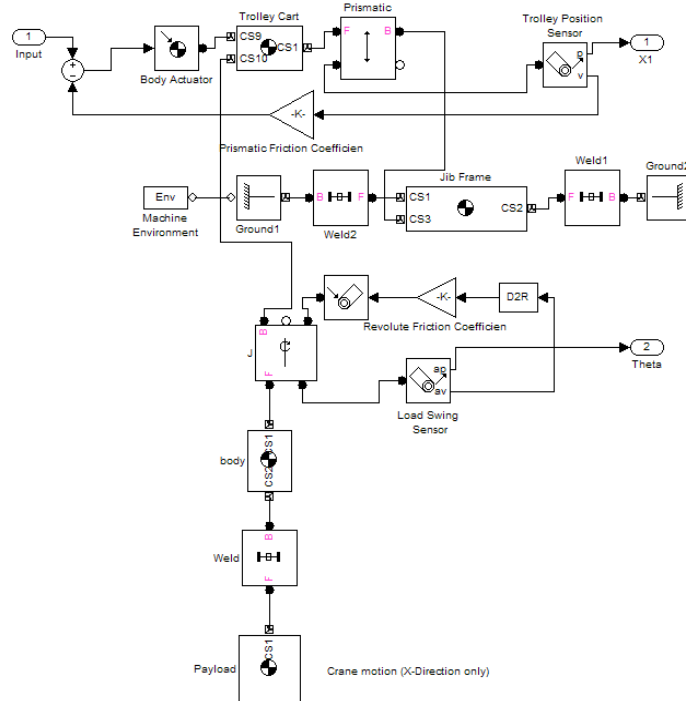


Figure (2,a): Mechanical Visualization of Overhead Crane

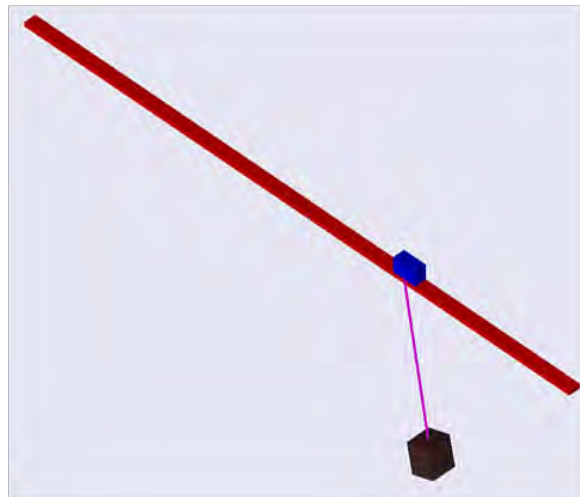


Figure (2,b): Mechanical Visualization of Overhead Crane

5. LINERIZATION OF 2D OVERHEAD CRANE USING LEAST SQUARE APPROACH

To linerize the model, adaptive perturbation approach with “linmod” command is used in Matlab simulink. That command will search equilibrium point (operating point) of the system where the net force is zero. Then, it generates linear time-invariant (LTI) state-space models. However, a simple step of creating model using “linmod” command without the details would make difficulty in analyzing the model. Therefore, instead of direct linearizing by MatLab, the mathematical model would be developed from collected dataset. The following steps have taken; model the input signal, collect the data set, and determine denominator/numerators using Least Square System Identification.

5.1 Modelling Input Signals Design

For x, y, and z motions, the system uses 3 different motors and therefore, different input designs have to be performed. Initially, other higher frequencies were tested but since, the frequency content of the input too high, the system does not have enough time to respond to changes in the input. In results, the response produced averaging effect. In current x-directional motion simulation, pseudo-random binary signal (PRBS) with 10 Hz sampling frequency and [1,-1] upper-lower bounds was designed, Fig (3). By varying the input signal and adjust longer pulse, it will enhance the statistics of the data, optimize the effectiveness of system identification as well as have visual respond to each input state.

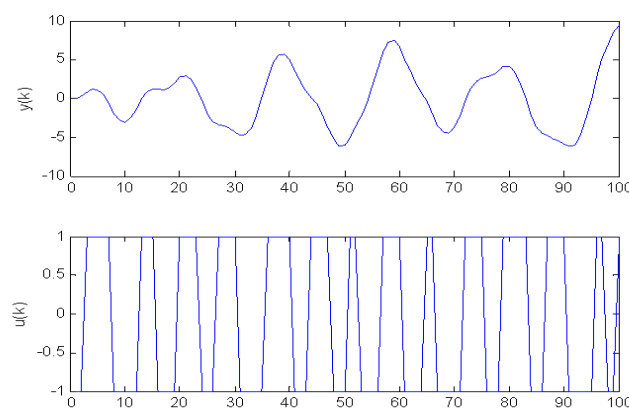


Figure (3): Input Signal at Frequency 10, range -1 to 1

5.2 Linear Least Square System Identification

Once the input/outputs dataset is collected, Least Square System Identification is applied to determine the number of parameters required for the system transfer function and find those parameters (b_1, b_2, \dots, b_m and a_1, a_2, \dots, a_n), Equ.(5), [1].

$$\Delta y(k) = \frac{b_1 z^{-1} + b_2 z^{-2} + \dots + b_m z^{-m}}{1 + a_1 z^{-1} + a_2 z^{-2} + \dots + a_n z^{-n}} \Delta u(k) \quad (5)$$

The output of the system represents the linear combination of past inputs and outputs, where, $\theta_1, \dots, \theta_m, \theta_{m+1}, \dots, \theta_{m+n}$ are the states of the system, Equ.(6), [1].

$$y(k) = -\theta_1 y(k-1) - \dots - \theta_m y(k-m) + \theta_{m+1} u(k-1) + \dots + \theta_{m+n} u(k-n) \quad (6)$$

$$y \begin{bmatrix} y(k) \\ y(k+1) \\ \vdots \\ y(k+N) \end{bmatrix} = \begin{bmatrix} -y(k-1) & \dots & -y(k-m) & u(k-1) & \dots & u(k-n) \\ -y(k) & \dots & -y(k-m+1) & u(k) & \dots & u(k-n+1) \\ \vdots & \ddots & \vdots & \vdots & \ddots & \vdots \\ -y(k-1+N) & \dots & -y(k-m+N) & u(k-1+N) & \dots & u(k-1+N) \end{bmatrix} \begin{bmatrix} \theta_1 \\ \vdots \\ \theta_m \\ \theta_{m+1} \\ \vdots \\ \theta_{m+n} \end{bmatrix}$$

$$y(k) = [-y(k-1) \ \dots \ -y(k-m) \ u(k-1) \ \dots \ u(k-n)]$$

$$y(k) = X\theta \quad (X \text{ is } m \times n \text{ with } m > n) \quad (7)$$

5.3 Denominator and Numerator Coefficients consideration

To compute 2 Denominator and 2 Numerator Coefficients, least square approach uses two simultaneous past inputs/outputs data to form X Matrix and therefore the following matrix would be formed, [10].

$$\begin{bmatrix} y(3) \\ y(4) \\ \vdots \\ y(100) \end{bmatrix} = \begin{bmatrix} -y(2) & -y(1) & u(2) & u(1) \\ -y(3) & -y(2) & u(3) & u(2) \\ \vdots & \vdots & \vdots & \vdots \\ -y(99) & -y(98) & u(99) & u(98) \end{bmatrix} \theta$$

5.4 Training and Checking Model

Initially, the collected dataset is divided into two parts, training and checking, Fig(4). The reason is, the developed model from the training part would be tested against checking output in order to verify how well the model matches. In this system, first half training dataset, y_{tr}, u_{tr} and X_{tr} have been developed to calculate Denominator and Numerator Coefficients, θ and produce Model Transfer Function.

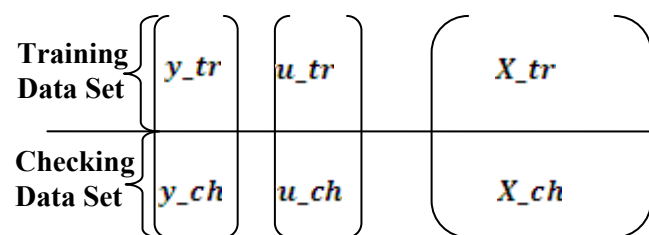


Figure (4): Training and Checking Data separation

Considering 2 Denominator and 2 Numerator Coefficients case, X_{tr} Matrix is identified and θ is computed using Equ.(7). The coefficients are estimated $\theta = x_{est} = [a_1, a_2, b_1, b_2]$ to form the following Model Transfer Function, [2].

$$X_{tr}^T * y_{tr} = (X_{tr}^T * X_{tr}) * x_{est}$$

$$x_{est} = [X_{tr}^T * X_{tr}]^{-1} * X_{tr}^T * y_{tr}$$

$$y_{Model_tr} = \frac{b_1 q^{-1} + b_2 q^{-2}}{1 + a_1 q^{-1} + a_2 q^{-2}}$$

5.5 Root Mean Square Error Calculation

Root-mean-square error (RMSE) is used to measure the differences between estimated values by the developed model, and actual outputs such as; y_{Model_tr} VS y_{tr} and y_{Model_ch} VS y_{ch} . Minimizing RMSE could produce better fit of the model and enhance approximation. RMSE is calculated in the following form, Fig(5);

Least Square General Form, [3]:

$$\|Ax - y\| = \left(\sum_{i=1}^m \left(\sum_{j=1}^n a_{ij} x_j - y_i \right)^2 \right)^{1/2} \quad (8)$$

$$\|X * x_{est} - y_{tr}\| = \|y_{Model_tr} - y_{tr}\| = \text{norm}(y_{tr} - y_{Model_tr})$$

$$RMSE = \frac{\text{norm}(y_{tr} - y_{Model_tr})}{\sqrt{\text{length of } (y_{tr})}} \quad (9)$$

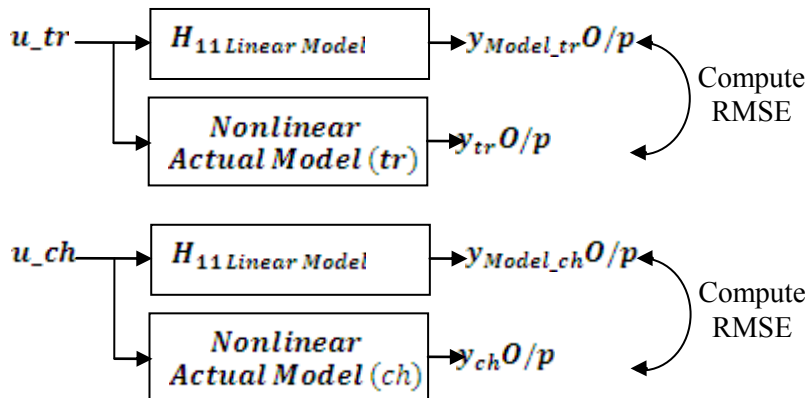


Figure (5): RMSE Comparison between actual and predicted models

Using Least Square System Identification; Den2Num2, Den3Num3, Den4Num4, Den2Num3, Den3Num2, Den4Num3, and Den3Num4 models are computed then followed by their respective RMSE. After comparing all RMSEs, lowest RMSE and its respective model would be picked up as the best linearly approximated model of the system. The following table shows, each model adjustment and calculated RMSE for both Training and Checking parts. Least Square System Identification with past consecutive inputs-outputs, Table (1);

Table(1): Least Square System Identification

Den	Num	Data Start from	Past data start from
2	2	y_3	$[-y2 \ -y1 \ u2 \ u1]$
3	3	y_4	$[-y3 \ -y2 \ -y1 \ u3 \ u2 \ u1]$
4	4	y_5	$[-y4 \ -y3 \ -y2 \ -y1 \ u4 \ u3 \ u2 \ u1]$
2	3	y_4	$[-y3 \ -y2 \ 0 \ u3 \ u2 \ u1]$
3	2	y_4	$[-y3 \ -y2 \ -y1 \ u3 \ u2 \ 0]$
4	3	y_5	$[-y4 \ -y3 \ -y2 \ -y1 \ u4 \ u3 \ u2 \ 0]$
3	4	y_5	$[-y4 \ -y3 \ -y2 \ 0 \ u4 \ u3 \ u2 \ u1]$

Since 1D overhead crane has Trolley cart's translational motion and load's swing angle outputs, the Least Square calculation produce two models for Trolley and load swing while each model has training RMSE and checking RMSE. After generating all RMSEs, lowest RMSE would be picked up from Trolley model and load swing model considering the best linear approximation. The following Table (2.a) and Table (3.a) show each computed RMSE(Training), RMSE(Checking), as well as its total RMSE for models (22,33,44,23,32,43,34) while Table (2.b) and Table (3.b) show lowest to highest computed RMSE in which Den 2 Num 2 model appears to have lowest RMSE not only in Trolley model but also in Load Swing model.

TrolleyCartRMSEDenNum				
RMSEs(Tr)	RMSEs(Ch)	RMSE	Den	Num
0.12645	0.13602	0.13123	2	2
0.09208	0.098917	0.095499	3	3
0.12587	0.13558	0.13073	2	3
0.12461	0.13458	0.12959	3	2
0.093626	0.098796	0.096211	4	3
0.092217	0.099155	0.095686	3	4
1.574e+008	1.6271e+008	NaN	4	4

Table(2.a): RMSE(Training) and RMSE(Checking) for Trolley

RMSEs(Trolley)	Den	Num
0.095499	3	3
0.095686	3	4
0.096211	4	3
0.12959	3	2
0.13073	2	3
0.13123	2	2
NaN	4	4

Table(2.b): from lowest to highest RMSE for Trolley Model

LoadSwingRMSEDenNum				
RMSEs(Tr)	RMSEs(Ch)	RMSE	Den	Num
0.82772	2.4455	1.6366	2	2
0.8423	2.4453	1.6438	3	3
0.82772	2.4455	1.6366	2	3
0.82771	2.4455	1.6366	3	2
5.4277	4.2815	4.8546	4	3
9.0589	16.653	12.856	3	4
1.574e+008	1.6271e+008	NaN	4	4

Table(3.a): RMSE(Training) and RMSE (Checking) for Load Swing

RMSEs(LS)	Den	Num
1.6366	3	2
1.6366	2	3
1.6366	2	2
1.6438	3	3
4.8546	4	3
12.856	3	4
NaN	4	4

Table(3.b): from lowest to highest RMSE for Load Swing

Trolley model, Den3 Num3, with lowest RMSE shows how well the linear approximation matches the actual output graph, Fig (6.a) in which, residuals are less than 0.08 and RMSE is only

0.095499. For the load swing model, Den3 Num2, with lowest RMSE produces residuals which are between (-0.4 to 0.4) while its RMSE is only 1.6366, Fig (6.b).

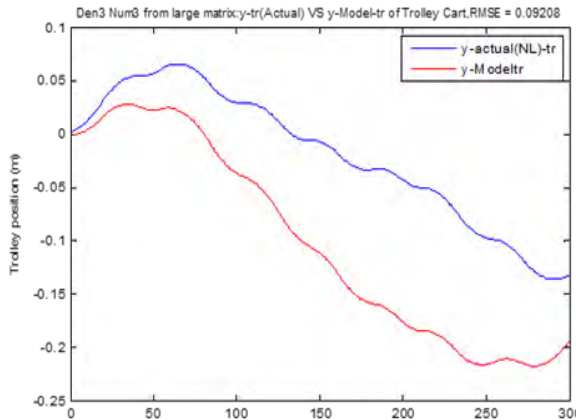


Figure (6.a): Den 2 Num 2 Trolley model

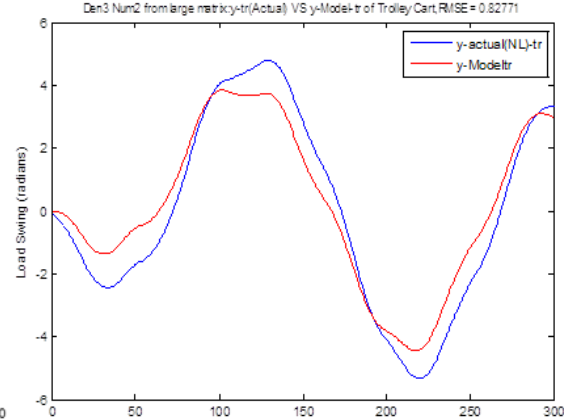


Figure (6.b): Den 2 Num 2 Load Swing model

6. LINEARIZATION OF THE CRANE USING MODIFIED LEAST SQUARE WITH 7 PAST INPUTS/OUTPUTS

To represent the X-translational motion of the load-attached trolley cart, the collected dataset is used to develop linear least square form of linearization. Usually, Linear Least Square approach uses linear combination of the past inputs/outputs dataset, for instant, $[y_3] = [-y_2 \ -y_1 \ u_2 \ u_1]$ and it can achieve only one Root Mean Square Error (RMSE) by comparing actual and estimated outputs. And that would be hard to analyze whether the model provides better approximation from the processed past inputs/outputs 4 dataset. Therefore, up to 7 past inputs/outputs dataset in the matrix X (mentioned below) have been applied in the linear least square which would produce more models, develop many RMSEs and eventually get better approximation of the model. The following X matrix shows how the 7 past inputs/outputs dataset are organized.

$$\begin{bmatrix} y(8) \\ y(9) \\ \vdots \\ y(100) \end{bmatrix} = \begin{bmatrix} 1 & \dots & 7 & 8 & \dots & 14 \\ -y(7) & \dots & -y(1) & u(7) & \dots & u(1) \\ -y(8) & \dots & -y(2) & u(8) & \dots & u(2) \\ \vdots & \ddots & \vdots & \vdots & \ddots & \vdots \\ -y(99) & \dots & -y(93) & u(99) & \dots & u(93) \end{bmatrix} \theta$$

6.1 Den and Num Coefficients consideration with Least Square modified approach

Selecting every possible combinations of the columns from a large matrix with 7 past inputs and 7 past outputs according to the model needs and forming X matrix to compute estimated states, are some of the essential tasks to look for better approximated model. For instance, to get Den 2 Num 2 model, X matrix with 2 outputs columns $-y(\textcolor{brown}{?})$ and 2 inputs columns $u(\textcolor{brown}{?})$ are required.

$$\begin{bmatrix} y(8) \\ \vdots \\ y(N) \end{bmatrix} = \begin{bmatrix} -y(\textcolor{brown}{?}) & -y(\textcolor{brown}{?}) & u(\textcolor{brown}{?}) & u(\textcolor{brown}{?}) \\ \vdots & \vdots & \vdots & \vdots \\ -y(\textcolor{brown}{?}+N) & -y(\textcolor{brown}{?}) & u(\textcolor{brown}{?}+N) & u(\textcolor{brown}{?}+N) \end{bmatrix} \theta, \\ y(k) = X\theta$$

From available 7 outputs columns, every possible 2 columns are picked at each time and same as every possible 2 from 7 inputs columns. That is, all possible 21 pairs of outputs/inputs columns can be picked to form 21 possible models. In previous session, $y_3 = [-y_2 \ -y_1 \ u_2 \ u_1]$ with only one

model could be formed while in this case there would be 21 models with Den2 Num2 coefficients which may produce better approximation

$$\begin{bmatrix} X_1 \\ X_2 \\ \vdots \\ X_{21} \end{bmatrix} = \begin{bmatrix} \text{Column 1} & \text{Column 2} & \text{Column 8} & \text{Column 9} \\ 1 & 2 & 8 & 9 \\ 1 & 3 & 8 & 10 \\ \vdots & \vdots & \vdots & \vdots \\ 6 & 7 & 13 & 14 \end{bmatrix}$$

For each X_1, X_2, \dots, X_{21} , estimated states are calculated to form estimated Models which would be compared against actual output. From, X_1 matrix;

$$X_1 = \begin{bmatrix} \text{Column 1} & \text{Column 2} & \text{Column 8} & \text{Column 9} \\ 1 & 2 & 8 & 9 \\ -y(7) & -y(6) & u(7) & u(6) \\ \vdots & \vdots & \vdots & \vdots \\ -y(7+N) & -y(6+N) & u(7+N) & u(6+N) \end{bmatrix},$$

$$\theta_1 = X_1^T * Y_1 \implies RMSE_1$$

Overall steps from selecting pairs, calculating estimated states and RMSEs for each case to computing lowest one from 21 RMSEs are shown in the following algorithm figure, Fig (7). For the Den2Num2 Model, the Algorithm could generate 21 RMSEs and respective models. After comparing all RMSEs, the lowest one and its related model would be picked up for further analysis. Figure, Fig(8), shows all highest to lowest RMSEs and their columns combinations.

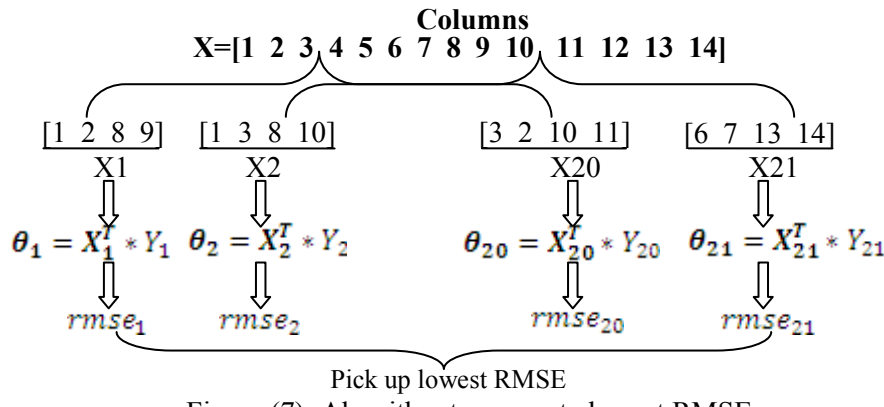


Figure (7): Algorithm to compute lowest RMSE

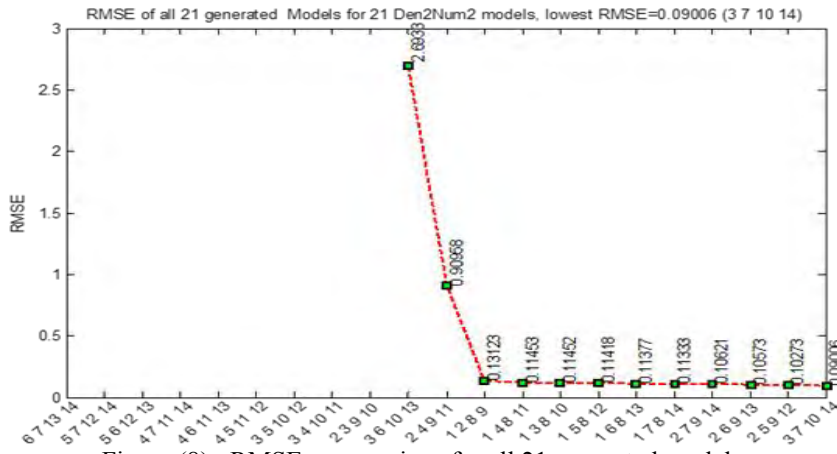


Figure (8): RMSEs comparison for all 21 generated models

For the other modeling cases such as; (Den 3 Num 3, Den 2 Num 3, Den 3Num 2, Den 4Num 3, Den 3 Num 4, Den 4 Num 4), the above-mentioned Algorithm is applied in which, all possible combination of columns pairs are first established then calculate estimated sates, generate Model Transfer Functions and compute RMSEs for all to pick up lowest RMSE with best approximation. The following Table (4,a) and Table (5,a) provide details of RMSE (Training part), RMSE (Checking part), and total RMSE each model for both Trolley and Load Swing simulations. Table (4,b) and Table (5,b) show the lowest RMSEs such as; RMSE=0.014485 for Trolley model Den 4 Num 4, and RMSE=1.616 for Load Swing Model Den 3 Num 4.

TrolleyCartRMSEDenNum				
RMSEs(Tr)	RMSEs(Ch)	RMSE	Den	Num
0.062355	0.11777	0.09006	2	2
0.062837	0.16689	0.036442	3	3
0.063118	0.11684	0.089978	2	3
0.058021	0.1539	0.10596	3	2
0.055614	0.10507	0.080342	4	3
0.092217	0.099155	0.095686	3	4
0.046732	0.13316	0.014485	4	4
0.06305	0.11571	0.08938	2	4
0.042649	0.11697	0.079812	4	2

LoadSwingRMSEDenNum				
RMSEs(Tr)	RMSEs(Ch)	RMSE	Den	Num
0.82772	2.4455	1.6366	2	2
0.82523	2.444	1.6346	3	3
0.82772	2.4455	1.6366	2	3
0.82771	2.4455	1.6366	3	2
0.81693	2.4393	1.6281	4	3
0.8021	2.43	1.616	3	4
0.82509	2.444	1.6345	4	4
0.82772	2.4455	1.6366	2	4
0.82751	2.4454	1.6364	4	2

Table(5.a): RMSE(Tr) and RMSE (Ch) for Load Swing

RMSEs(Trolley)	Den	Num
0.014485	4	4
0.036442	3	3
0.079812	4	2
0.080342	4	3
0.08938	2	4
0.089978	2	3
0.09006	2	2
0.095686	3	4
0.10596	3	2

RMSEs(LS)	Den	Num
1.616	3	4
1.6281	4	3
1.6345	4	4
1.6346	3	3
1.6364	4	2
1.6366	3	2
1.6366	2	4
1.6366	2	3
1.6366	2	2

Table(5.b): from lowest to highest RMSE for Load Swing

Using modified Linear Least Square with 7 past inputs/outputs data, Den 4 Num 4 trolley model provides lowest RMSE 0.046732, Fig (9,a) and while load swing model Den3 Num4; appeared to have better approximation with RMSE 0.08021, Fig (9,b).

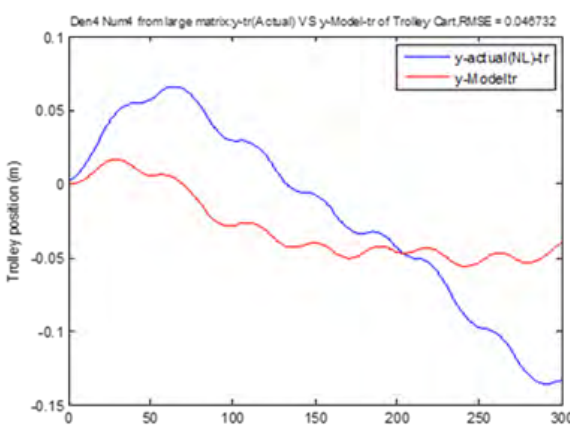


Figure (9,a): Den 4 Num 4 Trolley model

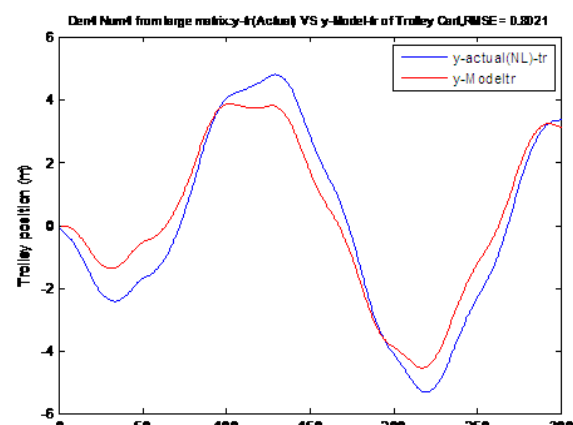


Figure (9,b): Den 3 Num 4 Load Swing model

6.2 Model Structure and RMSE comparison

From a simple Linear Least Square approach, trolley model structure with 3 Denominator 3 Numerator Coefficients appeared to have lowest RMSE=0.095495 while 3 Denominator 2 Numerator Coefficients load swing model has RMSE= 1.6366 respectively. Likewise in Least Square using 7 past inputs/outputs data approach, model structures with 4 Denominator 4 Numerator Coefficients appeared to have lowest RMSE (0.014485) while 3 Den 4 Num Load Swing model has lowest RMSE (1.616), as shown in Table (6). Those developed models from both approaches would be transformed into continuous state-space for control and performance comparison purposes.

According to the above simulation results, Linear Least Square with 7 past inputs/outputs data, produced lower RMSE than using simple linear least square approach which uses immediate past inputs/outputs data. Those selected models from both approaches would be implemented in controller designs and analyzed their responses.

	Den	Num	Model		RMSE
Least Square	3	3	Trolley	$\frac{4.924e - 005q^{-1} + 4.964e - 010q^{-2} - 4.924e - 005q^{-3}}{1 - 3q^{-1} + 3q^{-2} - q^{-3}}$	0.095499
Least Square	3	2	Load Swing	$\frac{-0.002723q^{-1} - 0.002722q^{-2}}{1 - 1.999q^{-1} + q^{-2} - 7.993e - 005q^{-3}}$	1.6366
Least Square with 7 past IOs	4	4	Trolley	$\frac{8.07e - 005q^{-1} + 1.321e - 005q^{-2} + 3.682e - 005q^{-3} - 2.993e - 005q^{-4}}{1 - 1.703q^{-1} + 1.026q^{-2} - 0.8826q^{-3} + 0.5598q^{-4}}$	0.014485
Least Square with 7 past IOs	3	4	Load Swing	$\frac{-0.002723q^{-1} - 0.002721q^{-2} + 2.736e - 006q^{-3} + 1.992e - 007q^{-4}}{1 - 2q^{-1} + 1.001q^{-2} - 0.0002781q^{-3}}$	1.616

Table(6): Model Structure and RMSE comparison

7. LQR CONTROLLER IMPLEMENTATION AND REFERENCE TRACKING

Linear quadratic regulation method is implemented for this overhead crane to determine the state-feedback control gain matrix K. LQR needs two parameters, Q and R weighting matrices which will balance the relative importance of the control effort (u) and error (deviation from 0), respectively, in the cost function J. Initially, $Q = \rho C^T C$ with $\rho = 1$ and $R = 1$ were assumed,[2]. The cost function corresponding to this and Q and R places equal importance on the control and the state variables outputs (cart's position x , and the pendulum's angle θ).

7.1 Q, R weighting matrices and Cost function J

Q and R matrices are considered as diagonal, $Q \propto I$. Matrix is positive-definite ($x^T Q x > 0$ for every nonzero vector, x) and were adjusted by hit and trial method to obtain the desired responses. The element in the (2, 2) position of Q represents the weight on the cart's position and the element in the (5,5) position represents the weight on the pendulum's angle. The input weighting R will remain at 0.001. In order to reach faster stabilization, it has been put more weights on the states as; $x = 30$, and $\theta = 20$ while R=0.001 to produce good controller gain K matrix. The following cost function J, Eq.(10), is considered to define the tradeoff between regulation performance and control effort of x-directional motion with the states $x, \dot{x}, \theta, \dot{\theta}$:

$$J = \int_0^{\infty} [x^T Q_x x + \theta_x^T Q_{\theta} \theta_x + u^T R u] dt \quad (10)$$

$$J = \int_0^{\infty} [x^T(t) \begin{bmatrix} 0 & 0 & 0 & 0 & 0 \\ 0 & 30 & 0 & 0 & 0 \\ 0 & 0 & 0 & 0 & 0 \\ 0 & 0 & 0 & 20 & 0 \\ 0 & 0 & 0 & 0 & 0 \end{bmatrix} x(t) + u^T(t) * 0.001 * u(t)] dt$$

The plant state equations can be written as follow;

$$\dot{x}(t) = Ax(t) + B_u u(t), \text{ and } y = Cx(t) + Du(t)$$

7.2 Linear Quadratic Regulator (LQR) Design

After Q, R weighting matrices are established and controller gain K values are computed, LQR Controller design, Eq.(11), with step response would run for the system performance, Fig (10). Initially, the system use Q (2,2)=Q (5,5)=1 and R=1 and it showed the plot was not satisfactory. Both cart and pendulum responses overshoot. To improve their settling times and reduce rise time, Q (2,2)= 30, Q (5,5)=20 and R=0.001 are selected after several trials.

$$\begin{aligned} \dot{x} &= Ax + B(-Kx), \text{ and } Y = Cx + D(-Kx), \\ u &= -R^{-1}B_u^T P(t)x(t) = -Kx \end{aligned} \quad (11)$$

$$\dot{x} = (A - BK)x, \quad Y = (C - DK)x$$

Whereby, the optimal feedback gain is, $K = -R^{-1}B_u^T P(t)$.

In the following Riccati Equation in which P is the steady state solution that yields a unique optimal control to minimize the cost function, J, [2].

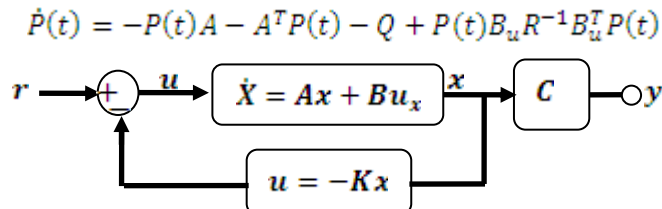


Figure (10): LQR Controller Design

In this overhead crane system, LQR performance of Trolley cart models, Den3 Num3 and Den4 Num4, are compared. The following figure, Fig(11) shows, Den4 Num4 model of modified Linear Least Square using 7past inputs/outputs dataset appeared to have shorter rise time and reach stability before 3 seconds while Den3 Num3 model of simple Least Square approach still fluctuating with longer rise time though the same Q and R weighting matrices have been applied.

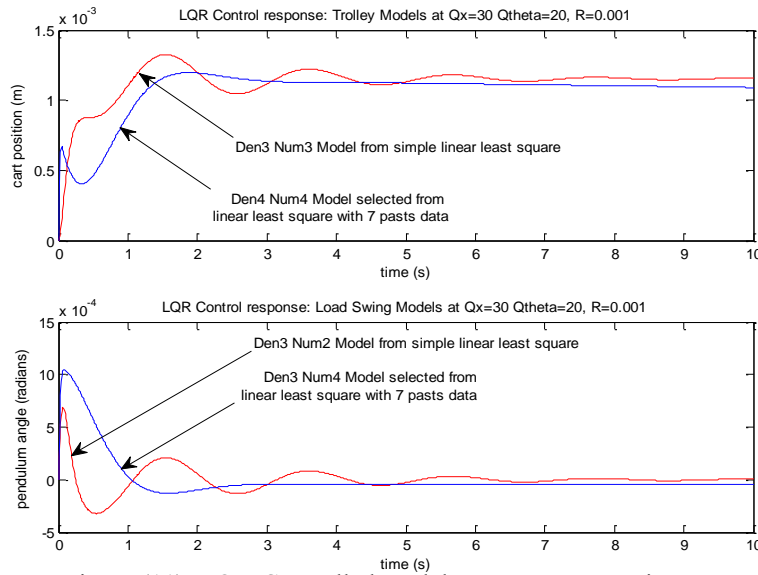


Figure (11): LQR-Controlled models response comparison

For Load swing performance, again Den3 Num4 from Linear Least Square using 7past inputs/outputs data appeared to reach zero swing angle in less than 3 seconds with less rise time and shorter settling time compared to Den3 Num2 model from simple least square. Besides, Linear Least Square using 7past inputs/outputs data produce more models, in this case up to 35 models have been analyzed before selecting the best fit model for control purpose. In this specific case of up to 600 data points, Den4 Num4 and Den3 Num4 models with lowest RMSEs have been picked for further reference tracking performance analysis. Though the controller response is better, steady-state errors still appear and therefore reference input tracking has been implemented to achieve desired inputs.

7.3 Reference Point tracking with full state feedback control

Adding the reference input to the system, $u=-Kx+r$ can lead to steady state errors. Pre-multiply r by carefully chosen matrix \bar{N} . In order to create pre-compensation \bar{N} , there are two possible ways such as; full-state feedback, and full-state feedback with full-order observer, [7]. In this case, full-state feedback reference input tracking would be used. The following equations, Equ(12) and Equ(13), and figures, Fig (12,a) and Fig(12,b) explain the pre-compensation \bar{N} calculation. Full-state feedback controller form is;

$$u = -Kx + \bar{N}r \text{ where } \bar{N} = N_u + KN_x \quad (12)$$

And therefore, full-state regulating input is; $u = -Kx + (N_u + KN_x)r$

$$u = N_u r - K(x - N_x r) \quad (13)$$

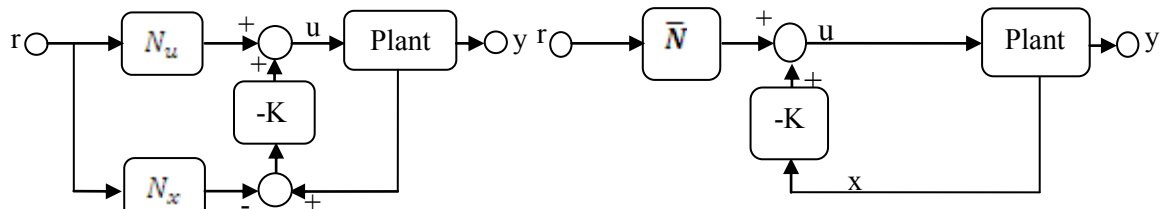


Figure (12.a): Full-state Feedback reference tracking

Figure (12.b): LQR Controller Design with pre-compensator

Full-state feedback would regulate steady-state output y_{ss} to desired steady-state value r_{ss} . In this trolley cart X directional motion, to track a constant desired position, x_{ss} (ss=steady-state) with control, u_{ss} , the control equation is;

$$0 = Ax_{ss} + Bu_{ss} \quad \{for steady state, \dot{x} = 0\}$$

$$y_{ss} = Cx_{ss} + Du_{ss}$$

By substituting

$$x_{ss} = N_x r_{ss}, \text{ and } u_{ss} = N_u r_{ss},$$

$$0 = AN_x r_{ss} + BN_u r_{ss}$$

$$y_{ss} = CN_x r_{ss} + DN_u r_{ss}$$

When $y_{ss} = r_{ss}$ in the steady-state

$$0 = AN_x r_{ss} + BN_u r_{ss},$$

$$r_{ss} = CN_x r_{ss} + DN_u r_{ss}$$

The above equations can be formed as state-space;

$$\begin{bmatrix} 0 \\ 1 \end{bmatrix} r_{ss} = \begin{bmatrix} A & B \\ C & D \end{bmatrix} \begin{bmatrix} N_x \\ N_u \end{bmatrix} r_{ss} \quad (\text{or}) \quad \begin{bmatrix} N_x \\ N_u \end{bmatrix} = \begin{bmatrix} A & B \\ C & D \end{bmatrix}^{-1} \begin{bmatrix} 0 \\ 1 \end{bmatrix}$$

However, when computing the large matrices inverse, $\begin{bmatrix} A & B \\ C & D \end{bmatrix}^{-1}$, it gives error. To be able to solve for larger matrices, this research applies the following way, Equ (14).

$$F = \begin{bmatrix} A & B \\ C & D \end{bmatrix}, Z = \begin{bmatrix} 0 \\ 1 \end{bmatrix}$$

$$N = \text{inv}(F^T * F) * (F^T * Z^T) \quad (14)$$

$$N = [N_x \ N_{u1} \ N_{u1} \ \dots \ N_{un}]^T$$

$$N_u = N_{u1} + N_{u2} + \dots + N_{un}$$

$$\bar{N} = N_u + KN_x, \text{ where K is the controller gain.}$$

The established full-state feedback pre-compensators Nu and Nx are then applied in LQR-controlled, Fig (13), to achieve the desired input. The robustness of reference tracking produces perfect control stability on both trolley motion and pendulum load swing. Each Trolley desired position has been achieved in less than 3 seconds while load swing could be suppressed in 2 seconds time compared to nonlinear high fluctuating pendulum output, Fig (14). It shows that, the developed trolley and load swing linear models using modified linear least square with 7 past inputs/outputs are more reliable and LQR with pre-compensator just make the whole system perfect.

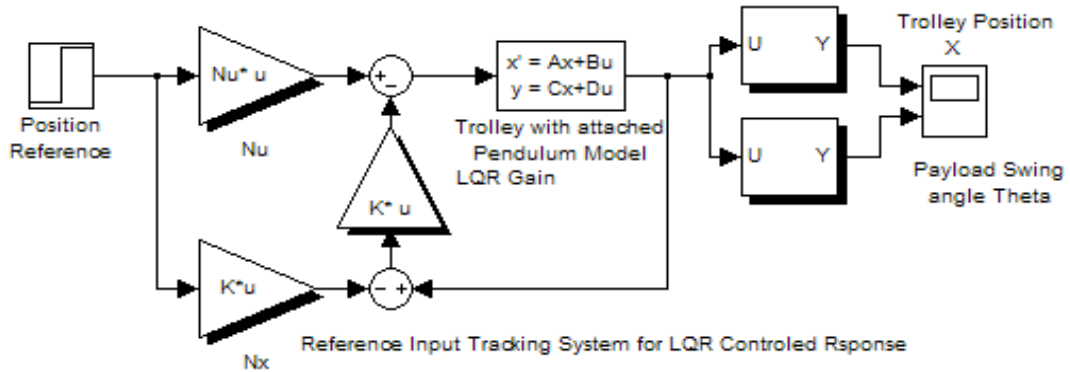


Figure (13): Reference Input Tracking with Full-state feedback

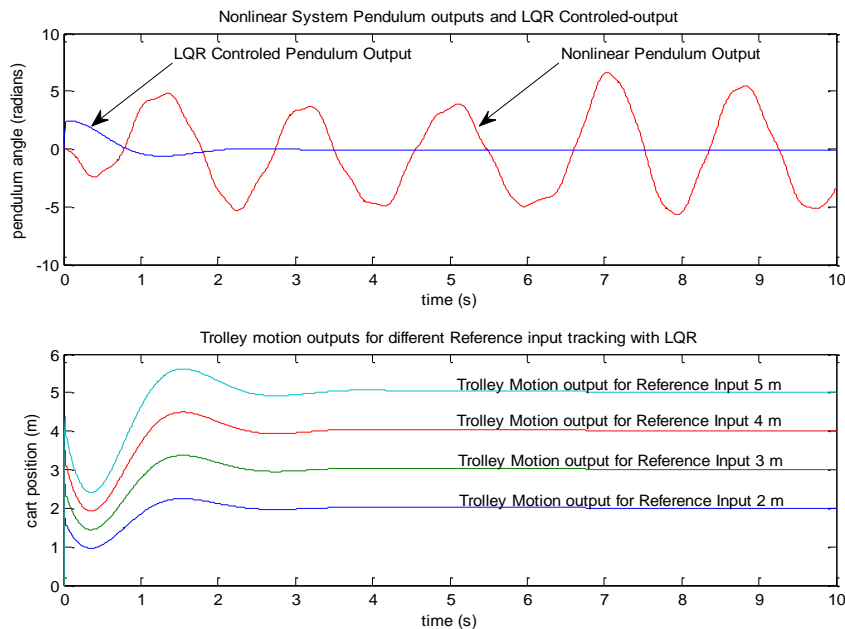


Figure (14): LQR Controlled response and Non-linear output

8. CONCLUSION

The main objective of this work is to design Overhead Crane experimental model using Simmechanic Visualization aiming not only to achieve real crane-like model feature but also to implement robust, fast and practical controller. Furthermore, it would also be a major milestone to deliver better crane modeling and control for the real operation instead of relying on lab-scaled model work. This development would close the gap between pure mathematical sketch with real time operation.

Throughout this work, trolley translational motion with attached pendulum is designed which represents exact lab model measurements and features. Practical considerations, such as joints actuation, moment of inertia, and the gravity, are taken into account. In addition, friction effects are included in the design using a friction-compensation technique.

To accomplish the objective, collected simulation data are then used in linear least square system identification to produce predicted models. To have better estimated model, 7 past outputs and 7 past inputs dataset matrix Algorithm was designed to produce more models. Root Mean Square

Errors checking has then been implemented to compare predicted models against the actual output.

Once the best fit linearized models have been established, those were implemented in reference input tracking-LQR controller design. The simulation result shows proposed control scheme guarantees both rapid damping of load swing and accurate control of crane position.

Since the major milestone of physical modeling using simmechanic visualization was achieved, the future step is to design 3D Tower Crane physical model which would have Trolley translation, Jib rotation, and Hoist up/down motion. Furthermore, jib oscillation would be thoroughly analyzed to suppress payload swing during the operation.

9. REFERENCES

- [1] Bei Na Wei, (2008). "An Innovative Approach to Overhead Crane Control". The University of New, South Wales, Sydney, Australia.
- [2] Hesketh T. Linear quadratic control. Elec9733 Real Time Computing and Control Lecture Notes, Apr 2008.
- [3] Ilse C. F. Ipsen. (2009). "Numerical Matrix Analysis: Linear Systems and Least Squares". North Carolina State University, Raleigh, North Carolina.
- [4] Inteco (2010). "Tower Crane Control User Manual", Inteco Ltd. (Inteco User Manual, Version 1.4.)
- [5] Lee H.H. Modeling and control of a three-dimensional overhead crane. Journal of Dynamic Systems, Measurement and Control, 120(4):471–476, Dec 1998.
- [6] Omar, H. M. (2003). "Control of Gantry and Tower Cranes", Virginia Polytechnic Institute and State University, Blacksburg, Virginia, USA
- [7] Oishi Meeko. (2012). "State Space Reference Tracking and other control problems".(Lecture Notes:EECE360). Electrical and Computer Engineering, The University of British Columbia.
- [8] Quanser (2010). "3 Degrees of Freedom Crane User Manual", Quanser Ltd. (Quanser User Manual)
- [9] Raul G. Longoria.(2002) "Modeling of Mechanical System for Mechatronics Applications". The University of Texas, Austin, USA.
- [10] R. S. Caprari (Robert S.). (1992). "Least squares orthogonal polynomial approximation in several independent variables". Flinders University of South Australia.
- [11] Sahan S. Hiniduma Udagama Gamage and Patrick R. Palmer. "Hybrid System Modeling, simulation and visualization; A crane system". Proceedings of SPIE Vol. 5097 (2003). Department of Engineering, University of Cambridge,UK
- [12] Shebel Asad, Maazouz Salahat,(2011). "Design of fuzzy PD-controlled overhead crane system with anti-swing compensation". Journal of Engineering and Computer Innovations Vol. 2(3), pp. 51-58, March 2011. Academic Journals
- [13] Schlotter Michael (2003). "Multi Body System Simulation with SimMechanics. Dynamic Seminar. Darmstadt University of Technology

Appendix E

“Response to Examiner (1) Report”

and
“Response to Examiner (2) Report”

Response to Examiners:

Response to examiner(1)' report

Name : Thein Moe WIN

SID : 3274820

Never Stand Still

Graduate Research School

RESPONSE TO EXAMINER 1

Examiner comments (please reproduce exactly as in the examiner report)	Response (include text added to revised thesis)	Section / Page (in original thesis thesis)	Section / Page (in revised thesis)	Reviewer's Comment (if applicable)
GENERAL COMMENTS				
1. Pages 1, 5, 6, 211. Abstract. "to deferent input conditions" - please check. Most likely "to different input conditions"	The typo error has been corrected as " to different input conditions "	Abstract / pp 1, vi, 211	Abstract / pp 1, vi, 221	
2. Page 20 (Chapter 1, #1). "In each crane operation like; hoist" - it seems that ":" is needed instead of ;. Please check usage of semicolons throughout the thesis.	The usage of ":" and ";" have been updated throughout the thesis. -In each crane operation like: hoist up-down motion..... -by a set of algorithms: Recursive Newton-Euler Algorithm -etc.	throughout the thesis	throughout the thesis	
3. Page 22 (#3). "Linear least square (LLS) is one useful way to" - is LSS really "a way"? Maybe LLS approach/method is a way? Please check.	It has been corrected as " LLS approach is one useful way "	Ch 1, p. 3	Ch 1, p. 3	
4. Page 31 (#12). "such as; (friction, noise and disturbance, actuator dynamic, and sensor, etc.)." - "such as: friction, noise and disturbance, actuator dynamic, and sensor, etc."	It has been corrected as " parameters such as: friction, noise and disturbance, actuator dynamic, and sensor, etc.. "	Ch 2, p. 12	Ch 2, p. 13	

Examiner comments <i>(please reproduce exactly as in the examiner report)</i>	Response <i>(include text added to revised thesis)</i>	Section / Page (in original thesis)	Section / Page (in revised thesis)	Reviewer's Comment (if applicable)
5. Page 32 (Chapter2,#13). "without having trouble in dealing with real cranes a working site." - maybe "without having trouble in dealing with real cranes ON a working site."	It has been corrected as " without having trouble in dealing with real cranes on a working site. "	Ch 2, p. 13	Ch 2, p. 14	
6. Page 33 (#14). "Lagrenge" - please check	"Lagrange" has been updated throughout the Thesis	Ch 2, p. 14 and throughout the thesis	Ch 2, p. 15 and throughout the thesis	
7. Page 34 (#15). Actually, (2.1), (3.24) are not transfer functions (as are named above in the manuscript). (2.1), (3.24) represent the plant model dynamics. The transfer function is a multiplier.	It has been corrected as " the plant model dynamics Eq.(2.1)." "the plant model dynamics Eq.(3.24)" .	Ch 2, p. 15 Ch 3, p. 57	Ch 2, p. 16 Ch 3, p. 58	
8. Page 41 (# 22). "One method to overcome this limitation is to implement the controller as a transfer function." - is not completely clear, because a transfer function is a form of the mathematical description for dynamical system.	This phrase "One method to overcome this limitation is to implement the controller as a transfer function." has been removed.	Ch 2, p. 22	Ch 2, p. 23	
9. Page 30 (Chapter 3,#30). "Using this derived nonlinear model equation (2)' and equation (3)'" - I haven't been able to find neither Eq. (2)' nor Eq. (3)' in the manuscript.	It has been updated as " Using these derived nonlinear equations Eq.(3.4) and Eq.(3.5), linearized models are developed in the next section. "	Ch 3, p. 30	Ch 3, p. 31	
10. Page 30 (Chapter 3,#31). "Equ(3.4)", "Equ(3.5);"	Rephrased as follow.			

Examiner comments (please reproduce exactly as in the examiner report)	Response (include text added to revised thesis)	Section / Page (in original thesis thesis)	Section / Page (in revised thesis)	Reviewer's Comment (if applicable)
references are not clear; Equ(3.6) and Equ(3.7) - the same	<p>Referring to the nonlinear dynamic force and torque equations Eq.(3.2) and Eq.(3.3), the following nonlinear equations of motions Eq.(3.4) and Eq.(3.5) are derived as</p> $\ddot{x}_t = \frac{1}{(M+m)} [F - ml(\dot{\theta} \cos \theta - \dot{\theta}^2 \sin \theta) - b\dot{x}] \quad (3.4)$ $\ddot{\theta} = \frac{1}{(I-ml^2)} [ml(\ddot{x}_t \cos \theta + g \sin \theta) - c\dot{\theta}] \quad (3.5)$ <p>Using this derived nonlinear equations Eq.(3.4) and Eq.(3.5), linearized models are developed in the next section.</p> <p>"Using these assumptions, the nonlinear mathematical equations Eq. (3.4) and Eq. (3.5) are linearized around the unstable equilibrium point and therefore, the following Eq. (3.6) and Eq. (3.7) have been obtained."</p>	Ch 3, p. 30	Ch 3, p. 31	
11. Page 51, 52 (#32, 33). meaning of "7.529e", "2.508e", "6.746e" in the transfer functions is not clear. Comparison with Simulink models Fig. 3.2a shows that they are misprints. By the way, writing numbers in the exponential form in mathematical expressions is not welcome (see also (4.9), (4.10)).	<p>Updated Fig. 3.2a and Transfer Functions</p> $\frac{x}{F} = \frac{0.5176 s^2 - (7.529 \times 10^{-6}) s + 5.54}{s^4 + 0.00412 s^3 + 15.23 s^2 + 0.04432 s}$ $\frac{\theta}{F} = \frac{-0.5647 s^2 + (2.508 \times 10^{-16}) s + 6.746}{s^4 + 0.00412 s^3 + 15.23 s^2 + 0.04432 s}$	Ch 3, p. 32	Ch 3, p. 33	Ch 3, p. 33
Transfer Functions (4.9), (4.10) in Chapter 4, p. 125 has also been updated as follow				

Figure3.2a Trolley-Payload Models Excitation

Examiner comments (please reproduce exactly as in the examiner report)	Response (include text added to revised thesis)	Section / Page (in original thesis thesis)	Section / Page (in revised thesis)	Reviewer's Comment (if applicable)
	$\frac{\theta_{yt}}{T_t} = \frac{(-2.72 \times 10^{-9})s^4 + (2.59 \times 10^{-7})s^3 - (4.104 \times 10^{-6})s^2 + (6.87 \times 10^{-6})s - (1.304 \times 10^{-4})}{s^4 + 31.34s^3 + 588.9s^2 + 109.3s + 1.32} \quad (4.9)$ $\frac{\theta_{xl}}{T_l} = \frac{(-2.76 \times 10^{-11})s^6 + (1.52 \times 10^{-9})s^5 - (1.67 \times 10^{-7})s^4 + (3.254 \times 10^{-6})s^3 - (1.95 \times 10^{-5})s^2 + (2.5 \times 10^{-4})s + (4.17 \times 10^{-4})}{s^6 + 92.1s^5 + 3206s^4 + 3.4e^4s^3 + 3.997e^5s^2 + 3.44e^4s + 4084} \quad (4.10)$	Ch 4, p. 123	Ch 4, p. 125	
12. Page 57 (Pg-38). "From L, 4" - reference is not clear.	<p>The wording has been rephrased as follows:</p> <p>"Based on the final Lagrange Equation above for "L", four dynamic equations ($\dot{\alpha}$, \dot{L}, $\dot{\phi}$, $\dot{\theta}$) are then obtained as follow."</p>	Ch 3, p. 38	Ch 3, p. 39	
13. Page 63 (#44). "Considering ... are considered as small." - please, consider paraphrase of this sentence.	<p>The wording has been rephrased as follows:</p> <p>"In the case of the system at an equilibrium point, load swing angles (θ, ϕ, α) and their velocities ($\dot{\theta}$, $\dot{\phi}$, $\dot{\alpha}$) can be assumed as small."</p>	Ch 3, p. 44	Ch 3, p. 45	
14. Page 64 (#45). "such as (load length change, frictions, noises and disturbances on actuators and sensors, etc.)" - brackets are not needed.	<p>Rearrange the sentence with ":".</p> <p>"such as: load length change, frictions, disturbances on actuators and sensors, etc."</p>	Ch 3, p. 45	Ch 3, p. 45	
15. Page 64 (#45). Please make a choice: "simmechanic", "Simmechanic" or "SimMechanic" throughout the manuscript	<p>To be consistent, this research uses "SimMechanics" throughout the Thesis</p>	Ch 3, p. 45 and throughout the thesis	Ch 3, p. 45 and throughout the thesis	

Examiner comments (please reproduce exactly as in the examiner report)	Response (include text added to revised thesis)	Section / Page (in original thesis thesis)	Section / Page (in revised thesis)	Reviewer's Comment (if applicable)
16. Page 68 (#49). "signal ... was designed in Fig. 3.10." - is not completely clear	<p>The wording has been rephrased as follows:</p> <p style="color: red;">"Using the specially designed pseudo-random inputs with sampling frequency 10-Hz as shown in Fig. 3.10, the load output movement in the X direction was obtained for the trolley translational motion."</p>	Ch 3, p. 49	Ch 3, p. 50	
17. Page 71 (#52). "The detail calculation ... is calculated below." - please, consider rephrasing.	<p>The wording has been rephrased as follows:</p> <p style="color: red;">"The detailed calculation of each rotational angle is shown below."</p>	Ch 3, p. 52	Ch 3, p. 53	
18. Page 86 (#67). (3.28) why "*" is used in the mathematical expression? (3.32), (4.3) - the same.	<p>The following mathematical expression with "*"has been removed.</p> $J = \int_0^{\infty} [x^T(t) \begin{bmatrix} 0 & 0 & 0 & 0 & 0 \\ 0 & 30 & 0 & 0 & 0 \\ 0 & 0 & 0 & 0 & 0 \\ 0 & 0 & 0 & 20 & 0 \\ 0 & 0 & 0 & 0 & 0 \end{bmatrix} x(t) + u^T(t) * 0.001 * u(t)] dt$ <p>And replaced by the following form.</p> $J = \int_0^{\infty} [x^T Q_x x + \theta_x^T Q_\theta \theta_x + u^T R u] dt \quad (3.28)$ $N = \text{inv} [(F^T F)(F^T Z^T)] \quad (3.32)$ $F_{ws} = PA \quad (4.3)$	Ch 3, p. 67	Ch 3, p. 68	
19. Page 87 (#68). "would run for the system performance" - "run for the performance" is not clear	<p>The wording has been rephrased as follows:</p> <p style="color: red;">"After Q and R weighting matrices are established and controller gain (K) values are computed, the system with step reference as shown in Fig.3.25, is controlled by LQR Controller, Eq.(3.29)."</p>	Ch 3, p. 68	Ch 3, p. 69	

Examiner comments (please reproduce exactly as in the examiner report)	Response (include text added to revised thesis)	Section / Page (in original thesis thesis)	Section / Page (in revised thesis)	Reviewer's Comment (if applicable)
20. Page 127 (#108). Reference in "gust wind (variable), Equ (1)." is not clear.	<p>The typo error has been corrected. It should be Equ (4.1).</p> <p style="color: red;">"The total wind load is actually a combination of static wind (mean) and gusts wind (variable), Equ (4.1)."</p>	Ch 4, p. 108	Ch 4, p. 108	
21. Page 149 (#130). (5.1) "whereby f is the function vector of state variables," - if this means that $f(\cdot)$ is a vector-function, it should be noticed that it depends not only on the state variable, but on the other ones	<p>It is clarified as follow.</p> $\dot{x} = f(x, w, u, t), y = Cx \quad (5.1)$ <p>whereby f is the function vector of state equations involving variables such as state ($x \in R^n$), external disturbance (w), control input (u), and time (t). Furthermore, the measurement (y) is the linear function of the state variables.</p>	Ch 5, p. 130	Ch 5, p. 132	
22. Page 149 (#130). The numerator in the first ratio below "system identification in [5]-[7];" is unclear and, most likely, erroneous.	<p>The examiner comment refers to the following transfer function and numerator ratio.</p> $\frac{y}{u} = \frac{(x, \dot{x}, \ddot{x}, \ddot{\dot{x}})}{F}$ $= \frac{-1.172e^{-7}s^4 - 4.761e^{-6}s^3 + 4.331e^{-6}s^2 + 0.002011s^1 + 0.01488}{s^4 + 54.86s^3 + 628s^2 + 586.2s^1 + 9.631}$ $\frac{x}{F} = \frac{0.01563}{s^4 + 54.86s^3 + 19.63s^2 + 4.58s^1 + 0.301}$ $p_{est} = [54.86; 19.63; 4.58; 0.301]$ <p>Let, $q_1 = x, q_2 = \dot{x}, \dots$ etc. the state space representation Eq.(5.2) can be expressed by</p> $\ddot{\dot{x}} = p(x, \dot{x}, w, u, t) \quad (5.2)$ <p>Trolley model transfer function mentioned above was from the journal references [5]-[7] which were earlier published as part of this research. Since it is nothing related to the control canonical form section, that part has been removed from the section 5.1.2.</p>	Ch 5, p. 130	Ch 5, p. 132	

Examiner comments (please reproduce exactly as in the examiner report)	Response (include text added to revised thesis)	Section / Page (in original thesis thesis)	Section / Page (in revised thesis)	Reviewer's Comment (if applicable)
23. Page 159 (#140). "Figure 5.7 LQR-Estimator-Integral Control" - an algebraic loop exists in the Simulink model. This causes questions.	<p>Figure 5.7 LQR-Estimator-Integral Control (LEIC) controller design illustration has the drawing mistake which shows "the algebraic loop with the control signal "u" feeding back to the block gain "K".</p> <p>The updated drawing Figure (5.7) is</p>	Ch 5, p. 140	Ch 5, p. 142	
24. Page 161 (#142). "As in (10)", "As in (13)", "As in (14)," - the references are not clear	<p>The following references have been corrected.</p> <p>"as in [10]", "as in [13]", "as in [14]"</p>	Ch 5, p. 137	Ch 5 p. 137, p. 142 p.143, p. 144	
25. Page 184 (#165). "Sliding model control" - most likely, "Sliding mode control" should be instead	It has been corrected as "Sliding mode control".	Ch 5, p. 165	Ch 5, p. 168	
26. Page 189 (#170). Please check usage of round brackets throughout the paper. In the most of cases they are placed mistakenly (cf. https://en.oxforddictionaries.com/punctuation/parentheses-and-brackets)	The bracket usage throughout Chapter 6 has been corrected.	Ch 6, pp 159- 174	Ch 6, pp 162- 178	

Examiner comments <i>(please reproduce exactly as in the examiner report)</i>	Response <i>(include text added to revised thesis)</i>	Section / Page (in original thesis)	Section / Page (in revised thesis)	Reviewer's Comment (if applicable)
27. There is some repetition at the beginning of each chapter, while summarizing motivation and key aspects of that chapter, see e.g. pages #4, #16, #107. This could have been done in order to keep each chapter self-contained. If the Committee opines that such repetition can be minimized, then suitable reduction of text can be done.	<p>The following section 1.4 remains unchanged</p> <p>1.4 Vibration Impact and Disturbance Rejection "Therefore, researchers have to rely on small model crane prototype to develop anti-sway control strategies. Ref. [8] envisages that, residual vibration would occur on completion of a trolley traverse due to the operator's manual control, different containers size and load lengths causing more friction and unstable load swing. In [9], transient sway and residual oscillation appear for certain types of payload and riggings, the payload mass is comparable to the cable mass, or the mass hangs from a hook without a cable in which the dynamics can become slightly different from a single pendulum due to the effects of inertia."</p> <p>Since the above-mentioned paragraph from section (1.4) was mistakenly repeated in sections (2.3), it has been replaced with the following paragraph.</p> <p>2.3 Vibration impact on tower crane "Having tall construction tower crane on standing tower hub, the vibration impact will be unavoidable. Since most of the researchers around the globe refer to the respective crane prototypes in proposing any control strategies, those developed models cannot provide reliable vibration impact analysis. There can be many forms of vibration impact on the crane due to: the crane unstable operation itself with higher load swing, the wind disturbance, unbalance counterweight and payload, trolley translational and tower rotation speeds, etc. In order to achieve the real</p>	Ch 1, p. 4	Ch 1, p. 4	

Examiner comments (please reproduce exactly as in the examiner report)	Response (include text added to revised thesis)	Section / Page (in original thesis)	Section / Page (in revised thesis)	Reviewer's Comment (if applicable)
	<p>crane automation and control, it is important to analyse the vibration impact on a reliable crane model in the case of real crane is inaccessible."</p> <p>The repeated paragraph from section (1.4) appeared in section (4.3) has been removed.</p>	Ch 4 p. 107	Ch 4 p. 108	
<p>28. The next relevant papers may be optionally added to the Reference list:</p> <p>1) Abdel-Rahman, E.M., Nayfeh, A.H., Masoud, Z.N. Dynamics and control of cranes: A review JVC/Journal of Vibration and Control. Volume 9, Issue 7, July 2003, Pages 863-908</p> <p>2) Beznos, A.V., Grishin, A.A., Lensky, A.V., Okhotsimsky, D.E., Formal'sky, A.M. A flywheel use-based control for a pendulum with a fixed suspension point. Journal of Computer and Systems Sciences International, Volume 43, Issue 1, January 2004, Pages 22-33.</p> <p>3) Aoustin, Y., Formal'sky, A. Simple anti-swing feedback control for a gantry crane. Robotica, Volume 21, Issue 6, November 2003, Pages 655-666.</p>	<p>The following new references have been added in the relevant chapters.</p> <p>[78] Abdel-Rahman, E.M., Nayfeh, A.H., Masoud, Z.N , Dynamics and control of cranes: A review, <i>Journal of Vibration Control (JVC)</i>, Volume 9 (Issue 7): pp. 863-908, July 2003</p> <p>[79] Beznos, A.V., Grishin, A.A., Lensky, A.V., Okhotsimsky, D.E., Formal'sky, A.M , A flywheel use-based control for a pendulum with a fixed suspension point, <i>Journal of Computer and Systems Sciences International</i>, Volume 43 (Issue 1): pp. 22-33, January 2004</p> <p>[80] Aoustin, Y., Formal'sky, A, Simple anti-swing feedback control for a gantry crane, <i>Journal of Robotica</i>, Volume 21 (Issue 6): pp. 655-666, November 2003</p>	Not in old thesis	Ch 6, pp 167-168	

Confirmation that required work has been completed and recommendation of Award Degree is made by:

Name: **Thein Moe WIN (3274820)**

Head of School OR Postgraduate Coordinator



**EXAMINER'S REPORT FOR THE
DEGREE OF DOCTOR OF PHILOSOPHY**
STRICTLY CONFIDENTIAL

Name of Candidate: Thein Win
School: School of Electrical Eng and Telecommunications
Title of Thesis: Robotic Tower Crane Modelling Control (RTCMC)
Report Due Date: 13 April 2017

**1 After examination of the thesis (and supporting papers) I recommend that:
(Please circle the letter next to the appropriate recommendation)**

A. The thesis merits the award of the degree.

This recommendation is appropriate if the thesis contains no faults that are apparent to the examiner. It is also appropriate where errors and omissions of an editorial nature are minor and, if left uncorrected, will not alter the conclusion that "the thesis merits the award of the degree".

or

B. The thesis merits the award of the degree subject to minor corrections as listed being made to the satisfaction of the Head of School.

The errors and omissions, which extend beyond those of an editorial nature, must be corrected if the thesis is to merit the award of the degree. The corrections are minor in that they do not change the structure or the conclusions of the relevant chapters of the thesis.

or

C. The thesis requires further work on matters detailed in my report. Should performance in this further work be to the satisfaction of the Faculty Higher Degree Committee, the thesis would merit the award of the degree.

The further work required should be sufficiently straightforward such that the examiner is happy to delegate approval of the revised thesis to the Higher Degree Committee. Examples of further work in this category could include: discussion and consideration of published work that is relevant to the conclusions of the thesis; consideration of alternative hypotheses that should reasonably be suggested by the candidate; presentation of additional experimental data that could be expected to be in the possession of the candidate; clearer specification of how the presented results/conclusions were arrived at.

or

D. The thesis does not merit the award of the degree in its present form and further work as described in my report is required. The revised thesis should be subject to re-examination.

Please indicate whether you are willing to review the resubmitted thesis Yes [] No []

The further work involves a major revision of the thesis on the same topic. The examiner is assumed to be satisfied with the candidate's capability and demonstrated competence for this further work. The comments and suggestions in the detailed report should be clear and helpful to the candidate. As the thesis is to be revised along the lines suggested by the examiners, it would normally be re-examined by the same examiners. Examples of further work in this category could include: further analyses or experiments where the scientific method as presented in the thesis has significant flaws; performance of additional experiments that are deemed vital to the conclusions drawn in the thesis.

Or

the candidate for a resubmitted thesis to achieve this merit.

The examiner should provide the basis of this recommendation in the detailed report.

2	I agree to my name being released to the candidate	Yes <input checked="" type="checkbox"/> No <input type="checkbox"/>
3	An Evaluation of the merits of the thesis is given overleaf (Attach additional pages if required) <i>Please see attached sheet</i>	

The examiner is requested to state concisely the grounds on which the recommendation is based, indicating where appropriate the strengths and weaknesses of the thesis. To assist the candidate with future work, this report may be released after a decision has been taken to award or not to award the degree.

Examiner: Professor Boris Andrievsky Signature:  Date: *01 March 2018*

Ph.D. Thesis Review
Title: Robotic Tower Crane Modelling Control (RTCMC)
Candidate: Thein Moe
UNSW Sydney
18 April 2016

This thesis deals with the topical problem of accurate positioning and swing minimization of payloads in large standing tall tower crane operation. The thesis topic is very relevant due to the widespread use of various kinds of cranes worldwide. Excitation of the payload oscillation is a serious problem, causes additional unnecessary efforts of crane operator, increasing crane's operational costs and time, not to mention the risk of damage to the surrounding environment and the destruction of the crane structure itself. Therefore, anti-swing control for cranes is theoretically and practically crucial, and many endeavors have been devoted to this direction. To date, there is no complete solution to this problem and the considered thesis is a good advance forward to automatic damping the crane payload oscillations. In the thesis, solutions to a class of swing suppression problem where it is critical to overcoming poor performance of highly nonlinear trolley-tower-payload crane operational control are presented.

In the thesis, the author successively proceeds from creation and studying of simpler to more complex models and methods of designing anti-swing and disturbance rejection controllers for crane payloads. After the problem description and the overview of existing results, the author presents various mathematical models of overhead, tower, and gantry cranes both in linear and nonlinear settings.

The Lagrangian formalism is widely and correctly used in the thesis for deriving the various mathematical models of the crane systems. The developed models are brought to the software implementation in the SimMechanic/MATLAB programming environment, which significantly expands the possibilities of their use for scientific research and solving practical engineering problems. In the thesis, for getting the correct virtual response of the simulation, moment of inertia tensors for each body part were carefully calculated and presented in the matrix form.

To measure the differences between estimated values by the developed model, and actual output, in the framework of the system identification problem, the author sensibly used the Root-mean-square error (RMSE) calculation which produces good fit of the model and enhances approximation. An interesting part of the work consists of the proposed improved version of the LLS algorithm, which could generate 21 RMSE and respective models. After comparing all RMSEs, the lowest RMSE and its related model would be picked up for further analysis. In the thesis this algorithm is successfully applied to estimate the cranes linearised model parameters based on the numerical input/output data. It seems that the proposed algorithm may found different applications for identification of the wide range of dynamical systems. However, in the present form, it looks rather heuristic, and it would be desirable in future studies to give him a better mathematical foundation, and to present recommendations to the choice of its parameters (number of columns, etc.).

The significant part of the work deals with vibration impact analysis on trolley translation with and without wind disturbance depending on the trolley position. On the basis of the given analysis, the quantitative characteristics of the influence of disturbances for different operating conditions are obtained. In the thesis, the reference point tracking with full state feedback Linear Quadratic Regulator (LQR) control is presented and the disturbance rejection observer as an adaptive alternative to integral action for enhancement the disturbance rejection properties of the feedback LQR controller is proposed, and is studied by the simulations in the framework of the built SimMechanic/MATLAB model. The simulation results demonstrate efficacy of the proposed control scheme.

The author has a sufficient number of scientific publications and poster presentations.

Summary Recommendation: The thesis merits the award of the degree subject to minor corrections as listed, being made to the satisfaction of the Head of School.

Specific Suggestions/Comments

The overall writing quality of the thesis is satisfactory, problems are clearly stated, the work seems to be technically correct, and different solutions are presented.

Despite the writing style is generally, crisp and clear, the thesis is not free from a row of misprints, unclear references and stylistically poor sentences. It is advisable to carefully proofread the thesis for eliminating them. For example:

1. Pages 1, 5, 6, 211. Abstract. "to deferent input conditions" - please check. Most likely "to different input conditions"
2. Page 20 (Chapter 1, #1). "In each crane operation like; hoist" - it seems that ":" is needed instead of ";". Please check usage of semicolons throughout the thesis.
3. Page 22 (#3). "Linear least square (LLS) is one useful way to" - is LSS really "a way"? Maybe LLS approach/method is a way? Please check.
4. Page 31 (#12). "such as; (friction, noise and disturbance, actuator dynamic, and sensor, etc.);" - "such as: friction, noise and disturbance, actuator dynamic, and sensor, etc."
5. Page 32 (#13). "without having trouble in dealing with real cranes a working site." - maybe "without having trouble in dealing with real cranes ON a working site."
6. Page 33 (#14). "Lagrenge" - please check
7. Page 34 (#15). Actually, (2.1), (3.24) are not transfer functions (as are named above in the manuscript). (2.1), (3.24) represent the plant model dynamics. The transfer function is a multiplier.
8. Page 41 (# 22). "One method to overcome this limitation is to implement the controller as a transfer function." - is not completely clear, because a transfer function is a form of the mathematical description for dynamical system.
9. Page 50 (#31). "Using this derived nonlinear model equation (2)' and equation (3)'" - I haven't been able to find neither Eq. (2)' nor Eq. (3)' in the manuscript.
10. Page 50 (#31). "Equ(4)", "Equ(5);"- references are not clear; Equ(6) and Equ(7) - the same
11. Page 51, 52 (#32, 33). meaning of "7.529e", "2.508e", "6.746e" in the transfer functions is not clear. Comparison with Simulink models Fig. 3.2a shows that they are misprints. By the way, writing numbers in the exponential form in mathematical expressions is not welcome (see also (4.9), (4.10)).
12. Page 57 (#38). "From L, 4" - reference is not clear.
13. Page 63 (#44). "Considering ... are considered as small." - please, consider paraphrase of this sentence.
14. Page 64 (#45). "such as (load length change, frictions, noises and disturbances on actuators and sensors, etc.)" - brackets are not needed.
15. Page 64 (#45). Please make a choice: "simmechanic", "Simmechanic" or "SimMechanic" throughout the manuscript
16. Page 68 (#49). "signal ... was designed in Fig. 3.10." - is not completely clear
17. Page 71 (#52). "The detail calculation ... is calculated below." - please, consider rephrasing
18. Page 86 (#67). (3.28) why "*" is used in the mathematical expression? (3.32), (4.3) - the same.
19. Page 87 (#68). "would run for the system performance" - "run for the performance" is not clear
20. Page 127 (#108). Reference in "gust wind (variable), Equ (1)." is not clear.
21. Page 149 (#130). (5.1) "whereby f is the function vector of state variables," - if this means that f(.) is a vector-function, it should be noticed that it depends not only on the state variable, but on the other ones
22. Page 149 (#130). The numerator in the first ratio below "system identification in [5]-[7];" is unclear and, most likely, erroneous.
23. Page 159 (#140). "Figure 5.7 LQR-Estimator-Integral Control" - an algebraic loop exists in the Simulink model. This causes questions.
24. Page 161 (#142). "As in (10)," , "As in (13):", "As in (14)," - the references are not clear

25. Page 184 (#165). "Sliding model control" - most likely, "Sliding mode control" should be instead
26. Page 189 (#170). Please check usage of round brackets throughout the paper. In the most of cases they are placed mistakenly (cf. <https://en.oxforddictionaries.com/punctuation/parentheses-and-brackets>)
27. There is some repetition at the beginning of each chapter, while summarizing motivation and key aspects of that chapter, see e.g. pages #4, #16, #126. This could have been done in order to keep each chapter self-contained. If the Committee opines that such repetition can be minimized, then suitable reduction of text can be done.
28. The next relevant papers may be optionally added to the Reference list:

- 1) Abdel-Rahman, E.M., Nayfeh, A.H., Masoud, Z.N. Dynamics and control of cranes: A review JVC/Journal of Vibration and Control. Volume 9, Issue 7, July 2003, Pages 863-908
- 2) Beznos, A.V., Grishin, A.A., Lensky, A.V., Okhotsimsky, D.E., Formal'sky, A.M. A flywheel use-based control for a pendulum with a fixed suspension point. Journal of Computer and Systems Sciences International, Volume 43, Issue 1, January 2004, Pages 22-33.
- 3) Aoustin, Y., Formal'sky, A. Simple anti-swing feedback control for a gantry crane. Robotica, Volume 21, Issue 6, November 2003, Pages 655-666.



B. Andrievsky
01, March, 2017

Response to Examiners:

Response to examiner(2)' report

Name : Thein Moe WIN

SID : 3274820

Never Stand Still

Graduate Research School

RESPONSE TO EXAMINER 2

Examiner comments (please reproduce exactly as in the examiner report)	Response (include text added to revised thesis)	Section / Page (in original thesis thesis)	Section / Page (in revised thesis)	Reviewer's Comment (if applicable)
GENERAL COMMENTS				
1. What are the assumptions for development of the mathematical model of the crane motion in the thesis?	<p>In chapter 3, there are several stages of mathematical model formations such as: 2D Nonlinear to Linear model and 3D Nonlinear to Linear model. In each case, assumptions in free-body diagram and linearization have also been explained.</p> <p>Using the nonlinear real-time data obtained from SimMechanic-Visualization based crane model simulation, linearized mathematical model is developed.</p> <p>In this mathematical model development process, this research developed improved version of Linear Least Square (LLS), considering to take 7 past inputs/outputs date instead of normal LLS approach. This assumption and approach gave the way to getting much reliable linear mathematical model.</p>	Ch 3, pp 57-66	Ch 3, pp 57-67	
2. How can the equations of motion (3.16)-(3.23) be evaluated for implementation to the crane during a motion?	<p>It is the Nonlinear Model Derivation for 3D model and Trolley-Payload Nonlinear Equations of motion scenario.</p> <p>The way joints and reactions forces are considered in the "Free-body Diagram Fig. (3.3) and equations of motions (3.16) -(3.23)", similar considerations have been taken in the SimMechanic-Visualization crane</p>	Ch 3, pp 35-44	Ch 3, pp 35-44	

Examiner comments <i>(please reproduce exactly as in the examiner report)</i>	Response <i>(include text added to revised thesis)</i>	Section / Page (in original thesis)	Section / Page (in revised thesis)	Reviewer's Comment (if applicable)
	model design.			
3. It's better to explain dynamical interaction between tower dynamics and crane dynamics in terms of load effects, such as wind, by considering different positions of the trolley on the crane.	<p>Glad to learn the examiner's helpful comment "to explain dynamical interaction...." and therefore the following additional section 4.7.1 is created.</p> <p>4.7.1 Vibration Impact Analysis on Tower Rotation-Trolley Translation with Wind Disturbance</p> <p>In this section, wind model disturbance has been applied on rotating tower crane while trolley translation throughout the jib tower. This simulation uses power input 6300W for tower to rotate (0 to 60 degree, maximum load 3000Kg, and the power input 3kW for trolley translation (0 to 20m). Wind model (1s notch) is reapplied to strike 3 times at certain time and spots. It is intended to identify vibration impact of the crane due to the dynamical interactions of tower rotation while trolley is translating. Interestingly, the simulation results contain vital information about the vibration impact of the crane in this scenario. The following Fig. 4.24a shows Tower rotation while Trolley translation is in process. During the operation, Wind pattern (static-gusts-pressure: 22-43-1017) is applied the same as before. However, due to the parallel tower-trolley run, swings angles fluctuations , Fig. 4.24b, and jibtip-hubtop oscillations are high. Fig. 4.24c obviously shows high oscillation reaching (-7 to 7 deg/se²) while reasonable amount of Hub-top oscillation appeared, Fig. 4.24d, which can cause the crane collapse. Therefore, this preliminary simulations results show running tower-trolley parallel operation is not recommended in real time.</p>	Not in old thesis	Ch 4, pp 120-121	

Examiner comments (please reproduce exactly as in the examiner report)	Response (include text added to revised thesis)	Section / Page (in original thesis)	Section / Page (in revised thesis)	Reviewer's Comment (if applicable)
	<p>Figure 4.24a Parallel Operation of Tower Rotation and Trolley Translation</p> <p>Figure 4.24c Jib-Tip Oscillation with Wind Pattern (22-43-1017)</p> <p>Figure 4.24b Swing angles in (X-Y-Z) directions</p> <p>Figure 4.24d Hub-Top Oscillation with Wind Pattern (22-43-1017)</p>			
4. How is the robustness of the control design in terms of sensor failures in the system?	<p>The following clarification in regards to "the robustness of the control design in terms of sensor failures in the system" has been added to the section 5.4 Summary.</p> <p>"Those developed controllers are considered to be robust for the crane system with all applicable sensors working condition. In the case of sensor failure during the operation, the robust controller is still usable but may have a slower response or become less effective to achieve the desire actuation and therefore, Fault Tolerant Control (FTC) is needed to be able to produce the desired effect, as in [77]. Since FTC is a combination of robust control and reconfigurable control, and further complexity in nature, it is recommended to implement in real crane operation though it has not been included in this stage of research."</p>	Not in old thesis	Ch 5, p. 161	

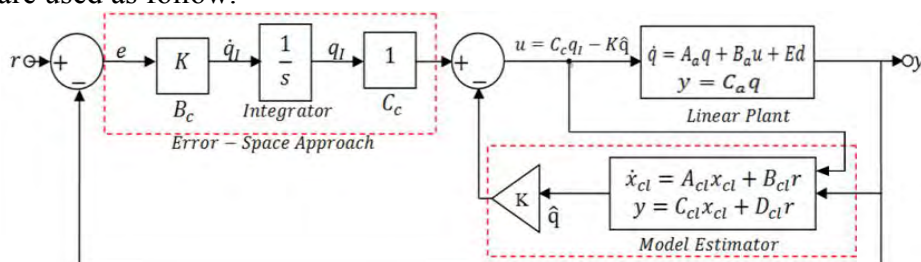
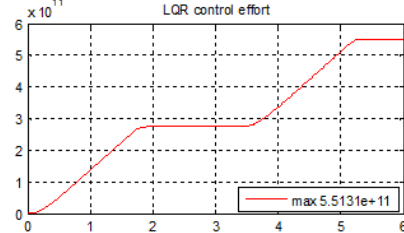
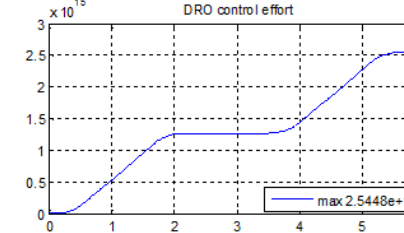
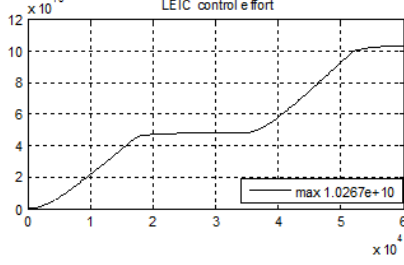
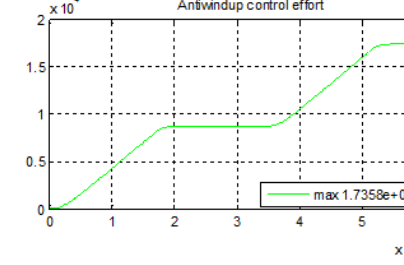
Examiner comments (please reproduce exactly as in the examiner report)	Response (include text added to revised thesis)	Section / Page (in original thesis)	Section / Page (in revised thesis)	Reviewer's Comment (if applicable)
6. Figure 4.11: could you explain what type of sensors can measure the angular accelerations in the order of 10^{-9} or 10^{-12} ?	<p>To view the angular accelerations and simulation results in Figure 4.11, the system needs certain type of sensors.</p> <p>Details of sensors implementation in Jib-tip/Hub-top and other essential locations are presented in section 3.4.13 with the Figure 3.47. Usually, those are position sensors draw angular position/velocity/acceleration during the operation making easier to analyse Jip-tip and Hub-top oscillations.</p>	Ch 3, p. 91	Ch 3, p. 92	
7. Considering some features such as short transfer time, why the finite-time LQR problem is not considered instead of the infinite-time case?	This thesis has only shorter rise time, shorter settling time, etc.. related to Figure 3.26. As the system is highly nonlinear time invariant, and states are infinite, this research has considered using infinite-time horizon approach.	Ch 3, p. 69	Ch 3, p. 70	
8. Page 140, Figure 5.7: What are the matrices F, G and H?	<p>The matrices F, G and H in Figure 5.7 refers to: $F = A_a$, $G = B_a$, and $H = C_a$ where A_a, B_a, and C_a are the augmented state spaces derived in section 5.2.</p> <p>However, to avoid confusion, the same derived augmented state spaces are used as follow.</p> 	Ch 5, pp 140-143	Ch 5, pp 141-145	

Figure 5.7 LQR-Estimator-Integral Control (LEIC) for Linear Model

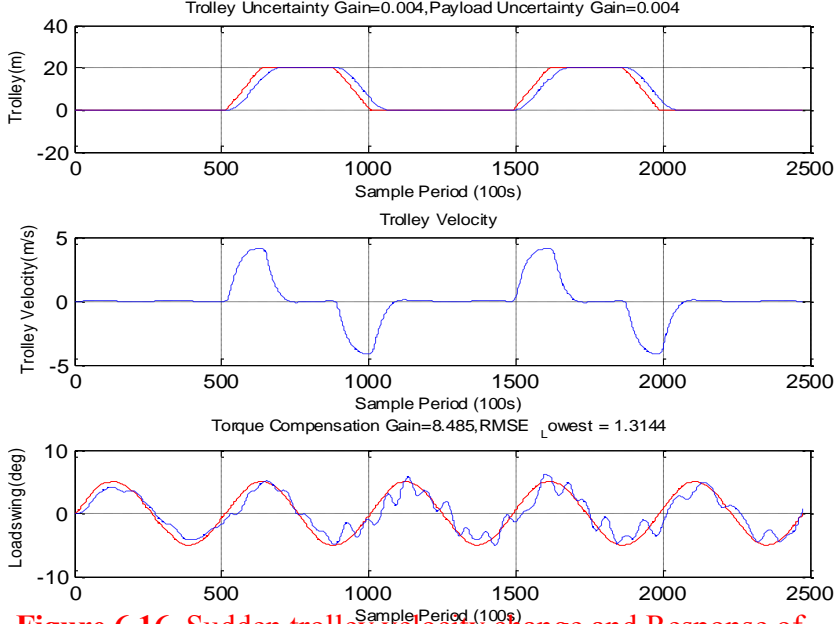
Examiner comments (please reproduce exactly as in the examiner report)	Response (include text added to revised thesis)	Section / Page (in original thesis)	Section / Page (in revised thesis)	Reviewer's Comment (if applicable)
How the reference signal 'r' is connected to the Model Estimator? Why both Linear Plant and Model Estimator (closed-loop system) are connected to each other in this block diagram, considering that the vector 'q' is already existed in the closed-loop state vector $x_{cl}(t)$.	<p>The reasons of using "reference signal "r" connected to the model estimator, in Figure 5.7" because, this research applies: the integral control approach with "$e = y - r$" in LQR-Estimator-Integral Control (LEIC) Development which is based on Franklin Powell 4th Edition Chapter 6 State-Space Design. The following Figure 5.8 has been modified to portray the LEIC in Simulink diagram.</p>	Ch 5, p. 143	Ch 5, p. 145	
9. In all control developments in the thesis, there is no constraints on the actuators. Could you explain how this effect can be considered in the design?	<p>This research has adopted a setpoint-following approach. This means that the LQ weights specify how closely the system follows the ideal response but they do not determine the control performance. Also, this deals in part with issues of actuator constraint as the actuations do not have to get the system output to the final setpoint.</p> <p>In the RTMC crane model, yes, constraints on the actuators have been discussed as follow.</p> <p>Section 3.4.15 "Trolley brake and Friction Design" discusses about four</p>	Ch 3, p. 93	Ch 3, p. 94	

Examiner comments (please reproduce exactly as in the examiner report)	Response (include text added to revised thesis)	Section / Page (in original thesis thesis)	Section / Page (in revised thesis)	Reviewer's Comment (if applicable)
	<p>constrain dampers which act as frictions for trolley translation.</p> <p>Section 3.4.16 "Input Tower Rotation Drive and Constrain Actuator" discusses about the implementation of one constrain damper which acts as a brake for Tower rotation actuator once tower exceeds the rotation limit.</p>	Ch 3, p. 94	Ch 3, p. 95	
10. Could you compare the control efforts for all cases LQR, LQR-DRO, LQR-LEIC, LQR-LEIC Anti-windup in Chapter 5?	<p>Thanks to the Examiner for this fruitful comment "to compare and discuss from the point of control efforts angle."</p> <p>Therefore, this research has added the following sub-section 5.3.7.</p> <p>5.3.7 Control Efforts Comparison</p> <p>This research further checks the control efforts of all developed linear controllers running in Trolley Translation controls. In order to do so, control signal from each design is squared-sum-integrate to analyze how good the control efforts are compared to each other. The following figures Fig. 5.18a provides the control effort of LQR with its peak value reaching $5.5131e^{11}$ while DRO control effort, Fig. 5.18b, takes largest control effort compared to others with its peak value $2.5448e^{15}$. Even though control effort in LEIC, Fig. 5.18c, further reduces to peak value with $1.0267e^{10}$, the significant changes happened in LEIC Anti-windup, Fig. 5.18d, with control effort takes up to $1.7358e^4$ only. Further simulations, improvements, and comparison would be made in payload swing control in the next section.</p>	Not in old thesis	Ch 5, p. 155	

Examiner comments (please reproduce exactly as in the examiner report)	Response (include text added to revised thesis)	Section / Page (in original thesis)	Section / Page (in revised thesis)	Reviewer's Comment (if applicable)
	    <p>Figure 5.18a LQR Control Effort Figure 5.18b DRO Control Effort Figure 5.18c LEIC Control Effort Figure 5.18d LEIC-Antiwindup Control Effort</p>			
11. How can the overshoot and undershoot of the trolley position response be minimized?	To minimize overshoot/undershoot, this research has done enormous trials adjusting the controller gain "K" and weighting matrices "Q and R". Several sections throughout chapter 5 discusses about the weighting matrices "Q-R" and control gain "K" trials.	Ch 5, pp 136-137 pp 141-142 pp 144-145 pp 149-150	Ch 5, pp 138-140 pp 143-144 pp 146-147 pp 151-152	
12. The simplified model of the tower train system is linearized around an operating point. As a future work, it is suggested to discuss the concept of linear parameter-dependent or parameter-varying model for	<p>Greatly appreciated for this comment.</p> <p>Yes, in the future work or further study, the concept of linear parameter-dependent or parameter-varying model for the system would be discussed</p>	Suggestion is for future work.	Suggestion is for future work.	

Examiner comments <i>(please reproduce exactly as in the examiner report)</i>	Response <i>(include text added to revised thesis)</i>	Section / Page (in original thesis)	Section / Page (in revised thesis)	Reviewer's Comment (if applicable)
<p>the system, which can be valid for a range of operating point conditions. In general, for the controller design developments in the thesis, the results are dependent on a constant simplified model.</p> <p>Can you present some possible strategies or ideas to improve it in your further study?</p>				
<p>13. In Figure 6.8, what are the sensors and their locations? And how the friction forces are derived?</p>	<p>Allocating necessary sensors and assigning friction forces are carefully considered during the trials-and-errors.</p> <p>Details investigation and implementation have been presented in the following sections:</p> <ul style="list-style-type: none"> -3.1.7 Nonlinear Model Derivation for 3D model - 3.4.2 Liebherr 71 EC Morrow Crane Datasheet -6.2 Cable structure impact on payload swing minimization -6.3 Reaction Forces and Torques Investigations -6.4 Joints, Sensors, and Actuators Implementation 	Ch 3, p. 35 Ch 3, p. 74	Ch 3, p. 34 Ch 3, p. 75	
<p>14. What is effect of the type of regressors selected in nalrx over the system response?</p>	<p>Several combinations of nonlinear regressors with different model orders were applied in order to get better fit model. The better the model fit in nalrx, the little control effort is only required to achieve the best control performance. Control effort comparison in section 5.3.7 has also been discussed.</p>	Ch 5, pp 145-158	Ch 5, pp 147-161	

Examiner comments (please reproduce exactly as in the examiner report)	Response (include text added to revised thesis)	Section / Page (in original thesis)	Section / Page (in revised thesis)	Reviewer's Comment (if applicable)
15. How the accuracy of the results in Figures 6.13 to 6.15 can be improved?	<p>To improve the accuracy of the results in Figures 6.13, Figures 6.14, and Figures 6.15, the essential parameters (Trolley Uncertainty Gain, Payload Uncertainty Gain, and Torque Compensation Actuator Gain) need to be fine tuned in the Nonlinear RTCMC design (Figure 6.11).</p> <p>Lowering the Root Mean Square Error (RMSE) can bring higher accuracy of the simulation results.</p> <p>Table 6.2 in section 6.8 discusses about the best suitable parameters chosen from trials-and-errors.</p>	Ch 6, pp 169-173	Ch 6, pp 172-177	
16. In Chapter 6, how the linear control LQR-DRO (i.e. single operating point) is computed for the Nonlinear RTCMC? If there is a sudden change in velocity of the trolley, how the nonlinear RTCMC will response?	<p>Several scholarly articles had provided the insight of LQR control for nonlinear systems. And, this research has also proved that LQR-DRO approach is possible to implement on Nonlinear RTCMC system due to;</p> <ul style="list-style-type: none"> -the best fit linear plant model developed by improved LLS approach. -the reliable LQR-DRO controller design -the implementation of sensors/actuators/reaction forces and torques/swing cables design/ and suitable parameters are all taken into consideration in order to achieve the nonlinear RTCMC control. <p>The Examiner's valuable comment about "Sudden change in velocity of the trolley, how the nonlinear RTCMC will response?" indeed helps this research to investigate RTCMC from another angle. Greatly appreciated.</p> <p>Therefore, this research has added the following section 6.9 "Sudden Trolley Velocity Change and Nonlinear RTCMC Response" in chapter 6.</p> <p style="color: red;">6.9 Sudden Trolley Velocity Change and RTCMC Response</p> <p style="color: red;">In real time operation, trolley translational position and tower angular rotation are the main trajectory concerns. The crane operator</p>	Ch 3, p. 67	Ch 3, p. 68	
	Ch 5, pp 136-138		Ch 5, pp 138-140	
	Ch 6, pp 160-169		Ch 6, pp 163-172	
	Not in old thesis		Ch 6, pp 176-177	

Examiner comments (please reproduce exactly as in the examiner report)	Response (include text added to revised thesis)	Section / Page (in original thesis)	Section / Page (in revised thesis)	Reviewer's Comment (if applicable)
	<p>needs to control the joy-stick to carry the payload based-on trolley position and tower rotation trajectories. Therefore, this research initially set reference trolley position and the payload swing reference constraints. The developed LQR-DRO control with actuator compensation will then perform the tracking process to achieve desire trolley position trajectory while keeping the payload swing within the reference constraints (5 to -5 degree). Even though the trolley velocity occurred sudden changes during the nonlinear RTCMC operations, trolley position control with payload swing suppression remains unaffected, Fig. 6.16. It is therefore proven that, the developed controller design is robust and reliable for the real time application.</p>  <p>Figure 6.16 Sudden trolley velocity change and Response of Nonlinear RTCMC</p>			

Examiner comments (please reproduce exactly as in the examiner report)	Response (include text added to revised thesis)	Section / Page (in original thesis)	Section / Page (in revised thesis)	Reviewer's Comment (if applicable)
<p>In addition, I would like to suggest the following minor comments in the document.</p> <p>-Quality, readability and visualization of some figures in the thesis should be improved, ex. Fig. 3.30, Fig. 4.12a, Fig. 4.15, so on.</p>	<p>Readability and visualization of the following figures have been improved.</p> <p>"Figure 3.30 Libherr 71-EC Morrow Tower Crane Datasheet"</p> <p>The figures (Fig. 4.12a, Fig. 4.12b, and Fig. 4.12c) shown in section 4.3 Vibration analysis comparison are regarded as unnecessary since those figures have been discussed in prior sections. Therefore, those figures have been removed.</p> <p>Fig. 4.15 has been improved but the figure number has been changed as Fig. 4.14 in revised thesis:</p> <p>"Figure 4.14 Wind Model Surface Area (x=0.12m,y=0.12m), 1-s notch wind strike"</p>	Ch 3, p. 75 Ch 4, p. 107	Ch 3, p. 75 Not in revised thesis	Ch 4, p. 111 Ch 4, p. 112
<p>- Page 57, below Equation 3.25, the vector $y(k)$ should be represented in bold and put in the equality sign '=' after $y(k)$ from the left side.</p>	<p>The vector $y(k)$ has been represented in bold in Equation 3.25.</p> <p>$\mathbf{y}(k) = -\theta_1 \mathbf{y}(k-1) - \dots - \theta_m \mathbf{y}(k-m) + \theta_{m+1} u(k-1) + \dots + \theta_{m+n} u(k-n) \quad (3.25)$</p>	Ch 3, p. 57	Ch 3, p. 58	
<p>-Page 134, Figure 5.3. The block diagram should be corrected as follows, please look at the disturbance input and ESO block (accordingly the block diagram in Figure 5.4 should be also corrected):</p>	<p>The following figures have been corrected accordingly to the Examiner's comment.</p>			

Examiner comments (please reproduce exactly as in the examiner report)	Response (include text added to revised thesis)	Section / Page (in original thesis)	Section / Page (in revised thesis)	Reviewer's Comment (if applicable)
	<p style="text-align: center;"><i>Disturbance Rejection Observer</i></p>	Ch 5, p. 134	Ch 5, p. 136	
	<p style="text-align: center;"><i>LQR-DRO Control</i></p>	Ch 5, p. 137	Ch 5, p. 139	

Examiner comments (please reproduce exactly as in the examiner report)	Response (include text added to revised thesis)	Section / Page (in original thesis)	Section / Page (in revised thesis)	Reviewer's Comment (if applicable)
<p>Some mathematical derivations are needed to elaborate LEIC- Antiwindup Control in bock diagram Fig. 5.14?</p>	<p>This LEIC-Antiwindup Control in bock diagram Figure. 5.14 is an extension of LEIC discussed in section 5.2 LQR-Estimator-Integral Control.</p> <p>All necessary mathematical derivations as well as parameters used have been presented in section 5.2 followed by the LEIC-Antiwindup development in sections 5.3.3 and 5.3.4 which discussed about the extension of "Integrator Antiwindup with Saturation".</p> <p>The following brief paragraph was added in section 5.3.4 "Weighting Matrices Q, and R" followed by the modified figure, Figure. 5.14.</p> <p>" This LEIC Anti-Windup approach is based-on LEIC structure with additional features (Saturation and integrator anti-windup). Anti-windup features are highlighted with red-dotted line in Fig. 5.14. Saturation values range are selected upon trial-and-errors to achieve the best control response."</p> <p>Figure 5.14 LEIC-Antiwindup Controller Design for Linear ARX Trolley Model</p>	Ch 5, pp 139-143	Ch 5, pp 141-145	

Examiner comments <i>(please reproduce exactly as in the examiner report)</i>	Response <i>(include text added to revised thesis)</i>	Section / Page (in original thesis)	Section / Page (in revised thesis)	Reviewer's Comment (if applicable)
<p>-For the vibration impact analysis, it is suggested to provide some comparative results in frequency domain for the load analysis or the tower crane system response.</p> <p>-Figures 6.2b, 6.3b are not clear and need to introduce the curves in color.</p>	<p>Thorough investigations and results comparisons regarding the Vibration impact analysis are presented in the following sections:</p> <ul style="list-style-type: none"> -4.5 Vibration Impact Analysis on Trolley Translation with wind Disturbance -4.6 Vibration Impact Analysis on Tower Rotation without Wind Disturbance -4.7 Vibration Impact Analysis on Tower Rotation with Wind Disturbance <p>Figures 6.2b, and 6.3b are generated in color. However, the printed pages (161-162) in thesis might have been in black-white by mistake. In revised thesis, it would be made sure to print all figures pages in color to be clear.</p>	Ch 4, pp 110-119	Ch 4, pp 111-122	

Confirmation that required work has been completed and recommendation of Award Degree is made by:				
Name:	Thein Moe WIN (3274820)			
Head of School	<input type="checkbox"/>	OR	Postgraduate Coordinator	<input type="checkbox"/>

**EXAMINER'S REPORT FOR THE
DEGREE OF DOCTOR OF PHILOSOPHY
STRICTLY CONFIDENTIAL**

Name of Candidate: Thein Win
School: School of Electrical Eng and Telecommunications
Title of Thesis: Robotic Tower Crane Modelling Control (RTCMC)
Report Due Date: 3 October 2016

**1 After examination of the thesis (and supporting papers) I recommend that:
(Please circle the letter next to the appropriate recommendation)**

A. The thesis merits the award of the degree.

This recommendation is appropriate if the thesis contains no faults that are apparent to the examiner. It is also appropriate where errors and omissions of an editorial nature are minor and, if left uncorrected, will not alter the conclusion that "the thesis merits the award of the degree".

or

B. The thesis merits the award of the degree subject to minor corrections as listed being made to the satisfaction of the Head of School.

The errors and omissions, which extend beyond those of an editorial nature, must be corrected if the thesis is to merit the award of the degree. The corrections are minor in that they do not change the structure or the conclusions of the relevant chapters of the thesis.

or

C. The thesis requires further work on matters detailed in my report. Should performance in this further work be to the satisfaction of the Faculty Higher Degree Committee, the thesis would merit the award of the degree.

The further work required should be sufficiently straightforward such that the examiner is happy to delegate approval of the revised thesis to the Higher Degree Committee. Examples of further work in this category could include: discussion and consideration of published work that is relevant to the conclusions of the thesis; consideration of alternative hypotheses that should reasonably be suggested by the candidate; presentation of additional experimental data that could be expected to be in the possession of the candidate; clearer specification of how the presented results/conclusions were arrived at.

or

D. The thesis does not merit the award of the degree in its present form and further work as described in my report is required. The revised thesis should be subject to re-examination.

Please indicate whether you are willing to review the resubmitted thesis Yes [] No []

The further work involves a major revision of the thesis on the same topic. The examiner is assumed to be satisfied with the candidate's capability and demonstrated competence for this further work. The comments and suggestions in the detailed report should be clear and helpful to the candidate. As the thesis is to be revised along the lines suggested by the examiners, it would normally be re-examined by the same examiners. Examples of further work in this category could include: further analyses or experiments where the scientific method as presented in the thesis has significant flaws; performance of additional experiments that are deemed vital to the conclusions drawn in the thesis.

Or

E. The thesis does not merit the award of the degree and does not demonstrate sufficient ability by

the candidate for a resubmitted thesis to achieve this merit.

The examiner should provide the basis of this recommendation in the detailed report.

2	I agree to my name being released to the candidate	Yes <input checked="" type="checkbox"/> No <input type="checkbox"/>
3	An Evaluation of the merits of the thesis is given overleaf (Attach additional pages if required)	

The examiner is requested to state concisely the grounds on which the recommendation is based, indicating where appropriate the strengths and weaknesses of the thesis. To assist the candidate with future work, this report may be released after a decision has been taken to award or not to award the degree.

Examiner: Professor Hamid Reza Karimi	Signature:	Date: 19/09/2016
---------------------------------------	------------	------------------

Please refer to the attachment.

Candidate's name: **Thein Moe Win**

Thesis title: **Robotic Tower Crane Modelling Control (RTCMC)**

The thesis by **Thein Moe Win** (TMW) consists of 259 clearly written pages in English and is covering 7 chapters with different sections and subsections and a bibliography and 4 Appendixes at the end. Besides this, the front matter covers 19 pages. TMW has cited 76 references in the thesis. This indicates that he has been aware of the literature relevant to the subject of his work. The document is easy to read and understand and can be briefly summarized as follows:

Chapter 1: In the introduction, TMW describes trends for the crane modeling, optimization, loading effects and motion control and the motivation for the work. the outline of the thesis is presented, which is followed by the TMW's achievements extracted from this thesis.

Chapter 2: This chapter reviews the related works in; tower crane modelling, system identification and linearization, anti-swing control strategies, and payload trajectory tracking controls.

Chapter 3: In this chapter the following results are presented: 2-dimensional overhead crane linear and nonlinear mathematical models, 3-dimensional tower crane nonlinear mathematical models, simmechanics-visualized 2-D overhead crane and 3D gantry crane models development, linearization and model optimization, simple Linear Quadratic Regulator (LQR) control for developed linear model, full-state feedback LQR control for reference tracking, and details of 3D Tower Crane Modeling using simmechanics-Visualization.

Chapter 4: In this chapter, the problem of vibration impact analysis is presented. More specifically, jib tower moment calculation, trials on both rigid-structure tower crane model and simmechanics-visualized 3-D tower crane, Wind disturbance model development based on Garonski approach, effect of wind disturbance on tower rotation, case studies on combinations of tower rotation speed-payload, identified and linearized worst case scenario, and finally implement full-state feedback LQR control.

Chapter 5: This chapter is devoted to control design. Firstly, the problem of LQR control design is proposed under Disturbance Rejection Observer (DRO) with Luenberger-based Extended State Observer to actively reject the disturbances caused by undesired source of inputs or unknown dynamics. Then, the following problems are address: 1) combination of error space approach with estimator as LQR Estimator-Integral Control (LEIC) for linear model, 2) the derivation of linear model using Nonlinear Autoregressive eXogenous (NARX) approach, 3) the development of LEIC-Antiwindup control to investigate robust reference tracking.

Chapter 6: In this chapter, Robotic Tower Crane Modelling Control (RTCMC) is addressed. Specifically, the following issues are presented in details: cable structure impact on payload swing minimization, investigation of reaction forces and torques, joints-sensors-actuators implementation, torque compensator design in swing minimization, complete nonlinear RTCMC, and comparison of trajectory tracking performance based on square reference and semi-hexagonal reference inputs.

Chapter 7: This chapter constitutes the conclusions and a review of further work.

In general, this doctoral study was initiated with tendency to investigate analysis and synthesis of Tower Crane Systems. However, the core concept of this research is to find competent solutions for dealing with the challenging topics of modeling and control of such systems under physical constraints.

The technical approaches developed in the thesis for the tower crane systems are technically sound, which make new contributions to the field of study. Some of the proposed approaches are numerically evaluated with the high fidelity software. During the Ph.D. study, TMW has published 3 articles in international journals and presented 4 articles in conferences. Therefore, the thesis presents substantial amount of original and good quality work, well beyond any threshold for qualification as a Ph.D. thesis.

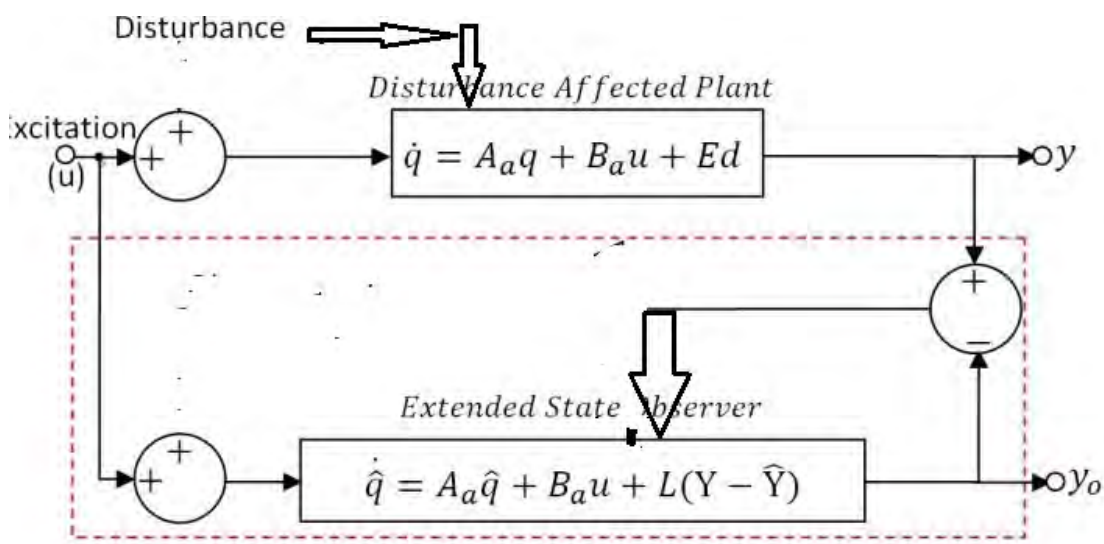
The writing is clear and in good style although the document has few minor grammatical and spelling errors. The general suggestions on the writing of the thesis are given as follows:

1. What are the assumptions for development of the mathematical model of the crane motion in the thesis?
2. How can the equations of motion (3.16)-(3.23) be evaluated for implementation to the crane during a motion?
3. It's better to explain dynamical interaction between tower dynamics and crane dynamics in terms of load effects, such as wind, by considering different positions of the trolley on the crane.
4. How is the robustness of the control design in terms of sensor failures in the system?
5. What performances or criteria should be considered in the control design? How can the cost function (3.28) fulfill a desired performance?
6. Figure 4.11: could you explain what type of sensors can measure the angular accelerations in the order of 10^{-9} or 10^{-12} ?
7. Considering some features such as short transfer time, why the finite-time LQR problem is not considered instead of the infinite-time case?
8. Page 140, Figure 5.7: What are the matrices F, G and H? How the reference signal 'r' is connected to the Model Estimator? Why both Linear Plant and Model Estimator (closed-loop system) are connected to each other in this block diagram, considering that the vector 'q' is already existed in the closed-loop state vector $x_{cl}(t)$.
9. In all control developments in the thesis, there is no constraints on the actuators. Could you explain how this effect can be considered in the design?
10. Could you compare the control efforts for all cases LQR, LQR-DRO, LQR-LEIC, LQR-LEIC Antiwindup in Chapter 5?
11. How can the overshoot and undershoot of the trolley position response be minimized?
12. The simplified model of the tower train system is linearized around an operating point. As a future work, it is suggested to discuss the concept of linear parameter-dependent or parameter-varying model for the system, which can be valid for a range of operating point conditions. In general, for the controller design developments in the thesis, the results are dependent on a constant simplified model. Can you present some possible strategies or ideas to improve it in your further study?
13. In Figure 6.8, what are the sensors and their locations? And how the friction forces are derived?

14. What is effect of the type of regressors selected in narlrx over the system response?
15. How the accuracy of the results in Figures 6.13 to 6.15 can be improved?
16. In Chapter 6, how the linear control LQR-DRO (i.e. single operating point) is computed for the Nonlinear RTCMC? If there is a sudden change in velocity of the trolley, how the nonlinear RTCMC will respond?

In addition, I would like to suggest the following minor comments in the document.

- Quality, readability and visualization of some figures in the thesis should be improved, ex. Fig. 3.30, Fig. 4.12a, Fig. 4.15, so on.
- Page 57, below Equation 3.25, the vector $y(k)$ should be represented in bold and put in the equality sign ‘=’ after $y(k)$ from the left side.
- Page 134, Figure 5.3. The block diagram should be corrected as follows, please look at the disturbance input and ESO block (accordingly the block diagram in Figure 5.4 should be also corrected):



- Some mathematical derivations are needed to elaborate LEIC- Antiwindup Control in bock diagram Fig. 5.14?
- For the vibration impact analysis, it is suggested to provide some comparative results in frequency domain for the load analysis or the tower crane system response.
- Figures 6.2b, 6.3b are not clear and need to introduce the curves in color.

Conclusions on the thesis

The thesis is well written and organized with a clear outline of the contributions. The effectiveness and advantage of the obtained results are illustrated by simulation studies. The conducted research covers a broad range of topics with a significant impact from the practical point of view, and may result in more good publications. In the thesis, TMW demonstrates that he has reached a mature scientific level and has a good overview over his field. I'm happy to recommend the candidate be admitted to the degree.